ANALYSIS AND DESIGN OF ANCHORAGE ZONES

IN POST-TENSIONED CONCRETE BRIDGES

by

OLIVIER LAURENT BURDET, B.S.C.E.

DISSERTATION

Presented to the Faculty of the Graduate School of

The University of Texas at Austin

in Partial Fulfillment

of the Requirements

for the Degree of

DOCTOR OF PHILOSOPHY

THE UNIVERSITY OF TEXAS AT AUSTIN

May 1990

Except the Lord build the house,
they labour in vain
that build it
Psalm 127:1

To my parents and my brother
Christophe, with love and
thankfulness.

Acknowledgements

At the conclusion of this work, I want to thank the many people who have made my coming to Texas possible and my stay pleasant and enriching. Dr. Jean-Claude Badoux of the Swiss Federal Institute of Technology in Lausanne encouraged me and helped me to come. Dr Marc Badoux gave me his advice and tutoring upon my arrival. Dr. John Breen deserves a special note for his warmth, his leadership and his patience as my supervisor during these three years. Dr. Gregory Fenves was willing to remain involved with the project in spite of his departure from the University.

I want to especially thank David Sanders for developing and maintaining a solid friendship in the midst of a lot of work. Most of the credit for our relationship belongs to David. I thank Carin Roberts, Gregor Wollmann, Brian Falconer and Tim Bradberry for their input and their willingness to listen to my sometimes lengthy developments. I thank Laurie Golding for her very competent handling of the administrative aspects of the project.

Finally, I want to thank God for his faithfulness through my years in Texas. I was not here by chance, but by design! To Him be the glory!

ANALYSIS AND DESIGN OF ANCHORAGE ZONES

IN POST-TENSIONED CONCRETE BRIDGES

Publication No. _____

Olivier Laurent Burdet, Ph.D.

The University of Texas at Austin, 1990

Supervisors: John E. Breen

Gregory L. Fenves

The current provisions of the AASHTO Bridge Design Specification do not address properly the problem of anchorage zones of post-tensioning cables, resulting in large differences in the design practice. Problems ranging from uncontrolled cracking to failure of the anchorage zone have been reported.

In this work, the Finite Element Method is used in conjunction with Strut-and-Tie Models based on the theory of plasticity of structures to investigate the behavior af anchorage zones of post-tensioning tendons. The anchorage zone is subdivided into two components: the local zone, consisting of the volume of concrete surrounding and immediately ahead of the anchorage device and the general zone consisting of the part of the member over

which the concentrated tendon force is laterally transmitted to the entire cross section. Three modes of failure relative to the various components are identified: failure of the local zone, tension failure of the general zone, and compression failure at the interface between the local zone and the general zone. The study concentrates on the last two modes of failure and on the analysis and design of the general zone.

The influence of the size of the anchorage device, of its eccentricity and, of the inclination and curvature of the tendon is investigated in parallel using the Finite Element Method and Strut-and-Tie Models. More complex configurations involving anchorage of multiple tendons and non-rectangular cross sections are also investigated. General guidelines for the development of the geometry of a Strut-and-Tie Model for the analysis of anchorage zones are developed and a specification proposal for the design of anchorage zones is presented.

The validity of the proposed analysis and design methodology is checked by comparing the analytical results with test results available from the literature, as well as with the test results of a companion experimental study in process at the University of Texas at Austin. The cracking loads of the anchorage zone predicted using the results of a linear elastic Finite Element Analysis are slightly too high. The ultimate load of the anchorage zone is conservatively approximated by the Strut-and-Tie Model.

Table of Contents

Chapter 1: Introduction

1.1   Post-Tensioned Concrete

Post-tensioning is a method of construction for concrete structures in which tendons of high strength steel are inserted in the structure in preformed ducts after the concrete is cast, as shown in Fig. 1.1. After the concrete has attained sufficient strength, the post-tensioning tendons are put under tension, inducing a field of compressive stresses in the concrete. Cement grout is generally injected in the tendon duct to protect the tendon from corrosion.
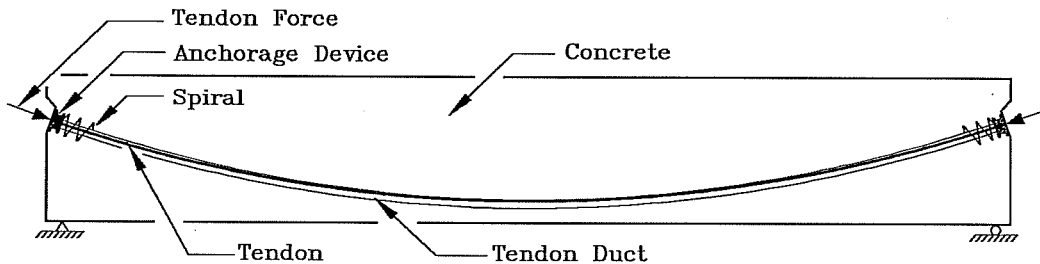
Figure 1.1   Principle of Post-Tensioned Concrete

Post-tensioned concrete presents several advantages over concrete reinforced with non-prestressed reinforcement only. The deflections under service loads are better controlled and cracks in the concrete are largely eliminated by the compressive stresses induced by the post-tensioning force. Economically, the combination of high strength steel in tension with high strength concrete in compression leads to an optimal utilization of both materials and allows for smaller cross sections.

1

Post-tensioned concrete is based on the principle developed in the late 1920's and early 1930's by the French engineer *Eugène Freyssinet* for prestressed, or pretensioned concrete. In pretensioned concrete, the reinforcement is generally in the form of individual wires or strands. The pretensioned reinforcement is put under tension using an external pre-tensioning frame before the concrete is cast; after the concrete has set, the connection between the pre-tensioning frame and the reinforcement is removed, and the pretensioned reinforcement (consisting generally of 7-wire strands) applies a compressive stress to the concrete. The tensile force of the pretensioned reinforcement is introduced into the concrete through bond stresses developing at both ends of the pretensioned strands.

In post-tensioned concrete, in contrast, the tendons are stressed only after the concrete has set, and the tendon force is introduced locally in the concrete through end anchorage devices. Post-tensioned concrete was first used in the late 1930's for the construction of bridges in Europe. The first post-tensioned concrete bridge in the United States was the *Walnut-Lane Bridge* in Philadelphia [111], built in 1948-49 by the Belgian engineer *Gustave Magnel*. Since then, thousands of others have followed.

1.2 Anchorage Zones

As mentioned in the previous section, the tensile force of the post-tensioning tendon is introduced into the concrete by end anchorage devices in the form of steel plates or castings. Fig. 1.2 shows various examples of anchorage devices. For practical reasons, the size of these anchorages is generally kept as small as possible, with the result that large forces are introduced very locally in the concrete. The *anchorage zone* is defined as the portion of the structure in which the concentrated

post-tensioning force is transferred from the anchorage device to the structure.

Because the primary reason for using post-tensioning is to introduce a significant compressive stress in the concrete, the tensile forces in the post-tensioning cables are typically very large. For example, in an ordinary bridge girder, the applied post-tensioning force is usually several times larger than the load applied on the bridge. It is not rare for an anchorage device
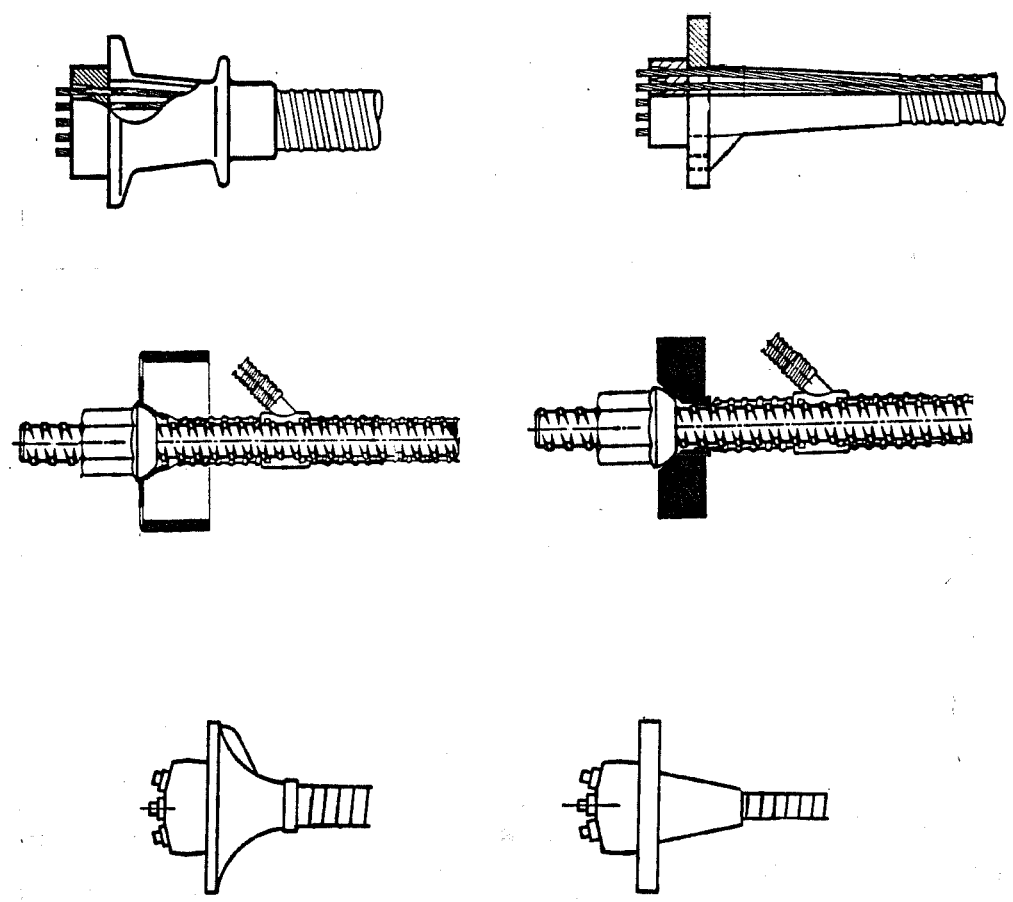
Figure 1.2   Examples of Anchorage Devices

with a cross sectional area of one square foot and weighing only 20 pounds to transfer a tendon force of 300,000 pounds.

The load-carrying mechanism of post-tensioned bridges relies primarily on the post-tensioning force. Therefore the anchorage zone is a very critical part of the structure, especially prior to bonding of tendons. The concrete is subjected to extremely high stresses in the anchorage zone, possibly more then anywhere else in the structure. Compressive stresses larger than the uniaxial compressive strength act in the immediate vicinity of the anchorage device. These high stresses are made possible by the favorable effect of confinement of the concrete. At a larger distance from the anchorage device, large tensile stresses develop which can lead to cracking of the concrete in tension.

1.2.1 Limit States Design

The general philosophy for the design of reinforced and prestressed concrete structures is formulated in terms of *limit states*. A limit state describes one set of conditions in which a structure must perform satisfactorily.

The *ultimate limit state* requires that the structure perform without collapse under the factored loads representing the largest expected overloading on the structure. At the ultimate limit state, it is impossible to apply more load to the anchorage than the actual ultimate force capacity of the tendon. In this limit state, the anchorage should not fail and still be able to transfer the tendon force, thus letting another, more ductile mode of failure take place.

The *serviceability limit state* requires that the structure have acceptable behavior under normal service loading conditions. Examples of acceptable behavior are a very limited amount of cracking, if any, and minimal displacements. Because one of the

primary purposes of using prestressed concrete is the subsequent limitation or suppression of cracks in the concrete, serviceability of anchorage zones is important. Ideally, no cracking is desired because it degrades the serviceability of the structure. However, if passive reinforcement is used to resist the tensile forces in the anchorage zones, reasonably large strains develop in both reinforcing steel and concrete. Thus it is likely that some cracks will form in the anchorage zone. Only lateral post-tensioning of the anchorage zone could entirely eliminate the cracks, but this solution is not always practical. The estimation of the cracking load of the anchorage zone and the provision of sufficient reinforcement to control cracking are important aspects of the serviceability design of the structure.

1.2.2 Modes of Failure of an Anchorage Zone

The design for the ultimate limit state is based on a series of checks that consider the various possible failure modes of the structure. Three principal modes of failures can be observed in anchorage zones.

The first mode of failure is a local failure in the immediate vicinity of the anchorage device, similar to the punching of an isolated foundation. The surface of rupture is often in the shape of a pyramid or cone, as shown in Fig. 1.3. The failure is caused by an insufficient compressive strength of the concrete or by lack of confining reinforcement.
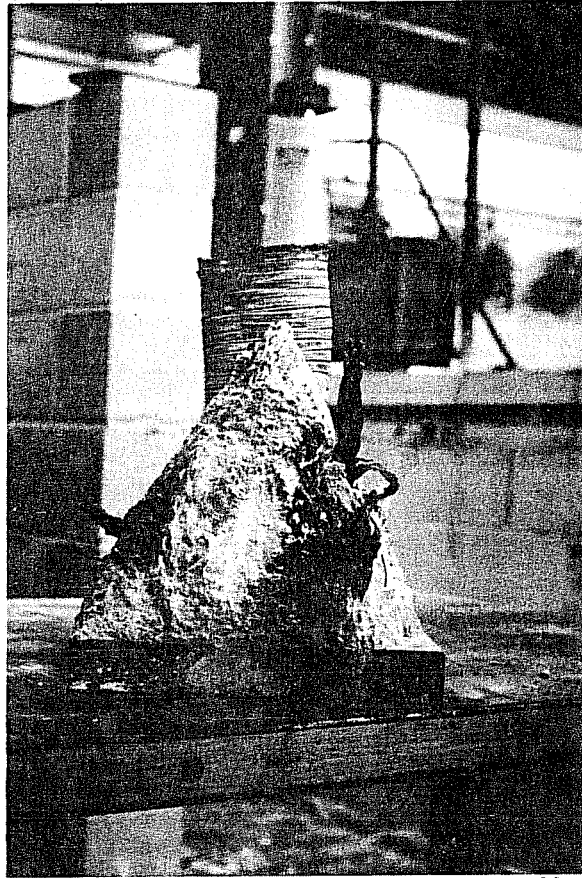
Figure 1.3   Compression Failure in the Local Zone with Cone of
             Concrete Characteristic of the First Mode of Failure
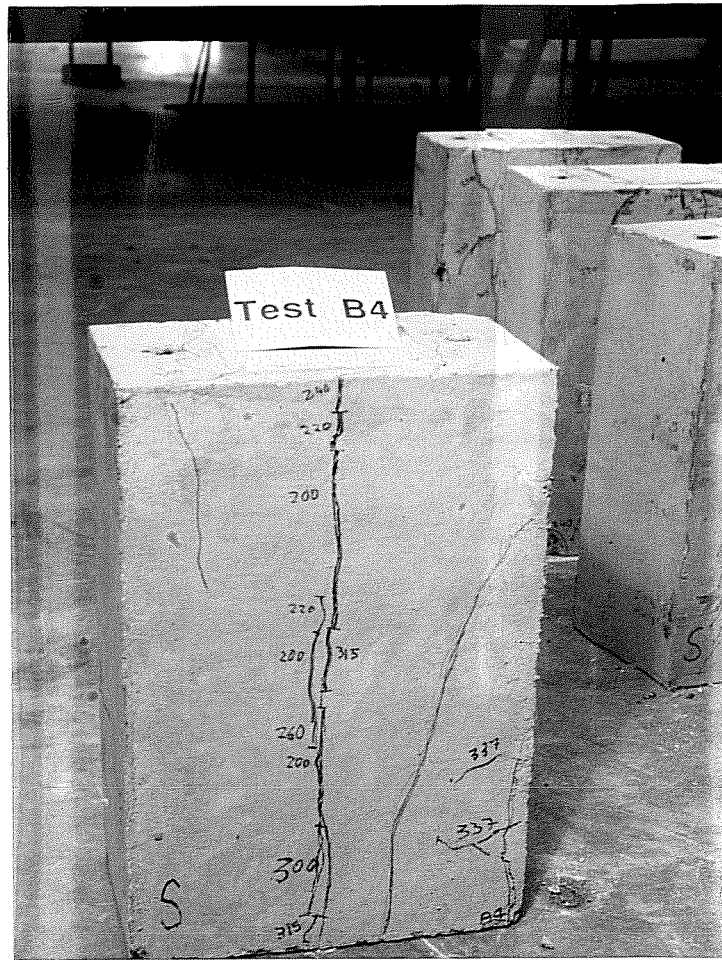
Figure 1.4   Large Cracks Along the Tendon Path Characteristic of
              the Second Mode of Failure (Tension Failure)

The second mode of failure occurs away from the anchorage device at a distance about one half of the depth of the member. It is characterized by large cracks running parallel to the post-tensioning duct and extending from the anchorage, as shown in Fig. 1.4. This mode of failure is caused by the inability of the transverse reinforcement to resist the transverse tensile forces in the concrete due to the lateral spreading of the post-tensioning force. This failure can occur at the time of first cracking or during subsequent loading.

Figure 1.5   Compression Failure at the Interface Between
Confined and Unconfined Concrete, Characteristic of
the Third Mode of Failure

The third mode of failure occurs at the interface between concrete surrounded by confining reinforcement in the immediate vicinity of the anchorage device and unconfined concrete. Because it involves a failure of concrete in compression, this mode of failure presents similarities with the first mode of failure. The main difference is that it occurs at a larger distance from the anchorage device. This mode of failure is characterized by cracks in the vicinity of the anchorage device and a bulging out of the concrete cover, as shown in Fig. 1.5.

As observed in tests by Sanders [153] and Stone & Breen [169], all three failure mechanisms exhibit a rather brittle behavior, even when the failure involves yielding of reinforcing steel. Because of this lack of ductility, any failure involving anchorage zones is undesirable. Ideally, the anchorage zones should be designed to safely transfer the tendon forces developed at ultimate, allowing a more ductile mode of failure to occur in another component of the structure.

To clearly distinguish between these three different modes of failure of the anchorage zone, it is helpful to define two distinct zones in the overall anchorage zone, the *local zone* and the *general zone*. The first mode of failure occurs in the local zone, the second mode of failure occurs in the general zone, and the third mode of failure occurs at the interface between the local zone and the general zone. The next subsections describe the characteristics of these two zones.

1.2.3 Local Zone

The local zone is the volume of concrete surrounding and immediately ahead of the anchorage device through which the concentrated force applied to the anchorage device is transferred to the general zone, as described in Section 1.2.4. Because the local zone is very close to the anchorage device, as shown in Fig. 1.6, its behavior is strongly influenced by the specific characteristics of the anchorage device. The geometry and the state of stress of the local zone are very complex, because of the duct hole, the confining reinforcement and the large tendon force. Large localized compressive stresses act at the interface between the anchorage device and the concrete of the local zone and tensile hoop stresses are induced by the lateral spreading of the concentrated tendon force.

a) Elevation

b) Plan View A–A
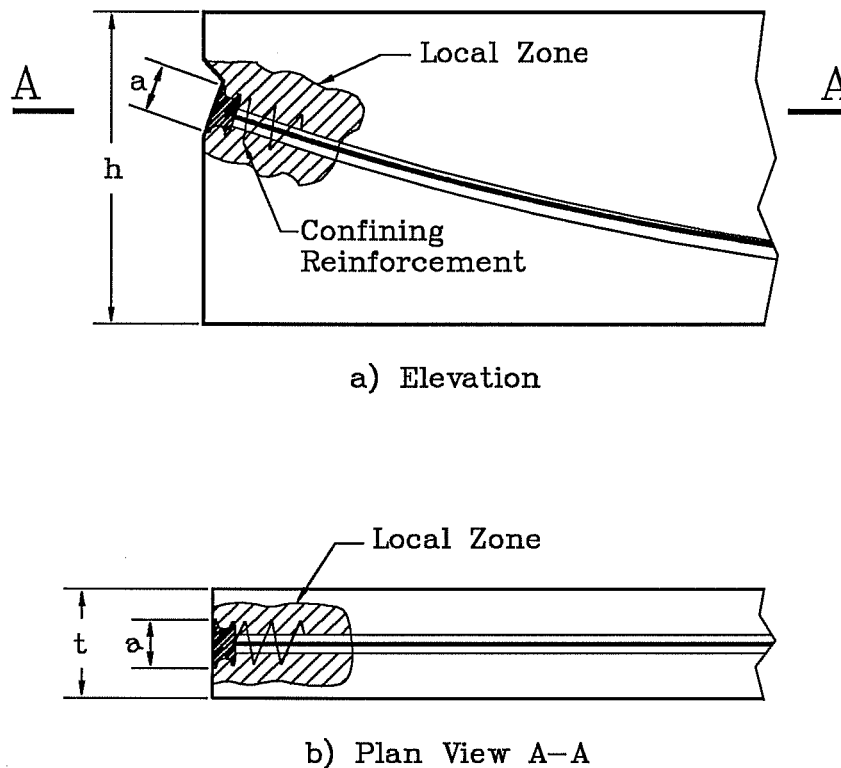
Figure 1.6   Definition of the Local Zone

The first mode of failure occurs in the local zone: the concrete fails, with a surface of rupture generally in the form of a cone or of a pyramid. The failure of the local zone is due to the lack of confinement, which can be provided by either confining reinforcement or surrounding concrete, allowing large lateral stresses to develop. The principal parameters governing the behavior of the local zone are the nominal bearing stress ahead of the anchorage device and the amount of confinement provided either by surrounding concrete or by confining reinforcement. The behavior and design of the local zone are not a direct part of this dissertation study. It is instead assumed that the design of the local zone is sufficient to prevent this mode of failure from occurring. As mentioned in Section 1.5, a separate component of the overall University of Texas research project was entirely

devoted to the subject of local zones and is described in [146]

1.2.4 General Zone

The general zone is the volume of concrete through which the lateral spreading of post-tensioning forces occurs from the highly concentrated force at the anchorage device to the more linear distribution across the entire cross section at some distance ahead of the anchorage device, as shown in Fig. 1.7. The extent of the general zone is approximately defined by Saint-Venant's principle, which states that the stresses tend to become uniform at a distance from a discontinuity equal to the largest transverse dimension of the member. In Fig. 1.7, the longitudinal extent of

a) Elevation

b) Plan View A–A
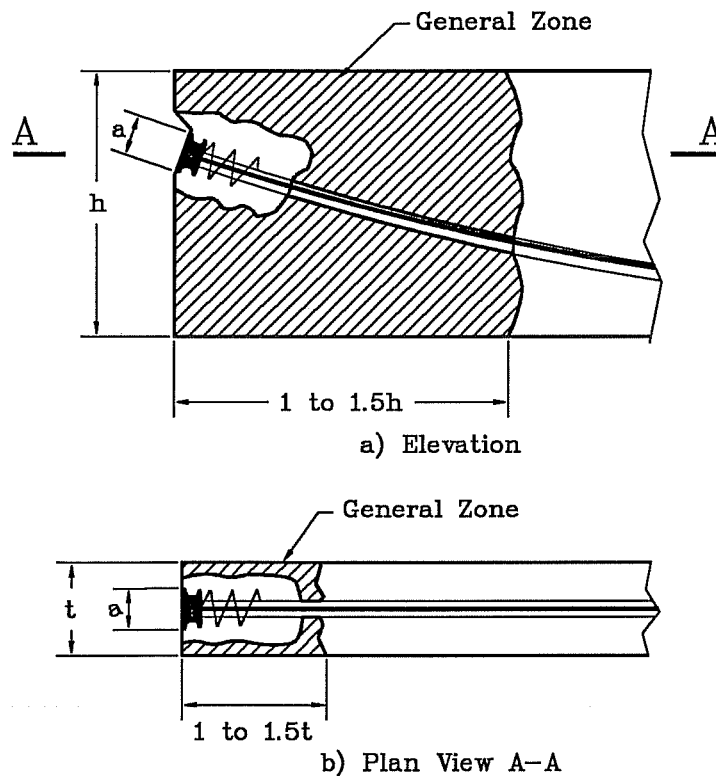
Figure 1.7   Definition of the General Zone

the general zone is shown to be between one and one and one- half times the transverse dimension of the member. The stresses in the general zone are not highly influenced by the specific anchorage device. In the transverse direction, the general zone extends for a distance about equal to the thickness of the member, as shown in Fig. 1.7b.

The second mode of failure occurs in the general zone. A tensile crack will form along the tendon path at some distance ahead of the anchorage device. After extension of the cracks along the tendon path, the reinforcing steel crossing the crack is highly stressed, and eventually yields. The cracks extend until no additional strength is available or the local deformation capacity of the anchorage zone is exhausted. At this point, the failure of the anchorage zone occurs.

a) Elevation

Spalling Stresses

Bursting Stresses

b) Plan View A—A
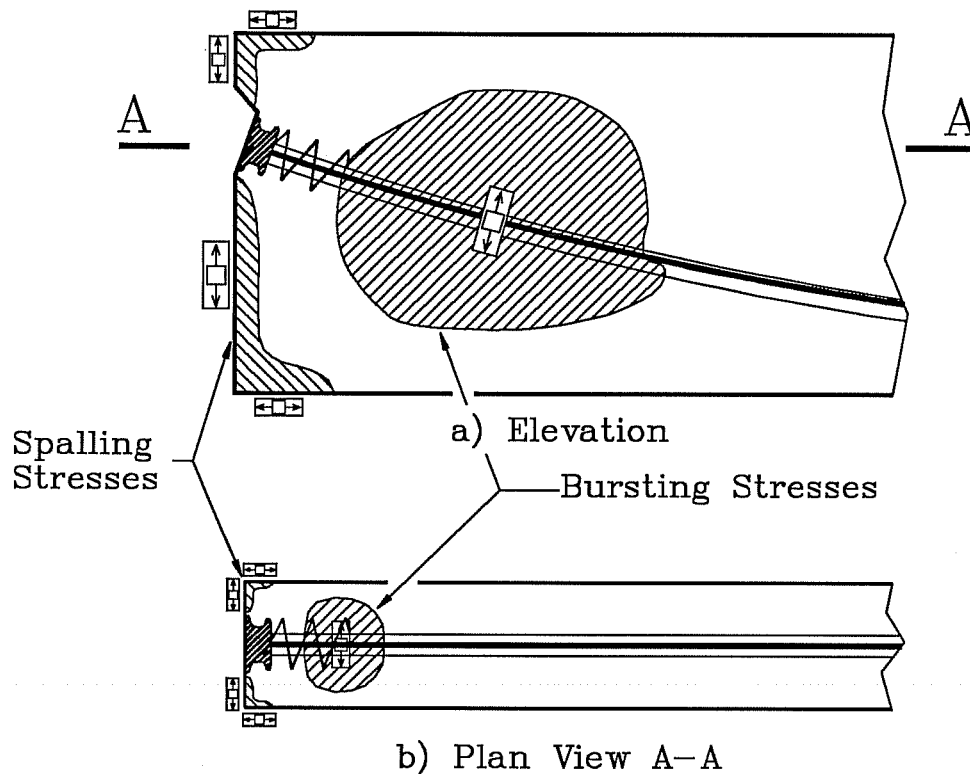
Figure 1.8   State of Tensile Stresses in the General Zone

The state of tensile stresses in the general zone exhibits several characteristics shown schematically in Fig. 1.8. The tensile stresses that act perpendicular to the tendon path in the concrete ahead of the anchorage plate are called bursting stresses. The tensile stresses that act parallel to the surface of the concrete on either side of the anchorage plate are called spalling stresses. Bursting stresses are caused by the lateral spreading of the tendon force from the concentrated location of the anchorage device to the entire cross section. Spalling stresses are mainly caused by the condition of compatibility of displacements. In cases where the tendon force is applied eccentrically, the spalling stresses are increased by components due to the overall flexure of the cross section.

1.2.5 Interface Between Local and General Zone

At the interface between the local zone and the general zone, the tendon force is transmitted from the confined concrete of the local zone to the concrete of the general zone. Depending on the size of the anchorage device and on the confining reinforcement provided in the local zone, the level of stresses at the interface between the local zone and the general zone can be very high. The third mode of failure occurs at the interface between the concrete of the local zone and the concrete of the general zone. The failure is caused by an excessive level of compressive stress transmitted from the concrete of the local zone, which is generally confined, to the concrete of the general zone, which is generally unconfined.

According to the descriptions given above, the local and general zones are overlapping, and there is a possibility of interaction between the behavior of the local zone and the behavior of the general zone. When the dimensions of the general

zone are much larger than the local zone, as in Fig. 1.7a, the modes of failure occur at different locations, and the interaction is small. In the case of smaller cross sections, or over the thickness of a thin specimen as shown in Fig. 1.7b, the local and the general zones tend to become identical. In such cases, the modes of failure controlling are failure of the local zone and failure at the interface between the local zone and the general zone.

1.3   Problems with Anchorage Zones

Most of the problems with anchorage zones described in the following subsections are observed at the time of the initial application of the post-tensioning force, or shortly thereafter. At that time, the post-tensioning force is at its largest, the strength of the concrete is at its lowest and the cement grout is not yet in place.   After the post-tensioning operations have been completed, the tendon duct is usually injected with a cement grout. The grouting is intended to protect the tendon against external corrosion attacks, but in the case of an internal tendon, the cement grout also provides a bond between the tendon and the concrete. This liaison between the post-tensioning tendon and the concrete structure makes a loss of resistance of the anchorage zone less critical, because the tendon forces can be transferred to the concrete through bond stresses, as in the cases of pretensioned concrete.

1.3.1 Excessive Cracking

The presence of tensile stresses in the concrete, both in the local and in the general zone, results in the potential for cracking of the concrete. Because of this, cracking has often been

observed when the post-tensioning force is first applied to the structure. If cracking occurs after the tensile capacity of the concrete is exceeded, it is necessary that a mechanism be available to resist the tensile forces acting in the structure. The use of passive reinforcement is a common and simple solution to resist tensile forces after cracking. If sufficient passive reinforcement is present in the anchorage zone and if it is located in the vicinity of the forming cracks, the progression and opening of the cracks will be stopped and the forces that were initially carried by the concrete in tension will be transferred to the steel. If, on the other hand, the reinforcement of the anchorage zone is insufficient or inadequately located, the cracks will propagate in the structure until eventually failure of the general zone occurs.

Excessive cracking is the most commonly observed problem with anchorage zones, particularly during the stressing of post-tensioning tendons. Even if the structure is uncracked after the tendons have been stressed, cracking may still occur at a later stage, due to creep of the concrete or external causes such as differential settlements or temperature effects.

1.3.2 Failure

Failure of the anchorage zone occurs when no stable state of equilibrium can develop to resist the tendon force. Failure will occur in the local zone if the concrete strength or the local confinement is insufficient. Failure will occur in the general zone if the concrete cracks in tension and if the reinforcement in the general zone is insufficient to resist the tensile forces. Failure will occur at the interface between the local zone and the general zone if the compressive strength of the concrete in the general zone is insufficient.

The number of reported failures in anchorage zones is significantly less than the number of reported cases where cracking occurred. Two main reasons can account for this trend. The first is the inherent toughness of anchorage zones. The load carrying mechanism exhibited by anchorage zones is complex and tests have shown that even apparently unimportant parts of the structure, like uncracked concrete in the general zone or reinforcing bars located at a large distance from the anchorage (outside the general zone as described in Section 1.2.4) can resist significant forces. Although these factors are not taken into account in the design, they can significantly enhance the strength of the anchorage zone. The second factor that can explain the small number of reported failures is the fact that, because the construction stage is generally the most critical case for anchorage zones, failure is likely to occur during construction. If a failure occurs during this phase, it will probably be promptly repaired and go essentially unreported.

1.3.3 Lack of Design Specifications

There has been comparatively little research done on anchorage zones of post-tensioning cables in the United States, resulting in a very limited number of practical design guidelines for anchorage zones. As a consequence, there is a lack of specifications for the design of anchorage zones of post-tensioning tendons. Most current design codes for post-tensioned concrete structures do not address the question of the design of anchorage zones in detail. As revealed by the CEB survey [29] described in Chapter 2, this lack of design specifications and guidelines results in an almost random variation of the designs of anchorage zones.

The problems related with anchorage zones are usually

unknown to the engineer and rarely appear in the literature. The few available design methods are often stretched beyond their range of application. Special cases like eccentrically introduced post-tensioning forces, inclined tendons or special geometries are often ignored.

1.3.4 Allocation of Responsibilities

Because of the lack of design and construction specification guidance on anchorage zones, the distribution of responsibilities in a project involving post-tensioning is often unclear. The parties involved are the engineer of record, the anchorage device supplier and the constructor. The engineer of record is responsible for the design of the project and for seeing that details carry out the design intent, but considerable flexibility is given to the constructor in the choice of the post-tensioning system used for construction. The supplier of the post-tensioning hardware may require that additional confining reinforcement to ensure proper performance of the anchorage devices. In practice, the design engineer has little control over the specific anchorage device hardware and without knowledge of the system and its required confining reinforcement he is not able to perform a complete design of the anchorage zone.

In a typical design process, the design engineer determines the required post-tensioning force and possibly proposes a system to resist the forces in the anchorage zone based on a post-tensioning system that he thinks is likely to be used. In a second stage, the constructor chooses the post-tensioning system suited to the circumstances and prepares the shop drawings. In a third stage, the supplier of the post-tensioning hardware may perform a check of the shop drawings for conformity with its standard detailing practice. In a final approval stage, the shop drawings

are submitted to the designer. Often, the designer has no specific criteria or experience on which to base the approval of the final details of the post-tensioning system. Because of the highly proprietary nature of the post-tensioning industry, it is possible that considerable variations will exist between the system originally conceived and the system installed in the structure.

In an attempt to clarify the areas of responsibilities for the design of anchorage zones, the research team involved in the current project proposed in the recent Post-Tensioning Institute (PTI) Final Report on Design and Construction Specifications for Segmental Concrete Bridges [141], now accepted as an American Association of State Highway Transportation Officials (AASHTO) Interim Specification, the concept of local and general zones. According to this concept, the constructor and the material supplier have the responsibility to ensure the proper behavior of the *local zone*, which is strongly hardware dependent. The design and specification of the reinforcement for the *general zone*, which is largely hardware independent is the responsibility of the engineer of record.

1.4   Specific Problems with Bridges

Highway bridges are particularly critical structures with respect to anchorage zones for several reasons that are discussed in the following sections. These reasons include the typical use of very large post-tensioning units and the frequent exposure to corrosive environments of deicing salt and salt water crossings.

In general, post-tensioned concrete bridges have cross sections as small as possible to limit the dead weight of the structure. The dimensions of the webs can often be reduced because the shear force is partly resisted by post-tensioning forces. However, as the web becomes thinner, the space to place anchorage

devices, confining reinforcement, shear reinforcement and general zone reinforcement becomes very congested, complicating the construction process and the casting of the concrete.

Highway bridges are located outdoors, in a potentially corrosive environment. Any crack can let corrosive mediums seep into the structure and attack the reinforcing steel. This is especially critical for bridge decks, girder ends and substructure elements. To limit corrosion of the reinforcement and degradation of the concrete, it is generally desirable to limit as much as possible cracking of bridge structures. One effective method is the use of lateral post-tensioning. Transverse post-tensioning of bridge decks is increasingly used in order to limit the extent of cracking and enhance the quality of the structure, but the anchorage zones of these cables must be themselves specially treated to avoid losing the advantage of post-tensioning.

As illustrated by the UT Survey on anchorage zones described in [24], there is a very large diversity in the design of anchorage zones in the US. This diversity is in itself a positive factor showing the innovative applications of post-tensioning. However, there is a need for specifications for post-tensioned anchorage zones to ensure more consistency in the design, more uniform reliability for the anchorage zones and a clearer assignment of design responsibilities.

1.5   UT Austin Research Project on Anchorage Zones

In response to the needs mentioned above, the *National Cooperative Highway Research Program (NCHRP)* initiated a research project on anchorage zones, of which this dissertation is a part. The research project seeks to identify and answer the questions related to the design of anchorage zones of post-tensioning tendons in concrete bridges. The investigation is pursued both

analytically and experimentally, with the intent of developing a general design philosophy and guidelines for the design of anchorage zones. Because of the extent of the project, several phases and components were defined within the overall project. In the first phase of the project, the analytical work of the present dissertation was pursued, focusing on the design of the general anchorage zone. A parallel experimental investigation program of the general zone was conducted under the supervision of Dr John Breen by David Sanders [153] while the specific subject of the design and acceptance testing of local zones was investigated by Carin Roberts [146]. In the second phase of the research project, more complicated geometries and loadings are being studied by Gregor Wollmann [189] while Brian Falconer [58] investigates the case of slab post-tensioning.

1.6   Goals of the Dissertation

The specific goals of the present dissertation are to investigate analytically the flow of forces in anchorage zones of post-tensioning cables and to establish a consistent methodology for the analysis and the design of anchorage zones. The applicability to the design of anchorage zones of Strut-and-Tie Models as well as the use of results from two- and three-dimensional linear Finite Element models are investigated. The development of Strut-and-Tie Models is supported by the results of Finite Element Analyses of the anchorage zone. Parametric studies using both the Finite Element Method and the Strut-and-Tie Model investigate the influence of the various parameters in the anchorage zone. The main parameters are the geometry of the anchorage device, the eccentricity and the inclination of the post-tensioning force as well as the material properties. In addition, the results of the Finite Element Analyses are used to

estimate the cracking load of the anchorage zone.

The models derived in the analytical study were used for the design of a series of experimental test specimens in companion study [153]. The validity of the proposed methodology is verified by comparing the analytical predictions with the results of experimental tests from the companion study and from a previous test program [172, 173, 174]. A series of practical recommendations for the analysis and the design of anchorage zones is presented and discussed.

1.7   Organization of the Dissertation

The overall organization of the dissertation can be seen from the chapter titles:

Chapter 1 : Introduction

Chapter 2 : State of the Art on the Analysis and Design of
            Anchorage Zones

Chapter 3 : Methodology for the Analysis of Anchorage Zones

Chapter 4 : Concentric Single Anchor Configurations

Chapter 5 : Other Single Anchor Configurations

Chapter 6 : Multiple Anchorages and Non-Rectangular Cross Sections

Chapter 7 : Summary of the Results and Specification Proposal

Chapter 8 : Conclusions

Chapter 2:   Literature Review of the Analysis and Design
              of Anchorage Zones

    The purpose of this chapter is to present an overview of the
technical literature for the analysis and the design of anchorage
zones. While many of the references date back from the 1950's and
1960's, there have been several important contributions since that
time. Stone and Breen [172] presented a comprehensive review of
the literature up to 1978. In the initial phase of this research
project, an extensive update of the literature was performed,
including more recent material, and was presented in the Interim
Report to NCHRP [24]. Although the bibliography at the end of this
dissertation includes all references presented in those two
documents, only references that have a direct bearing on this
dissertation are discussed in detail here.

    2.1   Overview of the Possible Solutions

    In the Interim Report to NCHRP [24], the following
classification was introduced for the possible approaches to the
problem of anchorage zones. This classification is also used in
the subsequent sections.
    1) Analysis using the theory of Elasticity,
    2) Equilibrium methods of analysis,
    3) Finite Element studies,
    4) Strut-and-Tie Models,
    6) Experimental investigations.
    Beside experimental investigations, the more recent studies
consist generally of either Finite Element studies or studies
using equilibrium-based Strut-and-Tie Models.

22

2.2   Analysis Using the Theory of Elasticity

Assuming that the reinforced concrete of the anchorage zone is a homogeneous, isotropic and elastic material, the anchorage zone can be analyzed as a concentrated force acting on an elastic body. This approach has been shown [67, 68] to be valid until the onset of visible cracking. Because the elastic analysis satisfies equilibrium, the distribution of elastic stresses indicates a possible load-carrying mechanism. If an appropriate criterion is chosen for the compressive and tensile stress limits, the elastic analysis results can be useful in determining the capacity of the anchorage zone. Linear elastic analyses usually do not consider the effect or distribution of anchorage zone reinforcement.
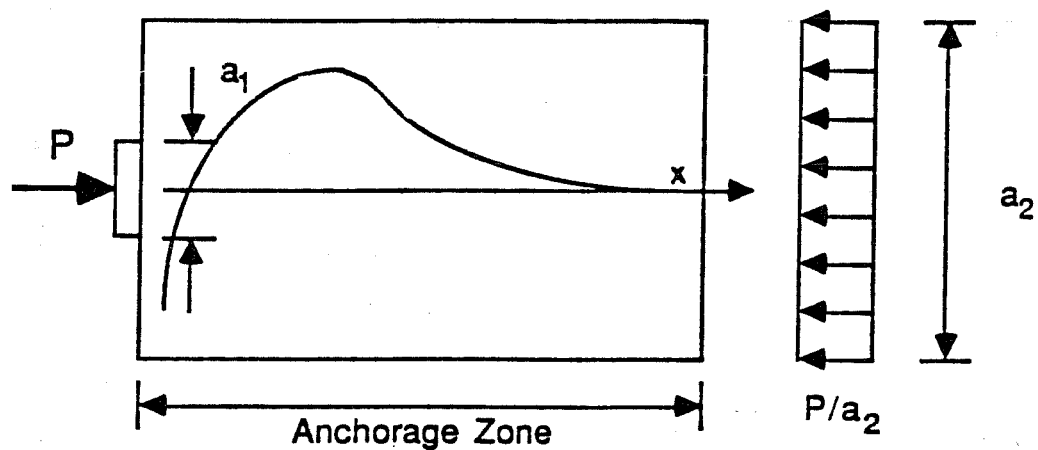
Figure 2.1   Geometry and Stress Distribution Along the Axis of a Concentric Anchorage Zone

Several authors have used two-dimensional elasticity for this approach, the most exhaustive and influential being Guyon [73, 74, 75]. Guyon solved the problem by using Fourier series, but also proposed simplified approaches and provided design aids for the determination of the stresses and forces acting in the anchorage zone. Fig. 2.1 shows the general anchorage zone of a
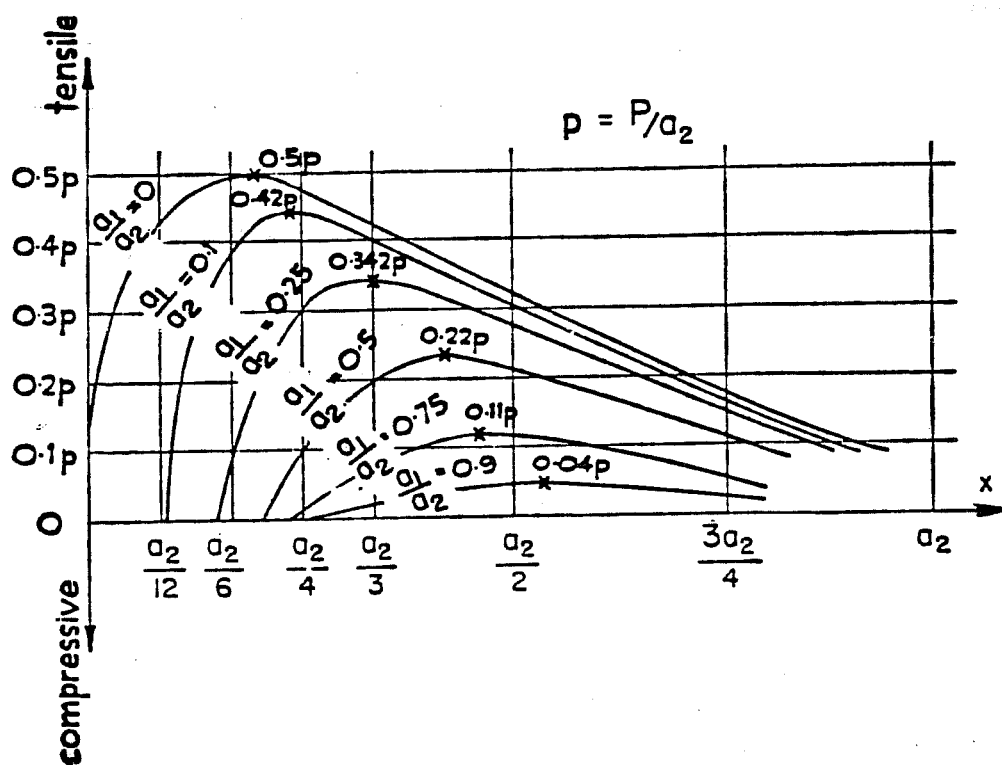
Figure 2.2   Bursting Stress Distribution According to Guyon [75]

rectangular beam subjected to a concentric tendon force. The longitudinal stresses induced by the post-tensioning force are uniformly distributed over the cross section at a distance approximately equal to the transverse dimension a_2 of the member. Guyon developed the design aid shown in Fig. 2.2, which gives the distribution of the tensile stresses perpendicular to the tendon

(bursting stresses, see Chapter 1) as a function of the ratio of the size of the anchorage device to the lateral dimension of the section, a_1/a_2. Fig. 2.3 shows another of Guyon's design aids, giving the total tensile bursting force as a function of the ratio of the size of the anchorage device to the lateral dimension of the section, a_1/a_2.

When the tendon force is applied eccentrically on the section, Guyon showed that the results obtained for a concentric prism can be still be used. To that end, the tendon load is assumed to act on a *symmetrical prism*, shown in Fig. 2.4 and defined as the largest symmetric prism that fits in the section with its centroid coinciding with the axis of the tendon. In the case of Fig. 2.4, the lateral dimension of the symmetrical prism is equal to twice the minimum distance from the centerline of the tendon to the closest edge of the concrete. The concept of symmetrical prism can also be applied to the case of multiple tendons acting on a cross section, as shown in Fig 2.5. In this case, the various symmetrical prisms are limited by either the distance to an edge of the concrete or by an adjacent prism.
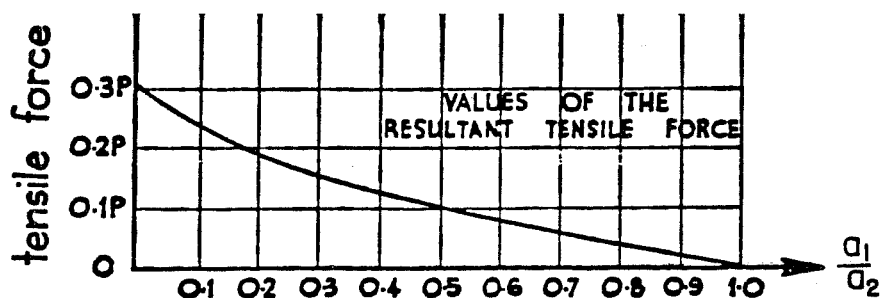
Figure 2.3   Bursting Force According to Guyon [75]

Table 2.1　Spalling Force According to Guyon [74]

a_1/a_2	0	0.1	0.25	0.5
Spalling Force	0.04P	0.03P	0.025P	0.02P
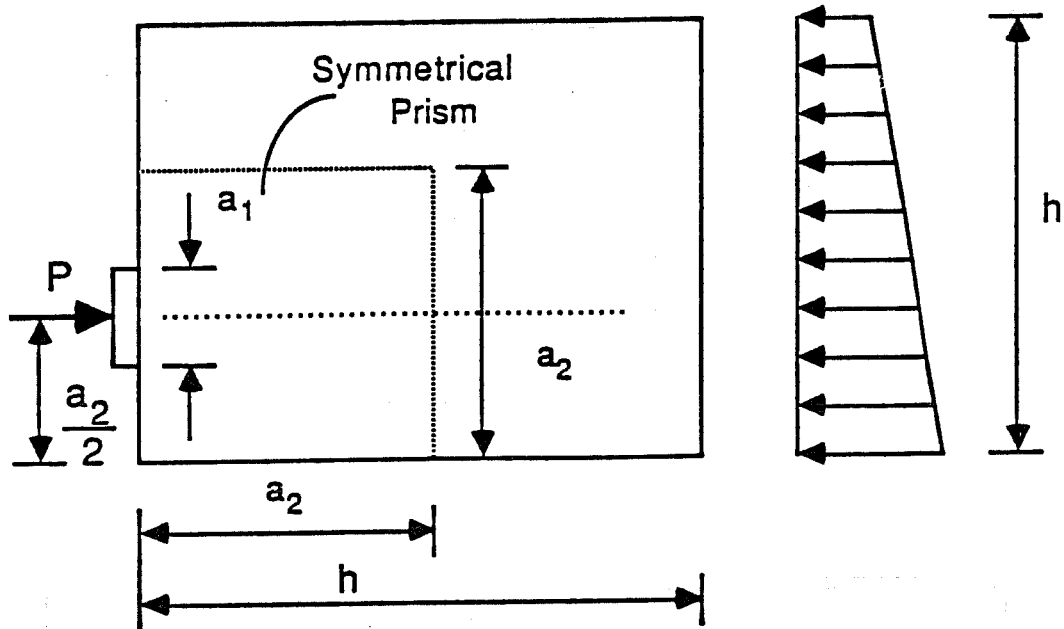
Figure 2.4　Guyon's Symmetrical Prism for Eccentric Anchorage Zone
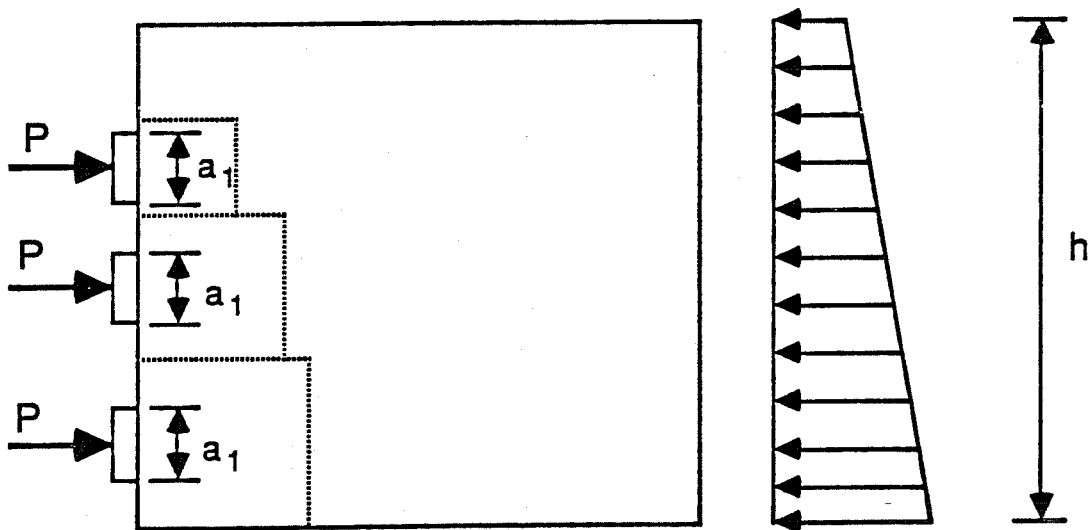
Figure 2.5   Guyon's Symmetrical Prism for Multiple Anchorage
             Zone

Based on photoelastic studies by Tesar, Guyon also determined the value of the spalling forces acting at the surface of the concrete on either side of the anchorage device. The values of Table 2.1 give the spalling force as a function of the relative plate size. As a matter of simplification, Guyon proposed to design for a constant value of 0.04P. The influence of the eccentricity of the load on the magnitude of the spalling force is not considered in this approach. In later editions of his textbook [74], Guyon introduced this effect, as shown in Eq. 2.1, where a is the distance from the tendon to the closest concrete edge, and a' is the distance to the furthest concrete edge.

$$T_s = (0.04 + |(a-a')/(a+a')|^3] \ P \qquad Eq. \ 2.1$$

Several other authors have studied the basic configurations investigated by Guyon, and have generally found Guyon's values to be correct [49, 52, 67, 68, 71, 192, 193].

2.3   Equilibrium Methods of Analysis

Equilibrium methods of analysis have been used to solve the problem of an anchorage zone after cracking has occurred. In a simplification of the real behavior, the cracks are assumed to be located at a known position, and the equilibrium of the structure is formulated. Fig. 2.6 shows the elastic foundation analogy proposed by Lenschow and Sozen [97]. Equilibrium methods have not been used in recent times, probably because the advent of nonlinear Finite Element solutions has decreased the need for approximate methods for modelling of cracking in concrete.
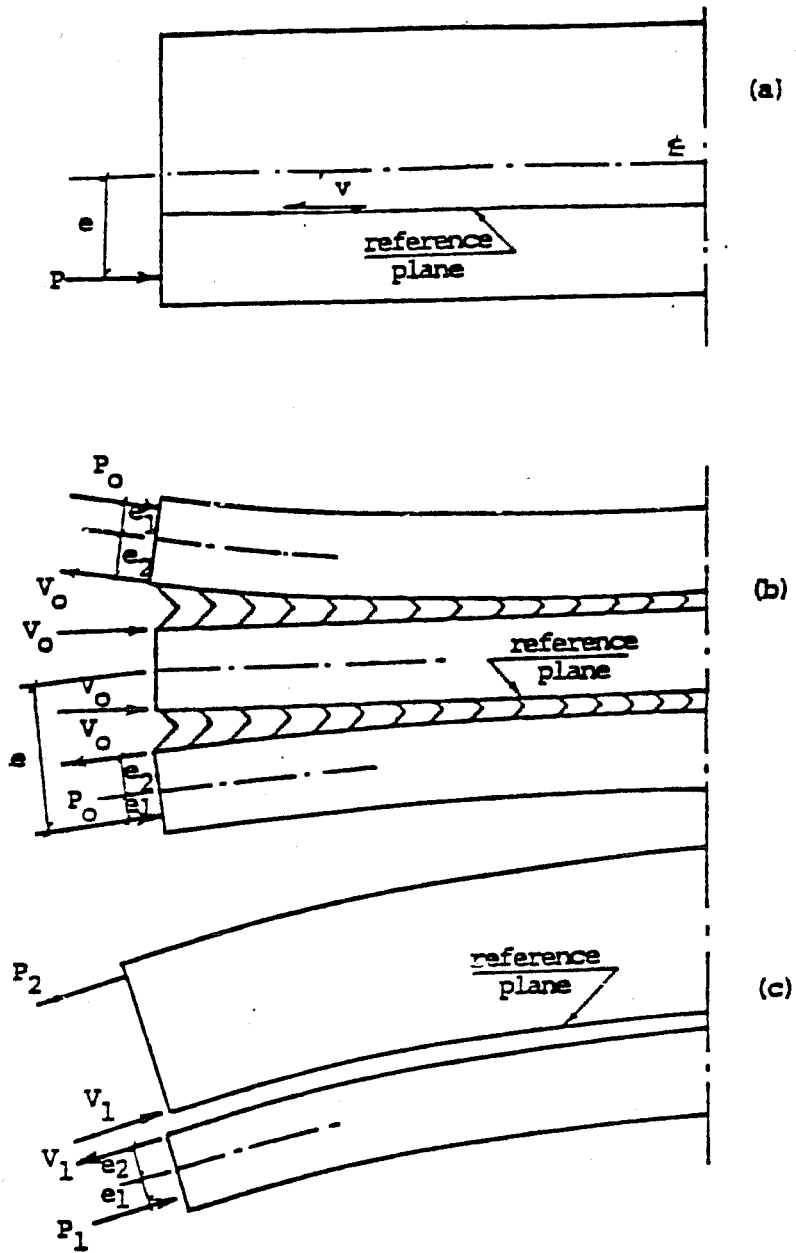
Figure 2.6   Analogy of a Beam on Elastic Foundation According to
            Lenschow and Sozen [97]

2.4 Photoelastic Investigations

Christodoulides [33, 34, 35, 36] performed two-dimensional photoelastic tests to explore the distribution of stresses in a rectangular block with two anchors symmetrically arranged about the centerline of the section. Christodoulides also conducted a three-dimensional photoelastic study on a concrete crane gantry to compare the photoelastic results with strain data. From his tests, he concluded that maximum stresses occur directly in front of the load. He determined that the Poisson's ratio had no effect on stresses because the results obtained on plastic models agree with the results from the concrete gantry test. According to Christodoulides' results, both Magnel and Guyon theories underestimate the stresses on the surface of the concrete.

Rasheeduzzafar and Al-Saadoum [143] conducted a three-dimensional photoelastic investigation of anchorage bearing stresses in rectangular blocks. The study looked at embedded anchors versus external anchors and the case of multiple anchors and the influence of the edge distance. The following trends were determined from their study. Embedded anchors allow part of the force to be transferred by shear and part by bearing, with about one-third of the force transferred by shear traction. Embedded anchors have smaller maximum tensions than external devices. Forces become essentially uniform after a longitudinal distance of two-thirds the depth of the block. The stresses that develop on the unloaded faces are very dependant on the location of the anchor; therefore, the authors predicted that a design formula that does not incorporate the distance between the anchor and the unloaded face will not be entirely successful in predicting stresses. In the tests, the geometry of the single and multiple anchorages were not exactly the same, but the stress data obtained suggested that, apart from an increase in the bursting tension on

the loaded face, there is no significant interaction between adjacent anchor units spaced by at least twice the largest anchor dimension. The authors concluded that in the absence of more comprehensive design criteria, the symmetrical prism approach of Guyon provides the most reasonable model for evaluating the bursting force.

2.5   Finite Element Studies

The development of comprehensive Finite Element analysis models has opened the way for powerful analytical studies. The linear finite element analysis has great promise for the determination of uncracked state stresses. Nonlinear Finite Element studies can model the anchorage zone in its cracked state. Yettram and Robbins [192, 193, 194] and Stone [169] have used two- and three-dimensional linear Finite Element models to investigate the state of stresses in the anchorage zone. They report stresses in accordance with Guyon's for concentric cross sections.

A broad investigation using the Finite Element Method was conducted by Yettram and Robbins [192, 193, 194]. The results of this research were presented in a series of three articles with the first addressing the simplest case of the stresses in a rectangular cross section with a concentric force. In this first study [192], both two-and three-dimensional cases were reported with the following conclusions. The distance to form a uniform normal stress field is 1.25 times the height of the prism. A variation of Poisson's ratio between 0.125 and 0.2 has little effect on the stress distribution. Iyengar's [87] and Guyon's [75] two-dimensional elastic analysis results give good values of the average stress when compared with Yettram, although they cannot indicate the transverse variations in the stress distribution. Yettram and Robbins compared their results with the experimental

results of Zielinski and Rowe [196, 197] , which are based on surface strain measurements. Zielinski and Rowe overestimate the maximum bursting stress for all ratios of bearing surface to cross section area.

In the second paper, Yettram and Robins [193] addressed the problem of anchorage zones in rectangular and non-rectangular cross sections. For the cases studied, it was determined that the symmetrical prism of Guyon gives a satisfactory representation of the bursting stresses for design purposes. They suggested that in the case of a non-rectangular section, if the symmetrical prism extends into either or both flanges, the bursting stresses extend further ahead of the anchorage device than in rectangular cross sections. They found also that, in non-rectangular cross sections, the flanges generally reduce the magnitude of the spalling stresses.

In their third paper, Yettram and Robbins [194] studied anchorage zone stresses in I-section members with end blocks. In the study, the length of the end block was the major variable. They concluded that in very short end blocks the transverse, out-of-plane bursting forces should be considered. A longitudinal taper between the block and the web is advantageous. Short end blocks are of little advantage because bending stresses overshadow the bursting stresses, causing an increase in transverse reinforcement and a greater congestion in the anchorage zone.

Egeberg [52] applied linear elastic Finite Element analysis to anchorage zones. The nonlinearities of the material, mainly the cracking of the concrete were modelled by manually introducing discrete cracks at locations of large stresses and performing a new analysis. Reinforcement was also modelled. Egeberg found a good agreement between his results and the results of Guyon [75] and Magnel [111]. He further determined that the bursting stresses for eccentric anchorage zones are almost identical to the bursting

stresses in concentric anchorage zones, simply shifted to a new location. The introduction of a crack at a predefined stress level of tensile stress in the concrete caused the stresses ahead of the crack to increase, thus propagating the crack. The addition of reinforcement significantly dropped the level of tensile stresses in the concrete as the tensile force was transferred to the steel.

Adeghe and Collins [4] used a non-linear Finite Element program to model specific details of reinforced concrete structures. The concrete model used is based on the compression field theory [184] which includes both tension and compression softening of the concrete. One of the detailing problems studied by Adeghe and Collins was the anchorage zone of a post-tensioning tendon.

Fig. 2.7 shows the distribution of the strains in the concrete along the tendon axis for the various configurations of the reinforcement shown in dashed lines. Fig. 2.8 compares the principal stress vectors in an anchorage zone modelled using a linear elastic model and a non-linear model. In the non-linear case, the principal stress vectors make a smaller angle with the axis of the tendon, but the difference is not extreme.
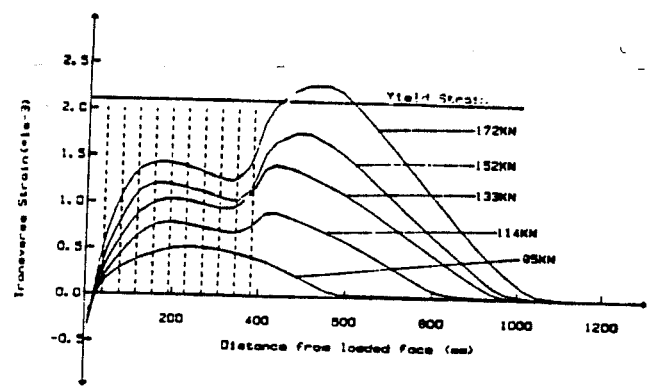
(a) Distribution of transverse strains for stirrup detail 1
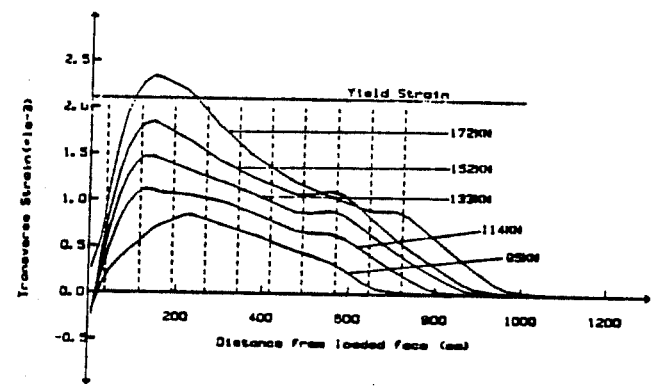
(b) Distribution of transverse strains for stirrup detail 2
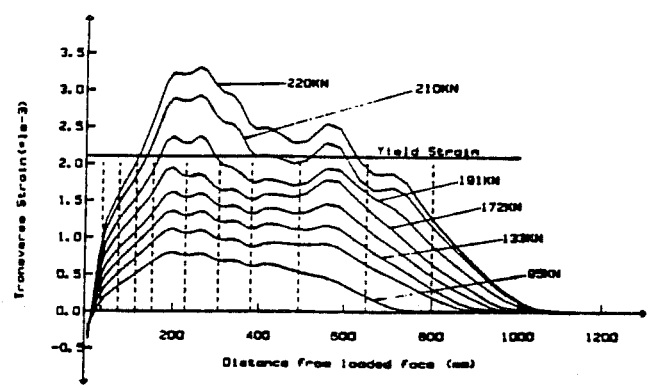
(c) Distribution of transverse strains for stirrup detail 3

Figure 2.7   Strain Distribution in the Concrete for Various

Disposition of the Reinforcement (dashed lines)

According to Adeghe and Collins [4]
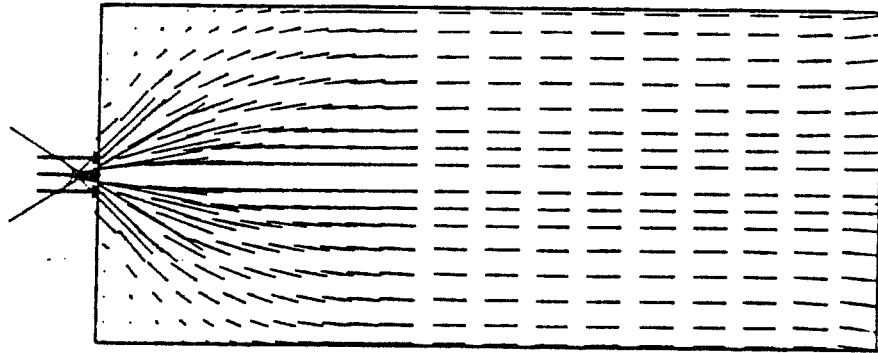
a - Compressive stress flow, Linear elastic analysis
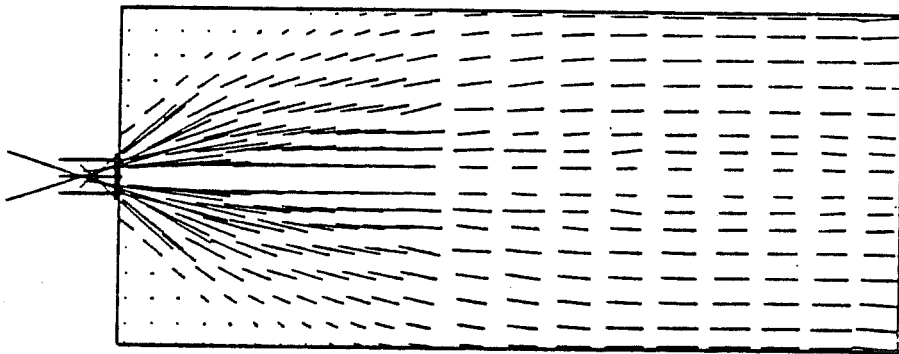
b - Compressive stress flow, Nonlinear analysis

Figure 2.8   Principal Stress Vectors for a Linear and a Non-
             Linear Model According to Adeghe and Collins [4]

2.6   Strut-and-Tie Model

The Strut-and-Tie Model, which is described in more detail
in Chapter 3, is a method based on the theory of plasticity in
which approximate stress fields are used to formulate an
equilibrium model consisting of compression struts and tension
ties connected at discrete nodes. The Strut-and-Tie Model stems
from the pioneering work of Ritter in 1899, who used such a model
to develop a truss analogy explaining the shear-diagonal tension

resistance in reinforced concrete beams. The Strut-and-Tie Model has been developed by many engineers from German-speaking countries such as Mörsch, Leonhardt, Thürlimann, and Schlaich.

$$Z_{tot} = \frac{F_0}{2} \cdot \frac{1 - \cos\alpha_0}{\sin\alpha_0} = \frac{F_0}{2} \cdot \tan\frac{\alpha_0}{2}$$
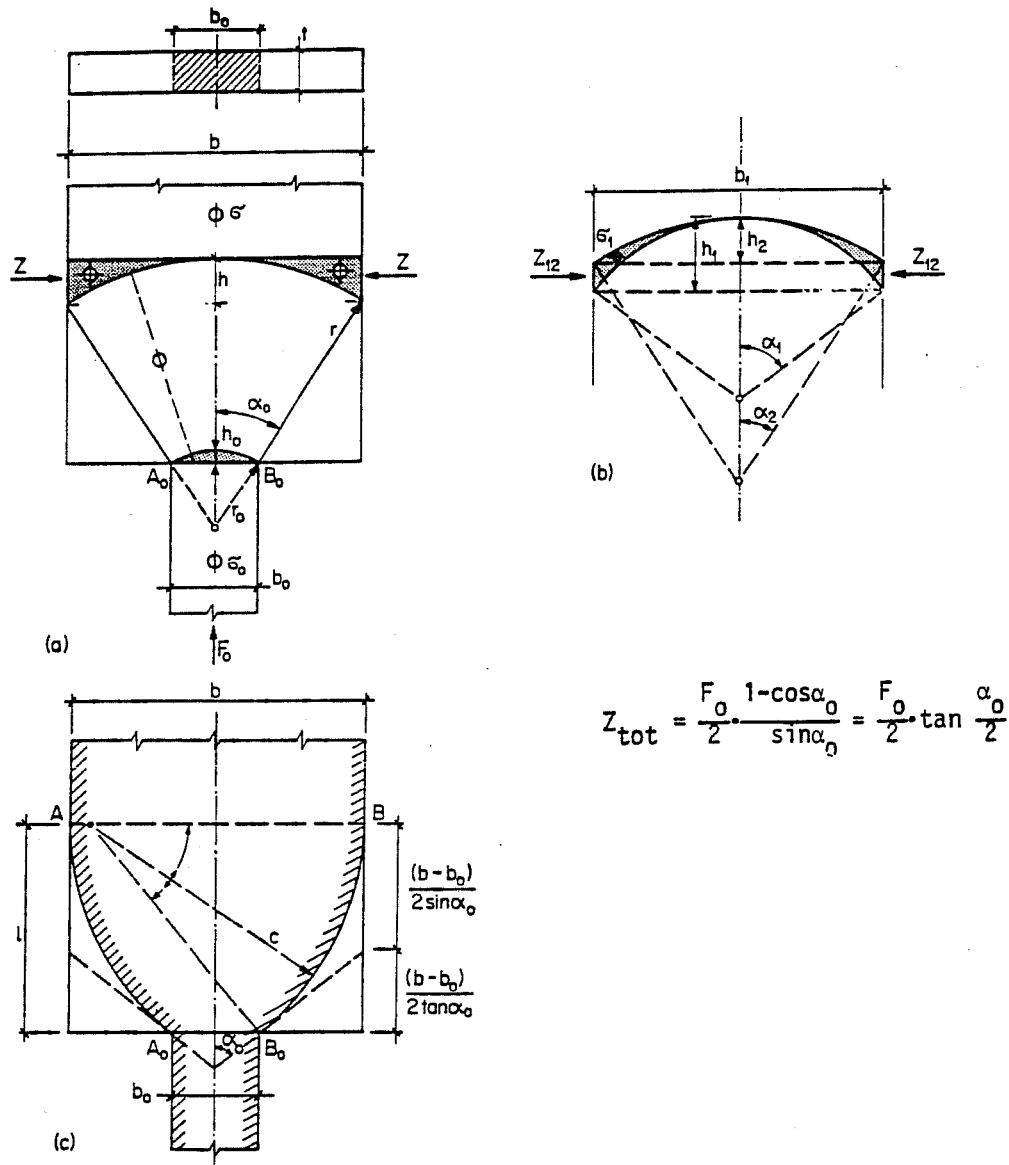
Figure 2.9   Plasticity Model for a Deep Wall on a Column
            Presented by Thürlimann [180]

The theoretical bases linking the theory of plasticity to

the Strut-and-Tie Model have been developed and demonstrated by Thürlimann and Marti [180, 114]. Various applications of the theory of plasticity to concrete structures, including the effects of bending, shear, torsion, local discontinuities in the geometry or the loading, and punching shear are presented in Ref. 180. Fig. 2.9 shows Thürlimann's solution to the problem of a deep wall resting on a column. This problem is similar to the local introduction of a post-tensioning force in a member. The tension force can be obtained by setting the diffusion angle for the stresses α_0 to a value between 22.5 and 45 degrees, with the larger angles being recommended. Interestingly enough, this approach predicts a tension force that is independent from the size b_0 of the column. The force predicted by this method is slightly less that the force predicted by Guyon and other authors for small sizes of the column (or anchorage device), but larger for cases with large columns.

The most comprehensive treatment of the Strut-and-Tie Model in English is the paper by Schlaich et al. [158], which shows many applications of the Strut-and-Tie Model including the modelling of an anchorage zone. Fig. 2.10 shows an example of the modelling of an eccentric anchorage zone using the Strut-and-Tie Model. Starting with the elastic stress trajectories shown in Fig. 2.10a, the Strut-and-Tie Model of Fig. 2.10c is developed. The force in the struts and ties can be compared to the elastic forces obtained from the elastic stresses shown in Fig. 2.10b. The Strut-and-Tie Model is gaining popularity because a designer can readily compute the required reinforcement of the general anchorage zone from such a model. Fig. 2.11 shows a Strut-and-Tie Model used by Mörsch in 1924 [122]. Even though the model is based on a very simplified assumed distribution of the forces, the value obtained for the tensile force Z is very close to the value given in many code provisions, and to the elastic calculations of Guyon [75].

Chapter 4 presents a more detailed discussion of this configuration. Even though little experimental research has been conducted into the application of the Strut-and-Tie Model for ultimate strength design of general anchorage zones, the technique holds much promise.
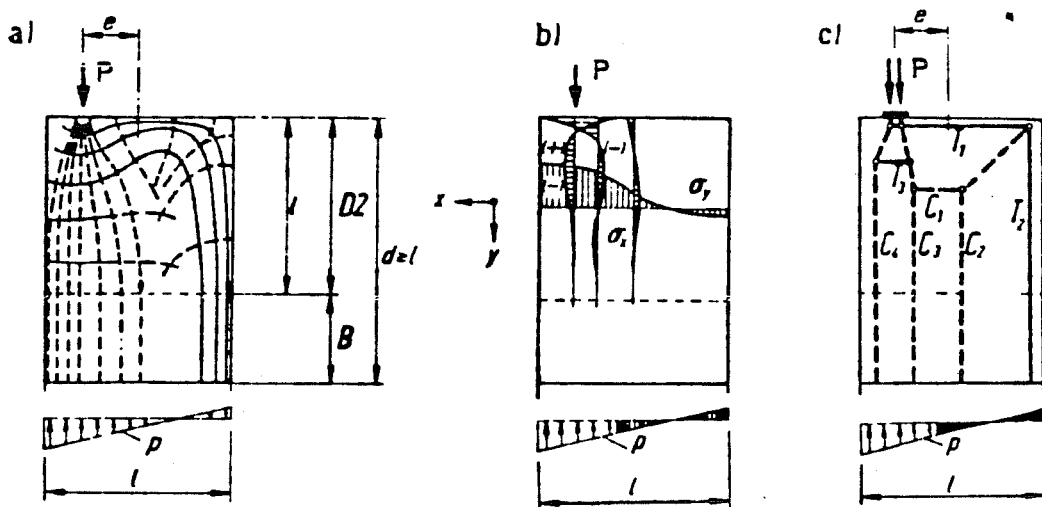
Figure 2.10   Strut-and-Tie Development from an Elastic Stress
Distribution According to Schlaich et al. [158]

In the 1989 edition of the German Beton Kalender [157], Schlaich and Schäfer expand on the use of the Strut-and-Tie Model for detailing of reinforced concrete, and describe a series of typical components generally encountered in the application of the Strut-and-Tie Model to structures. Fig 2.12 shows two details for the local introduction of pairs of forces in a concrete member.

39
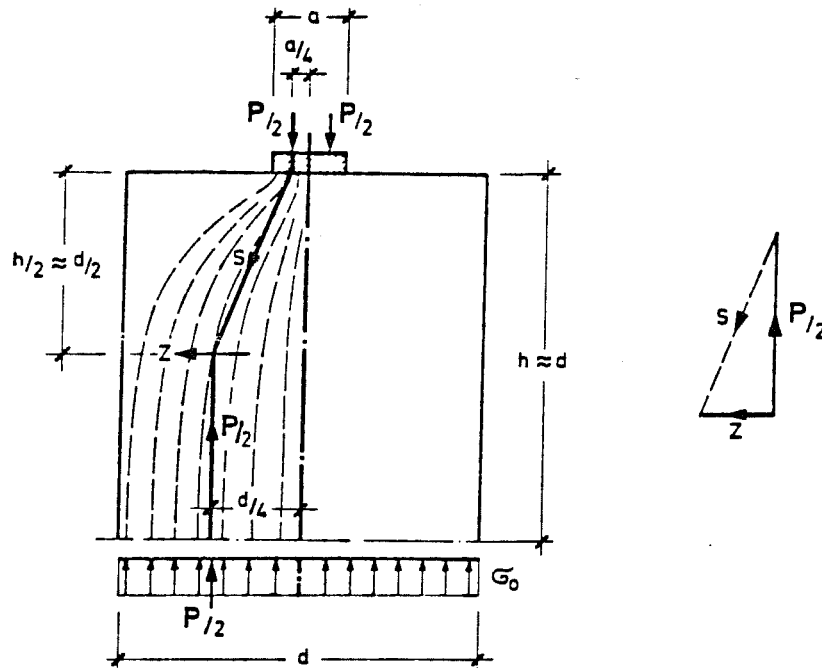
Figure 2.11   Strut-and-Tie Model According to Mörsch [122]

In many of the early applications of the Strut-and-Tie Model, the emphasis is on the calculation of the required tensile force in the reinforcement. Because it is a more brittle mode of failure, a failure of the concrete in compression is considered as undesirable, and the reinforcement is designed to yield before crushing of the concrete occurs [147, 20]. The compressive capacity of the concrete is checked and generally it is not critical. The failure of the nodes themselves is treated by using well proven construction details for the reinforcement. Several attempts have been made to define more complete and consistent design procedures that include cases in which the mode of failure includes the compression struts or the nodes. Such procedures are needed to permit the use of the Strut-and-Tie Model. Anderson [9] investigated the behavior of nodes involving two tension ties and one compression strut (CTT-nodes), and found that properly designed details are not critical. Bouadi [23] investigated the behavior of nodes with two compression struts and one tension tie

(CCT-node).

In a recent document, Bergmeister et al [20] present an exhaustive review of the available data concerning Strut-and-Tie Models and their application to detailing, including the design of compression struts and nodes. The proposed values for the compressive strength to be used when checking the compression struts are reviewed and evaluated in the light of the available test results. The strength of the concrete in the compression struts is generally expressed as a fraction of the uniaxial compressive strength of the concrete, f'_c. The coefficient, which reflects the type of loading and the extent and orientation of the cracking in the concrete is called the *efficiency factor* ν_e. The efficiency factor for compression struts typically ranges from 1.0 for uniaxial undisturbed state of stresses to 0.25 for severely cracked sections, in which the cracks make an angle of about 30 degrees with the struts [158, 110]. Most values are assuming that
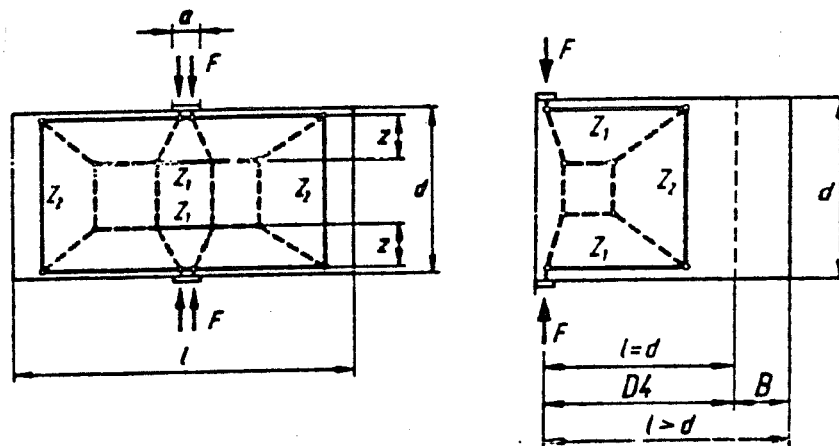
a) Concentric Configuration   b) Eccentric Configuration

Figure 2.12 Strut-and-Tie Models for Local Introduction of
Forces According to Schlaich and Schäfer [157]

the cracks are well distributed in the concrete. Because the struts tend to spread between the nodes [158], the critical section is in most cases located at the interface between the node and the strut. Table 2.2 summarizes the results of several investigators on efficiency factors. In the development of the *modified compression field theory*, formulas for the efficiency factor were developed to describe the non-linear properties of concrete in compression in presence of transverse tensile stresses [184, 37, 40]. Eq. 2.2 shows the formula proposed by Vecchio and Collins [184] which gives the maximum compressive stress in a strut f_{c2max} as a fraction of the uniaxial compressive strength of the concrete f'_c. The proportionality constant between the two is the efficiency factor.

$$f_{c2max} = 1/(0.8 - 0.34\epsilon_1/\epsilon_2) \; f'_c \quad \text{(Eq. 2.2)}$$

Where

f_{c2max} is the maximum compressive stress in the compression field

ϵ_1 is the average principal tensile strain

ϵ_2 is the average principal compressive strain, which can be assumed as -0.002 for concrete.

$$\epsilon_1 = \epsilon_x + (\epsilon_x + 0.002)/\tan^2\phi_{cs} \quad \text{(Eq. 2.3)}$$

Where

ϵ_1 is the average principal tensile strain

ϵ_x is the strain in the reinforcing bar, which can conservatively be taken as the yield strain

ϕ_{cs} is the angle between the tie and the strut

Table 2.2 Efficiency Factor According to Various Investigators, from [20]

Structural Member	Efficiency Factor ν_e		
	MacGregor and CEB [110]	Schlaich [158,30]	CSA [40]
Undisturbed uniaxial state of stresses		1.0	
Joints bounded by compressive struts and bearing areas	0.85		0.85
Joints anchoring tension ties in more than one direction, ties anchored by bearing plates			0.85
If tensile strains in the cross direction or tensile reinforcement may cause cracking parallel to the strut with normal crack width		0.8	
Joints anchoring one tension tie For skew cracking or skew reinforcement	0.65	0.6	0.75
Joints anchoring tension ties in more than one direction	0.5		0.6
Isolated compression strut in deep beam or D-region	0.5		
For skew cracks with extraordinary crack width, if the strut-and-tie departs from the elastic flow of forces		0.4	
Severely cracked webs or slender beams with reinforcement at yield: angle between strut and tie = 30° angle between strut and tie = 45°	0.25 0.45		0.31 0.55

Variations of this formula have been proposed, and can be found in the Canadian CSA code [40] and in Collins and Mitchell [37]. By setting the average principal tensile strain to the value given in Eq. 2.3 [37], assuming that the angle between the strut and the tie is 65 degrees, the efficiency factor for the concrete of an anchorage zone becomes 0.77, assuming that the cracks are well distributed.Most of the experiments on which the efficiency factors are based are tests of reinforced concrete panels subjected to shear, or shear with axial force. In general, the resulting stress field is fairly uniform, with the result that the cracks are well distributed. In the case of an anchorage zone, however, the tendon force is introduced locally, and the distribution of the tensile stresses is not uniform. In consequence, only a few cracks develop in the anchorage zone. This is detrimental for the compressive strength of the concrete, leading to a lower efficiency factor for the concrete.

As illustrated by the complexity of the truss models proposed by MacGregor [110], it is desirable to automate the calculation of the member forces in a Strut-and-Tie Model. Benabdallah et al. [19] describe the use of computer graphics on a minicomputer to alleviate the generation and calculation of a Strut-and-Tie Model. M. Schlaich [159] presents a similar program running on an engineering workstation. M. Schlaich's program incorporates an optimization algorithm (Simplex) to determine the most efficient load-carrying mechanism. The program also generates automatically a graphic representation based on simple components as a uniaxial compression member and a biaxial compression member of nodes at the intersection of compression struts (see Fig. 2.14).

Polygon of Forces

a) Node with five
Compression Forces

b) Node Decomposed into
Simple Components
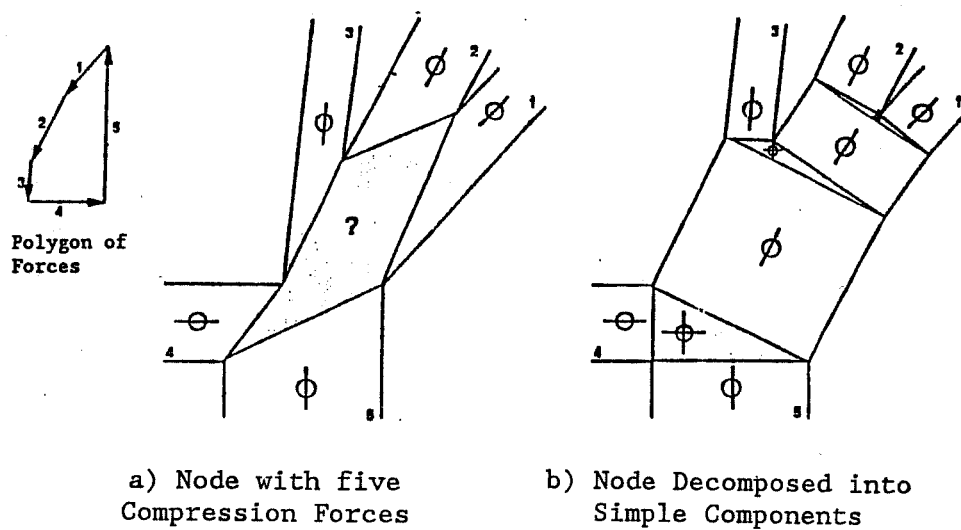
Figure 2.14 Decomposition of a Node at the Intersection of
Several Compression Struts According to M. Schlaich
[159]

2.7   Experimental Investigations

Stone and Breen [170, 171, 172, 174, 173] conducted an experimental and analytical study of single anchorage zones in thin web members. The experimental program investigated the influence of the eccentricity and inclination of the tendon, the height and the width of the section, the tensile strength of the concrete, the geometry of the anchorage device and the effect of supplementary anchorage zone reinforcement, both active (lateral post-tensioning) and passive. The experimental study consisted of forty-one quarter scale tests and ten full scale tests. The analytical study utilized both two-dimensional and three-dimensional linear Finite Element computer analysis to generalize the experimental results.

The conclusions of the investigators were:

1) For increased eccentricity and inclination, the cracking load decreases.

2) Bearing stresses as high as 2.5 times the compressive strength of the concrete can be reached.

3) Cracks can occur on the tendon path well outside the general anchorage zone where the tendon has a significant curvature and multiple strand tendons are used.

4) Tests on unreinforced concrete sections using various types of anchorages show that the geometry of the anchorage device has an influence on the cracking load. Anchorage devices with a stiff cone performed poorly when compared to plate anchors or bell anchors.

5) Spiral reinforcement is more effective than orthogonal reinforcement in increasing the cracking and the ultimate load of anchorage zones. (This conclusion is debatable, because Stone did not provide sufficient transverse reinforcement in the specimens with orthogonal

reinforcement. Most of Stone's failures were local zone failures, for which a spiral reinforcement is most efficient. However, as shown in [146] and [153], orthogonal reinforcement can be effective in preventing both local zone and general zone tension failure).

6) Lateral post-tensioning is the most effective method of preventing cracking of the anchorage zone. The best location is as close as possible to the loaded face. (This conclusion is correct in Stone's case, because the failure occurs in the local zone. If, however, a local zone failure is prevented by using an adequate detail for the local zone, the lateral post-tensioning will be more effective at a certain distance from the anchorage device, as discussed in Chapter 6).

Based on the conclusions of his research, Stone developed an empirical design procedure based on the cracking load of the concrete [171]. While applicable to sections similar to those investigated in the research, the empirical procedure can give misleading results for extreme values of variables such as eccentricity, section dimensions, tendon inclination and curvature.

In a companion study to this dissertation, Sanders and Breen [153] have tested a series of specimens of the general anchorage zone. Sanders' test results are used in the present dissertation to evaluate and calibrate the analysis. As another component of the present study, Roberts [146] studied the behavior and design of the local zone. Some additional details on Roberts' approach are given in Chapter 3.

2.8   Code and Design Guidelines

This section describes the design codes and guidelines for the design on anchorage zones. Generally, these codes do not specifically distinguish between local zone design and general zone design. Two main components are generally present in the specification, one being a limit on the bearing stresses under the anchorage device and the other some estimate of the tensile bursting force in the general zone. The major design codes and guides reviewed in this study are:

AASHTO Bridge Code 1983 [7]

ACI 318-83 [8]

Austrian Code 1979 [14]

CEB-FIP Model Code 1978/1990 [30]

CIRIA Anchorage Design 1976 [38]

FIP Recommendations 1981 [61]

Florida DOT Design Criteria [62]

German Code DIN 1045 [69]

North Carolina DOT Design Criteria [126]

Ontario Bridge Code 1983 [127]

PTI Segmental PT Guideline 1987 [141]

Switzerland Code SIA 162 [176]

VSL End Block Design 1975 [108]

Table 2.3 summarizes the limitations placed by the various codes on the maximum bearing stress under the anchorage device. None of these specifications takes into consideration the favorable influence of confining reinforcement that is usually present in the local anchorage zone, and the values are therefore relatively low. In practice, the limitation of 3000 psi under the bearing plate is seldom observed in the United States. Table 2.4 presents the values given by the various codes and design guidelines for the bursting tensile force in the general zone.

Table 2.3   Maximum Bearing Stress under the Anchorage Device
According to Various Design Codes and Guidelines

Code	Maximum Bearing Stress
AASHTO Bridge Code 89	SL: 3000 psi or $0.9f'_{ci}$
PTI	PT: $0.8f'_{ci}\sqrt{A/A_b}-0.2$ or $1.25f'_{ci}$ or 5000 psi SL: $0.6f'_{ci}\sqrt{A/A_b}$ or $1.25f'_{ci}$ or 6875 psi
CIRIA Guide defined	PT: $0.40f'_{ci}$ if bearing area is not well $0.80f'_{ci}$ if bearing area is well defined
Design Criteria for FL and NC	$F_{ck}/K\sqrt{A/A_b}$ or $3.3f_{ck}/K$ K=1.5 for normal loads K=1.3 for overload
Austrian Code	$0.75Kf'_c$ Where K is given by: A_b/A 0 0.20 0.40 0.60 0.80 1.0 K 1.6 1.23 0.93 0.69 0.51 0.40
German Code	$K/2.1\sqrt{A/A_b}$ or 1.4K where K is given by: f'_{cu} [MN/mm²] < 25 35 45 55 K $f'_{cu}/1.429$ 23 27 30
Swiss Code	$0.65f'_{cu}\sqrt{A/A_b}$ or $1.8\ f'_{cu}$

Where

A   is the area of concrete surrounding the anchorage device
        with a similar shape, representing the confinement
        provided by surrounding concrete

A_b is the area of the anchorage device

PT   is for the time of stressing of the tendons

SL   is under service loads

f'_{ci} is the concrete strength at stressing, but not more than f'_c

f'_{cu} is the concrete cube strength at stressing

f'_{ck} is the characteristic concrete cube strength

Table 2.4   Bursting   Force   According   to   Various   Codes   and Guidelines

Code	Bursting Force	Bursting Stress (max)
ACI 318-83 (ACI 358)	$0.70 \cdot P e^{-3(a_1/a_2)}$	
PTI	$0.35P\,(1-a_1/a_2)$	
CIRIA Guide	cP/K	
Design Criteria for FL and NC	$0.35P \cdot (1-a_1/a_2)$	$0.7P/bd\,(1-a_1/a_2)$
VSL Design Guide	$0.30P \cdot (1-a_1/a_2)$	Guyon, see Fig. 2.2
Ontario Bridge Code 1983	$0.70P \cdot e^{-3(a_1/a_2)}$	$P/(a_2)^2\,e^{-3(a_1/a_2)}$ $< 0.8f_t + 20A_r/(bd)$
CEB MC 78	$0.3P \cdot (1-a_1/a_2)$	
Austrian Code	$0.3P \cdot (1-a_1/a_2)$	
German Code	a) $0.25P \cdot (1-a_1/a_2)$ b) $0.30P \cdot (e/h-0.167)$	

Where

K is 1.0 for isolated anchors, 1.5 for anchors distributed in

one direction and 2.0 for anchors distributed in two directions

P is the tendon force

a_1 is the dimension of the anchorage device

a_2 is the lateral dimension of the member

c is given in function of $a_1/a2$:

a_1/a_2	<0.3	0.4	0.5	0.6	>0.7
c	0.23	0.20	0.17	0.14	0.11

b is the width of the section in the plane of potential bursting cracks

d is the effective depth of the anchorage zone, where the stresses become linear. Generally taken as the depth of the section

e is the eccentricity of the post-tensioning force measured from the centroid of the section

h is the depth of the section

Most formulas are based on an equation in the form $K \cdot P (1 - a_1/a_2)$, with K varying between 0.25 and 0.35. Most design codes give maximum values for the maximum tensile stress in the concrete of post-tensioned structures in the range from $5.0\sqrt{f'_c}$ to $7.5\sqrt{f'_c}$, but it must be noted that these values were determined for bending conditions that are very different from the stress distributions which occurs in an anchorage zone.

In a recent survey by the CEB [29], participants were asked to design a particular anchorage zone using their own national design code or handbook. The beam had six anchorages with a total force of 2,700 kN. The geometry of the anchorage zone is shown in Fig. 2.15. The participants were asked to calculate the tensile bursting force, the length of the bursting zone, and the cross sectional area of the required reinforcement. Six responses were received, and the range in the answers was very high, as

illustrated in Fig. 2.16. The average value of the tensile
bursting force is 193 kN, with a range of values from 49.5 kN to
440 kN. The values for the length of the bursting region ranged
from 170 mm to 850 mm with an average of 508 mm. The required
reinforcement ranged from 207 mm^2 to 2000 mm^2, with an average of
790 mm^2. The results of the survey make it clear that in the
domain of anchorage zones, the matter is not to refine the design
techniques to within 5% or 10%, but rather to achieve safe design
values that may still vary by 50% or 100%. According to the
proposed AASHTO Specification described in Chapter 8, the value of
the tensile force required for the example problem is at the upper
end of the answers from the survey with 612 kN and 2563 mm^2,
pointing to potentially unsafe designs in certain countries.

Concrete Grade C 3o
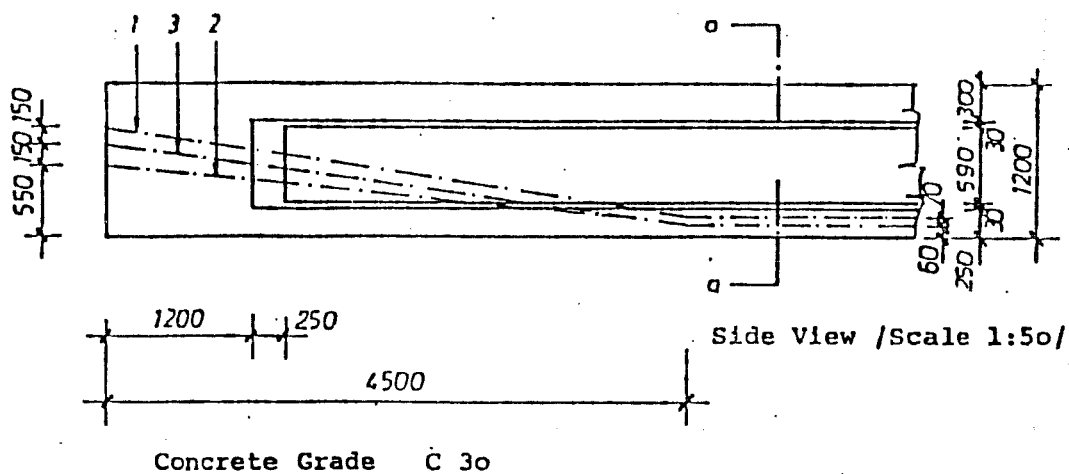
Figure 2.15 Geometry of the Anchorage Zone Problem from the CEB
            Survey [29]
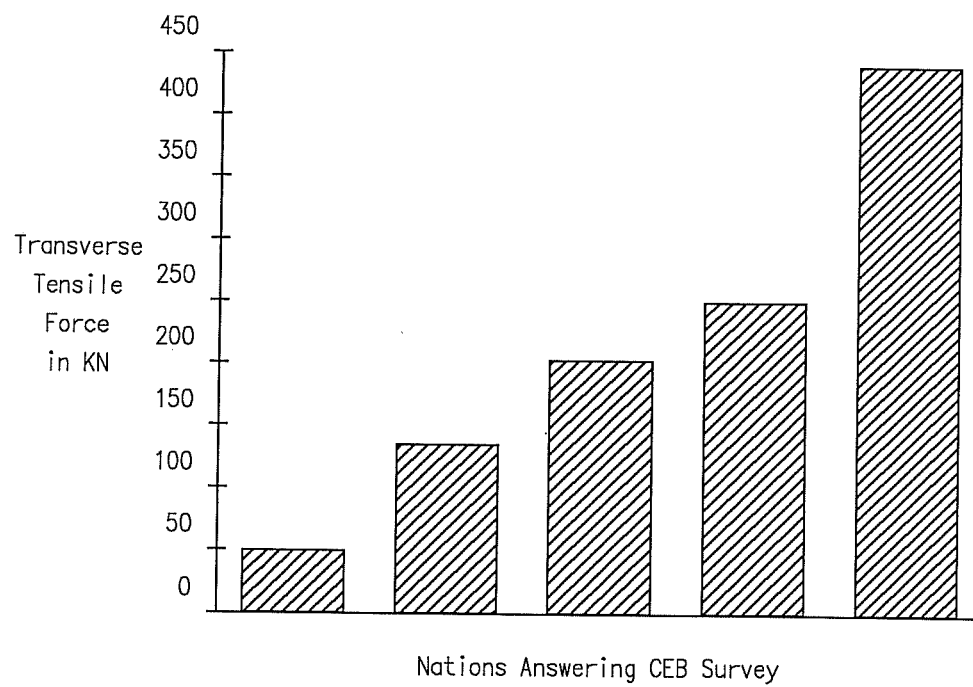
Figure 2.16   Tensile Bursting Force According to the Nations
Responding to the CEB Survey [29]

Chapter 3: Methodology for the Analysis of Anchorage Zones

This chapter presents the general methodology that is applied to the analytical investigation of anchorage zones. Two distinct procedures are presented and used for the analyses. The first procedure is an elastic stress analysis using the Finite Element Method and the second procedure uses Strut-and-Tie Models based on the theory of plasticity. The main parameters and the hypotheses underlying both methods are discussed.

Figure 3.1   Typical Anchorage Zone with four Tendons

Typical anchorage zones, as the drawing shown in Fig. 3.1 demonstrates, are extremely complex. Even the simplest possible geometry for an anchorage zone, a rectangular cross section loaded by a straight concentric tendon is more complicated than it appears. The tendon duct causes a void in the structure, the

reinforcement causes discontinuities in the material, and typical anchorage devices have a sophisticated geometry. Therefore, it is desirable to develop a general methodology for the analysis and the design of anchorage zones rather than to attempt to define guidelines to solve the entire problem.

3.1   Forces Acting on Anchorage Zones

Fig. 3.2 shows the forces acting on an anchorage zone. The principal force is the concentrated tendon force introduced at the anchorage device. In addition, the curvature of the tendon in the anchorage zone also induces deviation forces. Anchorages located near supports are also subjected to shear forces from the transverse reaction and possibly to bending moments. The resulting state of stresses is complex, making several simplifications necessary to analyze efficiently the anchorage zone.

Tendon Bearing Force

② Tendon Deviation Force

③ Transverse Reaction
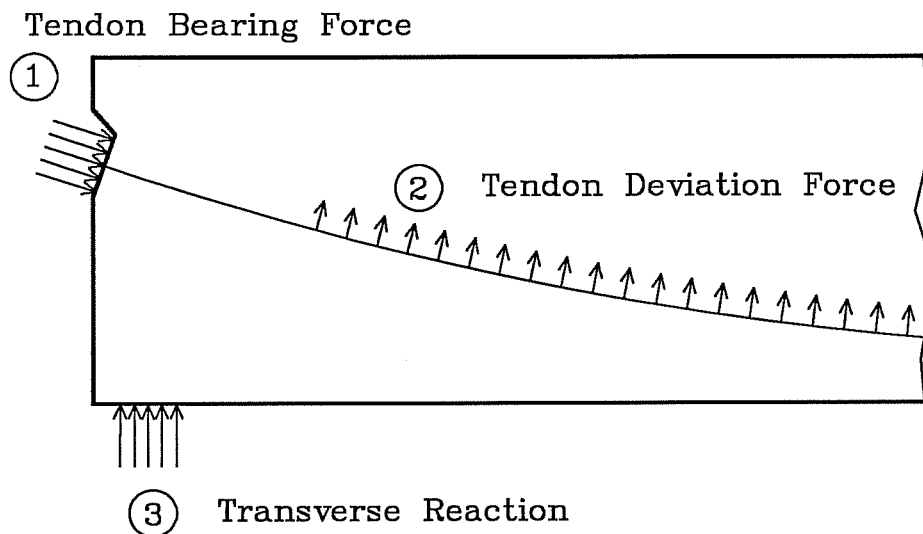
Figure 3.2   Forces Acting on an Anchorage Zone

In the present study, only the forces resulting from the direct application of the post-tensioning force on the structure are considered. This corresponds in many cases to the most critical condition for the structure, because a transverse reaction generally tends to counteract the effect of the bursting or spalling forces. Moreover, the most critical condition for the anchorage zone is when the structure is initially post-tensioned. At that time, the member is supported on some kind of scaffolding, and the only transverse reaction is caused by the fraction of the dead weight mobilized by the upward camber of the member due to the post-tensioning. This reaction is at most be equal to the reaction caused by the dead weight of the structure at that time, and neglecting this component will in many cases be conservative. In any case, the methodology presented in this chapter is general and can easily be expanded to include the effect of external forces acting on the anchorage zone.

3.2   Material Properties

In an anchorage zone, the concrete is stressed over a large range, from extremely high compression in the vicinity of the anchorage to tension and possibly cracking in the general zone. Reinforcing steel is provided to confine the concrete surrounding the anchorage and to resist the tension forces that are released upon cracking of the concrete. The next subsections describe the material properties of concrete and reinforcing steel.

3.2.1 Unconfined Concrete in Compression

Although the concrete of the general anchorage zone is reinforced, most of the concrete in the general zone is unconfined because reinforcement is generally not present in sufficient quantity over the transverse dimension of the cross section. To be

A — $-5.0\ \sigma_0$
B — $-4.5\ \sigma_0$
C — $-4.0\ \sigma_0$
D — $-3.5\ \sigma_0$
E — $-3.0\ \sigma_0$
F — $-2.5\ \sigma_0$
G — $-2.0\ \sigma_0$
H — $-1.5\ \sigma_0$
I — $-1.0\ \sigma_0$
J — $-0.5\ \sigma_0$
K — $0.0\ \sigma_0$
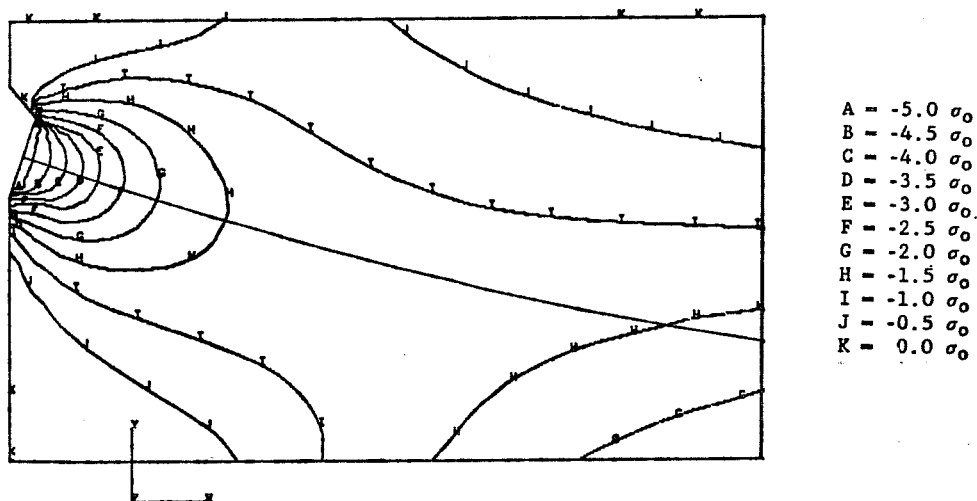
Figure 3.3   Contour Plot of the Minimum Principal Stress
(Maximum Compression) in an Anchorage Zone

effective, confinement needs to be provided in both directions normal to the axis of the tendon, in which expansion occurs under the compressive force. The absence of confinement is not a problem, because there is little need for confinement in the general zone, except for the concrete located in the immediate vicinity of the local zone. As shown in Fig. 3.3, the compressive

stress in the concrete decreases very rapidly with increased distance from the anchor. Assuming that the average compressive stress under the anchorage device (contour line A) is twice the uniaxial concrete strength f'_c, it is apparent that most of the concrete in the general anchorage zone is subjected to compressive stresses significantly less than 0.8 f'_c (contour line G), thus requiring no special confining reinforcement. Because the concrete of the general zone is subjected to relatively low compressive stresses, it can generally be considered as a linear elastic material.

Unconfined concrete can resist compressive stresses in the vicinity of its uniaxial compressive strength f'_c. In beam bending, the value is reduced to 0.85 f'_c. For anchorage zones, where the state of stresses is more complex, the maximum value is lower. Sections 3.4.4 and 3.5.7.2 give values of the maximum compressive stress for use in design procedures based on the Finite Element Method and the Strut-and-Tie Model respectively.

3.2.2 Confined Concrete in Compression

The average bearing stress ahead of the anchorage at the rated tendon capacity for the anchorage device is often greater than the uniaxial strength of the concrete f'_c. These large stresses can only be resisted by concrete confined by either surrounding concrete or confining reinforcement. Confining reinforcement is generally used for the concrete in the local zone in order to resist the large bearing stress near the anchorage device.

As discussed in Sections 1.2.2 through 1.2.6, one of the basic principles developed in this research is the distinction between failure in the local zone, failure in the general zone and failure at their interface. The present study focuses on the

investigation of the last two modes of failure, assuming that the design of the local zone is sufficient to resist the tendon force. This approach corresponds to the normal design procedure for anchorage zones, in which it is assumed that proper performance of the local zone has been demonstrated by the supplier of the anchorage device. The concrete confined in the local zone is therefore assumed to be able to transfer the concentrated post-tensioning force to the general zone.

In another component of the UT Research Project on Anchorage Zones, Roberts [146] has investigated the behavior of local zones with and without confining reinforcement. In her conclusions, she states that:

> *"The local anchorage zone in post-tensioned concrete presents a complex and critical problem for a designer. The high local bearing stresses imposed upon the concrete must be properly confined and effectively transferred to the rest of the structure.*

> *"The behavior of the local zone is primarily a function of the A/A_b ratio* [Note: A is the area of concrete concentric and similar to the anchorage device, and A_b is the area of the bearing plate], *the area confined by the primary confining reinforcement, and the volumetric ratio of the reinforcing steel to the confined concrete. The interaction of these variables dictates the overall local zone behavior.*

> *"The equation:*

$$F_{pu} = \phi \ [0.7 \ f'_c \ \sqrt{A/A_b} \ (A_b) + 4 \ f_{lat} \ A_{core} \ (1 - s/D)^2] \quad \text{(Eq. 3.1)}$$

$$\text{with } \phi = 0.7$$

Where

F_{pu} is the factored tendon force.

f_{lat} is the confining pressure produced by the reinforcement.

A_{core} is the area of the concrete surrounded by the confining reinforcement.

s   is the pitch of the confining reinforcement.

D   is the outer diameter of the confining reinforcement.
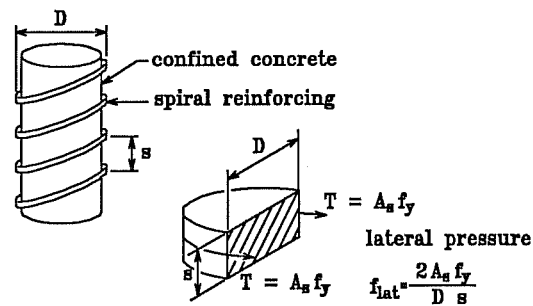
a) Lateral Pressure for Spirals
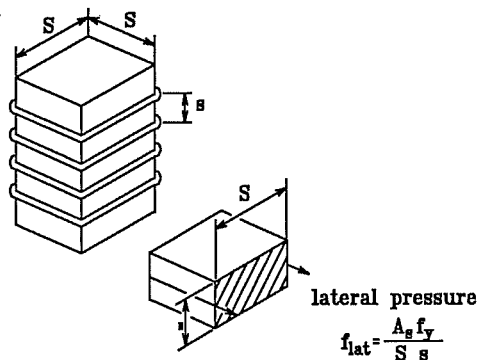
b) Lateral Pressure for Ties

Figure 3.4   Definition of the Quantities used in Roberts'
Formula for the Local Zone [146]

     "is reliable for the design of the local zone, with restrictions and recommendations on the various components of the equation [...] This equation is proposed only as a guideline for

design and not as a code equation. The proper performance of local zone details should be demonstrated through the test procedure described in Chapter [...]   .

Fig. 3.4 describes the quantities used in Equation 3.1, and shows how the confining pressure of the reinforcement is calculated for spiral and orthogonal confining reinforcement of the local zone. Because Roberts' investigation was conducted in parallel with the present study, these recommendations were not completely available at the time of design of the test specimens, but other available recommendations were used to avoid a failure in the local zone.

3.2.3 Concrete in Tension

As shown in Fig. 3.5, a large part of the anchorage zone is subjected to tensile stresses. Therefore the concrete of the general zone will be subjected to appreciable tensions. If the strains in the concrete reach the cracking strain, a crack opens and the tensile forces are transferred to the reinforcing steel. Fig. 3.6 shows typical stress-displacement curves for concrete in tension.

The tensile capacity of the concrete is generally neglected in the determination of the anchorage zone strength, because the concrete may crack during the lifetime of the structure due to other influences such as temperature or differential settlement.

K	=	0.0 σ_0
L	=	0.1 σ_0
M	=	0.2 σ_0
N	=	0.3 σ_0
O	=	0.4 σ_0
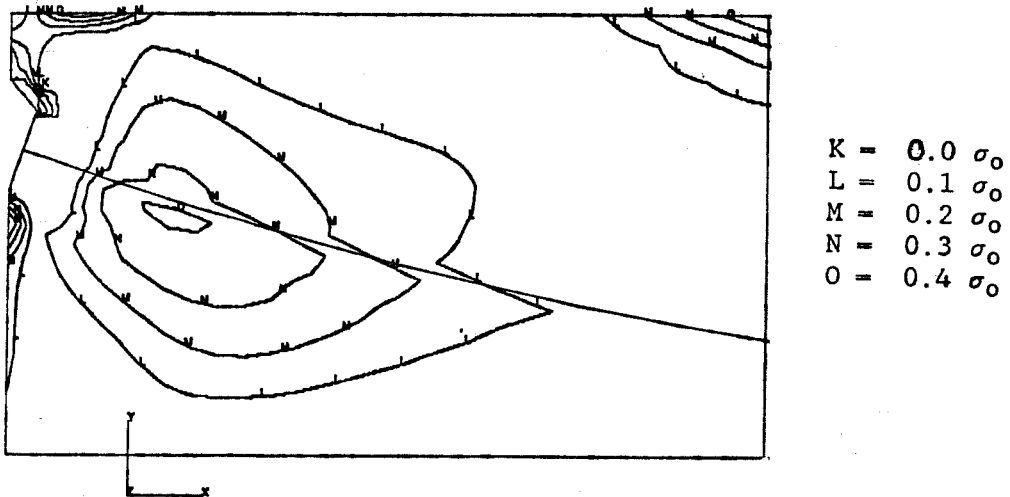
Figure 3.5   Contour Plot of the Maximum Principal Stress

(Maximum Tension) in an Anchorage Zone
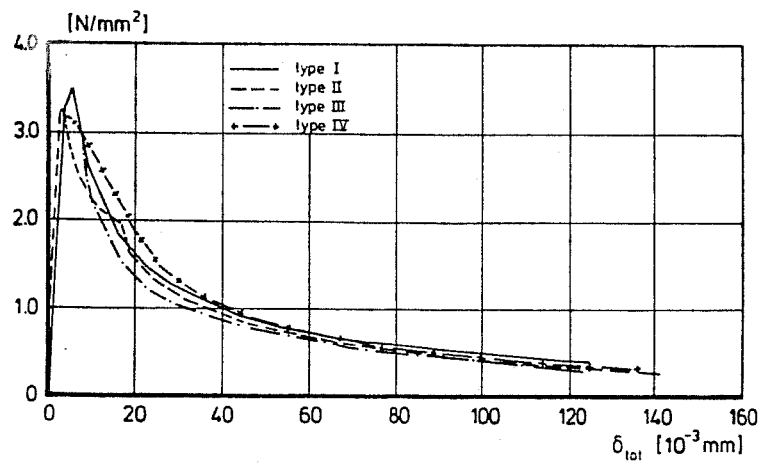
Figure 3.6   Stress-Strain Curves for Concrete in Tension

According to [191]

3.2.4 Reinforcing Steel in Tension

In most cases, the reinforcement of the anchorage zone is provided by rolled deformed reinforcing bars of Grade 60. The confining reinforcement, if it is in the form of a spiral, is sometimes made of smooth bars of Grade 40 steel. Before cracking of the concrete, the strains in the reinforcing steel are very small, and most of the tensile forces are resisted by the tensile capacity of the stiffer concrete section. After cracking occurs, the forces that were carried by the concrete are transferred to the reinforcing steel. When the reinforcing steel reaches its yield strength, the force in the bars ceases to increase. Only when the strains in the reinforcement become significantly larger will the steel strain harden. In most cases, the extensive cracking and the large deformations required to reach strain hardening of the reinforcement are not attained before another mode of failure takes place, or before the ductility of the anchorage zone is exhausted. For the study of anchorage zones, the reinforcing steel can therefore be considered as a bilinear material exhibiting a perfectly elastic behavior up to its yield point, and a perfectly plastic behavior beyond that point.

3.3   Three-Dimensional Effects

All structures are three-dimensional. However, in many instances, they can be represented using a simpler geometric model, such as a linear member for a beam. In anchorage zones, the concentrated force introduced by an anchorage device must be distributed to the entire cross section of the member, requiring a three-dimensional spreading of the forces. As a simplification, it is often sufficient to consider the spreading of the forces in two *principal planes* perpendicular to each other. In the simplest case of the distribution of a tendon force over a rectangular cross

section, the spreading of the post-tensioning force can be considered separately in the main plane of the structure (largest dimension) and over the thickness. The validity of this assumption is illustrated in the case of a linear stress analysis in Section 3.4.2.

In many cases in which post-tensioning is used, the cross section of the member is not a simple rectangle. Rather, it can be described as an assemblage of elements, each of which can be approximated as a thin rectangular cross section. Even though the overall problem is three-dimensional, the state of stresses in each component of the structure is essentially planar, with the
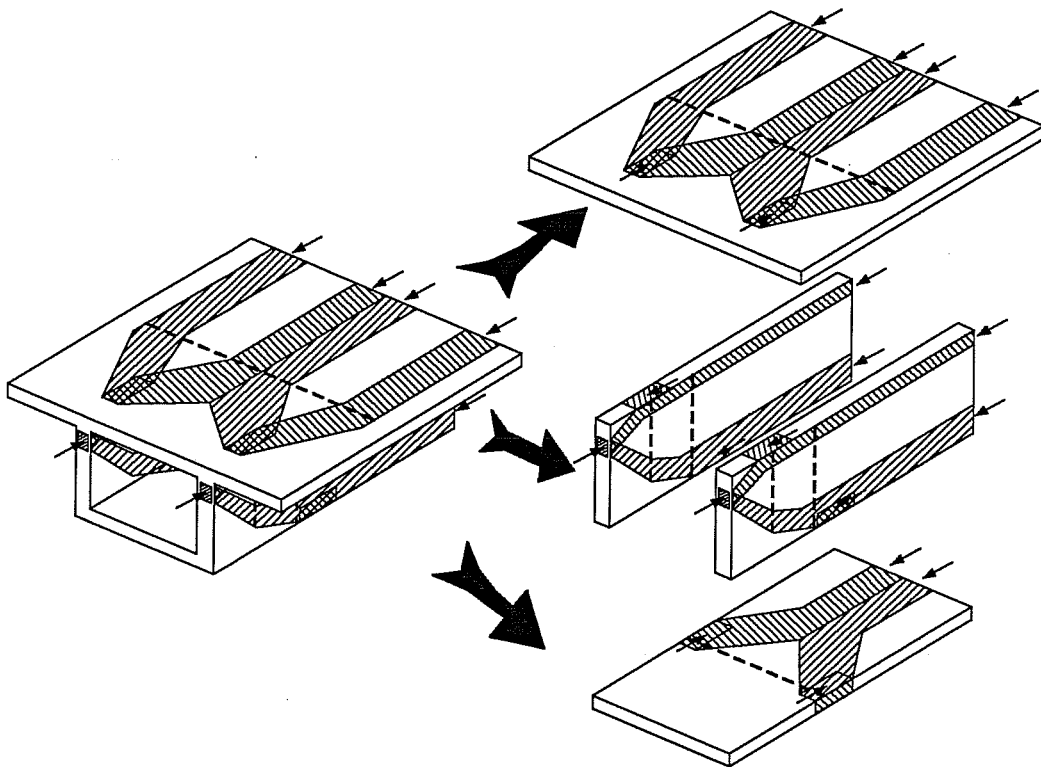
Figure 3.7   Principle of Decomposition of a Complex Cross
Section into Principal Planes

exception of the local zone and the interfaces between the various components.

As an example, Fig. 3.7 shows the case of the box-girder bridge. The top and bottom flanges as well as the webs can be considered as rectangular components of the cross section and the spreading of the tendon force can independently be investigated on each of the components of the cross section. This method of breaking down the section into planar element was proposed by Schlaich et al. [158] and is explained in more detail in Chapter 6.

3.4   Finite Element Analysis

The Finite Element Method has become increasingly popular over the last thirty years to calculate the detailed state of stresses in structures of arbitrary shape. Modern computer programs allow the user to model arbitrary structures and to define sophisticated material laws for the model. The principle of the Finite Element Method is to subdivide the structure to be analyzed in small parts, called Finite Elements, that have simple shapes. Examples of these shapes are straight lines, surfaces limited by second order parabolas or tetragons, as shown in Fig. 3.8. The displacements also are assumed to follow simple mathematical functions over the element. Using numerical methods, the individual stiffness of these elements can be computed. Subsequently the system of equations describing the equilibrium of the system is solved. In the case of nonlinear materials, the solution is iterative until the correct equilibrium for each load step is reached. Fig. 3.9 shows an example of Finite Element mesh, showing the subdivision of the anchorage zone into quadrilateral elements.

a) Line Elements
(Beam, Truss, Frame)

b) Surface Element
(Plane Stress, Plate Bending, Shells)

c) Volume Elements
(3D Solids)
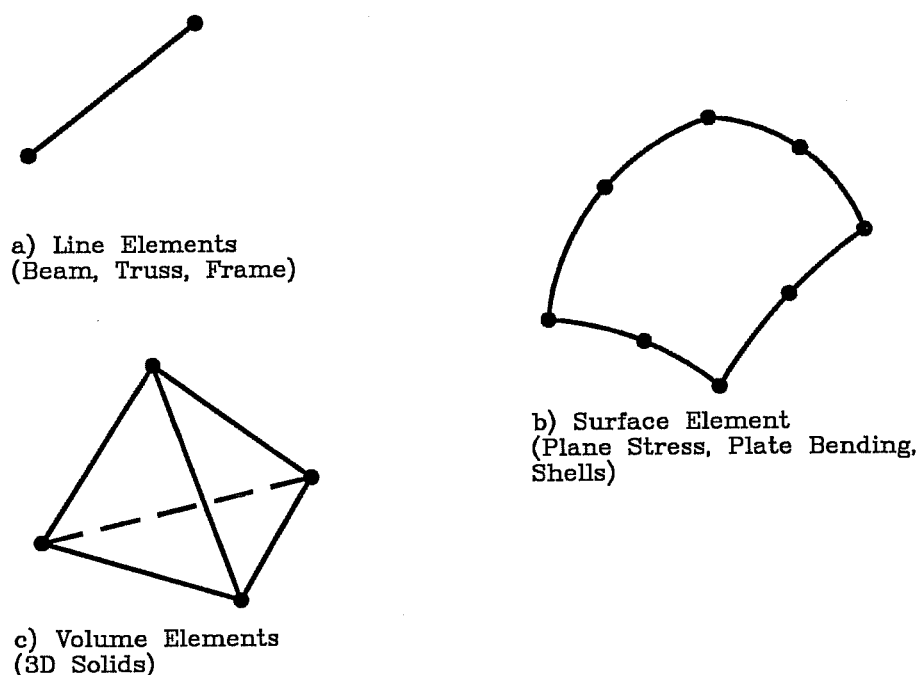
Figure 3.8   Examples of Shapes for Finite Elements

Application of the Finite Element Method is often limited by the lack of appropriate models for the behavior of the materials. This is especially true of the modelling of cracks in concrete. Cracks are usually not modelled as discrete discontinuities that extend as the load increases. Instead, the crack is considered as smeared over the considered elements, accordingly decreasing their stiffness [45]. While this hypothesis may be acceptable for large structures with a uniform distribution of reinforcement, it is much less accurate for small regions of reinforced concrete structures where the stresses in the reinforcing steel vary sharply at the cracks, as is the case for anchorage zones. Finite Element modelling of structural concrete is very much a field of research and rapid development at the present time [115]. For this research, the Finite Element Program ABAQUS [80] was used to perform the stress analysis. ABAQUS incorporates most of the

characteristics enumerated above. The generation of the Finite Element models was performed using PATRAN [130], a general purpose preprocessor for Finite Element analysis.
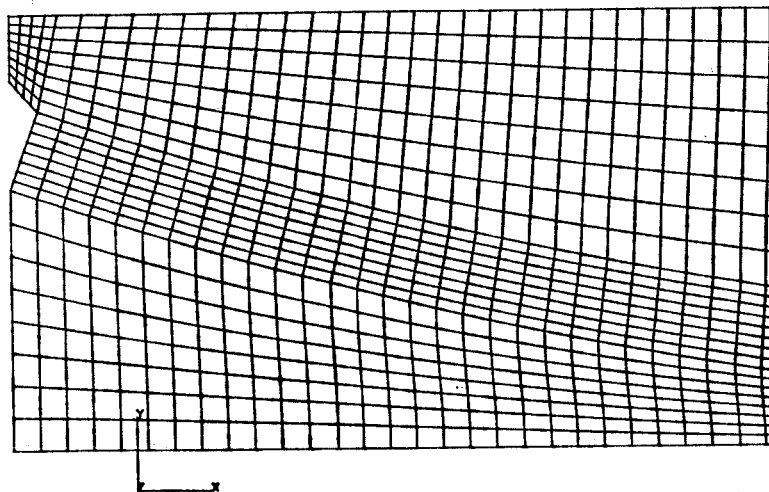
Figure 3.9   Example of Two-Dimensional Finite Element Mesh of an Anchorage Zone

The analyses performed during this phase of the project were exclusively linear elastic. This choice was made to simplify the individual analyses, allowing a wider range of geometries and load configurations to be investigated analytically. In a subsequent phase of the UT research project, nonlinear Finite Element Analysis will be used to more closely investigate some specific configurations.

3.4.1 Applicability of Linear Finite Element Analysis

As pointed out earlier, simplifying hypotheses are necessary for the analysis of the very complex behavior of anchorage zones. The simplest model is to assume the material to be linear elastic. The material properties are assumed to be the properties of concrete in compression, neglecting the presence of reinforcement and the non-linear properties of both concrete and steel.

Because the stresses in the concrete and the reinforcing steel are generally small up to the cracking of the concrete, a linear model is quite accurate to describe the behavior of the general zone of a specimen up to cracking [169]. Reasonable estimates of the cracking load of the general zone can therefore be obtained from a linear elastic stress analysis. The accuracy of the cracking load predictions could be influenced by the very large compressive stresses in the local zone. However, the presence of confining reinforcement is presumed to minimize this effect.

As will be shown in the subsequent chapters, the results of a linear elastic Finite Element Analysis can also be successfully used to determine the required amount of tensile reinforcement and to estimate the maximum compressive force that can be applied on an anchorage zone. Regardless of the method used to obtain the required amount of reinforcement, it is often desirable to pattern the tensile reinforcement according to the elastic stress distribution.

3.4.2 Modelling

Modelling is the process of idealizing a physical body into a model that can be analyzed by a given method. For the Finite Element analysis, modelling can be decomposed into several parts: modelling of the geometry, modelling of the loads and boundary

conditions, and modelling of the material properties. The latter will not be discussed here since it was discussed in the previous subsection.

Fig. 3.10 shows an example of an anchorage zone that is to be analyzed using the Finite Element Method. Because the structure and the loading are doubly-symmetric, only one quarter of the anchorage zone is considered. The geometric modelling of anchorage zones can be performed in several ways. The most rigorous representation is as a three-dimensional model as shown in Fig. 3.11a. For thin structures with a constant thickness, a simpler representation can be used by assuming that the structure is in a state of plane stresses, as shown in Fig. 3.11b. The
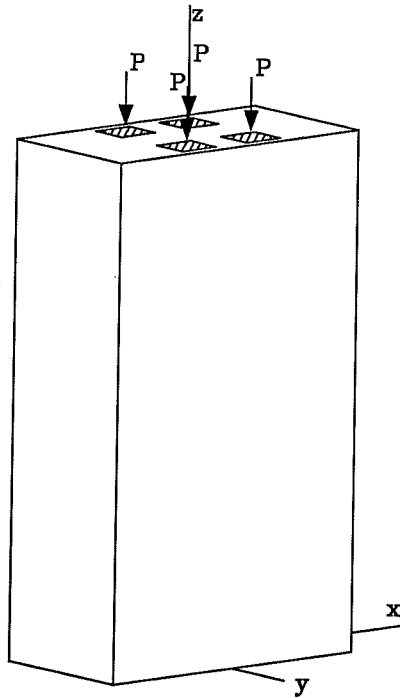
Figure 3.10 Example of Anchorage Zone to Model with Finite
            Elements

analysis in the transverse direction can be performed by using a simplified plane strain analysis, as also shown in Fig. 3.11c.
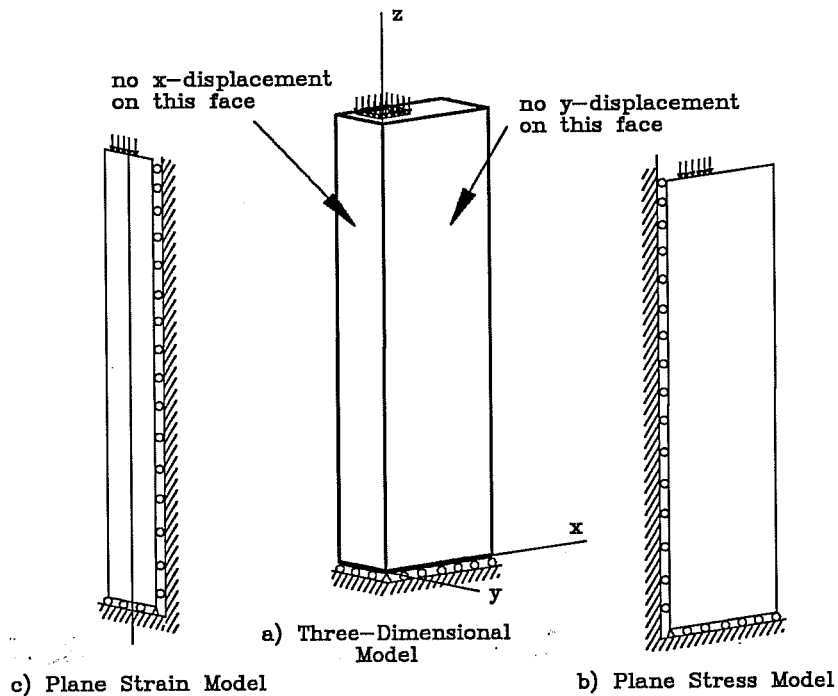
Figure 3.11   Three Possible Finite Element Models for the
Investigation of the Example Problem

Fig. 3.12a shows a contour plot of the stresses perpendicular to the tendon axis in the main plane of the anchorage zone, σ_{xx} on the quarter model of the anchorage zone modelled using three-dimensional brick elements (for more details on contour plots, see Section 3.4.3). In comparison, Fig. 3.12b shows a contour plot of the same stress obtained from the simpler plane stress analysis in the main plane. The distribution of stresses obtained by both models is very similar, with a slight tendency for the stresses on the outside of the three-dimensional model to be larger than the stresses in the plane of symmetry. As this example shows, the hypothesis of plane stress is valid even

for structures of relatively large thickness; in the example, the thickness in the transverse direction is 0.56 times the lateral dimension of the member. Fig. 3.13a shows the contour plot of the stress perpendicular to the tendon axis in the transverse plane, σ_{yy}, obtained from the three-dimensional analysis. In a similar fashion, Fig. 3.13b with the results obtained from a plane strain analysis. Although some differences can be observed, the results have similar distributions of stresses and magnitude of the maximum stress.

Modelling the loads and the boundary conditions can be a complicated operation because abstract quantities like a point load, a uniform pressure or an infinitely stiff body which are commonly used in Finite Element Analyses rarely occur in reality. Some studies of the sensitivity of the results to the influence of certain of these hypotheses are presented in Chapter 4. Great care was taken in designing the physical test specimens so that the boundary conditions assumed for the analysis were respected. For instance, lift-up of the base of a specimen during testing, which is a non-linear boundary condition, was avoided.

For the analysis of real structures, the boundary conditions should be chosen to represent the actual conditions of the structure. When only a part of the structure is analyzed using the Finite Element Method, it is appropriate to truncate the structure at a large distance from the anchorage zone to minimize the effect on the analysis of possible inaccuracies in the modelling of the boundary conditions. This distance should be at least one and one-half the larger cross-sectional dimension of the section. As will be seen in Chapter 5, this distance should be increased in the case of inclined and curved tendons.

$A = 0.00 \; \sigma_0$
$B = 0.05 \; \sigma_0$
$C = 0.10 \; \sigma_0$
$D = 0.15 \; \sigma_0$
$E = 0.20 \; \sigma_0$
$F = 0.25 \; \sigma_0$
$G = 0.30 \; \sigma_0$
$H = 0.35 \; \sigma_0$
$I = 0.40 \; \sigma_0$
$J = 0.45 \; \sigma_0$
$K = 0.50 \; \sigma_0$
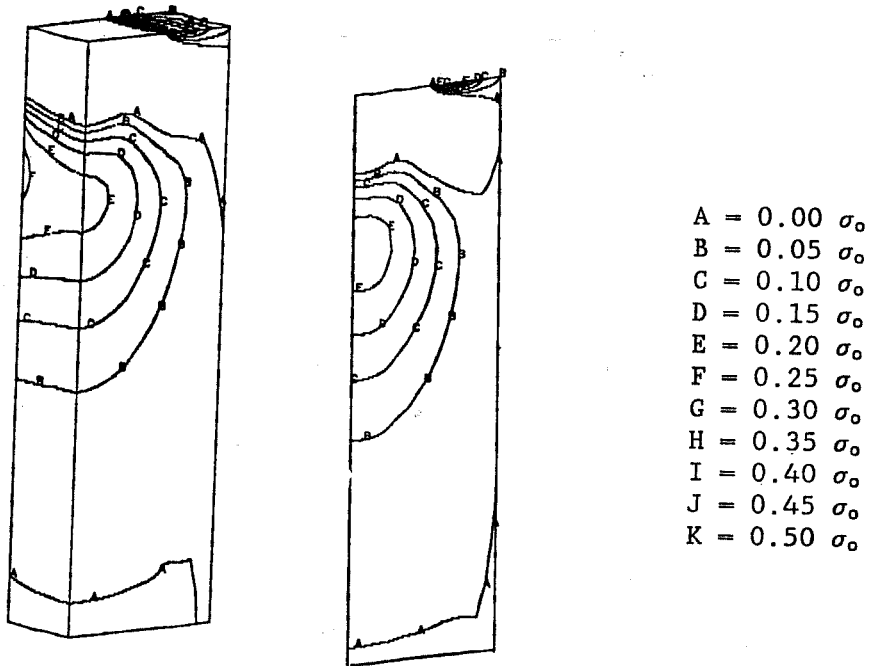
Figure 3.12   Approximation of the Three-Dimensional Stress Distribution with a Two-Dimensional Plane Stresses Model

A = 0.00 σ_0
B = 0.05 σ_0
C = 0.10 σ_0
D = 0.15 σ_0
E = 0.20 σ_0
F = 0.25 σ_0
G = 0.30 σ_0
H = 0.35 σ_0
I = 0.40 σ_0
J = 0.45 σ_0
K = 0.50 σ_0
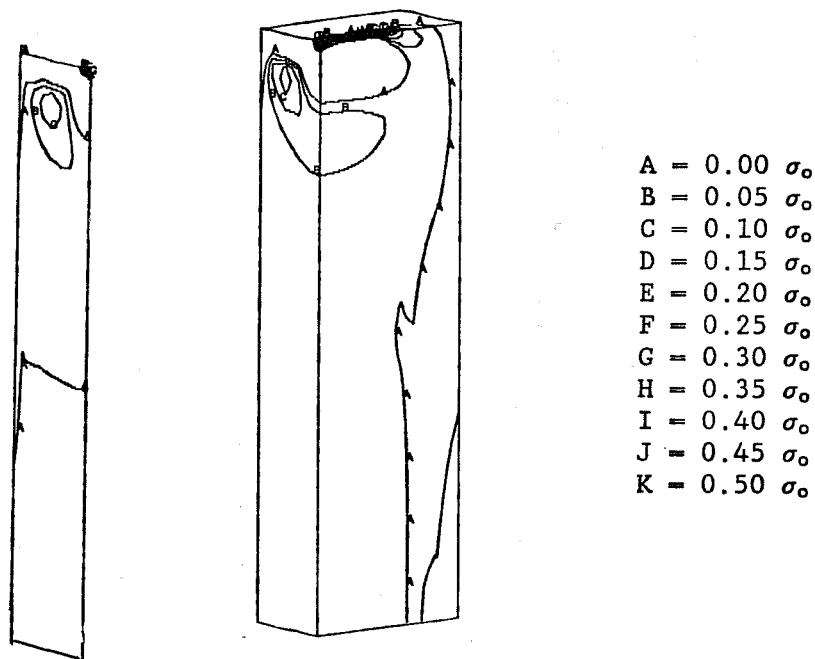
Figure 3.13   Approximation of the Three-Dimensional Transverse
              Stresses with a Two-Dimensional Plane Strain
              Analysis

3.4.3 Representation of the Results

Once a Finite Element Analysis has been performed, it is
best to represent the stress distribution in graphical form. This
allows for a quicker evaluation of analysis results. Several
representations exist, but no single representation has so far
been able to answer all the requirements of the analysis. Because

stress is a second-rank tensor, it seems best to combine several representations to present the results for evaluation.

A contour plot, as shown in Fig. 3.14, is a plot of lines of equal stresses. These lines are the equivalent of the lines of equal altitude that are found on topographic maps. However, because a stress function has several components, contour plots of one component give an incomplete picture of the state of stresses. In plane stress analysis, for example, a total of three contour plots are necessary to represent the three components of stresses in the plane, as shown in Fig. 3.14. Six plots would be necessary to represent the results of a three-dimensional analysis, even without considering the fact that several viewpoints and cuts through the model would probably be required. To limit the number of plots required to describe the state of stresses, contour plots of the Von Mises stress are often used to evaluate the results of the Finite Element Analysis. Unfortunately, this value is not very helpful for concrete structures, in which the maximum compressive stress can be an order of magnitude larger than the maximum tensile stresses, which are of interest. Contour plots of the principal stresses can also be used to evaluate the results of a Finite Element analysis, with the limitation that the direction of the principal stress is not shown on the plot.

Despite their limitations, contour plots are helpful, especially for simple configurations. One single plot of the stresses normal to the tendon path can yield sufficient information to design the bursting reinforcement for the general anchorage zone. Both ABAQUS and PATRAN offer facilities to generate contour plots of the stresses.

$$A = -5.0 \ \sigma_0$$
$$B = -4.5 \ \sigma_0$$
$$C = -4.0 \ \sigma_0$$
$$D = -3.5 \ \sigma_0$$
$$E = -3.0 \ \sigma_0$$
$$F = -2.5 \ \sigma_0$$
$$G = -2.0 \ \sigma_0$$
$$H = -1.5 \ \sigma_0$$
$$I = -1.0 \ \sigma_0$$
$$J = -0.5 \ \sigma_0$$
$$K = \ \ 0.0 \ \sigma_0$$
$$L = \ \ 0.1 \ \sigma_0$$
$$M = \ \ 0.2 \ \sigma_0$$
$$N = \ \ 0.3 \ \sigma_0$$
$$O = \ \ 0.4 \ \sigma_0$$
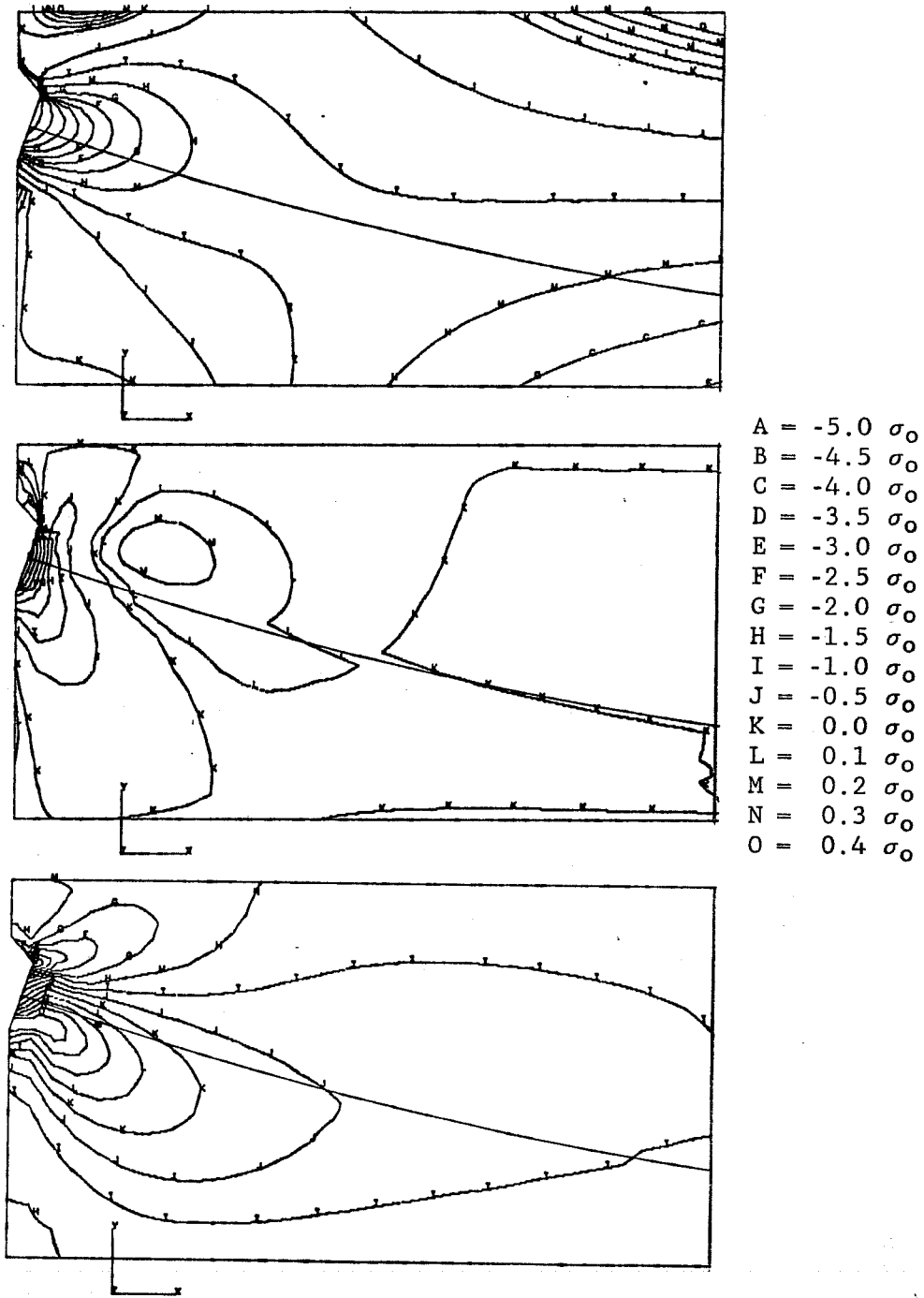
Figure 3.14   Contour Plot of the Normal Stresses σ_{xx} and σ_{yy} and of the Shearing Stress τ_{xy} in an Anchorage Zone
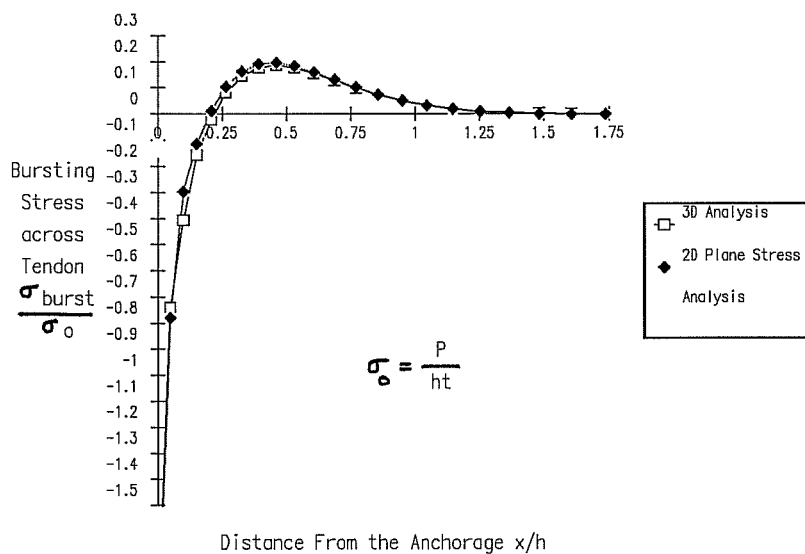
Figure 3.15   X-Y Plot of the Stresses Perpendicular to the Axis
of the Tendon σ_{xx} Represented Along the Axis
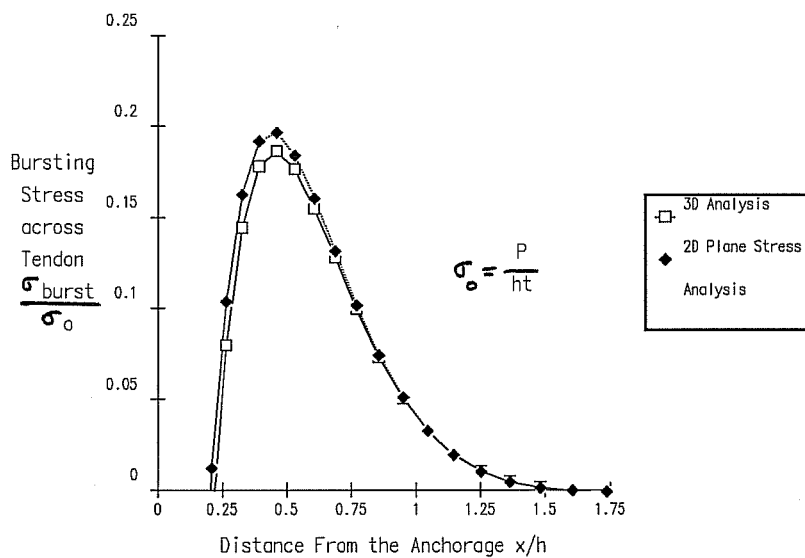
Figure 3.16   X-Y Plot of the Stresses Perpendicular to the Axis
of the Tendon Represented Along the Axis, Tensile
Stresses Only

An X-Y plot, such as the one shown in Fig. 3.15, is a plot of a given quantity, for instance stress, along a given line or curve. The X-coordinate, generally shown as the abscissa in the plot, is the distance along the line and the Y-coordinate, shown as the ordinate, is the value of the quantity being observed. To follow the analogy with topographic maps, an X-Y plot can be seen as a vertical slice through the mountain. Thus, an X-Y plot can easily be constructed from a contour plot of the corresponding quantity. In the example of Fig. 3.15, the stresses perpendicular to the axis of the tendon (σ_{xx}) are represented, and a comparison is made between the results of the three-dimensional analysis and the plane stress analysis. Because the compressive stress under the anchorage device is much larger than the tensile stresses observed at a larger distance from the anchor, and because tensile stresses are often of more concern for the designer, it is often convenient to only represent the tensile component of stresses, as shown in Fig. 3.16.

If the considered stress is perpendicular to the line, integrating the stress along the line gives the force acting perpendicular to it. As in the example presented in figures 3.15 and 3.16, X-Y plots are especially useful when comparing two or more configurations in which the other representations do not exhibit appreciable differences.

Isostatic lines as shown in Fig. 3.17a are lines that are at all points tangent to the direction of the principal stresses. They are similar to the equipotential lines of a flow net plot for underground fluid flow. Isostatic lines correspond to the intuitive idea of "spreading of forces" through a body. As a matter of fact, it is relatively easy to "guess" and draw isostatic lines for a simple configuration.

The tensorial nature of the stress function, in contrast to the scalar potential in fluid flow, renders an automated

computation of isostatic lines complicated. However, a plot representing a field of principal stress vectors as shown in Fig. 3.17b gives a visual idea that is very close to isostatic lines. The generation of principal stress vector plots can easily be automatized. If isostatic lines are desired, they can be drawn tangent to the corresponding vectors. If the vectors are scaled so that their lengths represent the magnitude of the stresses, plots of principal stress vectors also give indications of the relative magnitude of the stresses.
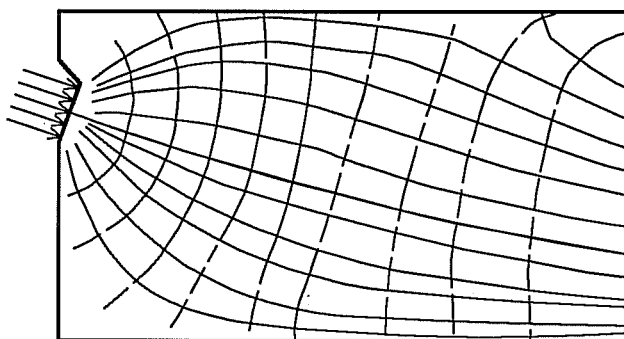
a) Isostatic Lines
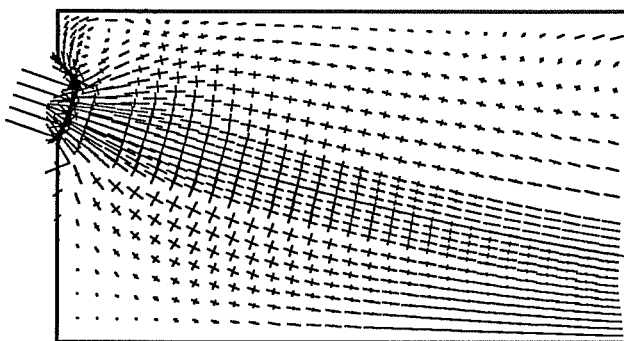
b) Principal Stress Vectors

Figure 3.17   Isostatic Lines and Principal Stress Vectors in an
              Anchorage Zone

A program to process the results of the Finite Element Analysis and to display the principal stress vectors and X-Y plots was developed on a microcomputer. This program allows a quick and easy interpretation of the results of a Finite Element Analysis and can export the results in several common file formats for further treatment. Because the program is based on a microcomputer and user-friendly, it has been extensively used in the design of specimens to evaluate the various design options.

3.4.4 Use of the Results from the Finite Element Analysis in the Design of Anchorage Zones

The results of a linear elastic analysis of the anchorage zone can be used for the design of the reinforcement in the general zone. Placing an amount of reinforcement corresponding to the calculated elastic tensile forces in the locations where the stresses in the concrete exceed the tensile strength allows an immediate load transfer when cracking occurs. The method of systematically placing reinforcement to resist any tensile stress in the model has often been used and is generally conservative. Furthermore, since the reinforcement is located exactly where it will be needed, it is expected that such a procedure will limit the extent of cracking. The knowledge of the elastic state of stresses in an anchorage zone is therefore a good starting point for design of reinforcement.

The compressive capacity of the anchorage zone can be estimated by computing the level of compressive stresses in the concrete under the factored tendon force. Because the confining reinforcement of the local zone generally extends for a length approximately equal to the lateral dimension of the anchorage device, the present study limits the stresses in the concrete at that location ahead of the anchorage device to 0.75 f'_c.

3.5   Strut-and-Tie Models

Strut-and-Tie Models (STM) constitute a simplified method to consider the state of equilibrium of a structure. [122, 181, 158]. As discussed in Section 3.4.3, the compressive stresses in the concrete flow naturally following the lines of principal stresses, or isostatic lines. In an approximation of the reality, the Strut-and-Tie Model assumes that the trajectories of principal stresses in the concrete are straight lines between points called nodes of the model. It is also assumed that the distributed compressive stresses can be represented by concentrated forces acting on compression members called **struts**. The tensile stresses are assumed to be entirely carried by reinforcing bars. Because the reinforcing bars are generally straight, the hypothesis of straightness is exactly valid for them, and the Strut-and-Tie Model is in this case closer to reality than an elastic stress analysis. The model generally lumps the effect of several reinforcing bars in a single tension member called a **tie**. The hypotheses of discrete struts and ties allows for a simplified analysis of the structure that is sometimes reduced to a **Truss Model**, which is an alternate, older designation for this method.

According to the theory of plasticity of structures, which is described in more details in the next section, such a model, if it satisfies the conditions of equilibrium and does not violate the material properties, predicts an ultimate capacity smaller or at most equal to the actual ultimate load of the structure [123, 181]. By definition, the nodes themselves are excluded from the overall plastic analysis. They are assumed to be able to rotate and transfer the member loads without causing failure. Some suggestions have been made on possible design criteria for nodes [181, 112, 113, 158, 9, 23]. Because the anchorage device itself is an obvious nodal point, it is clear that the Strut-and-Tie

Model will not give direct information on the mode of failure that occurs in the local zone. However, the Strut-ant-Tie Model can be used to a limited extent in separate evaluation of the local zone.

3.5.1 Plastic Design of Structures

Plastic design is a technique for estimating the maximum load a structure or a part of a structure can resist. The principal assumption of plastic design is that the components of the structure exhibit ductility, defined as the ability of a member to undergo a large amount of deformation (elongation or rotation) without a significant drop in strength. Ductility has long been known as a property of mild steel members as well as of reinforcing bars used in reinforced concrete [123, 181, 122].

At first sight, it would not appear that a reinforced concrete member is a very ductile structural component, but it can be made so. By properly selecting the amount of flexural
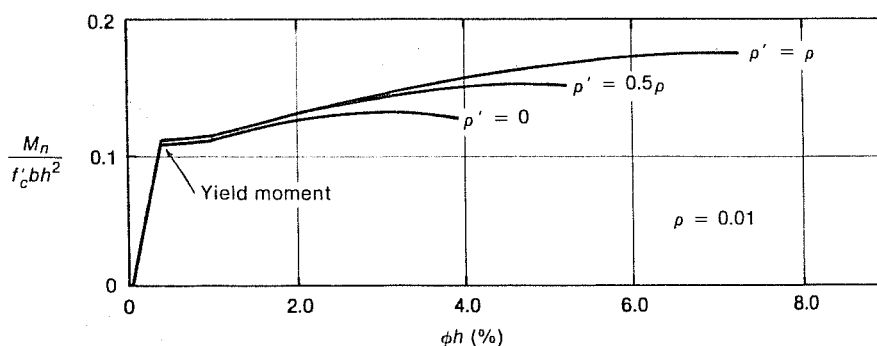
Figure 3.18   Moment-Curvature Relationship for a Rectangular
Concrete Section in Bending [110]

reinforcement, a reinforced concrete beam can be made ductile, because the reinforcing steel will yield in a ductile manner before the concrete fails in compression, as Fig. 3.18 shows. The various curves in Fig. 3.18 correspond to various amounts of compressive reinforcement φ'. The section described in the figure has a ductile behavior beyond the rotation corresponding to its plastic moment. The load carrying capacity increases slightly with the deformation beyond the plastic moment. Similar properties can be achieved for sections that are primarily subjected to shear and have adequate shear reinforcement proportioned so that the shear reinforcement yields before a compression failure occurs [181].

As in the case of steel structures, proper detailing is critical to achieve good ductility in a reinforced concrete section, especially to ensure that the required rotations can be developed. Proper detailing of reinforced concrete structures can provide a sufficient amount of ductility to allow the use of plastic design methods. For sections in bending, the contribution of concrete in tension can generally be ignored without significantly influencing the results. Experience with the application of plastic design methods to anchorage zones shows that the ductility of such structures is generally less than the ductility of members in bending. This behavior is in part caused by the comparatively large contribution of the concrete in tension to the load carrying mechanism of anchorage zones. As a consequence, when using the Strut-and-Tie Model for the design of anchorage zones, it is advisable to limit the demand on the ductility of the system by selecting Strut-and-Tie Model configurations that are close to the elastic stress distribution. The parametric studies of Chapter 4, however, show that a certain freedom is nevertheless available in the choice of the load-carrying system.

The theory of Plasticity of Structures rests on two major

theorems. These theorems are presented here first as they are were originally formulated for frame structures. They have however a more general validity, as a more general wording for the *Static Theorem* upon which the Strut-and-Tie Model is based will show.

(a) Static Theorem (Lower Bound Theorem)

A load corresponding to an equilibrium moment diagram with arbitrarily assumed values for the redundants is smaller than or at best equal to the ultimate loading if nowhere in the structure the moment exceeds the capacity of the section. [72]

(b) Kinematic Theorem (Upper Bound Theorem)

A load computed on the basis of an assumed mechanism will always be greater than or equal to the ultimate load.

The Static Theorem can be reworded in a more general fashion, showing that it is possible to obtain a conservative estimate of the capacity of a structure, or of a part of a structure, by assuming an internal stress distribution which respects the material properties. This is the principle on which the Strut-and-Tie Model rests.

The load computed based on an <u>assumed stress distribution</u> that satisfies the equilibrium condition and in no point exceeds the strength of the materials is a lower bound of the actual ultimate load.

3.5.2 Components of a Strut-and-Tie Model

This section describes in more detail the various components of the Strut-and-Tie Model that were introduced in Section 3.5. Fig. 3.19 shows the Strut-and-Tie Model of a concentric anchorage zone and identifies the various components. In the remainder of this document, compression struts will be graphically represented as solid lines, tension ties as dashed lines and nodes as donut shaped links.
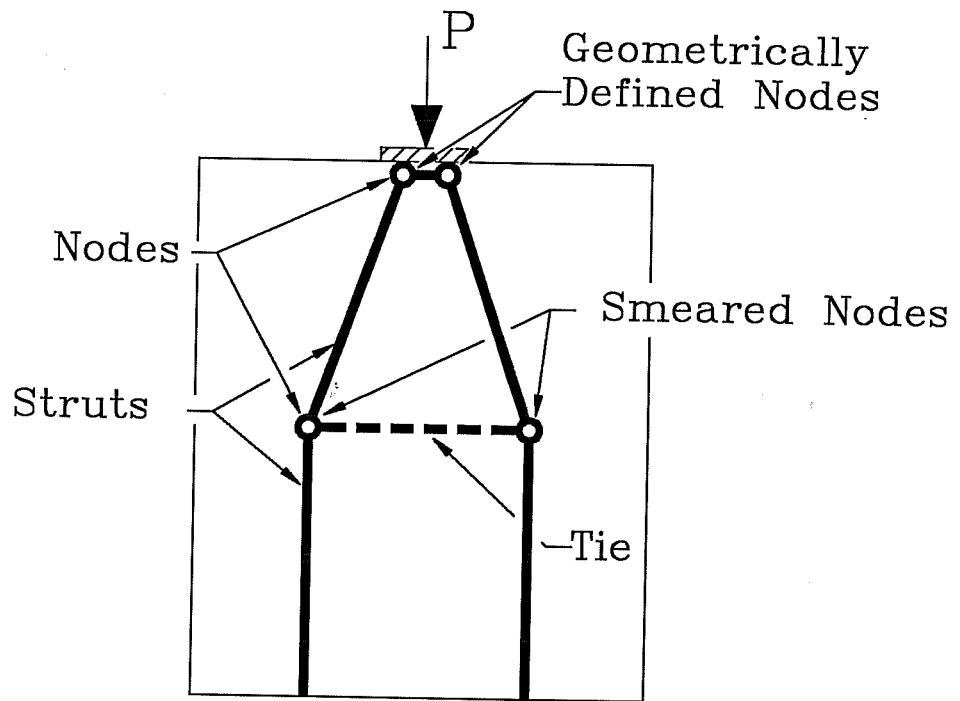

Figure 3.19   Components of a Strut-and-Tie Model

3.5.3 Nodes

Two kinds of nodes can be distinguished in developing Strut-and-Tie Models: nodes that are geometrically well defined by points of application of concentrated loads or reactions and nodes that need to be defined in areas of distributed loads or stresses.

To satisfy the equilibrium, it is necessary that the points of application of concentrated loads or reactions be represented as one or more nodes in the Strut-and-Tie Model, as shown in Fig. 3.19. This is for example the case with the local zone that surrounds the anchorage device. Geometrically defined nodes, also called singular nodes by Schlaich et al. [158], are subjected to strong gradients of stresses and are especially critical because there is no other load path to provide equilibrium of the structure.

The location of the nodes in regions where the stress distribution is smooth is not uniquely defined. These nodes can be considered as *smeared* over a certain area. If the chosen Strut-and-Tie Model is close to the elastic stress distribution, the actual stresses flow continuously and the stress gradients around the node are small, much like in the elastic model. These nodes are less critical because the stresses act on a larger area and there is a possibility of redistribution of the stresses around the node.

If, however, the chosen Strut-and-Tie Model is *not* close to the elastic stress distribution, sharp stress concentrations may be caused by the redistribution of forces and the cracking of the structure. The nodes then become geometrically defined by the cracks and are no longer smeared. Fig. 3.20 shows the detail of a dapped end beam, as described in [9, 158]. In this case, nodes C and E were originally located in an area of very low stresses, as can been observed from the principal stress vector plot. Because of diagonal cracking of the concrete, a redistribution occurred and nodes C and E became geometrically defined, and transfer a significant load.
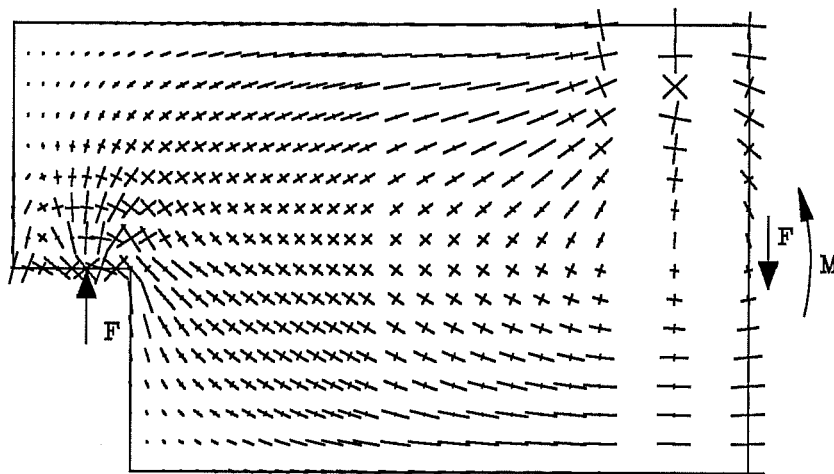
a) Principal Stress Vectors
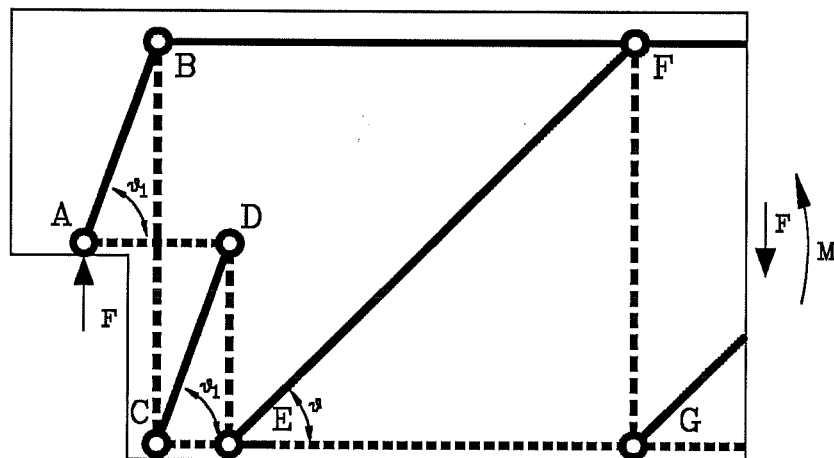
b) Strut—and—Tie Model

Figure 3.20   Principal Stress Vectors of a Dapped End Beam and
              Strut-and-Tie Model according to Schlaich et al.
              [158]

3.5.4 Struts

Concrete struts carry the compression forces from node to node in the Strut-and-Tie Model. As pointed out by Schlaich et al. [158], the stresses in the concrete tend to spread laterally between the nodes, as illustrated in Fig. 3.21. Because of the lateral spreading of the compressive stresses, the critical section for a concrete strut is generally located at the interface with the node, or at the location of a discontinuity in the thickness of the struts or in the confining reinforcement. Except in the vicinity of discontinuities, the thickness of the concrete struts can generally be taken equal to the thickness of the concrete section.
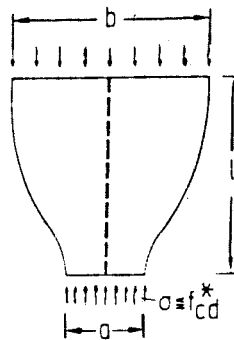
Figure 3.21   Bottle-Shaped Compression Struts According to [158]

3.5.5 Ties

The tension ties carry the tensile forces between nodes in the Strut-and-Tie Model. Tension ties are generally provided by non   prestressed   or   prestressed   reinforcing   steel.   The

reinforcement must be properly developed before or within the node, so that the full plastic capacity required by the Strut-and-Tie Model is available. The development of the reinforcement can be achieved through a regular development length, a hook or a mechanical connection.
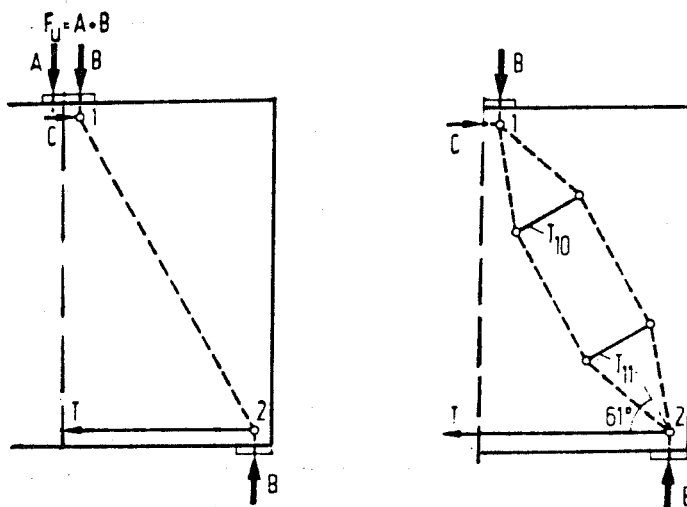
Figure 3.22   Secondary Strut-and-Tie Model in Compression Strut According to [158]

In certain cases, the tensile capacity is provided by concrete in tension. As pointed out by Schlaich et al. [158], reliance on the tensile capacity of concrete is implicit in any reinforced concrete design, even if this hypothesis is not stated. For example, the lateral spreading of compression forces mentioned in the previous subsection induces transverse tensile stresses perpendicular to the axis of the compression struts. These secondary tensile stresses can be either considered by means of secondary Strut-and-Tie Models, as illustrated in Fig. 3.22 or by concrete in tension, acting as a concrete tension tie.

3.5.6 Geometric Definition of the Strut-and-Tie Model

The single most important aspect of using the Strut-and-Tie Model is to define the geometry of the struts, ties and nodes. Once the geometry has been chosen, the calculation of the forces in the model is straightforward. Defining the geometry of the Strut-and-Tie Model is a crucial operation, because great freedom is available for locating the nodes, struts and ties. If the geometry is chosen solely to minimize the amount of reinforcement, the resulting Strut-and-Tie Model may well require a large amount of deformations and cracking before it can develop, thus producing an inadmissible solution because the large demand on ductility cannot be satisfied by the components of the Strut-and-Tie Model.

Only a few of the nodes of the Strut-and-Tie Model are unequivocally known because of their geometric location at points of local introduction of forces. Certain of the other nodes may be relatively easy to define, for example to represent the effect of distributed loads or of distributed reactions. In such cases, the distributed loads are lumped into several concentrated forces. Smeared nodes, that are internal to the structure, are usually less clearly defined. The geometry of the tension ties is usually constrained by constructive details. For example, it is often impractical to place reinforcement that would not follow the normal directions of the other reinforcement (orthogonal directions). On the other hand, the geometry of the concrete struts can be chosen more or less freely, since concrete is a continuous medium.

If the results of a linear stress analysis are available, the principal stress trajectories can be used in developing the Strut-and-Tie Model. The geometry of the compression struts should be chosen to be close to the trajectories of the principal compressive stresses to minimize the redistribution of forces.

This will ensure that the cracking under service loads remain limited and that the ductility requirements at ultimate will be small.

The ties are generally laid out on an orthogonal grid corresponding to the main reinforcement of the member. This method is adequate for cases where the direction of the stresses is close to the direction of the reinforcement. The centroid of the available reinforcement should be made to coincide more or less with the centroid of the tension forces as obtained from the linear analysis. In cases where the tensile forces are very large or if their orientation deviates strongly from the directions of the grid, it may be preferable to use oblique bars oriented in the direction indicated by the stress analysis.

If the results of a stress analysis are not available, it is still possible to develop a Strut-and-Tie Model. Given a simple problem, a structural engineer trained in the development of Strut-and-Tie Models should be able to sketch what is commonly called *force paths* of the forces in the body, which are similar to the isostatic lines shown in Fig. 3.17. These lines are a good basis to develop a Strut-and-Tie Model. In the present study, basic guidelines are developed to help in the systematic definition of the geometry of a Strut-and-Tie Model for the analysis of anchorage zone.

3.5.7 Use of the Strut-and-Tie Model in the Design of Anchorage Zones

Once the geometry of the Strut-and-Tie Model has been defined, the resulting truss structure can be analyzed. If the truss is statically determinate, the equilibrium equations can be solved in a manner similar to the analysis of truss structures. It frequently occurs that the resulting structure is *kinematic*, that

is that it is stable only for a specific loading. As a consequence, the model will need to be adapted for various loadings. If an analysis program is used to calculate the forces and deformations, additional members or boundary conditions must be added to make it stable.

Sometimes, the Strut-and-Tie Model is statically indeterminate. One possible solution is to assign reasonable values of forces to some members. By attributing to the force in a tension tie the strength of a given reinforcing bar, the corresponding unknown can be replaced by a known applied force. This procedure can be repeated until the structure becomes determinate [147]. It is also possible to perform a normal linear truss analysis of the indeterminate structure. Material properties and cross sectional areas are attributed to the struts and ties based on an assumed geometry of the members. Some iterations may be required before a satisfactory solution is reached.

The ultimate load predicted by the Strut-and-Tie Model is controlled by the failure of any one of the components, strut, tie or node. Each failure mode is discussed in the following sections.

3.5.7.1   Node Failure

Several propositions have been made concerning the mode of failure and the recommended design values for the nodes. Thürlimann, Marti and MacGregor [181, 112, 147] assume that the concrete in the node can resist a biaxial, hydrostatic compression with a pressure equal to the nominal concrete strength f'_c. Although there is little experimental evidence about this hypothesis,, it seems to be well accepted. The main problem in applying this philosophy is the design of nodes that involve tension ties. Schlaich et al. [158] present a model to explain the load transfer between the tension ties and the compression struts.

Anderson, Jirsa and Breen [9] have tested a series of nodes involving one compression force and two tension forces (CTT node). Bouadi, Jirsa and Breen [23] have tested nodes involving two compression forces and one tension force (CCT node).

With the exception of failures in the local zone, no failure of the nodes was observed in the tests of anchorage zones. This is most likely due to the fact that all nodes involved in Strut-and-Tie Models of anchorage zones, with again the exception of the local zone, are *smeared nodes*. In all test specimens however, the reinforcing steel of the ties was carefully detailed in order to be fully developed within or before the nodes. Failure of the anchorage zone in the local zone has been observed several times during the tests, but is not included in this dissertation as discussed in Section 1.2.3. Such failures would be prevented if the recommendations of Roberts [146] had been available and followed.

3.5.7.2   Strut Failure

In the general zone, stresses in the concrete are largest at the interface with the concrete of the local zone, which is generally confined. The critical section for the compression struts is generally located at the bottom of the confining reinforcement of the local zone. Its exact location varies because of the lateral spreading of stresses, which causes unconfined concrete to interact with confined concrete. For this study, a critical section located at one times the lateral dimension of the anchorage device ahead of the device was proposed. More details on the exact geometry of the critical section are given in Chapter 4.

Several values have been proposed for the maximum compressive stress in the concrete of compression struts [158, 181, 147, 110, 40]. Most of the studies were based on tests

performed on configurations involving either bending or shear, with no local introduction of force. The values proposed range from 1.0 f'_c to 0.3 f'_c depending of the state of stresses in the considered area and on the expected cracking pattern. For this study, the value of $0.6f'_c$ was used. This value is smaller than the value of 0.75 f'_c used with the results of Finite Element Analyses because the stresses obtained by the Strut-and-Tie Model are average values over the width of the strut, not peak values.

3.5.7.3   Tie Failure

A tension tie is considered as failed when all bars contributing to it have yielded. If the structure becomes a mechanism at this point, failure of the anchorage zone will occur. Failure of the steel ties in tension is the desired mode of failure because the yielding of steel is ductile. In the case of anchorage zones, this ductile behavior has not really been observed, because the contribution of uncracked concrete in tension is present until very late in the loading history.

Strut-and-Tie Models that rely explicitly on the tensile capacity of a concrete tie can fail if a concrete tension tie cracks and the crack propagates, releasing the tension force. Schlaich et al. emphasize that concrete ties should be relied upon only where no progressive collapse is expected. Because the anchorage zone is a critical part of the structure, it is undesirable to rely on any tensile capacity of the concrete for the design. However it was obvious when observing the behavior of laboratory test specimens that uncracked concrete has an appreciable contribution to the behavior of the anchorage zone even after cracking has occurred. Fig. 3.29 shows the load-deflection curve of the loading head of the testing machine for one specimen [153]. As can be observed in the figure, the onset of

cracking at a load of 345 kips has no obvious influence on the stiffness of the test specimen.

3.6 Serviceability of the Anchorage Zone

The purpose of the serviceability analysis is to ensure that the anchorage zone will perform satisfactorily under normal loading conditions. The performance is sufficient when the deformations of the anchorage zone are small and the extent and opening of cracks is limited.

Uncracked anchorage zones are very stiff members because of the massive section of concrete. As shown in Fig. 3.29, the
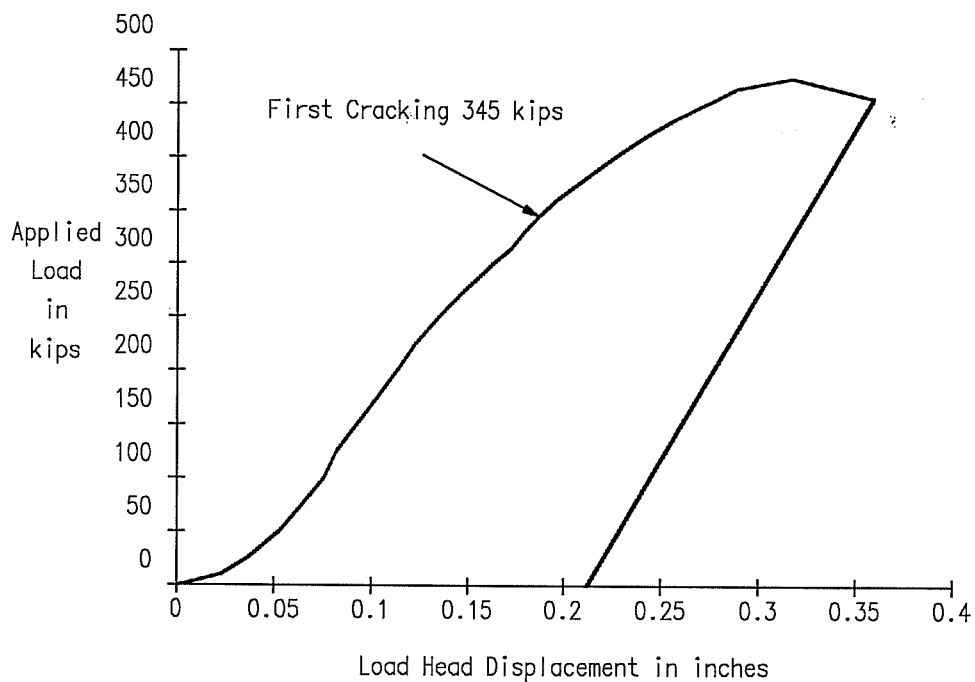

Figure 3.29   Load Deflection Curve Measured at the Loading Head
              for Specimen El [153]

presence of cracks does not dramatically reduce the stiffness of the anchorage zone. Even if the contribution of concrete in tension is neglected for the strength design of the anchorage zone, it will be present at service loads. Because the deflections of the anchorage zone under service loads are small, it is in general not necessary to compute them. If the deformations at ultimate are needed, they should be computed on the basis of the chosen Strut-and-Tie Model, assuming no concrete contribution. These deformations will be upper bounds of the real value. Because of the very large stiffness of the concrete compression struts, the stiffness of the Strut-and-Tie Model depends primarily on the stiffness of the tension ties. If the estimated deflections are excessive, they will be reduced by increasing the amount of steel in the ties.

It is unrealistic to expect that concrete will not crack at all in the anchorage zone of a member resisting service loads. The presence of post-tensioning forces in a structure will limit the opening of concrete cracks, but only in the direction of the prestressing force. Transverse stresses as caused by the tendon force in the anchorage zone, unaccounted external effects caused by differential settlements or impact loads as well as internal causes as shrinkage or temperature effects may well cause the concrete to crack anyway. It is therefore preferable to assume that the concrete *will* crack and to provide reinforcement that will both prevent the failure and limit the cracking. The main cracks in the general zone are caused by bursting stresses.

If the tensile stresses in the concrete are necessary for the equilibrium of the structure, as in the case of bursting stresses, the crack will extend until a new state of equilibrium is reached. For a given loading, the crack will stop propagating when the force in the reinforcing steel that crosses it compensate the tensile force resisted by the concrete before cracking. In

order to limit the opening of cracks, reinforcement must cross the crack close to the location where a crack is forming. The location of the reinforcement relative to a developing crack has a considerable influence on the growth of the crack. A reinforcement layout that follows relatively closely the elastic distribution of stresses will be most able to limit efficiently cracking. The tensile cracks in the concrete extend in the direction of the principal compressive stress and open perpendicular to it. Because the tendon path is a line of principal compressive stress, the reinforcement should be placed perpendicular to it.

Spalling stresses and stress concentrations in reentrant corners are primarily caused by the condition of compatibility. In these cases, the magnitude of the tensile stress is very large (theoretically infinite for a reentrant corner with an angle of 90 degrees), and cracking should therefore be observed first at these locations. However, examinations made during the experimental testing of specimens did not reveal an observable cracking of these areas before other areas cracked. Cracks in reentrant corners were only observed in the final stages of the loading. Some cracking other than cracking along the axis of the tendon (caused by bursting stresses) was observed during the testing of eccentrically loaded specimens with a large eccentricity, thus following the prediction of the elastic stress analysis. Fig. 3.27 shows Specimen E6 during testing. Cracks perpendicular to the surface of the concrete on the loaded face and on the side face away from the loading (closest to the camera in the picture) can be observed. Chapter 5 discusses in more detail the case of eccentrically loaded anchorage zones.

obtained from comparison with the results of the experimental test program.

Because of the large freedom given to the designer in the choice of the geometry of a Strut-and-Tie Model, it is necessary to define criteria by which, in the absence of physical test results, various Strut-and-Tie Model configurations can be compared and evaluated. At the same time, it should be recognized that in plastic design there is generally no unique solution to a given problem. Instead, the goal of the designer should be to obtain a safe design that performs satisfactorily under service loads and under ultimate loads.

As long as the concrete is uncracked, the chosen Strut-and-Tie Model and the associated reinforcement pattern have very little influence on the behavior of the anchorage zone. The stress distribution in the concrete corresponds essentially to the elastic stress distribution. As the anchorage zone starts to crack, the reinforcement provided by a well designed Strut-and-Tie Model will be located within close distance of the crack, and oriented in the proper direction. At ultimate, when no special attention needs to be given to corrosion protection, large cracks that result from important stress redistributions are permissible. A well designed Strut-and-Tie Model will use most efficiently the materials to resist the ultimate load without exhausting their ductility.

Schlaich et al. [158] propose that, according to the principle of minimum potential energy for linear elastic behavior of the struts and ties after cracking, the Strut-and-Tie Model that has the lowest level of strain energy in its members is the one to select. This criterion can be expressed as shown in Equation 3.2.

$$\Sigma F_i l_i e_{mi} = \text{Minimum} \quad \text{(Eq. 3.2)}$$
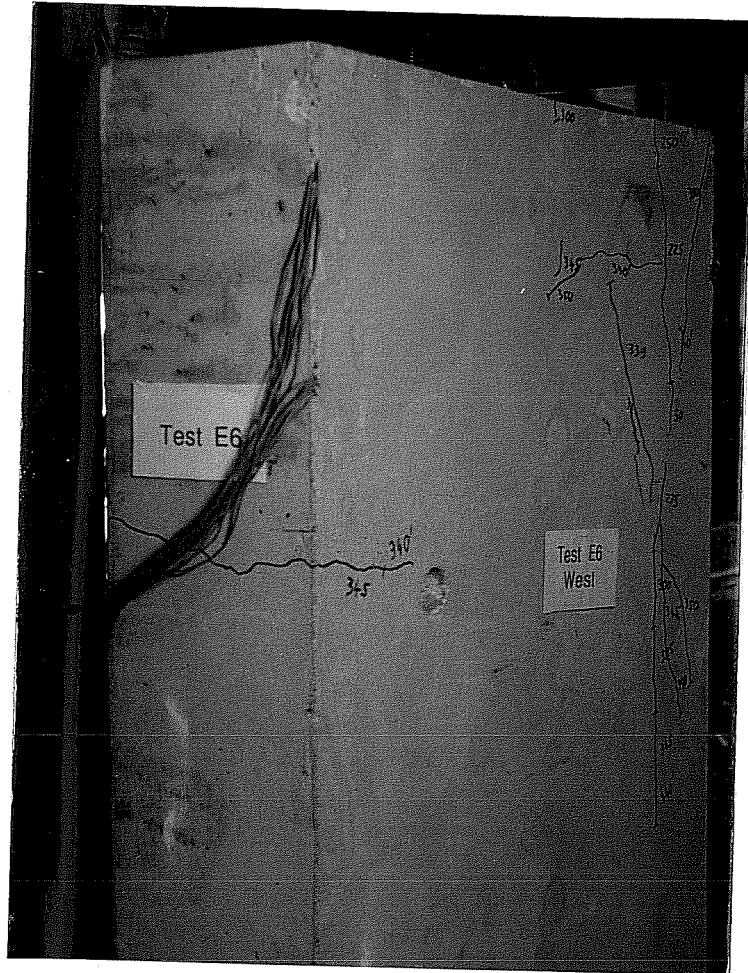
Figure 3.27   Cracking of Specimen E6 [153] with an Eccentricity
e = 0.25h

3.7   Evaluation of the Analysis Methods

In the subsequent chapters, both the Finite Element approach and the Strut-and-Tie Model approach are evaluated by comparing the predictions of either method with experimental test results. The methods are successively refined as more information is

Where

F_i is the force in a member

l_i is the length of the member

e_{mi} is the average strain in the member

Schlaich et al. further suggest that because the strains in the struts are usually very small, the strain energy of the concrete struts can be neglected. The optimal model is then the model that has the smallest strain energy in its tension ties. As Schlaich et al. [158] point out, there is no unique or absolute optimal solution and the engineer using this criterion should be looking for a satisfactory solution, not an optimal one.

If the chosen model strongly diverge from the elastic solution, the criterion of minimal strain energy in the ties can be inapplicable, as illustrated in Fig. 3.30. The Strut-and-Tie Model of Fig. 3.30a is relatively close to the elastic stress distribution and is a good solution with a distribution of the reinforcement that will limit cracking. The Strut-and-Tie Model of Fig. 3.30b has a lower strain energy than the model of Fig. 3.30a, and would therefore be selected on the basis of Equation 3.2. However, the extensive cracking of the anchorage zone required before the steel is mobilized makes this solution unacceptable for practical applications. The criterion of minimum strain energy in the ties is used in Chapter 4 to compare various Strut-and-Tie Model configurations that are all relatively close to the elastic stress distribution.

When the Strut-and-Tie Model has been applied to shear design of reinforced concrete beams [181, 176], limitations have been placed on the allowable angles for the compression struts. In a similar way, Schlaich et al. recommend that in any Strut-and-Tie Model the compression struts be chosen so as not to deviate more than 15 degrees from the direction of the elastic principal compressive stresses. This criterion is interesting, but it is

impractical to perform an elastic analysis for every anchorage zone. In the present study, since an elastic analysis of the structure was in all cases available, the criterion of *closeness* to the elastic stress distribution was used in evaluating the models proposed. However the methods subsequently proposed to obtain the Strut-and-Tie Models are in most cases independent of the elastic analysis itself. The principal stress trajectories from were used in defining the geometry of the Strut-and-Ties, but the proposed methodology does not require an elastic analysis.

The most important consideration in the development of a Strut-and-Tie Model for an anchorage zone is to locate the centroid of the tensile reinforcement (tension tie of the Strut-and-Tie Model) close to the elastic centroid of the tensile stresses. The specimens designed with Strut-and-Tie Models in which the reinforcing patterns followed the elastic stress distribution performed better in the experimental tests than the specimens with reinforcement departing more strongly from it.

a) Adequate
Strut—and—Tie Model

Strain Energy:

$$E = 0.15 \cdot P \cdot \frac{h}{2} \, \varepsilon_y$$

b) Inadequate
Strut—and—Tie Model

Strain Energy:

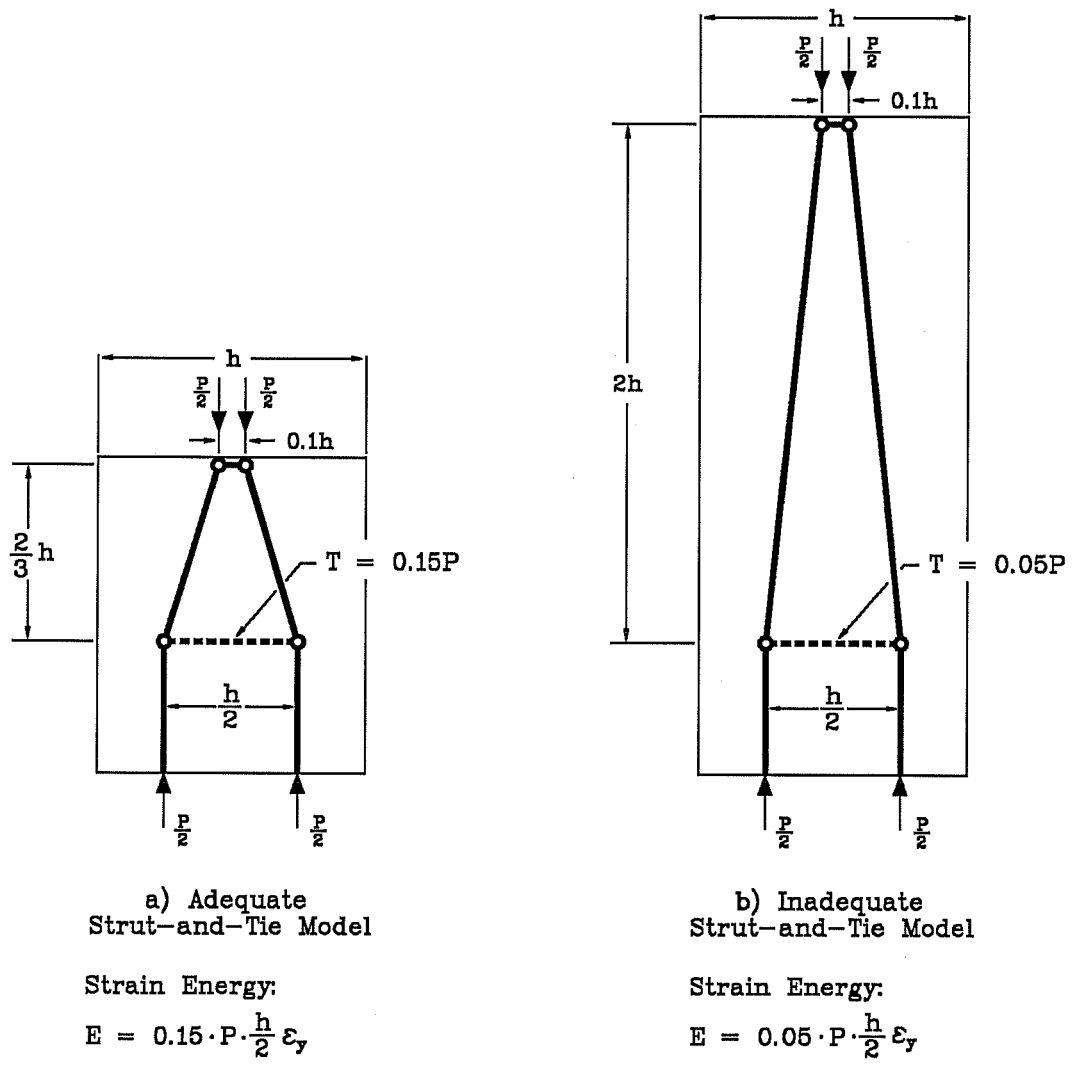$$E = 0.05 \cdot P \cdot \frac{h}{2} \, \varepsilon_y$$

Figure 3.30   Unsatisfactory Application of the Principle of
Minimum Strain Energy

4.   Concentric Single Anchor Configurations

Single anchors constitute the simplest configuration of anchorage zones. Because the number of parameters is reduced in comparison to multiple anchor configurations, the influence of the individual parameters can be more easily isolated for investigation.

In increasing order of complexity, as shown in Fig. 4.1, single anchor configurations can be loaded concentrically or eccentrically, the tendon can be parallel to the axis of the anchorage zone or inclined, the tendons can be curved, and the

a) Concentric   b) Eccentric   c) Inclined

d) Inclined and   e) Transverse   f) Transverse
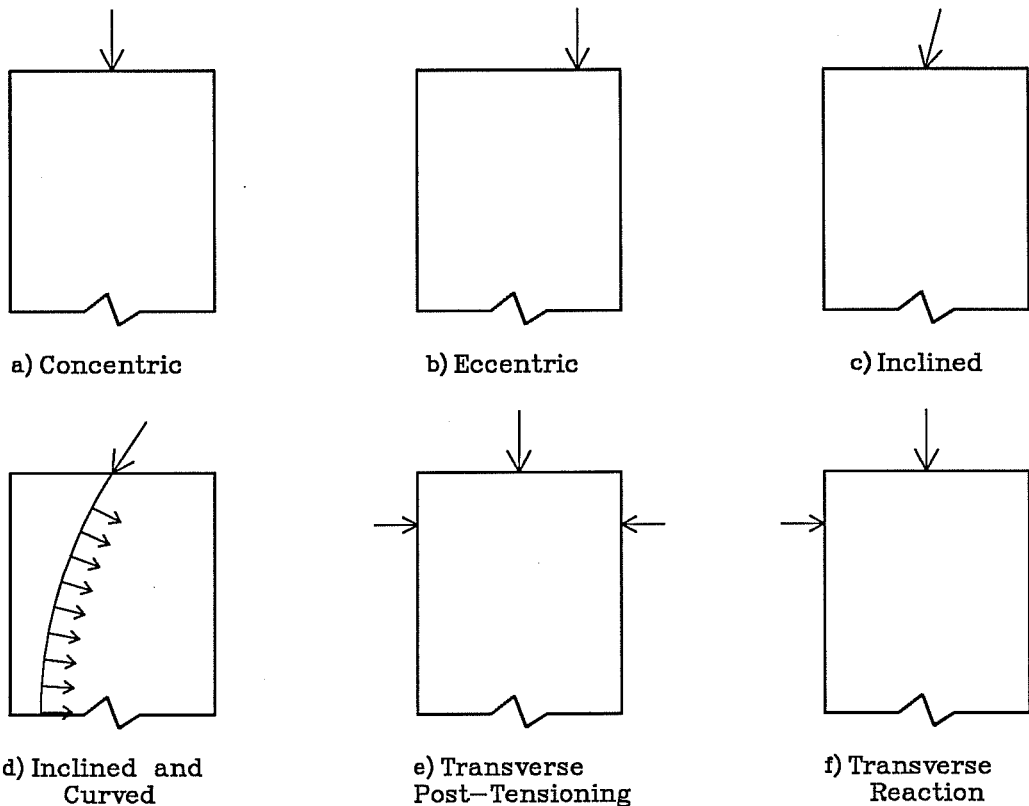   Curved   Post-Tensioning   Reaction

Fig. 4.1   Configurations for Single Anchors

anchorage zone can be subject to transverse post-tensioning or to transverse reactions. This chapter presents in detail concentric single anchor configurations. The basic principles developed in this chapter for the physical behavior of anchorage zones and for design using Strut-and-Tie Models will be expanded to more complex configurations in the subsequent chapters.

4.1   Interest in the Concentric Single Anchor Configuration

The behavior of an anchorage zone is controlled by the concrete strength and by the reinforcement. The layout of the reinforcement, the material properties of concrete, both in tension and in compression have a significant influence on the behavior of the general zone at service state and at ultimate. The behavior of the local zone is controlled by the compressive strength of the concrete and by the amount of confining reinforcement provided in the local zone.

The simplest configuration for anchorage zones is a single concentric anchor, as shown in Fig. 4.2. The governing parameter for the analysis of the general zone for a concentric anchorage is the width of the anchorage device relative to the width of the specimen (a/h).

The test specimens described in Section 4.4 were planned to specifically investigate the behavior of the general zone. Therefore, modes of failure that do not involve the general zone in the main plane of investigation are undesirable. As will be seen in subsection 4.2.2, the larger the anchorage device is relative to the concrete section (the larger the relative plate size a/h), the smaller the bursting force. In cases where the relative plate size a/h tends toward unity, a transverse failure due to bursting forces becomes impossible. This type of geometry, where one of the dimensions (the thickness) is small relative to

the other ones, and is approximately equal to the size of the anchorage plate, is quite common in practical applications of post-tensioning. Ordinarily, the general zone reinforcement will be determined for two or more *principal planes*, as outlined in Chapter 3 and developed in Chapter 6.
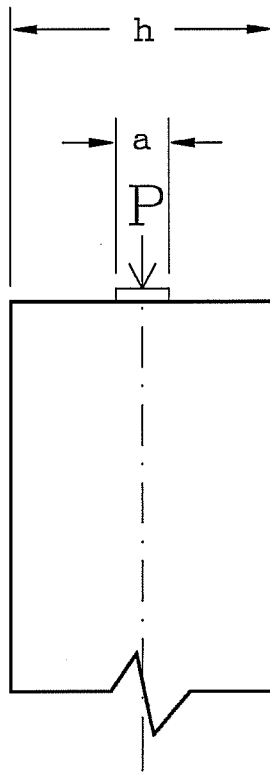
Therefore, in order to prevent a general zone failure due to bursting forces in the transverse direction, the experimental test specimens were built with a thickness as small as possible considering the transverse dimension of the anchorage device. The remaining possible modes of failure were then: failure in the general zone in the main plane, and failure in the local zone. The failure of the local zone can generally be prevented by limiting the nominal bearing stress under the anchor and by properly detailing the confining reinforcement of the local zone. Thus the only remaining mode of failure for the test specimens is a failure in the general zone of the main plane (largest dimensions) of the specimen. This failure can be due to a tension failure of the bursting reinforcement or a compression failure of the concrete. These two modes of failure are the object of the investigations in the subsequent sections.

Fig. 4.2   Geometry of Concentric Single Anchor

4.2 Finite Element Analysis

The Finite Element Method was used to determine the elastic state of stresses in anchorage zones with a single concentric tendon. Most analyses were performed on plane stress models, taking advantage of the fact that the thickness of the test specimens was small; some computations used three-dimensional models to investigate the influence of the hole caused by the tendon duct on the state of stresses. The results of the Finite Element Analysis performed will be compared with published results. The principal stress vector plots will be used in the construction of the Strut-and-Tie Models. The magnitude and location of the internal forces obtained from the Finite Element analyses will be used in the evaluation of the results from the Strut-and-Tie Model.

4.2.1 Finite Element Modelling

The mesh used for most of the investigations of single anchor configurations is shown in Fig. 4.3. Four-node isoparametric elements were used. The material properties used in the analyses are described in Table 4.1. The boundary conditions at the bottom allow for a lateral expansion of the specimen, which is the case that causes the largest bursting stresses.

The load was assumed to be applied as a pressure acting uniformly over the entire surface of the loading plate. The influence of this hypothesis and other possible assumptions for the modelling of the anchorage device are discussed in subsection 4.6.2. In a parametric study, the size of the anchor plate over which the loading is applied was varied from a = 0 (point load) to a = 1.0h.
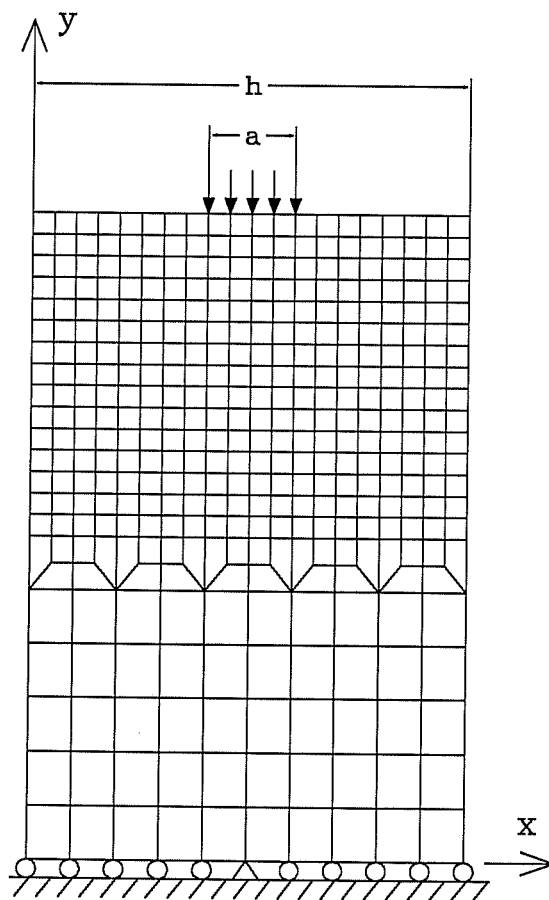
Fig. 4.3   Finite Element Mesh for Parametric Study

Table 4.1: Material Properties used for the Finite Element
            Analyses

Modulus of Elasticity for Concrete	$E = 4300$ ksi
Poisson's Ratio for Concrete	$\mu = 0.16$

A discussion of the accuracy of the Finite Element
computations and of the various hypotheses made for the analyses
is given in subsection 4.6.1. The results for a = 0 to a = 0.3h
were obtained using a finer mesh than the one shown in Fig. 4.3.

4.2.2 Elastic Distribution of Stresses and Internal Forces

Figure 4.4 shows the regions of a concentric anchorage zone subjected to bursting and spalling stresses. The bursting stresses act perpendicular to the tendon ahead of the anchorage device. The spalling stresses act on either side of the anchorage device, parallel to the free surface of the concrete. The magnitude of the spalling stresses (and of the corresponding forces) on the faces parallel to the tendon is much smaller than the magnitude of the spalling stresses on the loaded face, and no distress has been observed due to these stresses. In the subsequent sections, the term *spalling stresses* will therefore exclusively refer to the stresses acting on either side of the anchorage device parallel to the loaded surface. Figs. 4.5 and 4.6 show contour plots of the stresses in direction x-x, y-y and the shear x-y for the plate sizes a = 0.2h and a = 0.4h. All stresses are normalized to the average compressive stress at the end of the anchorage zone $\sigma_0 = P/(h\ t)$. The plots of the stresses in the x-direction show only the tensile stresses and the plots of the stresses in the y-direction show only compressive stresses. Figs. 4.7 and 4.8 show the corresponding principal stress vector plots.
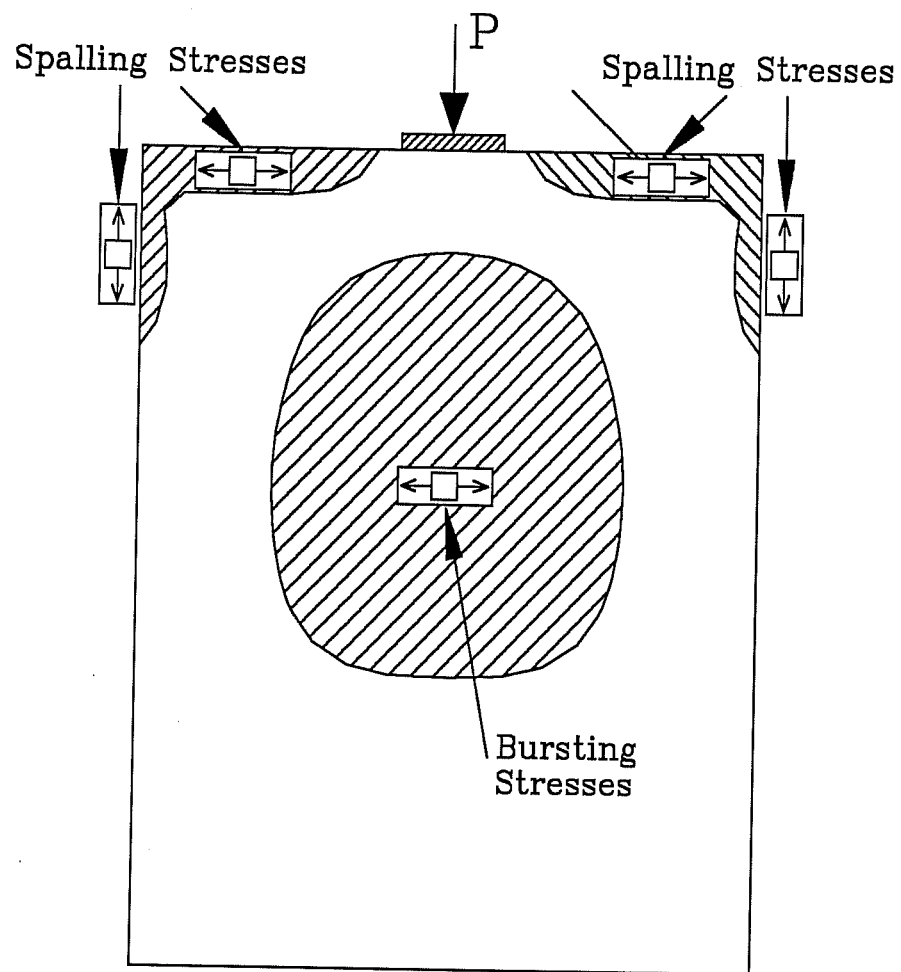
Figure 4.4   Areas of Bursting and Spalling Stresses in a
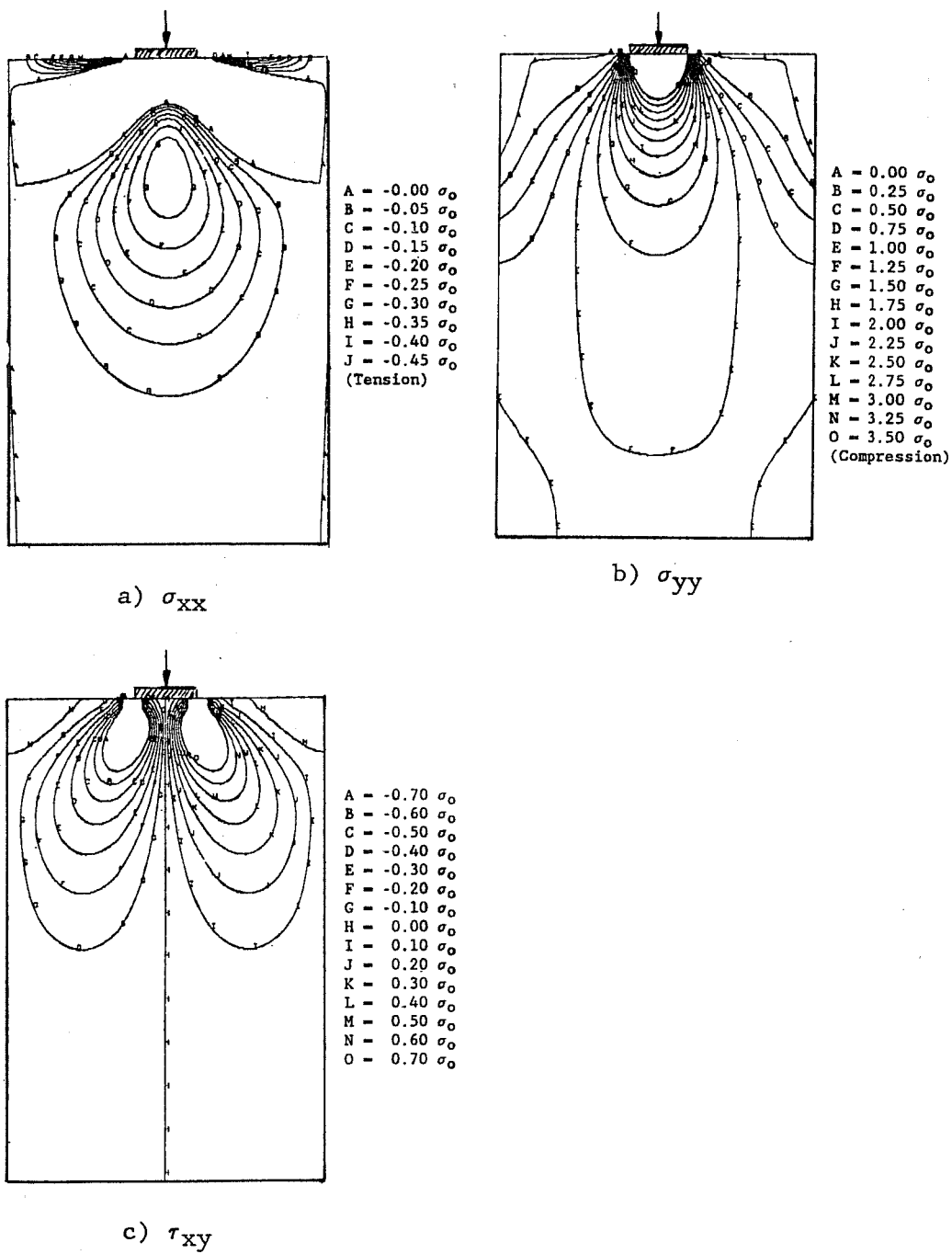Concentric Anchorage Zone

a) σ_{xx}

A — -0.00 σ_o
B — -0.05 σ_o
C — -0.10 σ_o
D — -0.15 σ_o
E — -0.20 σ_o
F — -0.25 σ_o
G — -0.30 σ_o
H — -0.35 σ_o
I — -0.40 σ_o
J — -0.45 σ_o
(Tension)

b) σ_{yy}

A — 0.00 σ_o
B — 0.25 σ_o
C — 0.50 σ_o
D — 0.75 σ_o
E — 1.00 σ_o
F — 1.25 σ_o
G — 1.50 σ_o
H — 1.75 σ_o
I — 2.00 σ_o
J — 2.25 σ_o
K — 2.50 σ_o
L — 2.75 σ_o
M — 3.00 σ_o
N — 3.25 σ_o
O — 3.50 σ_o
(Compression)

c) τ_{xy}

A — -0.70 σ_o
B — -0.60 σ_o
C — -0.50 σ_o
D — -0.40 σ_o
E — -0.30 σ_o
F — -0.20 σ_o
G — -0.10 σ_o
H — 0.00 σ_o
I — 0.10 σ_o
J — 0.20 σ_o
K — 0.30 σ_o
L — 0.40 σ_o
M — 0.50 σ_o
N — 0.60 σ_o
O — 0.70 σ_o

Fig. 4.5   Contour Plots of the Components of Stresses
            for a = 0.2h

a) σ_{xx}

A = -0.00 σ_0
B = -0.05 σ_0
C = -0.10 σ_0
D = -0.15 σ_0
E = -0.20 σ_0
F = -0.25 σ_0
G = -0.30 σ_0
H = -0.35 σ_0
I = -0.40 σ_0
J = -0.45 σ_0
(Tension)

b) σ_{yy}

A = 0.00 σ_0
B = 0.25 σ_0
C = 0.50 σ_0
D = 0.75 σ_0
E = 1.00 σ_0
F = 1.25 σ_0
G = 1.50 σ_0
H = 1.75 σ_0
I = 2.00 σ_0
J = 2.25 σ_0
K = 2.50 σ_0
L = 2.75 σ_0
M = 3.00 σ_0
N = 3.25 σ_0
O = 3.50 σ_0
(Compression)

c) τ_{xy}

A = -0.70 σ_0
B = -0.60 σ_0
C = -0.50 σ_0
D = -0.40 σ_0
E = -0.30 σ_0
F = -0.20 σ_0
G = -0.10 σ_0
H = 0.00 σ_0
I = 0.10 σ_0
J = 0.20 σ_0
K = 0.30 σ_0
L = 0.40 σ_0
M = 0.50 σ_0
N = 0.60 σ_0
O = 0.70 σ_0
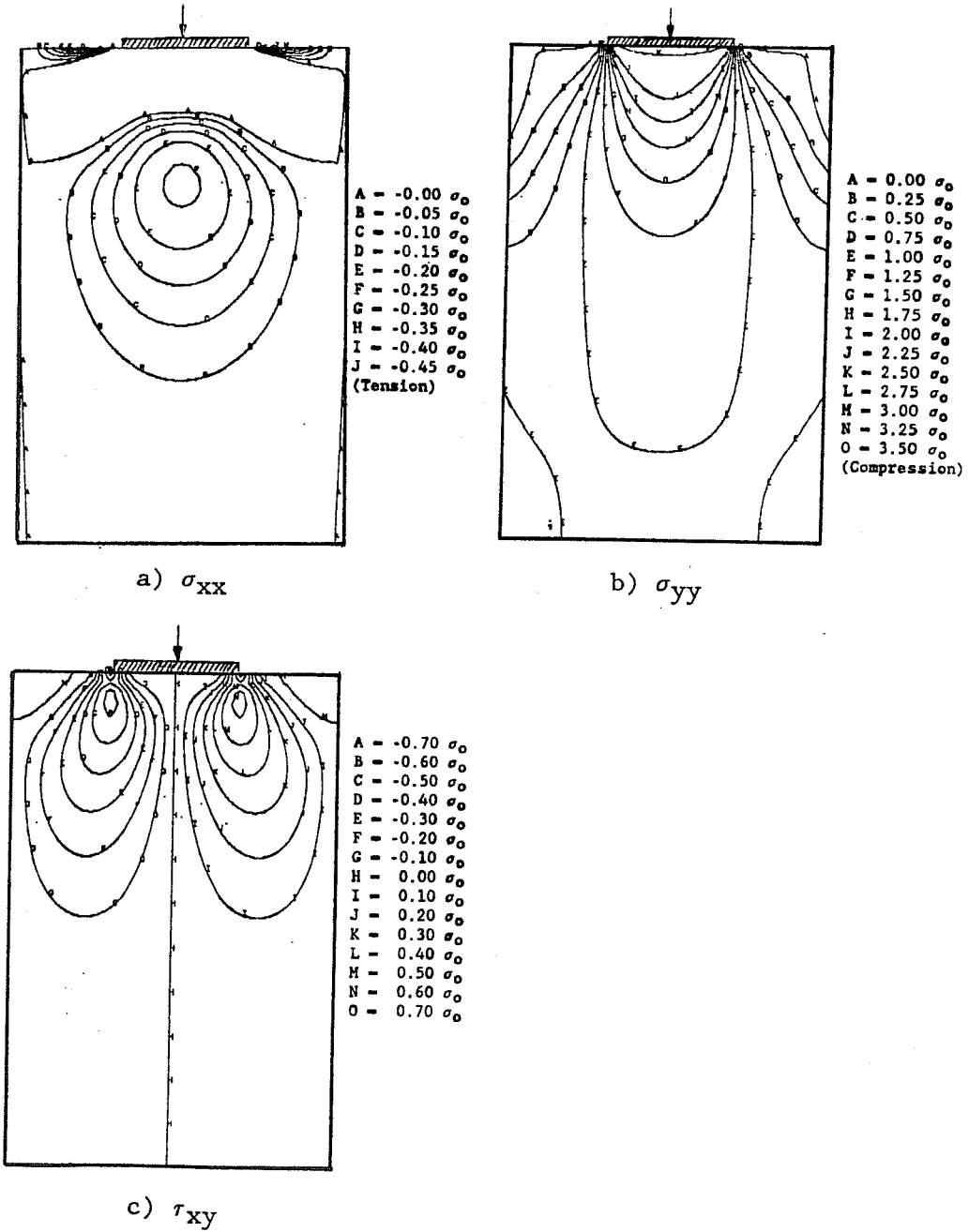
Fig. 4.6   Contour Plots of the Components of Stresses
            for a = 0.4h

a/h=0.2

a) Minimum Principal Stress
(compression)

b) Maximum Principal Stress
(tension)
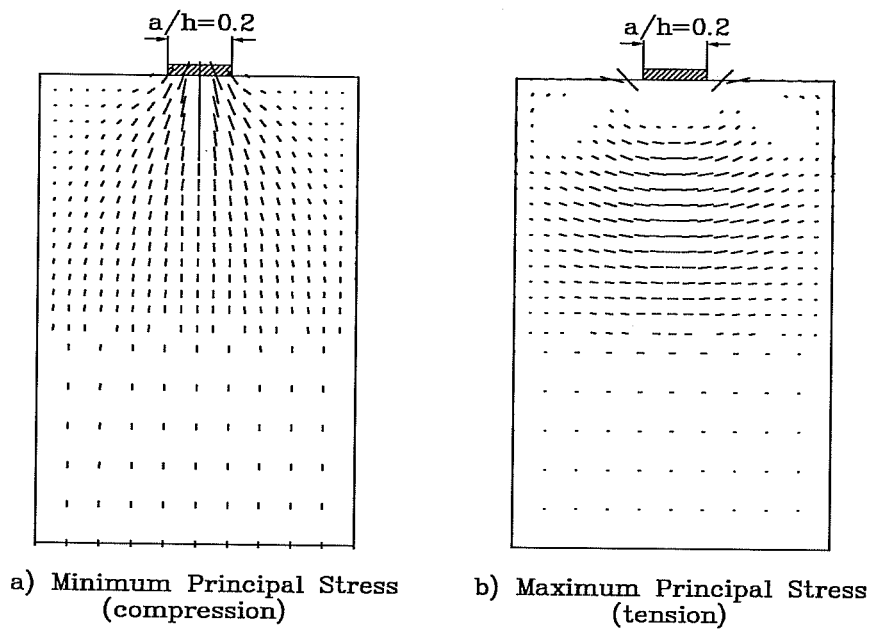
Fig. 4.7   Principal Stress Vectors Plot for a = 0.2h

a/h=0.4

a) Minimum Principal Stress
(compression)

b) Maximum Principal Stress
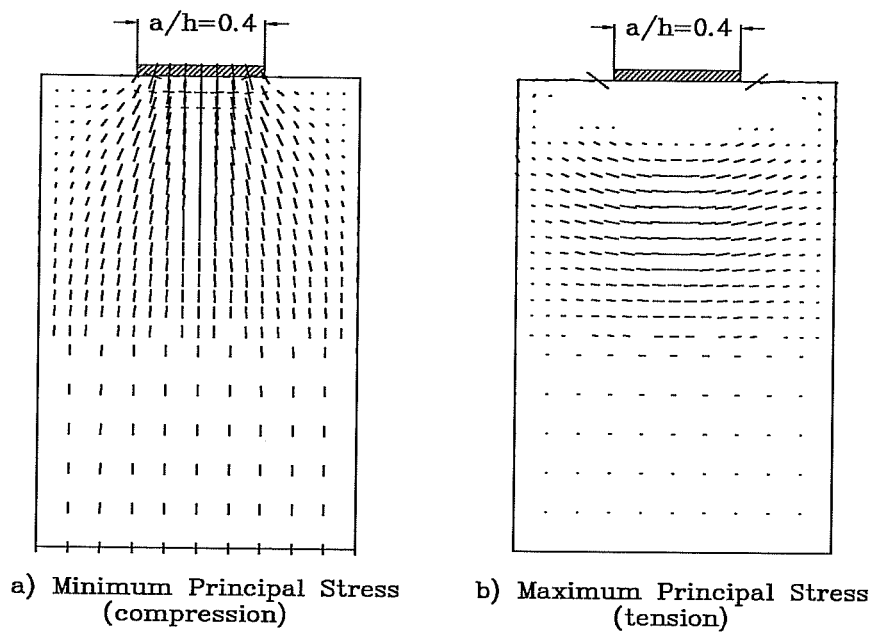(tension)

Fig. 4.8   Principal Stress Vectors Plot for a = 0.4h

4.2.2.1   Bursting Stresses

Fig. 4.9 shows the distribution of tensile bursting stresses along the tendon path for various ratios of the size of the anchor plate to the depth of the section.
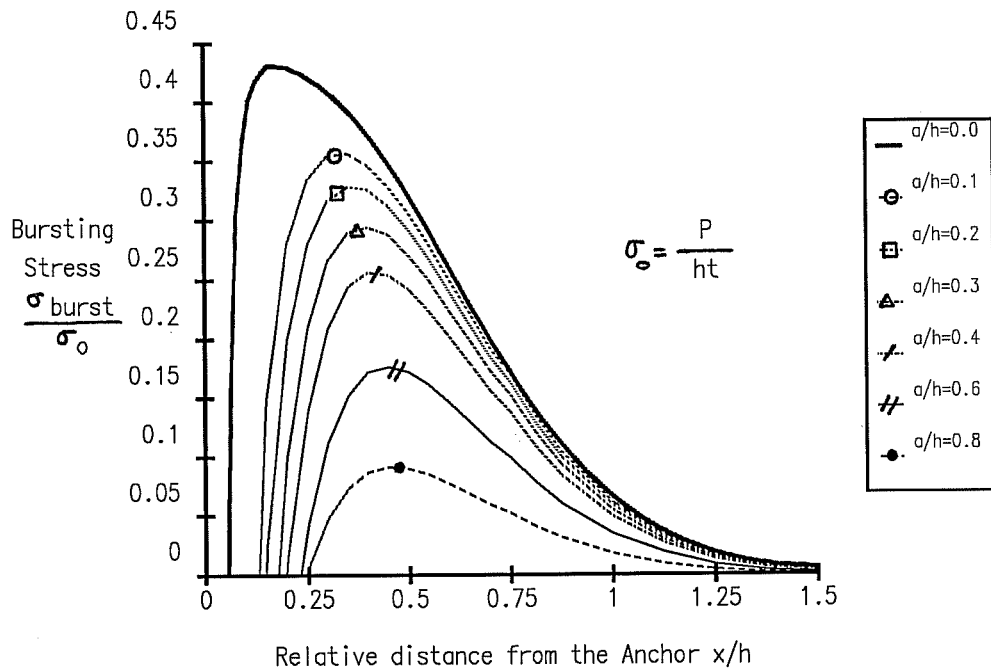

Fig. 4.9   Bursting Stress Distribution along the Tendon Path

Fig. 4.10 shows the maximum tensile stress perpendicular to the tendon path as a function of the relative size of the anchorage plate. There is a nearly linear relationship between the relative plate size a/h and the maximum stress. The slope of the line demonstrates the importance of this parameter. Fig. 4.11 shows the integrated value of the bursting force perpendicular to the tendon. Once again, there is a nearly linear relationship with a significant slope between the transverse bursting force and the relative plate size.
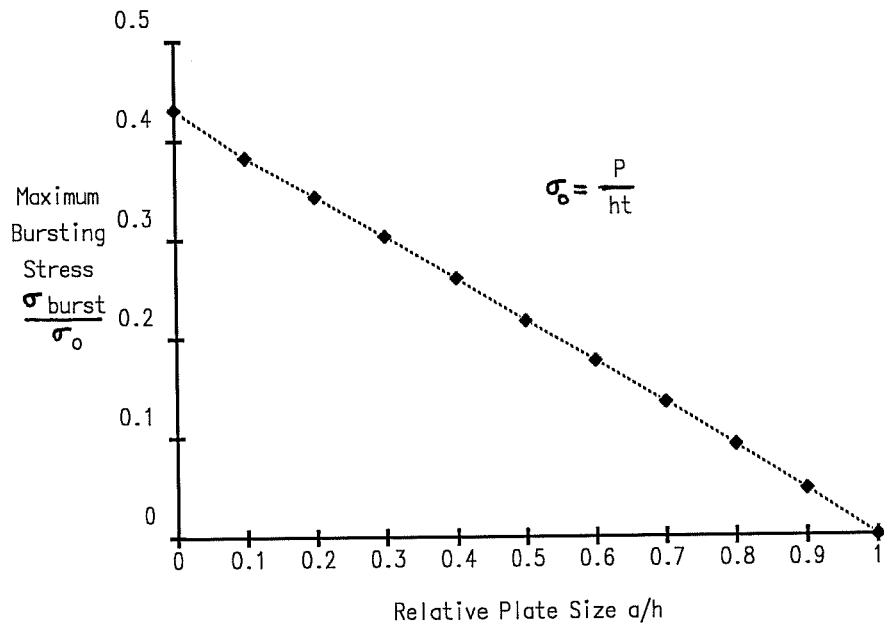
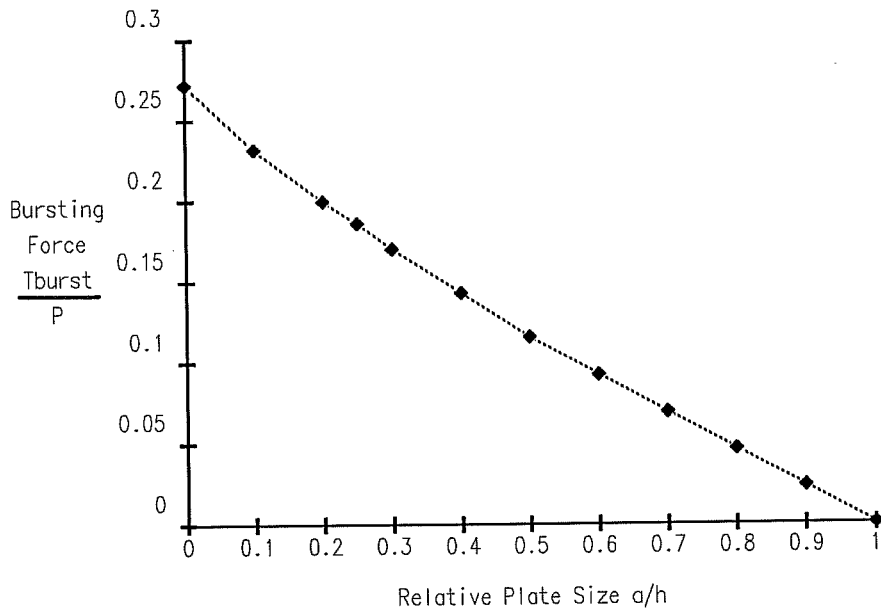Fig. 4.10 Maximum Bursting Stress as a Function of a/h

Fig. 4.11   Bursting Force as a Function of a/h

4.2.2.2   Compressive Stresses

Fig. 4.12 shows the distribution of compressive stresses acting along the tendon axis for various plate sizes. In cases where the relative plate size is small, the stresses reach very high level under the plate, but also decrease very rapidly at a small distance from the plate. The typical confining reinforcement of the local zone extends to about one to one and a half times the lateral dimension of the anchor. Assuming that the design of the local zone is satisfactory, the stresses in the concrete must be checked at the interface between the local zone and the general zone, at the bottom of the confining reinforcement. The exact location of the interface between the local zone and the general
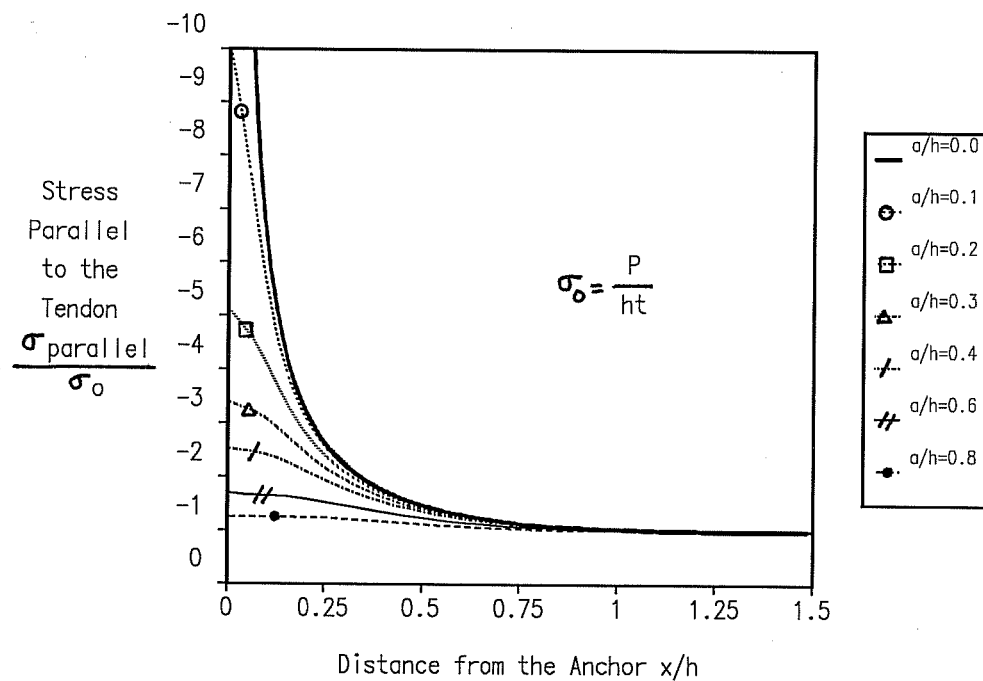

Fig. 4.12   Compressive Stresses along the Tendon Axis

zone may not be known at the time of design, and it was therefore decided to consider the stresses at a depth equal to the lateral dimension *a* of the anchorage device. Special attention will therefore be given to the magnitude of the compressive stresses at a depth *a* ahead of the anchorage device.
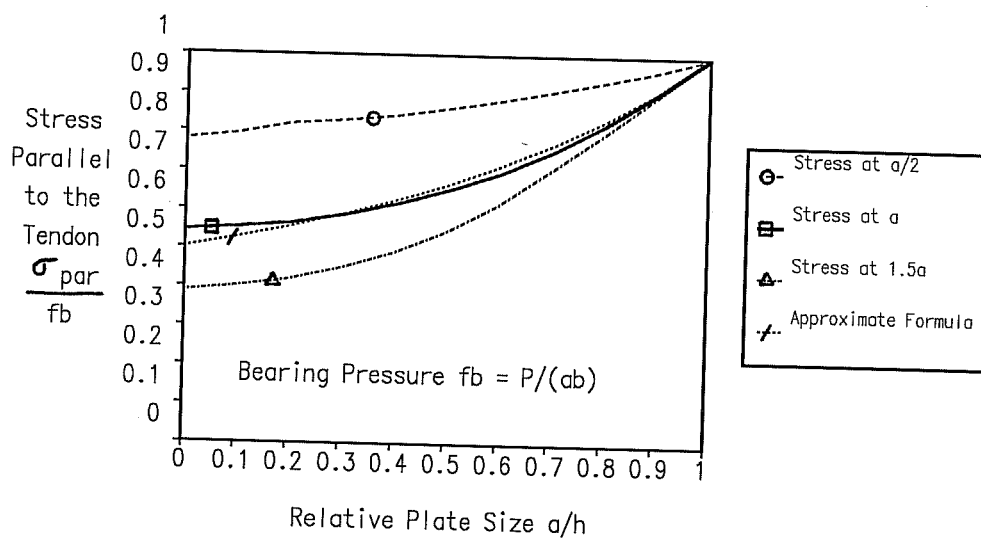

Figure 4.13   Compressive Stresses Ahead of the Anchor Normalized
to the Bearing Pressure as a Function of the
Relative Plate Size

Fig. 4.13 shows the compressive stress at a distance equal to 0.5a, 1.0a and 1.5a ahead of the anchorage device as a function of the relative plate size. The stresses are normalized to the bearing pressure f_b under the anchorage plate. Fig. 4.13 also shows the stresses at a depth *a* obtained from the simplified model described in Fig. 4.14. In this model the stresses are assumed to act on an effective width h_{eff} that is a linear function of the

depth x of the section considered. The effective width is equal to the width of the anchorage device just underneath the anchor (x = 0) and to the full width of the section at a depth equal to the width of the section (x = h). For a section located at x = a, the stresses are given by Equation 4.1. As can be seen from Fig. 4.14, Equation 4.1 predicts the elastic stresses at a depth a very well for plate sizes larger than approximately 0.15h. For plate sizes smaller than 0.15h, a constant value of $0.55f_b$ can be used as a better approximation.

$$\sigma(a) = f_b/(2-a/h) \quad \text{(Eq. 4.1)}$$

As can be observed from Fig. 4.13, the level of compressive stress at a small distance a from the anchorage plate is almost

$$h_{eff} = a\left[1 + x\left(\frac{1}{a} - \frac{1}{h}\right)\right]$$

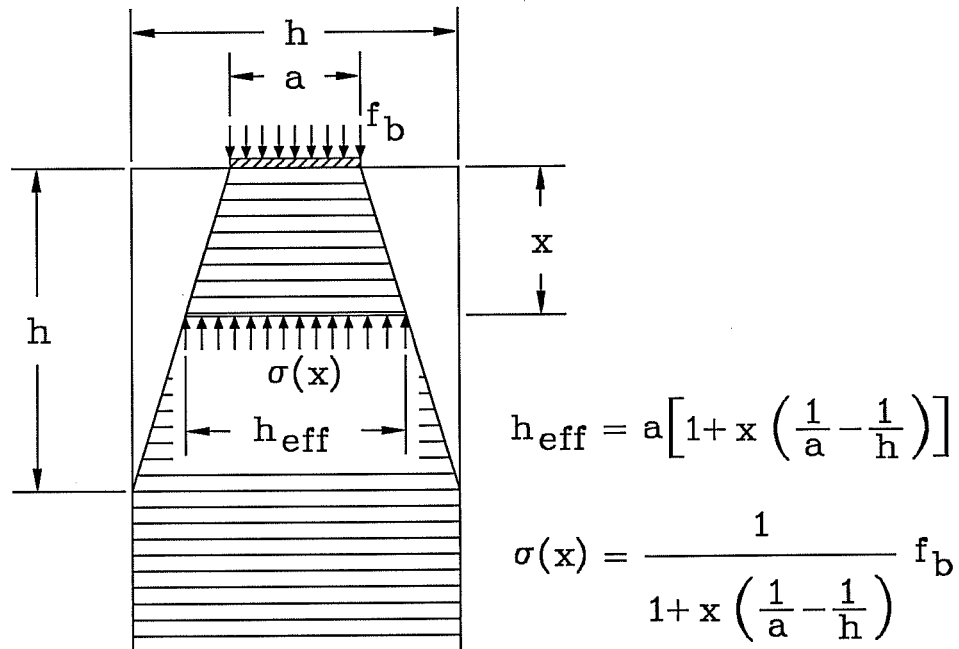$$\sigma(x) = \frac{1}{1 + x\left(\frac{1}{a} - \frac{1}{h}\right)} f_b$$

Figure 4.14   Assumed Spreading of Stresses for Approximate Computations of Compressive Stresses

constant for the range of plate sizes most often encountered in practice, between 0.1h and 0.4h. In this range, the compressive stress at a depth a can be taken as $0.6f_b$. The stresses at a depth *a* from the anchorage plate are of importance in this study, since this depth corresponds approximately to the expected location of the interface between the local zone and the general zone. In computing of curves of Figures 4.12 and 4.13, it is assumed that the transverse dimension of the anchorage device is the same as the thickness of the concrete section. In an actual structure, the anchorage device will be smaller than the thickness of the section, and the stresses will therefore be reduced by the transverse spreading. This effect can be taken into account by using Equation 4.1, or the curves of Figure 4.13 in both directions.

4.2.2.3   Spalling Stresses

Fig. 4.15 shows the magnitude of the largest spalling stress acting parallel to the loaded face of the specimen as a function of the plate size. Comparison with Fig. 4.10 shows that for the same plate size the spalling stresses are in most cases larger than the bursting stresses. Fig. 4.16 shows the magnitude of the largest spalling force as a function of the relative plate size a/h. The force are obtained by systematically integrating the stresses in the y-direction for various vertical planes and reporting the largest value. Because the area over which the spalling stresses act is quite small (typically less than h/20), the resulting spalling forces are very small.
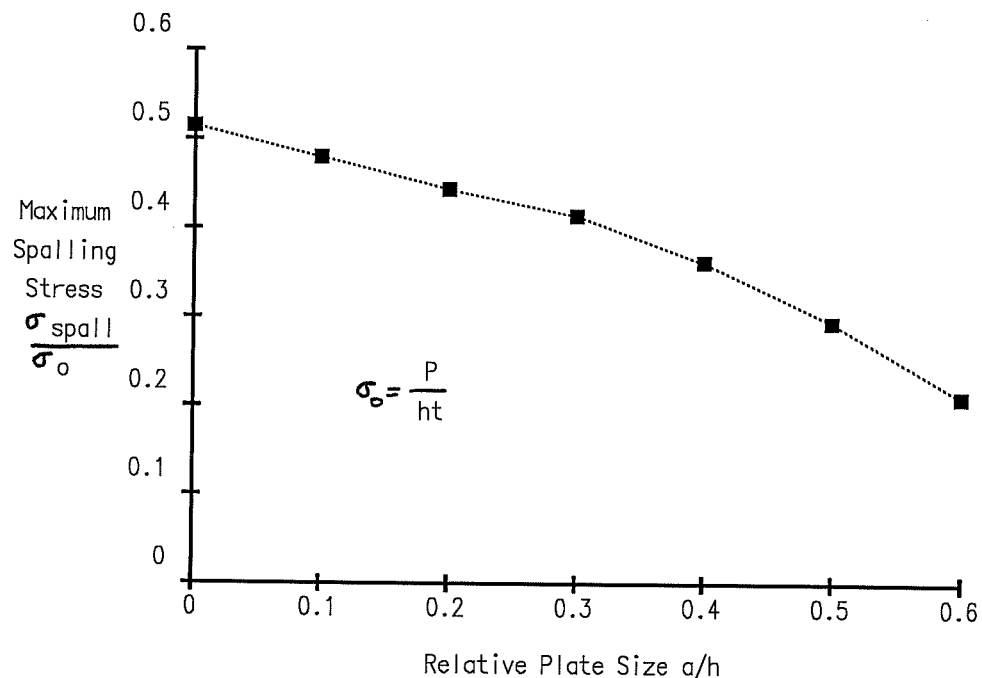
Fig. 4.15 Maximum Spalling Stress as a Function of the Plate Size

The areas subjected to spalling stresses are not on the direct path of the largest compressive stresses and could be removed without substantially changing the stress field otherwise, as illustrated in Figs. 4.17 and 4.18. These two figures show the stresses in a rectangular section compared with the stresses in a section where the areas of the concrete subjected to the largest spalling stresses have been removed. When the corners are removed, the spalling stresses practically disappear while the distribution of bursting stresses, as well as of compressive stresses (not shown) remain unchanged. Thus, the flow of forces is hardly modified when the areas of high spalling stresses are removed, either physically as in this example or by a loss of stiffness due to cracking of the concrete. This illustrates that the spalling

stresses are mainly induced by the condition of compatibility of displacements and not by the condition of equilibrium of the anchorage zone. This property will be further established by Strut-and-Tie Models and in the test results.
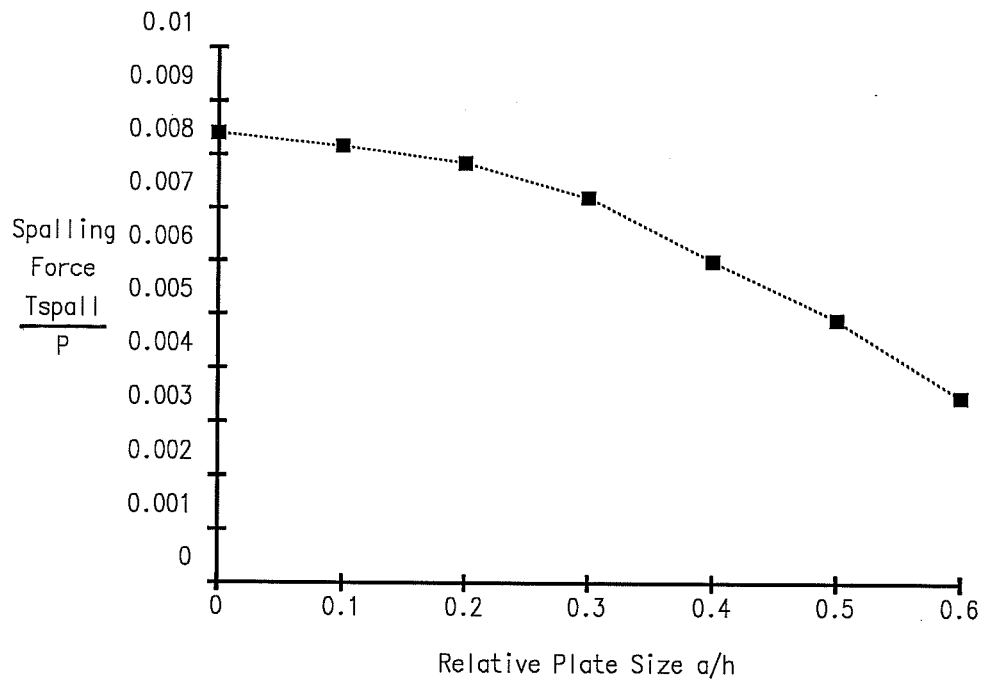

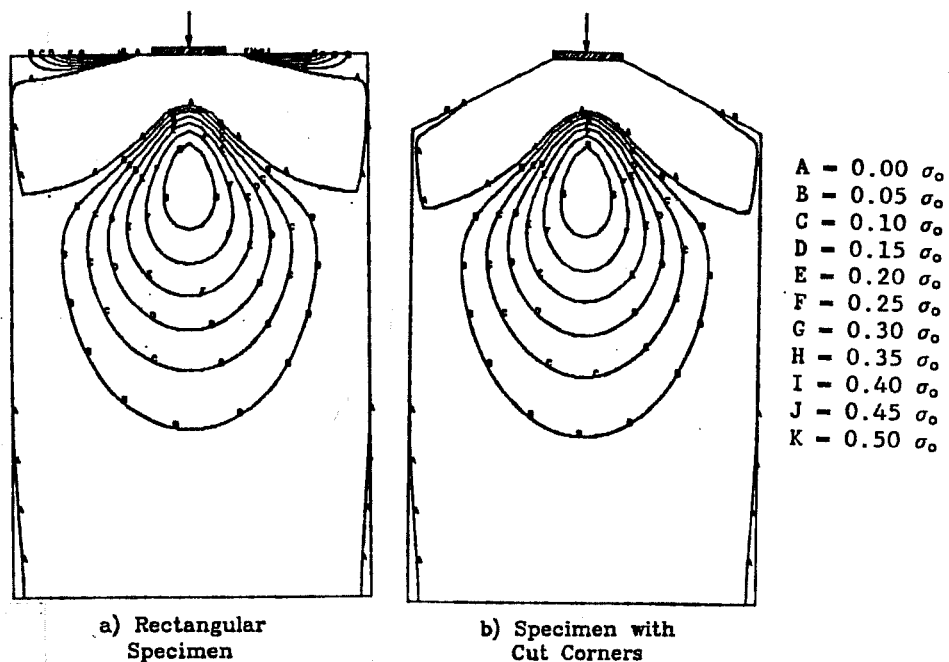Fig. 4.16   Spalling Force as a Function of the Plate Size

A = 0.00 σ_0
B = 0.05 σ_0
C = 0.10 σ_0
D = 0.15 σ_0
E = 0.20 σ_0
F = 0.25 σ_0
G = 0.30 σ_0
H = 0.35 σ_0
I = 0.40 σ_0
J = 0.45 σ_0
K = 0.50 σ_0

a) Rectangular
Specimen

b) Specimen with
Cut Corners

Fig. 4.17   Contour Plot of the Stresses Perpendicular to the

Tendon for a/h=0.2 Rectangular Section and Section

with Cut Corners

a) Rectangular
Specimen

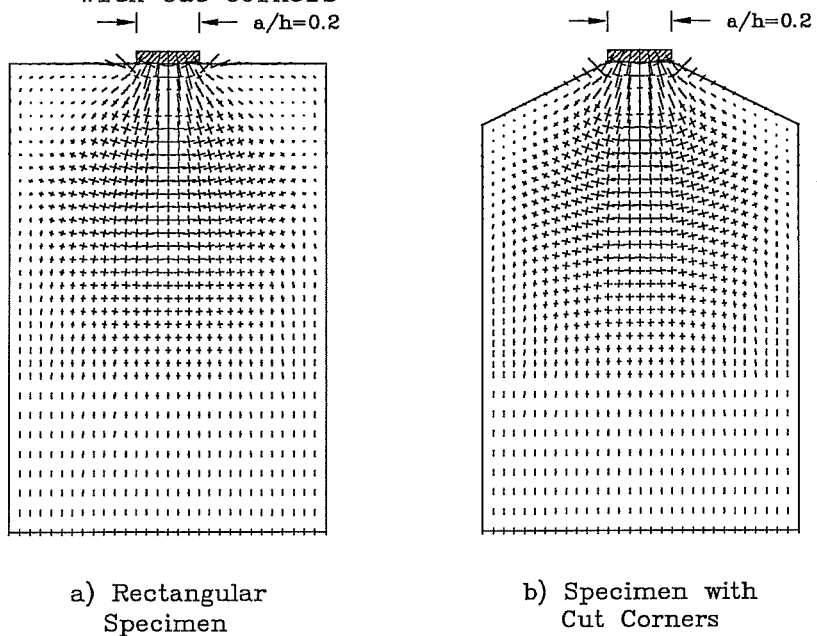b) Specimen with
Cut Corners

Fig. 4.18   Principal Stresses Vector Plot for a/h=0.2

Rectangular Section and Section with Cut Corners

4.2.3 Comparison with Published Results

Because of their relative simplicity, single anchor configurations have been investigated extensively. Many studies focus on the analysis of concentric configurations with straight tendons. The results of the Finite Element analyses are compared with the values of Guyon [75], Magnel [111], Lenschow & Sozen [97], Schleeh [160], Stone [169]. In Fig. 4.19, adapted from the paper by Lenschow & Sozen [97], the bursting stresses obtained from the present series of Finite Element analyses show a good agreement in the magnitude of the maximum bursting stress with the other solutions. The stress distribution is slightly different from the other solutions, particularly Magnel and Lenschow & Sozen, and is closest to the elastic solution obtained by Guyon using closed form solutions and Fourier series [75].

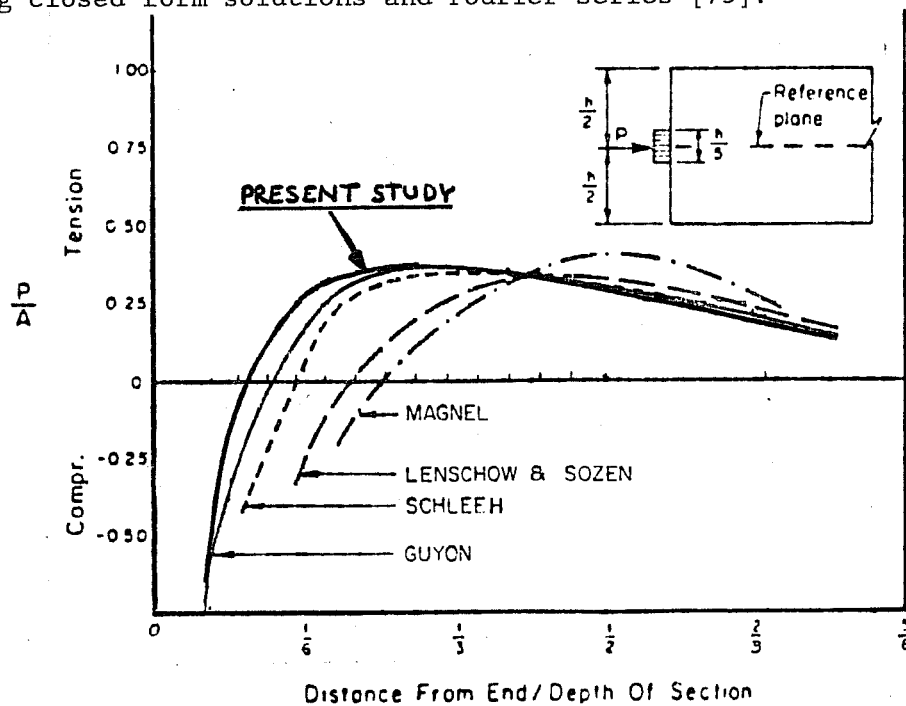Comparison of bursting stresses under a symmetrical load

Fig. 4.19   Comparison of Present Study with Previous Publications

Because Guyon published the most detailed results, including the variation of the total bursting force with the size of the plate, the results of the present Finite Element analyses will be compared with the results of Guyon. As shown in Fig. 4.20, the Finite Element solution corresponds fairly closely to the theoretical solution of Guyon. Also shown in Fig. 4.20 are two lines showing two linear approximations proposed by Guyon and described by Equation 4.2

$$T_{burst} = K \cdot P \ (1-a/h) \quad (Eq. \ 4.2)$$

The factor K in Equation 4.2 is proposed as 0.3 by Guyon, which leads to a solution that is conservative over the entire range of values for a/h. By taking K = 0.25, a better fit of the results is obtained, but the values are smaller than predicted by the elastic analysis for plate sizes smaller than approximately 0.15h.

The forces obtained from the Finite Element analysis are slightly larger than the forces obtained by Guyon, except for very small plates. Because of numerical problems for the case of a/h=0.0, (see Subsection. 4.6.1), it is assumed that Guyon's closed form elasticity solution is closer to the true elastic solution for a/h=0.0. Guyon's approximate formula (Eq. 4.2) gives a good approximation of the bursting force. Fig. 4.21 shows a comparison of the maximum bursting force obtained from the Finite Element Analysis with Guyon's results. There is a good agreement between both methods, except for small plate sizes for which the stresses obtained from the Finite Element analysis are noticeably smaller than the stresses of Guyon.
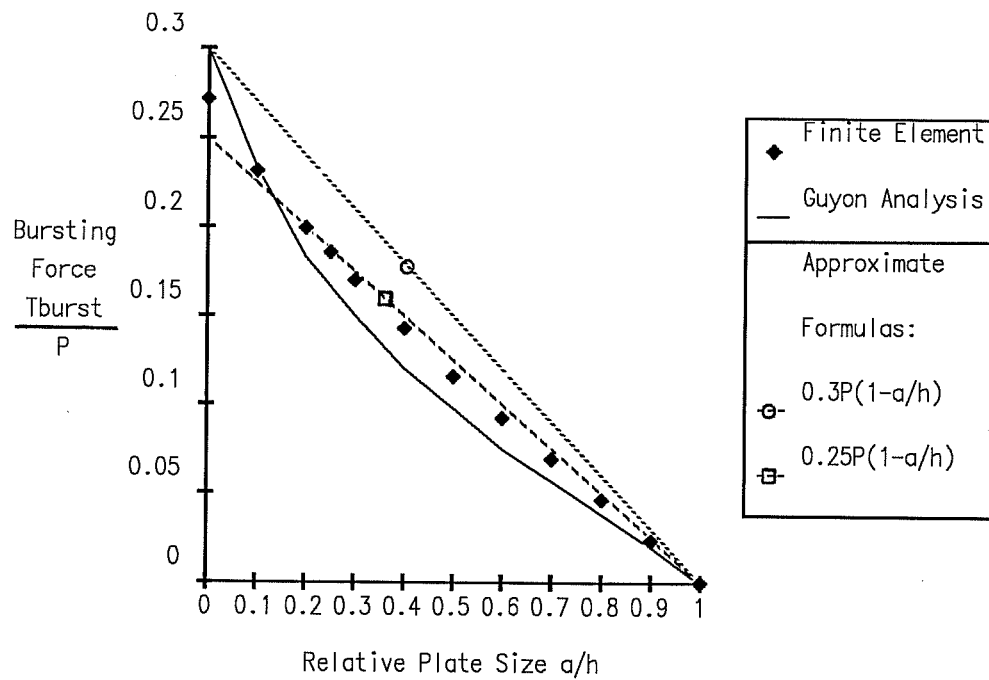
Fig. 4.20   Comparison of Finite Element Analysis with Published
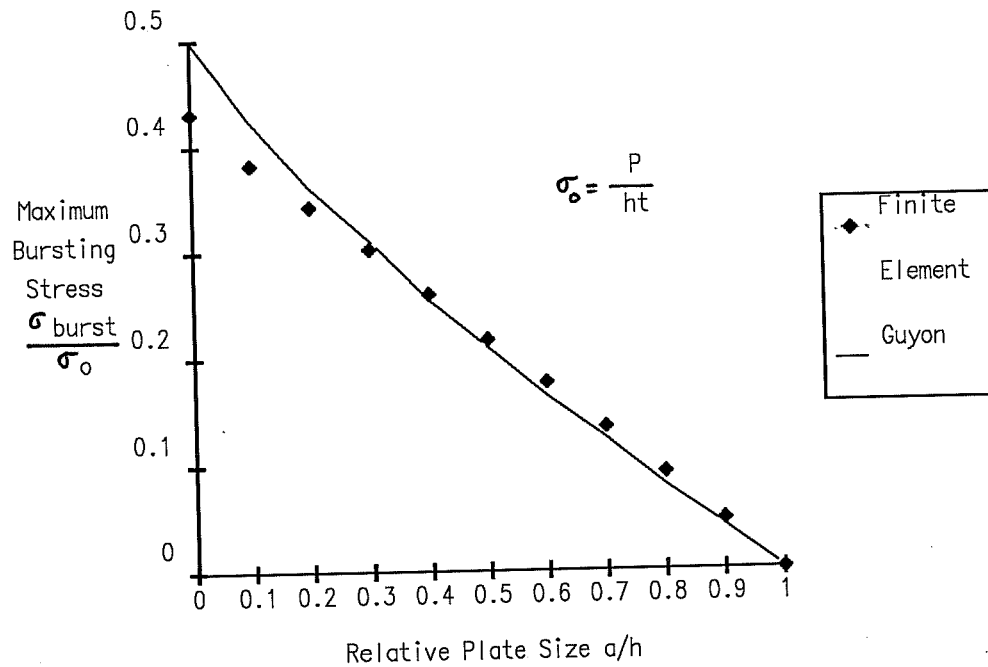   Results: Bursting Force

Fig. 4.21   Comparison of Finite Element results with Published
Results from Guyon: Maximum Bursting Stress

Guyon [75] is one of the few authors to address the case of spalling stresses. Even though he reports some calculated values for the spalling forces, he does not indicate a precise value as a function of the plate size, as in the case of bursting stresses. His recommendations are mostly of a practical matter, such as a constant value of 4% of the applied load recommended as a design value. According to Guyon, the reinforcement should be a fine mesh located underneath the anchorage device, as close to the surface of the concrete as possible. The purpose of that reinforcement is not clear, because it is to be placed underneath the anchor plate,

where theoretically only compressive stresses are acting. Because the maximum spalling stress generally occurs in the vicinity of the anchorage plate, it is possible that the intent of Guyon was twofold: to provide some confining steel in the vicinity of the plate to help resist the high local bearing pressures, and to provide reinforcement for the spalling stresses.

Fig. 4.22 shows the value of the spalling force obtained from the Finite Element analyses compared with the integrated values reported by Guyon and the constant value that he proposes for design purposes. Based on the results of the elastic Finite Element analysis, it appears that Guyon's solution is quite conservative.

Stone [169] places a large emphasis on spalling stresses. He mentions a decrease in the confining pressure of the local zone caused by spalling stresses as a possible cause for the initiation of the failure mechanism in the anchorage zone. As shown in subsection 4.4.2.2, it seems that the very high level of bearing stresses, combined with the reduction in confinement caused by the spalling stresses seems to be the cause of failure. In this case, the initiation of cracking will most likely be quickly followed by the failure of the anchorage zone.

As a conclusion of this comparison with published results, it is felt that the stresses from the Finite Element Analysis are reliable and accurate. More details on the convergence of the Finite Element solution can be found in section 4.6.1.
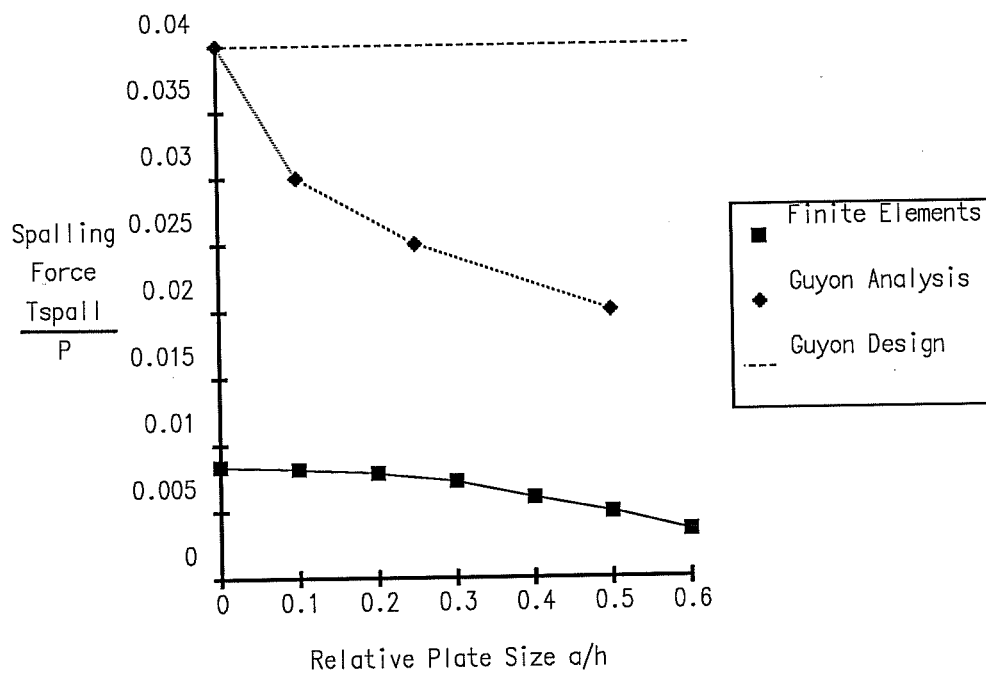
Fig. 4.22   Comparison of Finite Element results with Published
             Results from Guyon: Spalling Force

4.3 Strut-and-Tie Model

This section examines a variety of Strut-and-Tie Models to understand the flow of forces in a concentric, single tendon anchorage zone. A methodology to develop and evaluate Strut-and-Tie Models is described and applied to examples that incorporate the parameters for this configuration.

4.3.1 Geometric Definition of the Strut-and-Tie Model

The choice of a geometry for the Strut-and-Tie Model in a concentric anchorage zone is straightforward. However application of the Strut-and-Tie Model to complex configurations require a general methodology to construct the Strut-and-Tie Model and criteria to evaluate the adequacy of the model. The methodology is applied to the simple case of single anchor concentric configurations, where the number of possible solutions is limited.

When the Strut-and-Tie Model method has been described [181, 158], it is often assumed that the geometry of the model is a given or that it will be "chosen" by an engineer *trained in the application of the Strut-and-Tie Model*. While this is usually true, it is necessary to add some specificity to the definition of the model geometry. In the most frequent case, when no Finite Element analysis is available for the design of the anchorage zone, the engineer will "choose" a Strut-and-Tie Model based only on the geometry of the anchorage zone and on some calculations of equilibrium.

a) Geometry
and Loads

b) Forces
and Reactions

c) Force Paths

d) Compression Struts

e) Tension Ties
ans Solution

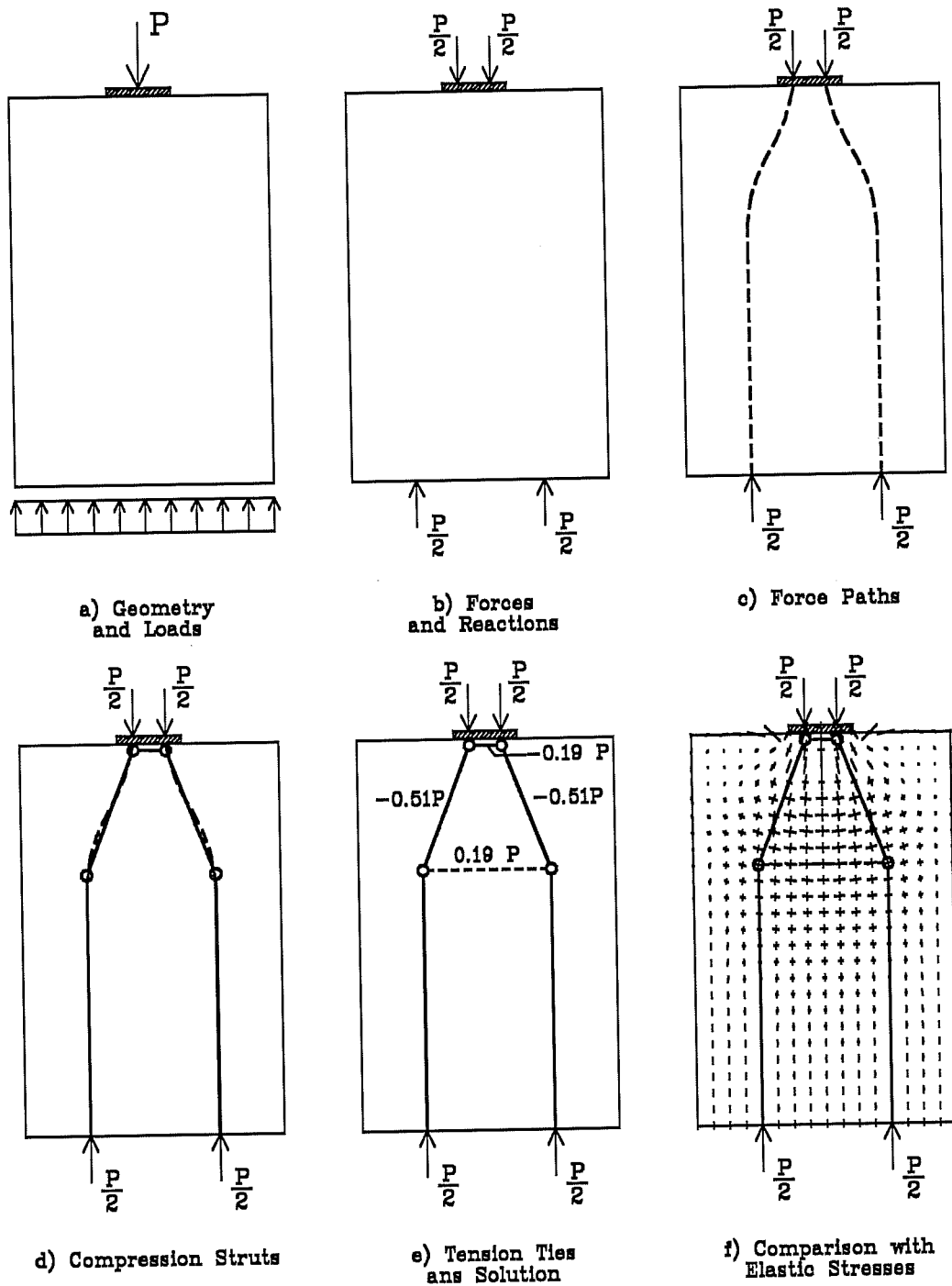f) Comparison with
Elastic Stresses

Fig. 4.23   Steps for the Development of a Strut-and-Tie Model

The first step to model the general anchorage zone is to cut the structure at the end of the discontinuity zone which is approximately 1.5 times the depth of the girder for rectangular cross sections, and draw the forces and reactions on the free-body. Because the cut is made at a reasonably large distance from the anchor itself, a simplified analysis such as simple beam theory can be used to determine the reactions (Fig. 4.23a).

The reactions at the extremity of the anchorage zone are then lumped into a series (at least two) of concentrated reactions. In most cases (except for tendons with a large curvature or inclination) it is recommended to separate the reactions that are "on one side" of the tendon from the reactions that are "on the other side". The tendon load on the anchor will also be represented by several components. However it seems unnecessary to use more than two nodes to represent the local zone around the anchor, because this gives an unjustified sense of accuracy to the modelling (Fig. 4.23b). In this example, the nodes modelling the anchor plate are located at the interface between the anchorage device and the concrete. This assumption has little influence on the results if the relative plate size is small (See more comments on this assumption in section 4.4.3).

At this stage, it is likely that a limited number of *main* reactions (two to four) will approximately sum up to the totality of the applied tendon load (at least 80% of it). Based on the knowledge of the location and magnitude of the main reactions, the engineer draws *force paths* from the anchor to the main reactions (Fig. 4.23c). Schlaich et al. recommend that the initial forces considered should exactly sum up to the tendon forces. Then in a second step the engineer should introduce the additional forces that result from eccentricities or other sources. While this requirement is helpful, it does not seem to be absolutely necessary to develop reasonable Strut-and-Tie Models for either

concentric or eccentric cases.

The compression struts follow the force paths. For best control of cracking, the angle between the axis of the tendon and the struts should be limited to between 20 and 35 degrees. If more than two struts are used, or if a *multiple level* or a *thrust-line model* (see next subsections) is used, larger angles may be allowed. The struts are to align exactly with the reactions at the extremity of the anchorage zone (Fig. 4.23d).

The tension ties balance the deviation of the forces in the struts. The ties can be oriented in the desired direction for the reinforcement. If necessary, the geometry of the struts may have to be adjusted for the possible locations of the ties. The forces in the ties can be closely estimated because the forces in the struts and the deviation angles are known. Because the Strut-and-Tie Model obtained so far includes only the main forces, every node may not be in equilibrium. It is therefore possible that two or more values are obtained for a given tie. At this point, it is conservative to choose the largest value (Fig. 4.23e).

Notice that the forces obtained up to this point resist the majority of the tendon force (80% or more), so that none of the remaining strut or tie forces is likely to dramatically change the load carrying mechanism of the model. However, these forces are necessary to satisfy the overall equilibrium conditions of the Strut-and-Tie Model. Notice also, that in the case of a concentric anchorage, there is no tension tie close to the anchorage at the surface, which would correspond to the effect of spalling forces. This is because spalling forces are compatibility induced and are not required for the overall equilibrium of concentric configurations.

At this stage, force paths are drawn for the remaining reaction forces and the corresponding struts and ties are incorporated in the Strut-and-Tie Model. In the case of the

concentric anchor example, all forces were considered as *main* forces, so that no additional forces are required to satisfy equilibrium.

If the results of a Finite Element analysis are available, the principal stress vectors can be used to help draw the force paths of Fig. 4.23c. The location of the tension ties can be adjusted to coincide with the centroid of the tensile stresses.

If no additional information is available, such as the results of a Finite Element analysis, it is generally difficult to assess the adequacy of a Strut-and-Tie Model. The designer should evaluate the sensitivity of the Strut-and-Tie Model to changes in the geometry. For example, larger angles between the tendon axis and the compression struts can be used. This gives larger tension forces in the ties and a larger compression force in the struts. There seems to be no reason, however, to use angles larger than 45 degrees, because they will lead to overconservative forces. The value of 45 degrees is often quoted in relationship to the diffusion of *stresses* in the concrete. If the stresses are diffusing at angles between 0 and 45 degrees, the average diffusion angle is 22.5 degrees, which is the angle of the compression strut. Taking the inclination of the strut as 45 degrees corresponds to taking the angle of diffusion of the stresses as 90 degrees.

If the stress trajectories (or principal stress vectors) are available for the anchorage zone, the adequacy of a Strut-and-Tie Model can be assessed by comparing the layout of the struts and ties with the elastic flow of stresses (Fig. 4.23f). In order for the structure to be well behaved at service state, it is desirable that the struts and ties follow the elastic flow paths closely (with a deviation of at most 15° from the elastic principal stresses, according to Schlaich et al. [158]) Although it is difficult to apply quantitatively, this requirement is especially

important for the main members, that carry a significant portion of the load. For the other members, that carry only a small portion of the load, a larger deviation is permissible. This implicitly takes into account the fact that in areas of low stresses, the concrete will remain essentially uncracked and will therefore be able to transfer elastically a portion of these stresses.

4.3.2 Practical Example

Fig. 4.24 shows the geometry of a simple but realistic problem involving one concentric anchorage with three layers of reinforcing bars of equal size. The goal is to determine the ultimate load for the anchorage zone. Simple plastic theory is used for this design, assuming that all reinforcing bars yield and

Example Problem:
d1 = 0.2h
d2 = 0.5h
d3 = 0.8h
a = 0.25h
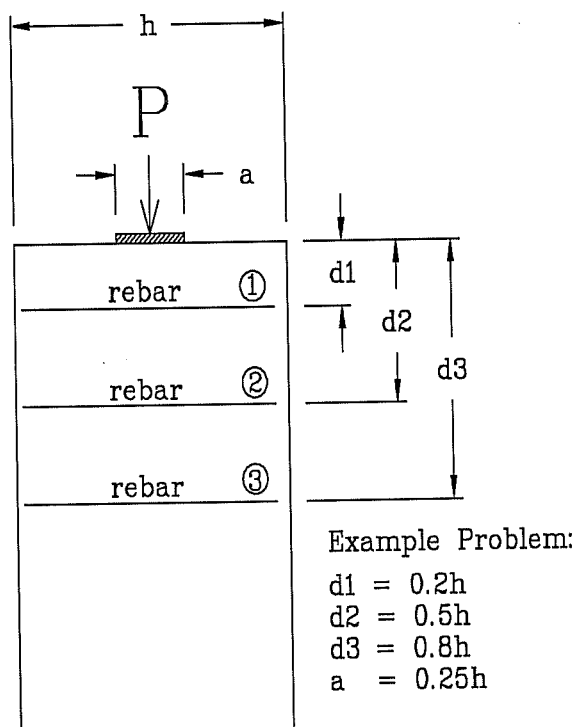
Fig. 4.24   Geometry of Sample Problem

carry the same force. This problem can actually be solved by simply formulating the conditions of equilibrium of a free-body obtained by cutting the specimen along the tendon line, as shown in Fig. 4.25.

$$T_1 = T_2 = T_3 = T$$

$$\sum F_y = 0 \quad \rightarrow \quad R = \frac{P}{2}$$

$$\sum M_A = 0$$

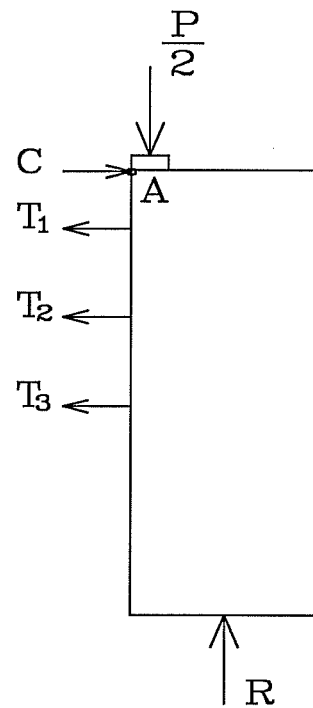$$\rightarrow \quad P = \frac{8T(d_1 + d_2 + d_3)}{(h-a)}$$

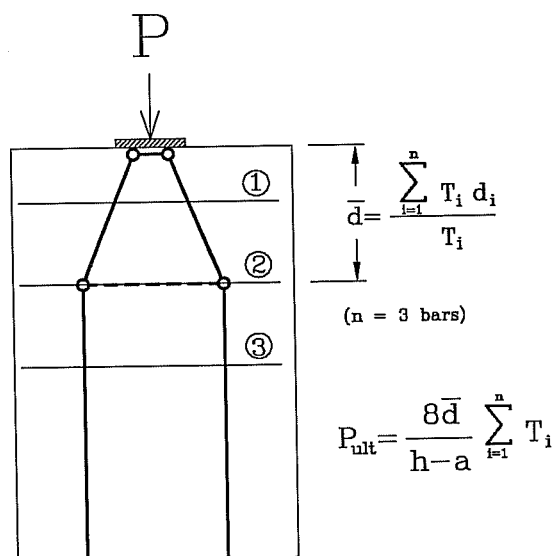Fig. 4.25   Free Body Solution for Concentric Anchorage Zone

4.3.3 Mörsch Strut-and-Tie Model

P

$$\bar{d} = \frac{\sum_{i=1}^{n} T_i \, d_i}{T_i}$$

(n = 3 bars)

$$P_{ult} = \frac{8\bar{d}}{h-a} \sum_{i=1}^{n} T_i$$

Fig. 4.26   Simple Strut-and-Tie Model for Example Problem

The basic Strut-and-Tie Model shown in Fig. 4.26 for the concentric anchor is quite simple and was initially proposed in the 1920s by Mörsch (see Fig. 4.27) [122]. The load is assumed to be applied as two loads of magnitude P/2 at the quarter points of the anchorage plate. The tension force Z results from the spreading of the compression struts toward the quarter points of the concrete section and is assumed to act at a depth of d/2.

The tension force can be simply calculated by equilibrium as:

$$Z = 0.25 \cdot P \cdot (1-a/d) \quad \text{(Eq. 4.3a)}$$

The ultimate load capacity for a given strength of the tension tie, Z, is:

$$P_u = 4 \cdot Z/(1-a/d) \quad \text{(Eq. 4.3b)}$$

The formula of Equation 4.1a is identical to the simplified formula proposed by Guyon, see Eq. 4.1 in section 4.2.2.2. This formula is used for example in the CEB code [30] and in recent PTI

recommendations [141] (both use the more conservative coefficient of 0.3 instead of 0.25 in the formula) [30]. The simple and powerful solution of this basic configuration illustrates the powerful tool offered by the Strut-and-Tie Model to solve anchorage zone problems. A more general representation for the Strut-and-Tie Model of Mörsch is shown in Fig. 4.26, with an expression for the ultimate load P_{ult}.
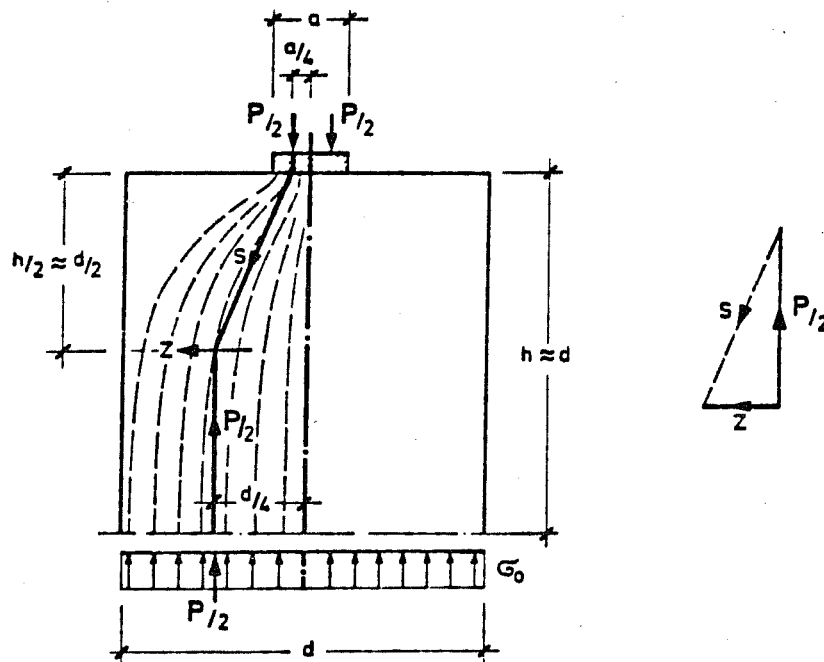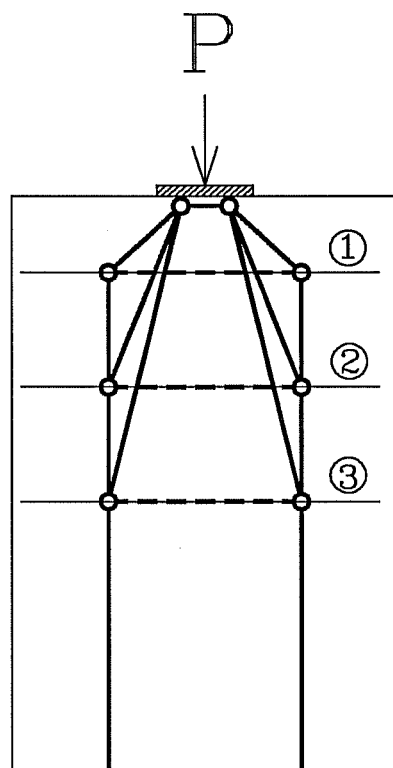

Fig. 4.27   Mörsch Strut-and-Tie Model

4.3.4 Multiple Level Strut-and-Tie Model

A more refined model for the same configuration is shown in Fig. 4.28. In this *multiple level Strut-and-Tie Model*, the applied force is transmitted through a series of compression struts directly to the individual reinforcing bars. The ultimate load

P_{ult} given in the figure is determined by summing the contribution of the individual struts.

4.3.5 Thrust-Line Strut-and-Tie Model

Fig. 4.29 shows still another Strut-and-Tie Model for the same configuration. In this *thrust line model*, the compression
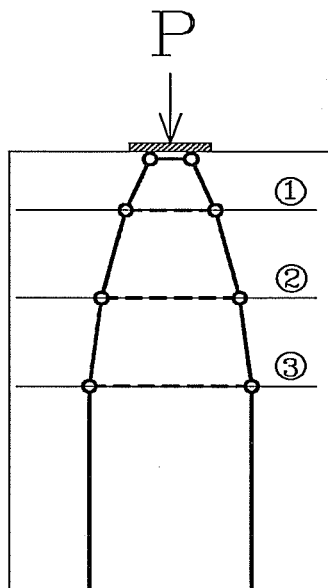

$$P_{ult} = \frac{8}{h-a} \sum_{i=1}^{n} T_i \, d_i$$

(n = 3 bars)

Fig. 4.28   Multiple Level Strut-and-Tie Model

force coming from the anchor is deflected each time it crosses a reinforcing bar, until it aligns exactly with the reactions at the end of the zone of introduction of forces. In practice, this model can be best constructed by starting at the side of the anchorage zone that is furthest from the anchor and moving toward the anchor. The ultimate load is obtained when the thrust lines reach the anchor plate at the quarter points. If the thrust lines cross the axis of the tendon line before reaching the plate, the load obtained is smaller than the actual ultimate load and is therefore conservative, because a thrust-line converging exactly to the quarter points of the plate could be constructed by assigning only a part of the yield force of each reinforcing bar. The ultimate load P_{ult} of the anchorage zone, given in the figure, can be obtained if the force in each bar is set to the yield value and the thrust lines reach the anchorage plate at the quarter points.

$$P_{ult} = \frac{8}{h-a} \sum_{i=1}^{n} \left[(d_{i-1} - d_i) \sum_{j=i}^{n} T_j \right]$$

$(n = 3 \text{ bars, } d_0 = 0)$

Fig. 4.29   Thrust-Line Strut-and-Tie Model

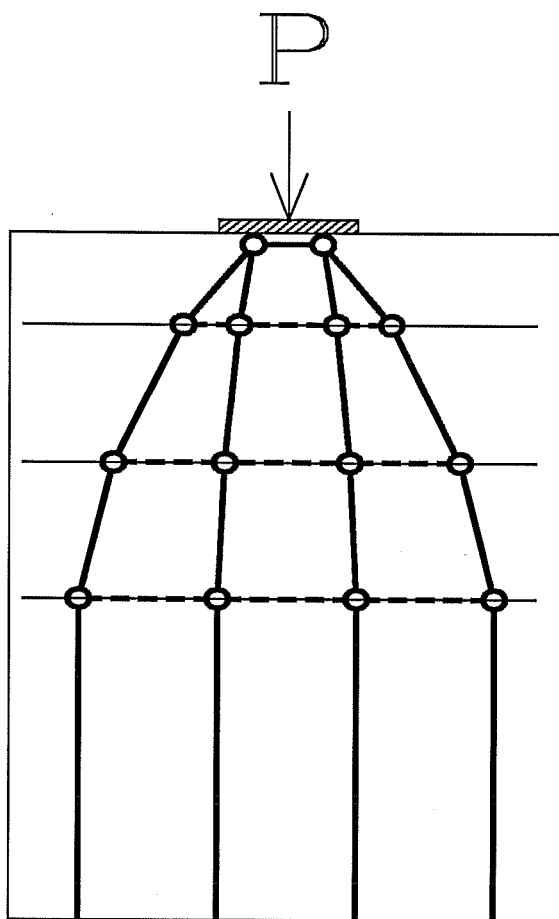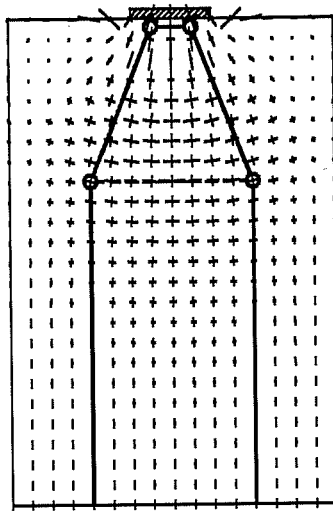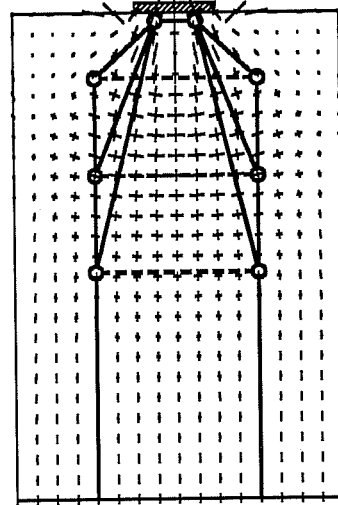## 4.3.6 Multiple Thrust-Line Strut-and-Tie Model

Fig. 4.30   Multiple Thrust Line Strut-and-Tie Model

The multiple Thrust-Line Model of Fig. 4.30 is an extension of the simpler model presented in the previous subsection. The multiple Thrust-Line Strut-and-Tie Model has the advantage of more closely following the flow of stresses in the concrete. As will be seen in subsection 4.5.2, this Strut-and-Tie Model also gives interesting information on the transfer of loads between the tension ties and the concrete.
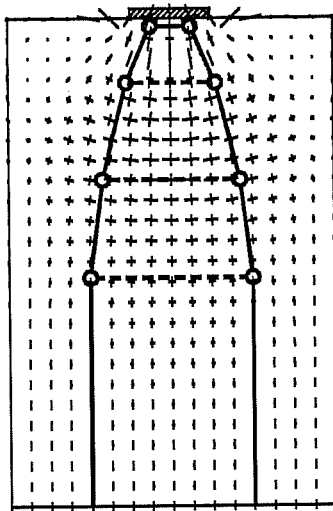
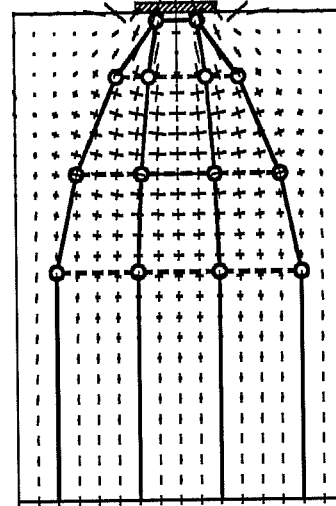4.3.7 Comparison of the Various Strut-and-Tie Models

a) Simple (Morsch)
Strut—and—Tie Model

b) Multiple Level
Strut—and—Tie Model

c) Single Thrust—Line
Strut—and—Tie Model

d) Multiple Thrust—Line
Strut—and—Tie Model

Fig. 4.31   Comparison of the Various Strut-and-Tie Model with
Principal Stress Vectors

Because the three equations obtained for the Strut-and-Tie

Models in Figs. 4.26 to 4.30 and the equation of equilibrium of the free-body all express the overall equilibrium of the structure, they logically give the same answer for the ultimate load P_u, as does the multiple thrust-line model, for which no explicit formula was developed. The assumption of complete yielding of the reinforcing steel at ultimate makes the problem determinate. As a matter of fact, the Strut-and-Tie Model equations of Fig. 4.28 and 4.29 are only sophisticated methods to compute the centroid of the tension force!

Fig. 4.31 summarizes the four Strut-and-Tie Models described in the previous subsections, superimposed on the principal stress vectors obtained from a Finite Element analysis. The simplest Strut-and-Tie Model of Fig. 4.31a is also very easy to establish, and may be used to crudely estimate the stresses in the concrete. However, it does not follow very closely the stress distribution. The multiple level Strut-and-Tie Model of Fig. 4.31b is clearly inadequate in describing the state of stresses in the concrete, and should therefore be avoided. The problems related to the computation of concrete stresses in Strut-and-Tie Models involving overlapping or crossing struts are difficult to solve. The thrust line Strut-and-Tie Models of Figs. 4.31c and 4.31d approximate more closely the elastic flow of stresses.

Fig. 4.32 shows as hatched zones the various concrete struts as they were used to compute the concrete stresses. Fig. 4.33 shows the stresses in the concrete struts as approximated by the thrust-line Strut-and-Tie Models compared with the stresses along the axis of the tendon (where the compressive stresses are maximum) obtained by an elastic analysis. Due to the inclination of the concrete struts, the stresses in the concrete are overestimated in the vicinity of the plate. The stresses are fairly well approximated by the internal strut and the single strut. The simple thrust-line Strut-and-Tie Model of Fig. 4.31c

actually gives better results than the more elaborate multiple thrust-line Strut-and-Tie Model of Fig. 4.31d. All four struts carry the same portion of the tendons force (P/4), but in order for the external struts which have a larger inclination to carry that force, a larger resultant is needed (P/4cos(α)). Therefore, contrarily to common sense and to the results of the theory of elasticity, the stresses in the external struts are larger than the stresses in the internal struts. This inaccuracy is compounded by the fact that only two nodes were used to represent the local zone.

According to Schlaich et al. [158], see Section 3.8, the best Strut-and-Tie Model is the configuration that minimizes the strain energy in the ties. Because the struts are assumed to be extremely rigid, the strain energy of the system will be concentrated in the ties. Minimizing the strain energy in the ties is therefore equivalent to applying the principal of minimum strain energy to the system. In this example, the thrust-line Strut-and-Tie Model of Fig. 4.31c has the lowest strain energy (see Table 4.2), and is therefore the best of the three models. The Multiple Level Strut-and-Tie Model is clearly the worst solution, because of the large plastic strains in the bars due to incremental yielding of the individual bars before the ultimate load is reached. In contrast, the other three models have all their bars simultaneously reaching the yield strength, thus minimizing the strain energy in the bars at ultimate. The differences between the three models are due to the slightly different lengths of the tension ties and to the fact that some parts of the reinforcement are not at yield in the multiple thrust-line Strut-and-Tie Model.

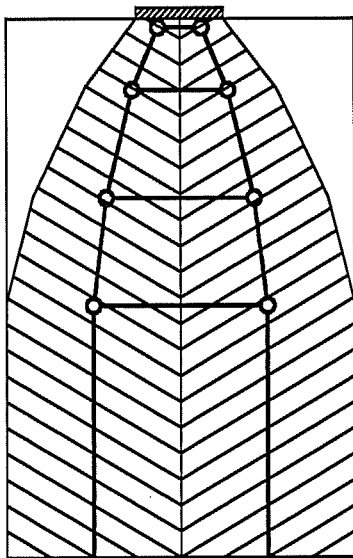Table 4.2:   Strain Energy at Failure for the Various Strut-and-Tie
Models

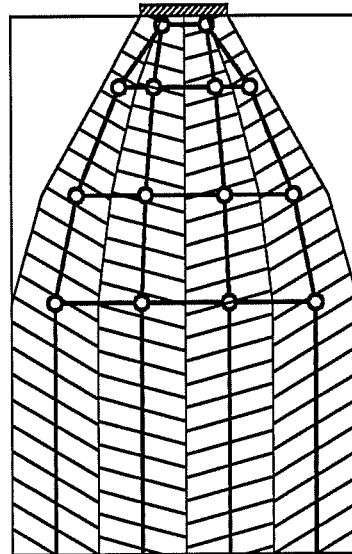| Strut-and-Tie Model (STM)	Strain Energy at Failure
Simple STM	$0.75\ h \cdot A_s \cdot f_y \cdot \epsilon_y$
Multiple Level STM	$2.0\ h \cdot A_s \cdot f_y \cdot \epsilon_y$
Thrust-Line STM	$0.6\ h \cdot A_s \cdot f_y \cdot \epsilon_y$
Multiple Thrust-Line STM	$0.7\ h \cdot A_s \cdot f_y \cdot \epsilon_y$
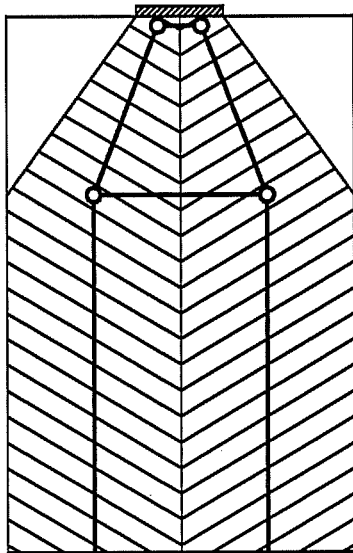
a) Simple (Morsch)
Strut—and—Tie Model
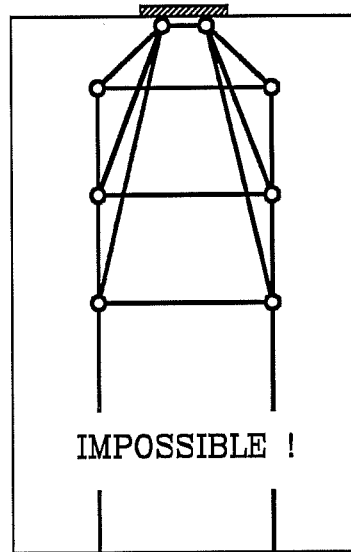
b) Multiple Level
Strut—and—Tie Model

c) Single Thrust—Line
Strut—and—Tie Model

d) Multiple Thrust—Line
Strut—and—Tie Model

Fig. 4.32   Geometric Definition of the Concrete Struts
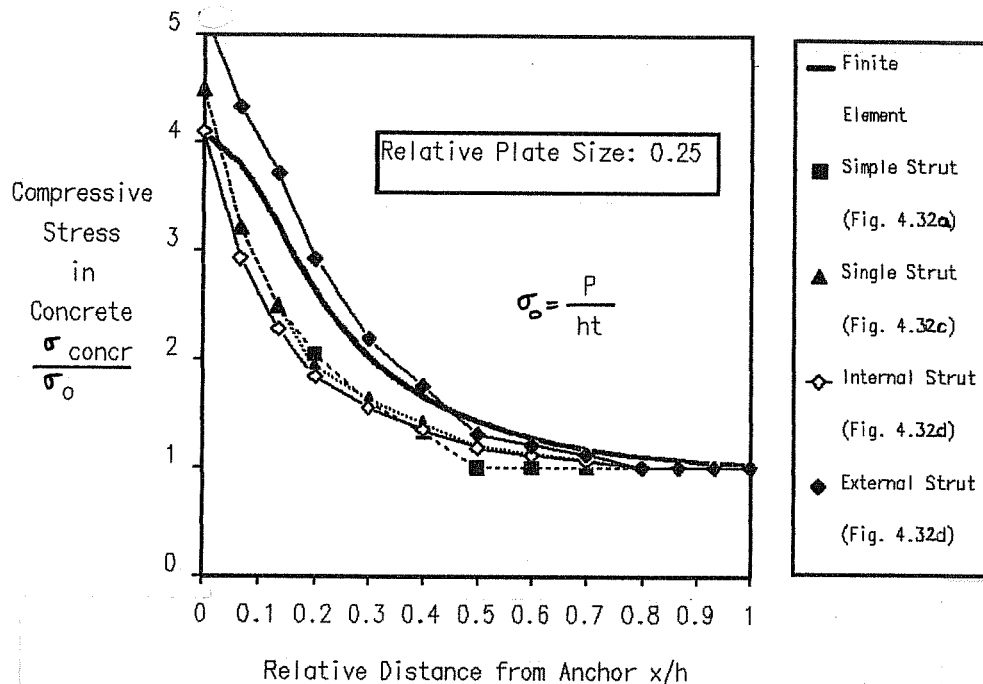
Fig. 4.33   Stresses in the Concrete Struts for the Various
             Strut-and-Tie Models Compared with the Stresses from
             the Finite Element Analysis

4.3.8 Location of the Centroid of the Tension Forces

In the example of Sections 4.3.2 to 4.3.7 it was assumed
that the location of the reinforcement is known. This may be true
in the case of the verification of an existing design, but this is
not the case in the general design process. Because equilibrium
can be satisfied with a variety of locations of the tensile
reinforcement, it is necessary that the designer locate the
reinforcement to effectively proportion the steel. The theory of
plasticity states that, as long as the deformation capacity of the
materials are not exceeded, any solution that satisfies

equilibrium is acceptable. From this point of view, any layout of reinforcement that would enable a Strut-and-Tie Model to carry the design load is acceptable.

However, the designer must consider serviceability conditions in order for the anchorage zone to perform satisfactorily during the lifetime of the structure. Cracking is an important component of the serviceability limit state for an anchorage zone. As mentioned earlier, the width of cracks will be effectively limited and the performance will be most satisfactory if the layout of the reinforcing steel follows closely the elastic stress distribution. Furthermore, as will be shown in subsection 4.4, the test specimens that were designed with a centroid of the reinforcement close to the elastic centroid of the bursting forces performed best.

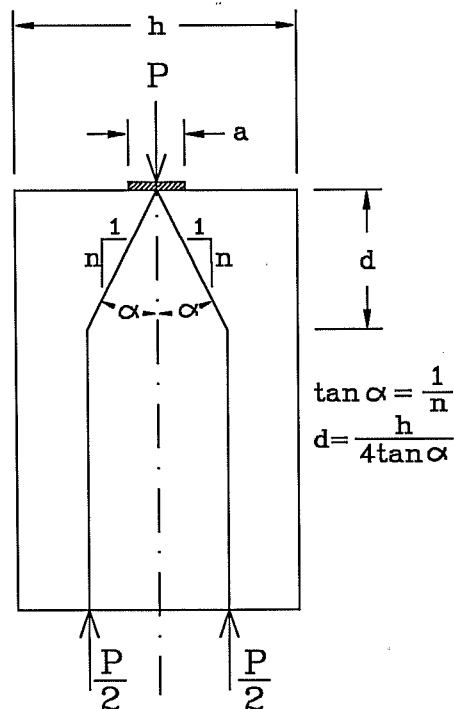$$\tan \alpha = \frac{1}{n}$$
$$d = \frac{h}{4\tan\alpha}$$

Fig 4.34   Definition of the Diffusion Angle

The location of the centroid of the elastic bursting stress

distribution is a valuable piece of information for design. Fig 4.34 defines the diffusion angle α from the center of the anchor. Fig. 4.35 shows the angle measured from the center of the anchor plate to the centroid of the elastic bursting forces as a function of the relative plate a/h. While the bursting force changes substantially with the size of the plate (Fig. 4.11), the location of the centroid is only slightly influenced by it. Because larger diffusion angles lead to larger values of the tensile force, the location of the elastic resultant can be estimated with sufficient accuracy for design by using a diffusion angle of 26.5 degrees (slope 1:2) from the axis of the tendon to the quarter points of the specimen. This solution is conservative for anchorage devices with ratios a/h greater than 0.15, and is reasonably close for ratios smaller than 0.15.
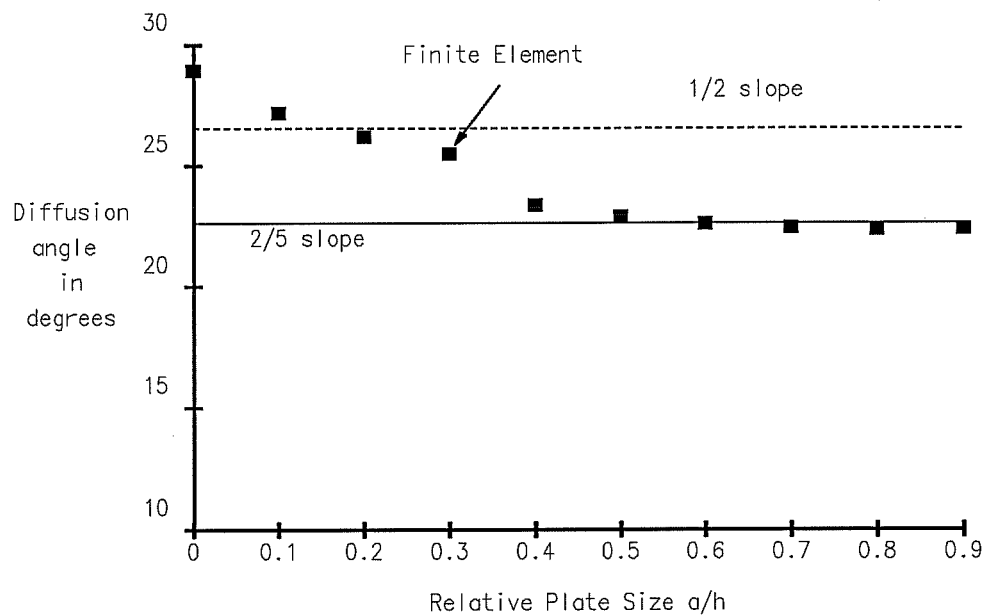
Fig. 4.35   Diffusion Angle as a Function of the Size of the Anchorage Plate

4.3.9 Compressive Stresses in the Concrete Struts

So far, the determination of the ultimate capacity of the anchorage zone using the Strut-and-Tie Model was only based on the capacity of the tension ties. Assuming that the local zone reinforcement is sufficient to prevent a failure in the local

$$w_s = a\left\{2(1-\frac{\tan\alpha}{2})\sin\alpha + \frac{1}{2\cos\alpha}\right\}$$
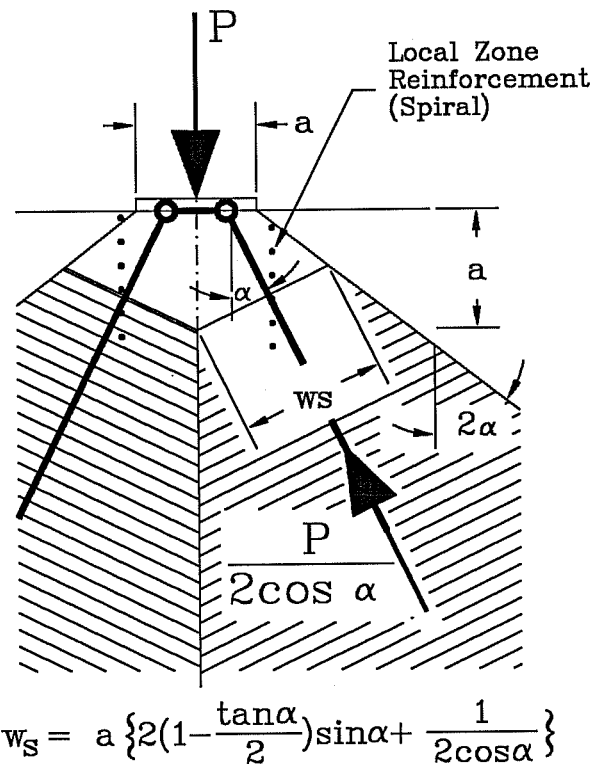
Figure 4.36   Definition of the Critical Section for the Concrete Struts

zone, a failure of the concrete in compression in the struts is possible, as mentioned in section 4.1. As was mentioned in section 4.2.2, the interface between the local zone and the general zone is located at a depth approximately equal to the lateral dimension of the anchorage device, depending on the

confinement provided for the local zone. Because the actual detail of the local zone device and confinement may not be completely known at the time of design, it is desirable that the *critical section* on which the stress in the compression struts is checked is as much as possible independent of the local zone details. For this study, the critical section is defined as a section perpendicular to the compression strut and intersecting the axis of the tendon at a depth equal to the lateral dimension *a* of the anchorage device. Fig. 4.36 shows the critical section and the concrete strut. The geometry of the strut is defined assuming that the outside of the strut is defined as a line of slope 2α from the corner of the anchorage device. The width w_s of the compression strut is given as a function of the strut angle α and the plate size a. Provided that a minimum edge distance (generally less than one and a half times the plate size) is respected so that the hypotheses made in defining the outside of the strut are met, the critical section is *independent* of the relative plate size a/h.

Fig. 4.37 shows the stress in the compression strut as a function of the angle of inclination of the strut. The compression strut is assumed to carry one half of the tendon force, and the increase in force due to the inclination of the tendon is taken into account. The stresses are normalized with respect to the bearing stress under the plate. For the diffusion angle of approximately 26 degrees recommended in section 4.3.8, the strut angle will generally between 15 and 25 degrees. In this range, the stresses are more or less constant at about $0.5f_b$. Compared to the elastic stresses shown in Fig. 4.13, the stresses predicted by the critical section defined for the Strut-and-Tie Model are smaller (an average value of $0.6f_b$ was indicated in section 4.2.2.2), which is normal because the Finite Element results give peak values, and the Strut-and-Tie Model gives average values over the width of the struts.
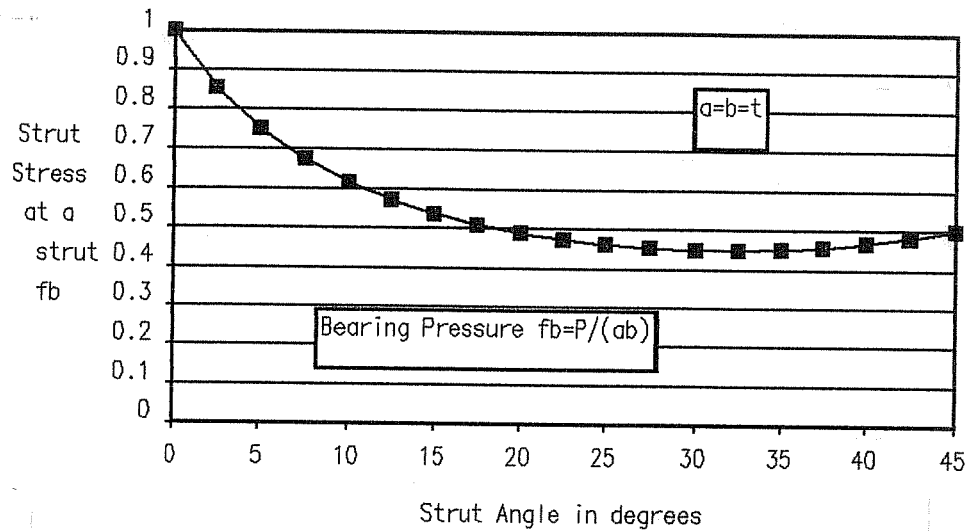
Figure 4.37   Stress in the Compression Struts at a Depth a as a
              Function of the Strut Angle

4.3.10   Conclusions from Example

The fact that all four Strut-and-Tie Models presented in the previous sections predict the same ultimate load for a given reinforcement simplifies the application of the Strut-and-Tie Model. Because the same amount of reinforcement is required for all four models, it is possible to use the simplest model to determine the required reinforcement and to then distribute the steel to follow more closely the elastic stress distribution. As long as the plastic centroid does not change, the ultimate load remains the same. Of course the reinforcement should not be placed too close to the anchor (within approximately one times the

dimension of the anchor), because it would be in a zone of transverse compression, where it will not be effective. The capacity of the strut varies slightly with the angle of inclination of the strut, but the changes in the predicted capacity between models is small as long as the centroid is located following more or less the elastic stress distribution.

4.4 Test Results

In a related task of the overall research project, a series of physical specimens was designed, fabricated and tested. The series consisted of eight specimens of single concentric anchorages (B1 through B8). The purpose of this test series was to investigate the behavior of simple concentric anchorage zones and to assess the validity of the Strut-and-Tie Model concept for these cases. This test series is described in more details in Ref. 153. The test results are used here to check the applicability of the Strut-and-Tie Model and the validity of the stress analyses for concentric anchorage zones.

The Strut-and-Tie Model was used in the design of the reinforcement for the test specimens. The cracking load was estimated on the basis of the expected tensile strength of the concrete using the elastic stress distribution from the Finite Element analysis.

4.4.1 Description of the Test Specimens of the UT Austin Research Project

The geometry of Sanders' test specimens for this series is shown in Fig. 4.38. In this series of tests, the relative plate size (a/h) of the specimen was held constant at 0.41. Fig. 4.38 also shows the local zone reinforcement in form of a spiral that was provided for all specimens, with the exception of B6. This

local zone reinforcement was designed so that the local zone would
not fail at a load lower than the anticipated ultimate load of the
general zone. Fig. 4.39 shows the distribution of tensile bursting
stresses from the Finite Element analysis along the axis of the
load and the corresponding layout of the bursting reinforcement in
the general zone for all specimens.
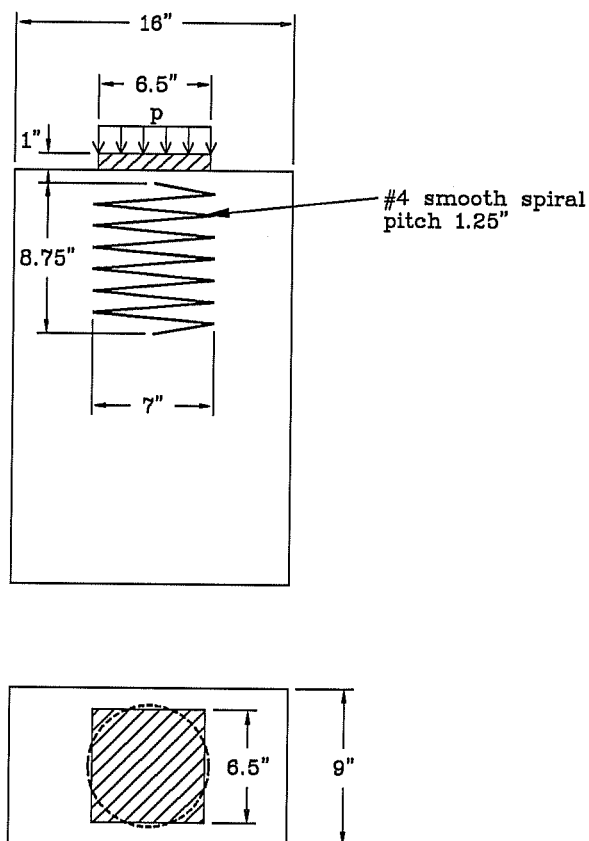

Fig. 4.38   Geometry and Local Zone Reinforcement of Specimens
             B1-B8

The primary goal of the first four tests of this series (B1 through B4) was to examine the influence of the layout of the reinforcement on the ultimate strength of the anchorage zone. The location of the centroid of the reinforcement and the distribution of the reinforcement along the tendon path were varied to achieve theoretically similar ultimate loads according to the Strut-and-Tie Model.

The remaining four specimens are variations on the specimen B4. Except for the specimen B5, that did not have any general zone reinforcement, the reinforcement of the general zone is identical to B4. Specimen B6 did not have any local zone reinforcement. While specimens B1 through B6 did not have a tendon duct, specimens B7 and B8 have a tendon duct with diameter 2.125 inch thus decreasing the area of concrete available to resist both the bearing force and the bursting force. Specimens B1 through B7 were uniformly loaded over the entire surface of the anchorage plate (Fig. 4.40a).

Specimen B8 was uniformly loaded through a circular area of 4 inches in diameter, concentric to the anchorage plate (Fig. 4.40b). This load more realistically represents an anchor loaded by a wedge plate attached to the tendon.
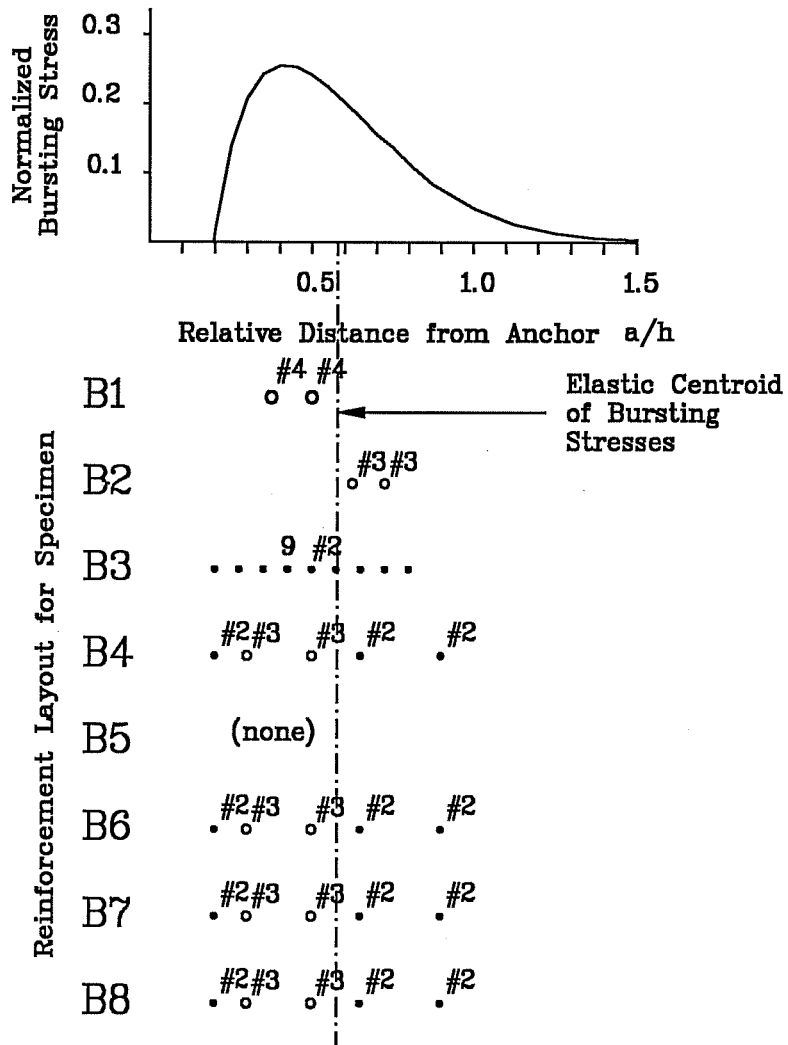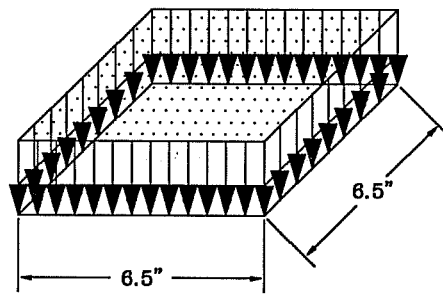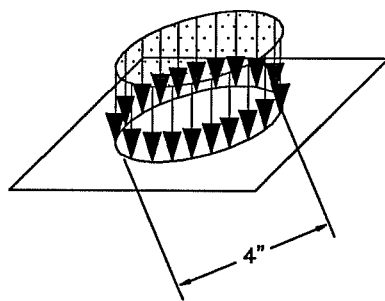
Fig. 4.39   Bursting Stress and Distribution of General Zone
             Reinforcement for Specimens B1-B8

a) Loading for Specimens B1—B7

b) Loading for Specimen B8

Fig. 4.40   Mode of Loading for Specimens B1-B8

4.4.2 Test Results

4.4.2.1   Results from the NCHRP UT Austin Program

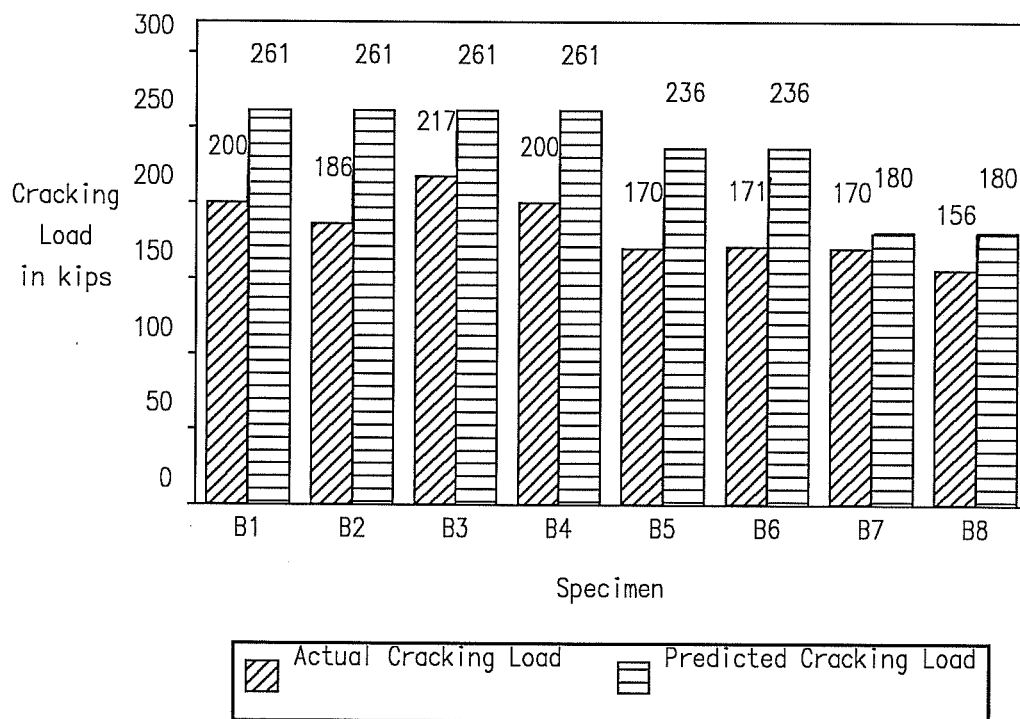| B1–B4 Various Reinforcement Distributions	B5 No General Reinforcement	B6 No Local Reinforcement	B7 Duct	B8 Small Plate

Fig. 4.41   Cracking Load for Specimens B1-B8

Figure 4.41 shows the cracking load of the eight test specimens and the corresponding predicted cracking load. The predicted cracking load was determined by setting the largest elastic tensile bursting stress obtained from a linear elastic

Finite Element Analysis to the measured tensile strength of the concrete, as obtained from split-cylinder tests. In all cases of this series, the predicted cracking load was larger than the observed value. The accuracy of the predictions was better for the specimens B7 and B8 which had a tendon duct.

Special attention was given to try to detect evidence of early cracking at the face of the specimen due to spalling stresses. However, no spalling cracks were observed in any of the specimens in this series. Because the cracks were detected by visual inspection, unobserved microcracks may have developed. In any case, no crack developed to a visible state at the face of the specimens, except for some cracks that surrounded the anchorage device in the later stages of the testing (Fig. 4.42).
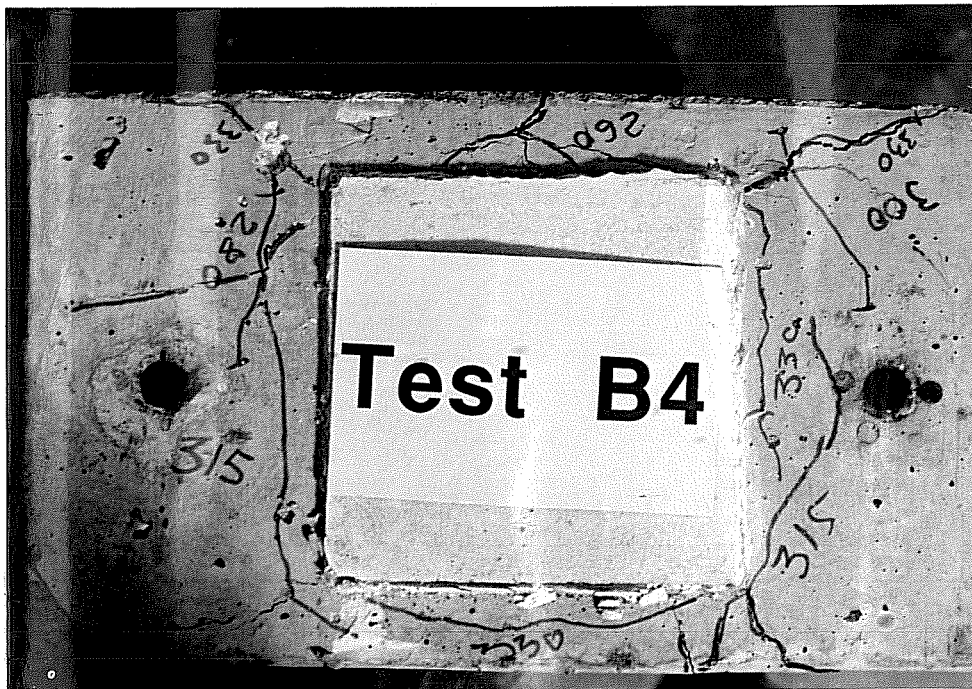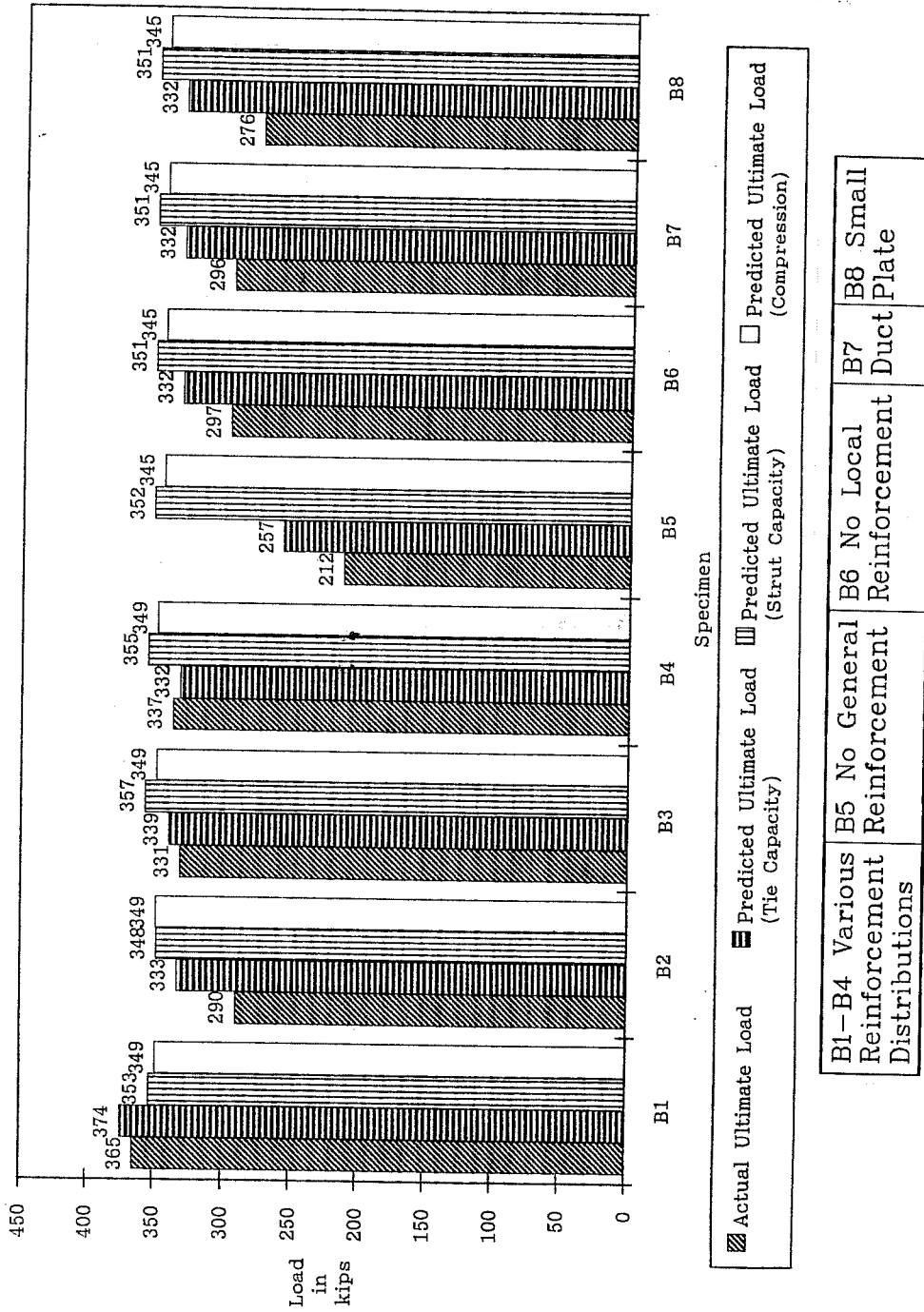

Fig. 4.42   Top Face of Specimen B4 after Testing

Fig. 4.43   Ultimate Load for Specimens B1-B8

| B1-B4 Various Reinforcement Distributions | B5 No General Reinforcement | B6 No Local Reinforcement | B7 Duct Plate | B8 Small Plate |

This observation confirms that spalling cracks are not critical for concentrically loaded anchorage zones. It is probable that the large spalling stresses shown in the elastic analysis do not develop because of an early development of microcracks in the spalling region. Once the spalling region has lost its stiffness, the condition of compatibility is relieved, and the anchorage zone behaves as if its regions of spalling stresses did not exist (see Fig. 4.17 and 4.18).

Figure 4.43 shows the ultimate load reached by the eight test specimens and the corresponding ultimate load predicted by the Strut-and-Tie Model. Two predictions of the ultimate capacity are shown for the Strut-and-Tie Model: the tie capacity is based on the tensile capacity of the reinforcement acting as a tension tie and the strut capacity is based on the compressive stress in the concrete at the critical section, as defined in section 4.3.9. The limiting effective concrete strength on the critical section was assumed to be 0.60 f'_c. The lowest of these two values is the ultimate capacity predicted by the Strut-and-Tie Model, P_{STM}. In this test series, with the exception of specimen B1, the capacity of the tie controls the design of all specimens. In addition, Fig. 4.43 gives a second estimate (labeled *Compression*) of the compressive capacity of the concrete based on the elastic stresses at a distance a ahead of the anchorage device. This value was obtained by setting the limiting effective compressive stress obtained from the Finite Element Analysis to 0.75 f'_c, a higher value than used for the Strut-and-Tie Model because the Finite Element solution obtains peak stresses, not average stresses. In the case of the specimens B1-B8, the two predictions of the compressive strength are very close to one another. As can also be seen from Fig. 4.43, the compressive failure load of all specimens was very close to the failure load based on the tension tie capacity.

B1–B4 Various Reinforcement Distributions	B5 No General Reinforcement	B6 No Local Reinforcement	B7 Duct	B8 Small Plate
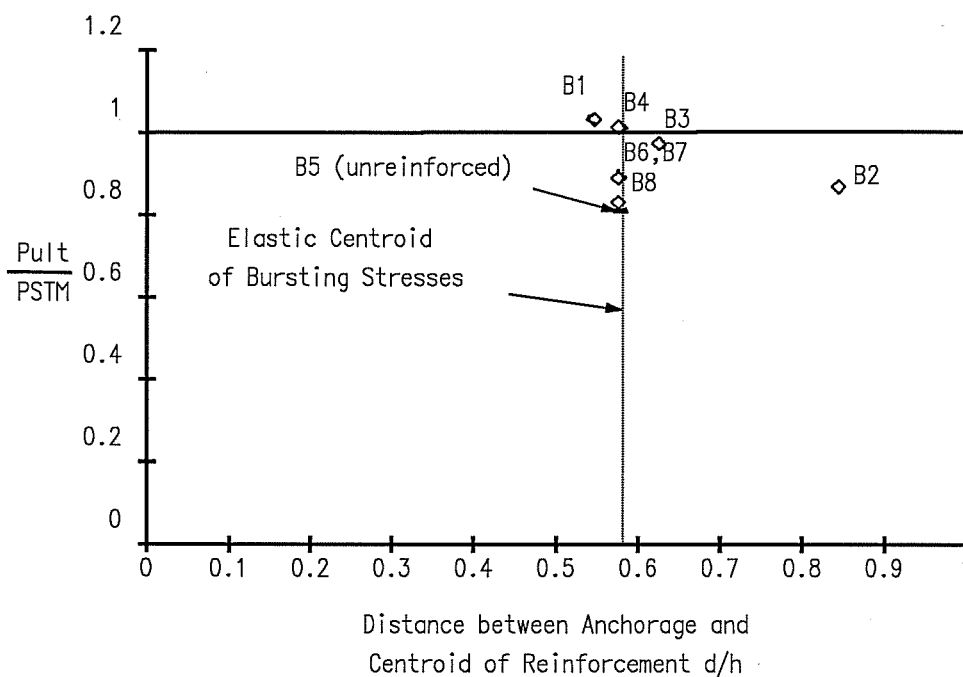
Fig. 4.44   Accuracy of the Strut-and-Tie Model as a Function of
        the Location of the Centroid

In order to allow an evaluation of the acceptability of the predictions of the Strut-and-Tie Model, it is interesting to normalize the ultimate load by the predicted ultimate load P_{ult}/P_{STM}. Figure 4.44 shows the normalized value P_{ult}/P_{STM} as a function of the relative location of the centroid. For specimen B5, which did not have any general zone reinforcement, the force in the tension tie was assumed to be equal to the force developed in the concrete in tension just before cracking. This tie force is considered as acting at the centroid of the tensile stresses.

The specimens B1, B3 and B4, which had reinforcement

patterns with a centroid close to the centroid of the elastic stresses, reached loads very close to the predicted load. Specimen B2, which had a reinforcement pattern that deviates considerably more from the elastic stress distribution nonetheless reached 87% of the load predicted by the Strut-and-Tie Model.

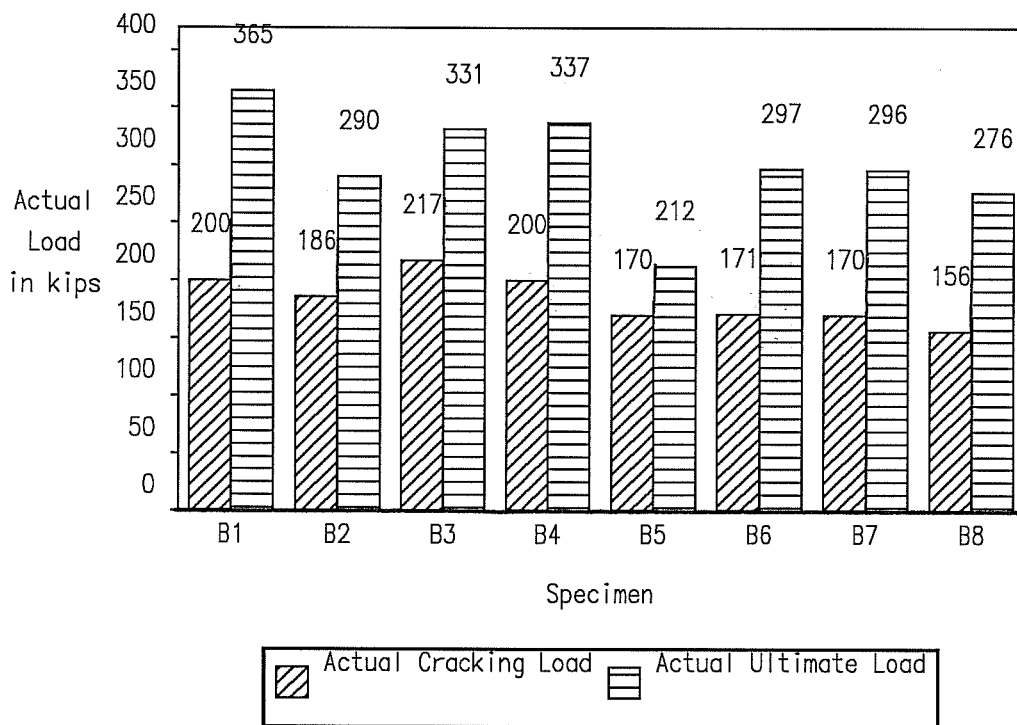| B1—B4 Various Reinforcement Distributions	B5 No General Reinforcement	B6 No Local Reinforcement	B7 Duct	B8 Small Plate

Fig. 4.45   Cracking Load and Ultimate Load for Specimens B1-B8

Figure 4.45 shows the cracking and ultimate loads for the specimens B1 through B8, which have the same reinforcement in the general zone (except for B5). Specimens B5 through B8 were cast separately from the first four specimens. The compressive strength of the concrete of specimens B5-B8 was comparable to the strength

of specimens B1-B4 at testing (5380 psi for B1-B4 vs 5320 psi for B5-B8), but the tensile strengths were appreciably different, 464 psi for B1-B4 and 420 psi for B5-B8. If the cracking load of B4 was normalized by the ratio of the tensile strength of the concrete, it would only be 181 kips, and compare better with the cracking loads observed for B5 and B6, as reported in Fig. 4.45.

The local or general zone reinforcement has little influence on the cracking load. This is expected because the strains in the reinforcement are small when the concrete is uncracked. The presence of a duct hole in specimen B7 does not have a large influence on the cracking load either, even though the loss in net area across the plane of the duct amounts to 23%. This is a surprising result considering that the first crack started along the path of the tendon duct. This apparently contradictory result may be caused by the large scatter normally exhibited by the tensile strength of concrete, and by the strength provided by the corrugated steel duct itself.

It is apparent from the considerably lower ultimate load of specimen B5 that the general zone reinforcement is crucial. If no general zone reinforcement is provided, the ultimate load is only 24% more than the cracking load. In all other cases, the ultimate load was between 52% and 82% larger than the cracking load.

Specimen B6 did not have any local zone reinforcement, but nonetheless reached 88% of the load of B4. The nominal bearing stress under the anchor plate was 1.3 f'_c at failure. This confirms the necessity of including local zone reinforcement in order to avoid a local zone failure and to develop the full strength predicted by the Strut-and-Tie Model.

Specimen B7 had exactly the same reinforcement as B4, but included a tendon duct. The ultimate load was 87% of the load of B4, and 90% of the load predicted by the Strut-and-Tie Model. The difference in ultimate strength may be caused by the high level of

bearing stresses under these plates (1.48 f'$_c$ for B4 and 1.43 f'$_c$ for B7), perhaps indicating a failure of the local zone.
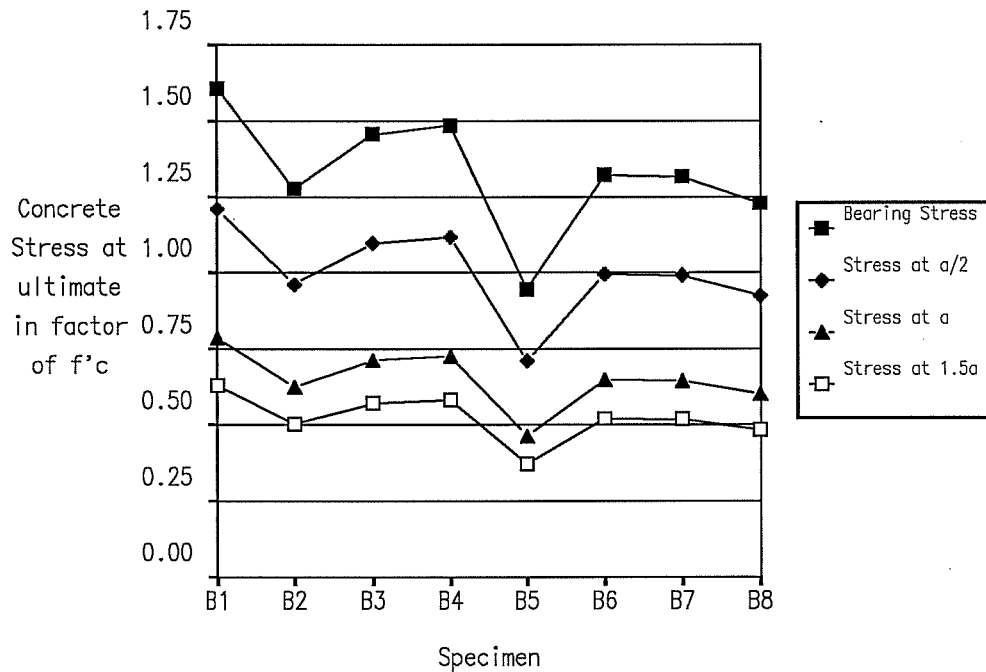
Fig. 4.46   Stresses in the Concrete Struts at Ultimate for
            Specimens B1-B8

Fig. 4.46 shows the compressive stresses at ultimate in the concrete under the bearing plate and at locations *a/2*, *a* and *1.5a* ahead of the anchorage. The level of compressive stresses in the concrete struts is very similar for specimens B4 and B7, once adjustments are made for the presence of the duct hole. The stresses at 1.0a, which corresponds to the critical section defined in section 4.3.9, are about 0.75 f'$_c$. Roberts [146] indicates this as a maximum stress for unconfined concrete in compression struts.

Specimen B8 is identical to Specimen B7, except for the having been loaded through a smaller surface (See Fig.4.40).

Specimen B8 reached a lower ultimate load than B7, presumably because the flexibility of the anchorage plate made the stress distribution under the plate nonuniform. To take into account the flexibility of the plate, it is possible to consider a plate smaller than it is in reality. Assuming a diffusion angle of the stresses of 45 degrees through the steel plate, the effective diameter of the loading plate would only be 6 inches. Using this value, the predicted ultimate load from the Strut-and-Tie Model is 315 kips and the corresponding cracking load is 174 kips. The ratio of the predicted ultimate load to the actual value is 0.88, which is very close to the result obtained for specimen B7 (0.89). This example shows that the flexibility of the anchorage device can be taken into account by considering a reduced anchorage size in the design. The results obtained from the Finite Element analysis as well as from the Strut-and-Tie Model show a better correlation if such a correction is used. Similar tendencies are described in Section 4.6.2, which presents the results of a more detailed analysis of the influence of the anchorage device.

4.4.2.2   Results from Other Investigators

Until the present NCHRP project, the largest number of large scale test specimens had been reported by Stone & Breen [172, 173, 174]. The results of concentric tests reported by Stone are shown in Fig. 4.46. The loads are normalized by the tensile strength of the concrete obtained from split cylinder tests, f_{sp}. The most striking fact about this figure is the very small increase in strength between the cracking load and the ultimate load. This type of behavior appears to have been frequently observed in the specimens reported by Stone and Breen.

As is shown in Fig. 4.47, the bearing stresses under the plate were very high in Stone's tests, significantly higher than

in the present test series. The compressive stresses in the concrete at the critical section were not computed for Stone's specimens, but based on the fact that the strut stresses at a depth a are usually approximately $0.5f_b$. If this is the case, the stresses at the critical section would be between $0.85f'_c$ and $1.3f'_c$ at failure, values which are clearly very high. It is therefore most likely that Stone's specimens failed in compression either in the local zone or at the interface between the local zone and the general zone. This is in agreement with the observation made by Stone that the reinforcement pattern in the general zone had little influence on the strength of the specimens.
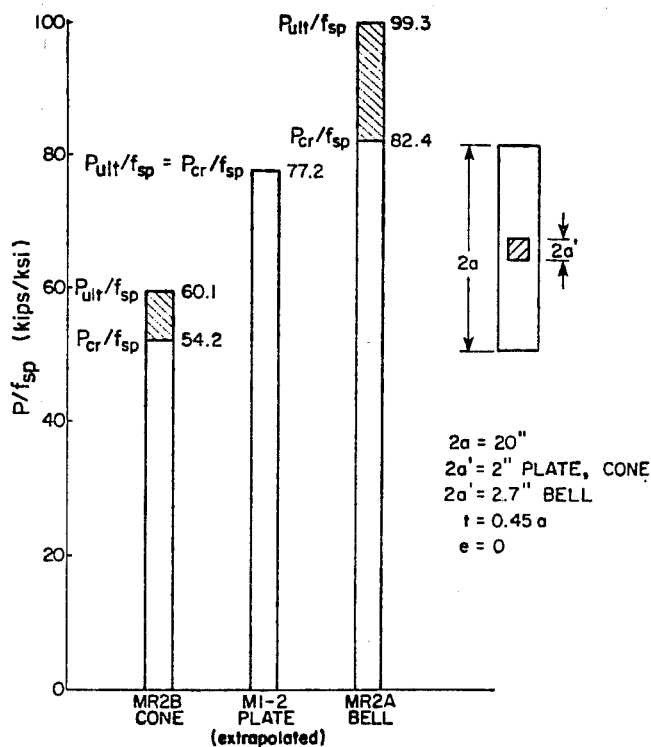

Fig. 4.46   Cracking and Ultimate Load for Stone's Concentric Specimens
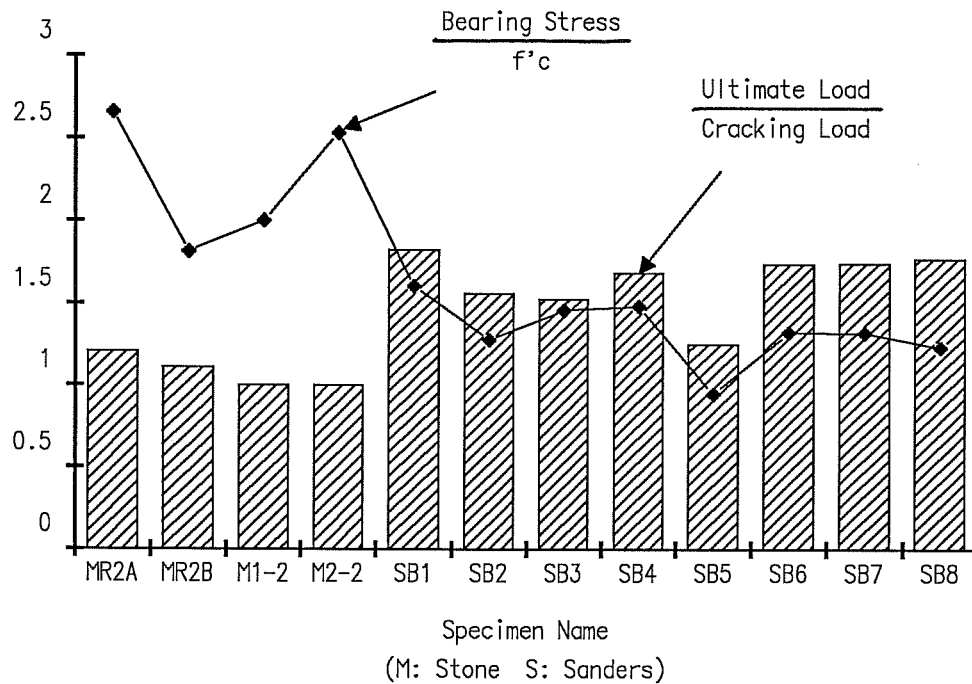
Fig. 4.47   Bearing Stress under Anchorage Device and Ratio of
            Ultimate to Cracking for Stone's and Sanders'
            Specimens

Stone attributed the initiation of failure of his specimens
to the spalling stresses that act at the surface of the specimen,
but also reports that spalling cracks were never observed. The
spalling stresses are rather thought to have had a detrimental
effect on the confinement provided by the concrete around the
anchor. Taking into account the high level of bearing stresses
acting under the anchorage device, this is a very likely
explanation. However, the spalling stresses alone are not causing
the failure of the specimen. Therefore it does not appear correct
to always relate the failure of an anchorage zone to spalling
stresses, provided the local zone is properly reinforced and the
compression struts are not subjected to excessive stresses.

4.4.3 Evaluation of the Analysis Method for Use in Design of Concentric Anchorage Zones

As shown in Fig. 4.41, the Finite Element analysis approximately predicts the cracking load although somewhat unconservatively. For the eight specimens, the average ratio of measured to predicted cracking load was an unconservative 0.792, with a standard deviation of 0.083. This error is not too surprizing because the tensile strength of the concrete has a large coefficient of variation. In addition, the detrimental effect of compressive stresses acting perpendicular to the tensile stresses was not taken into account. Ref. [129] indicates that the apparent reduction of the tensile strength of the concrete can be significant when the lateral compressive stresses are appreciable. More detailed predictions of the cracking load can be found in Ref. 153. Predictions of the cracking load that are within 25% of the observed value can be useful when one considers the present lack of knowledge in this general area. As shown in Fig. 4.45, except for specimen B5, which did not have any general zone reinforcement, the ultimate load is considerably larger than the cracking load. Also, the cracking load is close to the nominal capacity of a normal commercial anchorage device of comparable size. An anchor with dimensions 6.5 in. square can accommodate five 0.5 in. strands. The corresponding ultimate load is 265 kips, and the maximum tendon load (at 0.8 f_{pu}) is 212 kips. Based on this value, the cracking load was reached at loads between 74% and 102% of the maximum allowed stressing force. This indicates that for thin sections a limited amount of cracking is to be expected in the anchorage zone under normal circumstances.

As shown in Fig. 4.43, the ultimate load of the specimens of this series was fairly well predicted by the Strut-and-Tie Model. Excluding B5, which had no general zone reinforcement, the average ratio of measured to predicted was 0.931 with a standard deviation

of 0.078. The largest error was 17.5% for specimen B5, which did not have any general reinforcement. The second largest error was 16.9% for specimen B8 (without adjustment) that had a tendon duct and was loaded through a limited part of the plate. The next largest error is only 12.9% for the specimen B2.

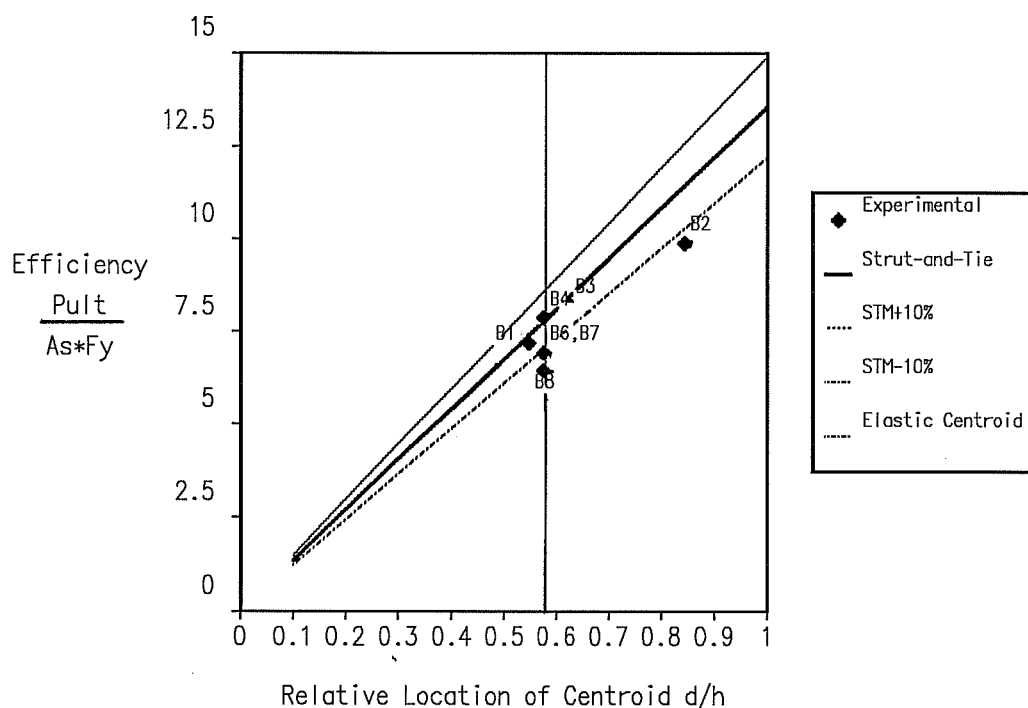| B1—B4 Various Reinforcement Distributions	B5 No General Reinforcement	B6 No Local Reinforcement	B7 Duct	B8 Small Plate

Fig. 4.48   Efficiency of the Reinforcement as a Function of the Location of the Centroid

Because the dimensions and material properties were well known, no understrength factor (ϕ-factor) was used for the evaluation of the test results. The fact that only two of the predicted loads were slightly larger than the effective ultimate

load (all other specimens were unconservative designs) indicates that the simplifying assumptions for the geometry of the Strut-and-Tie Model should be modified for better, more conservative results. As will be shown, the capacities predicted by the Strut-and-Tie Model are sensitive to the geometric definition of the model.

The "efficiency" of the reinforcement is defined as the ratio of the ultimate load reached by the specimen to the tensile capacity of the reinforcement provided. This quantity indicates how "efficient" the reinforcement is by describing the amount of ultimate load obtained for unit of reinforcement provided. The higher the ultimate load reached for a given amount of reinforcement, the more efficient is the reinforcement. Fig. 4.48 shows the efficiency of the reinforcement as a function of the location of the centroid of the reinforcement. The Strut-and-Tie Model predicts that the efficiency increases linearly as the centroid of the reinforcement gets farther from the anchor. As a consequence, the farther from the anchorage the reinforcement is located, the more efficient it is, and the less reinforcement is required for a given design load. This, of course, is only true as long as the failure is controlled by the failure of the tension tie. The experimental test results generally agree with this tendency, but indicate that a certain deterioration of the efficiency of the reinforcement is to be expected when the centroid of the reinforcement is not close to the centroid of the elastic stresses. However, it is remarkable that specimen B2 reached an ultimate load of 290 kips with only 59% of the steel required by specimen B4 which reached 337 kips. Additional testing would be required to assess the general validity and the limits of this property. It appears that in actual design situations the limit on admissible locations for the centroid of the reinforcement will be dictated mainly by serviceability

considerations. In many situations, it may be preferable to limit cracking to distribute the reinforcement according to the elastic distribution.

Fig. 4.48 shows again that the predictions of the Strut-and-Tie Model are slightly unconservative, because the predicted theoretical efficiency is exceeded only by Specimen B4. Fig. 4.49 shows the efficiency of the reinforcement as a function of the location of the centroid for a Strut-and-Tie Model in which the nodes for the compression forces under the plate are located not exactly at the surface of the concrete, as shown in Fig. 4.50a, but rather at a depth equal to 1/4 of the plate size, as shown in Fig. 4.50b.

As illustrated in Fig. 4.51 this minor adjustment to the Strut-and-Tie Model, that more realistically corresponds to the physical idea that the node should be "in" the concrete, leads to a much better correlation between the experimental values and the theory. Excluding B5,which had no general zone reinforcement, the average ratio of measured to predicted with node at a/4 was 1.110 with a standard deviation of 0.092.

Overall, these tests show that the Strut-and-Tie Model method is a valid concept for concentric anchorages. A consistent design can be achieved with various distributions of the tensile reinforcement, even if the distribution diverges from the elastic stress distribution. Specimen B4, which had a reinforcement pattern that followed closely the elastic stress distribution, performed best in this series, but was only marginally superior to specimens B1 and B3 that had simpler layouts for the reinforcement. The presence of a duct hole slightly decreases both the cracking load and the ultimate load. It is desirable to locate the nodes that represent the beginning of the spreading of the compression forces below the anchorage plate at a distance a/4 into the concrete to better represent the physical idea of the

nodes being part of the concrete structure.

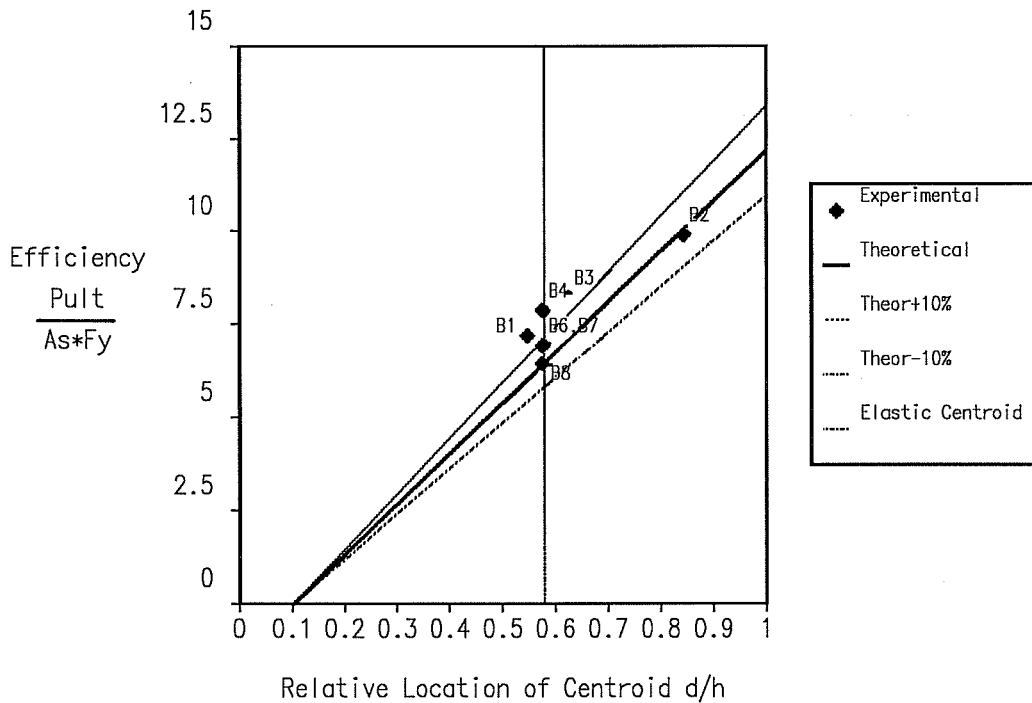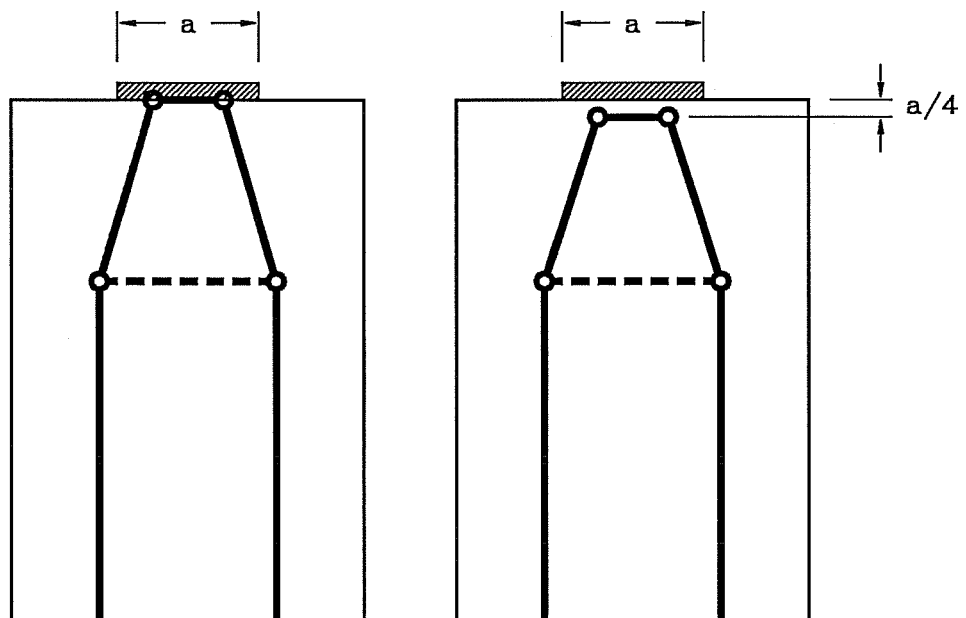| B1—B4 Various Reinforcement Distributions	B5 No General Reinforcement	B6 No Local Reinforcement	B7 Duct	B8 Small Plate

Fig. 4.49   Efficiency of the Reinforcement as a Function of the
Location of the Centroid with plate node at 0.25·a

a) Top Nodes at the
Surface of the Concrete

b) Top Nodes at a/4
in the Concrete

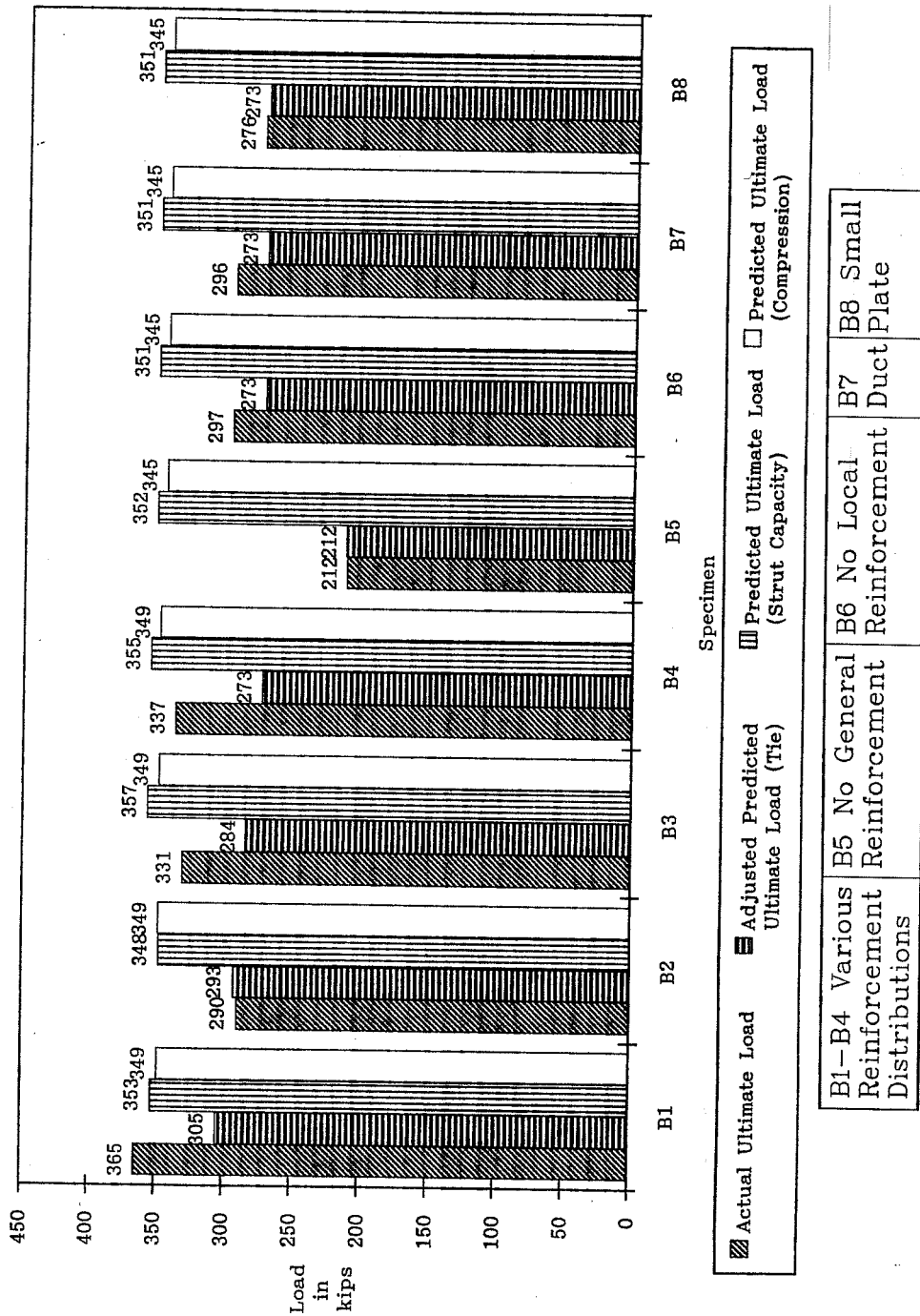Fig. 4.50   Geometric Location of the Nodes Representing the

Anchorage Plate

Fig. 4.51   Ultimate Load for Specimens B1-B8, with Adjusted
             Prediction for the Ultimate Load

4.5   Enhancement of the Strut-and-Tie Model

4.5.1 Tensile Concrete Contribution
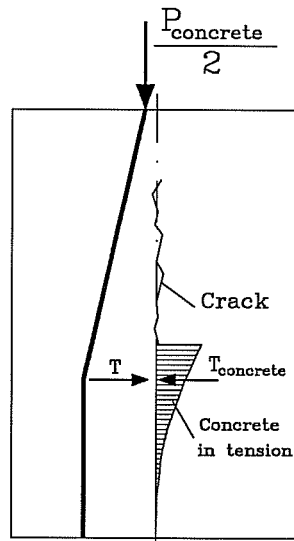
Fig. 4.52   Principle of the Tensile Concrete Contribution to the Load-Carrying Mechanism

The Strut-and-Tie Models presented so far do not account for the contribution of concrete in tension to the ultimate strength. This hypothesis is conservative and reasonable because the concrete may crack in the anchorage zone, for reasons independent of the post-tensioning forces. The test specimens of the series B were short and the use of Teflon sheets at the base ensured that negligible shear force was transmitted by friction between the reaction floor and the specimen. The specimens cracked extensively along the centerline, in such a manner that the contribution of concrete in tension to resisting the bursting force was effectively zero. Because the strength of the specimen depended mainly on the tensile reinforcement, a good correlation between the load predicted by the Strut-and-Tie Model and the effective ultimate load was observed.

In a real structure however, there is no clear separation

between the anchorage zone and the rest of the girder. The
uncracked part of the concrete in the main part of the girder may
be able to transfer a significant part of the load. A possible
model to describe the contribution of concrete in tension to the
ultimate capacity is presented conceptually in Fig. 4.52. The
uncracked concrete ahead of the crack has relatively large strains
(just lower than the cracking strain at the tip of the crack). The
resulting tension force is not very large, but it can contribute
to the ultimate load because of the favorable angle of the
corresponding compression struts. This load carrying mechanism,
since it involves uncracked concrete, will exhibit a considerable
stiffness, much larger than would be expected from a Strut-and-Tie
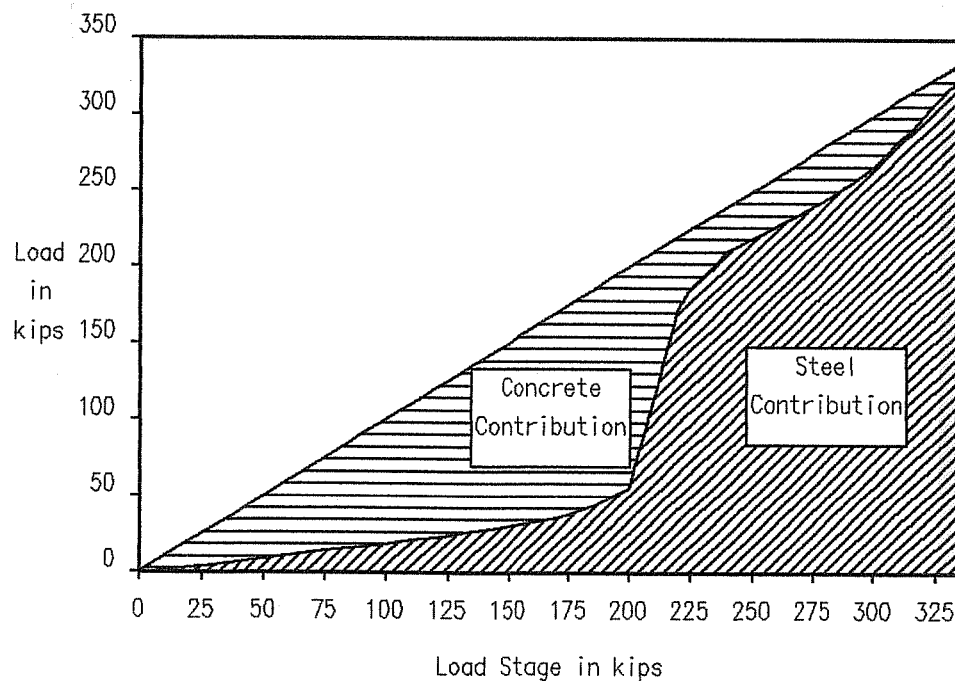Model involving only steel tension ties.

Fig. 4.53   Tensile Concrete Contribution to the Load-Carrying
             Mechanism of Specimen B4

Fig. 4.53 shows the relative contribution of the steel and the concrete in tension to the load-carrying mechanism of Specimen B4, as reconstructed from strain measurements on the reinforcing bars. For every load stage, the contribution to the Strut-and-Tie Model of the reinforcement is computed from the measured strains. The corresponding force is less than the applied force, and the rest of the load must therefore be carried by concrete in tension. Fig. 4.53 shows the two contributions as a function of the total applied load. Until cracking of the concrete occurs, at a load of about 200 kips, the load is mainly carried by the concrete. After cracking has occurred, the load is mainly carried by the reinforcement, but some concrete contribution is observed until the ultimate load is reached.

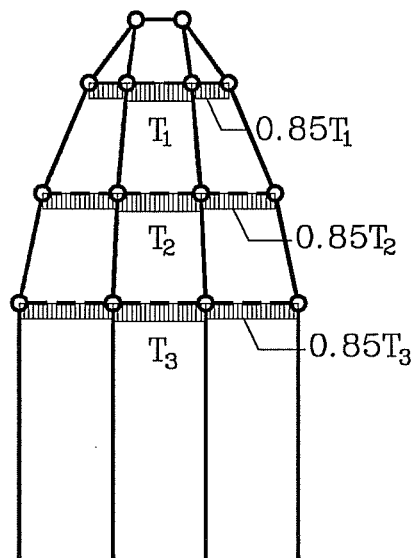### 4.5.2 Detailing of Smeared Nodes

Figure. 4.54 Residual Tension Force in the Ties

The detailing of *smeared* nodes can be better understood by considering the *multiple thrust line Strut-and-Tie Model* of Fig. 4.54 that shows how the force in the tension ties is gradually reduced in crossing the compression thrust lines. It is important to note that the force in the tension tie is not abruptly reduced

to zero when the node is reached. In fact, the force in the tie is progressively transferred to the concrete and remains large until the tie crosses the outermost compression strut. A comparatively large part of the load is transmitted by the outermost strut because it has the largest inclination. Because the geometry of the Strut-and-Tie Model can be freely chosen by the engineer, the force in the tension ties can vary considerably from one Strut-and-Tie Model to another. It is therefore difficult to define in a general manner what percentage of the load needs to be anchored on the outside of the node.
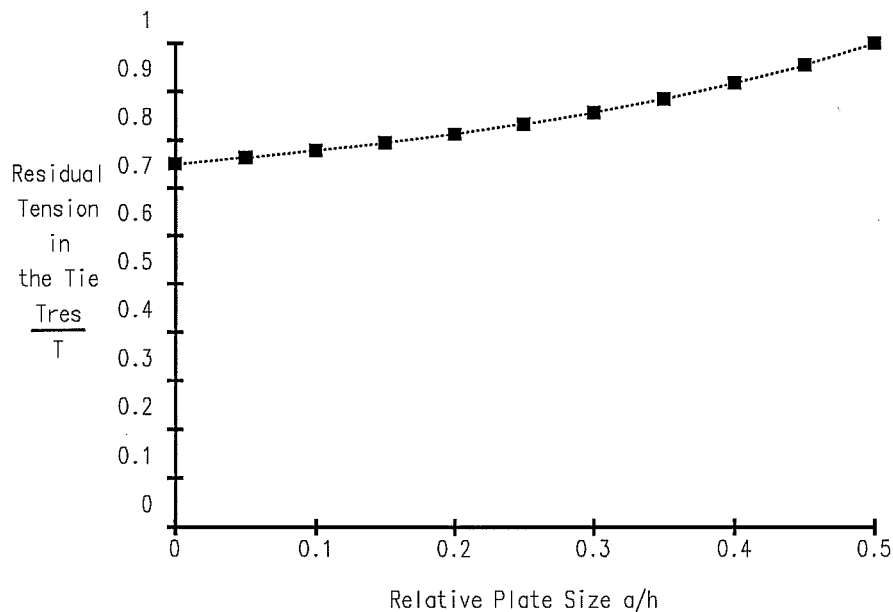
Fig. 4.55   Residual Tension in the Ties as a Function of the Plate Size

Some indications on the variation of the tension force was obtained from a parametric study based on the geometry of the example problem. The relative plate size (a/h) was varied from 0.0 to 0.5, and the ratio of the residual force transmitted to the

outer node to the force in the central portion of the tension tie was constrained to be the same for all three tension ties. Fig. 4.55 shows that in all cases, the value of the residual tension force is from 75% to 90%. This highlights the necessity of properly anchoring the reinforcement of tension ties that are connected to smeared nodes. Ordinarily, a detail like the one shown in Fig. 4.56 will provide the necessary development before the actual node. This type of detail was used throughout the test series described in Ref. 153 and no distress due to lack of development of the bars was observed.

Fig. 4.56   Typical Detail for Tension Ties in Anchorage Zones

4.6   Details of the Finite Element Modelling

4.6.1 Convergence of the Finite Element Solution

The convergence of the Finite Element solution using four-node isoparametric elements was investigated on the basis of the concentric configuration. The purpose of this convergence study was to gain some perception of the adequacy of a Finite Ele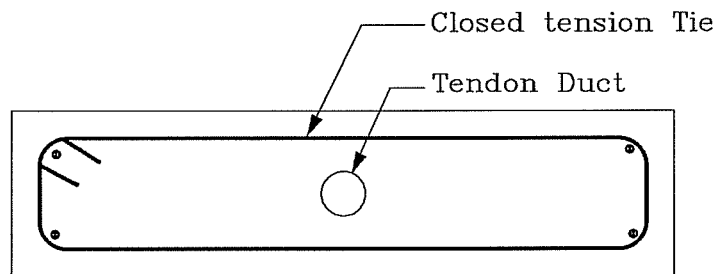ment mesh. The concentric configuration is very useful for such a study because it involves a limited number of parameters. The elastic solution of Guyon [75] was used in evaluating the results obtained by the Finite Element Method.

For this convergence study, the Finite Element mesh used to model a concentric anchorage zone was systematically refined by halving the dimensions of the elements. Fig. 4.57 shows the four meshes used with the corresponding number of degrees of freedom. The two load cases applied to the model are a point load and a uniformly distributed load with a relative plate size $a/h = 0.25$.

Fig. 4.58 shows the convergence of the maximum bursting stress and the bursting force as a function of the number of degrees of freedom for a point load. Both the bursting force and the maximum stress increase noticeably (by about 5%) between the last two meshes (32x48 elements and 64x96 elements.) This is further illustrated in Fig. 4.59 which shows the distribution of tensile stresses along the tendon axis for the various meshes. Also shown in Fig. 4.59 is the solution of Guyon [75] which predicts that in the case of a point load only tensile stresses exist along the tendon axis, except for an infinite compressive stress acting on an infinitesimal surface at the point of application of the load. It appears that the distribution toward which the Finite Element solution converges is close, but not identical to Guyon's solution. This is expected because the Finite

Element Method does not represent singularity, infinite stress at the load point.
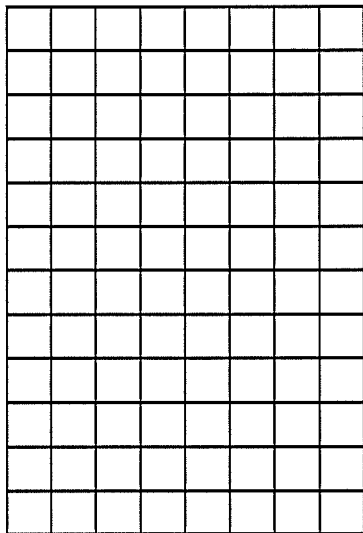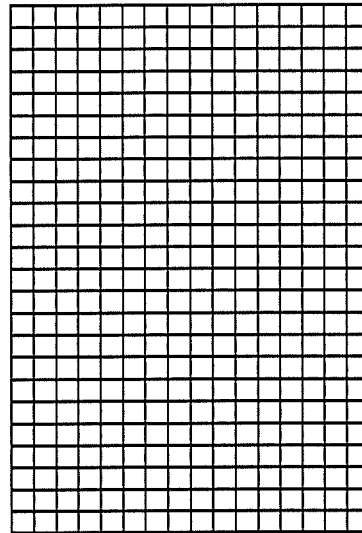
a) 8x12 elements   b) 16x24 elements
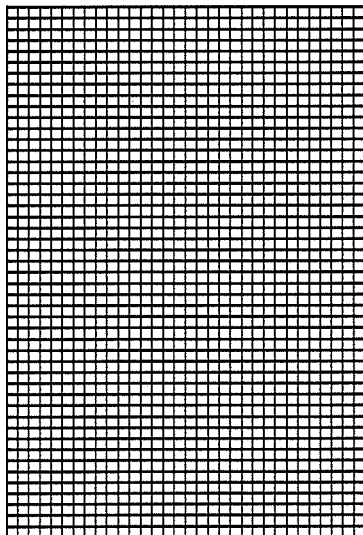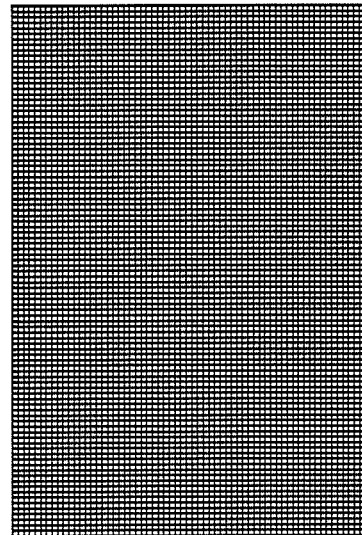
c) 32x48 elements   d) 64x96 elements

Fig. 4.57   Finite Element Meshes Used for Convergence Study
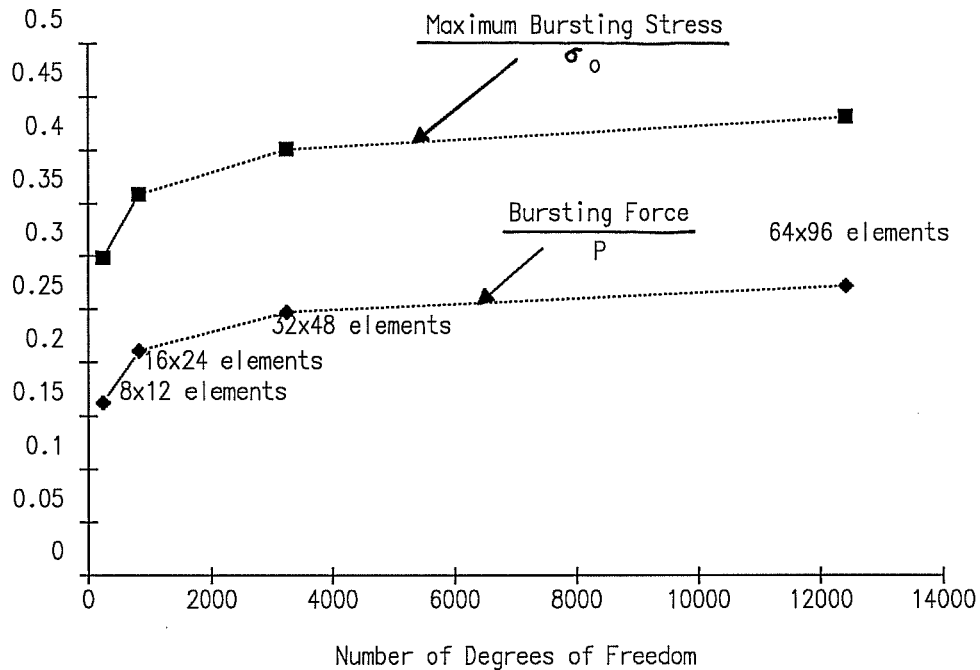
Fig. 4.58   Convergence of 4-node Finite Element Solution for a
             Point Load

Figs 4.60 and 4.61 show the convergence of the model
subjected to a uniform pressure acting on a plate of size
a = 0.25h. The results are much better for this load
configuration, with little change in the solution between the mesh
containing 16x24 elements and the mesh containing 64x96 elements,
as shown in Fig. 4.60 and 4.61. Again, the stress distribution
toward which the Finite Element solution converges is close, but
not identical to the stress distribution proposed by Guyon.
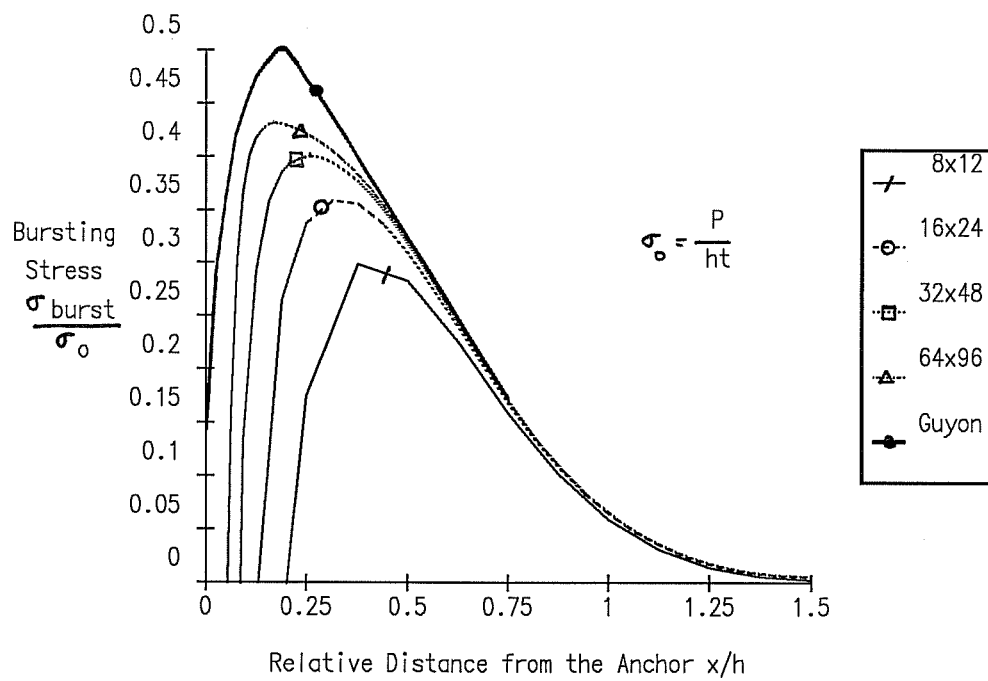
Fig. 4.59   Convergence of the Distribution of Bursting Stresses
along the Tendon Path for a Point Load
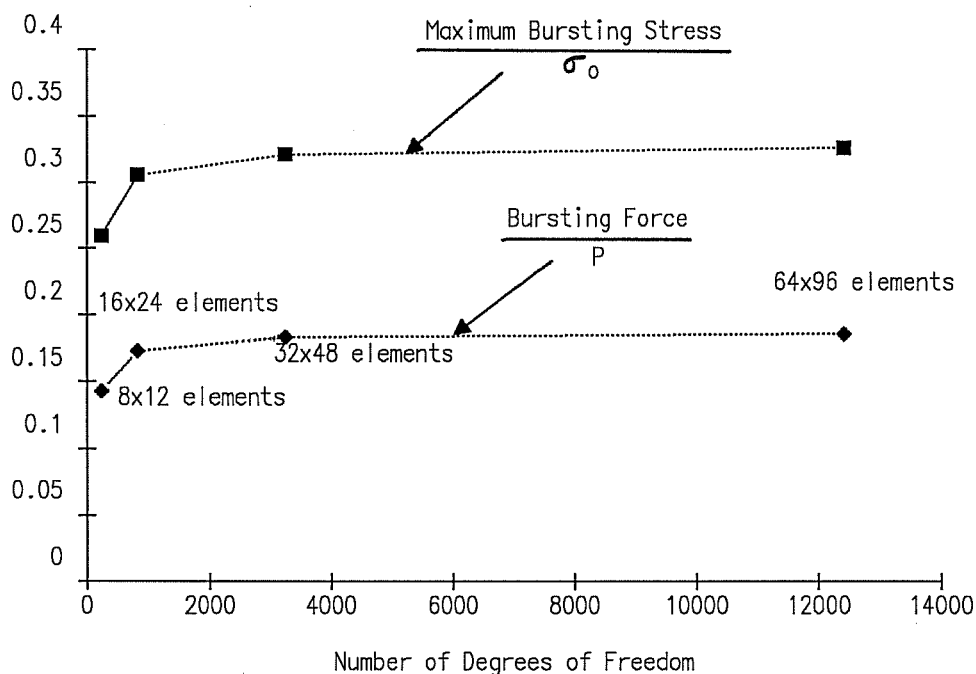
Fig. 4.60   Convergence of 4-node Finite Element Solution for a
            Distributed Load (a/h=0.25)

The convergence of the Finite Element solution for spalling stresses was found to be similar to the convergence of bursting stresses.

As a conclusion to this convergence study, it was found that for cases that do not include point loads the accuracy of the Finite Element solution is sufficient even for relatively coarse meshes, such as the one shown in Fig. 4.57b. A special attention should be given to cases in which the relative size of the anchorage plate a/h is small. In all the test specimens tested for this project, as well as for the majority of the practical application of post-tensioning, the relative size of the plate is larger than 0.1.
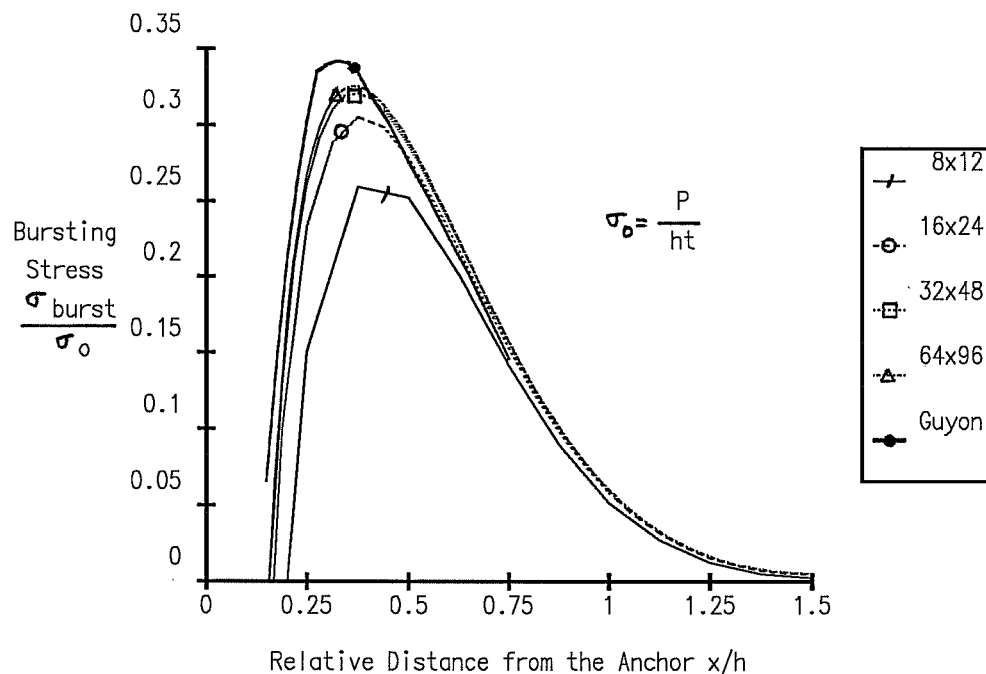
Fig. 4.61   Convergence of the Distribution of Bursting Stresses
along the Tendon Path for a Distributed Load
(a/h=0.25)

4.6.2 Modelling of the Anchor

As shown in Fig. 4.62, post-tensioning anchorage devices
have a wide variety of shapes from a steel plate to a complex
casting. Some devices have additional confining reinforcement in
the form of a spiral. This variety of geometries makes the
modelling of a "typical" device impossible. The modelling is
further complicated by the complexity of the boundary conditions
between the anchor and the surrounding concrete. In order to
understand the influence of the anchorage device on the state of

stresses, analyses were performed using a simple steel plate as an anchorage device.

The purpose of this investigation was to determine the influence of the anchorage device on the stresses from the Finite Element Analysis. To that end, various possible models of the interaction between the anchorage plate and the concrete were used. Fig. 4.63 shows the Finite Element mesh used for this examination. The steel plate has a length to thickness ratio of five which is typical for commercial plate anchors. The load is applied on the central third of the plate to simulate the effect of a typical wedge plate which introduces the tendon force near the center of the anchor.
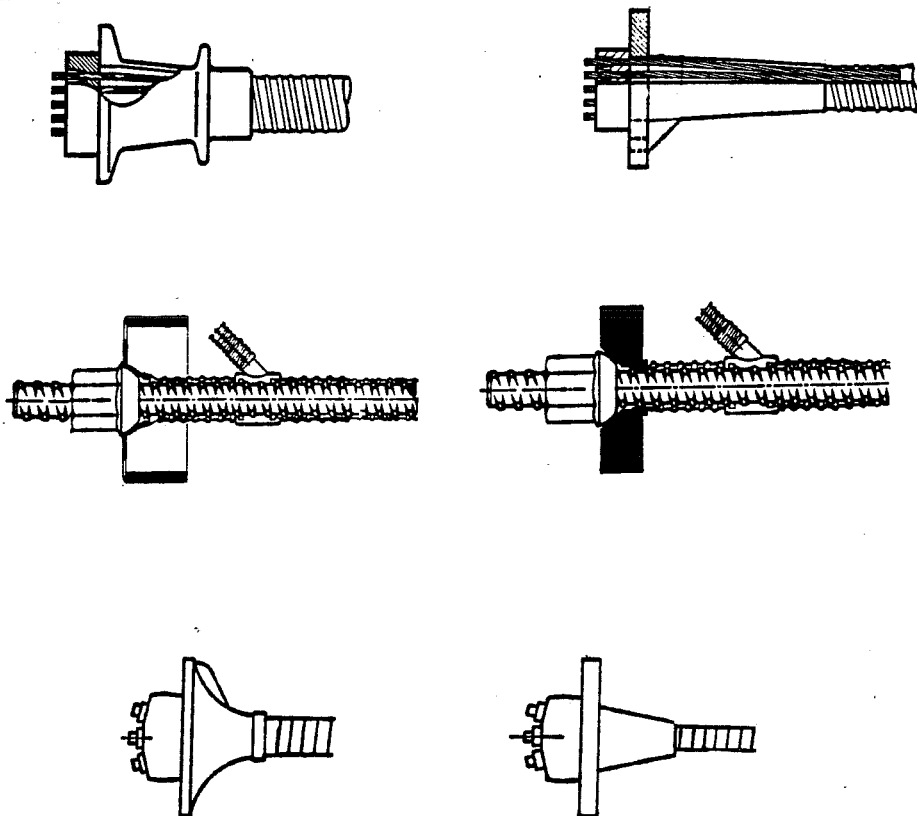
Fig. 4.62   Various Shapes of Anchorage Devices
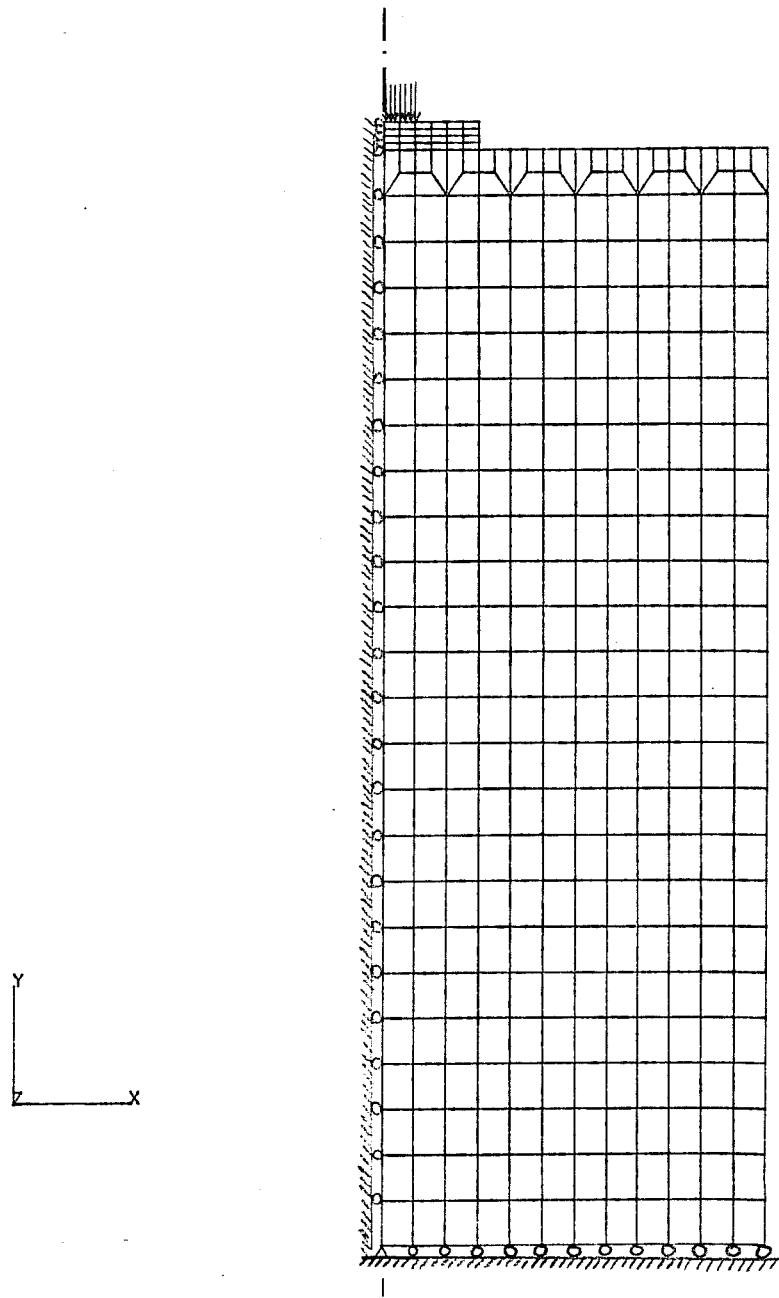
Fig. 4.63   Finite Element Model for the Analysis of the
             Influence of the Anchor Plate

a) Complete Bond   b) No Transverse Bond

c) Uniform Pressure   d) Rigid Plate
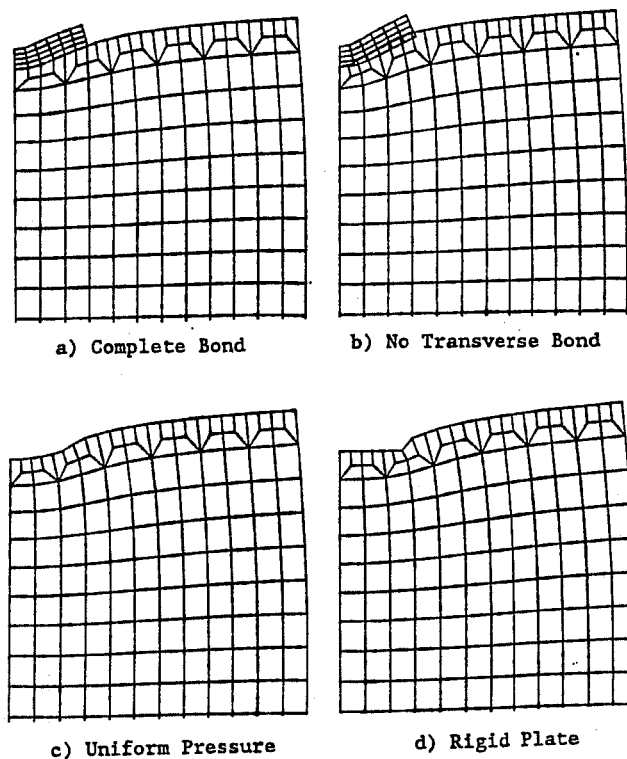
Fig. 4.64   Deflected Shape of Anchorage Zone for Various Models
of the Anchorage Plate

Fig. 4.64a shows a detail of the deflected shape
(exaggerated deformations) in the vicinity of the anchorage when a
full bond (in both x and y directions) is imposed between the
steel plate and the concrete. Fig. 4.64b shows the same detail
when only the compatibility of the longitudinal displacements (y
direction) is imposed between the plate and the concrete. Since
the transverse displacements (x direction) are not compatible, the
plate appears to penetrate the concrete. This does not occur in
reality (small displacement theory), but is due to the
magnification of the displacements in the drawing. Fig. 4.64c and
4.64d show the same detail of the vicinity of the anchor when the

anchor is modelled by a uniform pressure acting over the whole area of the anchor plate (Fig. 4.64c) or as being infinitely rigid (Fig. 4.64d). The anchor plate is not modelled in these cases, and does not appear in figures 4.64c and 4.64d.

Fig. 4.65 shows the contour of the stresses in direction x-x (transverse stresses) for all four cases. Notice that the stress distribution for the case where full bond is imposed between the steel plate and the concrete (Fig. 4.65a) is sensibly different from the stress distribution obtained in the other three cases. The entire concrete area along the tendon is subjected to tensile stresses. The compressive stresses necessary for equilibrium across the tendon axis are concentrated in the steel plate. As schematically shown in Fig. 4.66, the steel plate is subjected to bending under the applied load. In order to satisfy the compatibility of the transverse displacements, the concrete that is located at the interface with the steel plate must be in tension.

In all four cases, the largest bursting stresses occur along the axis of the tendon. Fig. 4.67 shows the distribution of bursting stresses along the tendon axis. The large tensile and compressive stresses occurring near the face are truncated. Notice again the considerable difference between the case where full bond is imposed between the plate and the concrete and the other cases. Fig. 4.68 shows the compressive stresses along the tendon axis. The two cases where the anchor plate is effectively modelled, and where the load is applied on one third of the surface, have the largest stresses directly under the plate. The rigid plate induces the smallest stresses along the tendon axis. Overall, the distribution of compressive stresses are unaffected by the modelling of the anchor plate at a distance equal to approximately one and a half times the size of the plate, which is approximately the size of the local zone [146].
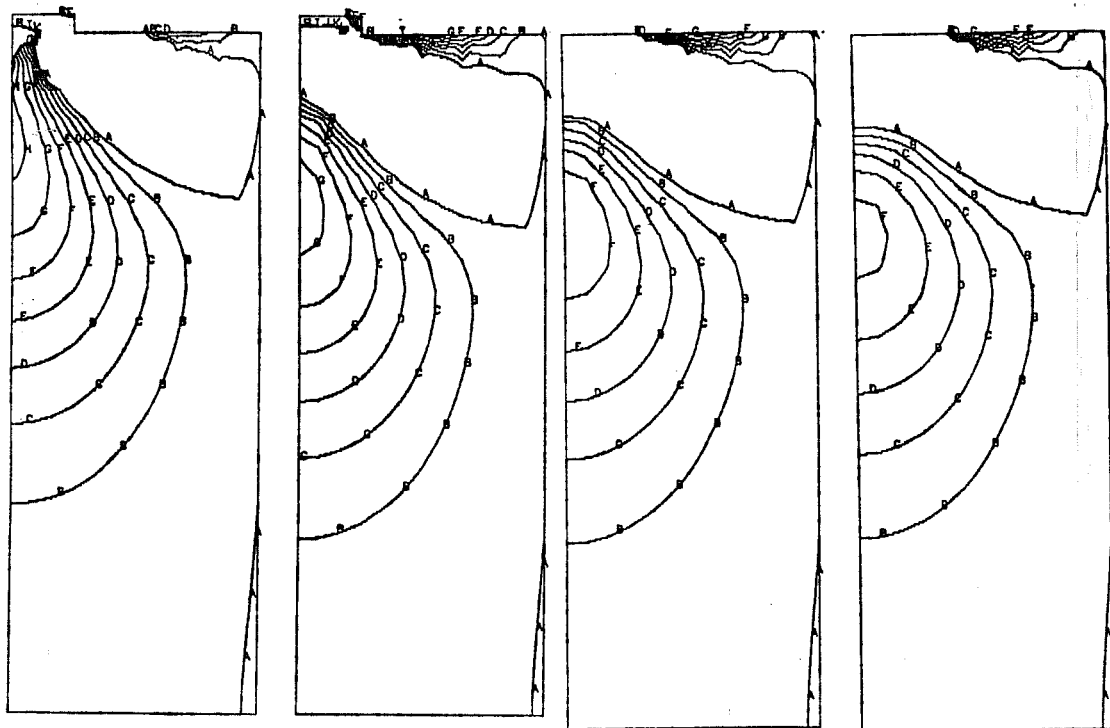
a) Complete Bond

c) Uniform Pressure

b) No Transverse Bond

d) Rigid Plate

A = 0.000 σ_0 B = 0.054 σ_0 C = 0.108 σ_0 D = 0.162 σ_0 E = 0.216 σ_0
F = 0.270 σ_0 G = 0.324 σ_0 H = 0.378 σ_0 I = 0.432 σ_0 J = 0.486 σ_0

Fig. 4.65   Contour Plot of Transverse Stress for Various Models of the Anchorage Plate

Applied tendon
load

Bending stresses
in the steel plate

Bearing
stresses

Steel plate

Tensile stresses
in the concrete
induced by
the bending of
the anchor plate
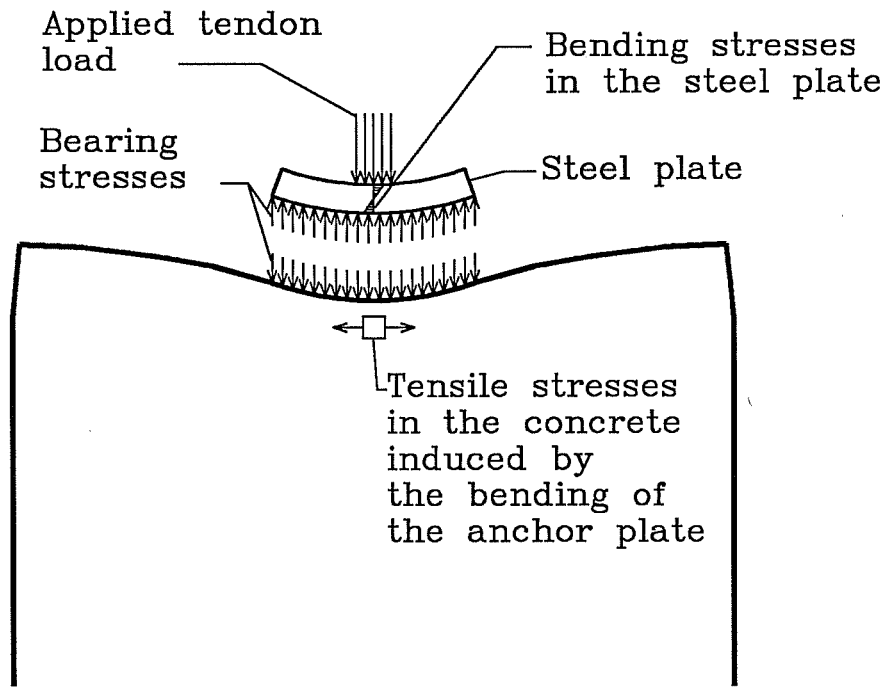
Fig. 4.66   Conceptual Model for the Full Bond Between the
             Anchor Plate and the Concrete

This study of the influence of the modelling of the anchor
plate shows that the anchorage device can have a substantial
influence on the state of stresses if a perfect bond exists
between the anchor plate and the concrete. If this is not the case
because of slip, of yielding of the anchor plate (the plate is
subjected to very high bending moments) or because of
microcracking of the concrete, then the stress distribution is not
considerably influenced by the modelling of the plate.

During the early part of the testing, careful attention was
given to try to observe evidence of a bond between the anchor
plate and the concrete. No conclusive proof was found to support
this assumption. Even though the bursting cracks along the tendon
axis usually extend all the way up to the anchor plate during the
test, these cracks are likely to be caused by the lateral

expansion of the concrete in the local zone. The cracks never appeared to be initiated at the anchor plate. Therefore it has been concluded that a full bond is not present between the anchorage plate and the concrete.

The available analytical solutions [75, 111, 169] generally consider the load as applied through a uniform pressure acting on the whole surface of the anchorage device. Even though no discussion of the reason for this choice was found, it appears from the available test results that such a model corresponds well to the reality.
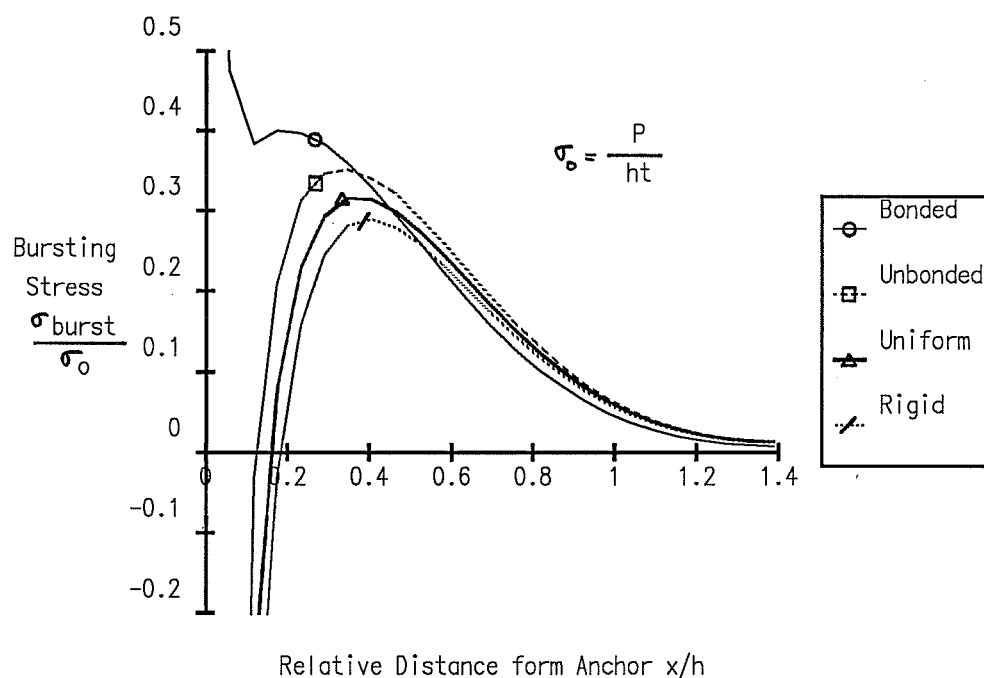
Fig. 4.67   Bursting Stresses along the Tendon Axis for Various Models of the Anchor Plate
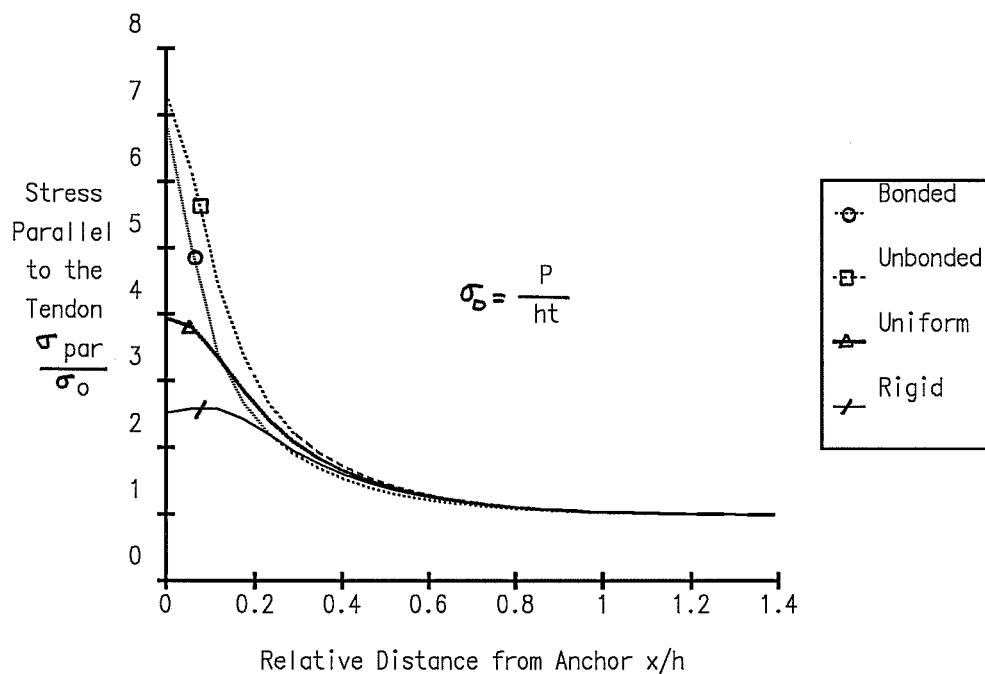
Fig. 4.68   Compressive Stresses Along the Tendon Axis for
             Various Models of the Anchor Plate

In the rest of this study, the loads are considered as applied through uniform pressures acting on the whole surface of the anchorage device. Even though this hypothesis is certainly not completely valid, especially for anchorages with multiple bearing planes, it was found experimentally that the accuracy of this assumption is sufficient, especially considering the other uncertainties in the analysis model. A more complete analysis should not only include the exact geometry of the anchorage device, but also a model for the slip at the interface between the concrete and the anchor, as well as the effect of the local zone confinement. Such an analysis is certainly possible, but goes beyond the scope of this investigation.

In subsection 4.4, it was proposed that to obtain

conservative solutions, it is possible to consider the anchorage plate as smaller than it is in reality. This will lead to larger bursting stresses, as well as larger bearing stresses. However, this type of procedure seems difficult to implement in practice because at time of design the engineer knows very little of the actual geometry of the anchorage device that will be finally used in construction.

4.6.3 Three-Dimensional Effects

It has been mentioned in section 4.2 that most of the Finite Element Analyses of this study were performed on two-dimensional plane models. The purpose of this subsection is to demonstrate the differences observed between the results of three-dimensional and two-dimensional analyses and to point out the limitations of the plane stress analysis.

While plane stress models can accurately represent the state of stresses in thin sections, they are unable to give information on the distribution of stresses through the thickness and to describe the local influence caused by a change in the cross sectional area such as the presence of a the tendon duct. Three-dimensional models using brick elements as shown in Fig. 4.69, with either 8 or 20 nodes, can more accurately model such changes. However this increase in accuracy comes at the expense of considerably longer computation times, due to the larger number of degrees of freedom as well as the larger bandwidth caused by the third dimension. For these reasons, it is not expected that three-dimensional solid analysis models will be used very often in practice for the design of anchorage zones.

Fig. 4.69   Finite Element Mesh for 3-D Analysis of Concentric
            Anchorage Zone
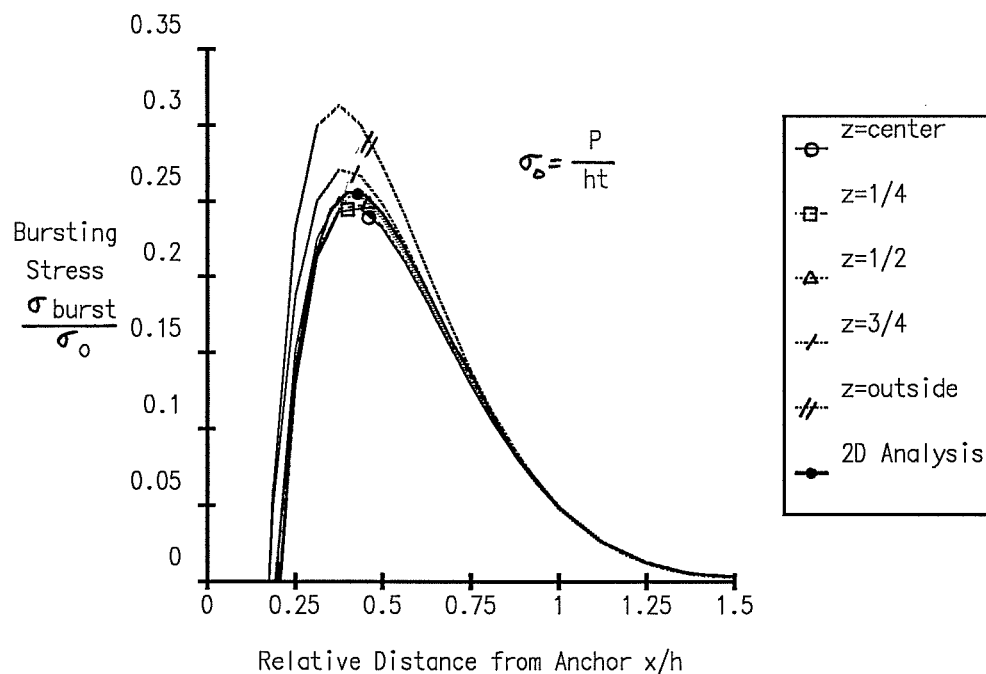
Fig. 4.70   Bursting Stresses: Comparison of 3-D Analysis with
             2-D Analysis

Fig. 4.70 shows the distribution of the bursting stress in the transverse plane containing the tendon axis as obtained from a 3-D analysis using 8-node brick elements. The distribution of bursting stresses obtained from a two-dimensional analysis is also shown in Fig. 4.70. The results of the three-dimensional analyses are generally close to the results previously obtained using a two-dimensional analysis. The stresses on the outside of the model, are higher than the stresses in the inside.

The strains reported by Zielinski and Rowe [196, 197], where the measurements were taken on the surface of the specimens, are consistently and noticeably larger than the values in this study. Although the exact configuration of Zielinsky and Rowe was not modelled, it is assumed that locally higher strains exist at the

surface of the concrete. But the average stress over the thickness, which is most important for the design, is lower than the values reported by Zielinsky and Rowe.

The influence of the duct hole on the stress distribution in the vicinity of the hole was investigated using the three-dimensional Finite Element model shown in Fig. 4.71. Only one quarter of the doubly symmetric anchorage zone was modelled. The tendon duct is represented by a square prism. This simplification in the geometry of the tendon duct was made in order to limit the complexity of the three-dimensional Finite Element model; except for areas of stress concentration close to the tendon duct, the stresses obtained from this model should give a good approximation of the stresses caused by a circular duct. The bursting stress distribution in the transverse plane including the tendon is shown in Fig. 4.72. These figures also include the results obtained from a two-dimensional analysis, adjusted by the ratio of the gross area to the net area across the tendon to account for the reduction of section caused by the tendon. The stresses obtained from the three-dimensional Finite Element analyses are higher than the stresses predicted by the simpler two-dimensional analyses. However the differences are comparatively small.

As a result of this investigation of the three-dimensional effects for thin specimens, it was concluded that the accuracy of two-dimensional analyses is sufficient for the majority of the specimens that are to be investigated in this phase of the project. For the more complex configurations that involve specimens whose dimensions are approximately equal in both directions, a 3-D analysis may become necessary.
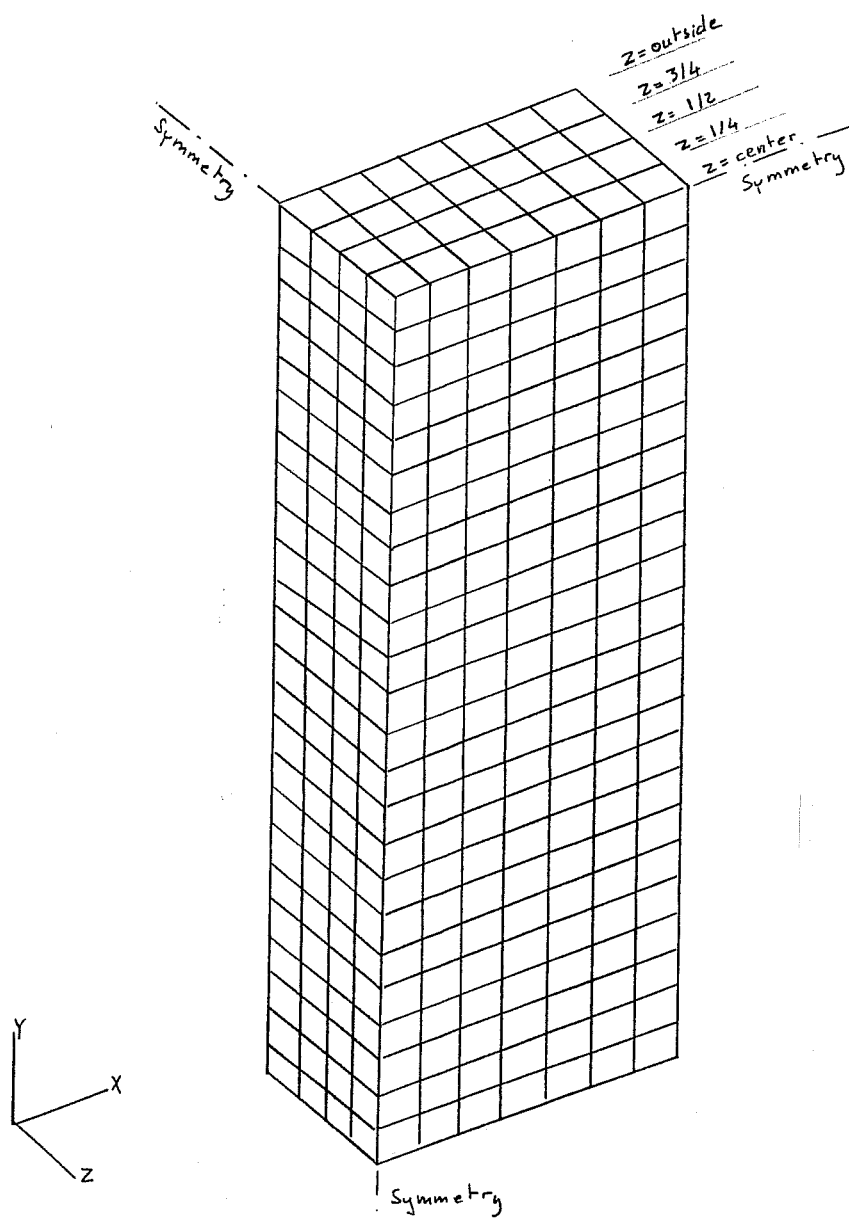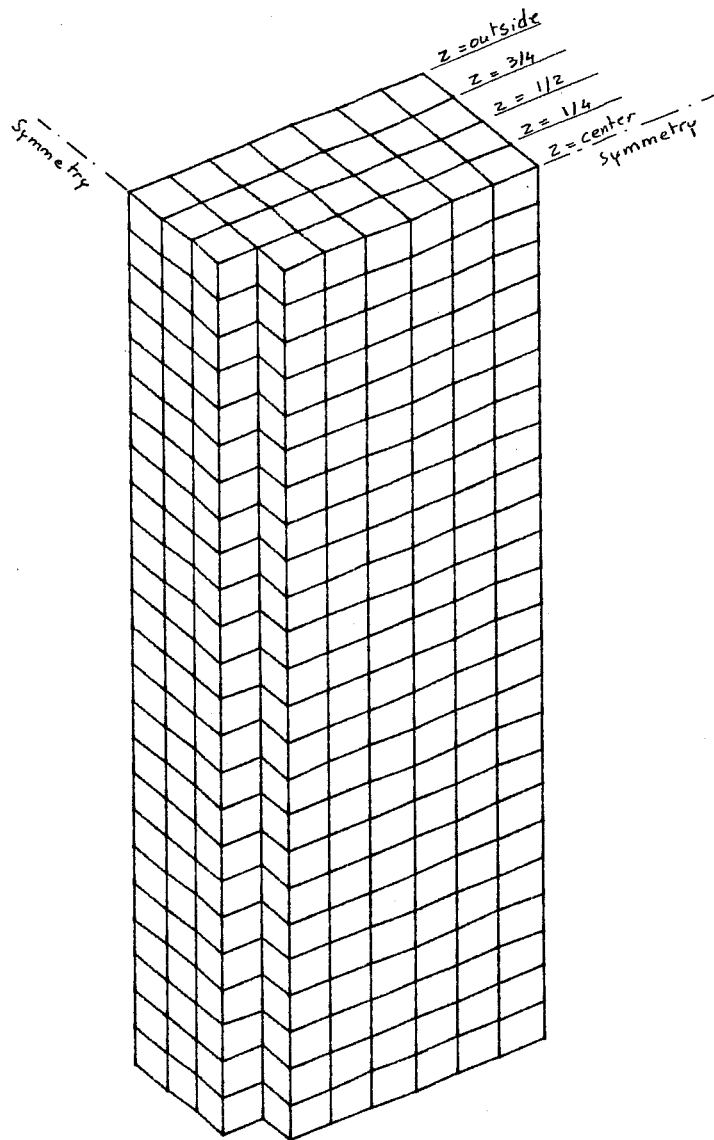
Fig. 4.71   Finite Element Mesh for 3-D Analysis of Concentric
            Anchorage Zone with Duct Hole
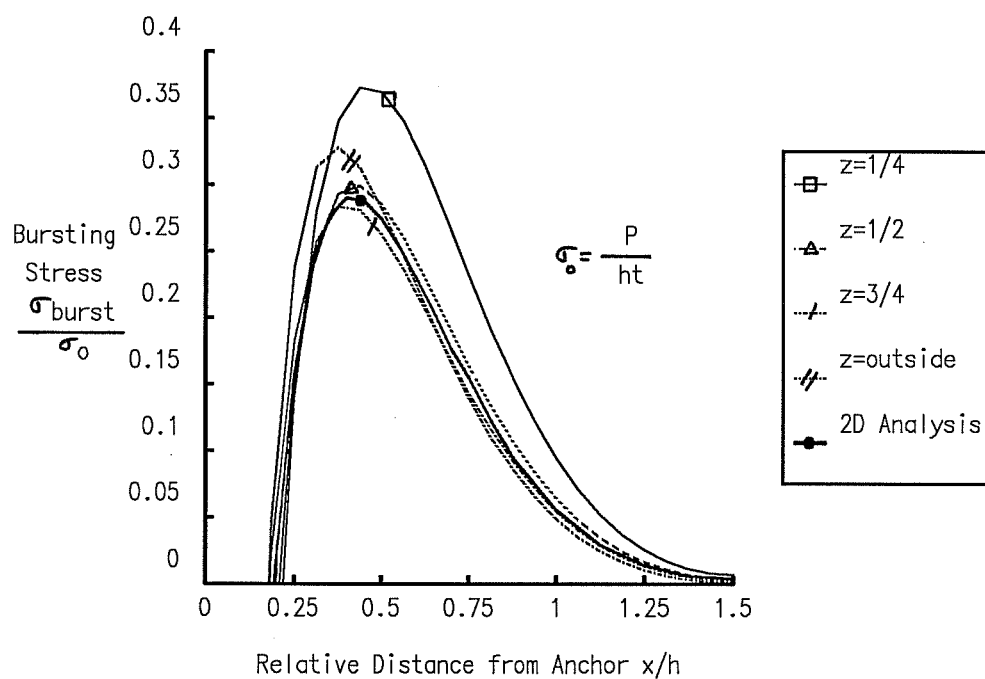
Fig. 4.72   Bursting Stresses: Comparison of 3-D Analysis
             Including a Duct Hole with 2-D Analysis (with
             Correction)

Chapter 5: Other Single Anchor Configurations

One of the main advantages offered by post-tensioning is the freedom available to the designer in the layout of the post-tensioning cables. The designer can select the trajectories and curvatures of the cables to correspond precisely to the specific requirements of the structure being built. In most cases, this leads to tendons with an eccentricity, an inclination, and possibly a curvature of the tendon in the anchorage zone (see Fig. 4.1 in Chapter 4). This chapter discusses these more complex configurations for single cable anchorage zones. The basic rules presented in Chapter 4 are expanded to include the case of eccentric, inclined and curved tendons.

5.1   Eccentric Anchorages

Anchorage zones with eccentric anchorages, as shown in Fig. 5.1, are very common in practice. If the eccentricity e of the post-tensioning force is small, that is if the load is applied within the kern of the section ($e/h \leq 0.167$ for a rectangular cross section), the state of stress in the anchorage zone is generally similar to that previously observed for concentric anchorages. There is an area of tensile bursting stresses along the axis of the tendon and two areas of tensile spalling stresses on either side of the anchorage plate, as shown in Fig. 5.2a.

If, however, the load is applied outside of the kern ($e/h > 0.167$ for a rectangular cross section), the state of stress in the anchorage zone is more complex. An additional area of tension parallel to the tendon path appears on the side face furthest from the anchorage device. This tension field results from the bending moment caused by the force applied outside of the kern of the section. The corresponding tensile stresses are called

flexural tensile stresses (Fig. 5.2b). Concurrently with the appearance of flexural tensile stresses, the spalling stresses and force increase considerably as the region subjected to spalling stresses becomes connected to the region subjected to flexural tensile stresses.
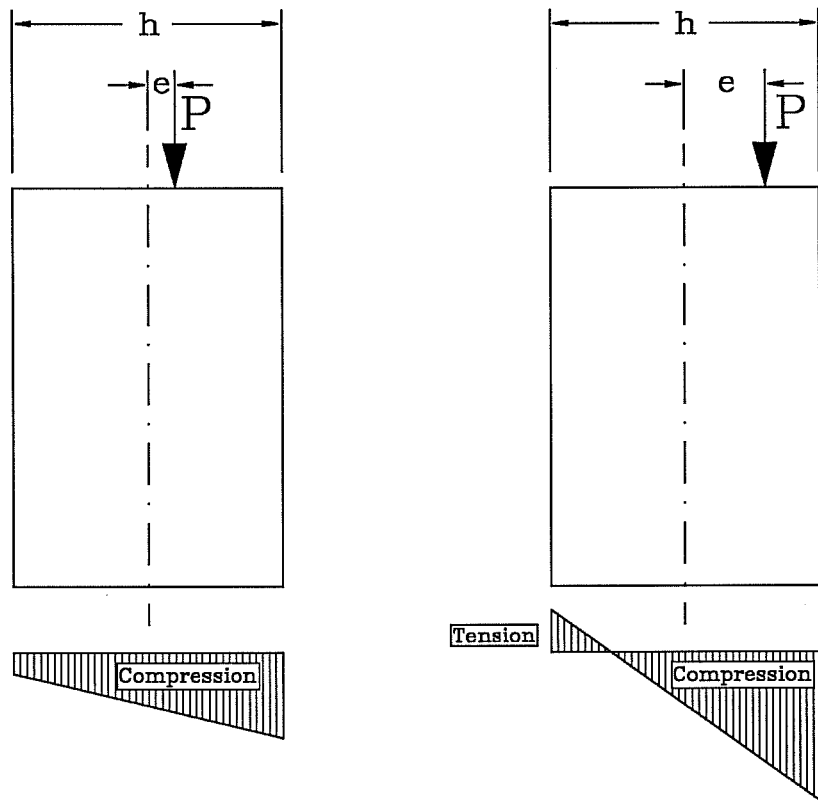
a) Load within the kern   b) Load outside of the kern

Figure 5.1   Load and Reactions for Eccentric Load Cases

Spalling Stresses   Spalling Stresses

Bursting Stresses

Bursting Stresses

Flexural Tensile Stresses

a) Load within the kern   b) Load outside the kern
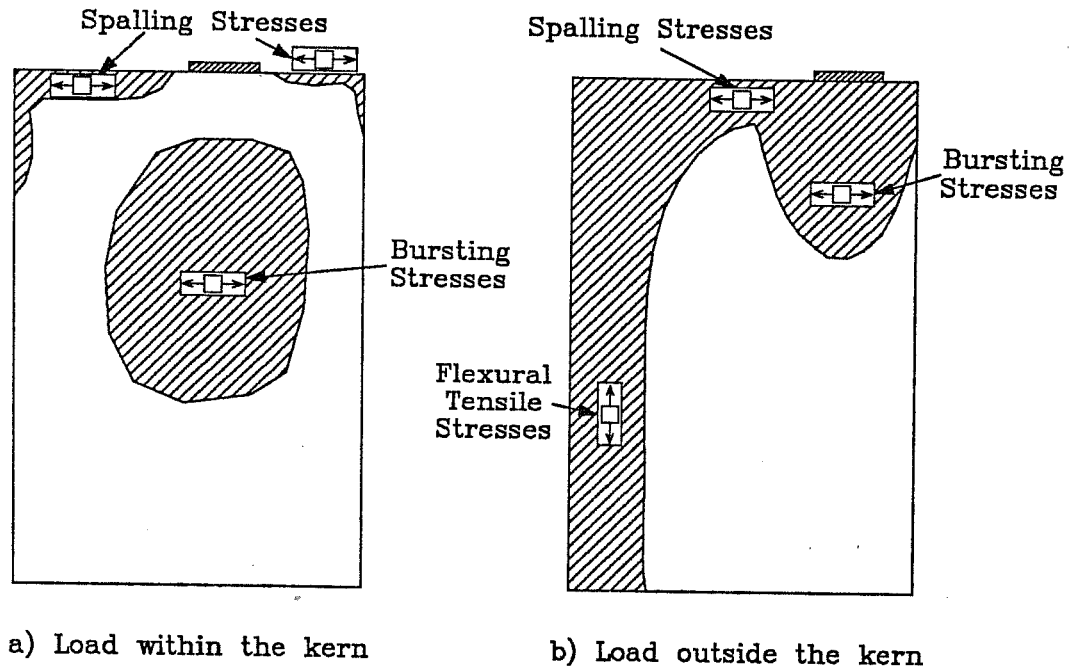
Figure 5.2   Areas of Bursting, Spalling and Flexural Tensile
             Stresses for Eccentrically Loaded Anchorage Zones

5.2   Finite Element Analysis of Eccentric Anchorages

In a manner similar to the approach used for concentric
anchorage zones, a series of Finite Element analyses was performed
for eccentric configurations. The Finite Element meshes used for
these analyses were mostly identical to the meshes used for the
concentric cases. Parametric studies were performed by varying the
relative eccentricity e/h of the loading from 0.0 (no
eccentricity) to 0.4. The largest theoretically possible
eccentricity is 0.5 (load on the edge of the section), but there
is a practical limitation because of the dimensions of the
anchorage plate. The relative size of the anchorage plate a/h was

also varied in the parametric studies. In all cases the load was introduced as a uniform pressure over the surface of the anchorage plate.

5.2.1 Bursting Stresses

The bursting stresses observed for eccentric configurations with straight tendons parallel to the centroidal axis of the section are similar in distribution and location to the bursting stresses for concentric anchorages. Close to the plate, there is a zone of very high compressive stresses, followed by a sharp gradient leading to the peak tensile stresses, and then a slower
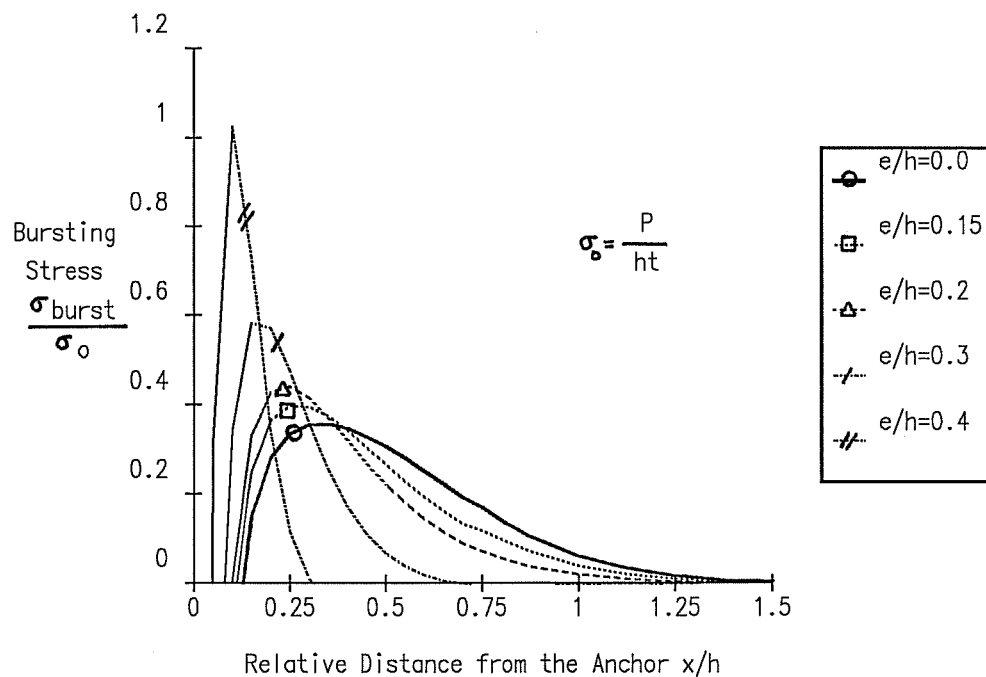
Figure 5.3   Bursting Stresses across the Tendon Axis for Various Eccentricities and a Relative Plate Size a/h=0.1

decrease of the stresses reaching zero at a certain distance from the anchor.

Figure 5.3 shows the distribution of tensile bursting stresses along the tendon axis for various eccentricities and a relative plate size a/h=0.1.
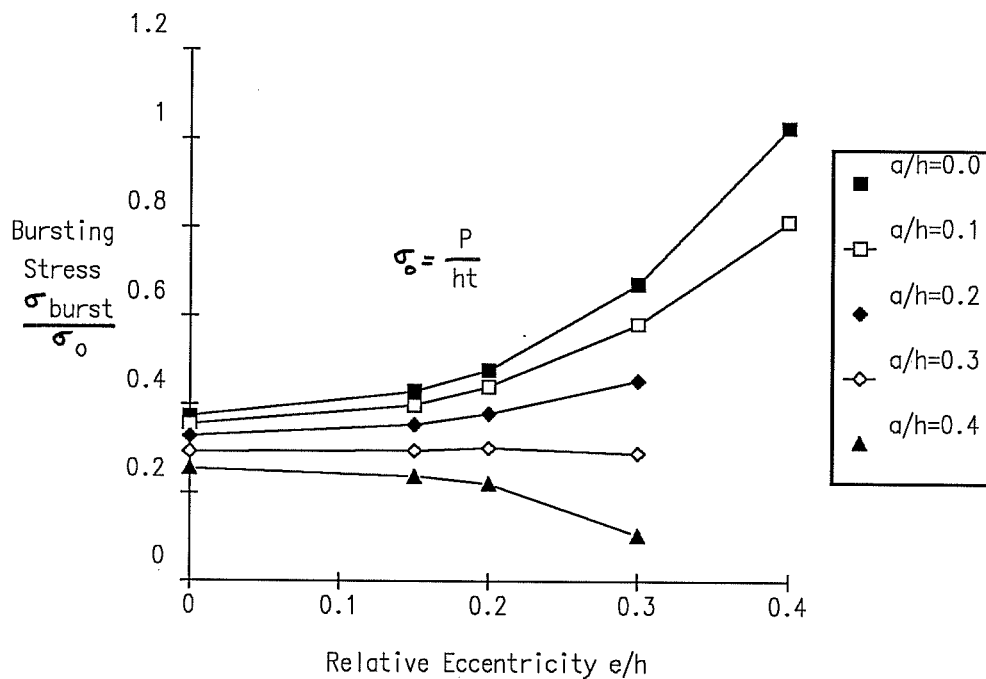
Figure 5.4   Maximum Bursting Stress across the Tendon Axis as a
             Function of the Eccentricity for Various Plate Sizes

In most cases, the magnitude of the peak tensile bursting stress increases with increased eccentricity, as shown in Fig. 5.4. However, the eccentric loading bursting stresses are acting over a reduced length when compared to concentric anchorages, as can be observed in Fig. 5.3. As a consequence, the bursting force actually decreases with increased eccentricity of the load. Fig. 5.5 shows the bursting force as a function of the

relative eccentricity and of the relative plate size. For a given plate size, the bursting force decreases almost linearly with increasing eccentricity of the loading. Because the largest bursting force occurs for zero eccentricity, a conservative estimate of the bursting force is to take it as the value obtained for no eccentricity. Fig. 5.5 shows by dotted lines the force obtained by the simplified formula given in Eq. 5.1, which was previously proposed for concentric specimens. Except for giving values just slightly under the elastic values for cases with no eccentricity, this simplified formula gives a generally conservative estimate of the bursting force for use in design.

$$T_{burst} = 0.25 \cdot P \cdot (1-a/h) \quad (Eq. \ 5.1)$$
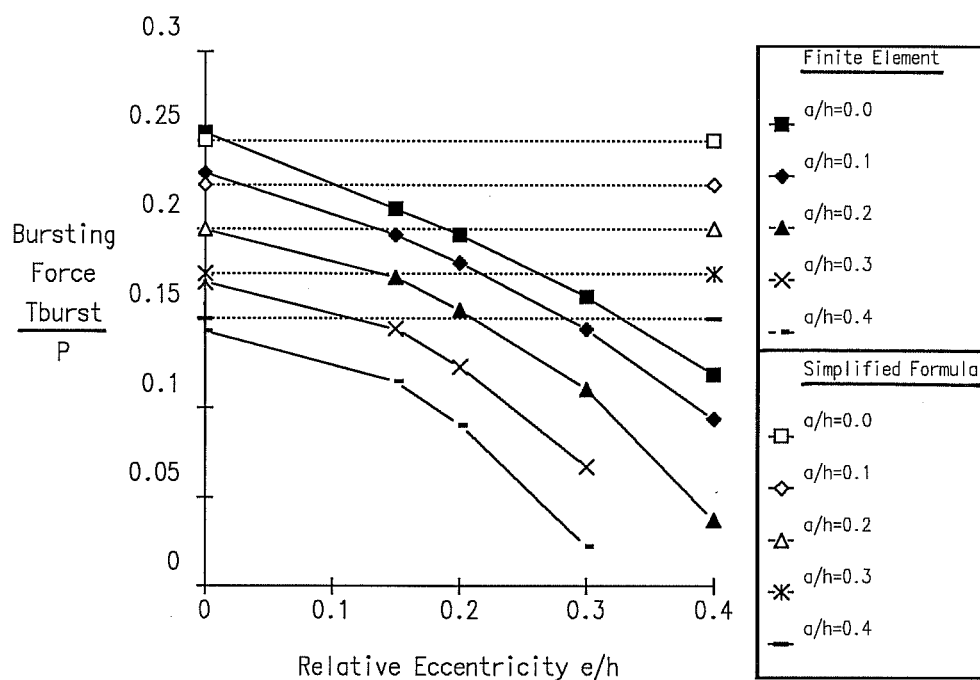
Figure 5.5   Bursting Force across the Tendon Axis as a Function of the Eccentricity for Various Plate Sizes

Fig. 5.6 shows the relative location of the centroid as a function of the eccentricity for various plate sizes. As already noted for concentric configurations, the location of the centroid is essentially independent of the plate size. The location of the centroid remains nearly constant for loads within the kern of the section. For larger eccentricities, the location of the centroid decreases almost linearly with the eccentricity.

5.2.2 Flexural Tensile Stresses

Flexural tensile stresses are the stresses induced by the
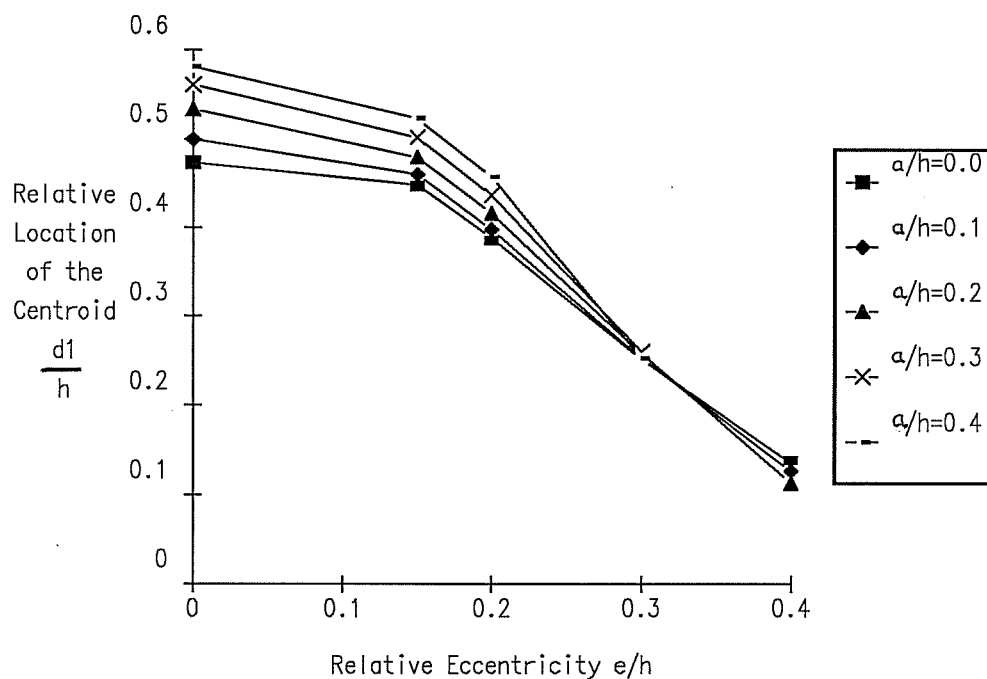
Figure 5.6   Relative Location of the Centroid of the Bursting Stresses as a Function of the Eccentricity for Various Plates Sizes

combined axial and flexural loading of the section under an eccentrically applied post-tensioning load (see Section 5.1). These stresses and the corresponding flexural tensile force can be determined using simple combined axial and flexural action theory. If the load is applied inside of the kern of the section, all stresses at the end of the general zone are in compression, as shown in Fig. 5.1a. However, if the load is applied outside the kern, tensile flexural stresses are induced at the end of the general zone opposed to the anchor, as shown in Fig. 5.1b.
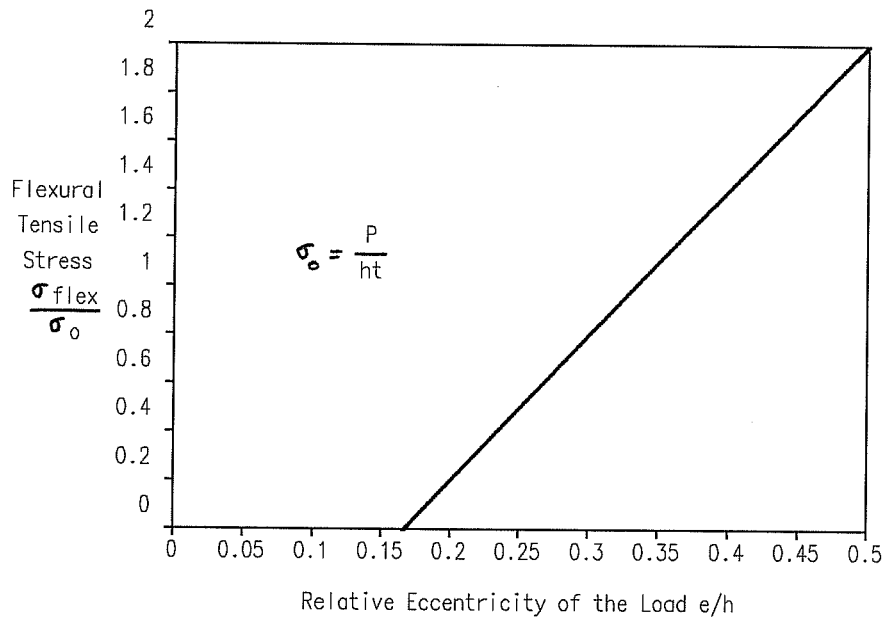
Figure 5.7 Maximum Flexural Tensile Stress Produced by Eccentric Loading as a Function of the Eccentricity of the Load (for a Rectangular Section)

The maximum value of the flexural tensile stress in a rectangular section is:

$$\sigma_{max} = 2 \cdot \sigma_0 \quad (Eq. 5.2)$$

with

$$\sigma_0 = P \ / \ (h \cdot t)$$

The corresponding maximum flexural tensile force is:

$$T_{max} = 0.333 \cdot P \quad (Eq. 5.3)$$
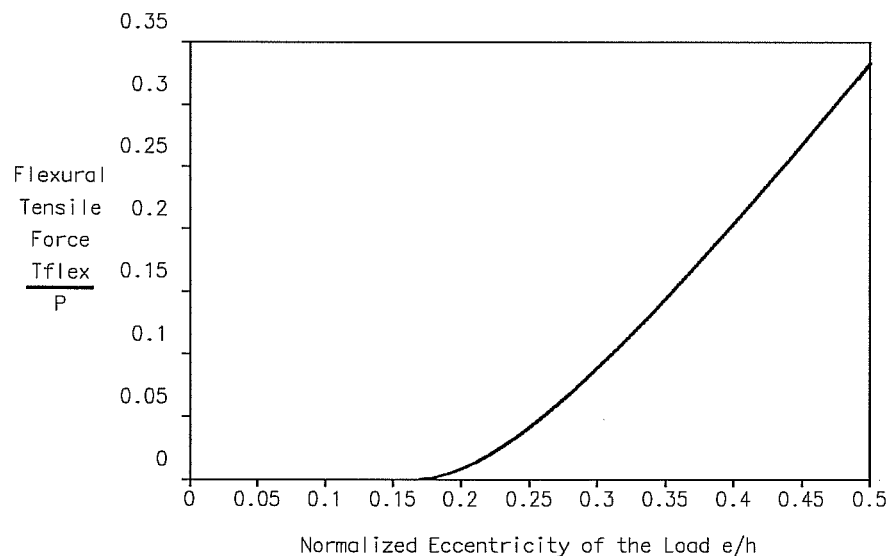
Figure 5.8   Flexural Tensile Force Produced by the Combined
              Axial and Flexural Action as a Function of the
              Eccentricity of the Load

Because the anchorage plate has finite dimensions, the values given by Eqs. 5.2 and 5.3 are upper bounds, and are only attainable with an infinitely small anchorage plate. Fig. 5.7 shows the maximum flexural tensile stress from combined stress

theory (in a rectangular cross section) as a function of the eccentricity of the load. Fig. 5.8 shows the flexural tensile force induced by the combined axial and flexural action as a function of the eccentricity of the load.

5.2.3 Spalling Stresses

As mentioned in Chapter 4, the spalling stresses in concentrically loaded anchorage zones are large but the corresponding spalling force is small. This observation remains valid for eccentric tendons with the load applied within the kern of the section. For larger eccentricities however, the spalling force increases rapidly to magnitudes close to the magnitude of the bursting force. For example, compare the values for the spalling forces in Fig. 5.9 with the values for the bursting forces in Fig. 5.5.

Fig. 5.9 also shows the flexural tensile force due to combined axial and flexural action on the section. For large eccentricities, the curve of the flexural tensile force is nearly parallel to the curve of the Finite Element spalling force results, indicating a linear relationship between the spalling force and the flexural tensile force. The contour plot of the maximum principal stress (in tension) shown in Fig. 5.10 and the vector plot of the principal stresses shown in Fig. 5.11 further illustrate the direct connection between the stresses induced by the overall bending of the section and the spalling stresses at the top surface.
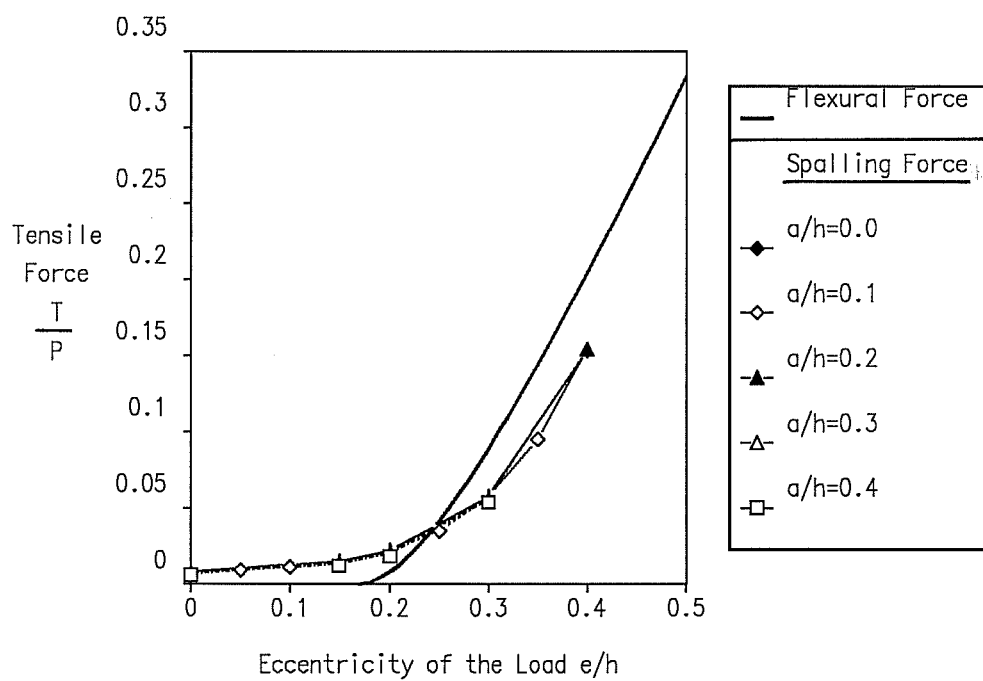
Figure 5.9   Flexural Tensile Force and Spalling Force as a
             Function of the Eccentricity of the Load for Various
             Plate Sizes
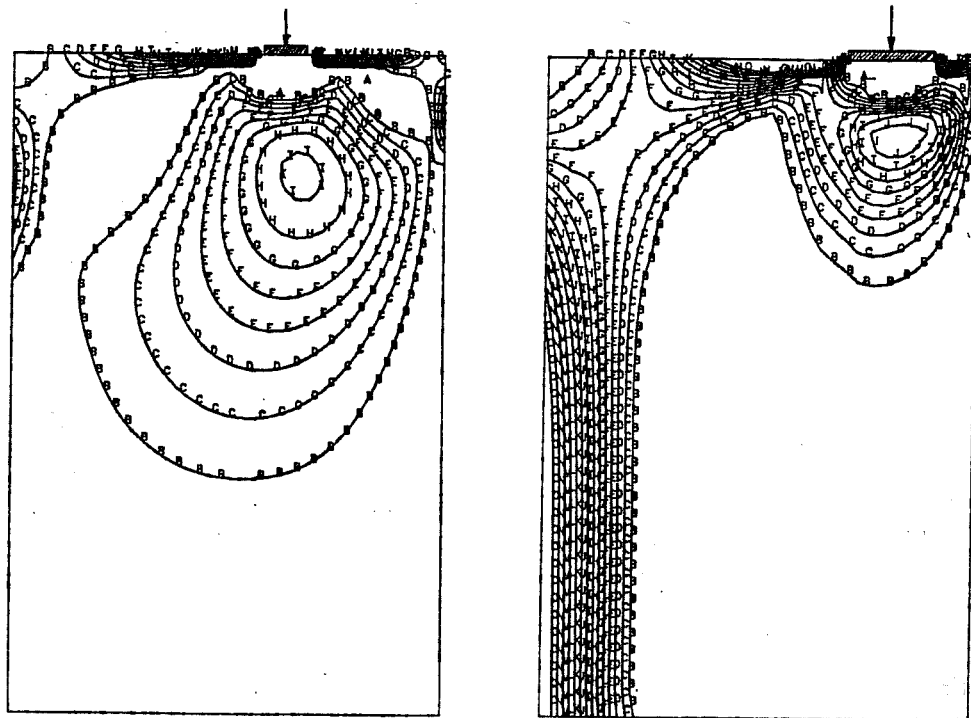
a) Eccentricity e=0.125h   b) Eccentricity e=0.250h

A = 0.00 σ_o B = 0.05 σ_o C = 0.10 σ_o D = 0.15 σ_o E = 0.20 σ_o F = 0.25 σ_o G = 0.30 σ_o
H = 0.35 σ_o I = 0.40 σ_o J = 0.45 σ_o K = 0.50 σ_o L = 0.55 σ_o M = 0.60 σ_o N = 0.65 σ_o

Figure 5.10   Contour plot of the Maximum Principal Stress for
              Eccentric Cases with Load Acting Within and Outside
              the Kern

a) Load within the kern
(e/h=0.125)
Maximum Principal Stress

b) Load outside of the kern
(e/h=0.25)
Maximum Principal Stress

c) Load within the kern
(e/h=0.125)
Minimum Principal Stress

d) Load outside of the kern
(e/h=0.25)
Minimum Principal Stress
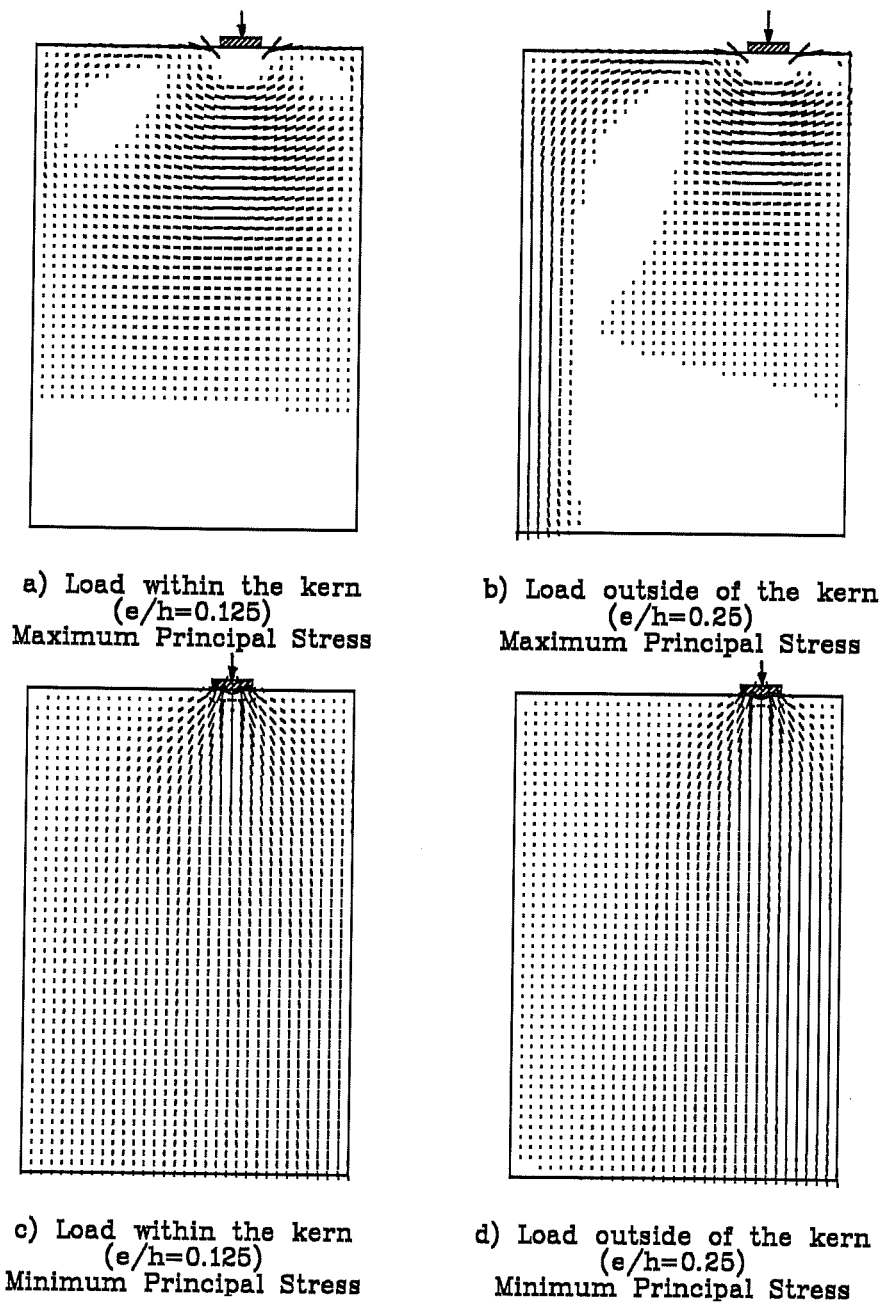
Figure 5.11   Vector Plot of the Principal Stresses for Eccentric
Cases with Load Acting Within and Outside the Kern

A	= 0.00 σ_0
B	= 0.05 σ_0
C	= 0.10 σ_0
D	= 0.15 σ_0
E	= 0.20 σ_0
F	= 0.25 σ_0
G	= 0.30 σ_0
H	= 0.35 σ_0
I	= 0.40 σ_0
J	= 0.45 σ_0
K	= 0.50 σ_0
L	= 0.55 σ_0
M	= 0.60 σ_0
N	= 0.65 σ_0
O	= 0.70 σ_0

a) Specimen with full Corners   b) Specimen with cut Corners
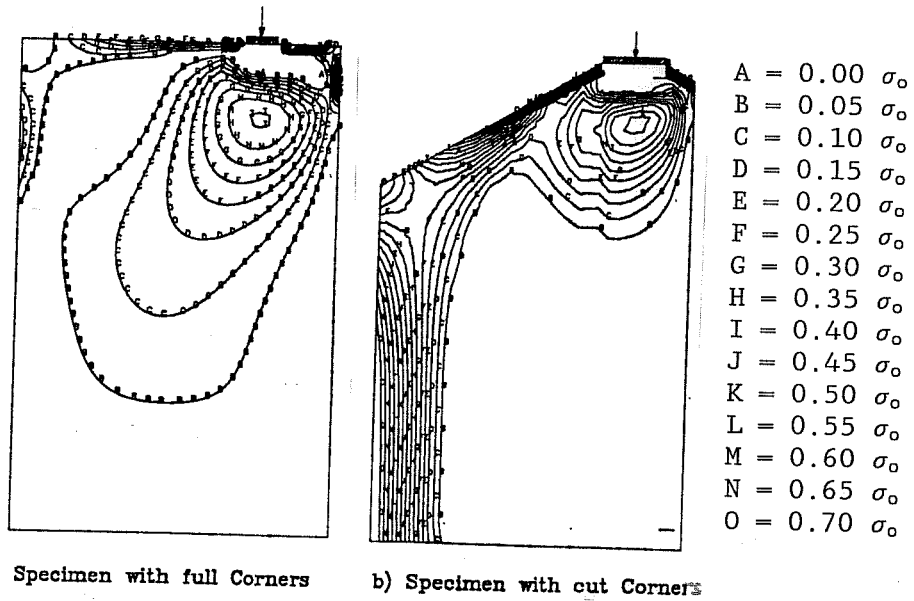
Figure 5.12   Contour Plot of the Maximum Principal Stress for Rectangular Section and Section with Cut Corners

a) Specimen with full Corners   b) Specimen with cut Corners
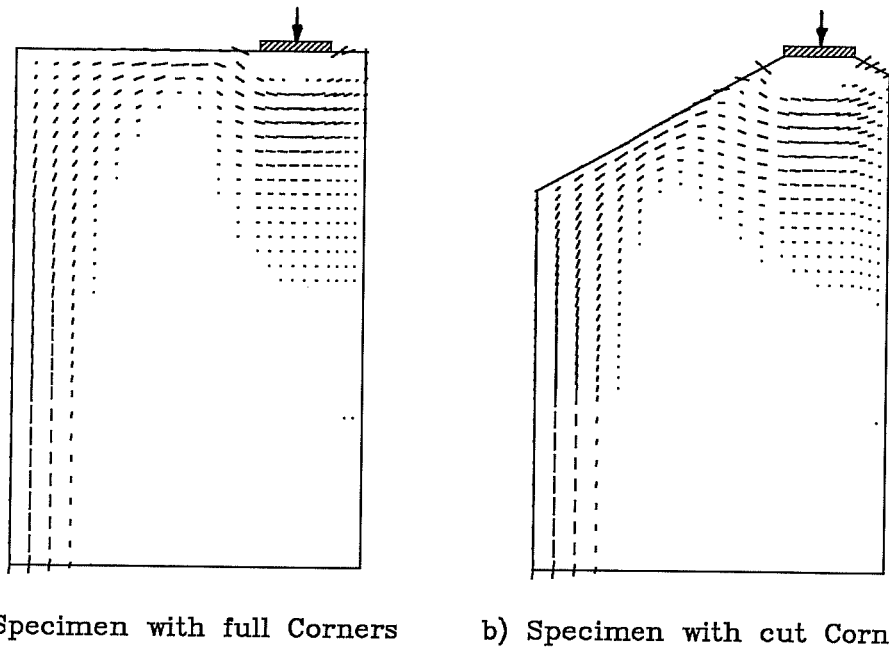
Figure 5.13   Vector Plot of the Principal Stresses for Rectangular Section and Section with Cut Corners

The flexural tensile forces are necessary for the overall equilibrium of the anchorage zone when the load is applied outside of the kern. The spalling forces are in this case strongly related to the flexural forces and are necessary for the overall equilibrium. Figures 5.12 and 5.13 illustrate that cutting the corners of the specimen does *not* eliminate the flexural and spalling stresses, because these stresses are induced not only by the conditions of compatibility, but are necessary for equilibrium of the section.

5.2.4 Comparison with Published Values

As in the case of concentric configurations, Guyon's work is the most complete and detailed for eccentric configurations. The fact, mentioned in Section 5.1, that the state of bursting stresses in eccentric configurations is similar to the state of stresses in simpler concentric configurations led Guyon [75] to introduce the concept of the *symmetrical prism*. The symmetrical prism, shown in Fig. 5.14 is defined as the largest prism that fits in the section with its symmetry axis coinciding with the axis of the tendon. The width a_2 of the symmetrical prism is limited by either an edge or by the boundary of a similar symmetrical prism of an adjacent tendon in the case of multiple tendons. If the tendon is placed concentrically in the middle of the section, the symmetrical prism will correspond to the depth of the member, in this case $a_2 = h$.
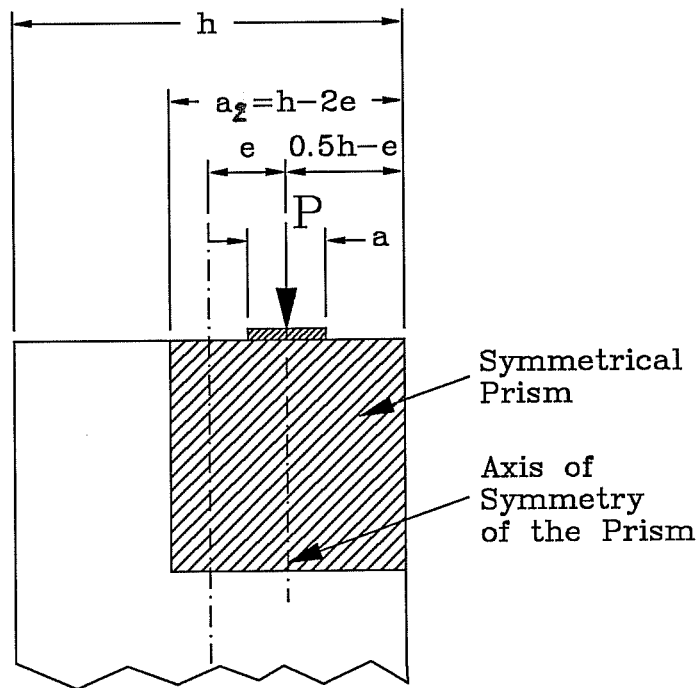
Figure 5.14   Geometric Definition of Guyon's Symmetrical Prism
              for Eccentrically Applied Post-Tensioning Forces

The symmetrical prism provides an approximation to the bursting stresses and forces for eccentric configurations by using the results for concentric configurations. The bursting stresses and forces acting on an eccentric configuration are computed as the bursting stresses and forces acting on the symmetrical prism defined in Section 5.2.4. Fig. 5.15 shows the value of the bursting force predicted by the symmetrical prism method compared to the results obtained from the Finite Element analysis, normalized to the ratio a_2/h instead of a/h to allow for comparison with the symmetrical prism. The Finite Element solutions are close to the simplified solution using the symmetrical prism. The largest discrepancies occur for small relative plate sizes, and are probably due to lack of convergence

of the Finite Element solution, as described in Chapter 4. The results for point loads have not been included in the figure. The linearized expression of Eq. 4.2 for the bursting force, with a factor of 0.25 is also shown in Fig. 5.15. As already observed for concentric configurations (see section 4.2.3), this expression gives very good results.

As pointed out by Stone, [172, 173] the symmetrical prism method, however, does not take into account the considerable difference in the spalling forces when the load is applied outside of the kern. Originally, Guyon indicated only a constant value of 4% of the tendon load as the design value for spalling forces.
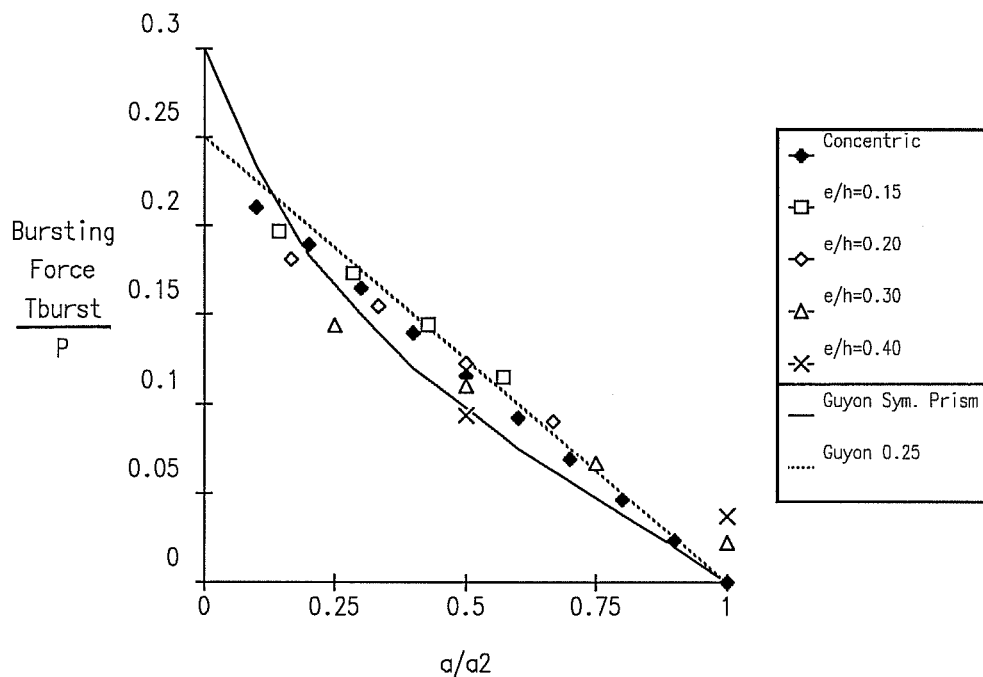
Figure 5.15   Comparison of the Bursting Force from Finite Elements Results with Guyon's Symmetrical Prism Theory

Fig. 5.16 shows that, for eccentricities larger than 0.25h this value is too small compared to the force obtained from Finite Element analyses. In later editions of his prestressed concrete textbook [74], Guyon addressed this point by suggesting that the total spalling force should be given by Equation 5.4 (rewritten for the notation used here).

$$T_S = (0.04 + 1.6 \cdot (e/h)^3) \cdot P \quad \text{(Eq. 5.4)}$$

This expression adds a term that is dependent on the eccentricity of the load to the constant 4% term. This equation is
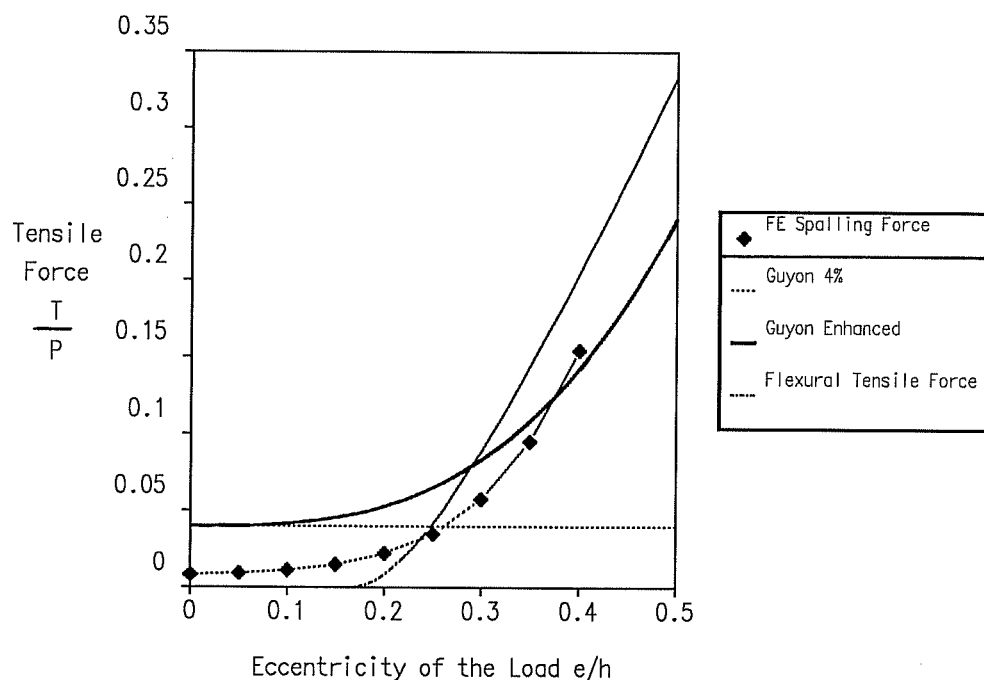
Figure 5.16   Spalling Force According to Guyon compared with Finite Elements Results and Bending Force

plotted in Fig. 5.16 along with the results of the Finite Element analyses and the tensile bending force obtained from simple beam theory. With the additional term, the improved Guyon formula is generally conservative, but it clearly overestimates the spalling forces for loads within the kern.

5.3   Strut-and-Tie Model for Eccentric Configurations

While the simple concentric Strut-and-Tie Model of Mörsch was proposed almost a century ago, Strut-and-Tie Models involving more complex configurations have only been proposed in relatively recent times. Schlaich et al [157, 158] give examples of Strut-and-Tie Models for eccentric configurations, as shown in Fig. 5.17.
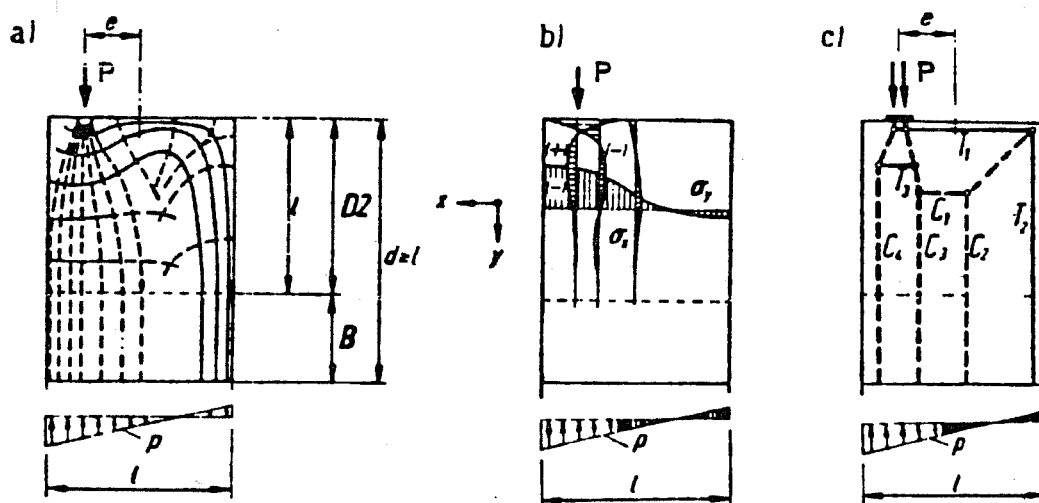
Figure 5.17   Strut-and-Tie Model for Eccentric Loading According
to Schlaich et al. [158]

5.3.1 Geometric Definition of the Strut-and-Tie Model

For the geometric definition of the Strut-and-Tie Model, the procedures described in Section 4.3.1 will be used. Fig. 5.18 shows the steps of the procedure to develop the Strut-and-Tie Model. The forces and reactions acting on the anchorage zone are first determined using simple beam theory (Fig. 5.18a), then lumped into discrete forces. The forces acting on one side of the post-tensioning cable are lumped separately from the forces acting on the other side; tension and compression forces are lumped separately. (Fig. 5.18b)

Force paths for at least 80% of the total force are drawn. Based on the force paths, corresponding struts and ties are drawn, and the forces in the members are calculated (Fig. 5.18c and d). Finally, the struts and ties corresponding to the remaining forces are introduced in the Strut-and-Tie Model (Fig. 5.18e). It is often necessary to slightly modify the geometry in order for the model to be stable, or at least kinematic, that is, stable for the given load case. These adjustments have usually only a small influence on the main forces.

As in the case of concentric tendons, simple equilibrium considerations would allow the determination of the ultimate load knowing the magnitude and the location of the tie force T_1, but the determination of the other tie forces, most notably T_3 would not be so evident. More elaborate Strut-and-Tie Models, including thrust-lines (see Section 4.3.5), can also be used with eccentric configurations. It is best to focus the use of thrust-lines on the limited number of struts that carry the majority of the load.

P

$\frac{P}{2}$ ↓↓ $\frac{P}{2}$

$\frac{P}{2}$ ↓↓ $\frac{P}{2}$

0.09P 0.26P
0.34P 0.49P

0.09P 0.26P
0.34P 0.49P

a) Geometry and
Loads

b) Forces and
Reactions

c) Force Paths

$\frac{P}{2}$ ↓↓ $\frac{P}{2}$

T1=0.19P

T3= 0.06P

$\frac{P}{2}$ ↓↓ $\frac{P}{2}$

T1=
0.19P

T2=
0.06P

T4=
0.09P

P

0.09P 0.26P
0.34P 0.49P

0.09P 0.26P
0.34P 0.49P

0.09P 0.26P
0.34P 0.49P

d) Main Compression
Struts

e) Tension Ties
and Solution

f) Comparison with
Elastic Stresses
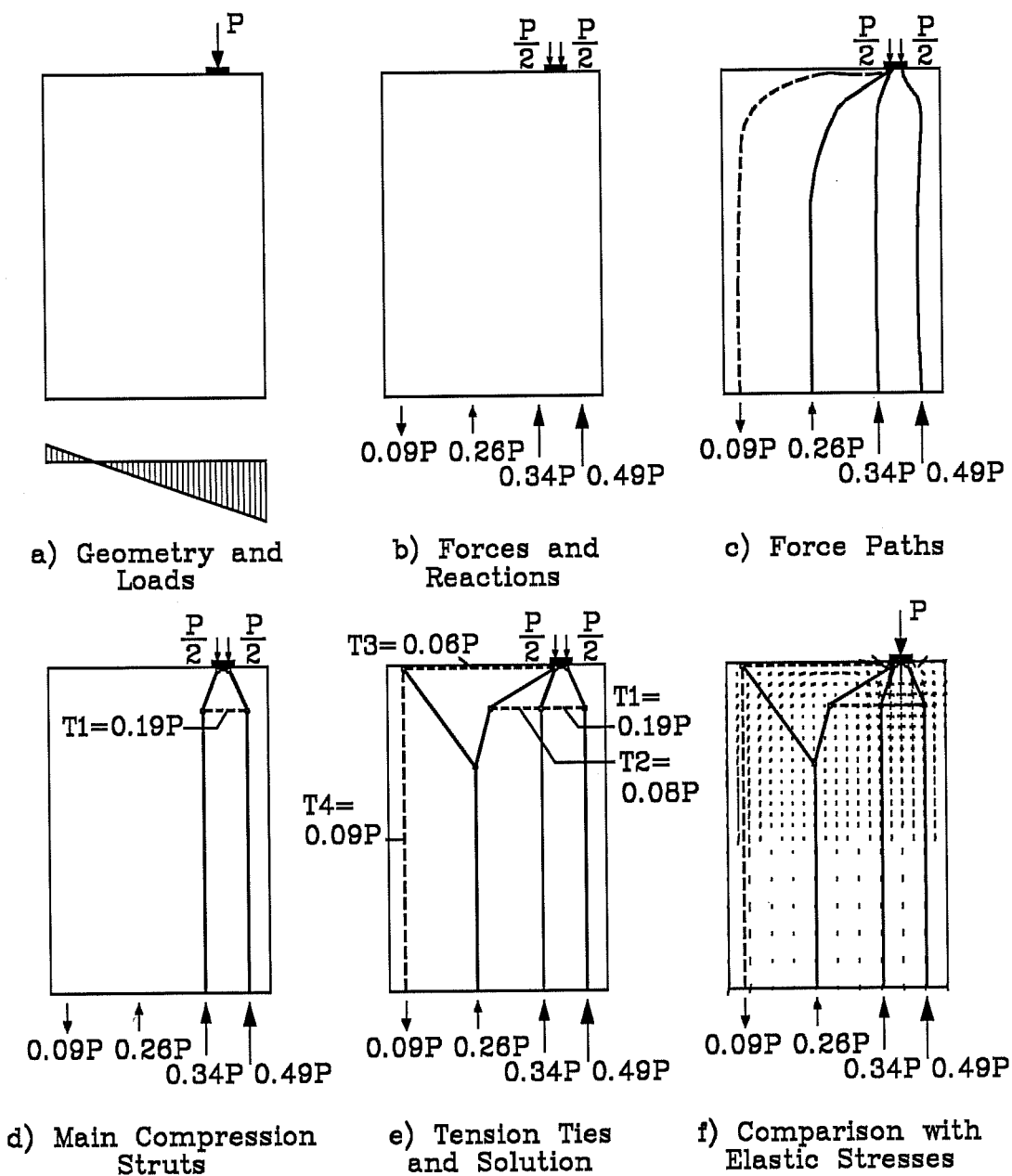
Figure 5.18   Steps for the Development of a Strut-and-Tie Model
for Eccentric Configurations

Because only equilibrium considerations are necessary to determine the ultimate capacity associated with a given bursting reinforcement pattern, the conclusions drawn in Chapter 4 for concentric configurations still apply. In order words, the ultimate capacity of the anchorage zone will not change if a simple Strut-and-Tie Model is replaced by a more elaborate model in the region of bursting stresses, as long as the centroid of the reinforcing steel does not change.

The region subjected to spalling and bending stresses involves forces smaller than the region subjected to bursting stresses. Therefore, it does not appear very effective to further refine the Strut-and-Tie Model in this area.

5.3.2 Parametric Study on the Influence of Eccentricity

A parametric study was performed using a Strut-and-Tie Model developed using the rules described in the preceding sub-section. Figure 5.19 defines the geometry of the Strut-and-Tie Model used for this parametric study and summarizes the additional constraints that were placed on the model. The depth d_1 at which the bursting force acts is defined as $(h/2-e)$, which corresponds to a diffusion angle of about 26 degrees. The relative plate size is $a/h = 0.2$. The width b_1 of the first compression strut (force P_1) is equal to the distance from the axis of the tendon to the edge of the concrete, $b_1 = h/2-e$. The width b_2 of the second strut (force P_2) is equal to the width of the compression strut b_1. The angle α_5 of the strut between nodes (5) and (7) is held constant at 35 degrees. This value is derived from the ratio of the spalling force to the bending force observed in Fig. 5.9 for large eccentricities. The location of the node (6) was iteratively adjusted so that the node would be in equilibrium without requiring a member between node (6) and node (5).
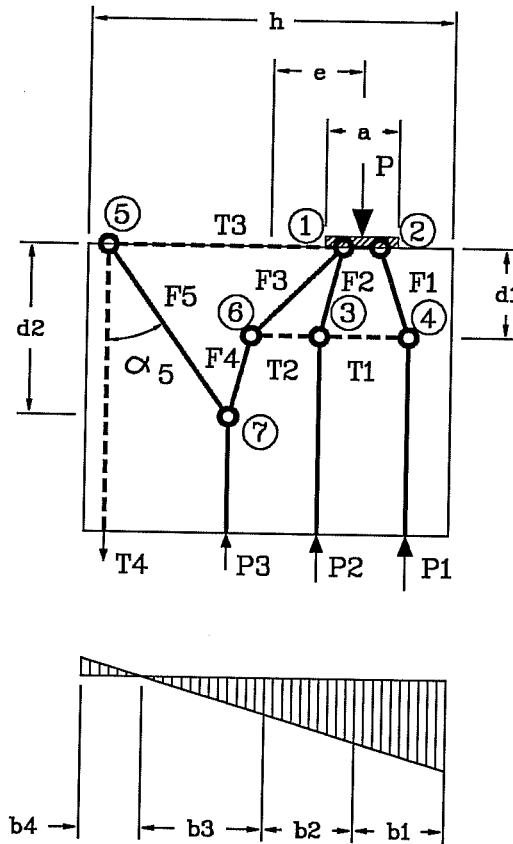
Figure 5.19 Geometric Definition of the Strut-and-Tie Model Used
for the Parametric Study of Eccentric Configurations

Fig. 5.20 shows the geometry as it evolves with increased eccentricity for a constant a/h = 0.2. Fig. 5.21 shows the forces in the struts and the ties as a function of the eccentricity.

a) No Eccentricity

b) Eccentricity e/h=0.1

c) Eccentricity e/h=0.3

d) Eccentricity e/h=0.4
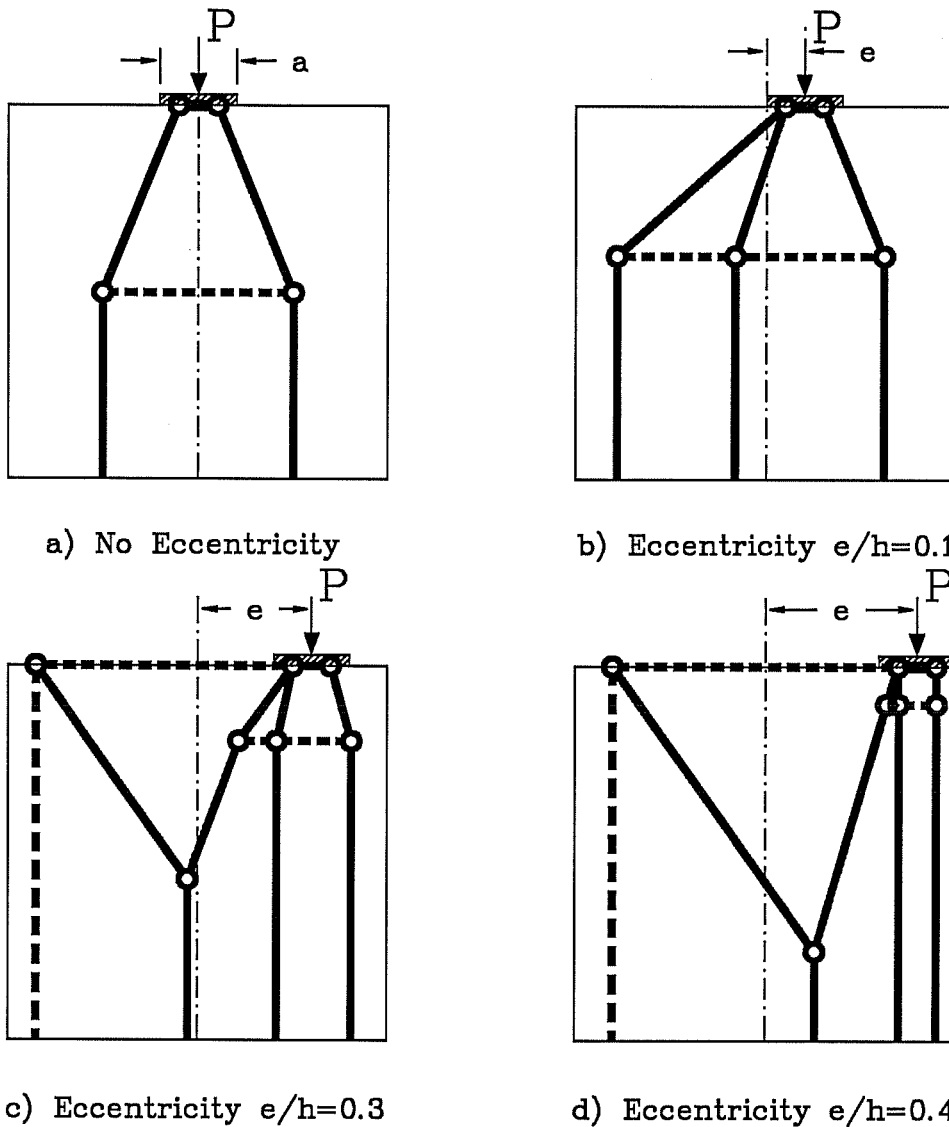
Figure 5.20   Geometry of the Strut-and-Tie Model Used in the Parametric Study for Various Eccentricities for a/h=0.2
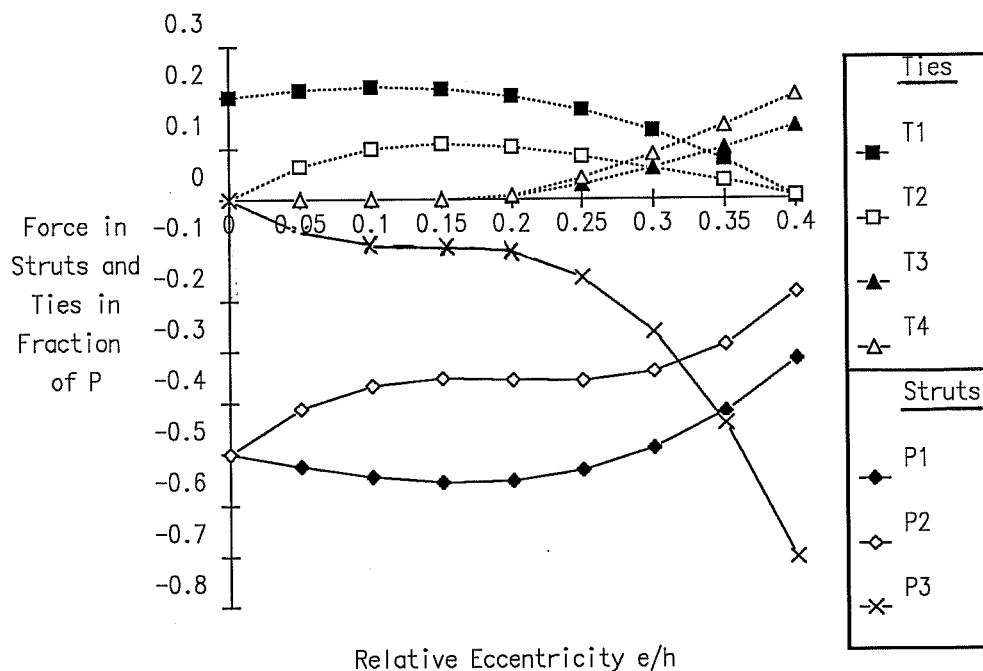
Figure 5.21   Forces in the Struts and Ties as a Function of the
              Eccentricity of the Load for a/h = 0.2

Fig. 5.22   shows the tension forces in the ties T_1 and T_2 as a function of the eccentricity, compared with the integrated bursting forces obtained from the Finite Element analysis. The correlation between the bursting force and T_1 is good, taking into account the relative simplicity of the model used. The magnitude of T_2, about one half of the bursting force T_1 for most eccentricities, indicates the necessity of extending the reinforcement laterally well outside of the region defined by the Guyon "symmetrical prism". Fig. 5.23 shows the flexural tensile force (T4) and the spalling force (T3) from the Strut-and-Tie Model compared to the results of the Finite Element analyses and Guyon's enhanced formula for spalling forces. The flexural tensile force obtained by the Finite Element method is not shown in the

figure, since it is identical to the value obtained by the Strut-and-Tie Model, and is defined by simple combined axial and flexural action theory. Here again, the correlation is good.
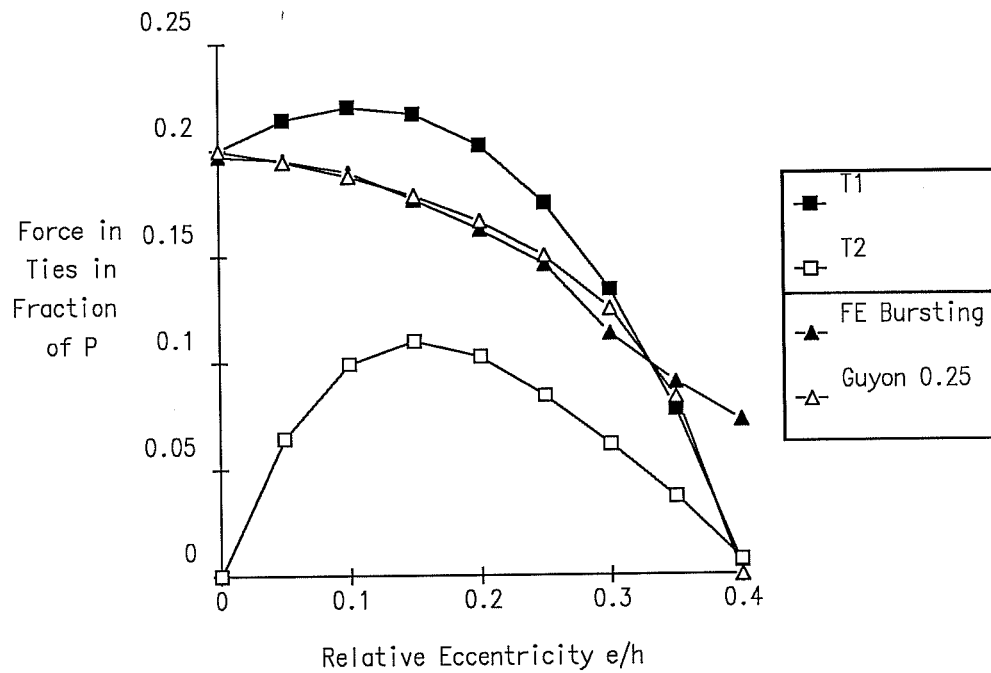
Figure 5.22 Tie Forces in the Bursting Region Compared with Finite Element Results and Guyon's Linearized Formula
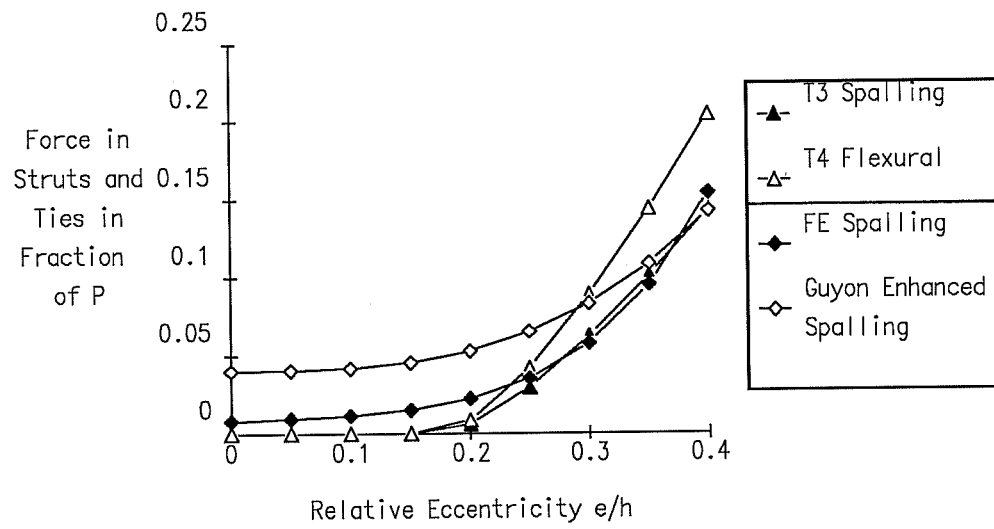
Figure 5.23 Tie Forces in the Spalling and Flexural Region
Compared with Finite Element Results and Guyon's
Enhanced Formula

5.3.3 Comparison with Test Results
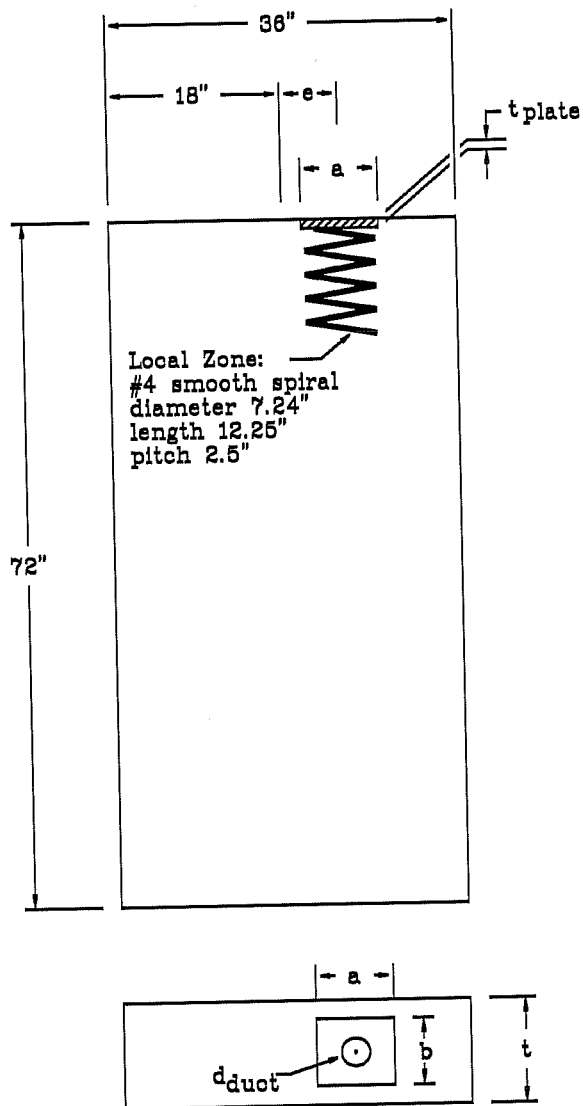
Figure 5.24   Geometry and Local
Zone Reinforcement of
Eccentric Specimens

In the overall UT Austin Research Project, a series of tests including eccentrically located anchorages was performed; the tests were labeled E1 to E6. In addition, one test of two anchors over the thickness of the specimen (M5) is also discussed in this section, because of the similitude of the geometry in the main plane of the specimen. The geometry of the specimens for these tests is shown in Fig. 5.24, along with the local zone reinforcement in form of a spiral. Table 5.1 summarizes the dimensions of the specimens and of the anchorage plate for the eccentric test series, as well as the concrete strength at testing. The outer diameter of the tendon duct is 2.9 inches. More details on the geometry, the reinforcement and the testing of Specimens E1-E6

and M5 can be found in [153].
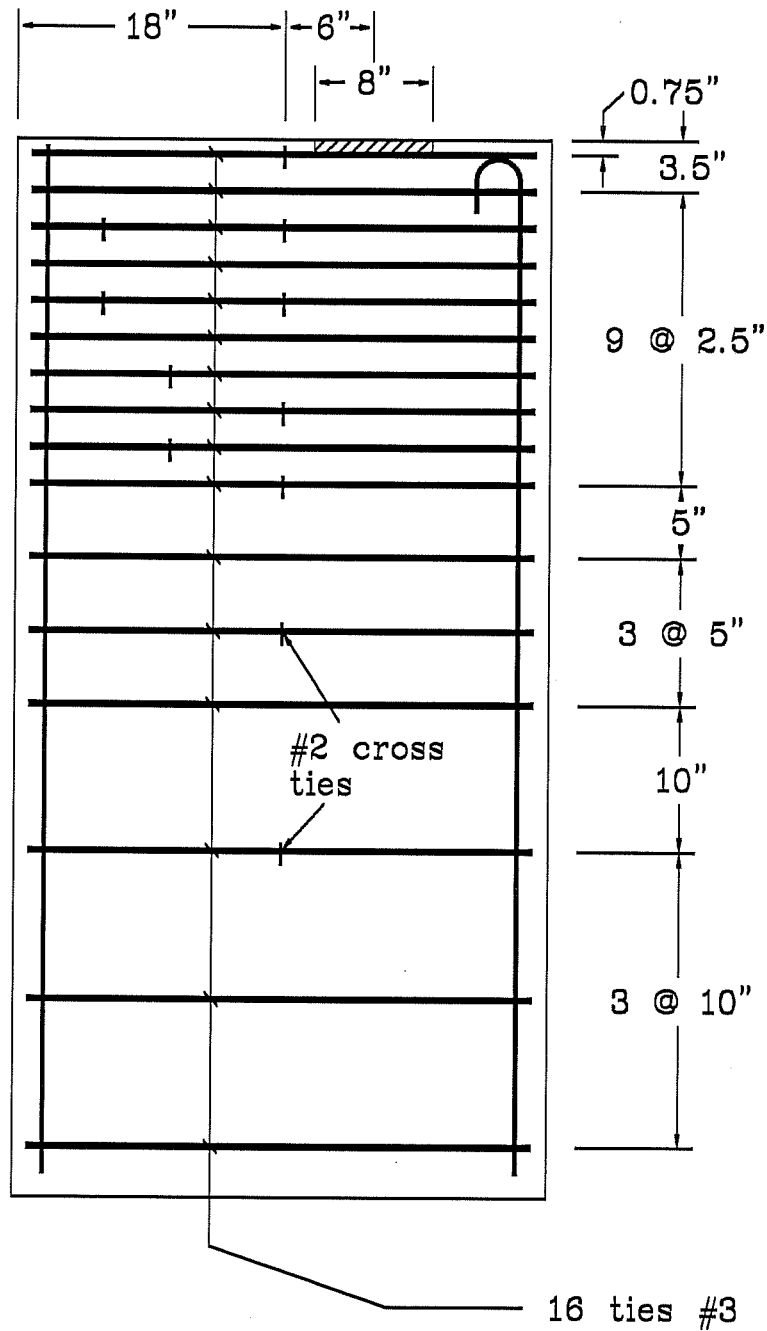
Figure 5.25   General Zone Reinforcement for Specimen E1

Table 5.1　Summary of the Dimensions of Eccentric Specimens with Dimensions of the Anchorage Plate and Concrete Strength

	Dimensions	Anchor	Concrete	
Specimen	$h \cdot w \cdot t \cdot e$ [in]	$a \cdot b \cdot t_{plate}$ [in]	f'_c [ksi]	f_{sp} [ksi]
E1	$72 \cdot 36 \cdot 11 \cdot 6$	$8 \cdot 7 \cdot 1$	5.45	0.428
E2	$72 \cdot 36 \cdot 11 \cdot 12$	$8 \cdot 7 \cdot 1$	5.95	0.460
E3	$72 \cdot 36 \cdot 11 \cdot 12$	$8 \cdot 7 \cdot 1$	6.13	0.492
E4	$72 \cdot 36 \cdot 11 \cdot 12$	$8 \cdot 7 \cdot 1$	5.69	0.475
E5	$72 \cdot 36 \cdot 8.5 \cdot 4.5$	$6 \cdot 6 \cdot 1.5$	5.71	0.459
E6	$72 \cdot 36 \cdot 10 \cdot 9$	$6.5 \cdot 6.5 \cdot 7^*$	5.68	0.444
M5	$60 \cdot 32 \cdot 17 \cdot 8$	$6.5 \cdot 6.5 \cdot 7^{**}$	4.67	0.330

*:　Multiplane Anchorage. Total depth of the anchor.

**:　Two Multiplane Anchors over the thickness. Dimensions of one anchor.

The reinforcement of the general zone for the Specimen E1 is shown in Fig. 5.25. The layout of the general zone reinforcement for the specimens E1-E6 and M5 is similar to the reinforcement of Specimen E1. Table 5.2 summarizes the reinforcement for all seven test specimens. The centroid of the bursting zone reinforcement was located at a depth of approximately h-2e from the anchorage plate; this reinforcement is shown as *main bursting reinforcement* in Table 5.2 and is the only reinforcement that was taken into account to determine the capacity of the section according to the Strut-and-Tie Model. In addition, some reinforcement was placed deeper in the section for specimens E1 to E4. This reinforcement is shown as *additional reinforcement* in Table 5.2 and was not considered when calculating the ultimate load capacity of the specimens. In order to better investigate the spalling and bending

forces, Specimen E3 was provided with crack formers in these areas.

Table 5.2   Summary of the Bursting, Spalling and Additional Reinforcement for Eccentric Specimens

	Main Bursting Reinforcement		Spalling Reinforcement		Additional Reinforcement		Spiral
Speci-	As*f_y	Centroid	As*f_y	Centroid	As*f_y	Centroid	diam/ pitch/ length
men	[kips]	[in]	[kips]	[in]	[kips]	[in]	[in]
E1	132.1	13.5	14.7	1	88.4	41.0	7.25/
E2	88.0	8.0	68.5	1	132.1	37.7	2.5/
E3	88.0	8.0	68.5	1	132.1	37.7	13.25
E4	88.0	8.0	0	N/A	132.1	37.7	
E5	58.7	13.0	14.7	2	N/A	N/A	6.5/2/8
E6	44.0	13.0	8.8	1	N/A	N/A	8/2/9.5
M5	39.4	15.3	6.6	1	N/A	N/A	7/2/10

Figure 5.26 shows the load causing cracking in the bursting region compared with the load predicted from the Finite Element analysis based on peak tensile stress and the split cylinder strength measured from companion cylinders. The actual cracking loads are generally slightly smaller than the predicted value. Disregarding the cracking load for specimen E3, which had crack formers, the average ratio of predicted to actual cracking load is 0.969, with a standard deviation of 0.106. The predicted cracking loads are much closed to the actual values than in the case of concentric specimens, for which the average ratio was 0.792 observed. The standard deviation is larger in the case of eccentric specimens, perhaps showing that the phenomenon of

cracking is more complex in eccentric specimens.

As in the test series for concentric specimens, two predictions of the ultimate capacity are shown for the Strut-and-Tie Model: the tie capacity is based on the tensile capacity of the reinforcement acting as a tension tie and the strut capacity is based on the compressive stress in the concrete at the critical section, as defined in Section 4.3.9. The maximum effective concrete strength on the critical section was assumed to be 0.60 f'_c. The lowest of the two values obtained is the ultimate capacity predicted by the Strut-and-Tie Model, P_{STM}. A limit based on the maximum stress in the concrete (labeled *Compression*) is also given as a second estimate of the compressive capacity of
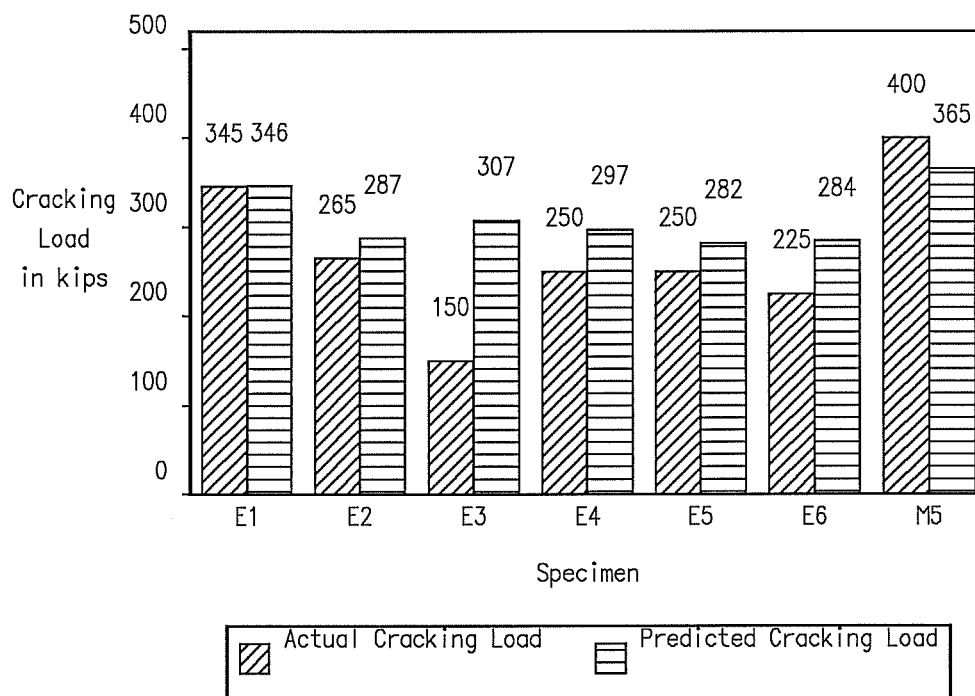
Figure 5.26 Actual and Predicted Cracking Load in the Bursting Region for Eccentric Specimens

the concrete. This value is obtained by setting the compressive stress at a distance a ahead of the anchorage device, as obtained from the Finite Element Analysis, to $0.75f'_c$

Figure 5.27 shows the ultimate load for the eccentric specimens compared with the ultimate load predicted by the Strut-and-Tie Model assuming tie failure, strut failure, and compression failure. It is apparent that the ultimate capacity of specimens E1-E4 is related to a failure of concrete in compression. The large amount of bursting reinforcement in specimens E2-E4 made such a mode of failure unavoidable. The fact that specimens E5, E6 and M5 failed at loads greater than calculated based on the tensile capacity of the available bursting reinforcement points out the importance of the tensile concrete contribution to the load carrying mechanism. Strain measurements in all eccentric specimens showed that several reinforcing bars in the bursting region did not yield during the testing. A prediction of the ultimate load based on the Strut-and-Tie Model and neglecting the contribution of the concrete in tension yields conservative strengths. The average ratio of measured ultimate load to predicted ultimate load (taking the lowest of the two values obtained from the Strut-and-Tie Model) is 1.26, with a standard deviation of 0.192. Without the value for M5 (that had a significant tensile concrete contribution that increased its ultimate load), the average is 1.20 with a standard deviation of 0.131. The lowest ratio of actual to predicted ultimate load is 1.006, slightly conservative. Because most specimens were controlled by the compressive strength of the concrete, the introduction of the correction suggested in Chapter 4 to consider the node as located at a distance $a/4$ in the concrete, would not significantly change the results. Figure 5.28 shows that, as in the case of concentric specimens, there is a substantial increase in load capacity between cracking and ultimate.
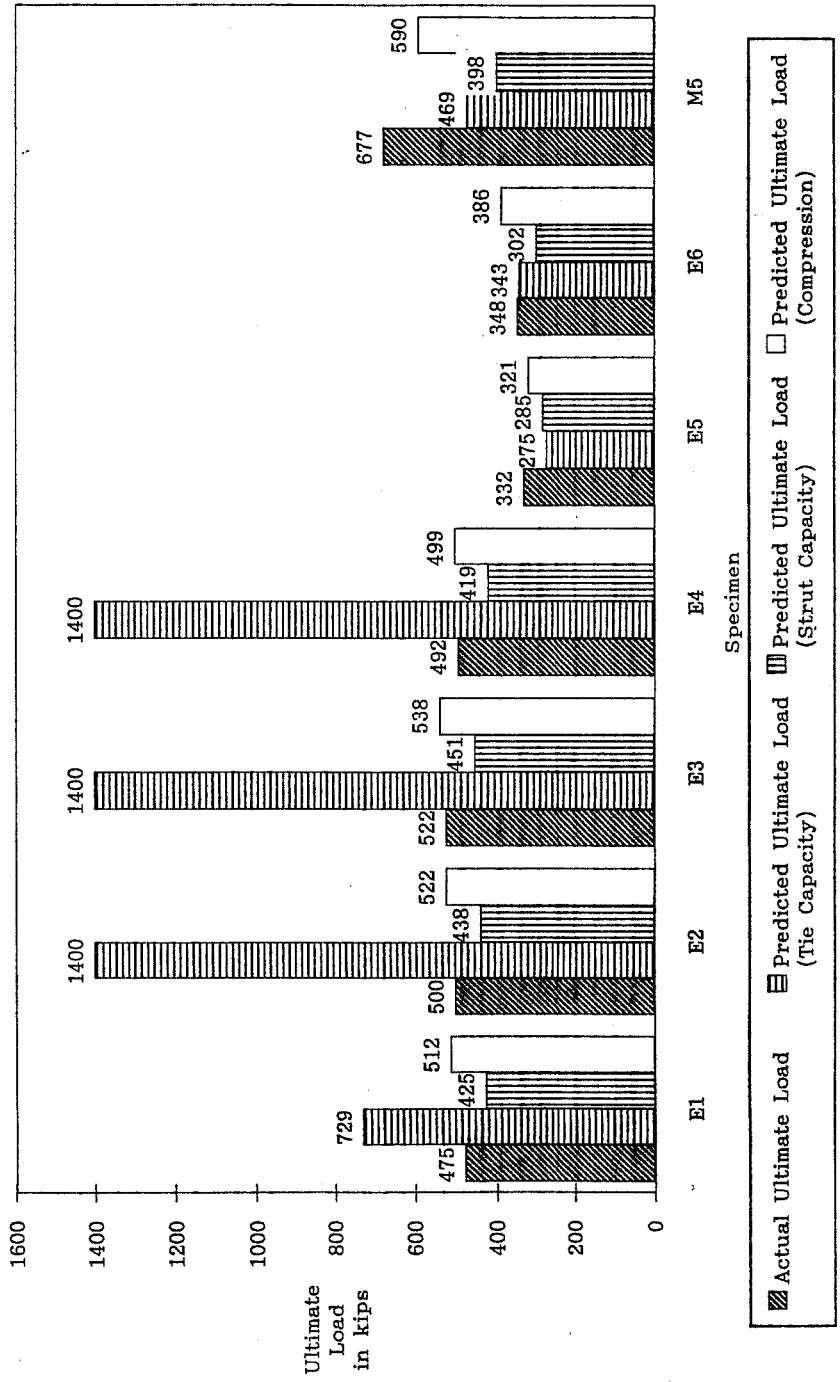
Fig. 5.27   Actual Ultimate Load and Ultimate Load Predicted by the Strut-and-Tie Model (Tie-Based Capacity and Strut-Based Capacity) for Eccentric Specimens
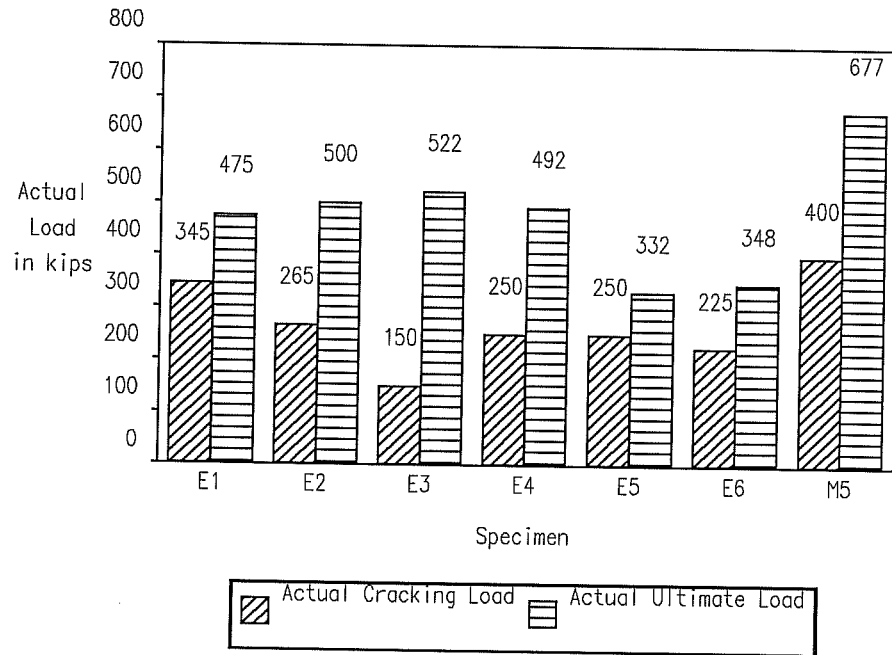
Figure 5.28   Actual Cracking and Ultimate Load for Eccentric
              Specimens

Figure 5.29 shows the actual cracking load in the spalling region compared to the cracking load predicted based on the peak spalling stress from the Finite Element analysis and the tensile strength of the concrete measured from split cylinder tests. Because spalling stresses reach extremely high values in eccentrically loaded specimens (with values ranging up to 5 or 6 times the average stress $P/(ht)$), the predicted cracking loads in the spalling region are extremely low. However, as shown in Fig. 5.29, the actual cracking loads in the spalling region were much higher, and appeared only in the specimens with the largest eccentricity $(e/h=0.333)$.

Correspondingly, the predicted ultimate load based on the capacity of the tension tie T_3 located in the spalling region has

little correlation with the actual ultimate load, as shown in Fig. 5.30. Specimens E2-E4 had identical reinforcement in the bursting region, and reached comparable ultimate loads, although the omission of the spalling reinforcement in specimen E4 should have reduced its ultimate strength to zero. These observations show that there is a considerable room for redistribution of the internal forces in the spalling region. As shown in Figs. 5.12 and 5.13, the stresses will be redistributed deeper in the cross section if the area of spalling stresses is removed or loses its stiffness. This was also observed during the testing, because the reinforcing bars located in the spalling region did not reach the stress levels expected from the Strut-and-Tie Model analysis, even for specimen E3 with crack formers.
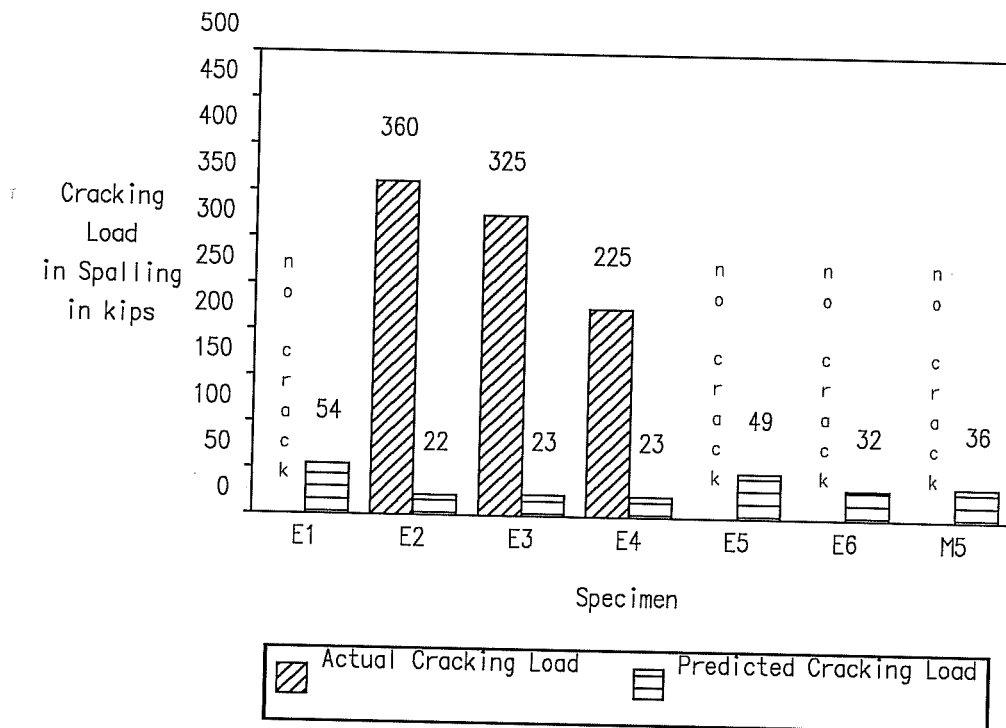
Figure 5.29 Actual and Predicted Cracking Load in the Spalling Region for Eccentric Specimens

The compressive stresses at the interface between the local zone and the general zone controlled the behavior and the ultimate capacity of most eccentric specimens of this series. Figure 5.31 shows the level of compressive stresses in the concrete at ultimate, based on the elastic stress distribution form the Finite Element Analysis. The bearings stresses under the anchorage are shown, as well as the compressive stresses at a distance equal to one half the plate size (a/2), one time the plate size (a), and as average over the compression strut P_1.
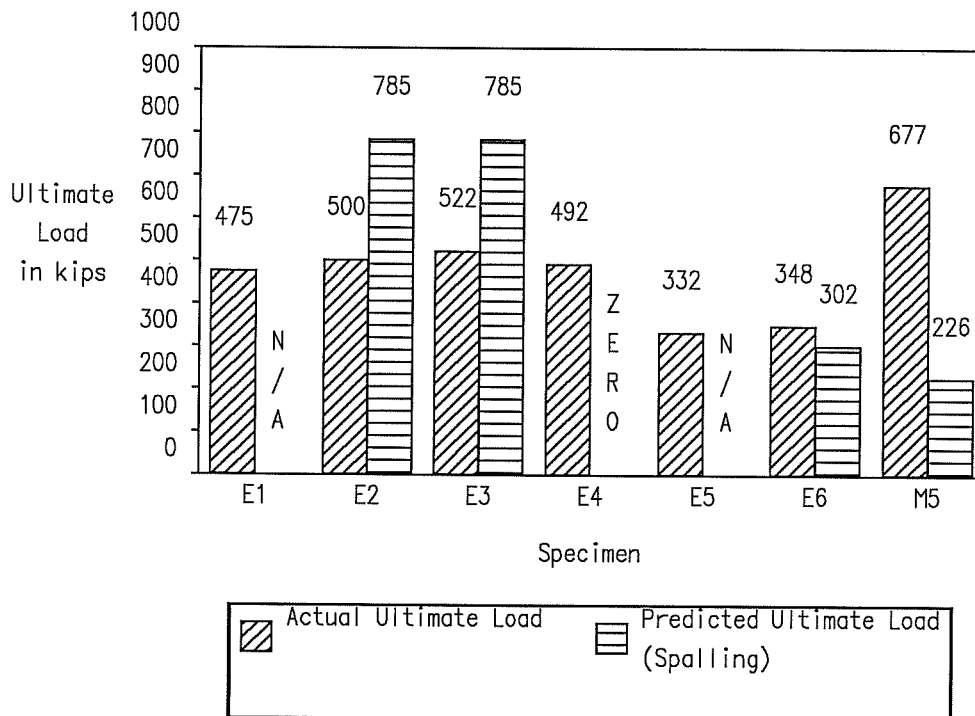
Figure 5.30   Actual Ultimate Load and Ultimate Load Predicted by the Strut-and-Tie Model in the Spalling Region (Tie Capacity) for Eccentric Specimens
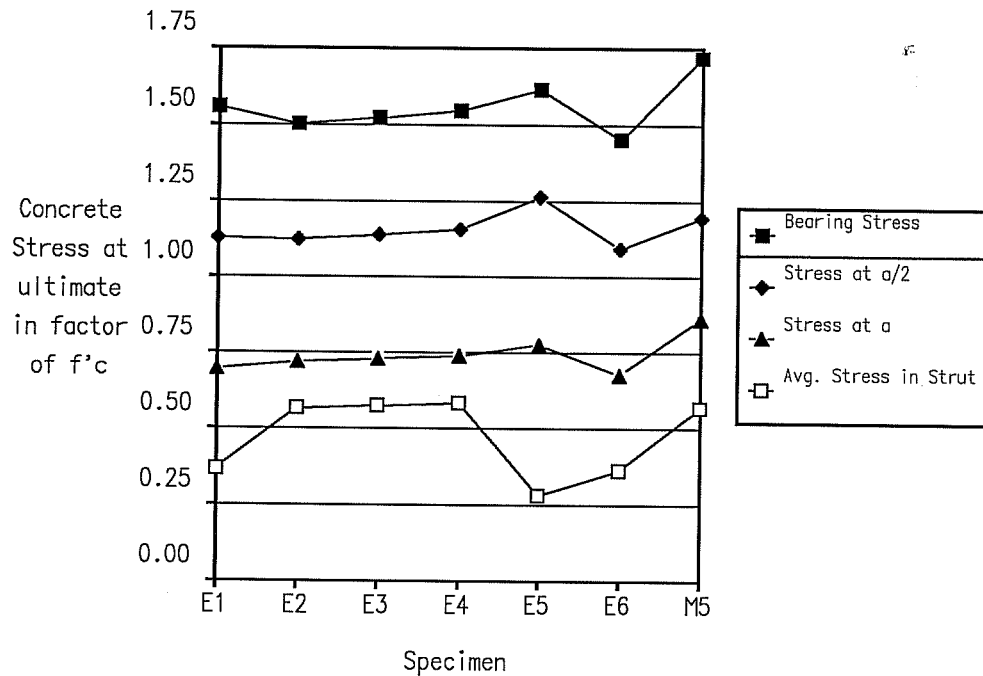
Figure 5.31   Compressive Stresses in the Concrete at Ultimate

While the average stresses in the compression struts remain at a relatively low level (less than 0.6 f'_c at ultimate), the stresses at a distance equal to the plate size are almost larger confirming the limiting value of 0.75 f'_c previously observed for concentric specimens.

5.3.4 Enhancement of the Behavior Model

As in the case of concentric specimens, a significant contribution of tensile force from uncracked concrete, and possibly of tensile force from reinforcement located at a larger distance from the anchor (the additional reinforcement of specimens E1-E4, shown in Table 5.2) was observed, resulting in a strength greater than expected from the strength of the tension

tie for specimens E5, E6 and M5. However, because the ultimate capacity of most of the eccentric tests was governed by the compressive capacity of the concrete struts, taking into account an increased capacity of the tensile ties would not have significantly the prediction of the ultimate load.

5.4   Inclined Tendons

In most cases, post-tensioning tendons have some inclination in the anchorage zone. In typical girder applications, this inclination is less than 20 degrees. Tendons also have a large radius of curvature in the vicinity of the anchorage device. Because the radius of curvature of the tendon is large, the deviation forces in the anchorage zone due to the curvature of the tendon can usually be neglected and the cable can be considered as straight for the purpose of analysis of the anchorage zone.

In special applications, however, the inclination can be very large. Configurations that include not only a large inclination, but also large deviation forces due to the curvature of the tendon will be described in Sections 5.7 to 5.9.

5.5   Finite Element Analysis for Inclined Tendons

A series of Finite Element analyses was performed on the basis of the geometry shown in Fig. 5.32. To limit the number of variables, the size of the anchor was kept constant at a = 0.125h. It is expected that tendencies similar to the tendencies observed for concentric tendons would be observed if the relative size of the plate was varied. The angles of inclination α investigated in this series are 10 and 20 degrees. Angles larger than 20 degrees would require that the tendon be curved in the anchorage zone.
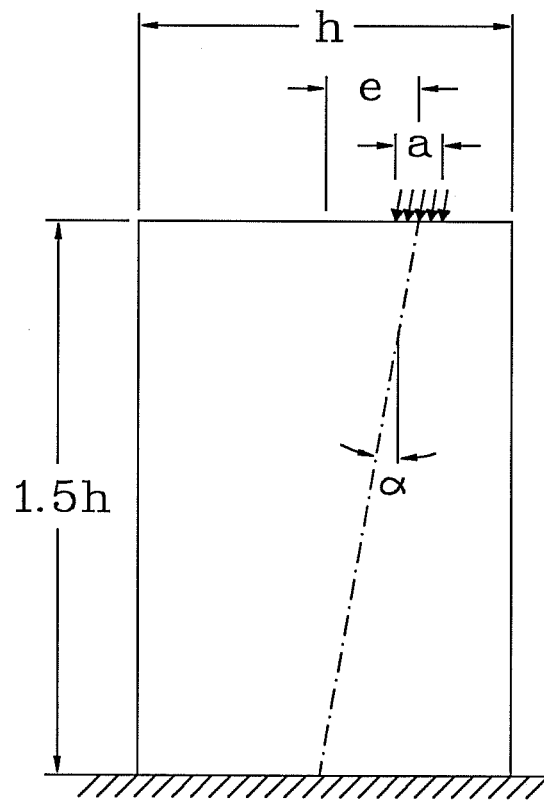
Figure 5.32   Geometry of Anchorage Zone with Inclined Tendon

5.5.1 Stress Distribution

The stress distribution due to tendons with a small inclination is similar to the stress distribution observed in concentric and eccentric configurations, with a zone of bursting stresses along the axis of the tendon and zones of spalling stresses on either side of the anchorage. However, the inclination of the tendon changes the orientation of the principal stresses. When the tendon is not inclined, the maximum tensile stresses in the bursting and in the spalling regions are observed perpendicular to the axis of the section. Therefore, plots of the stresses in the x direction delivered adequate information on the magnitude of the bursting and spalling stresses and forces. In configurations with inclined tendons, however, the maximum tensile stresses are no longer perpendicular to the axis of the section, but more or less perpendicular the axis of the tendon, depending on the angle of inclination. Contour plots of maximum principal stress, that incorporate the influence of the angular deviation from the specimen axes will be used in this section. Plots of principal stresses unfortunately do not deliver information on the direction in which the principal stresses are acting. The complementary information is delivered by the principal stress vector plots.

Fig. 5.33 shows the contour plot of the maximum principal stress (in tension) for inclinations of 0, 10 and 20 degrees with no initial eccentricity. Figure 5.34 shows the same contour plots for an initial eccentricity e = 0.25h. Fig. 5.35 and 5.36 show the corresponding principal stress vector plots which show the direction in which the principal stresses are acting.
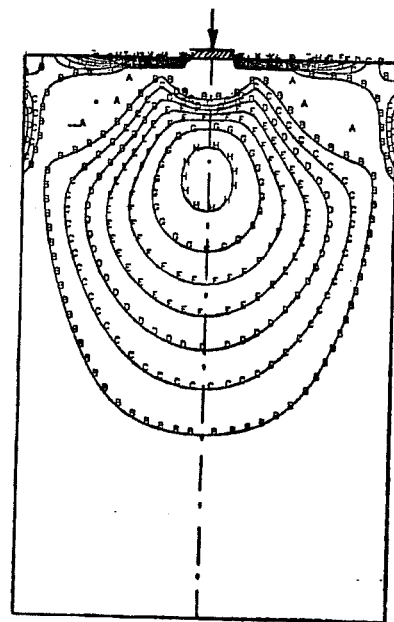
a) No Inclination
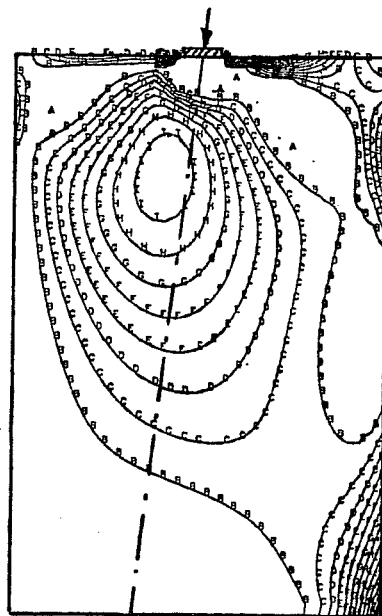
b) Inclination 10 degrees
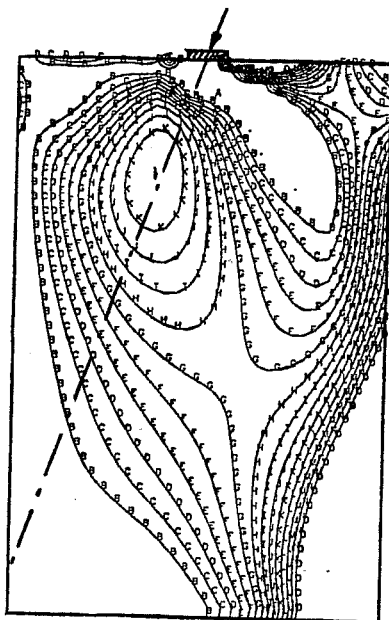
c) Inclination 20 degrees

A = 0.00 σ_o
B = 0.05 σ_o
C = 0.10 σ_o
D = 0.15 σ_o
E = 0.20 σ_o
F = 0.25 σ_o
G = 0.30 σ_o
H = 0.35 σ_o
I = 0.40 σ_o
J = 0.45 σ_o
K = 0.50 σ_o
L = 0.55 σ_o
M = 0.60 σ_o

Figure 5.33   Contour Plots of the Maximum Principal Stress (in Tension) for e/h=0.0 and Inclinations of 0, 10 and 20 degrees
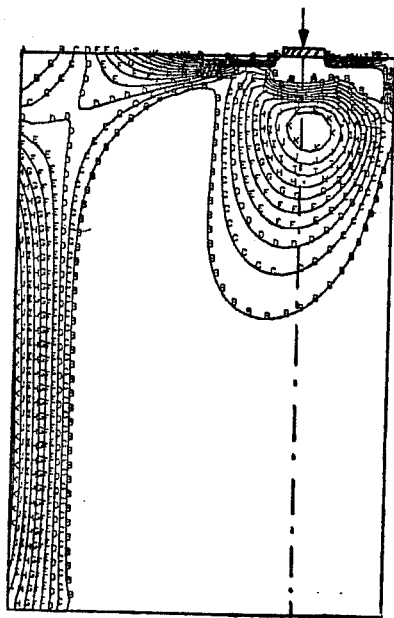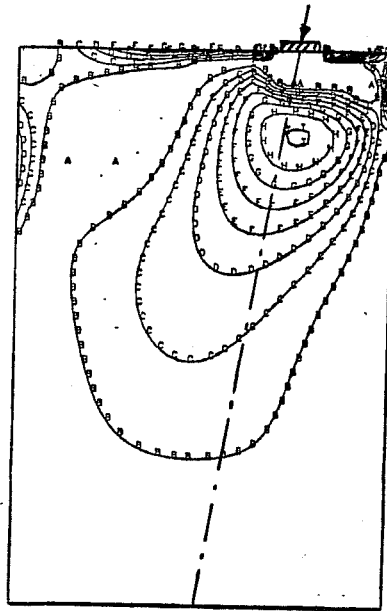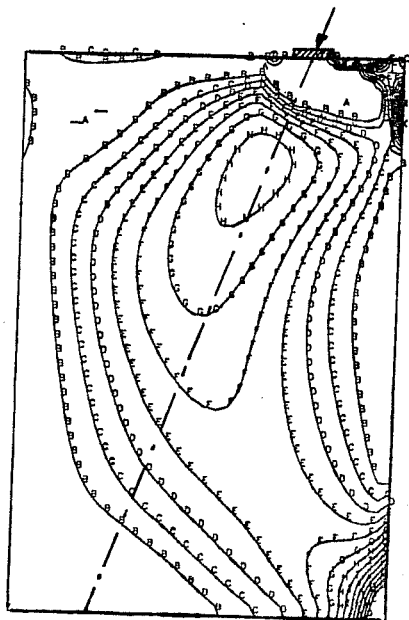
a) No Inclination

b) Inclination 10 degrees

c) Inclination 20 degrees

A = 0.00 σ_0
B = 0.05 σ_0
C = 0.10 σ_0
D = 0.15 σ_0
E = 0.20 σ_0
F = 0.25 σ_0
G = 0.30 σ_0
H = 0.35 σ_0
I = 0.40 σ_0
J = 0.45 σ_0
K = 0.50 σ_0
L = 0.55 σ_0
M = 0.60 σ_0

Figure 5.34 Contour Plots of the Maximum Principal Stress (in Tension) for e/h=0.25 and Inclinations of 0, 10 and 20 degrees
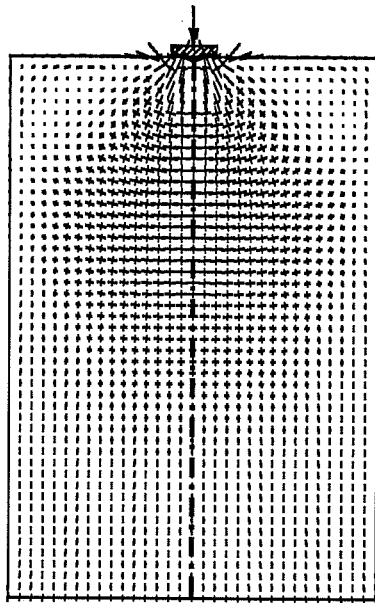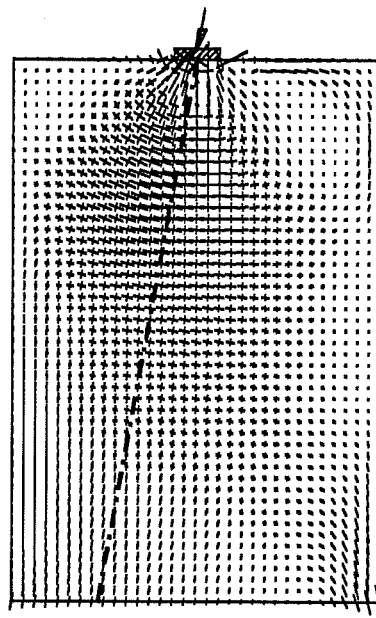
a) No Inclination
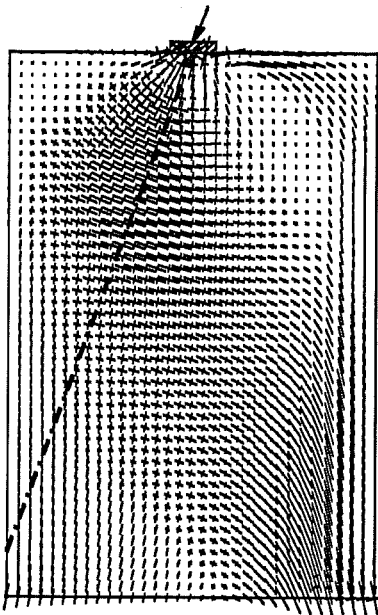
b) Inclination 10°

c) Inclination 20°

Figure 5.35   Vector Plots of the Maximum Principal Stress for
e/h=0.0 and Inclinations of 0, 10 and 20 degrees
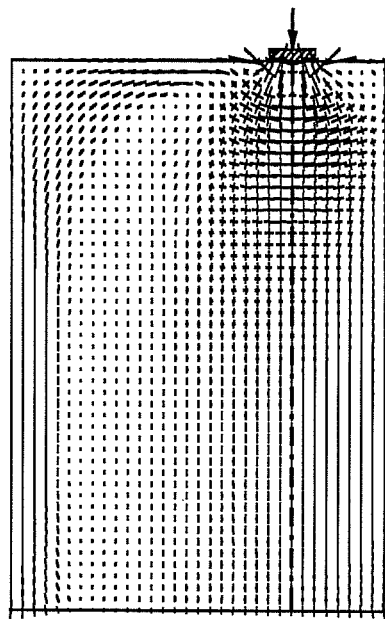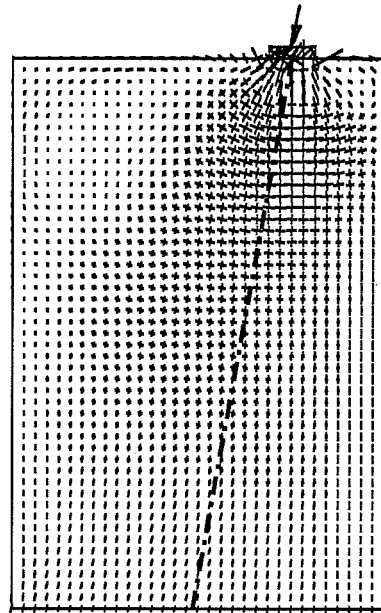
a) No Inclination
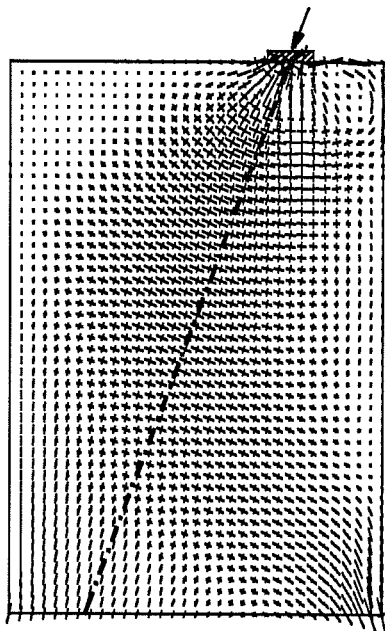
b) Inclination 10°

c) Inclination 20°

Figure 5.36   Vector Plots of the Maximum Principal Stress for
e/h=0.25 and Inclinations of 0, 10 and 20 degrees
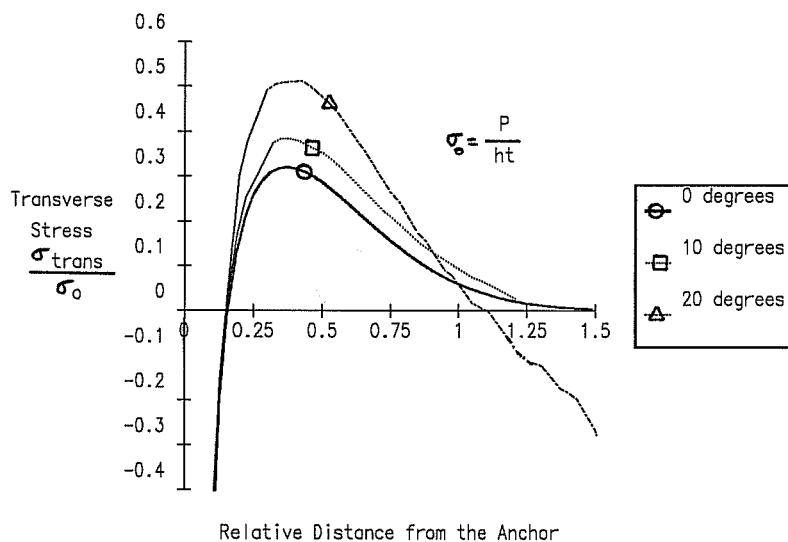
Figure 5.37   Stresses Perpendicular to the Tendon for Various
              Inclinations of the Tendon at an Eccentricity
              e/h=0.0
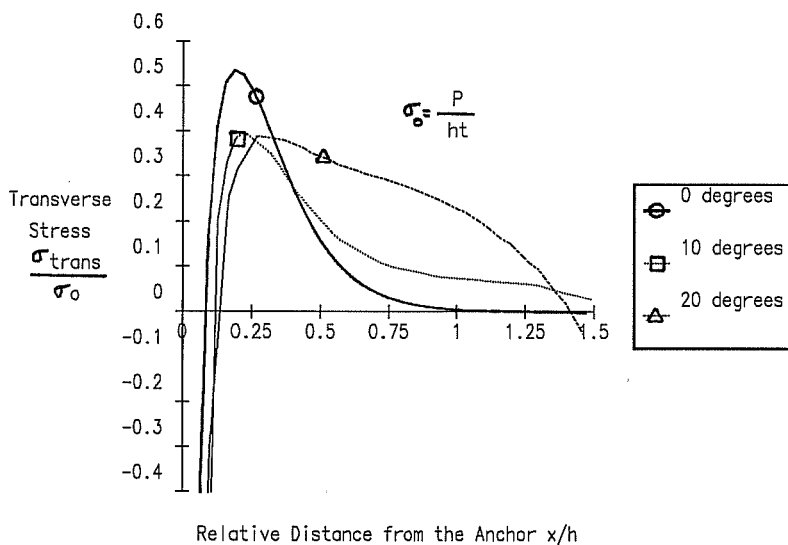
Figure 5.38   Stresses Perpendicular to the Tendon for Various
              Inclinations of the Tendon at an Eccentricity
              e/h=0.25
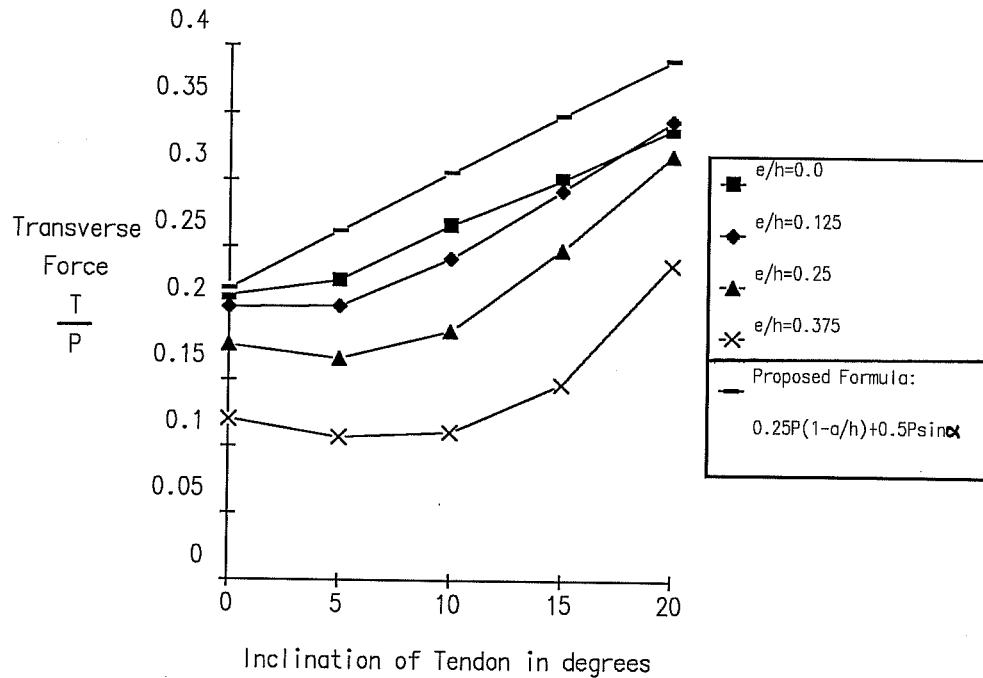
Figure 5.39   Transverse Force as a Function of the Inclination of the Tendon for Various Eccentricities of the Anchor and Proposed Simplified Formula

In configurations with inclined tendons, the largest principal stresses in tension and the largest transverse force are generally perpendicular to a line which approximately follows the axis of the tendon. Fig. 5.37 and 5.38 show the distribution of stresses perpendicular to the tendon for various eccentricities and inclinations of the tendon. It is important to notice that in the case of inclined tendons, the transverse stresses do not diminish to zero at a distance 1.5h from the anchor, as is the case for tendons without inclination. The remaining stresses, sometimes in compression and sometimes in tension depending on the initial inclination and initial eccentricity of the tendon, are caused by the transverse component of the tendon force, that does

not disappear. Fig. 5.39 shows the variation of the transverse force as a function of the inclination of the tendon for various eccentricities. This force was obtained by integrating the stresses perpendicular to a line going from the middle of the anchor to a point located in a section at a distance $h/cos\alpha$ from the anchor. Integrating over another length would lead to slightly different results, due to the presence of shear stresses. In general the transverse force, that is a combination of bursting force and shearing force, increases with increased inclination of the tendon. The figure also shows the values given by the proposed simplified formula described in the next paragraph.

The change in the transverse force is due to the presence of the transverse shear induced by the inclination of the tendon. Fig. 5.40 shows the change in transverse force due to the inclination of the tendon for various eccentricities, along with the shear induced by the inclination of the tendon. This illustrates the relationship between the increase in transverse force and the shear force induced by the tendon. For angles of inclination larger than about 5 degrees, the increase in transverse force becomes significant. As an approximation, the effect of the inclination of the tendon on the transverse (bursting) force can be estimated as one half the transverse component of the post-tensioning force. This approximation is shown in Fig. 5.40 as "Proposed Increase". Introducing this contribution into Eq. 5.1 gives the formula of Eq. 5.5.

$$T_{burst} = 0.25 \cdot P \cdot (1-a/h) + 0.5 \cdot P \cdot sin(\alpha) \quad (Eq.\ 5.5)$$

The formula of equation 5.5 is plotted in Fig. 5.39 as "Proposed Formula". The formula is generally conservative, especially for cases with a large eccentricity, because the effect of the eccentricity on the magnitude of the transverse bursting

force is neglected in Eq. 5.1.
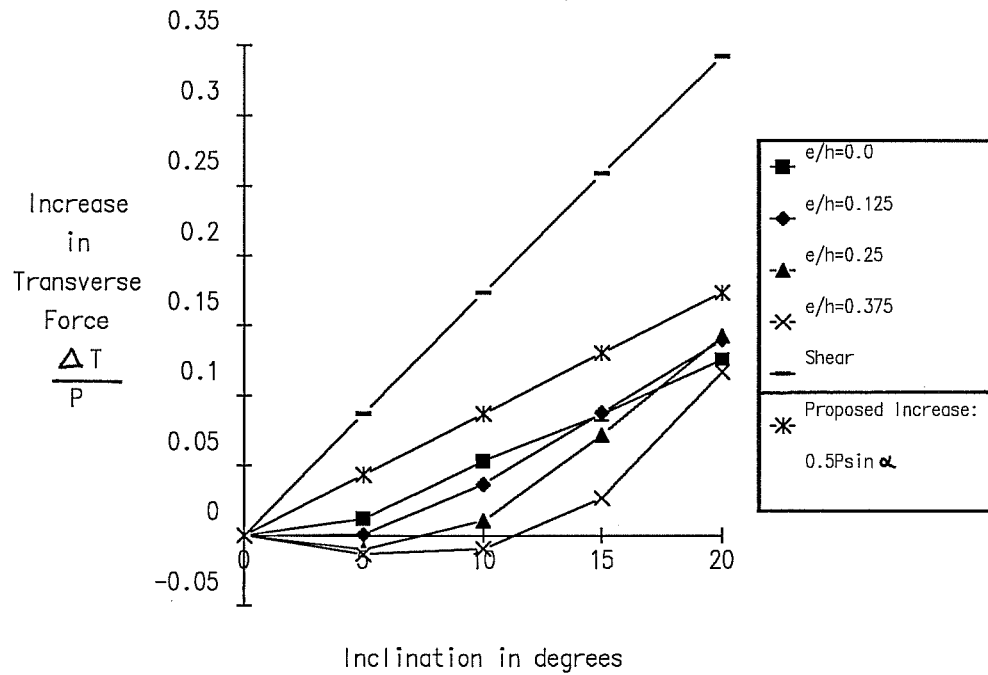
Figure 5.40　Change in Transverse Force as a Function of the
Inclination of the Tendon for Various Eccentricities
of the Anchor and Proposed Formula for the Change
due to the Inclination of the Tendon

The approximate location of the centroid of the bursting force as measured along the axis of the tendon can be estimated using the expression given in Eq. 5.6. Fig. 5.41 shows the centroid of the transverse force as a function of the inclination of the tendon and the values obtained by using the approximate formula. Although the formula is very simple, the correlation is rather good.

$$d_{centr} = 0.5 \cdot (h-2e) + 5 \cdot e \cdot \sin(\alpha) \qquad (Eq. \ 5.6)$$
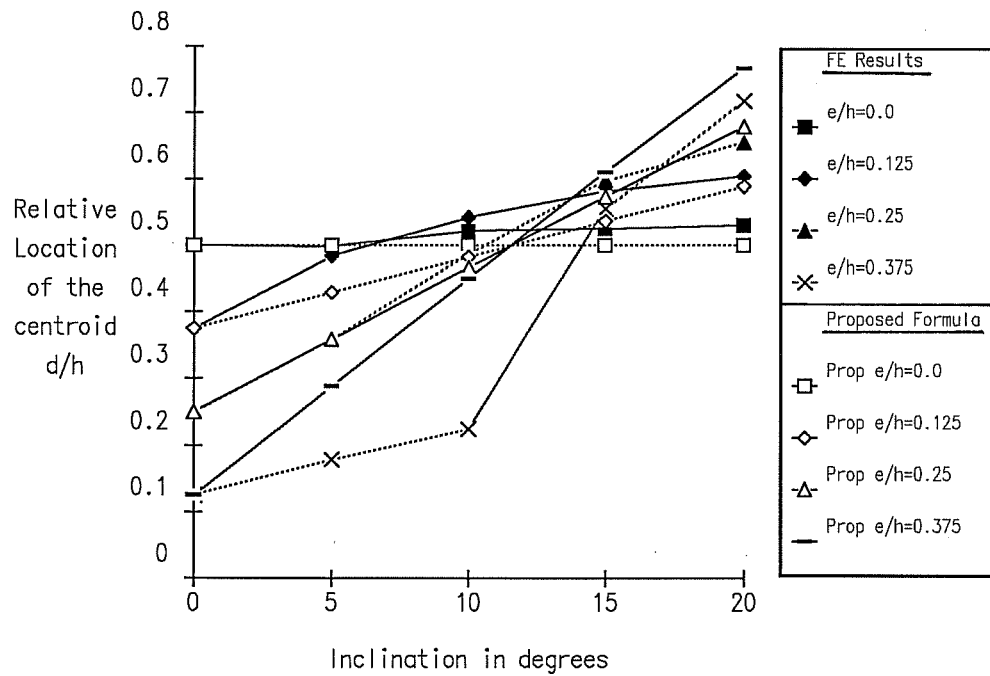
Figure 5.41   Centroid of the Transverse Tension Force as a
              Function of the Inclination of the Tendon for
              Various Initial Eccentricities and Proposed
              Simplified Formula

5.5.2 Comparison with Published Values

There are very few previously published studies dealing with inclined tendons. Guyon [75] has some analytical results for a force applied transversely to the section, but his investigations are limited to small inclinations of about 1:10 (5.7 degrees). As a consequence, he reports no noticeable changes in the stress distribution for tendons with a small inclination. This observation confirms the tendency shown in Fig. 5.40 where the transverse force changes little for such small inclinations of the tendon.

Leonhardt [99] shows the results of a study by Sargious [154] with an inclination of the tendon of 6.3 degrees (Figure 5.42). The maximum transverse stress as well as the transverse bursting force correlate well with the results obtained in the present study. For the angles investigated, which were up to 6.3 degrees, Leonhardt reports that no significant increase in the transverse stresses and forces were observed.
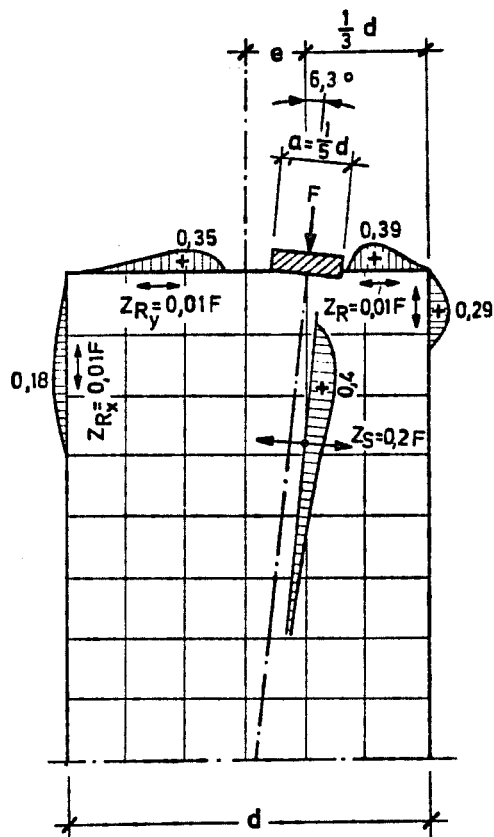
Figure 5.42   Distribution of the Transverse Stresses and Transverse Force According to Sargious [99, 154]

5.6   Strut-and-Tie Model for Inclined Tendons

Figure 5.43, shows the geometry, loads and reactions acting on a free-body diagram of an anchorage zone with an inclined, eccentric tendon. The reactions at the end of the general zone include an axial component and a moment caused by the eccentrically applied tendon force, as well as a transverse force (shear) due to the inclination of the tendon. Because the tendon is inclined relative to the axis of the section, the moment caused by the post-tensioning force depends on the location l where the cut is made at the end of the general zone. For the parametric study of this section, the cut was made at one times the depth of the section, $l=h$.
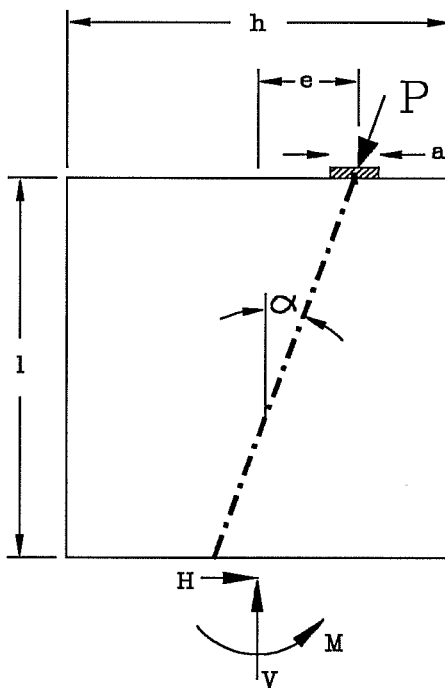
Figure 5.43   Geometry and Loads of an Anchorage Zone with
Inclined Tendons

5.6.1 Geometric Definition of the Strut-and-Tie Model for Inclined Tendons

Figure 5.44a shows the elastic stress trajectories for the case of an eccentric and inclined tendon along with the Strut-and-Tie Model developed on the basis of these stress trajectories. The eccentricity of the anchorage is 0.25h and the inclination of the tendon is 20 degrees. Diagonal members were added in order to make the Strut-and-Tie Model assemblage stable, but as can be seen in Fig. 5.44b, the corresponding forces are comparatively small. The total tensile transverse force is approximately 26% of the post-tensioning load. Such a model can easily be drawn and forces calculated to obtain design values for the transverse force.

a) Strut—and—Tie Model with Stress Trajectories

b) Forces in the Struts and Ties
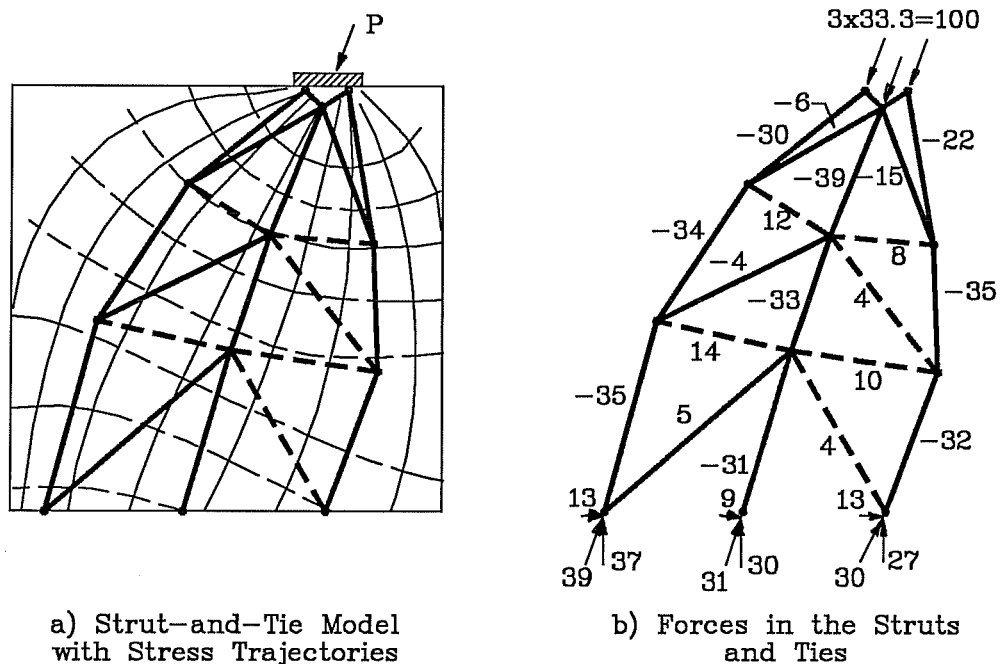
Figure 5.44   Strut-and-Tie Model Developed on the Basis of the Elastic Principal Stress Trajectories

As can be observed in Fig. 5.44b, the presence of a transverse component of force due to the inclination of the tendon leads to at least some inclined compression struts at the end of the general zone. While the vertical component of the reaction can be readily obtained by integrating the axial stresses as in the previous cases, the question of the distribution of the transverse force between the struts is of importance, and will be further developed in the next section.

In the Strut-and-Tie Model of Fig. 5.44, the transverse force at the end of the general zone is distributed unevenly between the compression struts, with a smaller force, 9% of the applied load coming through the middle strut than through the external struts which each carry 13% of the applied load. Adequate transverse reinforcement should be placed at the interface between the general zone and the rest of the beam in order to distribute these forces to the entire cross section.

5.6.2 Parametric Study of the Influence of Inclination

To understand the influence of important parameters, a Strut-and-Tie Model simpler than the one presented in the previous section was developed, and is shown in Fig. 5.45. The reinforcement was assumed to be lumped in one single tie oriented perpendicular to the tendon. The total diffusion angle (sum of the diffusion angles on either side of the tendon axis) was constrained to 52 degrees, which corresponds to twice the value obtained in Chapter 4 for the diffusion angle on one side of the tendon.

Because the Strut-and-Tie Model is based on the theory of plasticity, arbitrary distributions of the transverse force at the end of the general zone are possible, as long as overall equilibrium is satisfied. This is also the case for the axial

force, for which it was found satisfactory and practical to simply use the resultants from the elastic stress distribution. Once the method for distributing the transverse force has been chosen, the geometry of this model is entirely defined, with the exception of the force carried by each strut. For the Strut-and-Tie Model to be in equilibrium, the location of the interface is iteratively modified, until equilibrium is satisfied. It appears that for the given constraints, only one equilibrium solution exists.
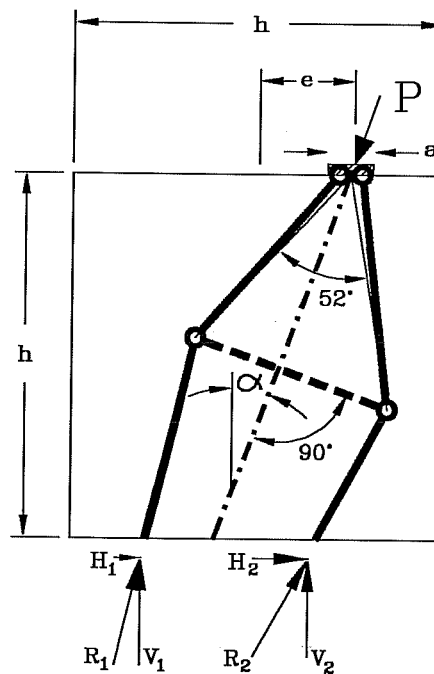
Figure 5.45   Geometry of the Strut-and-Tie Model Used for the
              Parametric Studies

No Eccentricity
Inclination 10 degrees

Eccentricity 0.25h
Inclination 20 degrees

a) Transverse Force
Distribution based on
Parabolic Distribution

b) Transverse Force
Distribution based on
Strut Area

c) Transverse Force
Distribution based on
Axial Force in Strut
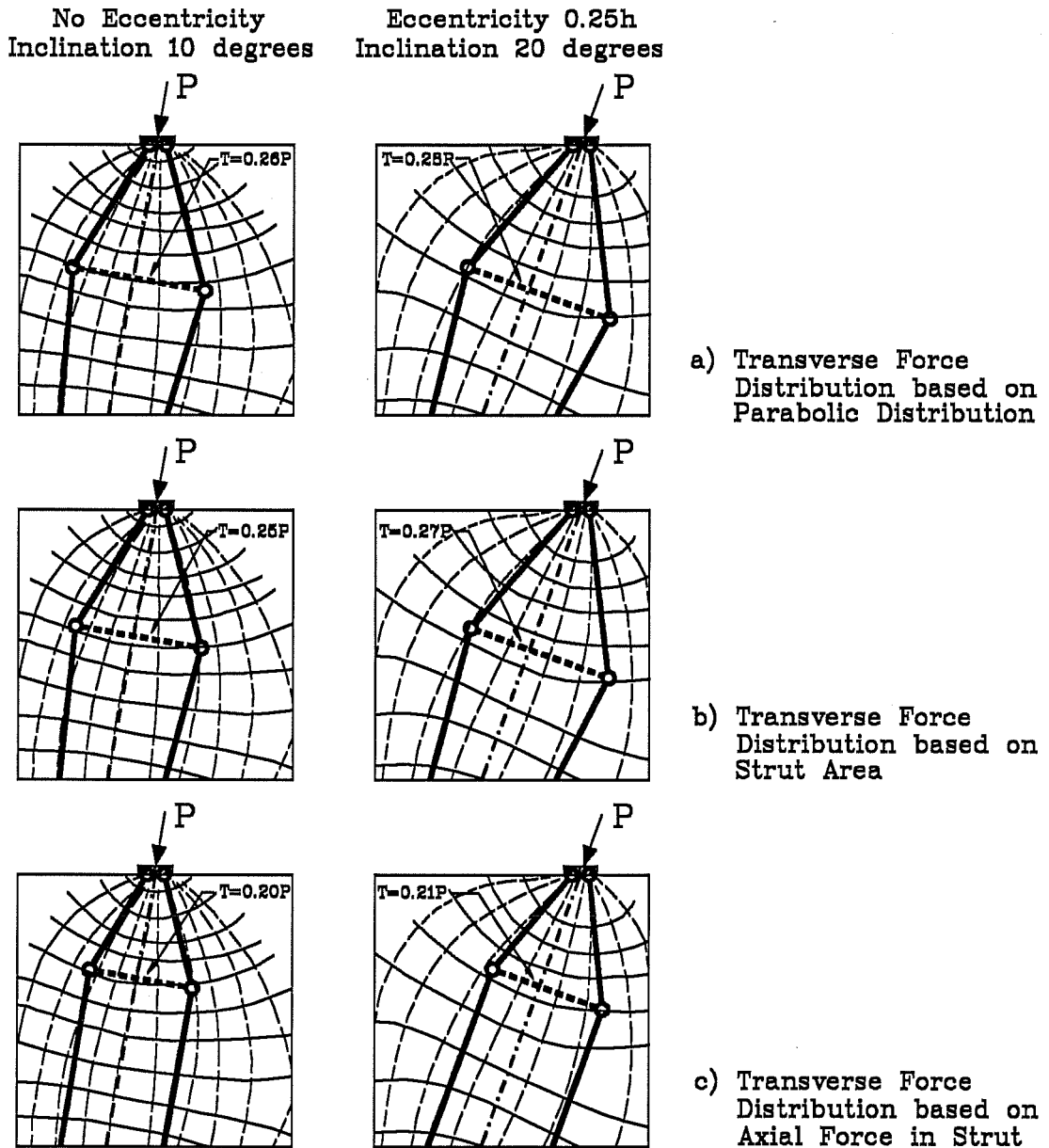
Figure 5.46 Elastic Principal Stress Trajectories and Strut-and-
Tie Models Based on the Various Assumptions on the
Distribution of the Transverse Reaction two Initial
Eccentricities and Inclinations

Fig. 5.46 shows three series of two Strut-and-Tie Model, each series being based on a different assumption for the distribution of the transverse force. The Strut-and-Tie Models are superimposed on the stress trajectories from the theory of elasticity. The first Strut-and-Tie Model in each series is for no initial eccentricity and a tendon inclination of 10 degrees; the second Strut-and-Tie Model is for an initial eccentricity of 0.25h and a tendon inclination of 20 degrees.

Fig. 5.46a shows two Strut-and-Tie Models based on a distribution of the transverse reaction corresponding to the parabolic distribution of the shear stresses as obtained from the theory of elasticity. The transverse forces are not proportional to the axial forces, leading to different inclinations of the struts and reactions at the end of the general zone.

Fig. 5.46b shows two Strut-and-Tie Models derived based on the hypothesis that the transverse reaction carried by the struts is proportional to their width (measured perpendicular to the axis of the member). This corresponds to a uniform (rectangular) distribution of the shear stresses at the end of the general zone. Here again, the inclinations of the struts at the end of the general zone are not equal.

In the solution presented in Fig. 5.46c, the transverse reaction carried by the compression struts is proportional to the amount of axial force that they are carrying. In this case, the inclination of the compression struts at the end of the general zone is the same, and is the same as the inclination of the tendon.

Because all Strut-and-Tie Models shown in Fig. 5.46 fulfill the conditions of equilibrium, they can all be considered valid plastic solutions. A parametric study of the value obtained for the tie force T will show the relative advantages of the various hypotheses.
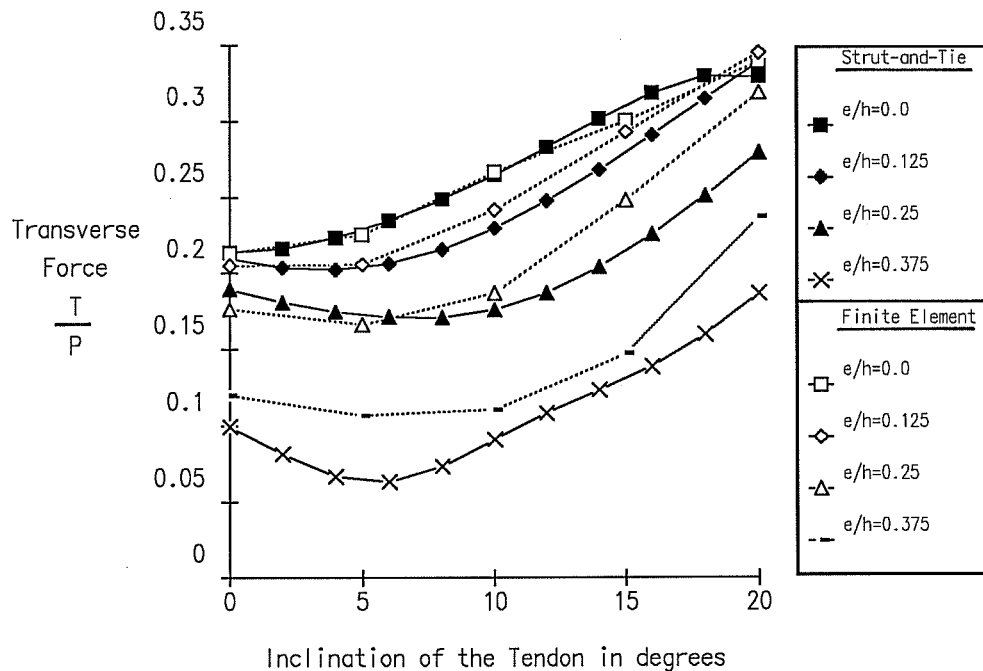
Figure 5.47 Tie Force as a Function of Inclination and
            Eccentricity for a Parabolic Distribution of the
            Transverse Reaction

Figure 5.47 shows the transverse force predicted on the
basis of a parabolic distribution of the transverse reaction as a
function of the inclination of the tendon for various
eccentricities of the anchor. The correlation with the results of
the Finite Element analyses is good. The tendencies observed in
the Finite Element solution are well represented by the Strut-and-
Tie Model. At the largest eccentricity, the values obtained are
less than the elastic values from the Finite Element Analysis.

    Fig. 5.48 shows the tie force based on a uniform
distribution of the transverse reaction. The results are in less
agreement with the results from the Finite Element study compared
to the parabolic distribution. The results indicate the same

tendencies as the Finite Element Solution with the exception of the largest eccentricity, for which the slight decrease in transverse force for angles between 5 and 10 degrees is not predicted.
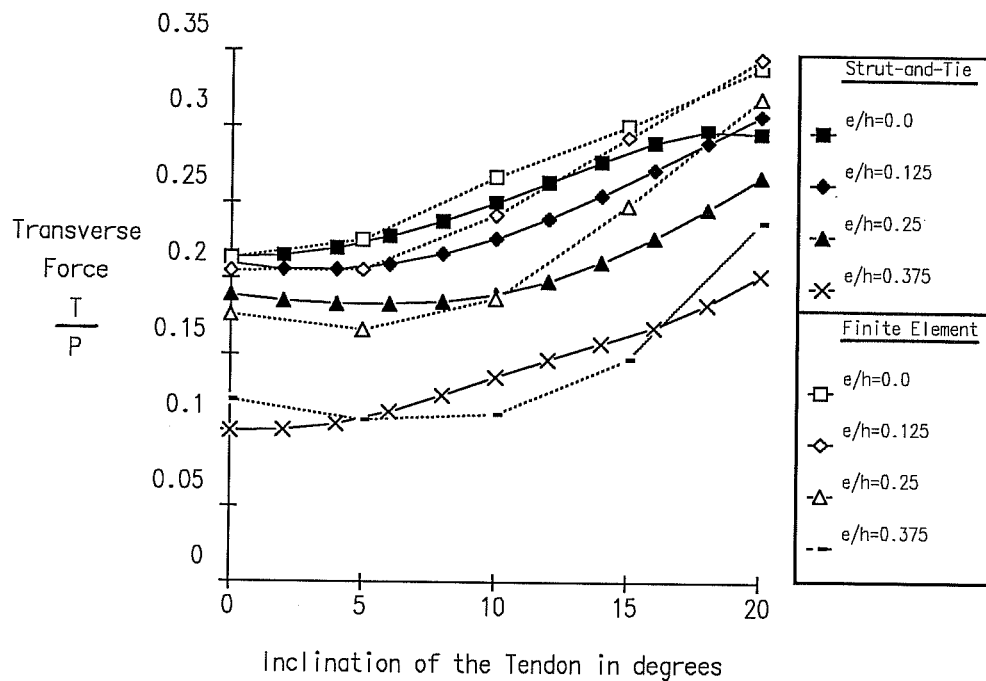
Figure 5.48   Tie Force as a Function of Inclination and Eccentricity for a Distribution of the Transverse Reaction in Proportion to the Width of the Struts

Figure 5.49 shows the tie force predicted by the Strut-and-Tie Model that assumes that the struts carry a shear force proportional to their axial load. The results are not in very good agreement with the results of the Finite Element analyses. Certain tendencies are reversed, as in the case of no eccentricity (e/h=0.0).
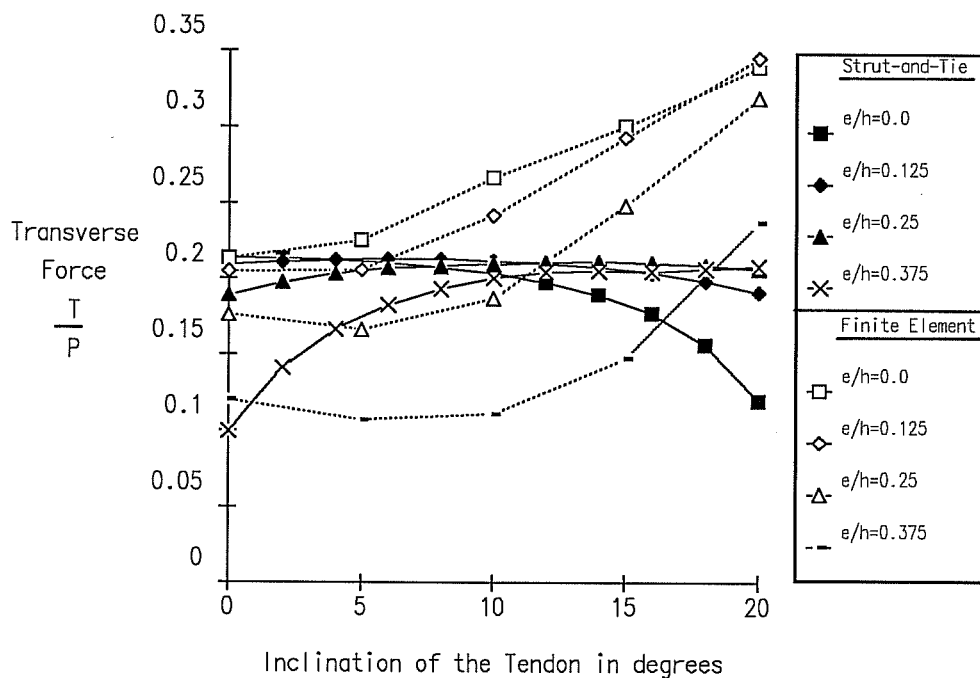
Figure 5.49   Tie Force as a Function of Inclination and
              Eccentricity for a Distribution of the Transverse
              Reaction Proportional to the Axial Force in the
              Struts

It should be emphasized, however, that the differences are not as pronounced as they appear. The location of the resultant of the transverse forces is not at the same location in the section. This latter set of Strut-and-Tie Models, by assuming that the struts carry a part of the shear proportional to their axial force, assumes that there is some additional resistance to transverse forces available at the end of the general zone to absorb the asymmetry induced by the model. This had already been mentioned for the Strut-and-Tie Model presented in Section 5.6.1

and is not a problem in itself, as long as this difference is not overlooked and the necessary reinforcement is provided. If the reinforcement necessary to re-center the resultant of the shear forces is added to the reinforcement required to resist the combined bursting and shearing forces in the general zone, the results are much more comparable with the results of the previously presented models. This example shows how important it is to consider the Strut-and-Tie Model in a global context, not only using it as a tool to obtain a given force, such as the transverse force in the general zone, but also considering how the reaction forces resulting from the Strut-and-Tie Model will be resisted by the rest of the structure.

No tests were performed on anchorage zones with inclined tendons without curvature, mainly because of the practical difficulty of developing a test setup that would be able to realistically model the boundary conditions involving different transverse force distributions at the end of the general zone. Therefore, the results of the Strut-and-Tie Model were compared only with the results of the Finite Element Analysis based on the theory of elasticity in determining what geometric definition is most suitable for the analysis.

5.6.3 Strut-and-Tie Model with Tie Perpendicular to the Axis of the Beam

a) No Eccentricity
Inclination 10°

b) Eccentricity 0.25h
Inclination 20°
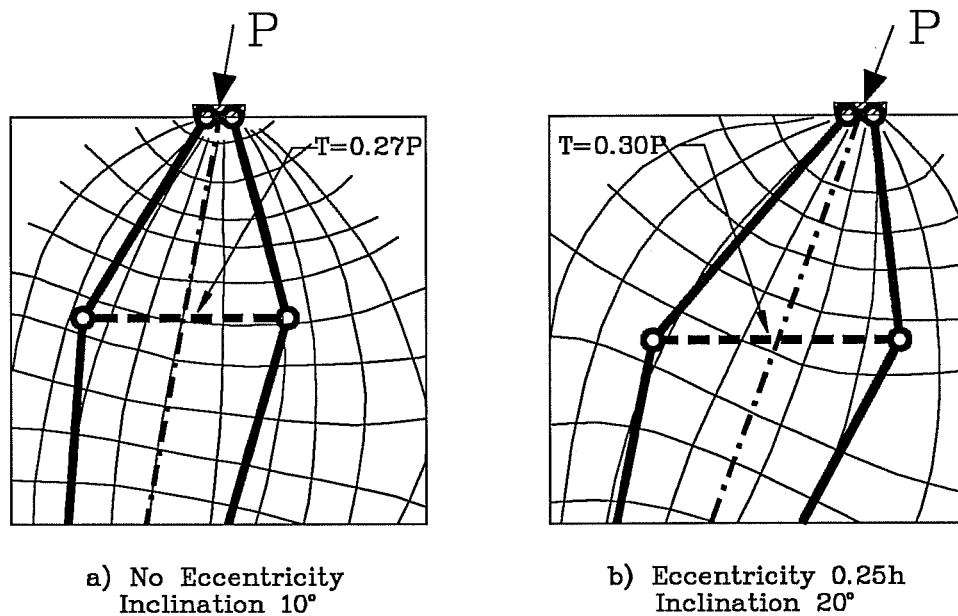
Figure 5.50 Strut-and-Tie Models Based on the Assumption of a Parabolic Distribution of the Transverse Reaction, Tie Perpendicular to the Axis of the Section

In practical applications, it may not be very convenient to place reinforcement perpendicularly to the axis of the tendon, as was assumed in the previous subsection. Instead, it appears desirable to place the reinforcement to resist the transverse forces in the same orientation as the rest of the reinforcement, most notably the stirrups that are typically perpendicular to the axis of the member. Based on the results presented in Section 5.6.2, values of the required transverse force to be resisted perpendicular to the tendon can be obtained and then distributed into components parallel and perpendicular to the axis of the beam, leading to design values for the tie forces. However, the

Strut-and-Tie Model can directly account for the effective orientation of the reinforcement, avoiding the intermediate step.
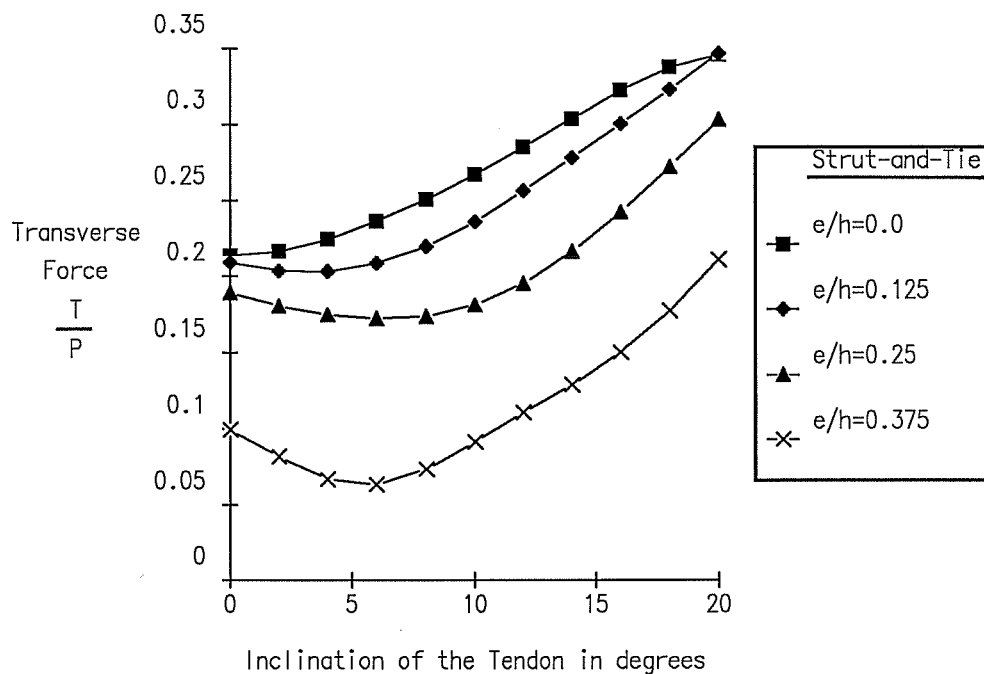
Figure 5.51 Transverse Force as a Function of the Inclination of the Tendon for Various Eccentricities. Tension Tie Perpendicular to the Axis of the Section

Fig. 5.50 shows two Strut-and-Tie Models based on a parabolic distribution of the transverse force at the bottom, a total diffusion angle of 52 degrees and a tension tie perpendicular to the axis of the section. Fig. 5.51 shows the variation of the transverse force as a function of the inclination of the tendon for various eccentricities. Notice that the values are only slightly greater than the values presented in Fig. 5.47.

5.7 Curved Tendons

5.7.1 Application with Curved Tendons in the Anchorage Zone

Anchorage zone configurations involving curved tendons occur in diaphragms, in segmental box girder bridges built using the free cantilevering method and in cantilever pier caps. Intermediate anchors located close to the supports in continuous bridges may have curved tendons in the anchorage zone. In general, anchorage zones that involve curved tendons also involve an inclination of the tendon at the anchorage. Stone and Breen [172, 173] describe applications of post-tensioning in segmental box girders bridges with inclinations of the cables at the anchorage up to 45 degrees. Applications with such an extreme inclination are rather rare, but cases with inclinations of up to 30 degrees are more common in practice.

5.7.2 Influence of Tendon Curvature on the State of Stresses in the Anchorage Zone

The presence of the deviation forces due to the curvature of the cable complicates the state of stresses by introducing discontinuities in the stress field near the tendon. Fig. 5.52 shows the deviation forces induced by a tendon with a radius of curvature R. The part of the structure located on the inside of the tendon is subjected to compressive stresses acting in the radial direction that are induced by the curvature of the tendon. These stresses decrease the tensile transverse stresses caused by the lateral spreading of the concentrated tendon force and by the inclination of the tendon. On the other hand, assuming that no cracking has occurred, the part of the structure located on the outside of the tendon sees an increase in the tensile transverse

stresses due to the radial tensile force caused by the curvature of the tendon.
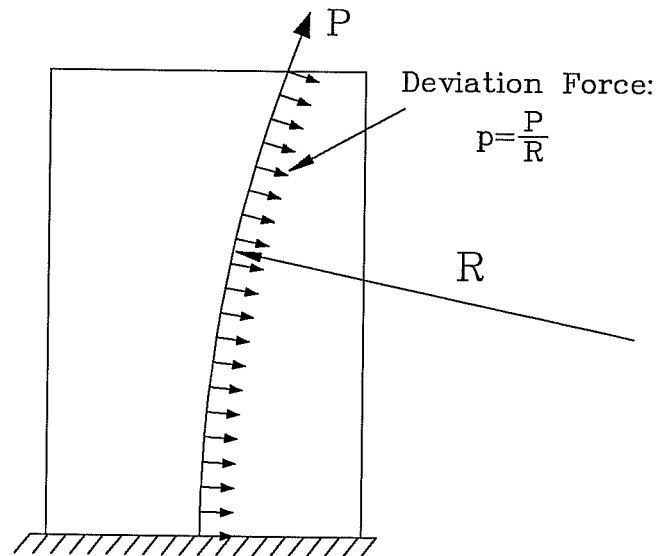
Figure 5.52   Tendon Force and Deviations Forces Induced by the Curvature of the Tendon

In an elastic body, like the ones studied using the elastic Finite Element Method, the deviation force is transmitted in part as a compression force to the inside of the tendon and in part as a tension force to the outside of the tendon, in proportion of the relative stiffness of both sides. In a real concrete structure, especially in thin sections like girder webs, a crack is likely to form along the axis of the tendon, because the largest transverse tensile stresses are observed perpendicular to the tendon. This is more likely to happen in thin sections, because the duct hole additionally decreases the area of concrete available to resist these stresses.

Once a crack forms along the tendon axis, the distribution of the deviation force from the tendon depends exclusively on the reinforcement that crosses the tendon axis. Thus, in addition to resisting the lateral spreading of forces, the transverse

reinforcement has to tie part of the deviation force of the tendon back across the crack. In practice, it is possible to use two different sets of reinforcing bars to fulfill the two functions, using one set of bars to provide the *tie-back* reinforcement and another set of bars to provide the *spreading* reinforcement, or to simply design the transverse reinforcement to resist both components. As will be seen in the subsection dealing with Strut-and-Tie Models for anchorage zones with curved tendons, it is important to consider both contributions in the design of the general zone reinforcement.

5.8 Finite Element Analysis of Curved Tendon Configurations

The influence of the curvature of the cable was investigated using the geometry described in Fig. 5.53. The inclinations
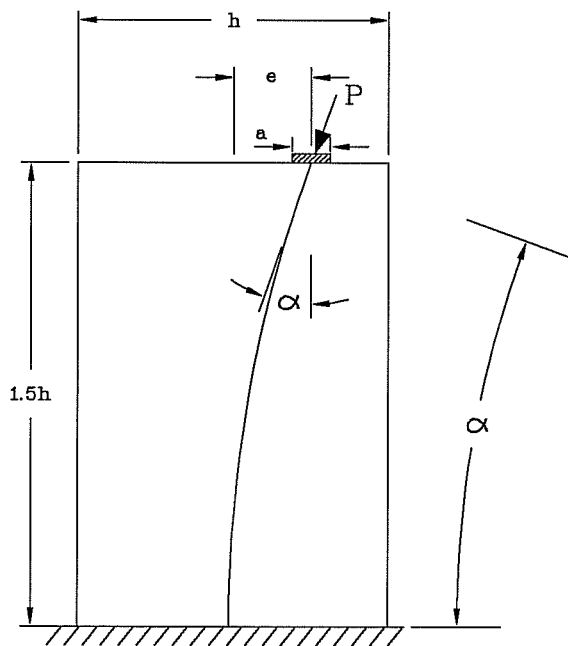
Figure 5.53 Geometry used in the Study of Anchorage Zones with Curved and Inclined Tendons

investigated were 0, 10, 20 and 30 degrees, and the eccentricities
considered were e = 0.0 and e = 0.25h. In each case, the radius of
curvature was chosen so that the tendon is parallel to the member
axis at a distance 1.5h from the anchor. The radii of curvature
are 8.638h for 10 degrees, 4.386h for 20 degrees and 3.0h for
30 degrees initial inclination. The deviation forces are applied
as a uniform pressure at the location of the tendon.

In addition to the parametric studies, Finite Element
analyses based on the actual geometry of the experimental test
specimens described in Section 5.9.3 were performed, and used in
the design of the specimens.

Fig. 5.54 shows the distribution of maximum principal stress
(in tension) for four cases with no eccentricity and with initial
inclination of the tendon of 0, 10, 20 and 30 degrees. The
contours are shown only for a length of 1.2h. As can be seen, the
maximum transverse stress increases with increased inclination and
curvature of the tendon, and its location tends to move slightly
closer to the anchorage device. The length over which tensile
stresses are acting tends to remain the same with increased
initial inclination of the tendon. The discontinuity in the stress
field caused by the introduction of the radial deviation forces of
the tendon appears clearly. Fig. 5.55 shows the corresponding
principal stress vectors for the same four specimens. Because the
axis of the tendon is a line of principal stress, the
discontinuity in the stress distribution at the location of the
tendon does not show very clearly in principal stress vector
plots, except by the fact that the vectors representing tension
stresses on the outside of the tendon are much larger.

a) No Inclination
No Curvature

b) Initial Inclination 10 degrees
Radius 8.64h

$A = 0.00\ \sigma_0$
$B = 0.05\ \sigma_0$
$C = 0.10\ \sigma_0$
$D = 0.15\ \sigma_0$
$E = 0.20\ \sigma_0$
$F = 0.25\ \sigma_0$
$G = 0.30\ \sigma_0$
$H = 0.35\ \sigma_0$
$I = 0.40\ \sigma_0$
$J = 0.45\ \sigma_0$
$K = 0.50\ \sigma_0$
$L = 0.55\ \sigma_0$

c) Initial Inclination 20 degrees
Radius 4.39h

d) Initial Inclination 30 degrees
Radius 3.0h

Figure 5.54   Contour Plot of the Maximum Principal Stress (in tension) for Tendon Inclinations of 0, 10, 20 and 30 degrees and no Initial Eccentricity
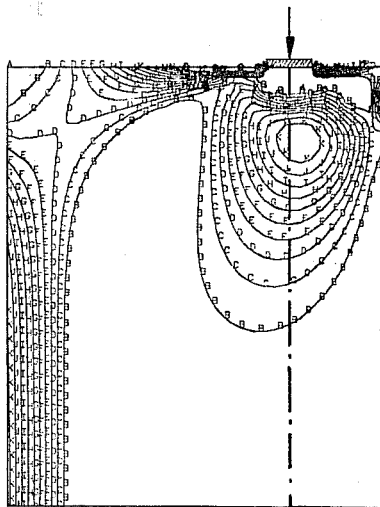
a) No Inclination
No Curvature
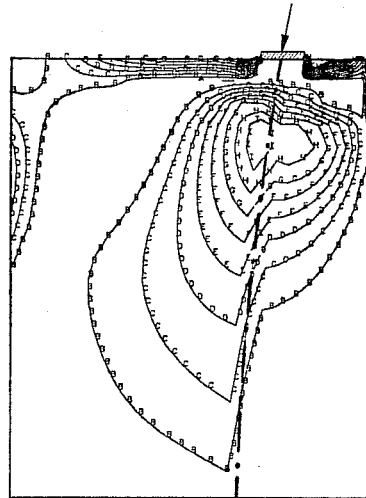
b) Initial Inclination 10 degrees
Radius 8.64h

c) Initial Inclination 20 degrees
Radius 4.39h

d) Initial Inclination 30 degrees
Radius 3.00h
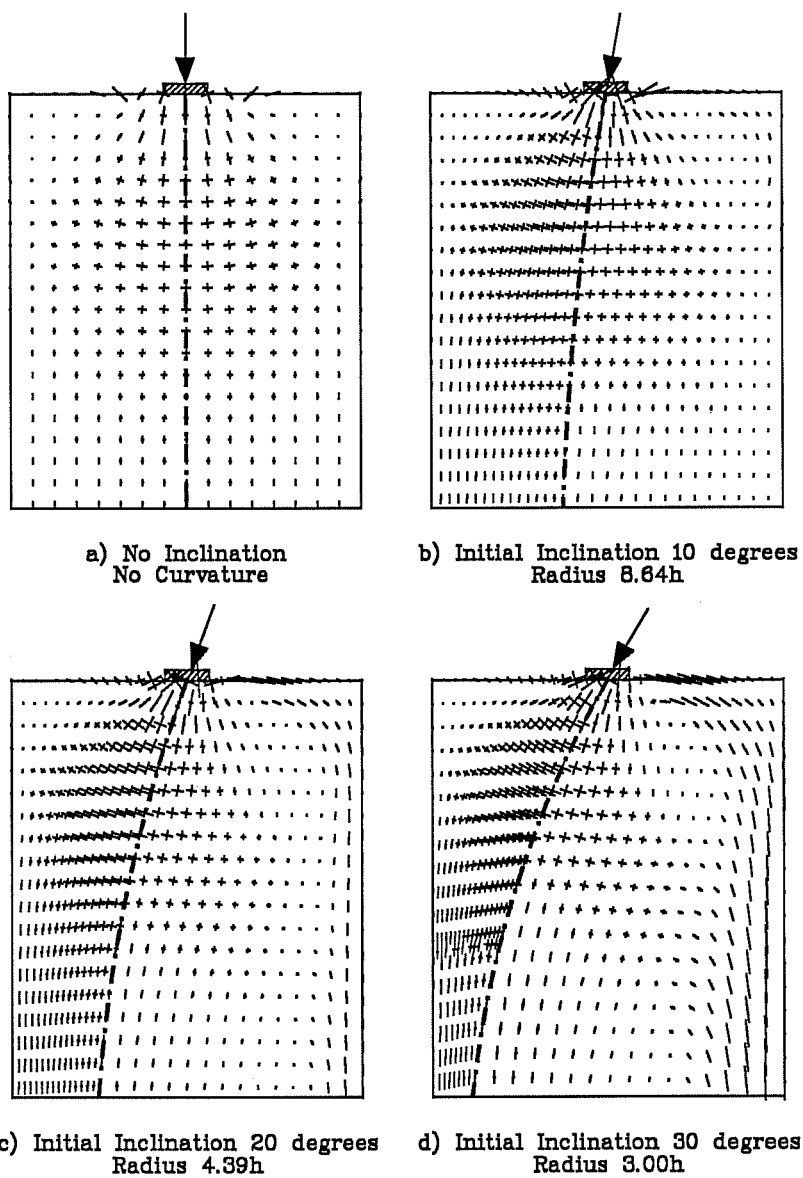
Figure 5.55 Vector Plot of the Principal Stresses for Tendon
Inclinations of 0, 10, 20 and 30 degrees and no
Initial Eccentricity

a) No Inclination
No Curvature

b) Initial Inclination 10 degrees
Radius 8.64h

A = 0.00 σ_0 B = 0.05 σ_0C = 0.10 σ_0 D = 0.15 σ_0 E = 0.20 σ_0 F = 0.25 σ_0 G = 0.30 σ_0
H = 0.35 σ_0 I = 0.40 σ_0 J = 0.45 σ_0 K = 0.50 σ_0 L = 0.55 σ_0 M = 0.60 σ_0 N = 0.65 σ_0

c) Initial Inclination 20 degrees
Radius 4.39h

d) Initial Inclination 30 degrees
Radius 3.0h

Figure 5.56   Contour Plot of the Maximum Principal Stress (in tension) for Tendon Inclinations of 0, 10, 20 and 30 degrees and Initial Eccentricity e = 0.25h

a) No Inclination
No Curvature Eccentricity 0.25h

b) Initial Inclination 10 degrees
Radius 8.64h Eccentricity 0.25h

c) Initial Inclination 20 degrees
Radius 4.39h Eccentricity 0.25h

d) Initial Inclination 30 degrees
Radius 3.0h Eccentricity 0.25h
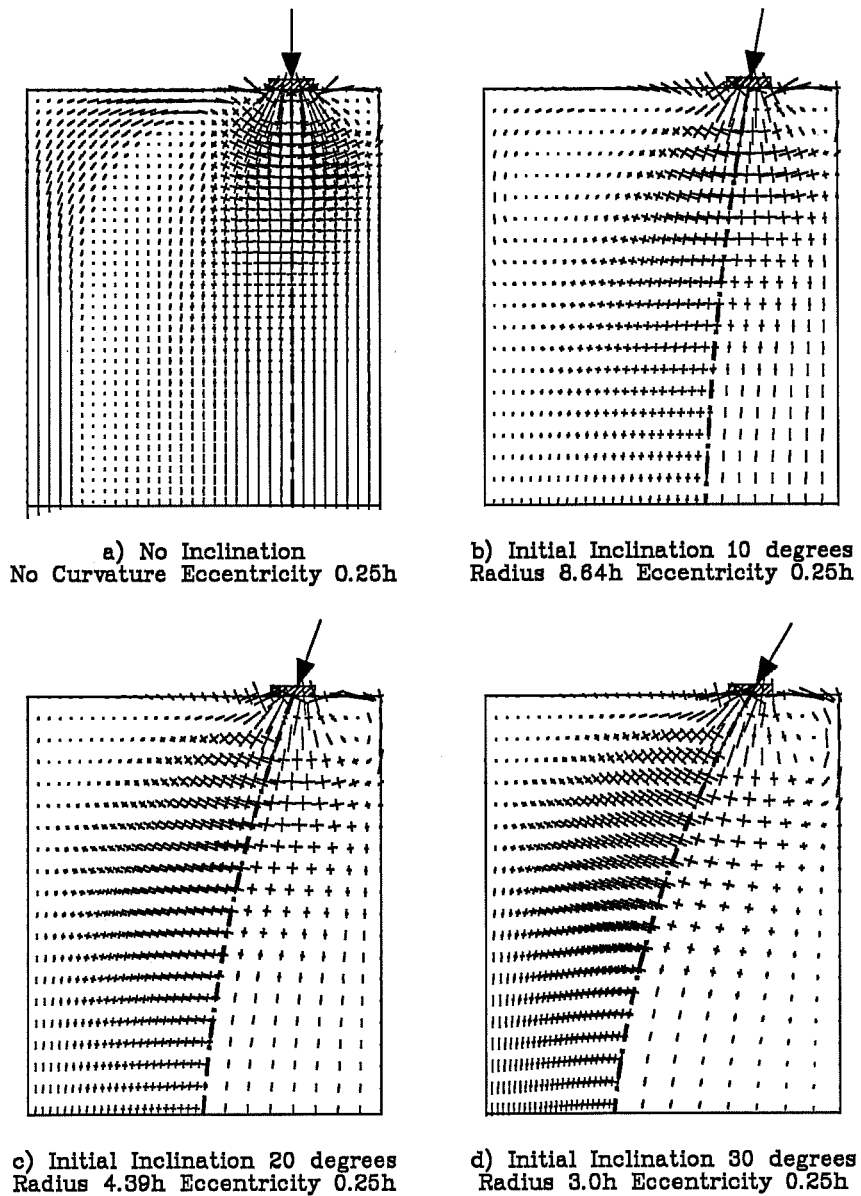
Figure 5.57   Vector Plot of the Principal Stresses for Tendon
Inclinations of 0, 10, 20 and 30 degrees and Initial
Eccentricity e = 0.25h

Fig. 5.56 shows the contour plot of the maximum principal stress for an eccentrically located tendon (e = 0.25h) and for the four initial inclinations of 0, 10, 20 and 30 degrees. Fig. 5.57 shows the corresponding principal stress vector plots. The maximum tensile stress does not change noticeably with the inclination, but the length over which transverse tensile stresses are acting increases with increased initial inclination. For an initial inclination of 20 degrees or more, the transverse stresses across the tendon have still not completely vanished at a distance 1.2h from the anchor. This is more than double the length observed for an eccentric tendon with no inclination, (compare with Fig. 5.10.)

Figure 5.58 shows the distribution of transverse stresses along the tendon axis for three initial inclinations of 10, 20 and 30 degrees and the corresponding curvatures of the tendon. The distribution is shown along three lines, instead of only one as previously for straight tendons. Because there is a discontinuity in the stress field at the location of the tendon, it is necessary to look at the stresses along the axis of the tendon, along a line slightly on the inside of the tendon axis, and along a line slightly on the outside of the tendon axis to obtain a complete picture of the state of stresses close to the tendon. The line corresponding to the axis of the tendon is shown for completeness, but it does not have much meaning, since this location is at the discontinuity and the stresses are automatically averaged by the Finite Element program. The other two lines give valuable information. They are separated by what is approximately the value of the deviation force of the tendon (P/r). The line located slightly to the inside of the tendon, where the deviation forces induce compressive stresses, shows smaller values of the transverse tensile stress than the line located slightly to the outside of the tendon, where the deviation forces induce additive tensile stresses. As a consequence, the controlling section for

cracking and design of the reinforcement is located just to the outside of the tendon, where cracking is more likely to initiate. Similarly, the transverse reinforcement should be designed on the basis of the force acting on the outside of the tendon.

Figure 5.59 shows the distribution of transverse stresses for initial inclinations of 10, 20 and 30 degrees and an initial eccentricity of 0.25h. The stresses on the outside of the tendon are larger than the stresses on the inside, as in the case with no initial inclination. The length over which tensile stresses act perpendicular to the tendon tends to increase with increased initial inclination. For the case of Fig. 5.59c, with an initial inclination of 30 degrees and a radius of the tendon of 3.0h, the transverse stresses become zero at a distance roughly equal to 1.5 times the depth h of the member. The tensile transverse stresses are located at a larger distance from the anchor than for the cases studied previously. These tensile stresses are mainly due to the deviation forces introduced by the cable, and could therefore be interpreted as a separate problem from the specific anchorage zone problem because they would be present without an anchorage zone. However, the fact that these stresses are in areas near the transverse stresses induced by the lateral spreading of forces makes it logical to consider both cases simultaneously. Fig. 5.60 and 5.61 show the transverse force integrated along the three lines, on the inside, the axis and the outside of the tendon, for no initial eccentricity and an initial eccentricity of e = 0.25h respectively. Most significant is the force integrated just outside of the tendon, where the largest values are observed. The figures also show the transverse force previously obtained for an inclined tendon that would be tangent to the curved tendon at the location of the anchor, as well as the values given by Eq. 5.5 for inclined tendons (see section 5.5.1).
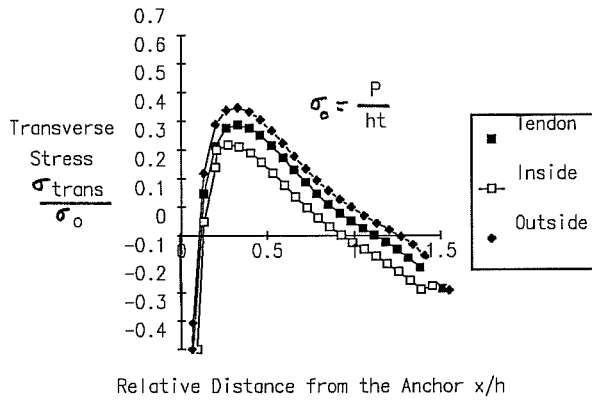
a) Initial Tendon
   Inclination
   10 degrees, Radius
   8.54h, no Eccentricity
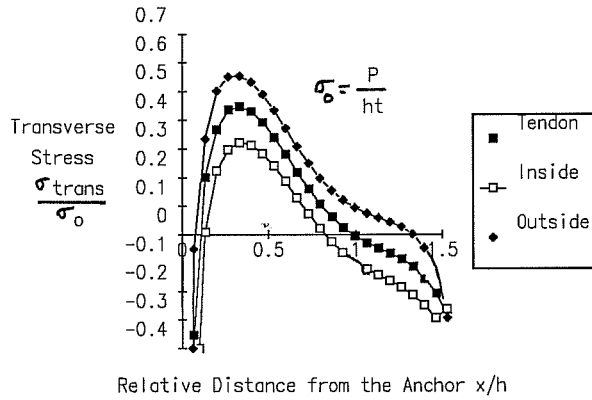
b) Initial Tendon
   Inclination
   20 degrees, Radius
   4.39h,
   no Eccentricity
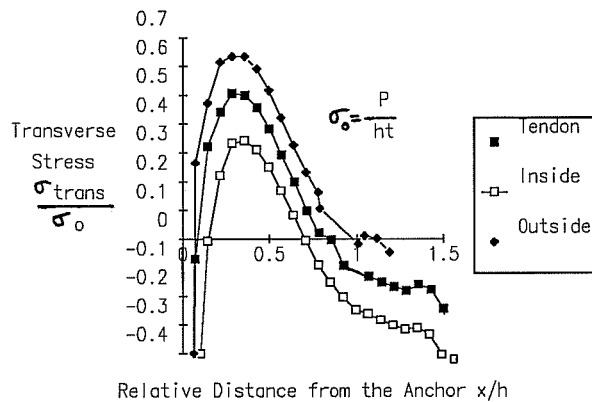
c) Initial Tendon
   Inclination
   30 degrees, Radius
   3.0h, no Eccentricity

Figure 5.58   Distribution of the Transverse Stresses across Lines
              Close to the Tendon as a Function of the Distance
              from the Anchor for Various Tendon Geometries with
              no Initial Eccentricity
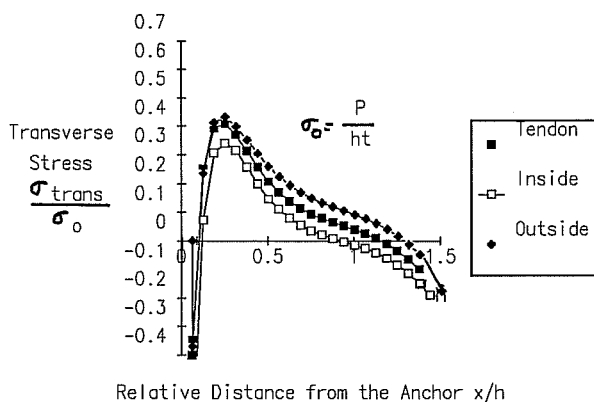
a) Initial Tendon Inclination 10 degrees, Radius 8.54h, Eccentricity 0.25h
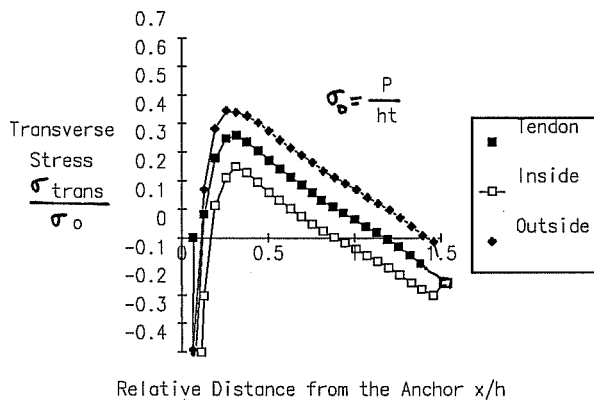
b) Initial Tendon Inclination 20 degrees, Radius 4.39h, Eccentricity 0.25h
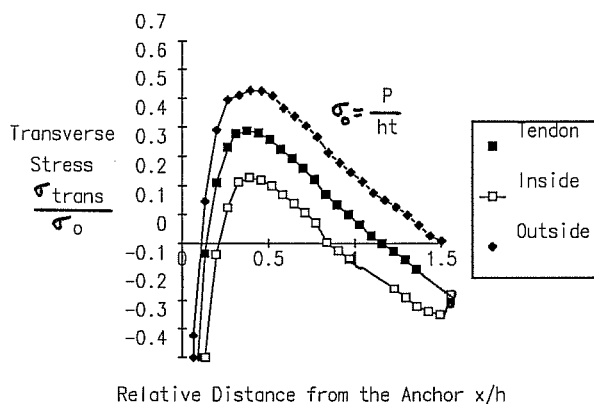
c) Initial Tendon Inclination 30 degrees, Radius 3.0h, Eccentricity 0.25h

Figure 5.59   Distribution of the Transverse Stresses across Lines Close to the Tendon as a Function of the Distance from the Anchor for Various Tendon Geometries with Initial Eccentricity e = 0.25h

The values obtained for the transverse force with initial inclination and curvature of the tendon are significantly larger than the values obtained for straight cables with no inclination. They are slightly larger than the results obtained for straight cables with an initial inclination, with the increase more pronounced for the eccentric case. Overall, the deviation forces do not significantly change the final result, at least for initial inclinations up to 20 degrees and radii of more than 4.5h. The transverse force for larger initial inclinations and smaller curvatures increases sharply, especially for the case with an initial eccentricity. The formula of Eq. 5.5 is generally conservative.
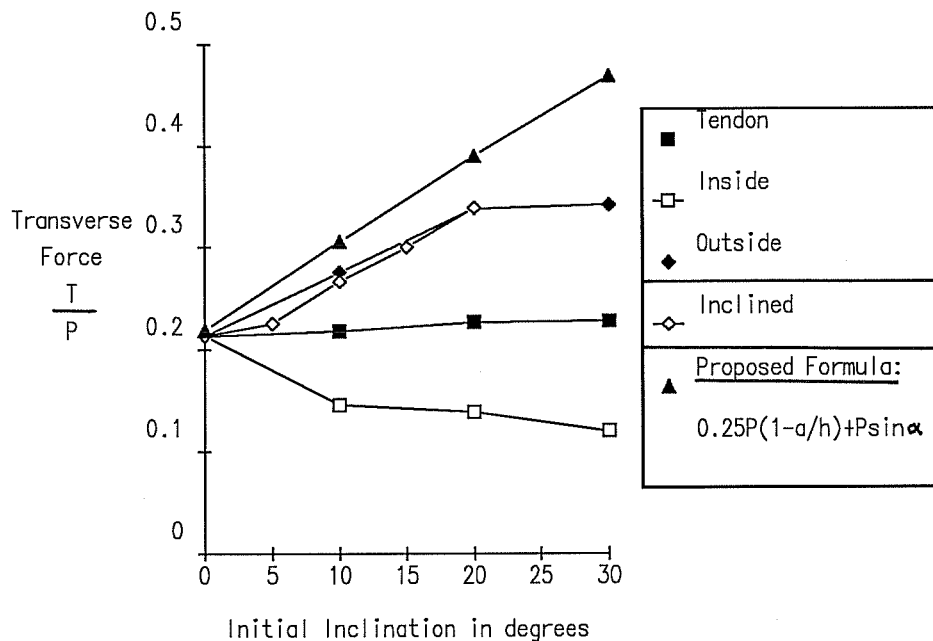
Figure 5.60   Integrated Tensile Force Across Integration Lines
              Close to the Tendon as a Function of the Initial
              Inclination of the Tendon
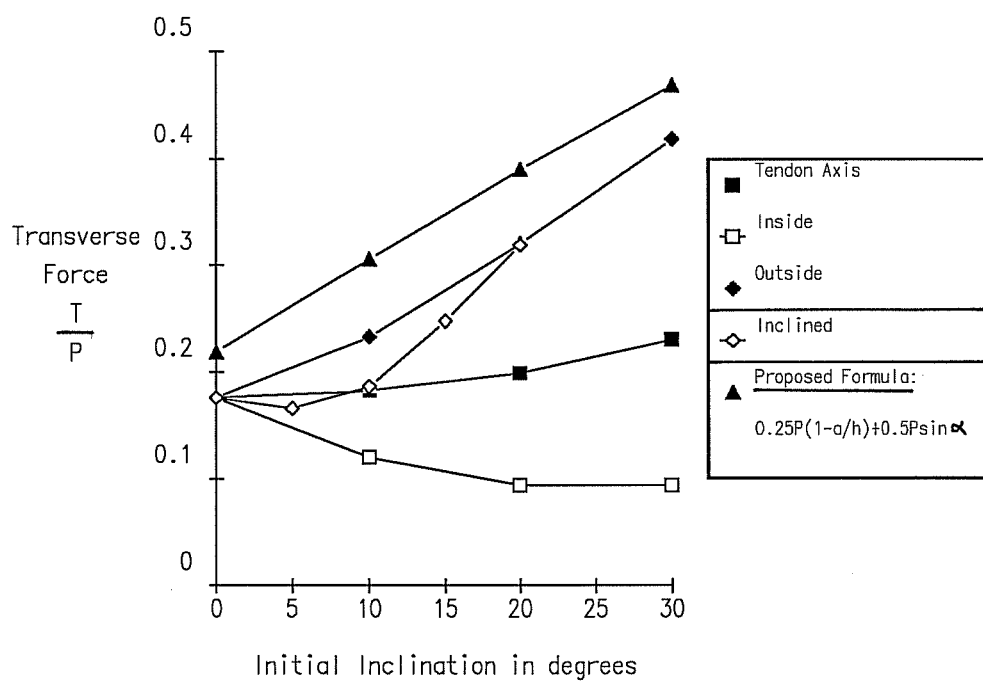
Figure 5.61 Integrated Tensile Force Across Integration Lines
            Close to the Tendon as a Function of the Initial
            Inclination of the Tendon for an Initial
            Eccentricity e = 0.25h

5.9   Strut-and-Tie Model for Curved Tendons

In anchorage zones with curved tendons, deviation forces caused by the curvature of the tendon are present in addition to the tendon load applied at the anchorage. Fig. 5.62 shows free bodies of an anchorage zone with a curved tendon. Under the assumption of no tensile concrete contribution across the tendon axis (as it is likely a crack will form at that location), and if no separate tie-back reinforcement is provided to anchor all or part of the deviation force, the tendon deviation forces will be distributed only to the part of the anchorage zone located to the inside of the tendon (Fig. 5.62a). The struts located to the inside of the tendon are curved because of the deviation forces, while the struts located to the outside of the tendon are straight between the reinforcing bars (Fig. 5.62c). The transverse reinforcement obtained by solving the Strut-and-Tie Model based on this hypothesis will resist the combination of both the lateral spreading of the concentrated anchorage load and the deviation forces.

If dedicated reinforcement is provided to anchor back part or all of the deviation forces induced by the curvature of the tendon force, as shown schematically in Fig. 5.62b, the deviation forces will be distributed to the struts located both to the inside and to the outside of the tendon, in proportion of the amount of force that is anchored back. Due to these deviation forces, the compression struts are curved between the transverse reinforcing bars (Fig. 5.62d). The transverse reinforcement obtained from the Strut-and-Tie Model based on this hypothesis will only resist the lateral spreading of forces; it requires that additional tie-back reinforcement be provided to resist the deviation forces.

a) Free Bodies with no
Tie—Back Reinforcement

b) Free Bodies with
Tie—Back Reinforcement

c) Strut—and—Tie Model
with no
Tie—Back Reinforcement

d) Strut—and—Tie Model
with
Tie—Back Reinforcement
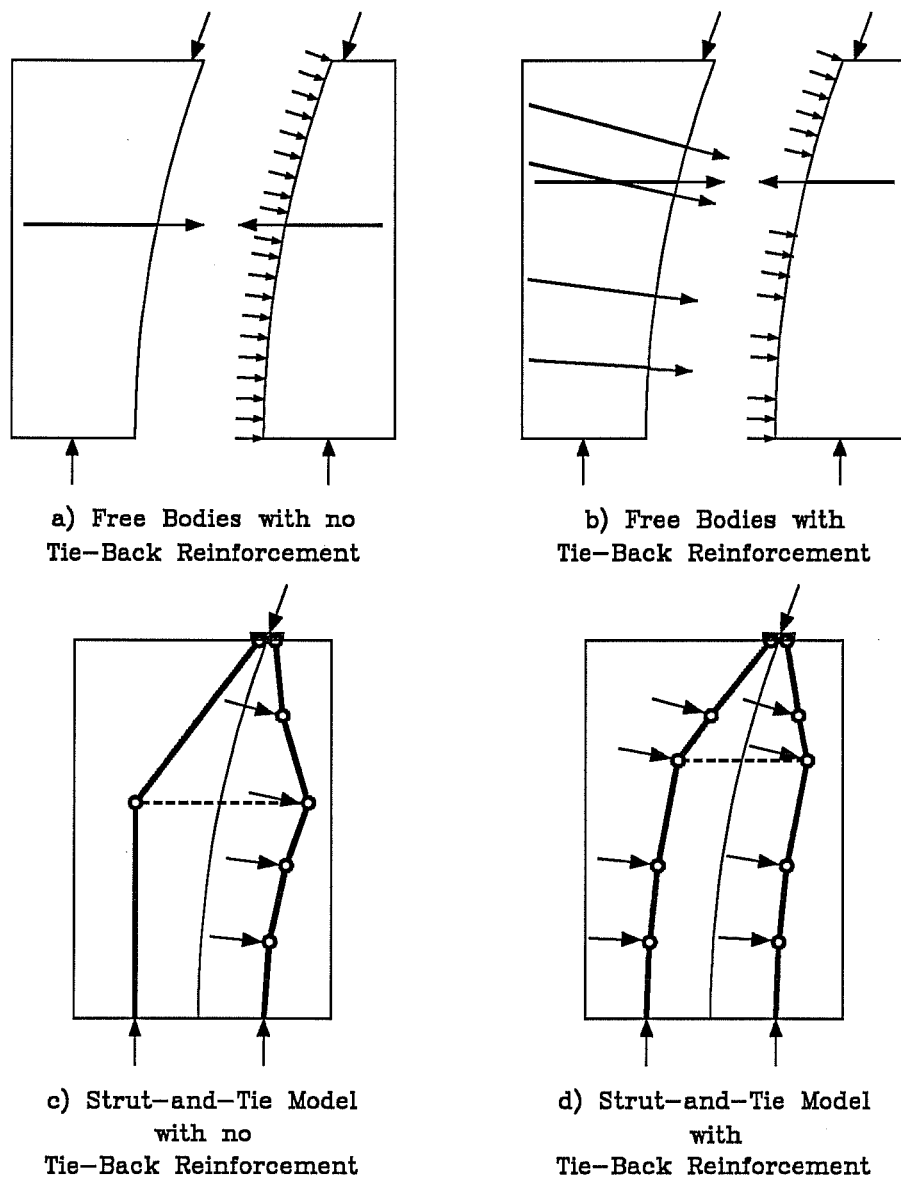
Figure 5.62   Free Bodies and Strut-and-Tie Models for Curved
Tendons with and without Tie-Back Reinforcement

For a meaningful comparison between the various possibilities, it is necessary to add both lateral spreading and tie-back of the deviation forces when comparing the forces obtained by the Strut-and-Tie Model.

In the next sections, the influence of the tie-back reinforcement will be investigated on the basis of Strut-and-Tie Models. The variable used to quantify the amount of tie-back reinforcement provided is defined as the ratio F of the available tie-back force to the deviation force produced by the curvature of the post-tensioning tendon. Fig. 5.63 shows how the deviation force from the tendon is distributed on both sides of the tendon, with an amount F being tied back to the outside of the tendon and the rest of the deviation force $(1-F)$ being introduced as a compression on the inside of the tendon. If no tie-back reinforcement is provided, the tie-back ratio $F = 0$. For the parametric studies, the value of the tie-back ratio F was defined
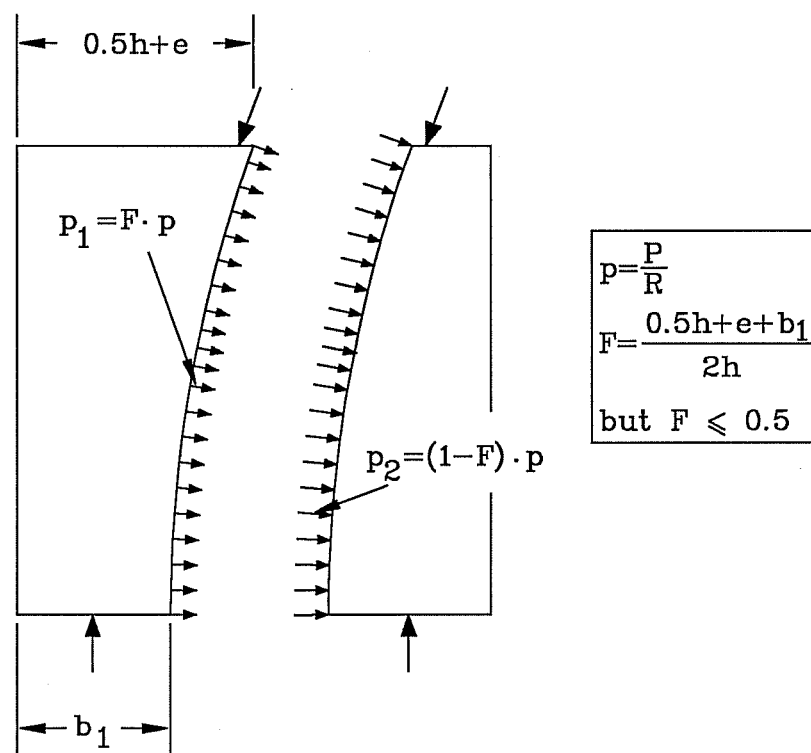
Figure 5.63 Definition of the Tie-Back Ratio F for Anchorage
Zones with Curved Tendons

as indicated in the formula of Fig. 5.63. The tie-back ratio is given by the average part of the section that is located outside of the tendon relative to the overall depth of the section, with a limit of one half of the deviation force induced by the tendon. The limit of one half on the tie-back reinforcement seems reasonable for most cases because the transfer of more than 50% of the deviation force to the back of the general zone would most likely cause very wide cracks near the tendon. Tie-back ratios greater than 0.5 are sometimes used in applications where the tendon is located on the inside of a curved shell. The limitation to 0.5 for this study includes standard applications of post-tensioning to girders.

5.9.1 Geometric Definition of the Strut-and-Tie Model for Curved Tendons

The presence of deviation forces and the hypotheses on the distribution of the deviation forces have a significant influence on the geometry of the Strut-and-Tie Model. In this section, only thrust-line Strut-and-Tie Models were considered because of their flexibility in handling complex loading conditions. Starting at the end of the anchorage zone, two resultants are determined for the forces to the left and to the right of the tendon. Then, working toward the anchor, the deviation forces and the effect of transverse reinforcement are introduced in the compression struts at given locations in the general zone, according to the tie-back ratio. A satisfactory Strut-and-Tie Model is obtained when the thrust-lines converge to the quarter points of the plate. The process is iterative, but can be stopped as soon as the thrust-lines actually cross each other before reaching the plate. A conservative (if not optimal) design is then obtained. For a precise analysis of the ultimate load capacity of a given

configuration, several iterations are required.

Fig. 5.64 shows two examples of Strut-and-Tie Models for curved tendons with an initial eccentricity of 0.25h and an initial inclination of the tendon of 20 degrees. The Strut-and-Tie Model in Fig. 5.64a assumes that no tie-back reinforcement is available, while the Strut-and-Tie Model in Fig. 5.64b has a tie-back reinforcement to resist half the deviation forces. When the contributions of all the reinforcement that crosses the axis of the axis of the tendon are summed, the Strut-and-Tie Model with no

a) Strut–and–Tie Model
with no Tie–Back
Reinforcement (F=0)

b) Strut–and–Tie Model
with Tie–Back
Reinforcement (F=0.5)

Figure 5.64   Strut-and-Tie Models of Anchorage Zone with a Curved
Tendon of Initial Inclination 20 degrees and Initial
Eccentricity 0.25h, for Tie-Back Ratios F=0 and
F=0.5

tie-back reinforcement requires 37% of the tendon load, while the Strut-and-Tie Model with tie-back reinforcement requires a total of 38% of the tendon load, showing how close the results of the two methods are.

5.9.2 Parametric Study of the Influence of the Curvature

A parametric study was performed on the influence of initial inclination and curvature of the tendon using thrust-line Strut-and-Tie Models. Fig. 5.62c and 5.62d show the geometry used for this study. In order to simplify the model, the reinforcement was assumed to be located in one layer perpendicular to the axis of the member. Because reinforcement is usually detailed perpendicular to the axis of the member, this does not appear to be restrictive. As in the previous parametric studies, the diffusion angle from the center of the plate to the centroid of the reinforcement was constrained to be 52 degrees. The parametric study was performed for two values of the tie-back force: no tie-back reinforcement (F=0) and tie back reinforcement as defined in Fig. 5.63, equal to the average distance from the tendon axis to the back of the anchorage zone, but not larger than 0.5 (F=F(e) in Figs 5.65 to 5.68).

Fig. 5.65 presents the transverse force obtained from the Strut-and-Tie Model as a function of the initial inclination of the tendon for the two hypotheses on the tie-back reinforcement (F=0 and F=F(e)) as well as the integrated forces obtained from the Finite Element analyses for no initial eccentricity and the approximate formula proposed in Section (?). Fig. 5.66 shows similar curves for a case with initial eccentricity of the tendon (e = 0.25h). The values obtained by the Finite Element method and the approximate formula are also shown in the figures.

The results obtained by both Strut-and-Tie Models are very close if the tie-back reinforcement is included in the total transverse force. There is a satisfactory correlation between the force obtained by the Strut-and-Tie Model and the force obtained by integrating the elastic stresses. Both methods predict a sharp increase in the required transverse reinforcement as the initial inclination of the tendon increases (and the radius of curvature decreases).
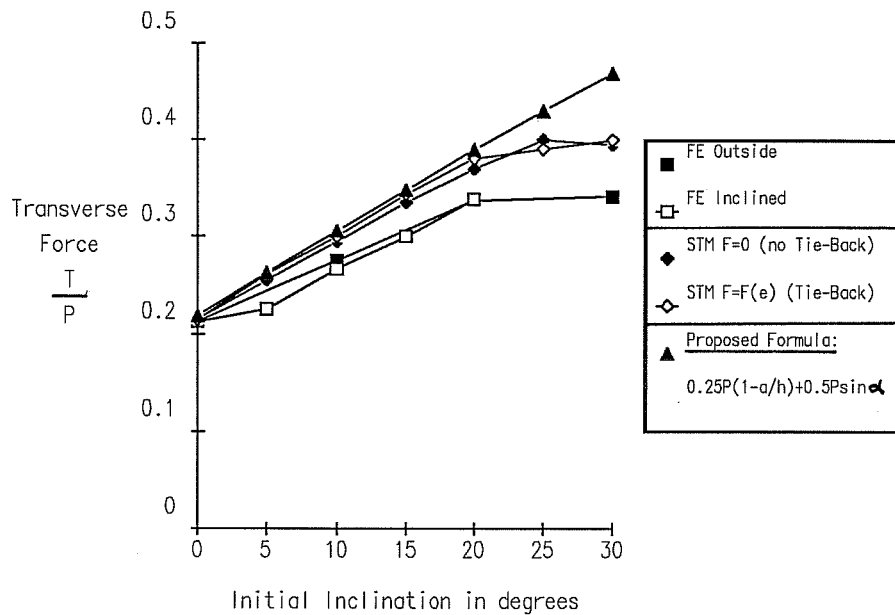
Figure 5.65   Transverse Force Obtained from the Strut-and-Tie
             Model as a Function of the Initial Inclination for
             Various Ratios of the Tie-Back Reinforcement with no
             Initial Eccentricity
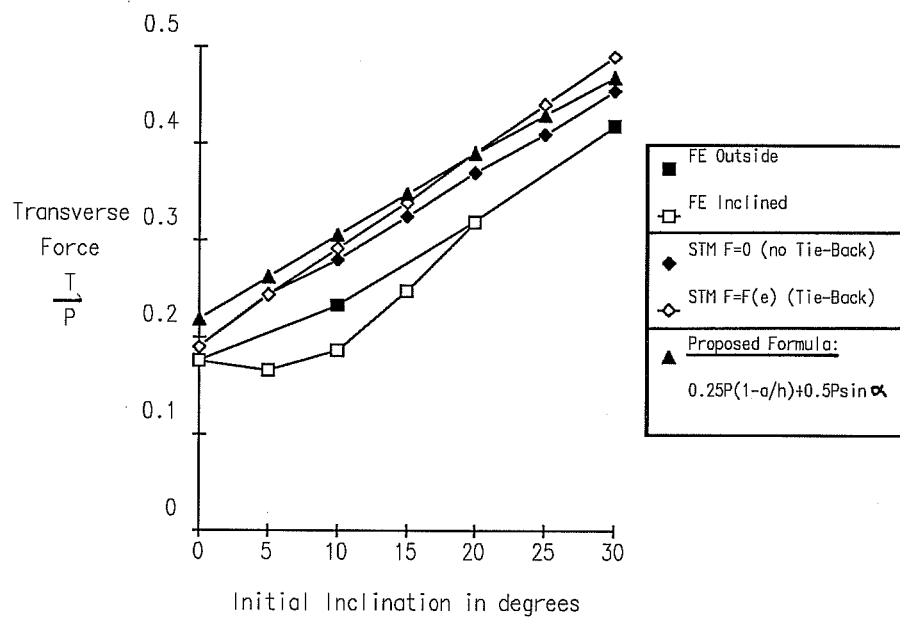
Figure 5.66   Transverse Force Obtained from the Strut-and-Tie
              Model as a Function of the Initial Inclination for
              Various Ratios of the Tie-Back Reinforcement with an
              Initial Eccentricity e = 0.25h
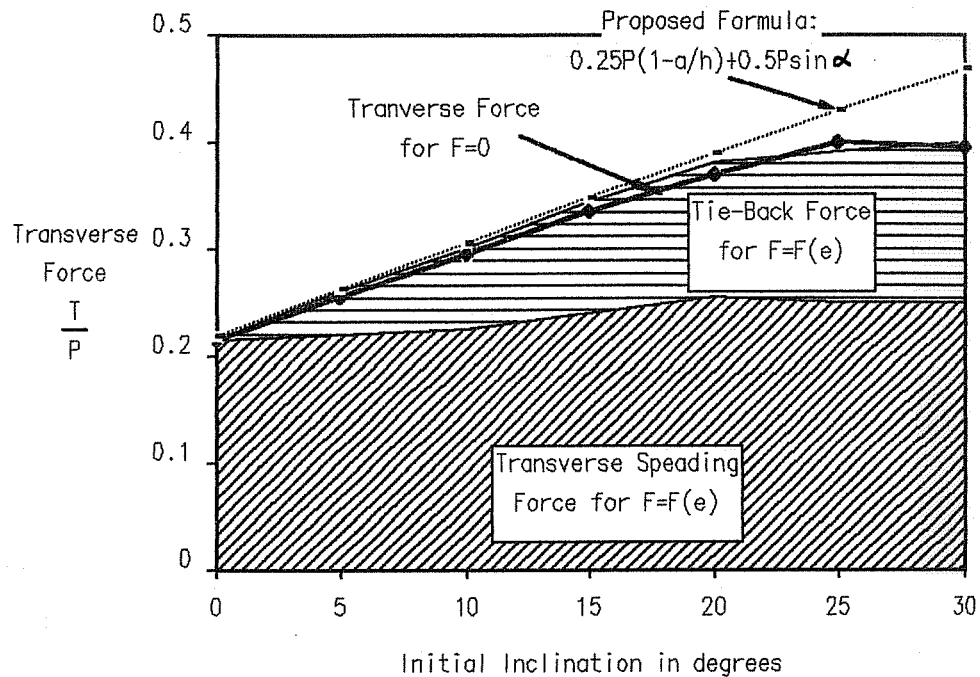
Figure 5.67   Components of the Transverse Force as a Function of
the Initial Inclination for no Initial Eccentricity

Figures 5.67 and 5.68 show a comparison of the two Strut-
and-Tie Models used for this parametric study. The thick line
represents the transverse force required by the Strut-and-Tie
Model with no tie-back reinforcement, while the shaded areas
represent the two components present in the Strut-and-Tie Model
with tie-back reinforcement. As can be seen in the figures, the
component of the transverse force caused by the lateral spreading
of forces (labeled Transverse Spreading Force in the figures) is
nearly constant with increased inclination, while the contribution
due to the deviation force causes the majority of the increase in
the total transverse force. The approximate formula proposed to
estimate the magnitude of the transverse force is shown as a
dotted line. This formula is generally conservative for angles of

inclination up to 20 degrees. For most practical application, the results of the formula are conservative. A more detailed analysis is recommended for configurations involving angles in excess of 25 degrees and large eccentricities.
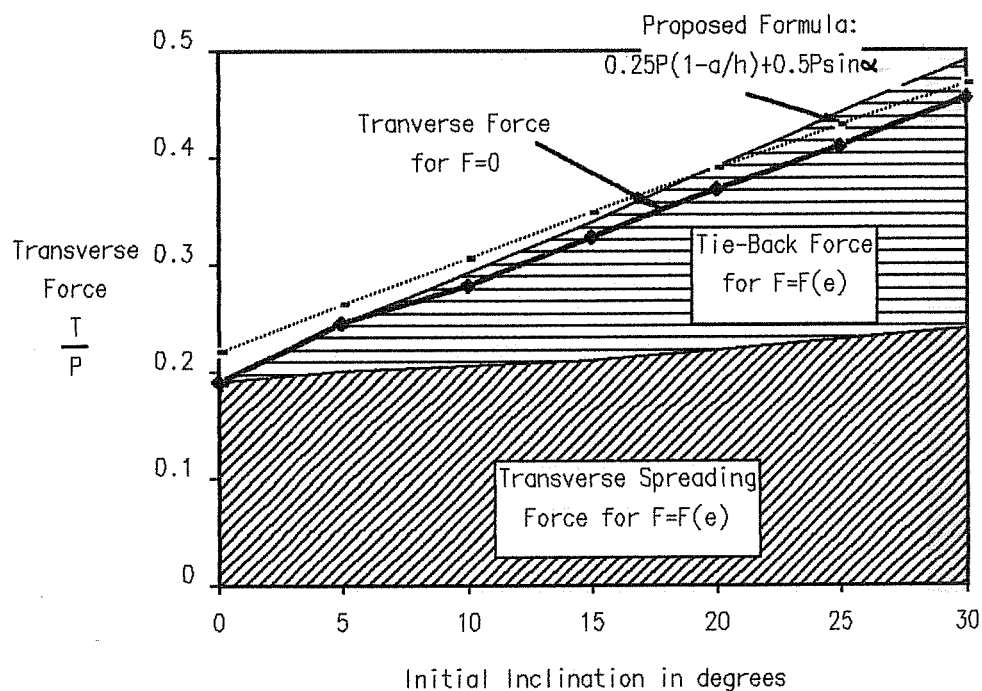
Figure 5.68   Components of the Transverse Force as a Function of the Initial Inclination for Initial Eccentricity e = 0.25h

5.9.3 Comparison with Test Results of the UT Austin Research Project

A series of four test specimens, labeled I1 through I4, were built and tested to investigate the influence of inclination and curvature of the tendon in the anchorage zone. Fig. 5.69 shows the

geometry of the specimens in this series of tests. Table 5.3 summarizes the dimensions, the tendon layout and the properties of the concrete.

Fig. 5.70 shows the layout of the reinforcement in the general zone for the specimen I1, which is typical of the reinforcement used for this test series. The transverse reinforcement consists of closed stirrups of high strength #2 ties (Tensile capacity 3.57 kips for one bar) at a distance of four inches. The tie-back reinforcement consists of five closed stirrups of the same high strength steel placed around the tendon. The detailing of the tie-back reinforcement, with the ties just
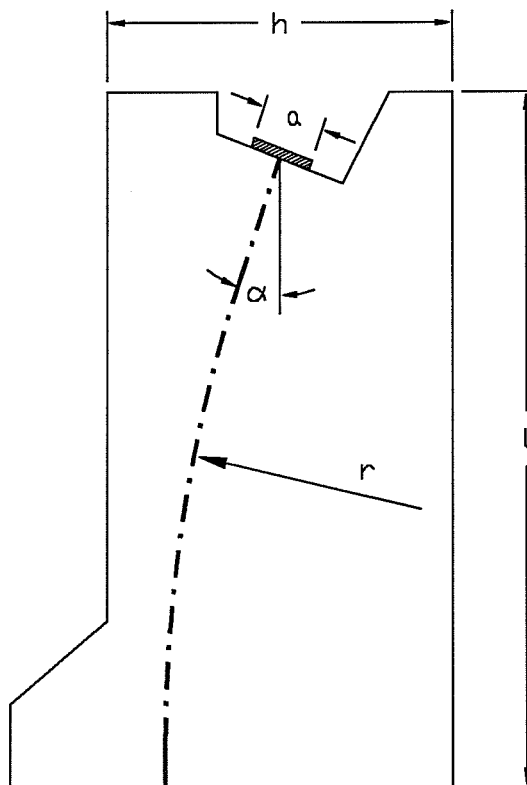
Figure 5.69 Geometry of Specimens with Curved Tendons

surrounding the tendons and being anchored somewhere in the middle of the outside compression strut is not recommended for practical applications. It was used for the experimental tests because it allowed for a better separation between the functions of the two types of reinforcement. For practical applications, it is recommended that tie-back reinforcement of greater length be used. The tie-back reinforcement should enclose the entire compression strut, to ensure that the tensile force is properly introduced into the strut. Table 5.4 summarizes the total yield force and centroid for the two types of reinforcement, as well as the sum of both. More details about the test setup and the testing procedures can be found in Ref. 153.

Table 5.3   Summary of the Dimensions of Specimens with Curved Tendons with Dimensions of the Anchorage Plate and Concrete Strength

	Dimensions	Tendon	Concrete	
Specimen	$h \cdot w \cdot t$ [in]	α/radius/eccentricity [degrees]/[in]/[in]	f'_c [ksi]	f_{sp} [ksi]
I1	66·36·10	20/130.7/0	5.72	0.358
I2	66·36·10	20/130.7/9	6.41	0.423
I3	66·36·10	10/238.6/0	4.51	0.348
I4	66·36·10	20/130.7/9	6.17	0.393
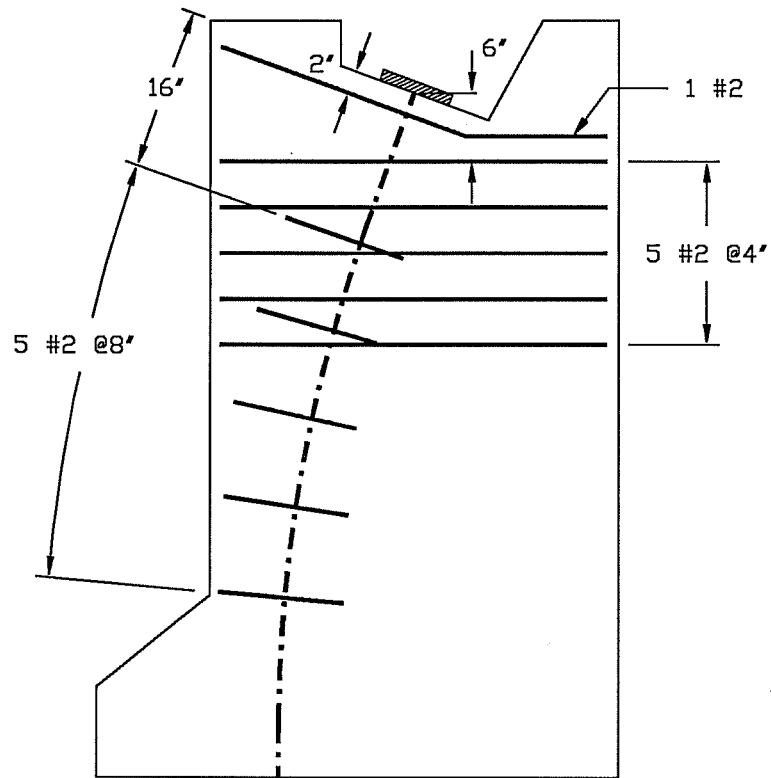
Figure 5.70   Transverse and Tie-Back Reinforcement of Specimen I1

Table 5.4   Summary of the Transverse and Tie-Back Reinforcement
             for Specimens with Curved Tendon

	Transverse Reinforcement		Tie-Back Reinforcement		Total Reinforcement	
Specimen	As*fy [kips]	Centroid [kips]	As*fy [in]	Centroid [kips]	As*fy [in]	Centroid [kips]
I1	39.4	12	32.8	32	72.2	21.1
I2	39.4	12	71.2	32	110.6	24.9
I3	39.4	12	26.2	30	65.6	12.2
I4	32.3	12	N/A	N/A	32.3	12

Figure 5.71 shows for the four specimens with curved tendons the actual cracking load and the cracking load predicted based on the peak tensile stress in the bursting region obtained from the Finite Element Analysis and the concrete tensile strength as measured in a split cylinder test. The actual cracking loads in this test series were greater than the predicted values, with an average ratio from actual to predicted of 1.25 and a standard deviation of 0.157. Fig. 5.72 shows the ultimate strength of the specimens with curved tendons and the predicted strength based on the Strut-and-Tie Model for both tie and strut failure, as well as the compression failure based on elastic stress calculations. For all specimens, the failure of the tension tie controls the design. However, as can be observed from Fig. 5.72, the actual ultimate
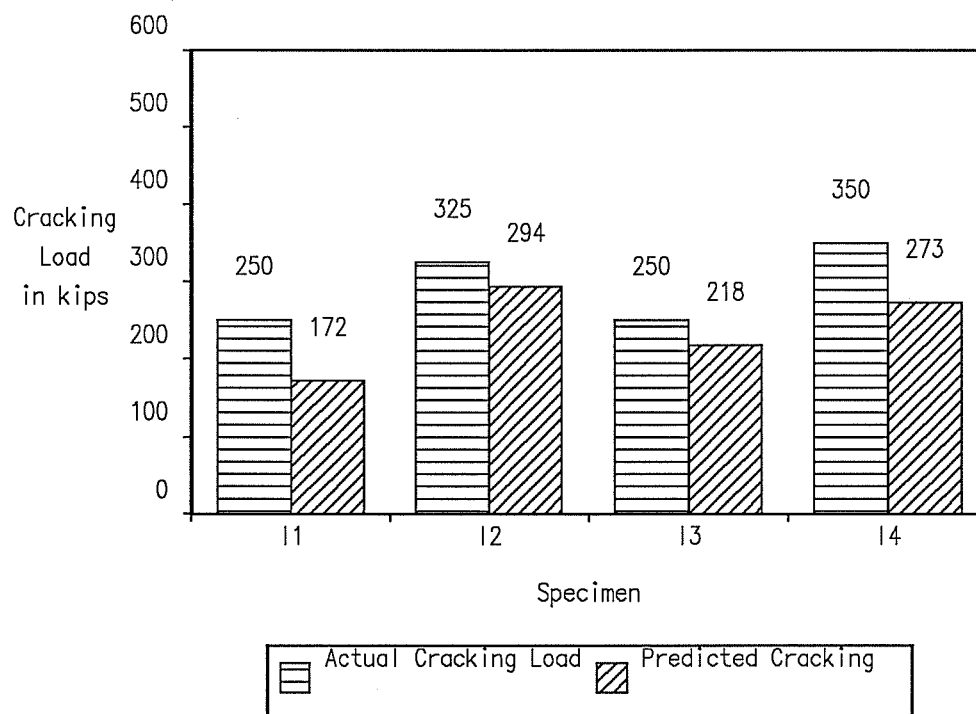
Figure 5.71   Actual and Predicted Cracking Load for Specimens with Curved Tendons

load is considerably higher than predicted, and close to the value predicted by a failure of concrete in compression. This may be due to a contribution of concrete in tension to the load-carrying mechanism. As a consequence, the results predicted by the Strut-and-Tie Model are quite conservative, much more than for the previous configurations. This is especially true for specimen I4, which did not have any tie-back reinforcement.
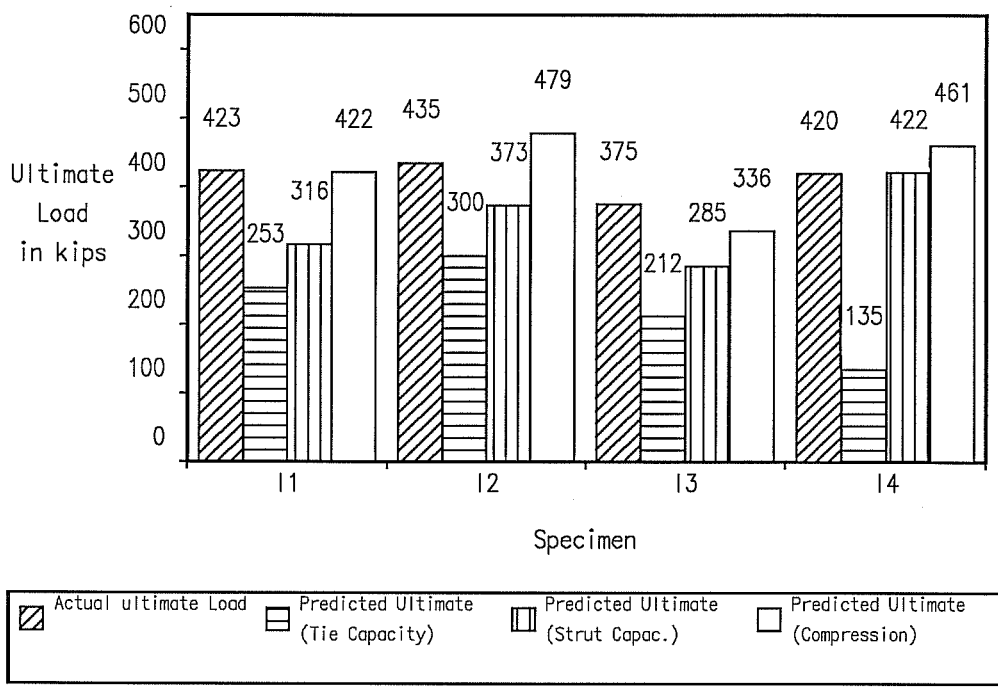
Figure 5.72   Actual Ultimate Load and Ultimate Load Predicted by
              the Strut-and-Tie Model (Tie-based Capacity and
              Strut-based Capacity) for Specimens with Curved
              Tendons

Fig. 5.73 shows the actual cracking and ultimate load for all four specimens. There is still a sizeable increase in strength between cracking and ultimate loads, but this increase is only of 20 percent for specimen I4. Specimen I4 is essentially identical

to specimen I2, except that it does not have any tie-back reinforcement. According to the Strut-and-Tie Model the absence of tie-back reinforcement should drastically reduce the load carrying capacity of the specimen, but this was not observed in the test specimen.
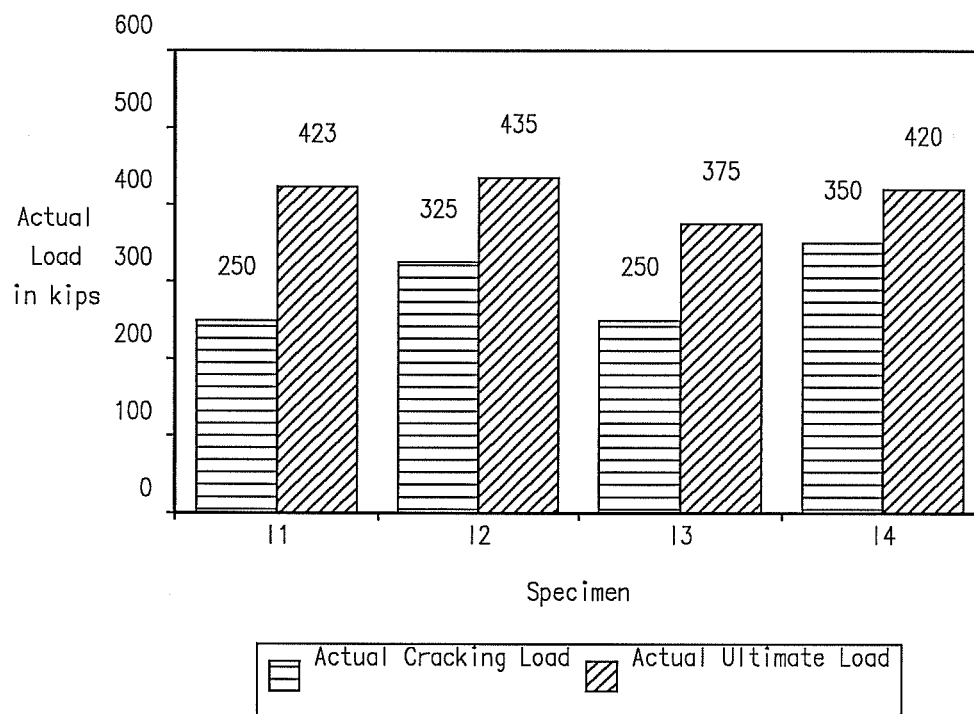
Figure 5.73   Actual Cracking and Ultimate Load for Specimens with Curved Tendons

Fig. 5.74 shows the ratio of the actual ultimate load to the predicted ultimate load from the Strut-and-Tie Model as a function of the ratio of the actual location of the centroid of the reinforcement to the location of the elastic centroid. The figure shows two series of points. The first takes into account both the transverse and the tie-back reinforcement. The second takes into account the transverse reinforcement only. If both types of reinforcement are included, the points for Specimens I1 to I3 are

well distributed around the abscissa of 1.0, corresponding to the elastic centroid, while the point for I4 is at an abscissa of 0.4, meaning that the reinforcement is located much closer to the anchor. The apparent diffusion angle from the center of the plate to the centroid of the reinforcement obtained by the Strut-and-Tie Model is approximately 85 degrees, compared with the 52 degrees used for the parametric studies, and recommended for design.
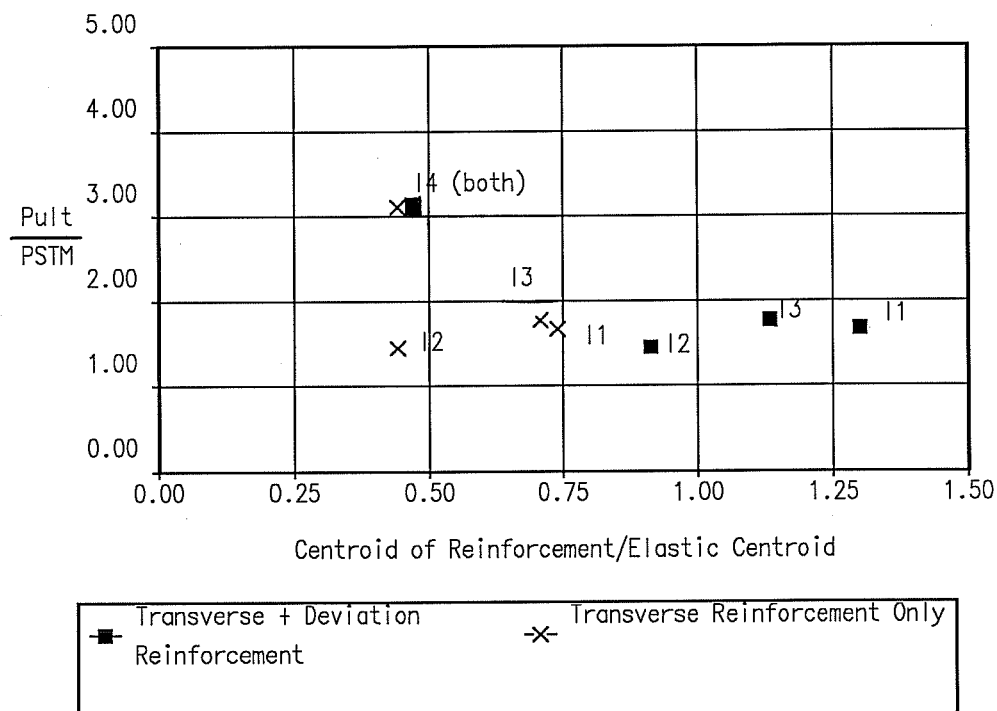
Figure 5.74 Ratio of the Actual Ultimate Load to the Predicted Ultimate Load as a Function of the Ratio of the Actual Centroid to the Elastic Centroid

The average ratio of actual ultimate load to predicted ultimate load is 2.00, with a standard deviation of 0.752 if all specimens are taken into account. If only specimens I1 to I3 are considered, the average ratio is 1.63 with a standard deviation of 0.163. In all cases, the design values obtained by the Strut-and-

Tie Model are conservative, albeit too much so. Additional investigations would be needed to identify the possible additional effects that cause such discrepancies.

5.9.4 Comparison with Other Test Results

A series of test specimens with inclined and curved tendons has been reported by Stone and Breen [172, 173, 174]. Table 5.5 summarizes the dimensions and concrete strength for five specimens with curved tendons reported by Stone. Table 5.6 gives the total reinforcement provided for the specimens. Fig. 5.75 shows the cracking and ultimate loads of Stone's specimens. In this case, a sizeable increase from the cracking to the ultimate load was observed. This is accentuated by the fact that the ultimate load reported for Specimens FS2A, FS2B and FS4A are not actual failures of the anchorage zone, but rather failures of the tendon. Fig. 5.76 shows the ultimate load of Stone's specimens compared to the ultimate loads predicted by the Strut-and-Tie Model for both tie and strut capacity. As can be clearly seen, Stone's specimens were heavily reinforced. The tie based capacity is typically in excess of three times the predicted strut capacity. This is confirmed by looking at Table 5.6 which shows the transverse reinforcement provided: the tensile capacity of the reinforcement is of the same order of magnitude as the actual ultimate load. In contrast, the ultimate load of the specimens reported in Section 5.9.3 is on average seven times greater than tensile capacity of the reinforcement. Thus, it is more than likely that Stone's specimens experienced a compression failure, which is confirmed by the relative closeness of the actual ultimate load and the ultimate load predictions based on the strut capacity.

Table 5.5   Summary of the Dimensions and Characteristic Strengths
of the Concrete for Stone's Specimens with Curved
Tendons

	Dimensions	Tendon	Concrete	
Specimen	h·w ·t [in]	α/radius/eccentricity [degrees]/[in]/[in]	f'c [ksi]	fsp [ksi]
MI2	20.5·48*·3	30/65**/0	5.31	0.582
MI3	20.5·48*· 3	30/65**/0	5.21	0.606
FS2A	82·125*·12	15/500**/0	5.04	0.532
FS2B	82·125*·12	30/260**/0	4.27	0.455
FS4A	82 ·125*·12	30/260**/0	5.2	.513

*:   approximate value, depending on the specimen

**: assumed average radius. The radius is not constant in
Stone's Specimens

Table 5.6   Summary of the Transverse Reinforcement for Stone's
Specimens with Curved Tendons

	Transverse Reinforcement	
Specimen	As*fy [kips]	Centroid [in]
MI2	52.8	16.6
MI3	52.8	49
FS2A	720	49
FS2B	720	49
FS4A	820	49
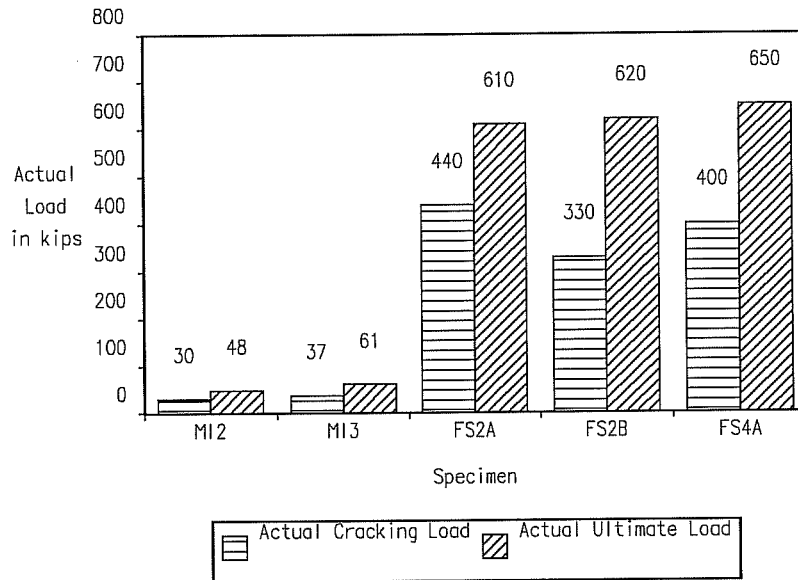
Figure 5.75   Cracking Load and Ultimate Load for Stone's Curved
              Specimens
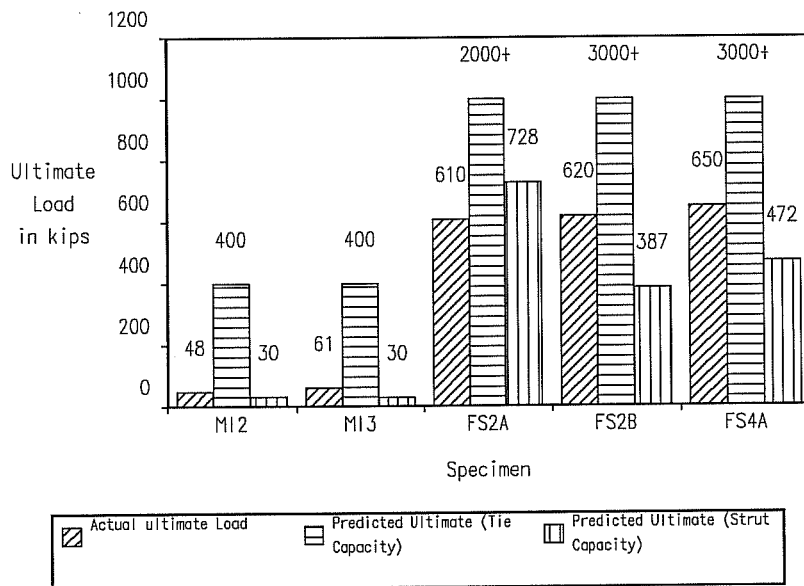
Figure 5.76   Actual Ultimate Load and Ultimate Load Predicted by
              the Strut-and-Tie Model for Stone's Curved Specimens

5.9.5 Enhancement of the Behavior Model

It appears that some unaccounted load carrying mechanism is involved in configurations with curved tendons, causing the ultimate load to be significantly larger than the load predicted on the basis of the Strut-and-Tie Model. An additional load carrying mechanism possibly involving concrete in tension, may cause this increase, although all specimens appeared to be cracked all the way down to the base along the tendon axis before failure occurred. The assumption that concrete contribution is causing the increase in strength, especially for specimen I4, is partly confirmed by the fact that specimen I4 had a smaller increase in load between cracking and ultimate than the other specimens. In all cases, the design values obtained by the Strut-and-Tie Model are conservative, albeit seemingly too large. Additional investigations would be needed to identify the possible additional effects that caused such discrepancies. If they are due to concrete contribution, they should probably be neglected in the design, because cracking due to other load effects may reduce or eliminate this contribution. The application of the proposed design methodology to Stone's curved specimens was successful, but not completely satisfactory because several of Stone's specimens did not fail in the anchorage zone but rather had a tendon failure.

Chapter 6: Multiple Anchorages and Non-Rectangular Cross Sections

In Chapters 4 and 5, basic configurations of anchorage zones involving one tendon acting on a rectangular cross section were discussed. In most practical applications of post-tensioning, however, several tendons are used to stress the member, which is
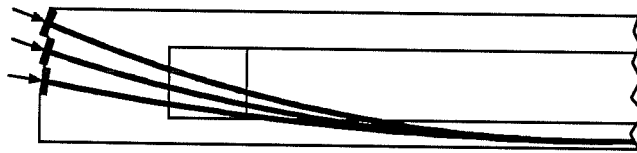
a) Multiple Anchorage Devices at
End of Girder
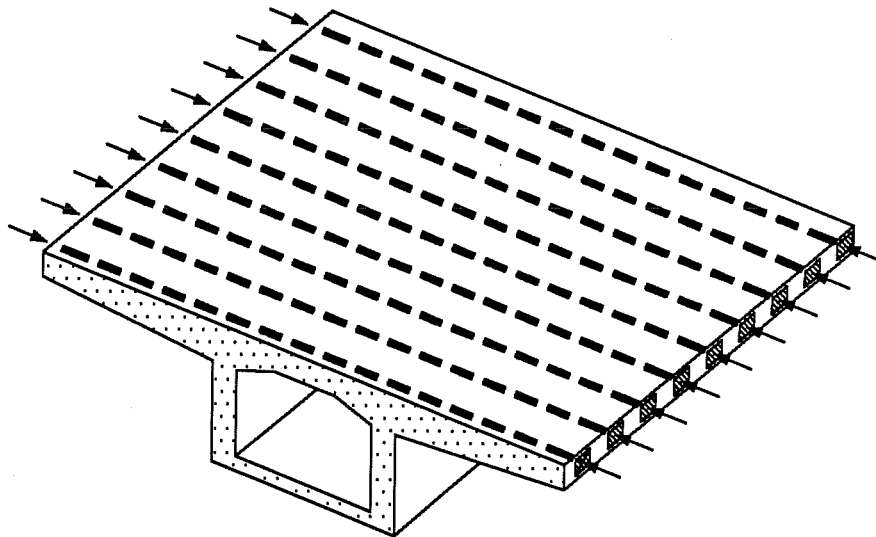
b) Multiple Anchorages for
Transverse Deck Post—Tensioning

Figure 6.1   Examples of Applications Involving Multiple Tendons

generally not rectangular in cross section. This chapter deals with the more general aspects of anchorage zones, such as multiple anchorages, transverse post-tensioning of the anchorage zone, and T-shaped cross sections.

6.1   Multiple Anchorages

Multiple anchorages are generally used to provide a post-tensioning force that is not readily achieved with a single tendon, as in the case of the post-tensioned girder of Fig. 6.1a or to introduce a distributed post-tensioning force as in the case of the transverse deck post-tensioning of Fig. 6.1b. The purpose of the present section is to investigate the stress field in

a) Concentric Resultant   b) Eccentric Resultant
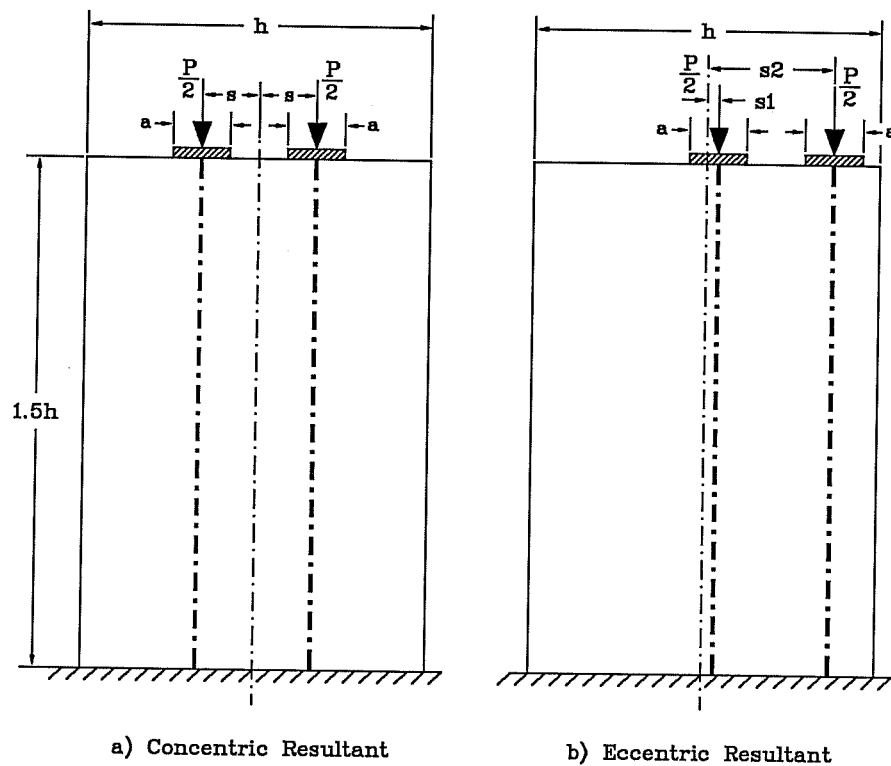
Figure 6.2   Geometry of Anchorage Zone with Two Anchors

anchorages zones with multiple tendons and to compare the deviation forces and stresses to the forces and stresses acting on an anchorage zone with a single tendon.

This study will focus on configurations involving two anchors. Although the methodology and design philosophy are of general applicability and can be applied to any anchorage zone problem, cases with more than two tendons in the anchorage zone are not investigated here. Configurations involving more than two tendons (or two groups of tendons) tend to be less critical from the standpoint of the general zone, because the forces are already partially distributed over the cross section, inducing less transverse spreading of forces in the general zone. The case of transverse deck post-tensioning is the subject of continuing current experimental and analytical research at The University of Texas at Austin [58]. From the preliminary results of these studies it appears that, as would be expected, the general anchorage zone tends to be less critical for structures with a large transverse dimension or a large number of anchorage devices, with the exception of the first few anchorages located close to an edge. Problems with the local zone, or possible transverse failure are more likely to be the main cause of failure in this type of applications.

Fig. 6.2 shows the geometry of an anchorage zone with two tendons in a concentric and in an eccentric configuration. The variable chosen to characterize the location of the tendons is the distance between the centroid of the section and the axis of each individual tendon. This quantity corresponds to the eccentricity as defined in Chapter 5 for a single tendon. In the concentric configuration of Fig. 6.2a, s corresponds to half the spacing between the center of the plates. In the eccentric configuration shown in Fig. 6.2b, the two variables are s_1 and s_2. For the normalization of the stresses and forces, each anchorage device is

subjected to a load of 0.5P, for a total load of P acting on the entire anchorage zone. Thus the average stress on the cross section due to post-tensioning is $\sigma_o = P/(ht)$.

6.2   Finite Element Analysis of Multiple Anchorages

A parametric study of the influence of the distance between the two anchors in a concentric configuration was performed using the Finite Element method, based on the geometry described in Fig. 6.2a. The size of each anchorage plate was held constant at 0.167h. Some additional cases with an eccentric resultant were also investigated.

6.2.1 State of Stresses in a Concentric Configuration

Fig. 6.3 shows the contour plots of the stresses in the x direction for various spacings $2s$ of the plates in configurations where the resultant of the tendon forces is concentric. For cases where the two anchorages are close (up to one plate size between the plates), as for example Fig. 6.3a, the stress distribution in the bursting region is similar to the stress distribution observed for a single concentric anchorage in Chapter 4 (see Fig. 4.5 for example). Figure 6.5 compares directly the distribution of bursting stresses along the tendon axis for a single anchor plate of size 0.3h, 0.4h or 0.5h with the bursting stresses produced by two anchor plates of size 0.167h at a half tendon spacing of 0.111h or 0.167h. The latter give an overall width of the area defined by the outside of the two plates of 0.278h and 0.333h. In these cases, the bursting stresses produced by two plates are less than the bursting stresses produced by a single plate of width equal to the total width of the two plates.

As the half spacing between the tendon axes increases beyond

one plate size, two clearly separated areas of bursting stresses appear, one ahead of each anchorage device, along the axis of the tendon (see Fig. 6.3c-f). The bursting stresses along the tendon axis in configurations with two concentric tendons acting outside the quarter points are comparable to the bursting stresses induced by a single eccentric tendon load, as can be seen from Fig. 6.6 (see also Fig. 5.10 in Chapter 5). Once again, the stresses produced by two plates are less than the stresses produced by a single anchorage plate.

When the distance between the plates increases beyond approximately the size of the plate, spalling stresses develop between the two plates. As the distance further increases, the area subjected to tensile bursting stresses decreases while the area subjected to spalling stresses increases (Fig. 6.3e,f). When the point of application of the forces moves outside the quarter points of the section, the spalling forces are combined with flexural tensile forces. Fig. 6.7 from Schlaich and al. illustrates how the behavior of an anchorage zone with tendons located outside the quarter points is similar to the behavior of a deep wall supported on isolated columns or footings. In the case presented by Schlaich, three tendons are acting on an anchorage zone, two of which are acting on the outside of the section. This configuration is analogous to a deep wall supported by three supports subjected to a uniform loading, illustrating the fact that the tensile forces in the spalling region are caused by the flexure of the cross section in the transverse direction.

a) Distance 2s=0.111h   b) Distance 2s=0.222h   c) Distance 2s=0.167h

d) Distance 2s=0.278h   e) Distance 2s=0.333h   f) Distance 2s=0.389h

A = 0.00 σ_o B = 0.05 σ_o C = 0.10 σ_o D = 0.15 σ_o E = 0.20 σ_o F = 0.25 σ_o G = 0.30 σ_o
H = 0.35 σ_o I = 0.40 σ_o J = 0.45 σ_o K = 0.50 σ_o L = 0.55 σ_o M = 0.60 σ_o N = 0.65 σ_o
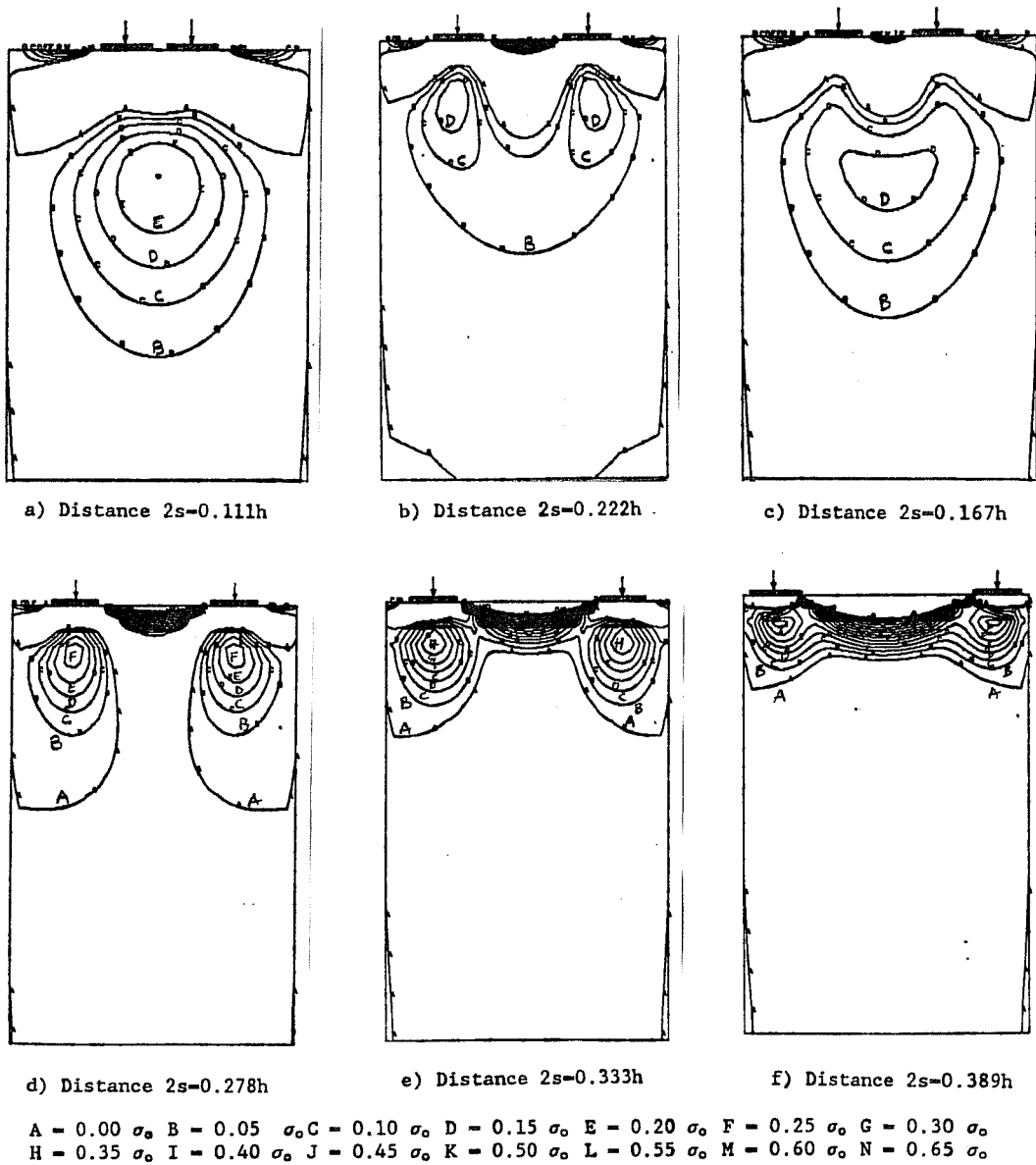
Figure 6.3   Contour Plot of the Tensile Stress in the x
              Direction (Perpendicular to the Tendon) for Various
              Spacings of the Anchorage Devices
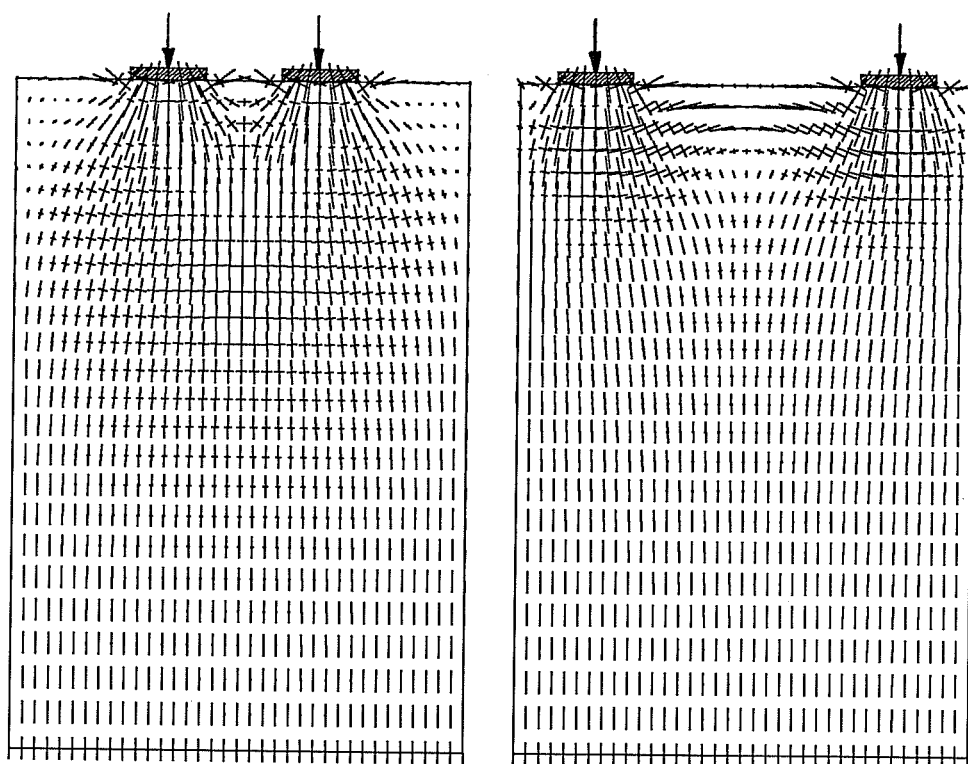
a) Plates Inside Quarter Points
2s = 0.333h

b) Plates Outside Quarter Points
2s = 0.667h

Figure 6.4   Principal Stress Vector Plot of Multiple Anchor
Configuration with 2s = 0.333h and 2s = 0.667
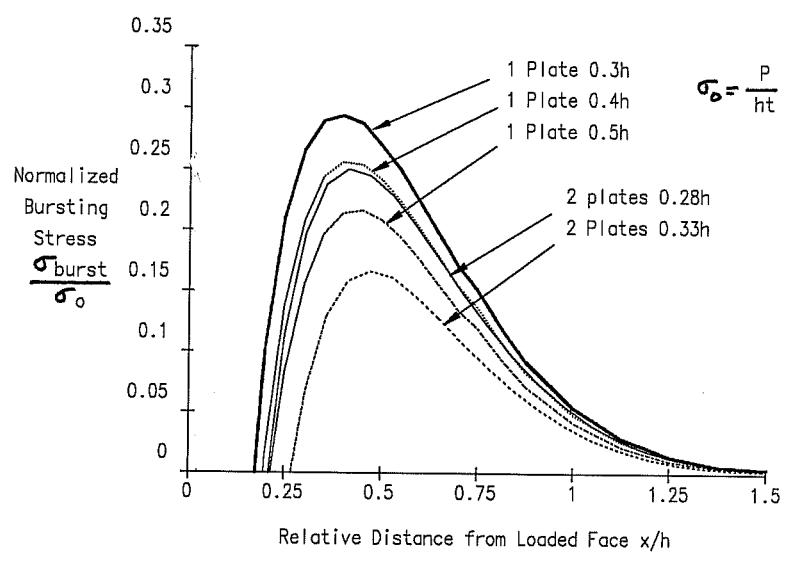
Figure 6.5   Bursting Stresses Along the Centerline of the Section for One or Two Plates with Similar Overall Areas
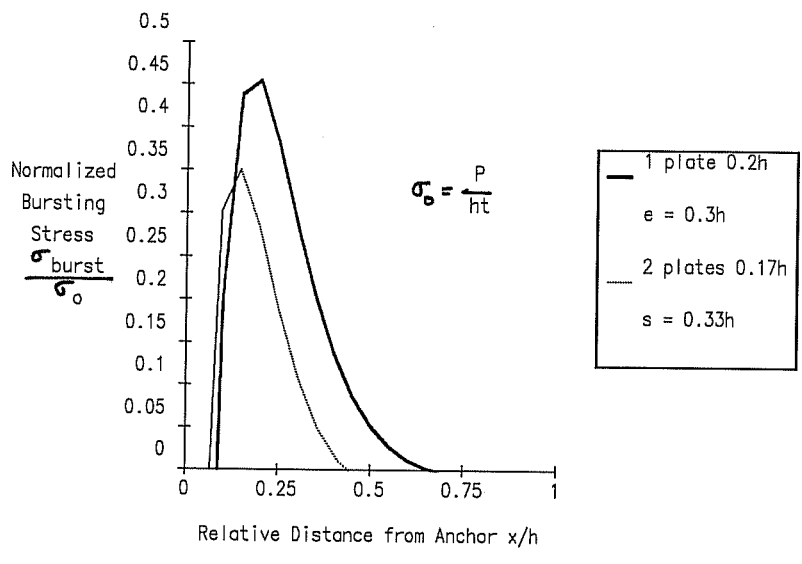
Figure 6.6   Bursting Stresses Along the Tendon Axis for One or Two Plates Outside the Quarter Points with Similar Eccentricities and Plate Sizes
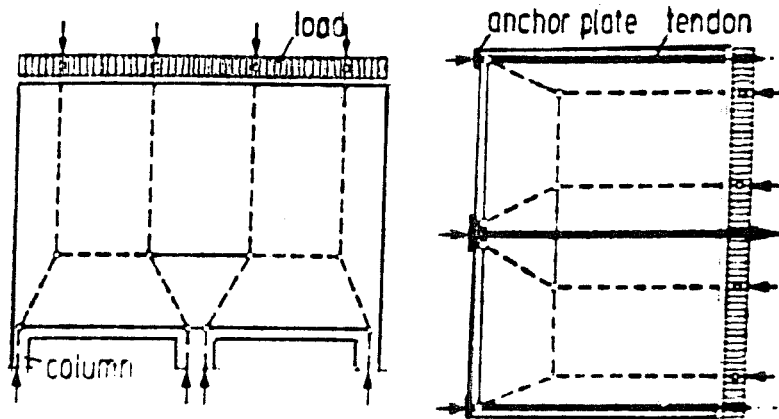
Figure 6.7   Analogy Between a Deep Wall and an Anchorage Zone
              with Multiple Tendons (from Schlaich and al., [158])

Tendon loads acting outside the quarter points increase the tensile stresses induced by transverse flexure very rapidly with increasing spacing of the plates, as can be seen in Fig. 6.3e and f. For very large spacings, it becomes difficult to distinguish between the spalling and flexural stress area and the bursting stress area, because they merge together. The large difference in principal stress vector plots is shown in Fig 6.4 for the cases of 2s = 0.167h and 2s = 0.333h.

Fig. 6.8 shows the location of the main tensile and compressive transverse forces in an anchorage zone with two tendons. Travelling along the tendon axis from the anchorage, a compression force close to the plate and a tension force further ahead are observed, as in the case of a single tendon. For cases in which the tendons are located within the quarter points, two distinct zones of tension exist along the centerline, one close to the surface and one deeper down, as shown in Fig. 6.8a. They are separated by a compression zone. For the case of tendons located

outside the quarter points Fig. 6.8b shows that there is only one tension zone acting near the top of the centerline, with a compression force acting further down.
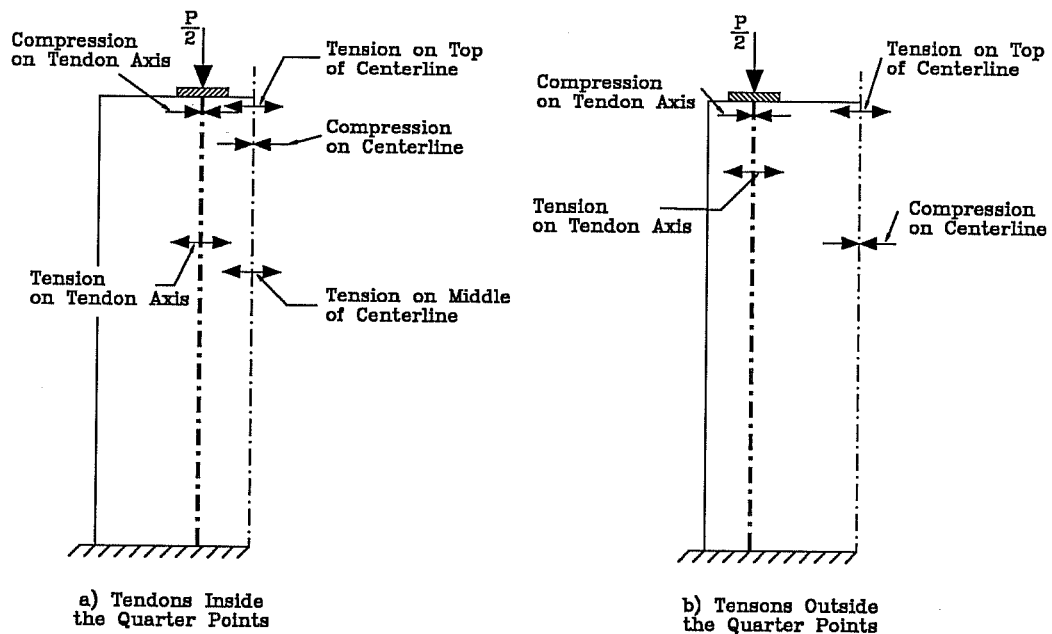
Figure 6.8   Definition of the Main Transverse Forces Acting on an Anchorage Zone with Multiple Tendons

Fig. 6.9 shows the variation of these forces as a function of the half spacing s between the axes of the tendons. For small spacings, the value of the tension force acting on the tendon axis is comparable to the tension force acting on the middle of the centerline. However, the tension force acting on the middle of the centerline disappears when the tendon loads are acting outside the quarter points. The tension force at the top of the centerline increases slowly with increased spacing of the loads as long as the loads are applied within the quarter points, and then

increases rapidly with increased spacing. The magnitude of the compression forces is equal to the sum of the corresponding tension forces.
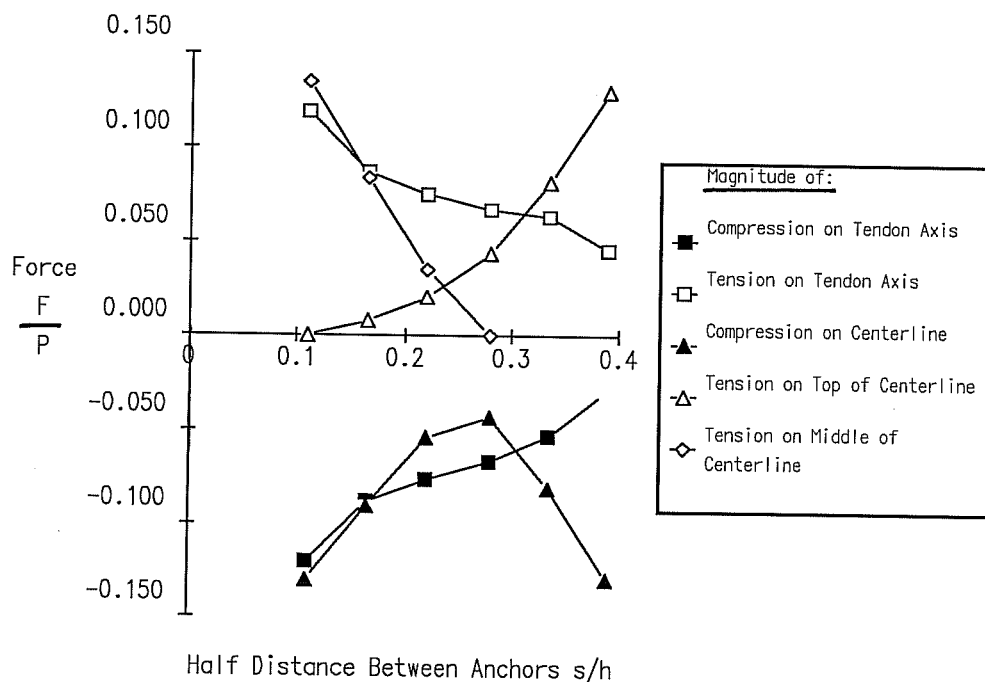
Figure 6.9   Variation of the Main Forces in an Anchorage Zone with two Tendons in a Concentric Configuration as a Function of the Half Spacing between the Anchorage Devices

6.2.2 State of Stresses in an Eccentric Configuration

Figure 6.10 shows the contour plot of the stresses perpendicular to the axes of the tendon for an anchorage zone with two tendons applying a total load of P with an eccentric

resultant. The size of the anchorage device is a = 0.167h as in the cases with a concentric resultant, and the relative location of the anchorage plate is given by s_1 = -0.111h and s_2 = 0.333h. The distance between the anchorage devices is larger than one plate size and the areas of bursting stresses ahead of each anchorage device are clearly separated, as was observed in the case of concentric tendons (see Fig. 6.3d).

$$A = 0.00 \ \sigma_o$$
$$B = 0.05 \ \sigma_o$$
$$C = 0.10 \ \sigma_o$$
$$D = 0.15 \ \sigma_o$$
$$E = 0.20 \ \sigma_o$$
$$F = 0.25 \ \sigma_o$$
$$G = 0.30 \ \sigma_o$$
$$H = 0.35 \ \sigma_o$$
$$I = 0.40 \ \sigma_o$$
$$J = 0.45 \ \sigma_o$$
$$K = 0.50 \ \sigma_o$$
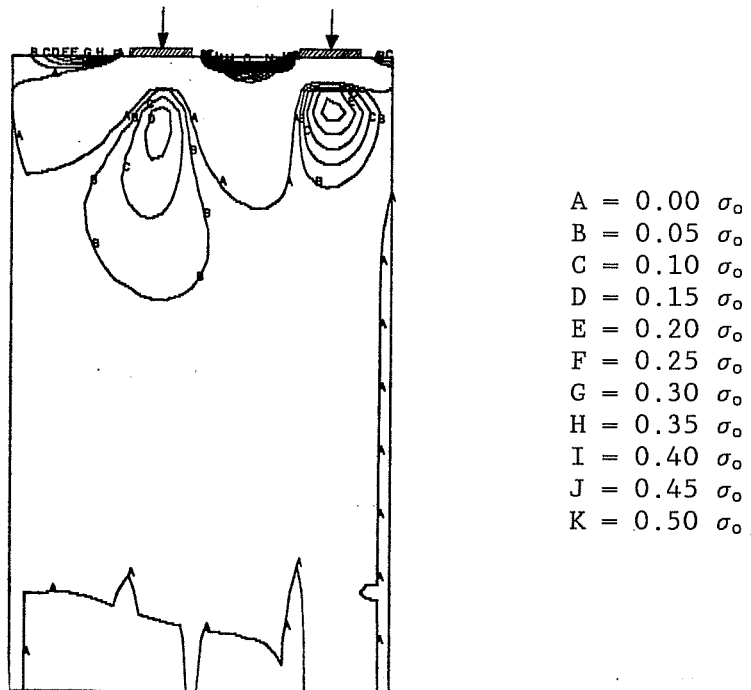
Figure 6.10   Contour Plot of the Tensile Stresses Perpendicular to the Tendon Axes for Specimen ME1 with two Tendons and an Eccentric Resultant

6.2.3 General Remarks on the State of Stresses for Configurations with Multiple Anchorages

Anchorage devices located within a short distance from one another may be considered as one single plate for the purpose of analysis. It is of course necessary to consider the actual stressing sequence in determining the amount of reinforcement. By choosing an appropriate stressing sequence, the cracking of the general zone can be minimized, as well as the amount of reinforcement necessary in the general zone.

In cases where the post-tensioning is to be distributed evenly over the entire section, the analogy between an anchorage zone with multiple tendons distributed over the cross section and a deep wall is helpful in assessing the required reinforcement for the spalling/flexural region of the anchorage zone. From this analogy, it is evident that for a given total post-tensioning force the required reinforcement in the spalling/flexural region decreases rapidly with increased number of endons.

6.3 Strut-and-Tie Model for Concentric Configurations with Multiple Anchorages

The basic principles used to develop Strut-and-Tie Models for single anchor configurations will be used to develop Strut-and-Tie Models for multiple anchor configurations. For the Strut-and-Tie Models presented in this section, the reactions at the end of the general zone were obtained by dividing the cross section into struts separated by the axes of the tendons and by the centroid of the section. Fig. 6.11 shows the geometry for configurations with two tendons with a concentric resultant. Fig. 6.11a shows the geometry of the Strut-and-Tie Model when the tendon loads act within the quarter points. Fig. 6.11b shows the geometry of the Strut-and-Tie Model when the tendon loads act

outside the quarter points.

Figs. 6.11c and Fig. 6.11d show how the location of the transverse ties is determined. For the load within the quarter
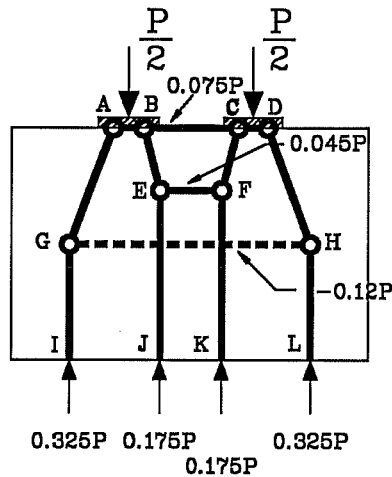
a) Load within the
Quarter Points
(s = 0.175h)
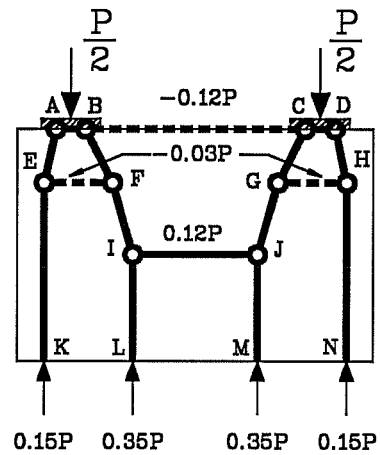
b) Load Outside the
Quarter Points
(s = 0.35h)
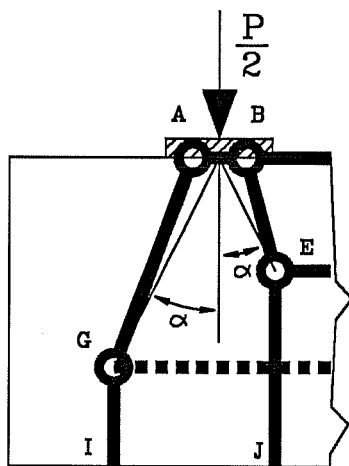
c) Detail of the
Geometry of a)
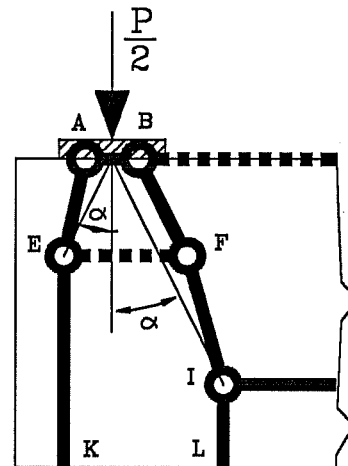
d) Detail of the
Geometry of b)

Figure 6.11   Definition of the Geometry of the Strut-and-Tie
Models for Anchorage Zones with Two Tendons

points, as shown in Fig. 6.11a and c, the two internal struts (BE and CF) converge until they reach the line of action of their respective resultants (JE and KF), at which points they are deviated by the same amount, creating a compression strut (EF) between the two internal struts. The internal struts do not require a tension tie for equilibrium. The two external struts are balanced by a tension tie (GH) crossing the internal struts. The horizontal equilibrium of the anchorage requires a compression strut (BC) between the two plates. In the configuration with the load outside the quarter points, shown in Fig. 6.11b and d, the two external struts (AE and DH) extend to the line of action of their resultants (KE and NH) from the end of the general zone, and are balanced by tension ties (EF and GH) anchored back into the corresponding internal struts (BFI and CGJ). The horizontal equilibrium of the nodes at the anchorage device requires a horizontal tension tie (AD) between the anchors close to the surface of the concrete. This tie corresponds to the transverse flexural tension stress previously observed in the results of the Finite Element Analysis.

6.3.1 Parametric Study of an Anchorage Zone with Two Anchorages

A parametric study was performed based on the geometry defined in the previous section. The deviation angle was held at 26 degrees for the outside strut, while the angles of the internal struts were so chosen that the average angle α from the plate to the point where the internal struts becomes parallel to the axis was also 26 degrees. The size of the plates used for this parametric study was a = 0.167h, the same value used for the Finite Element analyses.
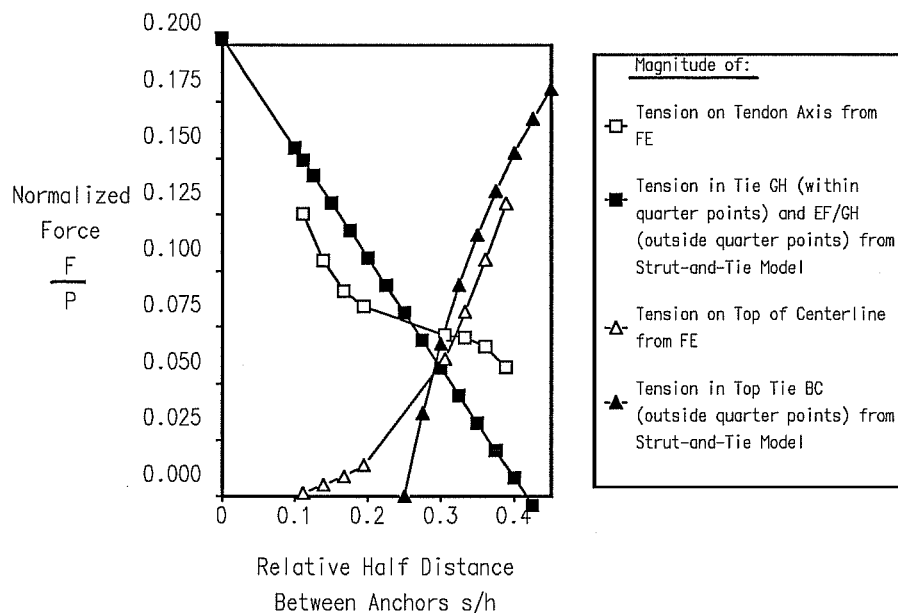
Figure 6.12   Tension Forces Obtained from the Strut-and-Tie Model
               for an Anchorage Zone with Two Concentric Tendons
               Compared with the Results from the Finite Element
               Analyses

    Figure 6.12 shows the horizontal forces in the tension ties
obtained from the parametric study performed using the Strut-and-
Tie Model described above, as well as the results from the Finite
Element analyses. Overall, there is a fair agreement between the
two methods, with a good prediction of the bursting force for the
case with small spacing between the plates and a good prediction
of the flexural tensile force for the larger spacings. When the
loads are located outside the quarter points, that is for half
spacings larger than 0.25h, the bursting force predicted by the
Strut-and-Tie Model is less than the value obtained by the Finite
Element method, probably because the Strut-and-Tie Model does not
consider the fact that the spalling and flexural forces tend to

merge with the bursting force at large eccentricities. However, this difference is probably not a serious concern because the reinforcement provided for the flexural tensile force and the spalling force would most likely extend all the way through the bursting region and be anchored on the edge of the section. In such a case, it is most likely that the reinforcement would be designed on the basis of the larger of the two forces.

Because they are induced by the condition of compatibility, the Strut-and-Tie Model does not predict any tensile forces at the surface of the concrete between the anchorage plates for cases where the anchorages are located within the quarter points. Furthermore, the Strut-and-Tie Model tends to underestimate the magnitude of the tensile force in cases where the anchorages are located just outside of the quarter points. No test data are available for two anchorages with a half spacing of about 0.25h, so it is not possible to determine if these forces actually develop. Data available for smaller spacings shows that, even though the calculated elastic tensile stresses at the surface of the concrete between the anchorages are very high, no early cracking of the concrete was observed in this area. This indicates that these compatibility induced stresses may be released by microcracking and not develop to the level predicted by elastic theory. In all cases, it appears prudent to at least provide some reinforcement to distribute and limit the opening of possible cracks in this region of the anchorages zone.

6.3.2 Strut-and-Tie Model for a Configuration with Two Tendons and an Eccentric Resultant

The Strut-and-Tie Model corresponding to the configuration of a specimen with two tendons and an eccentric resultant is shown on Fig. 6.13, superimposed on the principal stress vectors corresponding to the elastic stress distribution. In this specific case, the Strut-and-Tie Models corresponding to each tendon do not need to be connected by struts or ties to achieve equilibrium. The locations of the tension ties were obtained by assuming a diffusion angle of 26 degrees from the center of the anchorage devices to the corresponding *external* struts.
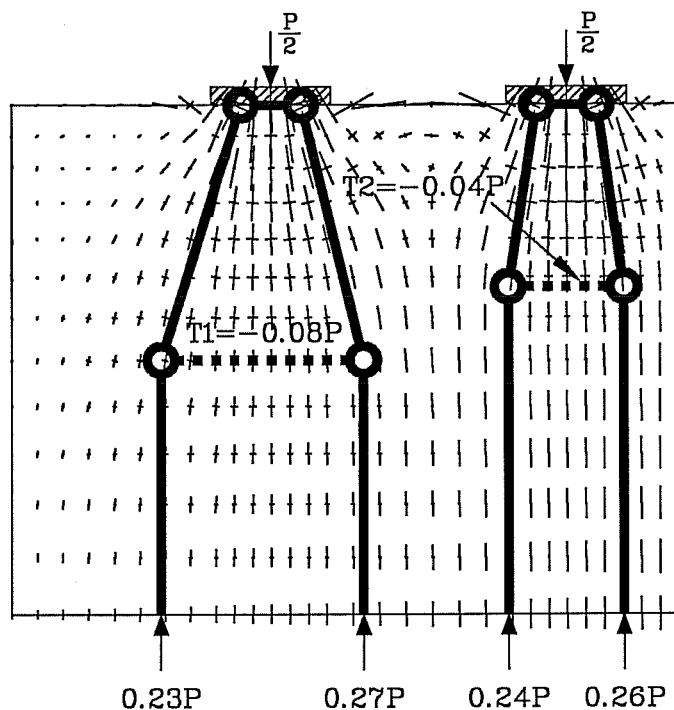
Figure 6.13   Principal Stress Vector Plot and Strut-and-Tie Model for Specimen ME1 with two Tendons and an Eccentric Resultant

6.3.3 Comparison with Test Results for Concentric Configurations
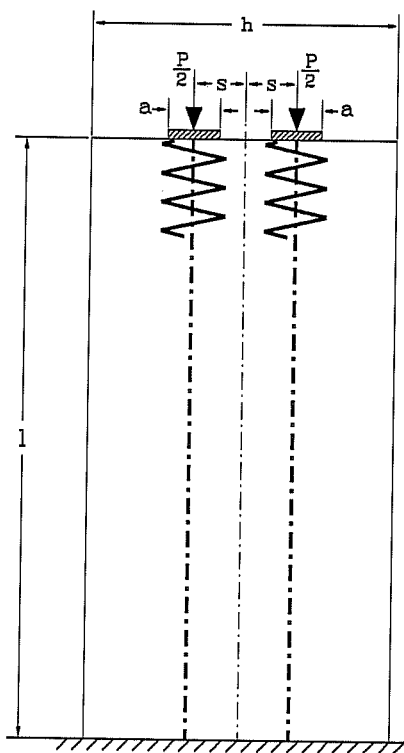
Figure 6.14 Geometry and Local Zone Reinforcement for Specimens with Multiple Tendons

A series of physical test specimens with multiple tendons was investigated by Sanders [153]. The specimens were labeled M1 to M6. Only Specimens M1 to M4 and M6 will be discussed here. Because M5 which had two anchors side by side was already discussed in Chapter 5 with eccentric single anchor configurations. Fig. 6.14 shows the geometry of the test specimens. Table 6.1 gives the dimensions and concrete properties for each specimen. Due to problems with the capacity of the original test setup, tests M2, M3 and M4 were performed twice. Only the relevant values were used in the comparison of cracking loads and ultimate loads: the concrete tensile strength at the time of the first loading for the computation of the cracking load and the concrete compressive strength at the time of the second loading for the computation of the ultimate load. Fig. 6.15 shows the reinforcement layout for specimen M2, which is typical of this series. The reinforcement of all specimens is summarized in Table 6.2.

1#3 @2"

6"

4#3 @4"

8"

2#3 @8"

37"
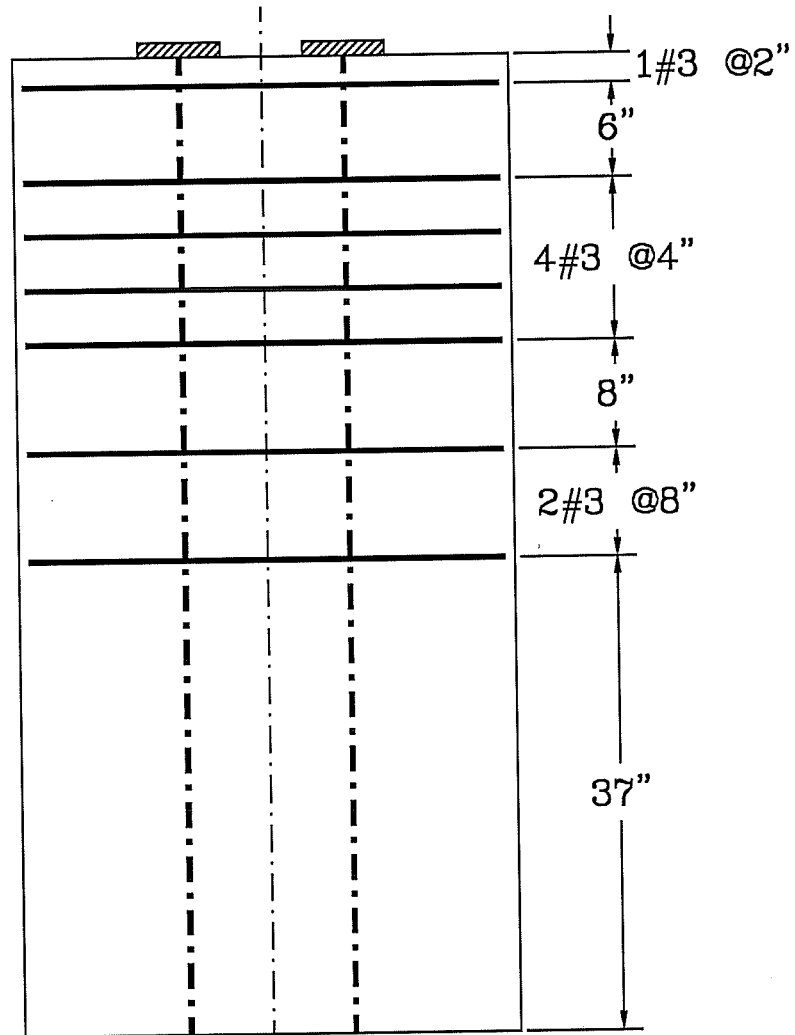
Figure 6.15 General Zone Reinforcement for Specimen M2

Table 6.1   Summary of the Dimensions and Concrete Properties of
            Specimens with Multiple Tendons

	Dimensions	Anchor	Concrete First Test		Concrete Second Test	
Specimen	$h \cdot w \cdot t \cdot s$ [in]	$a \cdot b \cdot t_{plate}$ [in]	f'_c [ksi]	f_{sp} [ksi]	f'_c [ksi]	f_{sp} [ksi]
M1	$72 \cdot 36 \cdot 8.5 \cdot 4$	$6 \cdot 6 \cdot 1$	5.94	0.441	N/A	N/A
M2	$72 \cdot 36 \cdot 8.5 \cdot 6$	$6 \cdot 6 \cdot 1$	5.33	0.497	5.73	0.500
M3	$72 \cdot 36 \cdot 8.5 \cdot 12.5$	$6 \cdot 6 \cdot 1$	5.33	0.497	5.73	0.500
M4	$72 \cdot 36 \cdot 8.5 \cdot 6$	$6 \cdot 6 \cdot 1$	5.57	0.441	6.62	0.571
M6	$60 \cdot 32 \cdot 17 \cdot 4$	$6.5 \cdot 6.5 \cdot 7^*$	4.75	0.415	N/A	N/A

*:   Four Multiplane Anchorage. Total depth of the anchor.

Table 6.2   Summary of the Bursting, Spalling and Additional
            Reinforcement for Specimens with Multiple Tendons

	Bursting Reinforcement		Spalling Reinforcement		Local Zone (Spiral) Reinforcement	
Specimen	A_s*f_y [kips]	Centroid [in]	A_s*f_y [kips]	Centroid [in]	A_s*f_y [kips]	diam/pitch/length [in]
M1	105.6	26.9	N/A	N/A	12.0	6/1.5/8
M2	92.4	16.6	N/A	N/A	12.0	6/1.5/8
M3	91.7	17.6	50.9	2	12.0	6/1.5/8
M4	70.0	10.8	N/A	N/A	12.0	6/1.5/8
M6	57.1	17.6	N/A	N/A	12.0	7/2/9.5

Fig. 6.16 shows the measured cracking load and the predicted cracking load based on the maximum bursting stress obtained from the Finite Element Analysis and the concrete tensile strength measured in a split cylinder test for this series of specimens. To limit the contribution of concrete in tension to the load carrying mechanism, crack formers were introduced for a length of 12 inches along the axes of the tendons in specimens M1 and M4, so the cracking load was not recorded. The three tests for which a cracking load was recorded exhibit a large scatter in the accuracy of the prediction. The average ratio of actual to predicted is
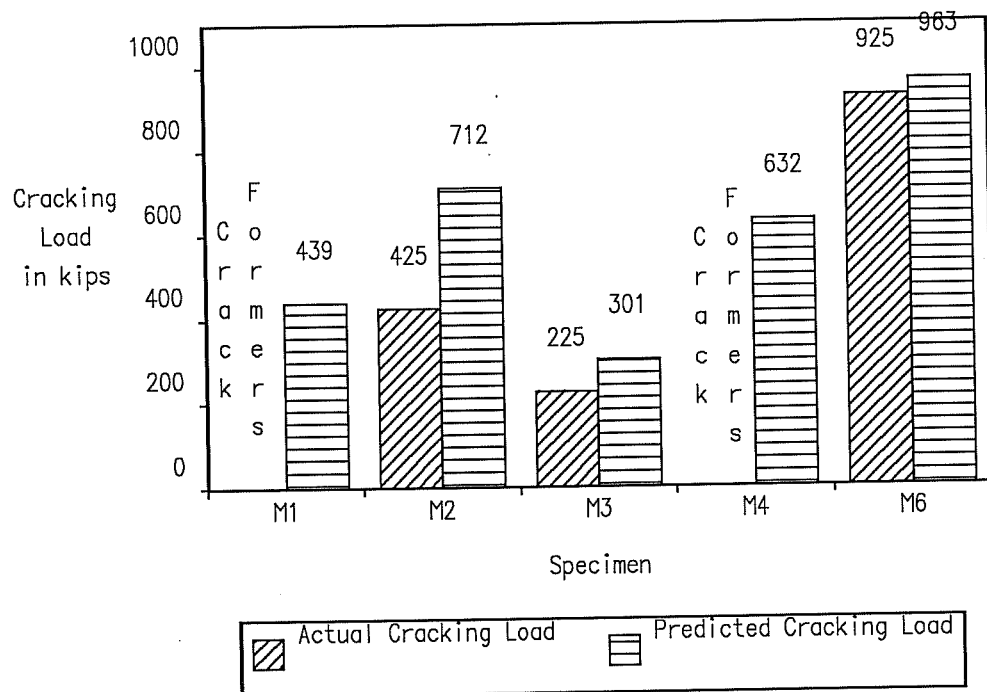
Figure 6.16 Actual Cracking Load and Predicted Cracking Load for
Specimens with Multiple Tendons

0.625, with a standard deviation of 0.323.

Fig. 6.17 shows the actual ultimate loads for the specimens with multiple tendons compared to the theoretical values. The first two theoretical values were predicted by the Strut-and-Tie Model based on the tie capacity and on the strut capacity. The last value is the compression capacity, which was computed based on a maximum effective concrete compression stress of $0.75f'_c$, determined by using the stress at a distance a from the anchor from the Finite Element solution. For specimens M1 and M2, the strut capacity controls the prediction of the ultimate capacity by the Strut-and-Tie Model. For specimen M3, the capacity of the tension tie in the spalling area controls the design. For specimens M4 and M6 the tie capacity in the bursting region controls the design. Taking all values into account, the average ratio of actual to predicted is 1.71 with a standard deviation of 0.140. It is apparent from Fig. 6.17 that the tie-based capacity is not the best indication of the capacity of the anchorage zone. The compression strength as predicted based on the Finite Element Analysis gives a much better estimate of the ultimate load. The relatively low (and conservative) values of the strut capacity given in the figure are a consequence the relative simplicity of the model used to define the critical section of the struts. In general, the external strut controls the strut capacity, while the internal strut still has some reserve capacity. A model that would define the width by redistributing part of the area attributed to the internal strut to the external strut would give larger values for the strut-based capacity
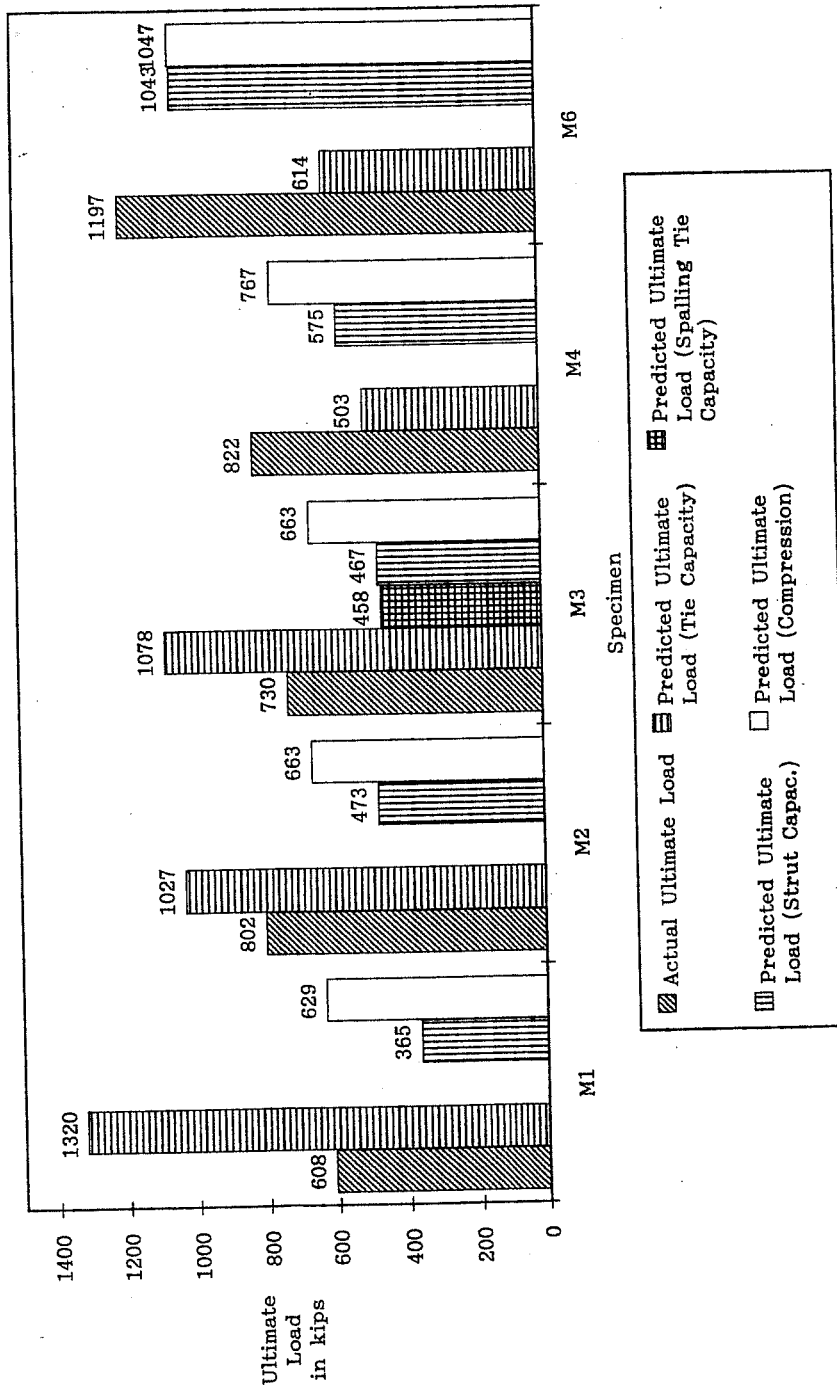
Fig. 6.17   Actual Ultimate Load and Ultimate Load Predicted by the Strut-and-Tie Model for Specimens with Multiple Tendons

For closely spaced anchorage devices, the elastic state of stresses is similar to the state of stresses for a single anchorage device. Fig. 6.18 shows the ultimate load reached by specimen M1, M2, M4 and M6 compared to the ultimate load predicted by the Strut-and-Tie Model considering only one plate. The critical section for the strut capacity was located at the less of the equivalent plate size or the thickness of the cross section. The results are conservative, with an average ratio of actual to predicted ultimate of 1.87 and a standard deviation of 0.91.

Figure 6.18   Actual Ultimate Load and Ultimate Load Predicted by the Strut-and-Tie Model for Specimens with Multiple Tendons, Using a Single Tendon for the Strut-and-Tie Model

A large contribution of the concrete in tension (below the

crack former in the case of M4) apparently prevented an early failure due to yielding of the ties. This hypothesis is reinforced by the very high cracking load observed for specimen M6. In the case of M6 which had a significantly larger cross-sectional area, it is also possible that increased friction at the base of the specimen could have increased the ultimate load capacity. If the ratio of actual to predicted ultimate load is taken as the ratio of actual to strut-based predicted ultimate load for M4 and M6, the average ratio for all specimens becomes 1.098, with a standard deviation of 0.090. This indicates a much better correlation between the experimental and theoretical values.
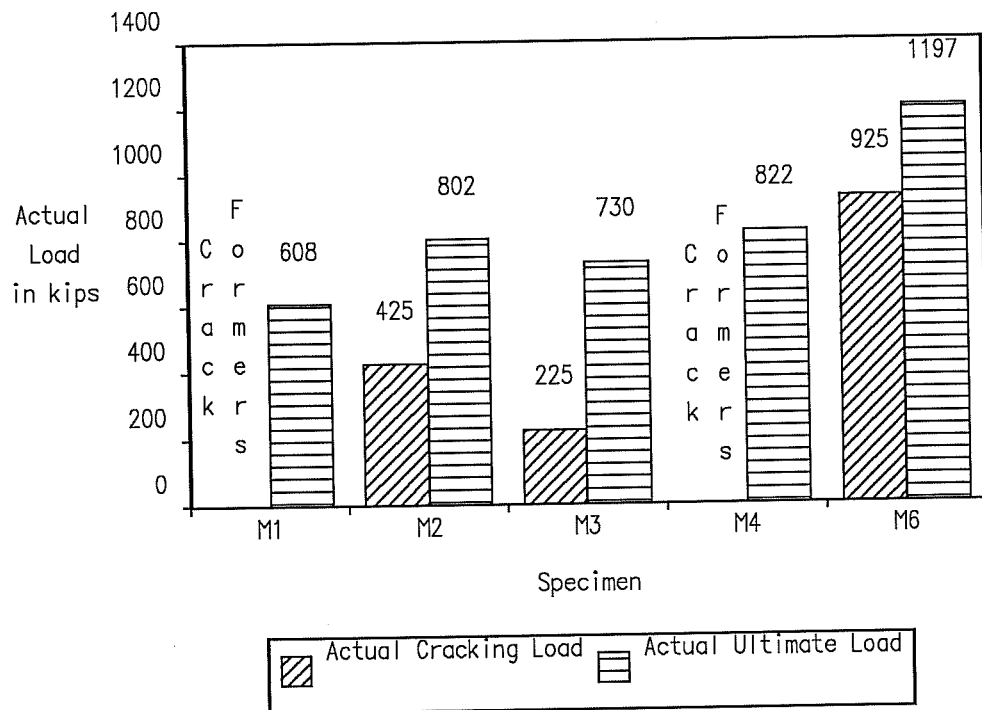
Figure 6.19   Actual Cracking and Ultimate Load for Specimens with Multiple Tendons

Fig. 6.19 shows the actual values of the cracking load and of the ultimate load for specimens with multiple tendons. A marked

increase in capacity between cracking and ultimate is observed in all cases, even for specimen M6 that was actually underreinforced because its tie-based capacity was less than its expected (and actual) cracking load.

6.3.4 Comparison with Test Results for the Eccentric Configuration

One specimen with two tendons in an eccentric configuration was investigated in the experimental program. Fig. 6.20 shows the geometry and reinforcement used for this test specimen. Fig. 6.21 shows the actual and predicted values of the cracking load. The predicted cracking load was based on the elastic stress distribution and the tensile strength of the concrete as obtained from a split cylinder test. The actual cracking loads were greater than the predicted cracking loads. Cracking initiated along the axis of the left tendon, that is the tendon furthest from the edge of the section, although the elastic stress distribution indicated that the stresses would be higher along the axis of the right tendon, that is closer to the edge of the section.
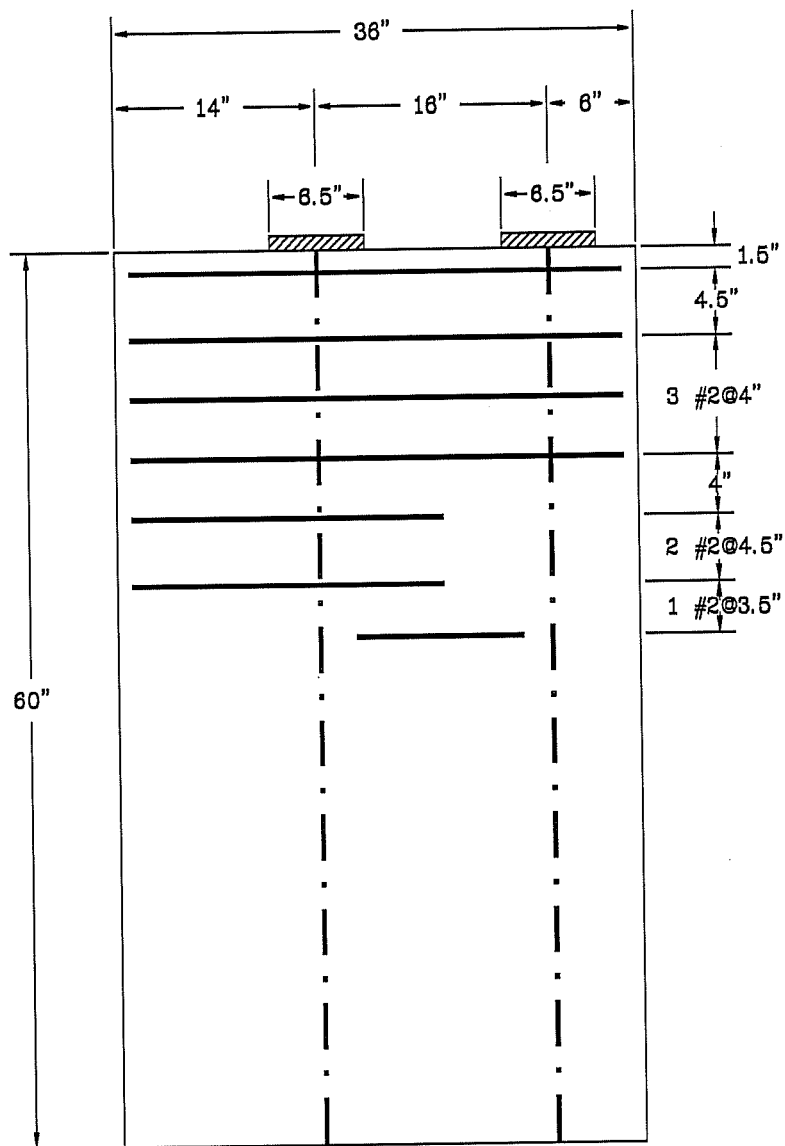
Figure 6.20   Geometry and Reinforcement of Specimen ME1 with two
Tendons and an Eccentric Resultant
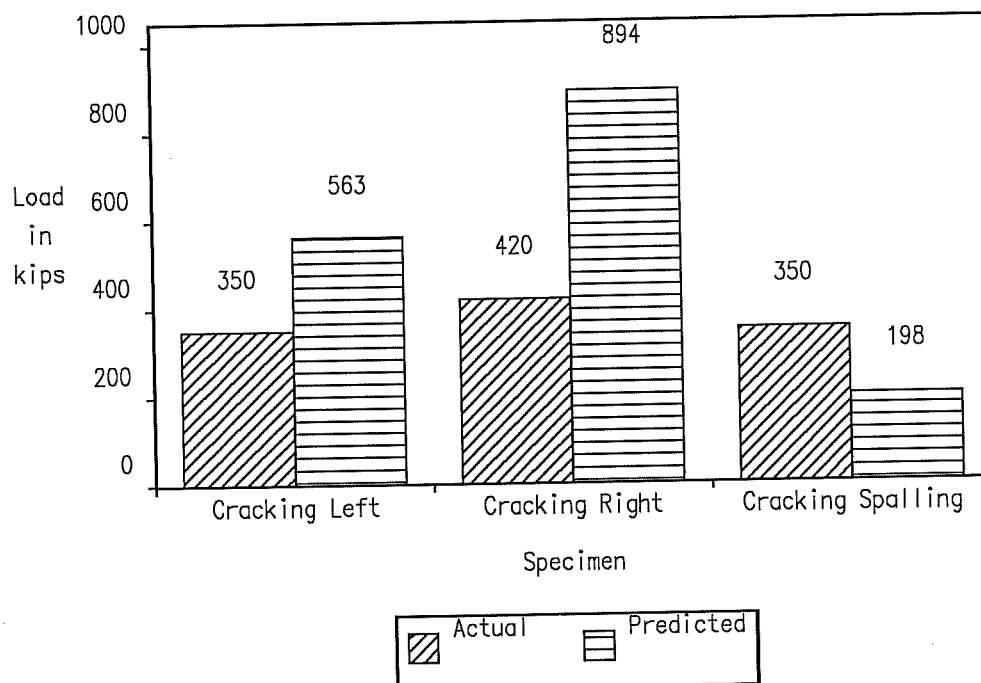
Figure 6.21   Actual and Predicted Cracking Load for Specimen ME1
with two Tendons and an Eccentric Resultant

Fig. 6.22 shows the actual ultimate load reached by the specimen compared with the predicted ultimate load. The ultimate load predicted by the tie capacity considers the reinforcement that crosses each tendon axis. The strut capacity was calculated using a nominal stress of 0.6 f'_c at the critical section located at a distance a from the anchorage. Because two struts converge at each anchorage plate, a total of four strut capacities were obtained. Only the smallest value is reported for each anchorage plate. Of course, the smallest value controls the design, in this case the capacity of the left tension tie. The compression capacity was obtained on the basis of the elastic stress at a distance from the anchorage equal to the lateral dimension of the

anchorage device and using 0.75 f'c as the limiting stress.

The actual ultimate load was greater than the ultimate load predicted by the tie capacity of either the left Strut-and-Tie Model or the right Strut-and-Tie Model. It is presumed that concrete in tension contributed to this increase in strength. Extensive cracking was observed along the axis of the left tendon at ultimate. When the crack extended all the way to the base of the specimen, the tension force contributed by concrete was released, leading to the failure of the anchorage zone.
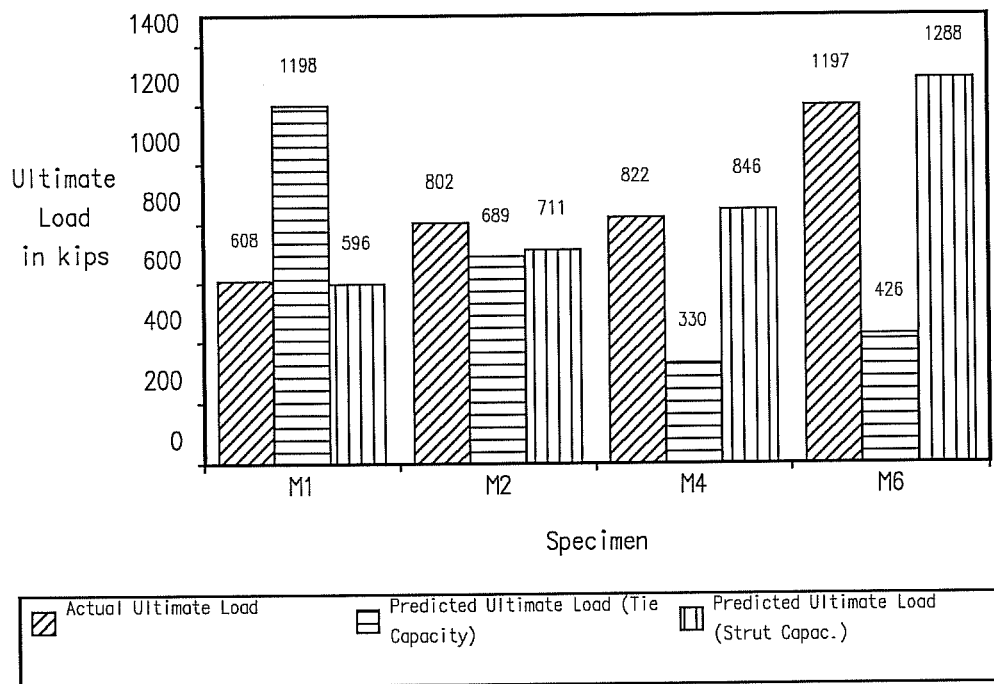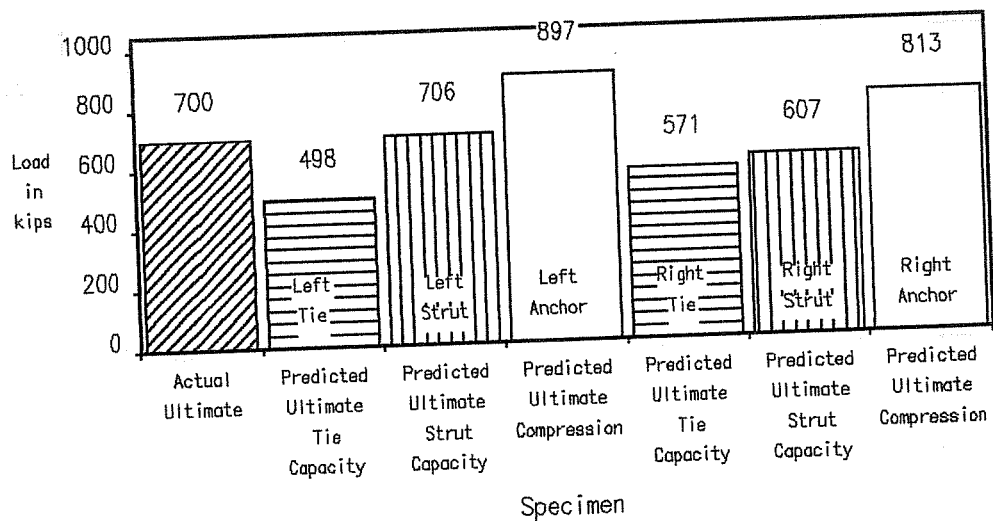

Figure 6.22 Actual Ultimate Load and Ultimate Load Predicted by the Strut-and-Tie Model for Specimen ME1 with two tendons and an Eccentric Resultant

6.4   Lateral Post-Tensioning of the Anchorage Zone

One of the major advantages of post-tensioned concrete is the reduction, and ideally the suppression of cracks in the concrete under service loads. Unfortunately, the local introduction of post-tensioning forces in the anchorage zone produces transverse tensile stresses that can lead to cracking of the concrete. The main post-tensioning of the structure cannot suppress this effect since it produces stresses that act perpendicular to it. If non-prestressed reinforcement is used to resist the transverse forces in the general anchorage zone, large strains in the steel are necessary, leading to cracking of the concrete. In cases where cracking is highly undesirable, one solution is to add secondary *lateral* (or *transverse*) post-tensioning in order to provide a compression in the concrete that will counteract possible tensile stresses induced by the lateral spreading of the main tendon forces. This section deals specifically with the use of lateral post-tensioning in anchorage zones.

6.4.1 Finite Element Analysis of Anchorage Zones with Lateral Post-Tensioning

A series of Finite Element analyses were performed for concentric single anchor configurations as shown in Fig. 6.23. The main parameter investigated in this study was the amount of transverse post-tensioning and its distance d relative to the location of the main anchor. Fig. 6.24a shows a contour plot of the maximum principal stresses in tension caused by lateral post-tensioning alone with a magnitude of $P_{lat} = 0.2P$, P being the capacity of the main tendon. Fig. 6.24b shows the maximum principal stresses resulting from the combination of the main tendon load P and the lateral post-tensioning $P_{lat} = 0.2P$.

Fig. 6.25 shows the corresponding principal stress vectors.
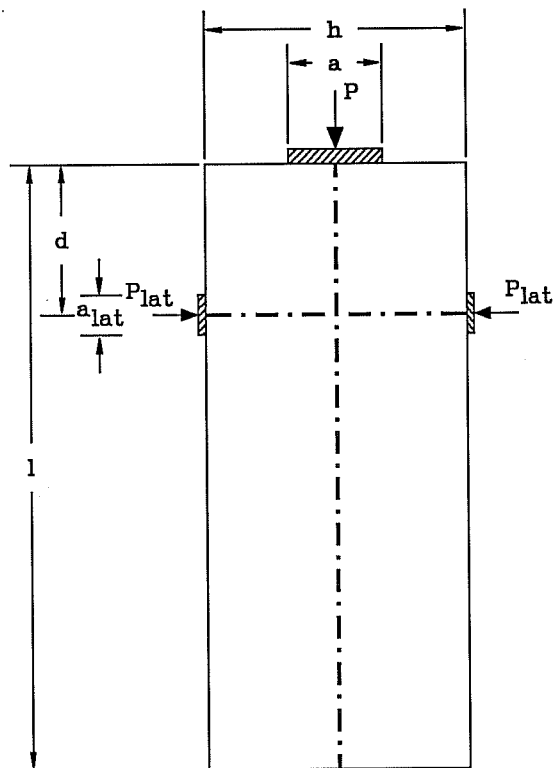
Figure 6.23 · Geometry of an Anchorage Zone with Lateral Post-
          Tensioning
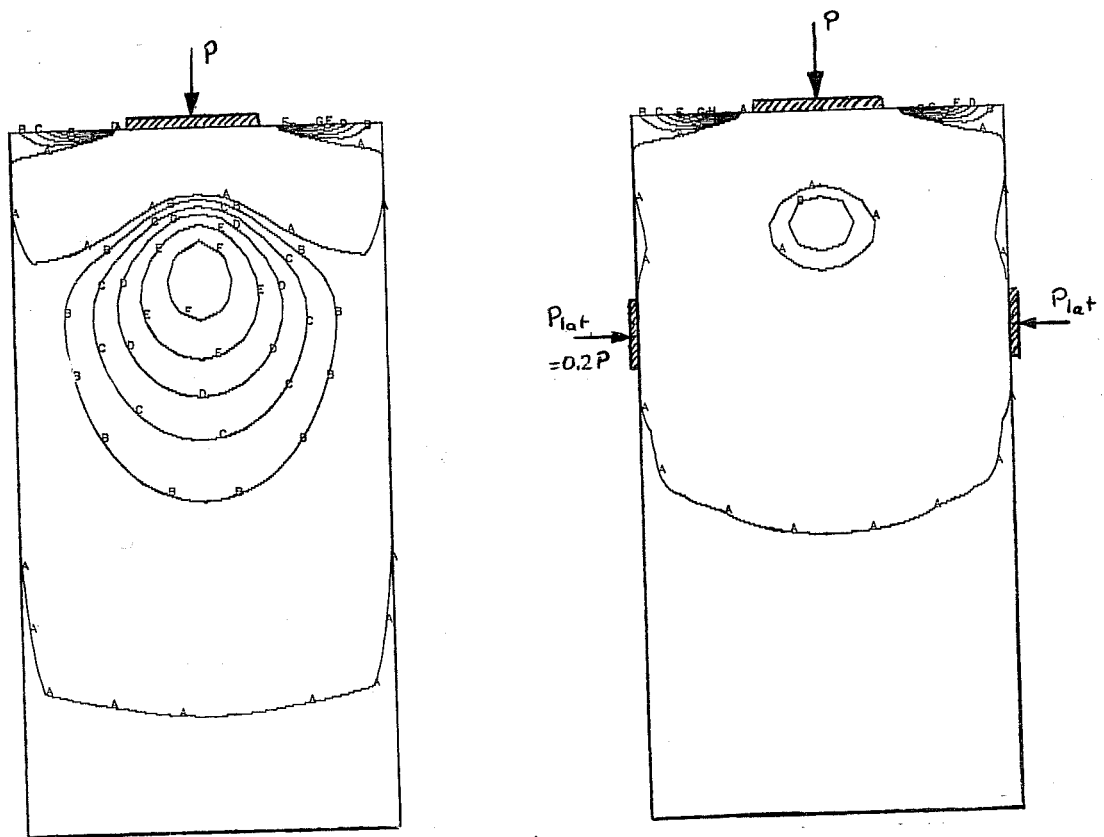
A = 0.0 σ_0 B = 0.05 σ_0 C = 0.1 σ_0 D = 0.15 σ_0 E = 0.2 σ_0 F = 0.25 σ_0
G = 0.3 σ_0 H = 0.35 σ_0 I = 0.4 σ_0 J = 0.45 σ_0 K = 0.5 σ_0 L = 0.55 σ_0

Figure 6.24   Contour Plot of the Maximum Principal Stress (in
Tension) for Lateral Post-Tensioning Only and for
Lateral Post-Tensioning and Main Post-Tensioning
(Plat = 0.2P)

a) Lateral
Post—Tensioning Only

b) Main Post—Tensioning
(100K)
and Lateral Post—Tensioning
(20K)
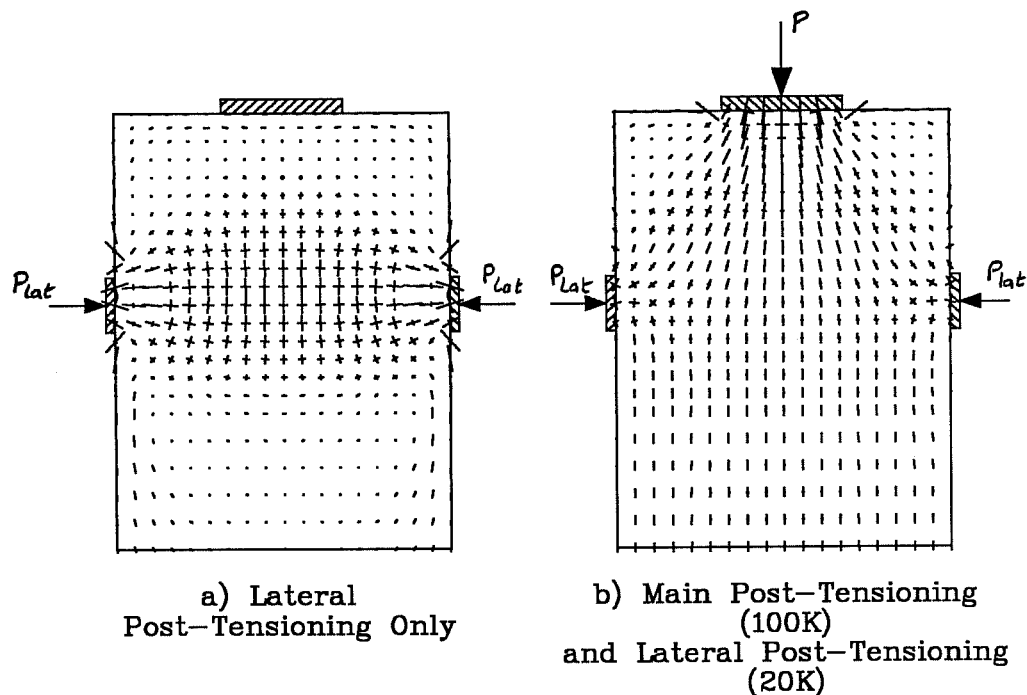
Figure 6.25   Vector Plot of the Principal Stresses for Lateral
Post-Tensioning Only and for Main Post-Tensioning
and Lateral Post-Tensioning (P_{lat} = 0.2P)

Fig. 6.26 shows the distribution of transverse stresses
along the tendon axis caused by a lateral post-tensioning load.
The distribution of transverse tensile stresses along the tension
axis caused by a tendon load applied on a plate with size a =
0.36h is also shown in the figure. It is apparent that the most
efficient location for the transverse post-tensioning is a
location at about 0.5h from the main anchor. This location
corresponds more or less to the location of the centroid of the
tensile bursting stresses caused by the main post-tensioning. For
depths of the lateral post-tensioning greater than approximately
0.2h, the maximum compressive stress becomes constant. The
normalization of the stresses is based on the transverse dimension
h of the specimen described in Section 6.4.3, while the

distribution of transverse stresses due to lateral post-tensioning is not directly dependent on the transverse dimension. The magnitude of the curves in Fig. 6.26 would be significantly different for other proportions.

Bursting Stresses from Main Anchor
with no Lateral Post-Tensioning

Transverse Stress $\dfrac{\sigma_{trans}}{\sigma_0}$

Stresses from Lateral Post-Tensioning

d/h=0.167
d/h=0.222
d/h=0.178
d/h=0.333
d/h=0.444
d/h=0.556
d/h=0.667

$\sigma_0 = \dfrac{P}{ht}$

Distance from the Anchor x/h
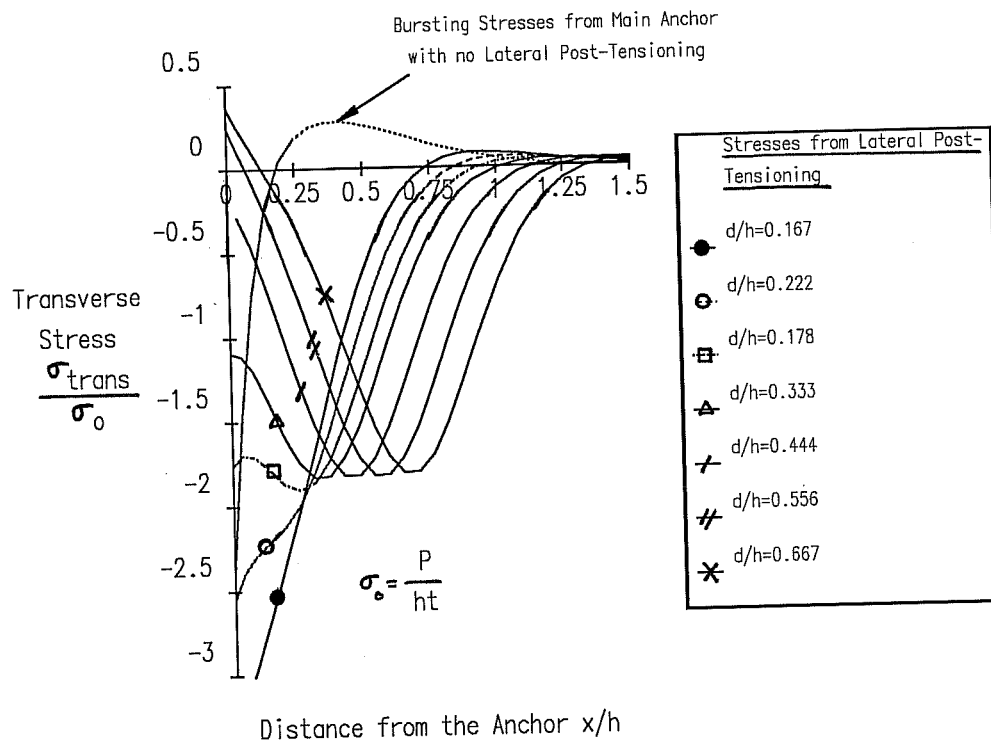
Figure 6.26   Distribution of Stresses Perpendicular to the Tendon Axis Caused by Various Locations of the Lateral Post-Tensioning Force

Previous studies by Stone and Breen [172, 173, 174] proposed to locate the lateral post-tensioning as close as possible to the main anchorage device. As discussed in Chapter 5,

Stone's specimens were generally overreinforced in the general anchorage zone, forcing the failure to occur in the local zone or at the interface between the local zone and the general zone, close to the anchorage device. It is logical that, under these circumstances, the conclusion mentioned above was drawn. A transverse compressive force will indeed increase the capacity of the local zone. In addition, the large inclination of the main tendons at the location of the anchorage in Stone's specimens induced high spalling stresses, which were greatly reduced by the lateral post-tensioning. Under more typical circumstances, however, the local zone is sufficiently reinforced to transmit the tendon force to the general anchorage zone and the level of stress in the concrete struts at the interface between the local zone and the general zone is not excessive. If these hypotheses are met, taking into account that cracking usually initiates at some distance ahead of the anchorage device, the best location for the transverse post-tensioning is at a distance of about 0.4h from the main anchor for anchorage zones with a small to moderate inclination of the tendon (up to 25 degrees).

6.4.2 Strut-and-Tie Model for Anchorage Zones with Lateral Post-Tensioning

Figure 6.27a shows the principle of the Strut-and-Tie Model for use with lateral post-tensioning. The lateral post-tensioning is considered as an external force acting on the anchorage zone. Its effect is to deviate the flow of forces coming from the anchorage device. The Strut-and-Tie Model of Fig. 6.27a also incorporates a layer of non-prestressed reinforcement that will contribute to the ultimate strength. Fig. 6.27b shows a two level thrust-line Strut-and-Tie Model with two layers of non-prestressed reinforcement.

The top layer has the same capacity as the force introduced by the lateral post-tensioning. Notice that, with the exception of the compression strut coming from the anchorage devices for the lateral post-tensioning, both Strut-and-Tie Models are identical. This means that the methods previously developed for anchorage zones using conventional, non-prestressed reinforcement can be directly applied to anchorage zones using lateral post-tensioning. It appears prudent to take the nominal post-tensioning force ($0.7A_pf_{pu}$ in the current code) and not the yield value, as for conventional non-prestressed reinforcement. During the physical tests of such specimens [153], the strains in the unbonded strands used for the lateral post-tensioning were measured. Although some

a) Strut—and—Tie Model with Lateral Post—Tensioning

b) Strut—and—Tie Model with Non Prestresssed Reinforcement
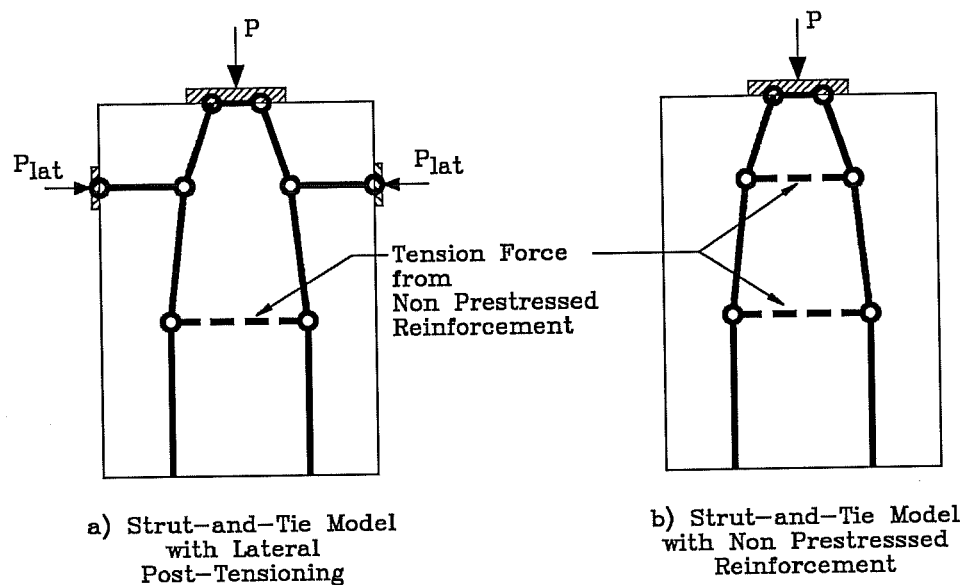
Figure 6.27   Strut-And-Tie Model for an Anchorage Zone with Lateral Post-Tensioning Compared with an Anchorage Zone with Non-Prestressed Reinforcement Only

increase in strains was observed between the initial condition and failure, the increase was not sufficient to ensure that the full yield capacity of the tendons would be reached. Because the tendons used for the lateral post-tensioning would most likely not be grouted when the main post-tensioning is applied, it seems reasonable to count only on the effective lateral post-tensioning force at the time of stressing of the main tendons.

The main differences between non-prestressed and prestressed lateral reinforcement for the anchorage zone lie in the presence of secondary local zones at the anchors for the transverse post-tensioning and the lateral spreading of forces due to the lateral post-tensioning before the main post-tensioning is applied. Once the main post-tensioning is in place, the anchorage zone will be essentially subjected to compressive stresses. However, as shown in Figures 6.24a and 6.25a tensile stresses acting parallel to the main tendon axis are induced by the lateral post-tensioning. Although these forces should not be very large, because the lateral post-tensioning required to prevent cracking is only a fraction of the main tendon force, it is possible to use a Strut-and-Tie Model to determine the forces caused by the spreading of the lateral post-tensioning load.

6.4.3 Comparison with Test Results

A series of four experimental specimens were prepared and tested in the overall anchorage zone investigation. The location d and the amount of transverse post-tensioning were varied, and compared with the results obtained for a specimen reinforced with non-prestressed reinforcement. The geometry of the test specimens is the same as the geometry shown in Fig. 6.23.
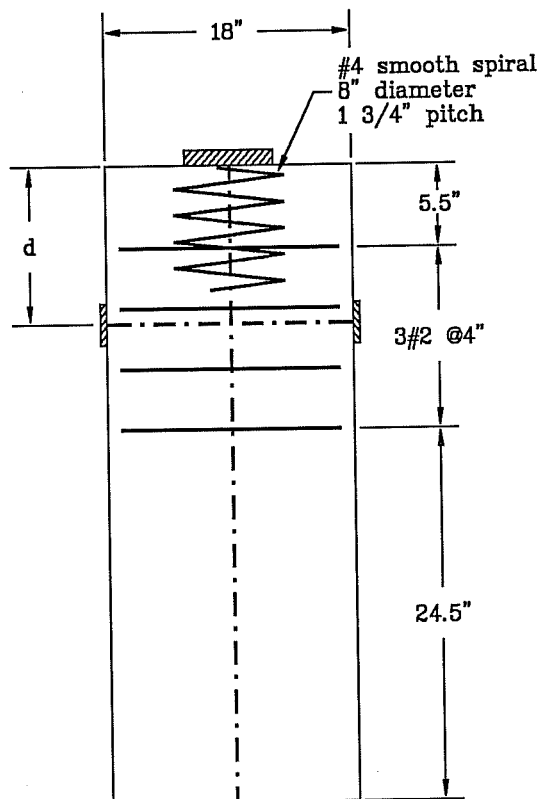
Figure 6.28   General and Local Zone Reinforcement of Specimen
              TPT2

Table 6.3   Dimensions and Concrete Properties for Specimens with
Lateral Post-Tensioning

	Dimensions	Anchor	Concrete	
Specimen [in]	$h \cdot w \cdot t \cdot d$ [in]	$a \cdot b \cdot t_{plate}$ [ksi]	f'_c [ksi]	f_{sp} [ksi]
TPT1	$42 \cdot 18 \cdot 10 \cdot$ N/A	$6.5 \cdot 6.5 \cdot 7^*$	4.95	0.326
TPT2	$42 \cdot 18 \cdot 10 \cdot 10.5$	$6.5 \cdot 6.5 \cdot 7^*$	4.95	0.326
TPT3	$42 \cdot 18 \cdot 10 \cdot 5.5$	$6.5 \cdot 6.5 \cdot 7^*$	5.15	0.409
TPT4	$42 \cdot 18 \cdot 10 \cdot 5.5$	$6.5 \cdot 6.5 \cdot 7^*$	4.95	0.326

*: Multiplane Anchorage. Total depth of the anchor.

Table 6.4   Non-Prestressed and Prestressed Reinforcement for
Specimens with Lateral Post-Tensioning

	Non-Prestressed Reinforcement		Lateral Post-Tensioning	
Specimen [kips]	As^*f_y [in]	Centroid [kips]	$0.7A_p^*f_{pu}$ [kips]	Centroid [in]
TPT1	28.6	11.5	N/A	N/A
TPT2	28.6	11.5	10.15	10.5
TPT3	28.6	11.5	28.92	5.5
TPT4	28.6	11.5	20.30	5.5

Table. 6.3 summarizes the geometry and the material properties of the concrete at time of testing. Fig. 6.28 shows the layout of the reinforcement for Specimen TPT2, and Table 6.4 summarizes the prestressed and non-prestressed reinforcement for the specimens in this series.

Fig. 6.29 shows the predicted cracking loads based on the

largest tensile stress from the Finite Element Analysis and the
concrete tensile strength measured in a split cylinder test for
the various specimens, along with the actual values. Specimens
TPT1 and TPT2 reached cracking loads greater than the predicted
values. The average ratio of predicted to actual cracking load is
1.02, with a standard deviation of 0.204. Fig. 6.31 compares the
actual test results with the ultimate load predicted based on the
capacity of the tension tie (both non-prestressed and prestressed
reinforcement), the ultimate load predicted based on the capacity
of the struts, as well as a compression limit obtained by setting
the elastic compressive stress at a distance a from the anchorage
device to $0.75f'_c$.
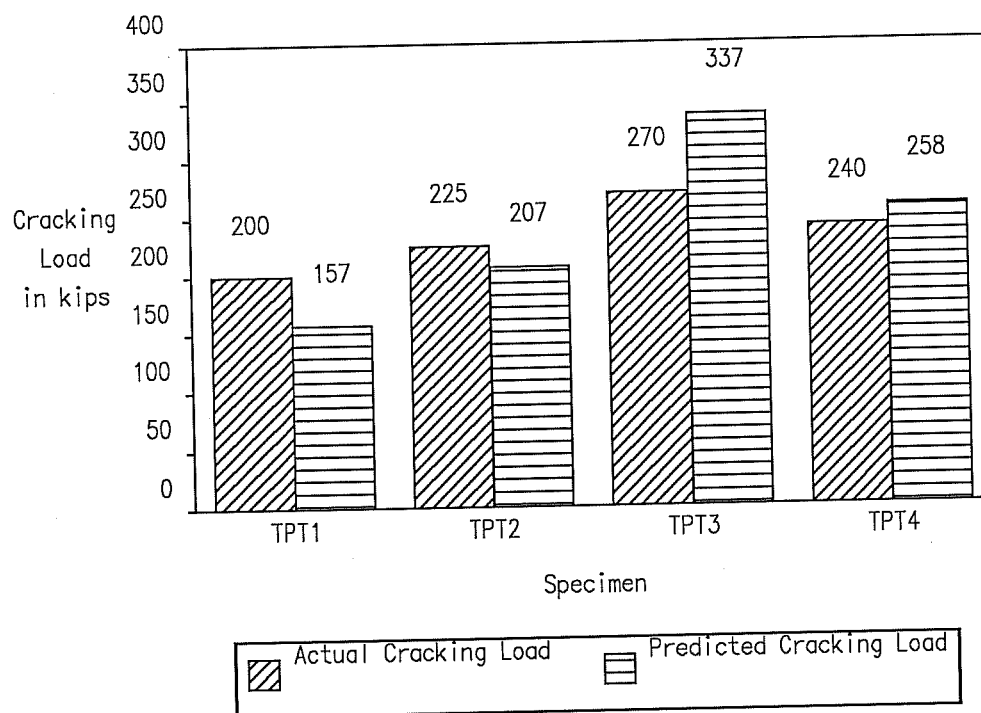
Figure 6.29   Actual and Predicted Cracking Load for Specimens
with Lateral Post-Tensioning
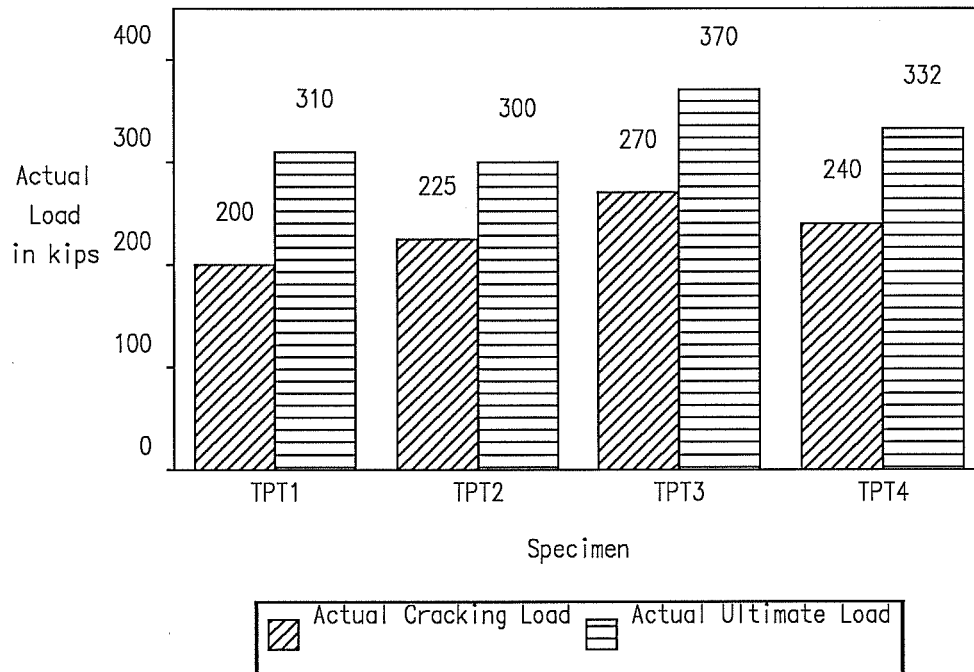
Figure 6.30 Actual Cracking and Ultimate Load for Specimens with Lateral Post-Tensioning

Specimen TPT1 reached an ultimate load larger than specimen TPT2 with the same non-prestressed reinforcement and an additional lateral post-tensioning. This behavior is probably due to a large contribution of concrete in tension to the tie capacity, which is also indicated by the comparatively high cracking load of Specimen
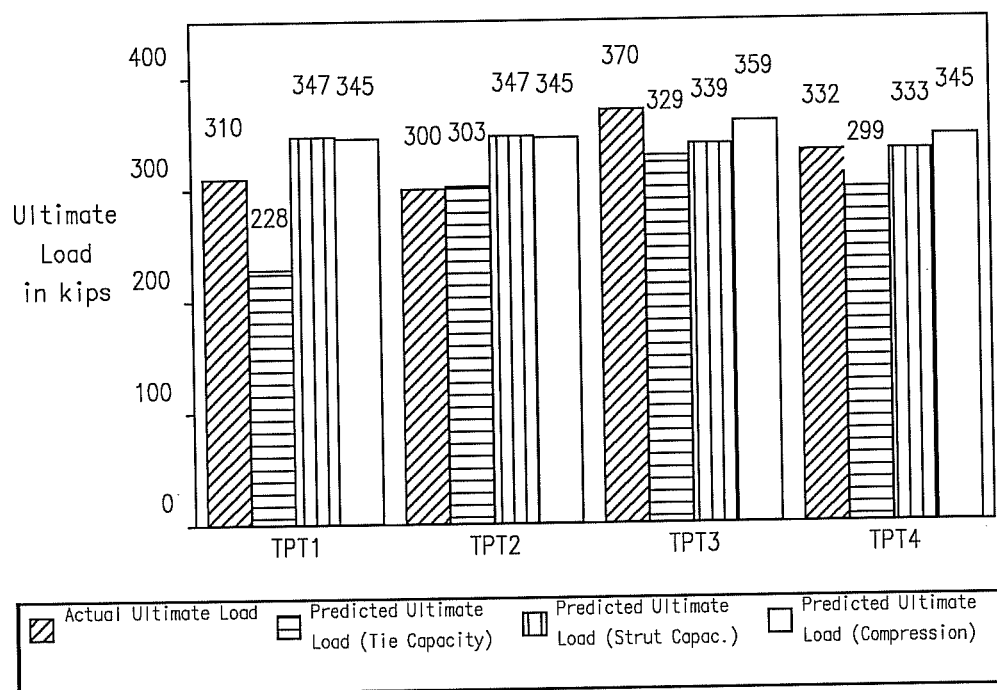
Figure 6.31 Actual and Predicted Ultimate Load for Specimens with Lateral Post-Tensioning

TPT1. A reloading of all specimens reached approximately the same load for Specimens TPT2 to TPT4, while Specimen TPT1 reached only 240 kips, very close to the predicted ultimate load based on the tie capacity. The strut capacity seems to control the load capacity of most specimens of this series, although the tie

capacity is very close. The average ratio of predicted to actual ultimate load is 1.14, with a standard deviation of 0.158. Fig. 6.30 shows the actual cracking and ultimate loads for all specimens of the TPT series. As in previous tests, a significant additional capacity is observed between the cracking load and the ultimate load.

6.5   Non-Rectangular Cross Sections

In most applications of post-tensioning, especially for bridge girders, the cross section over which the post-tensioning acts is not rectangular. In typical bridge applications, the post-tensioning forces are applied to the webs and distribute over the entire cross section. Fig. 6.32 illustrates how two tendon forces acting on the webs of a box girder section are distributed first to the web, and then to the top and bottom flanges. The distribution of forces in the various components of the cross section is similar to the distributions observed for rectangular cross sections. The top and bottom flanges are only indirectly subjected to the tendon forces, which are introduced over a certain distance. This is significant because it indicates that the local introduction of forces into members not directly subjected to the post-tensioning forces is not as severe as in members which are directly subjected to the post-tensioning force. The tendon force acting on these components of the cross section is not applied at one concentrated location, but rather is introduced over a certain length. Notice also that the forces acting on the top and bottom flanges are applied at a larger distance from the anchorage device than in the case of rectangular cross sections. As a consequence, the general anchorage zone will be longer in the case of a cross section made of several components than in a rectangular cross section.
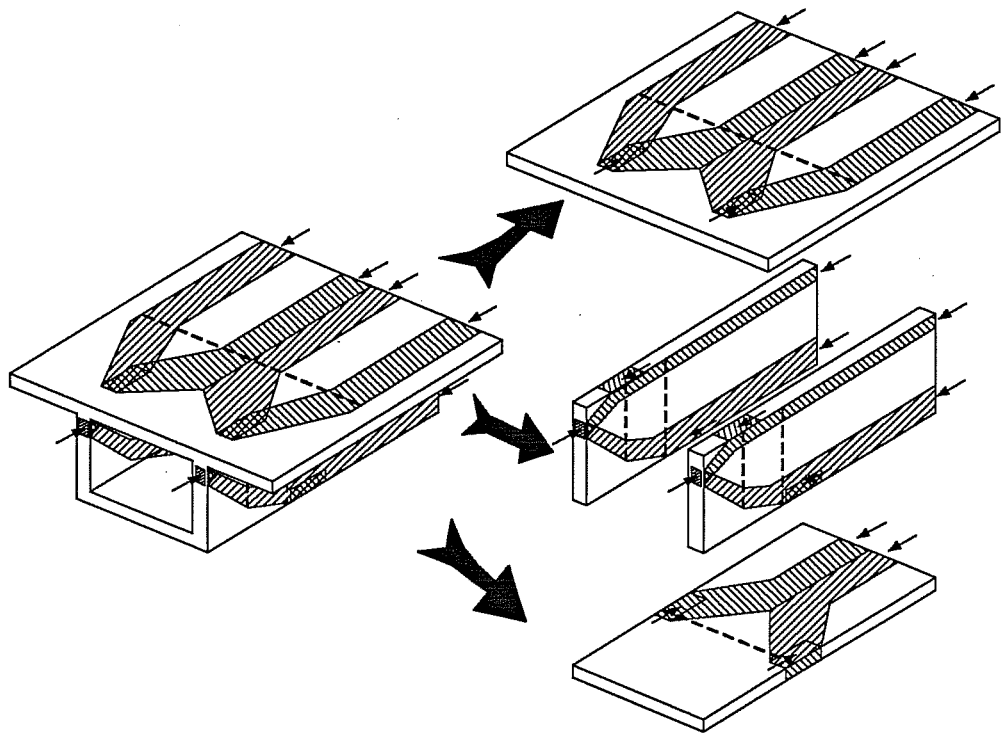
Figure 6.32   Flow of Forces in the Anchorage Zone of a Box Girder
Cross Section
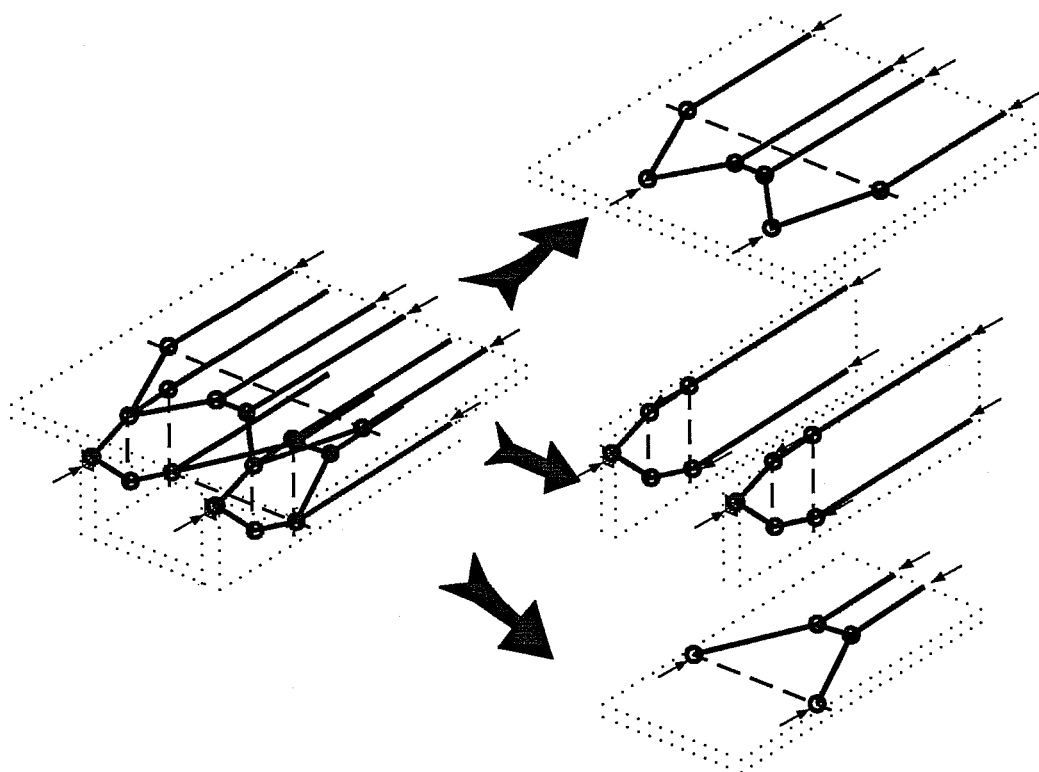
Figure 6.33   Three-Dimensional Strut-and-Tie Model of the
                Anchorage Zone of a Box Girder Cross Section

Fig. 6.33 shows a Strut-and-Tie Model of the same box girder cross section, where all struts and ties are represented as thin lines, and all nodes are considered as points. This type of Strut-and-Tie Model is appropriate for calculations of the forces in the various components of the cross section, but it should be kept in mind that some struts and nodes actually are distributed over areas larger than suggested by this representation. It is advantageous whenever possible to analyze separately the individual components instead of solving the complex three-dimensional Strut-and-Tie Model. The principles for developing Strut-and-Tie Models for cross sections involving several components are the same as for the rectangular cross sections presented in the previous sections. Starting at the end of the

general zone, the stresses can be determined based on simple beam theory. The resultant forces on the various components on the cross section are computed as resultants of these stresses. It has been found practical to have at least two struts corresponding to each anchorage device, with the tendon axis acting as line of separation between the two. A path for the post-tensioning force from the anchorage device to the end of the general anchorage zone can then be drawn. Once the magnitude and point of application of the forces acting on each component on the section are known, each component can be analyzed and designed independently using the methods presented for rectangular cross sections. Alternatively, a single, three-dimensional Strut-and-Tie Model can be developed.

The transfer of forces from one component of the cross section to another component occurs over a certain distance, as shown conceptually in Fig. 6.32. Components that do not have an anchorage device acting directly on them, properly speaking, do not have an area of local introduction of forces corresponding to the local zone. For the sake of simplicity, the Strut-and-Tie Model used for the design of the component (for example the top flange of Fig. 6.33) assumes that the force is introduced completely at a specific point, which would correspond to the local zone in a rectangular cross section. However, the concentration of forces in this area is much less severe than the concentration that occurs in the vicinity of an anchorage device. Fig. 6.34 shows a detail of the special *smeared* node at the interface between the web and the top flange. This type of node is essentially subjected to compression forces. Provided that the web reinforcement is properly detailed so as to go *around* the node, this reinforcement will introduce a compression force in the node. Assuming that the levels of stresses in the compression struts in the web and the top flange are acceptable, the node itself will not be critical. In a similar fashion, the tensile tie forces

obtained from such a Strut-and-Tie Model will probably differ from the values obtained from an elastic analysis because of the larger uncertainties in defining the geometry of the Strut-and-Tie Model.
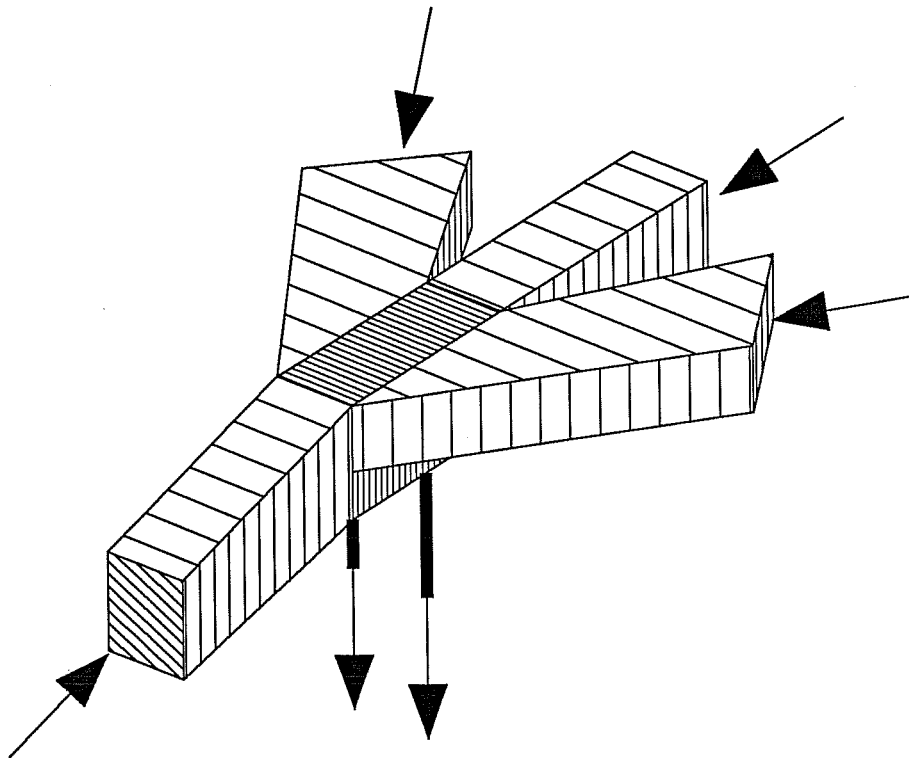
Figure 6.34   Three-Dimensional Representation of the Node at the
              Intersection of the Flange and the Web

The simplest non-rectangular section is a *"T-shaped"*, or *flanged* cross section, that consists of two rectangular plates. This is a very common cross section for bridge girders, and it will be the main focus of the investigation of the state of stress and the tensile forces in the anchorage zone in non-rectangular cross-sections.

6.5.1 Finite Element Analysis of a Flanged Section

A series of Finite Element analyses were performed on flanged sections to investigate the influence of the presence of the flange on the overall state of stresses. Fig. 6.35 shows the geometry of the flanged section used for the parametric studies. Shell elements were used to model the structure. Fig. 6.36 shows
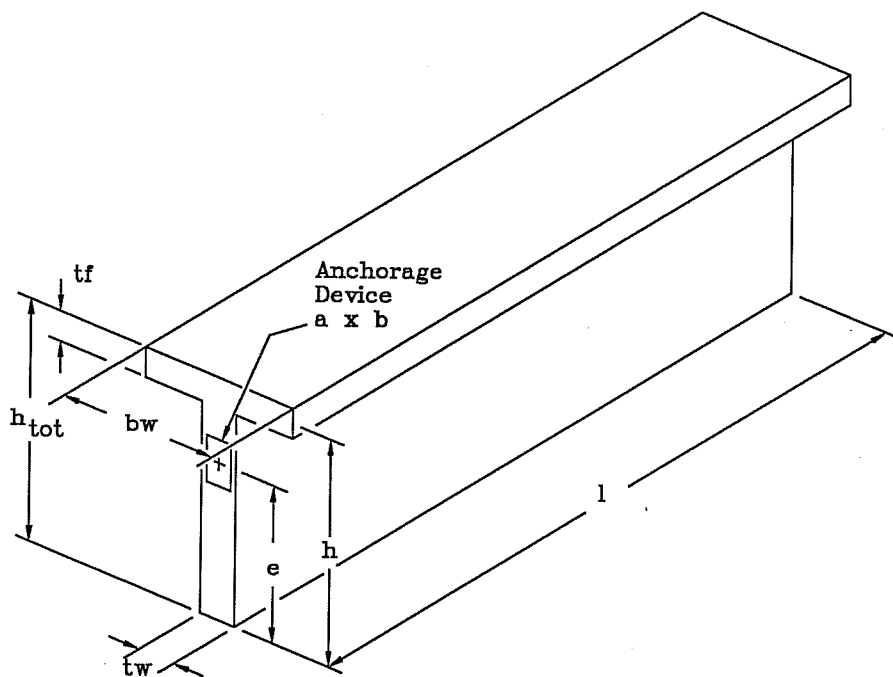
Figure 6.35   Geometry of the Model Used for the Finite Element
             Analyses of Anchorage Zones in Flanged Cross
             Sections

the Finite Element mesh used for the parametric studies. To facilitate the parametric studies, the height of the web was kept constant up to the middle of the top flange (labeled h in Fig. 6.35), instead of the total height (h_{tot} in Fig. 6.35). The location e of the tendon load is defined as the distance from the bottom of the cross section to the center of the tendon. For the

Finite Element Analyses that investigated the effect of two anchorage plates, the centroid of the two forces is given as e. The output of the Finite Element program was processed to allow the use of the program used previously for the display of principal stresses of two-dimensional structures.
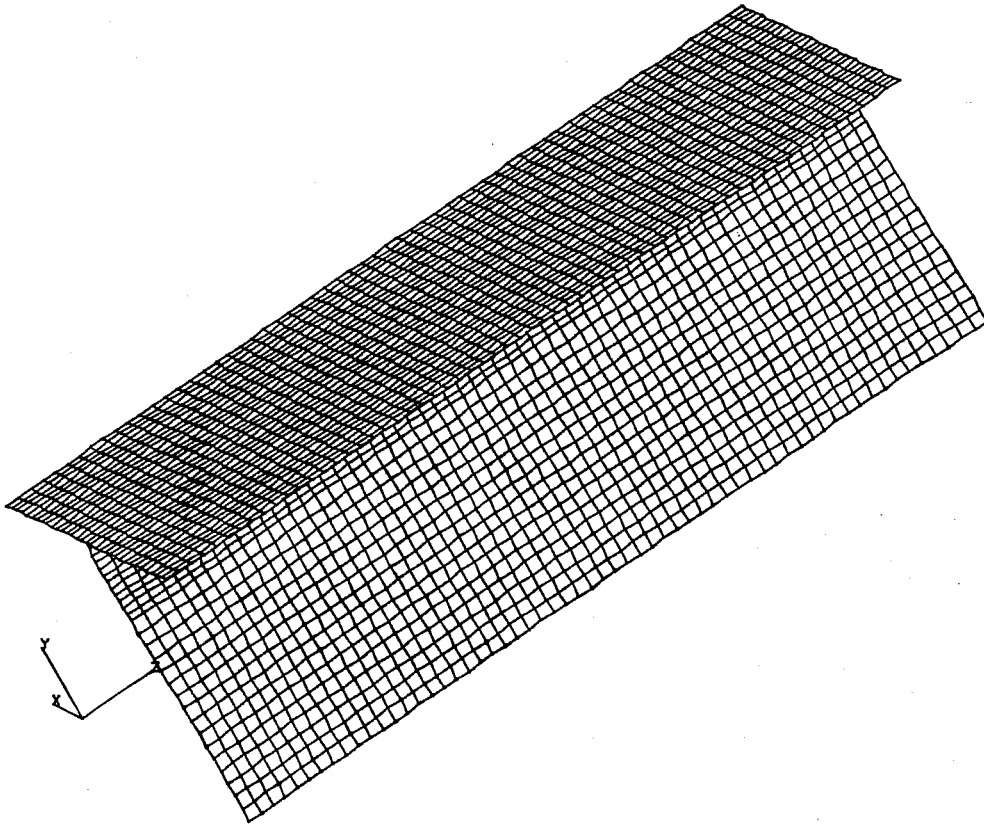
Figure 6.36 Finite Element Model Used for the Analysis of
Flanged Configurations
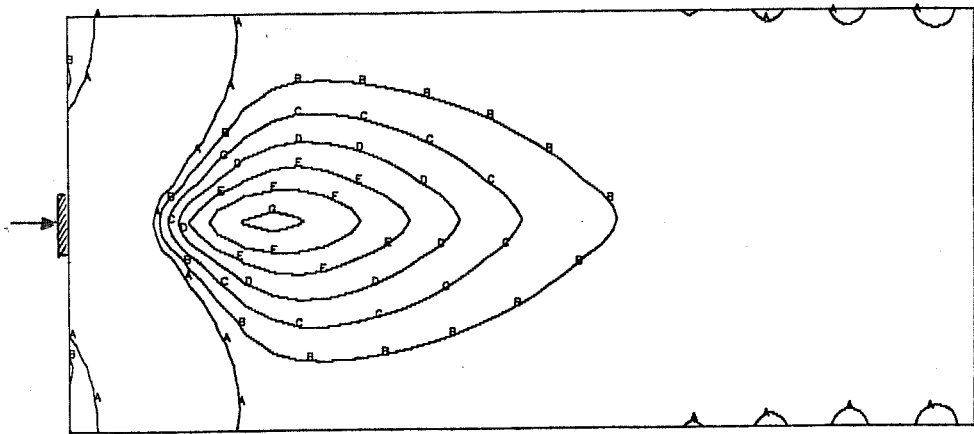
a) Top Flange
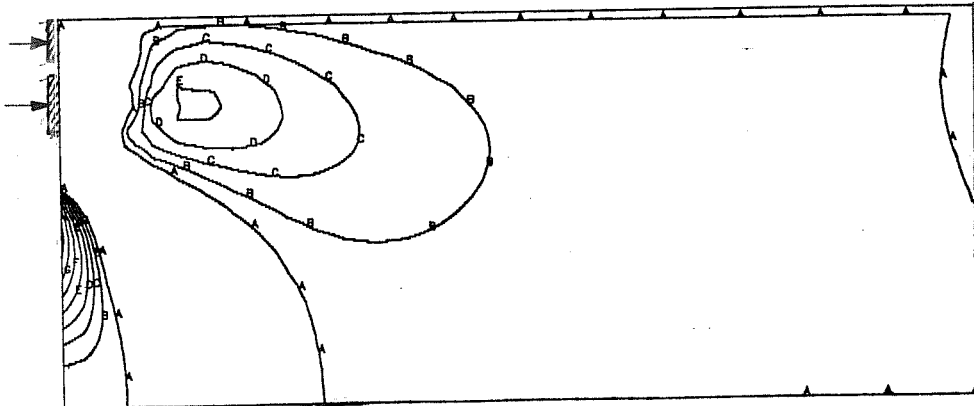
b) Web

A = 0.00 σ_0 B = 0.05 σ_0C = 0.10 σ_0 D = 0.15 σ_0 E = 0.20 σ_0 F = 0.25 σ_0 G = 0.30 σ_0
H = 0.35 σ_0 I = 0.40 σ_0 J = 0.45 σ_0 K = 0.50 σ_0 L = 0.55 σ_0 M = 0.60 σ_0 N = 0.65 σ_0

Figure 6.37   Contour Plot of the Transverse Stresses
              Perpendicular to the Tendon Axis in an Anchorage
              Zone of a Flanged Cross Section

Fig. 6.37 shows the contour plot of the stresses perpendicular to the tendon axis for a configuration with two anchorage plates of size 0.19h located at 0.65h and 0.88h from the bottom of the cross section. The state of stresses in the web is similar to the state of stresses in an eccentrically loaded rectangular cross section, while the top flange presents similarities with a concentrically loaded rectangular cross section. Fig. 6.38 shows the two corresponding plots of principal stress vectors.
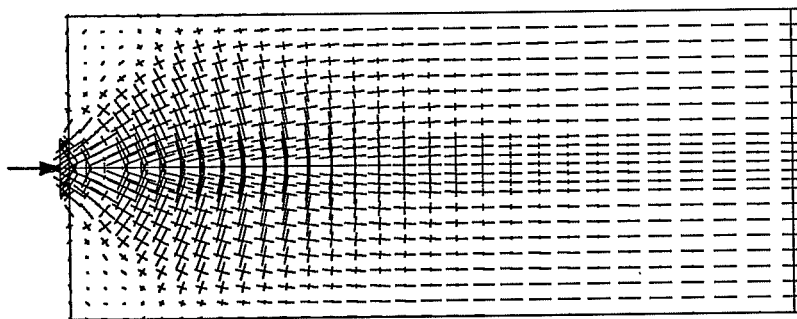
a) Top Flange
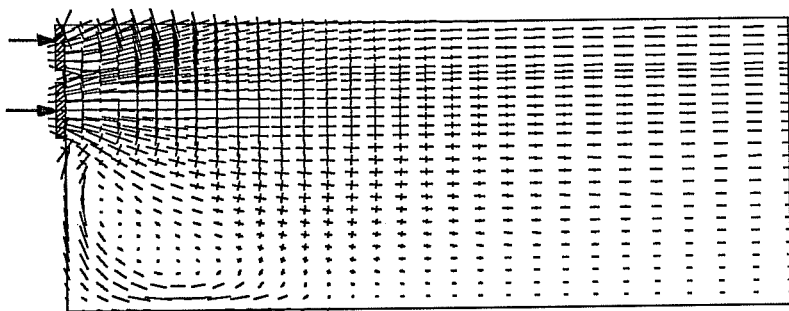
b) Web

Figure 6.38   Vector Plot of the Principal Stresses in the
             Anchorage Zone of a Flanged Cross Section

Fig. 6.39 shows the distribution of tensile stresses along

the axes of the two tendons, along the interface between the flange and the web, and along the centerline of the flange. Notice how the distribution of the stresses in the top flange is shifted away from the anchorage device, compared to the curves of the stresses in the web. The length over which the tensile stresses are appreciable is large than in rectangular cross sections. It is approximately equal to the sum of the lateral dimensions of the cross section.
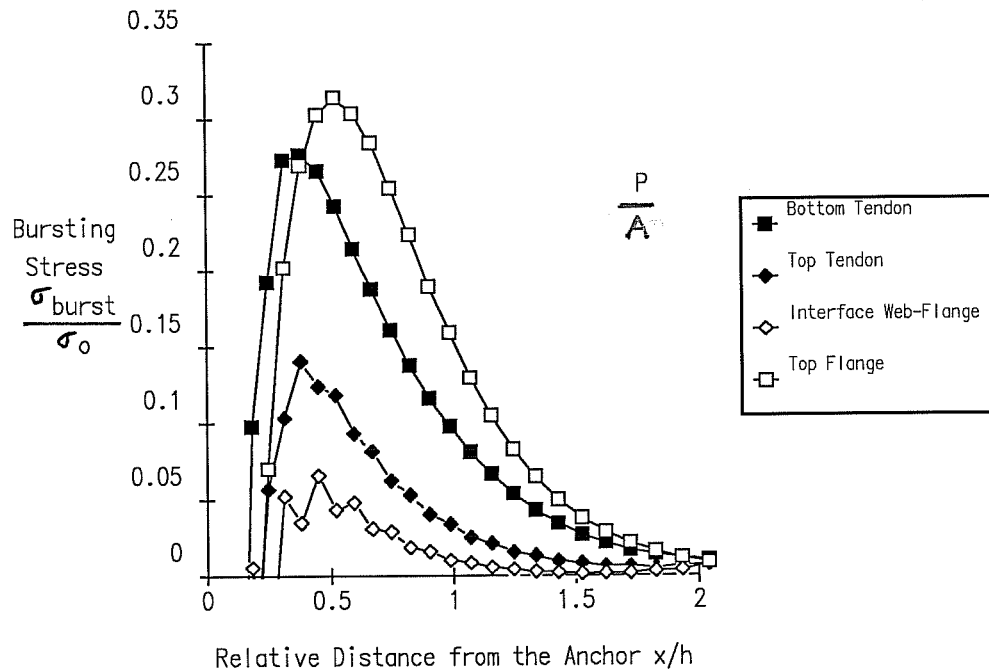
Figure 6.39   Transverse Bursting Stresses along Various Lines
              Parallel to the Axes of the Tendons in an Anchorage
              Zone of a Flanged Section

Because more area is available in a non-rectangular cross

section for the distribution of stresses, each component of the cross section has to resist a force smaller than it would have to resist in a similar rectangular cross section subjected to the same post-tensioning force. Therefore, the contribution of concrete in tension will have an larger influence on the actual behavior of the anchorage zone. Because of the large contribution of concrete in tension, it is expected that the design of the local zone and the compressive stresses in the concrete at the interface between the local zone and the general zone will control the behavior of anchorage zones in non-rectangular cross sections.
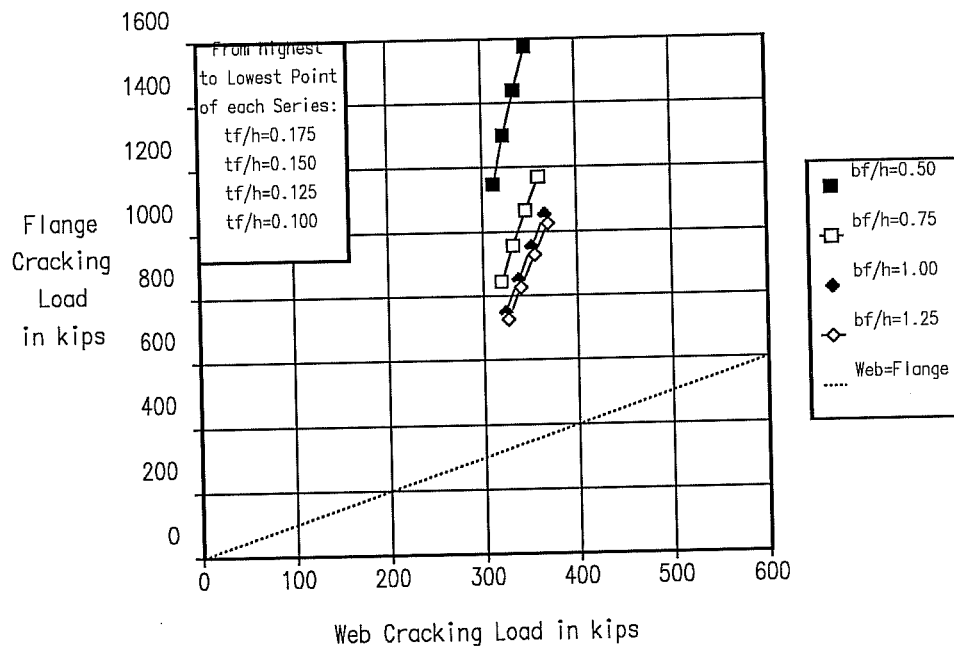
Figure 6.40   Influence of the Flange Dimensions on Predicted Cracking Loads for the Flange and the Web of a Flanged Cross Section with an Overall Depth h_{tot} = 36 inches and an Assumed Tensile Strength Capacity of the Concrete of 0.4 ksi

Furthermore, a substantial contribution of concrete in tension to the load capacity had been observed in experimental tests [153]. To ensure that the flanged test specimen would not fail without cracking of the cross section, an extensive series of Finite Element Analyses was conducted, investigating the influence of various geometric and loading parameters on the cracking loads of the web and the flange. Fig. 6.40 shows the predicted cracking loads for the flange of the specimen as a function of the predicted cracking load for the web of the specimen. The parameters under investigation are the width and the thickness of the top flange. The results of are normalized for an overall depth h_{hot} of the section of 36 inches.

The cracking loads are obtained by setting the largest calculated tensile stress in the web and in the flange to the tensile strength of the concrete, assumed to be 0.4 ksi. The reduction in cross section of the web caused by the tendon duct was neglected in this parametric study. To be able to observe the development of a Strut-and-Tie Model in the test specimen, it was desirable that both the flange and the web have similar cracking loads. In the previous tests [153], it had been observed that the ultimate strength of the specimens was less than twice the first cracking load. According to this criterion, none of the configurations presented in Fig. 6.40 were suitable for a test specimen. From this parametric study, it was found that, beyond a ratio b_f/h of 1.0, there is little change in the state of stresses in the top flange. The thickness of the top flange has a certain influence, but, for the considered test setup, ratios t_f/h smaller than 0.125 were not practical.

Fig. 6.41 shows the influence of additional parameters like the point of application of the load, the thickness of the web and the number of tendons on the cracking loads of the web and the flange. The most important changes occur when the load is applied through two plates, with one plate acting mainly on the top flange and the other acting on the web. Based on this parametric study, the dimensions of the test specimen described in Section 6.5.3 were chosen to follow the proportions of the configuration shown as a black triangle in Fig. 6.41.
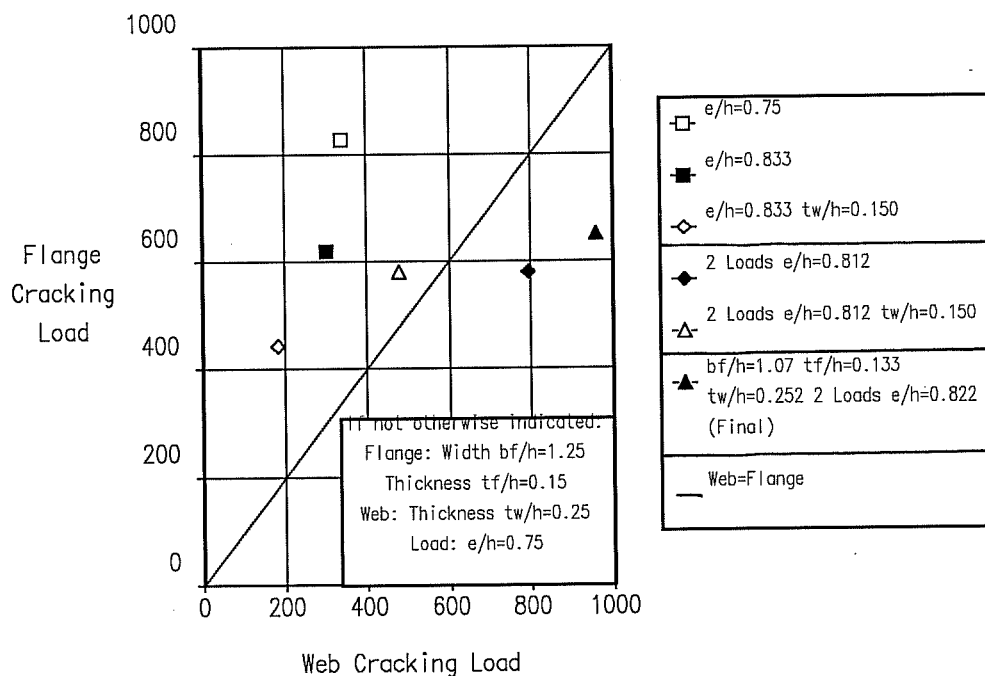
Figure 6.41   Influence of the Web Thickness and of the Loading on Predicted Cracking Loads for the Flange and the Web of a Flanged Cross Section with an Overall Depth h_{tot} = 36 inches and an Assumed Tensile Strength Capacity of the Concrete of 0.4 ksi
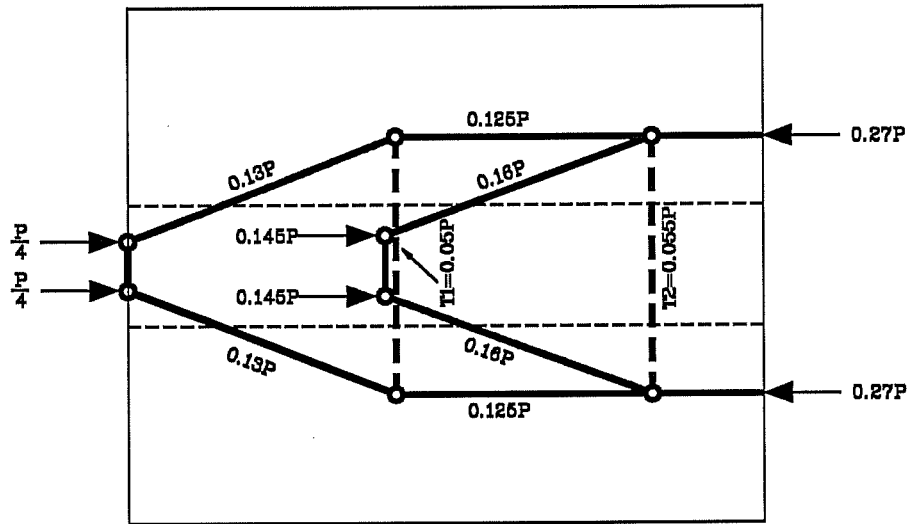
a) Top Flange
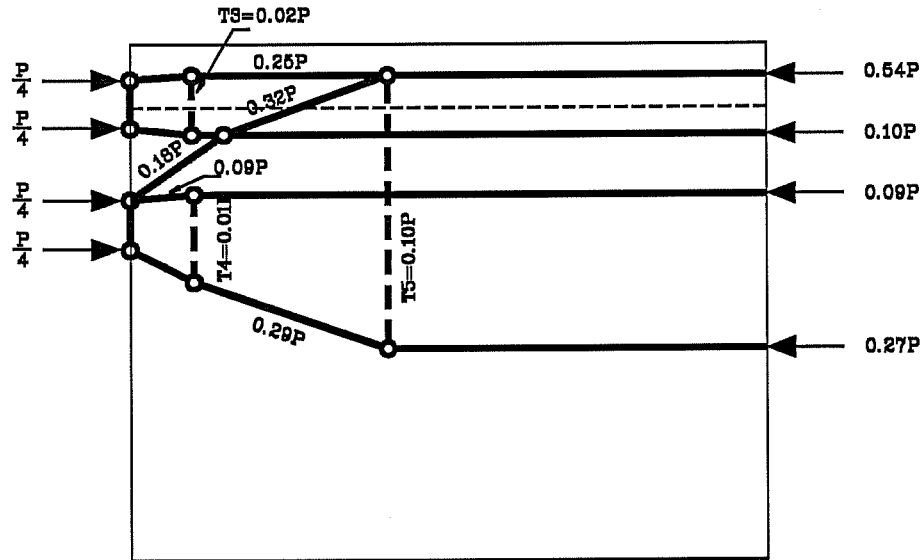
b) Web

Figure 6.42   Strut-and-Tie Model of Anchorage Zone in Flanged
             Cross Section

6.5.2 Strut-and-Tie Model for a Flanged Section

The general principles for the development of Strut-and-Tie Models for non-rectangular cross sections, as presented in Section 6.5 were applied to the test specimen described in Section 6.5.3. The angle used for the diffusion of the compressive forces was 26 degrees, as in the previous models. Minor adjustments were made to simplify the geometry. Fig. 6.42 shows the Strut-and-Tie Model with the force in the main members. The total transverse force in the web is 0.11P, compared with 0.085P from the Finite Element solution, and the total transverse force in the flange is 0.105P, compared with 0.082P from the Finite Element analysis. Considering the number of assumptions necessary to obtain a Strut-and-Tie Model of this level of complexity, the results of the Strut-and-Tie Model are quite close to the elastic valued obtained from the Finite Element Analysis.
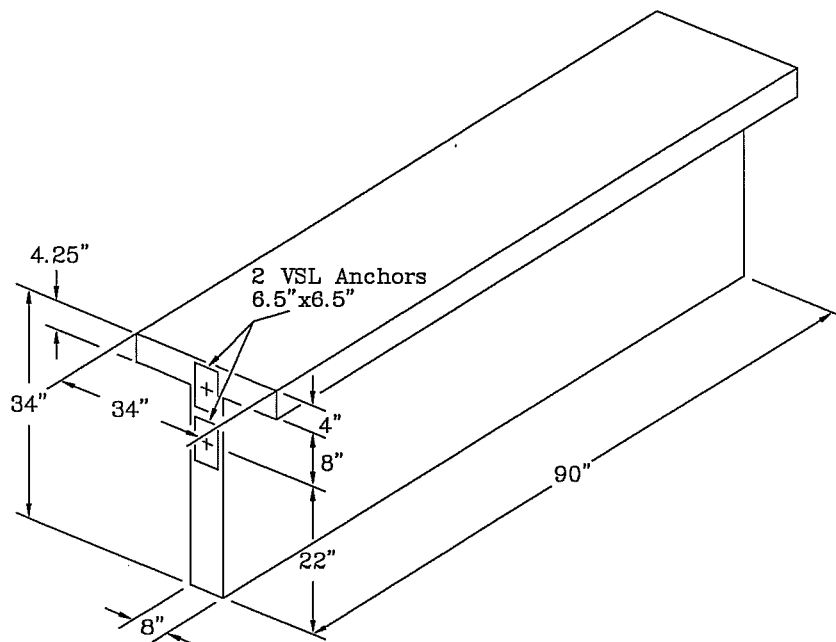
Figure 6.43   Geometry of Specimen F with Anchorage Zone in a Flanged Section

6.5.3 Comparison with Test Results

One specimen with a T cross section was tested [153]. The geometry of the specimen and the reinforcement of the local zone are shown in Fig. 6.43. The reinforcement of the general zone is shown in Fig. 6.44. The local zone reinforcement consists of a #4 spiral with a diameter of 7 inches, a pitch of 1.5 inches and a length of 8 inches. The compressive strength of the concrete at testing was 4.54 ksi, and the split cylinder tensile strength was 0.316 ksi.
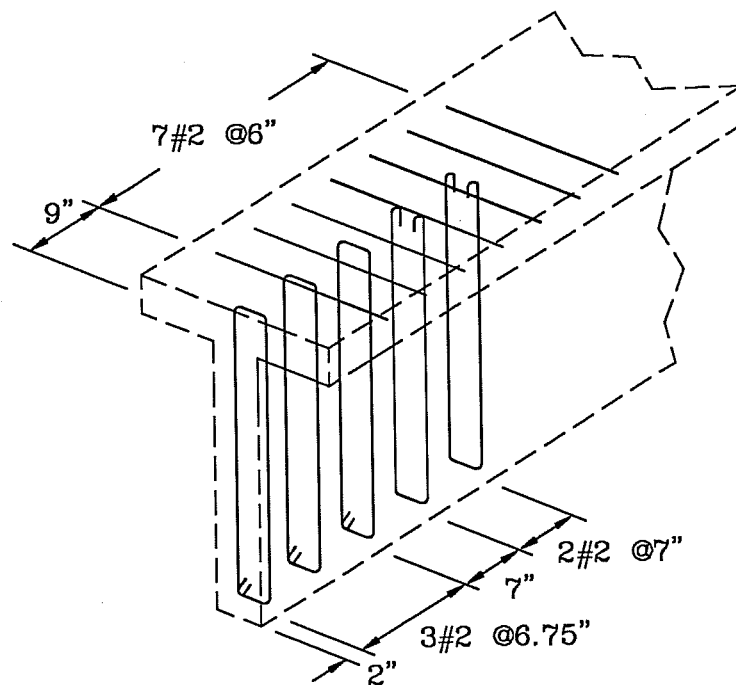
Figure 6.44 General Zone Reinforcement of Specimen F with Anchorage Zone in a Flanged Section

Fig. 6.45 shows the cracking loads for the specimen, compared with the values predicted based on the results of the Finite Element Analysis and the tensile strength of the concrete measured in a split cylinder test. The first cracking occurred at

the interface between the flange and the web, at a load much less than predicted. This is probably because the results of the shell model are not very accurate at the interface between the components of the section. The cracking load of the flange was close to the predicted value, but the web never really cracked.
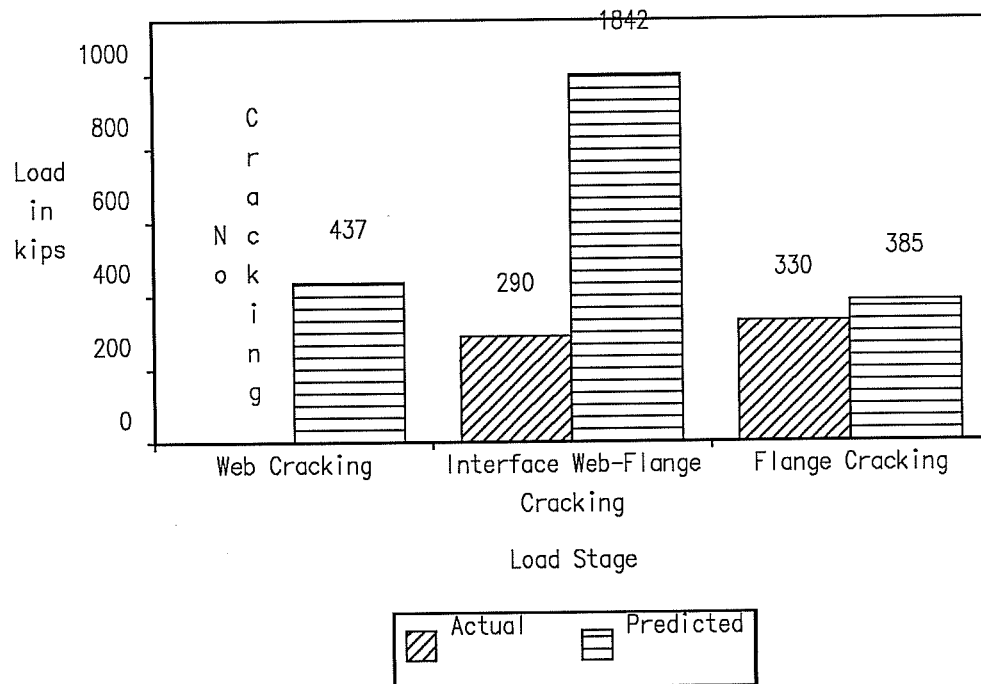
Figure 6.45   Actual and Predicted Cracking Load for Specimen with Flanged Cross Section

Fig. 6.46 shows the ultimate load reached by the flanged specimen compared to the load prediction based on the Strut-and-Tie Model and on the elastic stress compression capacity. The strut capacity was obtained by setting the average stress to $0.60f'_c$ on the critical section located at a distance a from the anchorage device. The compression stress capacity was obtained by setting the compressive stress at a distance a from the anchor obtained from the Finite Element Analysis to $0.75f'_c$. The ultimate

load exceeded the loads predicted based on the tie capacity only, but was less than both the strut capacity and the compression capacity. The failure occurred suddenly, after that longitudinal cracks developed in the top flange. It is assumed that the failure was due to the release of the tensile stresses in the concrete of the top flange caused by the progressive cracking.
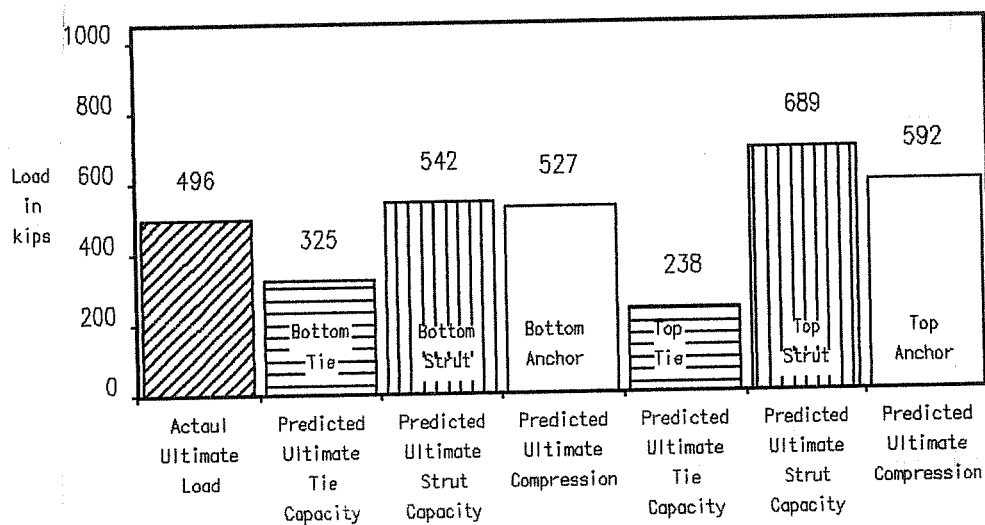
Figure 6.46   Actual Ultimate Load and Ultimate Load Predicted by
the Strut-and-Tie Model for Specimen with Flanged
Cross Section

6.6 Conclusions of the Study of Multiple Anchorage Zones and Non-Rectangular Cross-Sections

The methodology developed in Chapters 4 and 5 was applied to more complex configurations involving multiple anchorages, lateral post-tensioning and no-rectangular cross-sections. The general methodology for the development of Strut-and-Tie Models for the design of anchorage zones was found to be applicable for these more complex configurations. The predictions of the Strut-and-Tie Models were compared with the results of physical tests, and the method was found to be conservative. In most cases, the ultimate load predicted based on the capacity of the tension ties was exceeded by the test specimens, probably due to the effect of tensile stresses in the concrete. In such cases, the strut capacity was found to be an upper limit for the actual capacity of the anchorage zone. For plates located within a small distance from one another (the spacings investigated were up to 1.23 times the plate size), it is possible in design to consider the plates as one large anchorage device.

Chapter 7: Summary of the Results and Specification Proposal

The results of a total of 30 experimental test specimens from the study by Sanders [153] were used to calibrate and evaluate the analytical predictions based on the results of the Finite Element Analyses and the Strut-and-Tie Model, as described in the previous chapters. In this chapter, the results from the analysis and the experimental test results of anchorage zones are summarized. The accuracy of the predictions and the influence of the various hypotheses made in the analysis are evaluated. As a part of the overall UT Austin research project on anchorage zones, a new AASHTO specification for the design and analysis of anchorage zones is proposed. The development of this specification proposal for the design and analysis of the general anchorage zone is part of the present dissertation. The parts of the proposed specification that are directly related to the present work are discussed.

7.1   Prediction of the Cracking Load

The cracking load was predicted based on the maximum elastic tensile stress obtained from a Finite Element Analysis and the tensile strength of the concrete as measured in a split cylinder test. Fig. 7.1 shows the measured and the predicted cracking loads for all test specimens. For most specimens, the actual cracking load was slightly less than the predicted value. This is further illustrated in Fig. 7.2 which shows the ratio of the actual cracking load to the predicted value for all specimens. Fig. 7.3 shows the statistical distribution of the ratio of the actual cracking load to the predicted value. The average ratio of actual to predicted cracking loads is 0.907 with a standard deviation is 0.220. Considering the complexity of most configurations and the

357
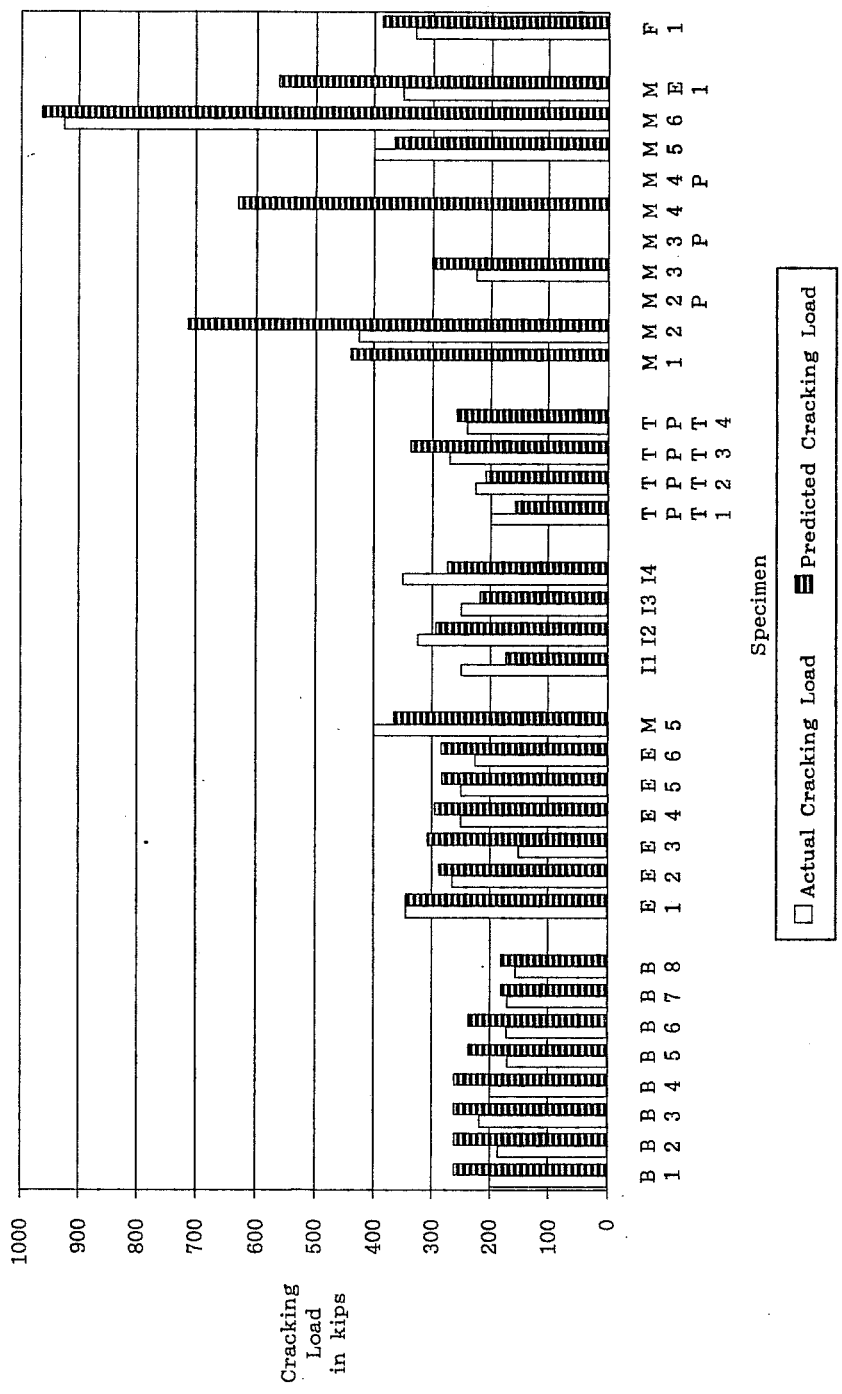
Figure 7.1   Actual and Predicted Cracking Load for All Test Specimens
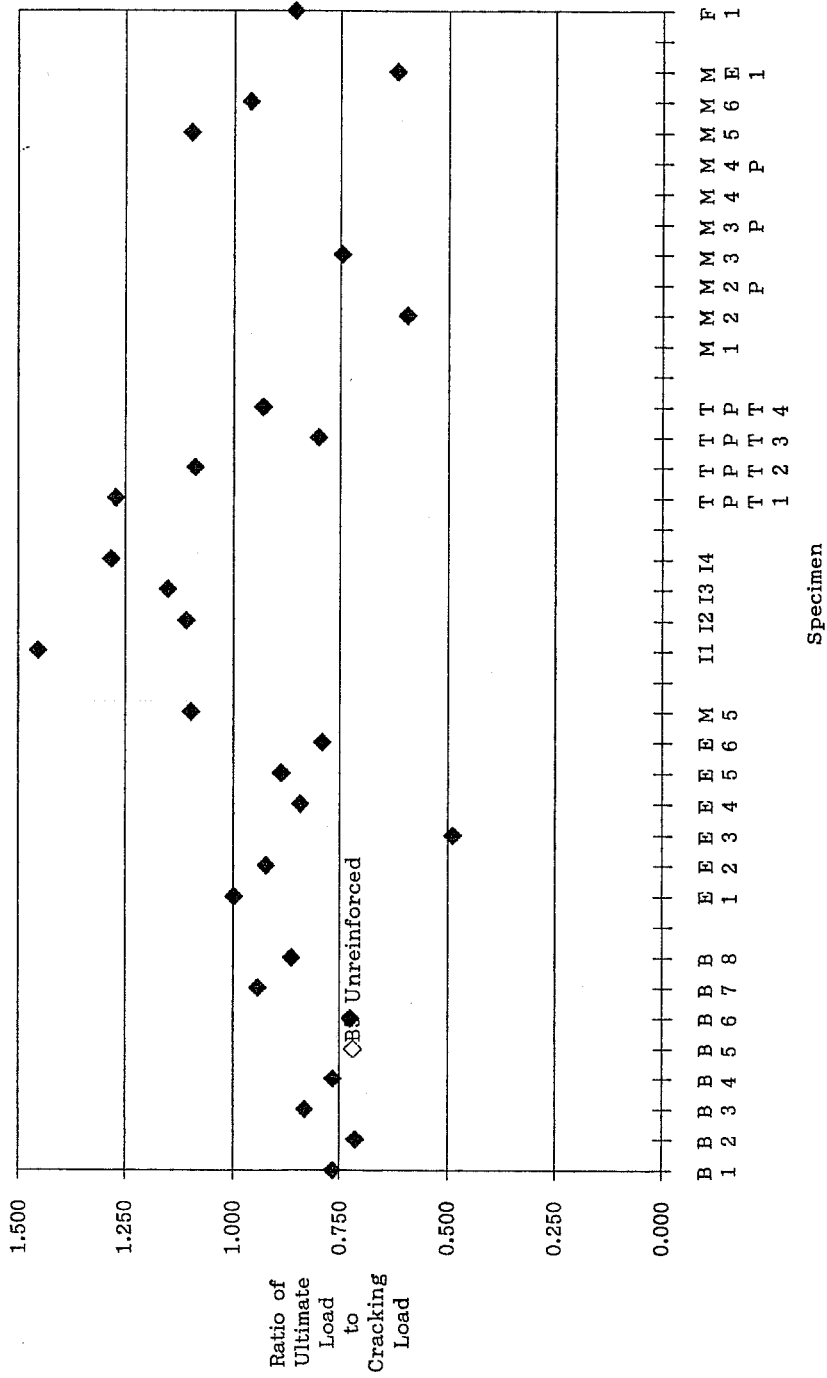
Figure 7.2 Ratio of the Actual Cracking Load to the Predicted Cracking Load for All Specimens
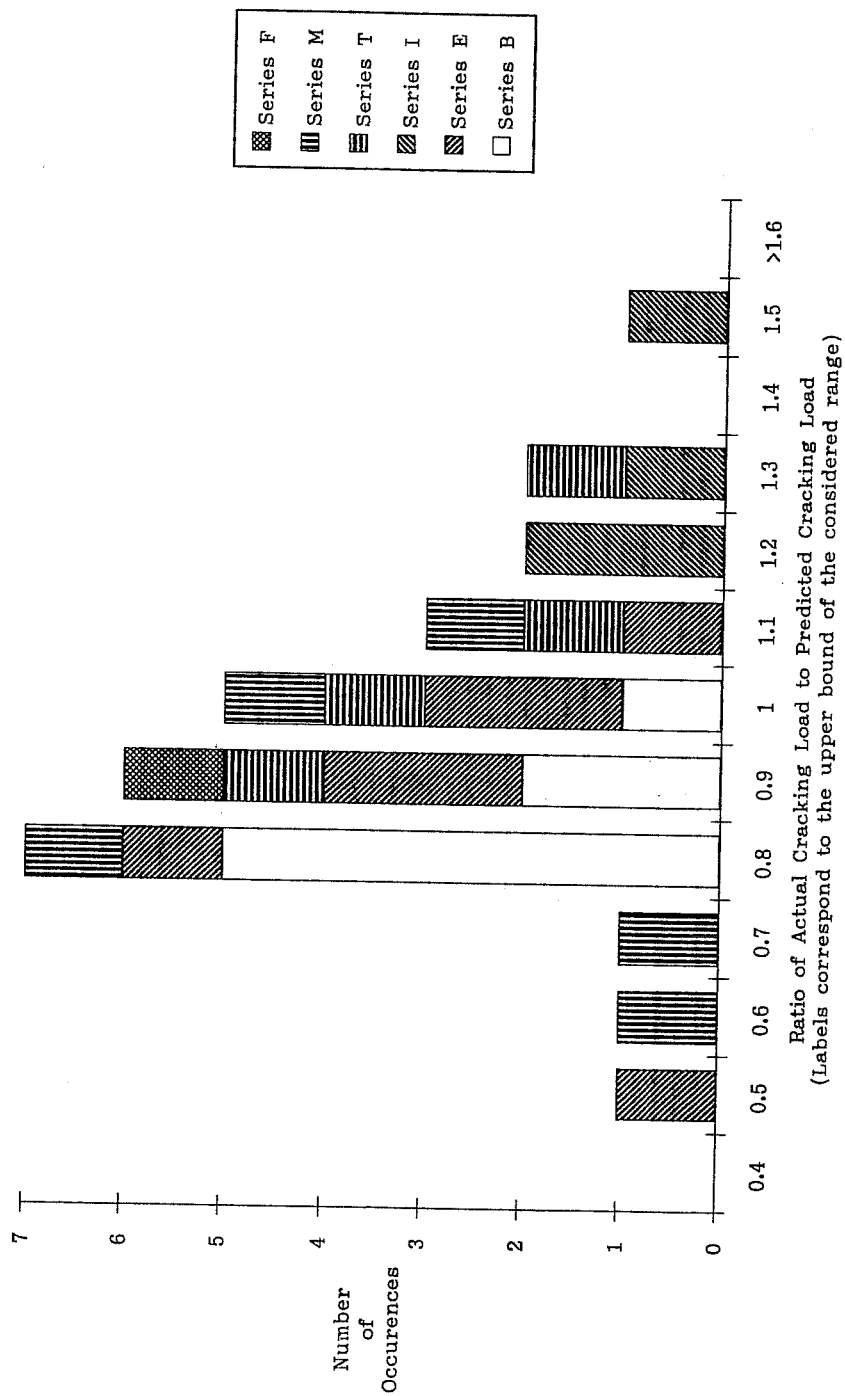
Figure 7.3   Statistical Distribution of the Ratio of the Actual Cracking Load to the
Predicted Cracking Load for All Specimens

uncertainties usually related with the prediction of cracks in concrete, these results are satisfactory. It could be possible to improve the estimate of tensile failure of the concrete by considering an appropriate biaxial stress failure theory such as that suggested by Ottosen [129]. Because the level of compressive stress along the tendon axis is fairly high, this would lower the tensile strength below the split cylinder value and would improve the average. However the scatter of the predictions would still be appreciable. The results of a Finite Element analysis of the anchorage zone can therefore be used to estimate the cracking load of the anchorage zone. Because the tests were of short duration, a smaller value of the concrete tensile strength should be used if it is desired that the anchorage zone remain uncracked for the lifetime of the structure.

7.2   Prediction of the Ultimate Capacity

Two distinct modes of failure can occur in the general anchorage zone. The first mode of failure is caused by insufficiency of tensile reinforcement to resist bursting forces. The second mode of failure is caused by an excessive level of compressive stresses in the concrete, typically occurring at the interface between the local zone and the general zone. The first mode of failure was predicted using the tensile force obtained from the Strut-and-Tie Model. Two methods were proposed to predict the second mode of failure. The first method is based on the Strut-and-Tie Model and the second uses the elastic stresses as determined from a Finite Element Analysis. Fig. 7.4 shows the actual ultimate load reached by the test specimens and the ultimate load predicted by the Strut-and-Tie Model. In most cases the ultimate load predicted by the Strut-and-Tie Model is less than the actual ultimate load. This is also clear when considering

Fig. 7.5, which shows for all specimens the ratio of the actual ultimate load to the ultimate load predicted by the Strut-and-Tie Model. The very large ratio obtained for Specimen I4 is due to the fact that this specimen had very little bursting reinforcement, but nonetheless reached a high capacity due to the presence of tensile stresses in the concrete. Specimen B5 is shown with the value of the predicted ultimate load based on an assumed tensile capacity of the concrete acting as a tension tie.

Fig. 7.6 shows the statistical distribution of the ratio of the actual ultimate load to the ultimate load predicted by the Strut-and-Tie Model. The average ratio of actual to ultimate is 1.44 with a standard deviation of 0.44. In the figure, thick lines surround those test specimens for which the compressive capacity of the concrete struts controlled the design. Fig. 7.7 shows the statistical distribution of the results obtained if the compressive capacity is estimated based on the elastic stresses obtained from the Finite Element Analysis. The estimation of the ultimate load is slightly improved, with an average ratio of 1.32, but the standard deviation is essentially the same at 0.45. Because most of the designs are controlled by the capacity of the tensile ties, for which the results of the Strut-and-Tie Model are used for both figures, the improvement obtained by using an improved model for the prediction of the compressive stresses is not substantial. However, the prediction of the ultimate load based on the results of the Finite Element Analysis is substantially improved when the mode of failure is a compressive failure of the concrete at the interface between the local zone and the general zone.

Fig. 7.8 shows for all specimens the two values of the ultimate load predicted by the Strut-and-Tie Model. The lowest value controls the design. The actual ultimate load is also shown with a horizontal dash. Because in most cases the actual ultimate

load is larger than the lowest of the design values, the method is conservative. It is interesting to consider the cases where the ultimate load is substantially larger than predicted. This is the case for Specimens I1-I4, M2, M2-M6, ME1 and F1. Except for M2 and M3, the tie capacity controls the design of these specimens. However, probably because of a substantial contribution of concrete in tension, the actual ultimate load is much larger. In all cases, the actual ultimate load does not increase to values much greater than the predicted strut-based capacity of these specimens. It is likely that in such cases a compression failure occurs, and not a tension failure as predicted. The most obvious example is specimen M6 which reached almost twice the ultimate load predicted based on the capacity of the tensile reinforcement. A possible exception is presented by Specimen I4, which exhibited a very brittle behavior and probably failed when the tensile cracks in the bursting region propagated to the end of the specimen.

All specimens exhibited a substantial increase in load between first cracking and ultimate. This fact is illustrated by Fig. 7.9 which shows the ratio of the ultimate load to the cracking load for all specimens. This result contradicts Stone's [169] finding that the cracking load and the ultimate load are close for anchorage zones. As indicated previously, it is likely that many of Stone's observed failures were not failures caused by bursting forces, but rather failures of the local zone, which were carefully avoided in the present study, or compressive failures at the interface between the local zone and the general zone.
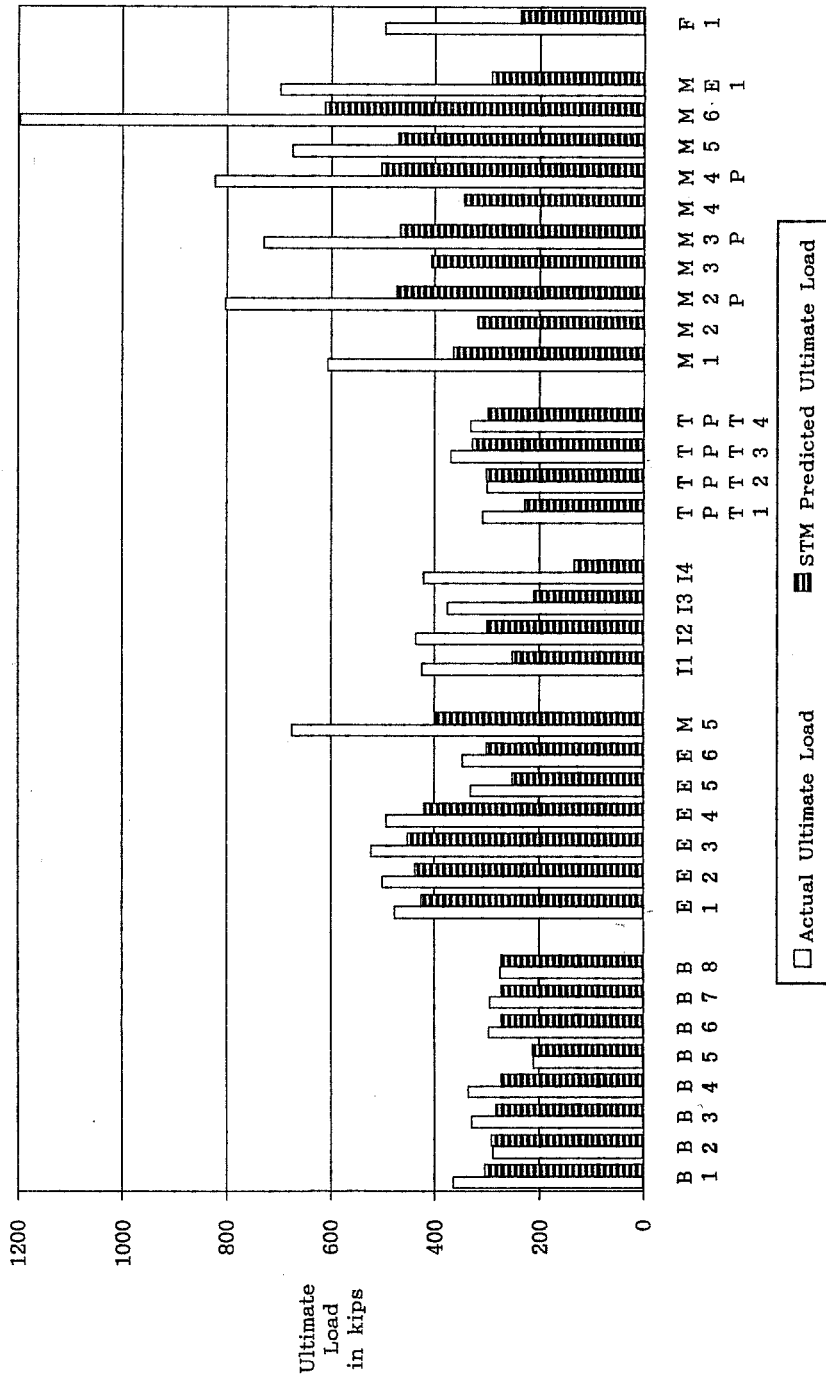
Figure 7.4   Actual Ultimate Load and Ultimate Load Predicted by the Strut-and-Tie Model for All Specimens
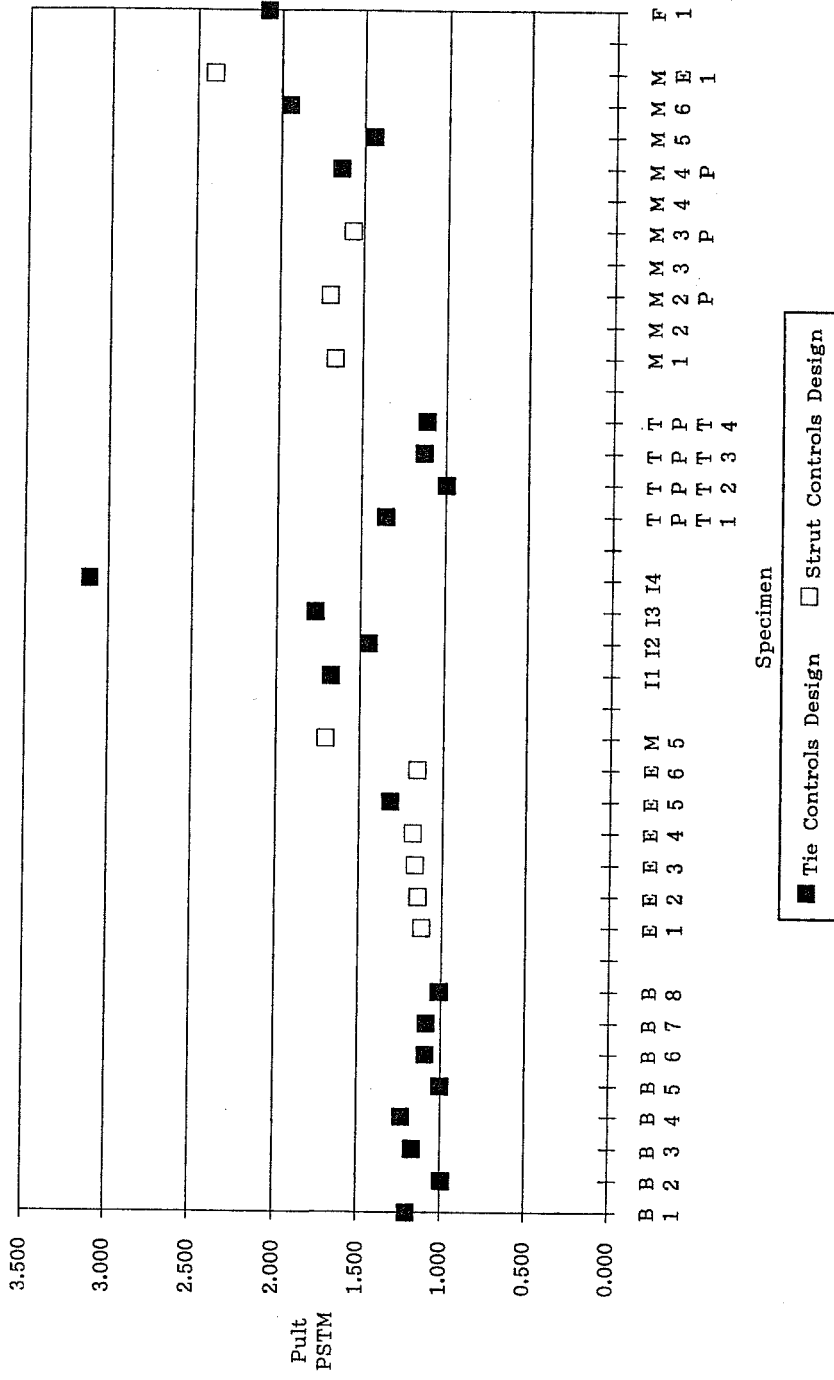
Figure 7.5   Ratio of the Actual Ultimate Load to the Ultimate Load Predicted by the Strut-and-Tie Model for All Specimens
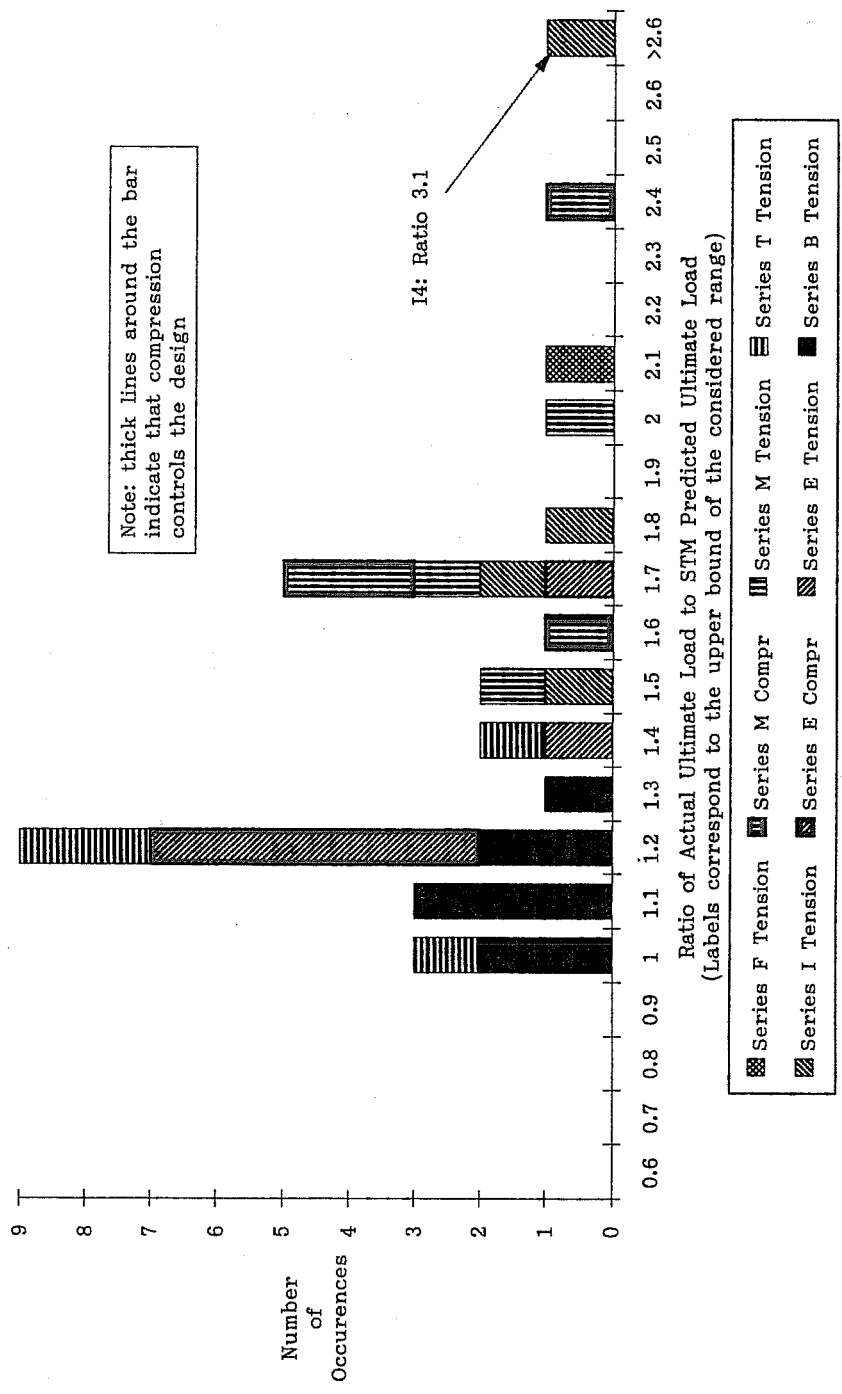
Figure 7.6   Statistical Distribution of the Ratio of the Actual Ultimate Load to the Ultimate Load Predicted by the Strut-and-Tie Model for All Specimens
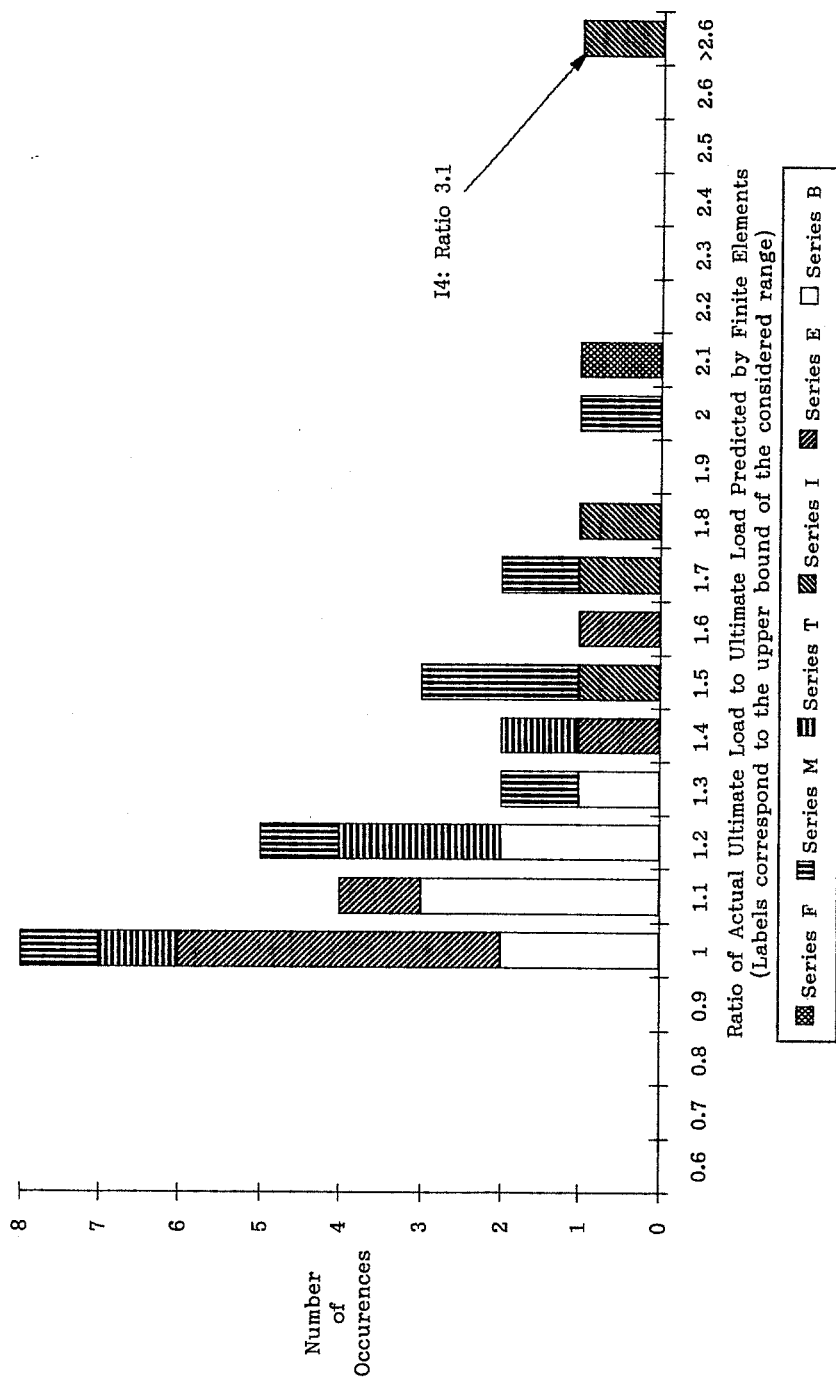
Figure 7.7 Statistical Distribution of the Ratio of the Actual Ultimate Load to the Ultimate Load Predicted Based on the Finite Element Results (compression capacity) for All Specimens
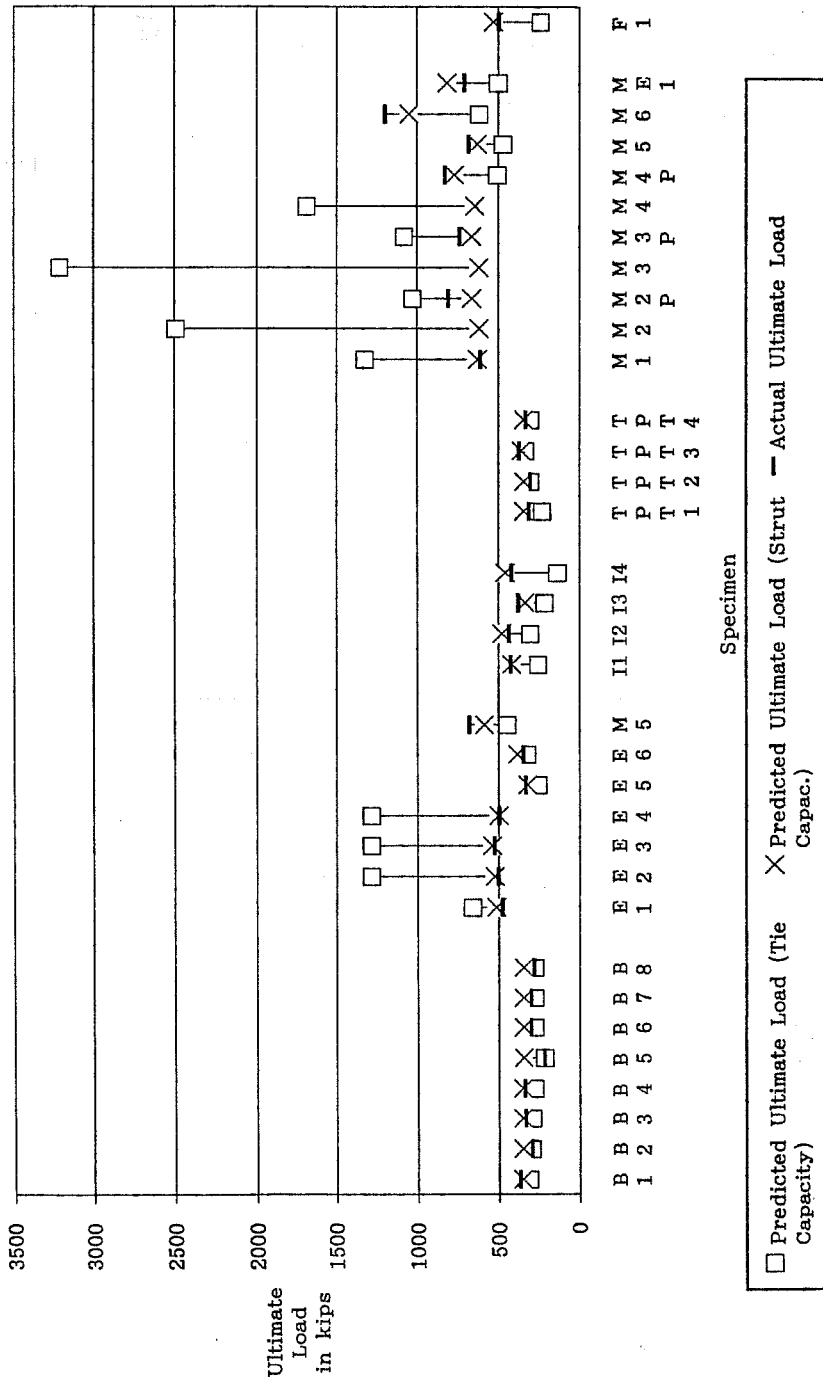
Figure 7.8   Strut-based and Tie-Based Capacity Compared with the Actual Ultimate Load for All Specimens

369
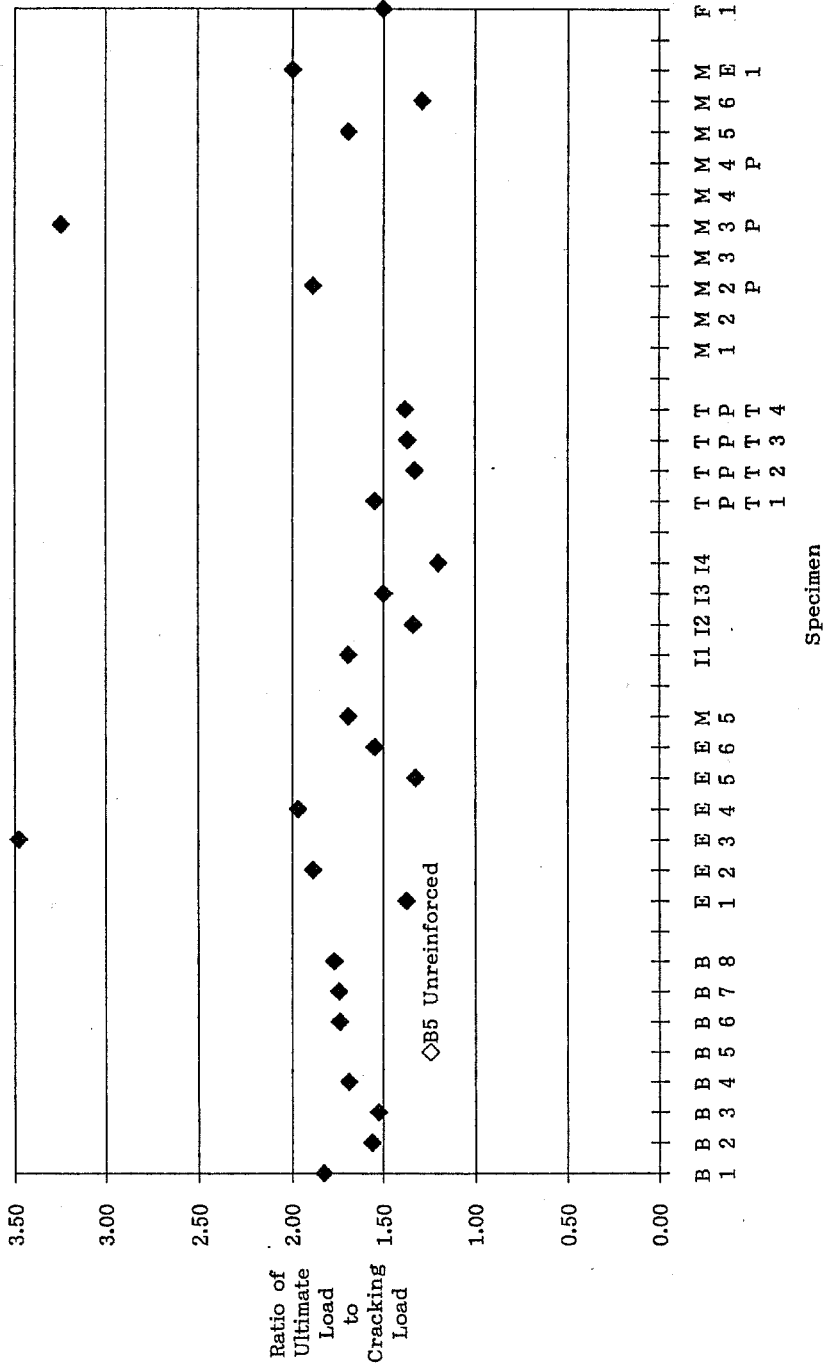
Figure 7.9   Ratio of the Actual Ultimate Load to the Cracking Load for All Specimens

7.3 Proposed AASHTO Specification for the Design of Post-Tensioned Anchorage Zones

As part of the overall UT Austin research project on anchorage zones, a specification proposal was developed for the analysis and design of anchorage zones. Part of this proposed specification deals with local zone requirements and is reported by Roberts [146]. The parts of the proposal that are directly related to the general zone and stem from this dissertation are presented and discussed in the next sections. The numbering of the sections of the specification proposal corresponds to the numbering in the current AASHTO Bridge Design Specification [7]. The text of the Specification proposal is shown with margins wider than the normal margins in the next sections. Only limited portions of the proposal concerning the design of the local zone are included in this discussion, for discussion of the geometry of the local zone. Most of the new provisions are inserted in Chapter 9 of Division I, *Design* of the AASHTO Bridge Design Specification. The procedures for the testing of anchorage zones will be inserted in Chapter 4 of Division II, *Construction*.

7.3.1 Notations

A few notations frequently occurring in the design of anchorage zones of post-tensioning tendons need to be inserted in Section 9.1.2.

9.1.2 Notations   [add to current Section 9.1.2]

f_b average concrete compressive stress under bearing plate of anchorage device

F_{pu} guaranteed ultimate strength of the prestressing tendon, $A_s * f_{su}'$

P_u factored tendon force

7.3.2 Load and Resistance Factors

9.14   Load Factors [add to current Section 9.14]

The computed strength capacity shall not be less than the largest value from load factor design in Article 3.22. For the design of anchorage zones and regions of large tendon curvature a load factor of 1.3 shall be applied to the maximum tendon jacking force.

The following strength reduction factors shall be used:

. . .

For anchorage zones $\phi = 0.75$

For effects of tendon curvature $\phi = 0.75$.

The proposed load factor of 1.3 is ordinarily applied to the maximum tendon jacking force of $0.8F_{pu}$, so that the anchorage zone is designed to resist a force larger (by about 4%) than the maximum force that the tendon can develop. This value takes into account the possibility that more strands, or strands of a larger diameter or tensile strength inadvertently could be fitted into a given anchorage device.

The ϕ-factor of 0.75 is relatively low, reflecting the importance of the anchorage zone, the desire that failure of the anchorage zone be avoided, the brittle nature of compression strut failure and the uncertainties related to the design of anchorage zones.

7.3.3 Definitions

The purpose of this section is to present in a concise manner the concepts used in the analysis and design of anchorage zones. The order of the articles in this definition section has been reorganized to allow for a more logical presentation of the

items. In the final specification, the various definitions are organized alphabetically for more convenient use.

> 9.1.3 Definitions [add to current Section 9.1.3]
>
> Anchorage Device - The hardware assembly used for transferring a post-tensioning force from the tendon wires, strands or bars to the concrete.
>
> Anchorage Zone - The portion of the structure in which the concentrated prestressing force is transferred from the anchorage device onto the concrete (Local Zone), and then distributed more widely into the structure (General Zone).
>
> End Anchorage - Length of reinforcement, or mechanical anchor, or hook, or combination thereof, beyond point of zero stress in reinforcement. [Delete remainder of current definition]
>
> Intermediate Anchorage - Anchorage not located at the end surface of a member, for tendons that do not extend over the entire length of the member; usually in the form of embedded anchors, blisters, ribs, or recess pockets.

The definition of the anchorage device is very broad, allowing for any type of device transferring a force to the concrete. End anchorages of post-tensioning cables are incorporated in the existing definition for end anchorages, while intermediate anchorages are the object of a separate definition. Only end anchorages were investigated in this study, but intermediate anchorages are currently under investigation by Wollmann [189].

General Zone - Region within which the concentrated
prestressing force spreads out to a more linear stress
distribution over the cross section of the member
(Saint Venant Region).

Local Zone - The volume of concrete surrounding and
immediately ahead of the anchorage device, subjected
to high local bearing stresses.

Because the general zone is geometrically identical to the
anchorage zone itself, and is never directly used in the design
procedure, no separate definition of the anchorage zone is needed.

7.3.4 Geometry of the Anchorage Zone

9.21 Post-tensioned Anchorage Zones

9.21.1   Geometry of the Anchorage Zone

9.21.1.1   The anchorage zone is geometrically
defined as the volume of concrete throughout which the
transverse spreading of the prestressing force occurs
from the concentrated load at the anchorage device to
a more linear stress distribution across the entire
cross section at some distance from the anchorage
device.

9.21.1.2   For anchorage zones at the end of a
member, the transverse dimensions may be taken as the
depth and width of the section, but not larger than
the longitudinal dimension of the member or segment.
The longitudinal extent of the anchorage zone in the
direction of the tendon shall be at least equal to the
larger of the transverse dimensions of the anchorage
zone and shall not be taken as more than one and one
half times that dimension.

9.21.1.3   For intermediate anchorages the anchorage zone also extends in the direction opposite to the anchorage force for a distance at least equal to the larger of the transverse dimensions of the anchorage zone.

9.21.1.4   For design purposes, the anchorage zone shall be considered as comprised of two regions; the general zone as defined in Section 9.21.2.1 and the local zone as defined in Section 9.21.2.2.

9.21.2   General Zone and Local Zone

9.21.2.1   General Zone

The general zone is identical to the overall anchorage zone and includes the local zone. Design of general zones shall meet the requirements of Sections 9.14 and 9.21.3.

9.21.2.2   Local Zone

9.21.2.2.1 The local zone is defined as the rectangular prism (or equivalent rectangular prism for circular or oval anchorages) of concrete surrounding and immediately ahead of the anchorage device and any integral confining reinforcement. The dimensions of the local zone are defined in Section 9.21.5.

9.21.2.2.2 Design of local zones shall meet the requirements of Section 9.21.5 or shall be based on the results of experimental tests required in Section 9.21.5.3 and described in Section 4.33.11 of Division II. Anchorage devices based on the acceptance test of Division II, Section 4.33.11, are referred to as special anchorage devices.

The anchorage zone is defined very broadly as the zone of transition between the concentrated introduction of forces at the anchorage device and the rest of the structure. The width of the general zone is generally the larger of the depth or the thickness of the cross section. If the length of the member is smaller than one of its transverse dimensions, the width of the general zone will be taken as the length of the member. This condition was added to take into account cases where one of the lateral dimensions of the member is essentially infinite, as in the case of transverse post-tensioning of a bridge deck. The length of the general zone is one to one and one half times the width of the general zone ahead of the anchorage device. In the case of intermediate anchorages, tensile forces occur behind the anchorage device as well. In this case, the anchorage zone extends behind the anchorage for a distance equal to the width of the general zone.

The distinction is made between the local zone and the general zone. The general zone is identical to the entire anchorage zone, including the local zone.

7.3.5 Responsibilities for the Analysis, Design and Execution of the Anchorage Zone

9.21.2.3   Responsibilities

9.21.2.3.1 The engineer of record is responsible for the overall design and approval of working drawings for the general zone, including the specific location of the tendons, anchorage devices, and general zone reinforcement as well as the specific stressing sequence.

9.21.2.3.2 If special anchorage devices are used, the anchorage device supplier is responsible for

furnishing anchorage devices which satisfy the acceptance test requirements of Section 9.21.5.3 and of Division II, Section 4.33.11. The anchorage device supplier shall provide records of the acceptance test by an accredited independent testing agency in conformance with Division II, Section 4.33.11.8 to the engineer of record and shall specify auxiliary and confining reinforcement, minimum edge distance, minimum anchor spacing, and minimum concrete strength at time of stressing required for proper performance of the local zone.

9.21.2.3.3 The responsibilities of the constructor are specified in Division II, Section 4.33.17.

As mentioned in Chapter 1, there are several unclarities in the present distribution of responsibilities for the analysis, design and execution of anchorage zones. This section of the proposed specification attributes clear responsibilities to the three parties involved. The design engineer has the specific responsibility to indicate the location of the individual tendons and anchorage devices, and not simply the desired centroid of the tendon force. Should the designer initially choose to indicate only total tendon force and eccentricity, the designer retains the responsibility of approving the specific tendon layout submitted by a post-tensioning specialist or the constructor. The designer is responsible for the proper design of general zone reinforcement required by the approved tendon layout. The responsibility for the adequacy of the anchorage device and for the proper reinforcement of the local zone is assigned to the supplier of the hardware. It is expected that anchorage device suppliers will deliver specific product information indicating the required cover, edge distance and concrete strength to the designers in the form of manuals, in

a manner similar to the current practice in European countries. In addition, it is expected that the supplier will furnish independent verification of the adequacy of those details. The constructor is responsible for the proper execution of the instructions of both the engineer of record and the anchorage device supplier. A warning is given in Section 4.33.17 about the necessity to follow the stressing sequence indicated by the engineer.

7.3.6 Methods for the Design of Anchorage Zones

9.21.3   Design of the General Zone
9.21.3.1   Design Methods
The following methods may be used for the design of general zones:

    (1) Equilibrium based plasticity models, generally termed "Strut-and-Tie Models" (see Section 9.21.4)

    (2) Elastic stress analysis (Finite Element Method or equivalent)

    (3) Approximate methods for determining the compression and tension forces given in Sections 9.21.3.4 to 9.21.3.9, where applicable.

The effects of stressing sequence and three-dimensional effects shall be considered in the design. Three dimensional effects may be approximated by considering two or more planes independently.

The list of methods that can be used to compute the various forces acting in the anchorage zone does not pretend to be exhaustive, but corresponds to the state of the art for the analysis of anchorage zones. The emphasis on the three-dimensional

nature of the spreading of forces is important, because it was observed that transverse reinforcement is often neglected by designers (for example across the web of a girder). This leads to designs that must rely completely on tensile stresses in the concrete to distribute the force transversely, which is undesirable.

9.21.3.2 Nominal Material Strengths

9.21.3.2.1 The nominal tensile strength of bonded reinforcement is limited to f_{sy} for non-prestressed reinforcement and to f_y^* for prestressed reinforcement. The nominal tensile strength of unbonded prestressed reinforcement is limited to $f_{se} + 15,000$ psi.

9.21.3.2.2 The effective nominal compressive strength of the concrete of the general zone, exclusive of confined concrete, is limited to $0.7f'_c$. The tensile strength of the concrete shall be neglected.

9.21.3.2.3 Unless otherwise specified, stress shall not be transferred to concrete until the compressive strength of the concrete as indicated by test cylinders, cured by methods identical with the curing of the member, is at least 3,500 psi.

9.21.3.3 Use of Special Anchorage Devices

Whenever special anchorage devices which do not meet the requirements of Section 9.21.5.2 are to be used, additional confinement reinforcement similar in configuration and equivalent in volumetric ratio to that used in satisfying Division II, Section 4.33.11.3 shall be placed in the portion of the general zone ahead of the local zone for that anchorage device.

The specification allows a compressive stress on the concrete of $0.7f'_c$, compared with $0.6f'_c$ used earlier in this dissertation. Considering the statistical distribution of the results presented in Fig. 7.6, this value seems a little high. Only one of the specimens of Series E would have reached this level of stresses. The other specimens of this series failed with strut stresses between 0.65 and $0.68f'_c$, which is close to the value proposed in the code. In other tests, strut stresses in excess of $0.7f'_c$ were observed, showing that this value is not highly unconservative.

It is important to notice that reliance upon tensile stresses in the concrete to resist the tensile forces in the anchorage zone is explicitly forbidden. For practical applications, this means that anchorage zone reinforcement should be provided in all three directions. Section 9.21.5.3 specifies that if a given anchorage device has been tested in a testing block involving confinement outside the local zone, a similar reinforcement must be placed in the general zone of the actual structure.

> 9.21.3.4   Compressive Stresses
> 9.21.3.4.1 The compressive stresses in the concrete ahead of the anchorage device shall be checked at a distance measured from the concrete bearing surface equal to the smaller of:
>> (1) The depth to the end of the local confinement reinforcement.
>> (2) The smaller lateral dimension of the anchorage device.
>
> If these stresses are obtained from an elastic stress analysis, local stress maxima can be averaged over an area equal to the bearing area of the anchorage

device. Section 9.21.4.3 defines the critical section if a Strut-and-Tie Model is used.

9.21.3.4.2 In the absence of a more accurate analysis, the concrete compressive stresses induced by isolated anchorage devices in rectangular cross sections can be approximated by Equation (9-32), provided the smaller edge distance of the anchor, measured parallel to the larger dimension of the cross section of the member, is at least one times the corresponding lateral dimension, a, of the anchorage device. The compressive stress induced by closely spaced anchorage devices with a center to center spacing of the anchorage devices less than two times the lateral dimension of the anchorage device are estimated by increasing the stress at the interface between the local zone and the general zone f_{ca} by the correction factor κ given in Equation (9-33). In the case of anchorages disposed in several rows, Equation (9-33) shall be applied to both transverse directions.

$$f_{ca} = \kappa \cdot 0.6P/[a\ b(1 + a(1/b-1/t))] \quad (9\text{-}32)$$
$$\kappa = 1 + [2 - (s/a)] \cdot [0.3 + n/15] \leq 2.0 \quad (9\text{-}33)$$

where

f_{ca} is the concrete compressive stress ahead of the anchorage device;

a is the lateral dimension of the anchorage device measured parallel to the larger dimension of the cross section;

b is the lateral dimension of the anchorage device measured parallel to the smaller dimension of

the cross section;

P_u is the factored tendon load;

t   is the thickness of the section;

s   is the center to center spacing of the anchorage
        devices;

κ is the correction factor for closely space
        anchorage devices, taken as 1.0 for isolated
        anchorages.

The critical section is defined at one times the lateral dimension of the anchorage device in the concrete, as proposed in the present dissertation. An allowance is made for the fact that the stresses obtained from a Finite Element Analyses are local peak values, by permitting the stresses to be averaged over an area equal to the area of the anchorage device. This specific method of averaging was not used in the present work, but a higher compressive stress in the concrete $(0.75f'_c)$ was used. The method of averaging the stresses on a certain area appears to be preferable because only one value needs thus to be prescribed for the compressive strength of the concrete.

Equation (9-32) is based on Fig. 7.10 (same as Fig. 4.37), which shows the compressive stress in a concrete strut at a depth a ahead of the anchorage device. The value $0.6P/(a \cdot b)$ was obtained by assuming that the strut angle is approximately 12 degrees. In the case of strut angles less than this value, the stress obtained from Equation (9-32) will be slightly unconservative.

Fig. 7.11 shows the ratio of the compressive capacity predicted by the approximate formula to the compressive capacity predicted by the Finite Element Solution and the strut capacity predicted by the Strut-and-Tie Model. The approximate formula gives results close to the values predicted by the Finite Element Method. The formula approximates the strut capacity predicted by

the Strut-and-Tie Model with more scatter. As shown in Fig. 7.12, the results are slightly unconservative for the cases in which compression controls the design (Specimens E1-E4 and M1).
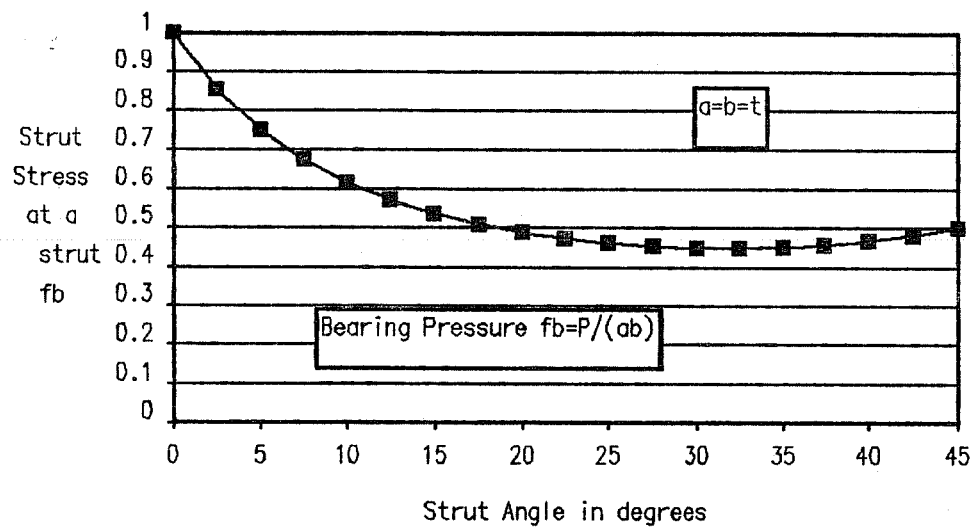
Figure 7.10   Stress in the Compression Struts at a depth a as a
Function of the Strut Angle
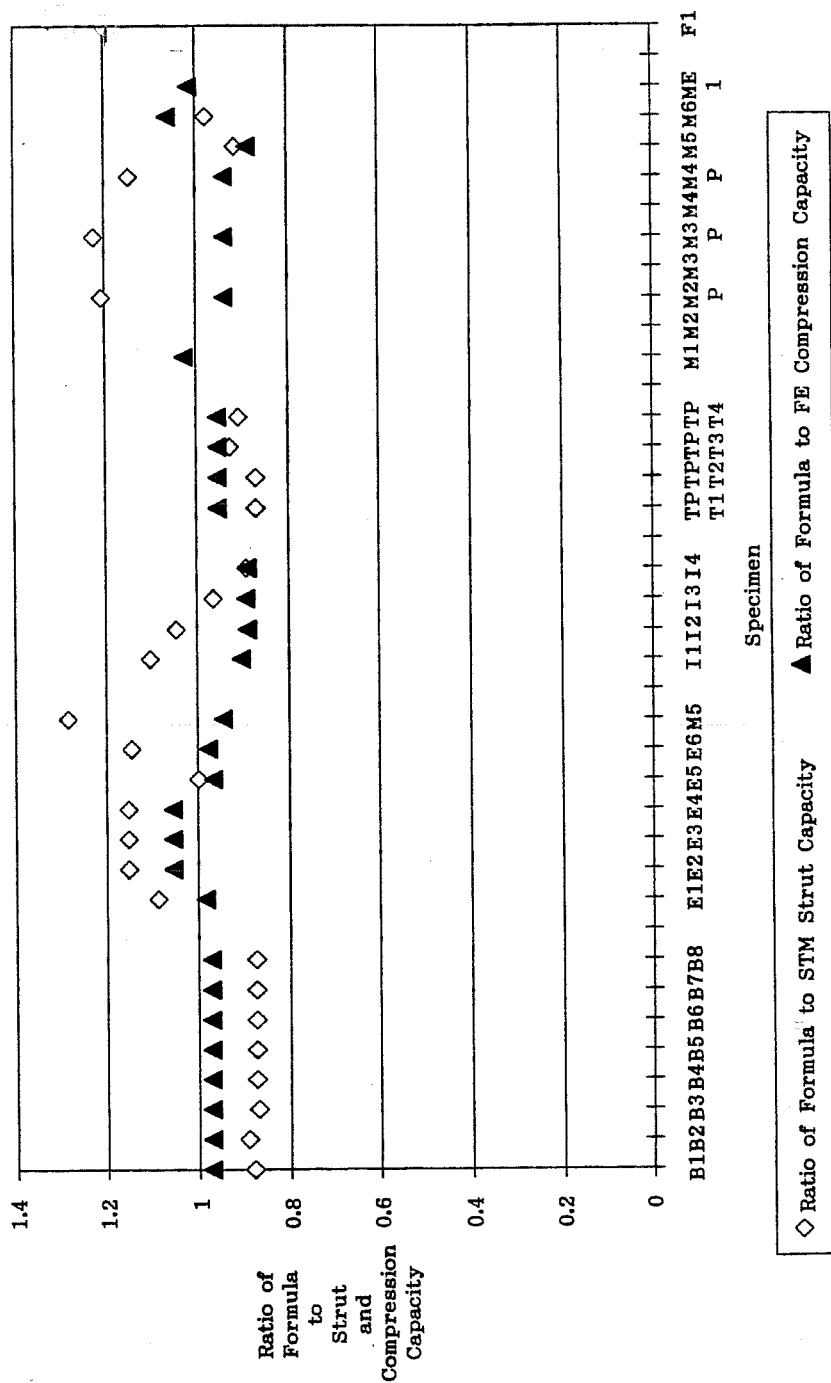
Figure 7.11 Ratio of the Compressive Capacity Predicted by the Code Formula to the Compressive Capacity Predicted by the Finite Element and the Strut Capacity Predicted by the Strut-and-Tie Model

Figure 7.12   Ratio of the Actual Ultimate Load to the Ultimate Load Predicted Using the Approximate Code Formula
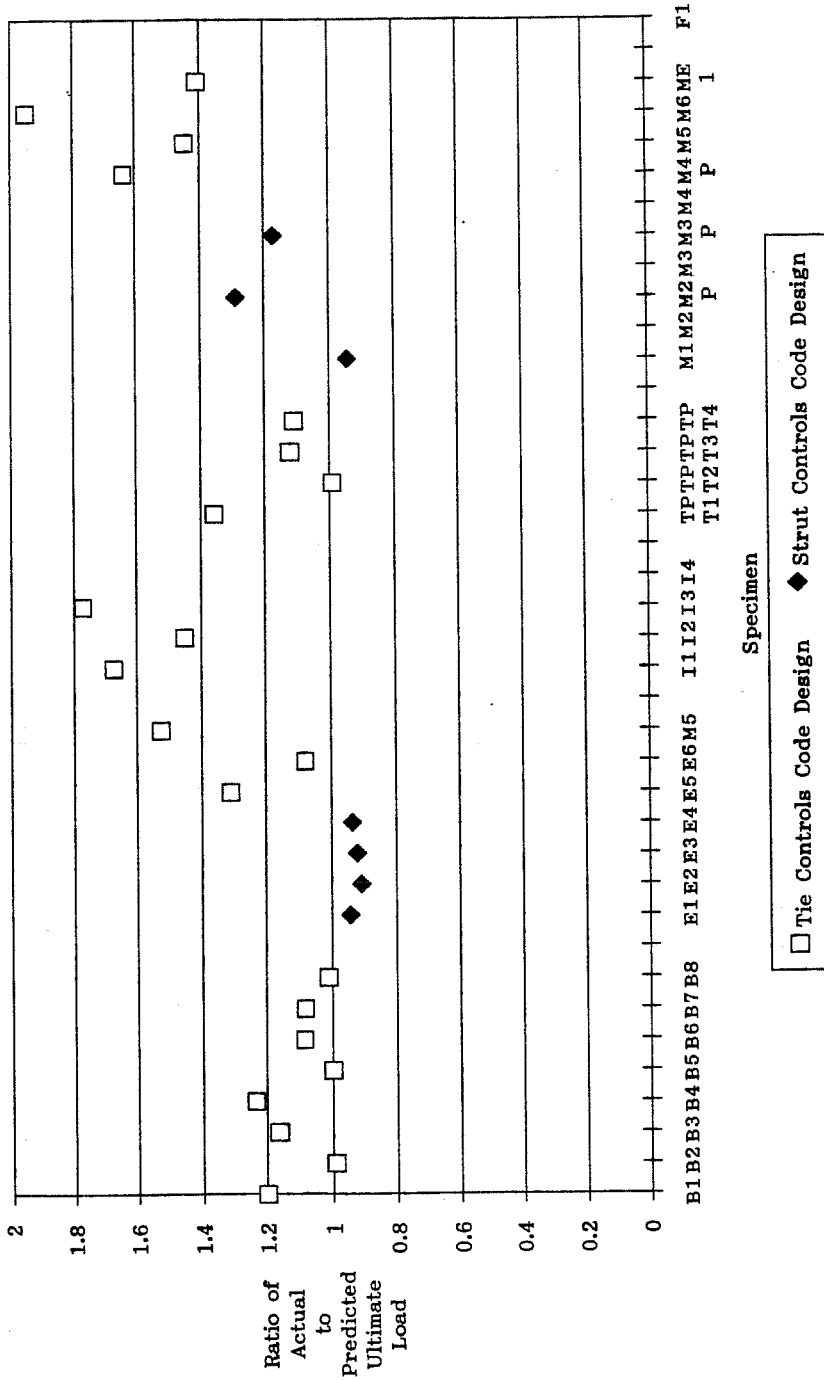
The derivation of the corrective factor 1/(1 + a(1/b - 1/t)) is shown in Fig. 7.13 (same as Fig. 4.14), and corresponds to the lateral spreading of the stresses. Recognizing that the term P/(a b) is the bearing pressure under the anchorage device and setting the strut stress to the maximum value of $0.7f'_c$, Equation (9-32) can be rewritten as Equation 7.1 which gives a limit on the bearing stress under the anchorage device.

$$f_{b,max} = 1.17\phi f'_c \cdot (1 + a \cdot (1/b - 1/t)) \quad (Eq.\ 7.1)$$

In the most unfavorable case where the transverse dimension of the anchorage device is identical to the thickness of the member, the maximum stress is $1.17\phi f'_c$, or $0.88f'_c$. Fig. 7.14

$$h_{eff} = a\left[1 + x\left(\frac{1}{a} - \frac{1}{h}\right)\right]$$

$$\sigma(x) = \frac{1}{1 + x\left(\frac{1}{a} - \frac{1}{h}\right)} f_b$$
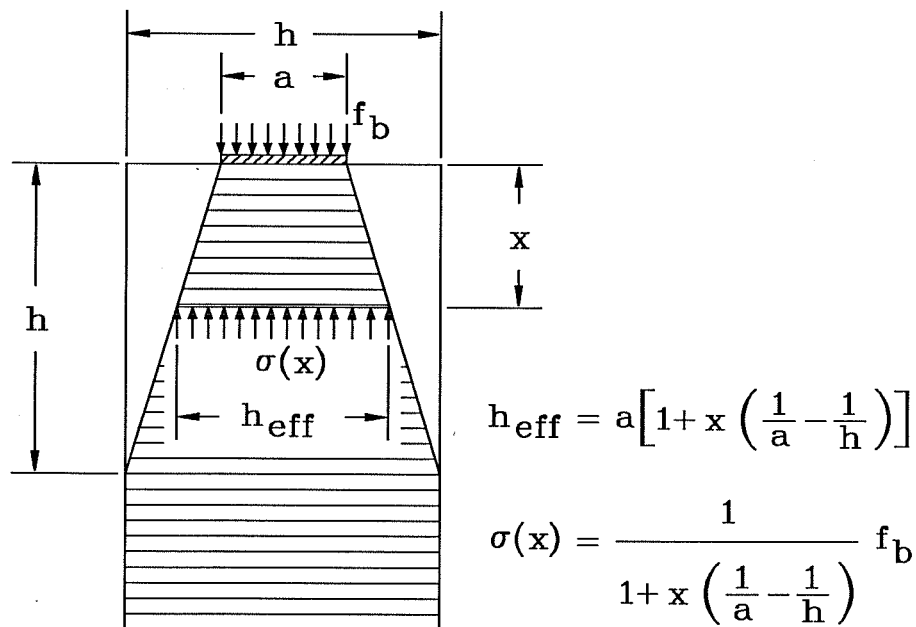
Figure 7.13   Assumed Spreading of Stresses for Approximate
Computations of Compressive Stresses

shows the value of the maximum bearing stress as a function of the available concrete cover for various typical anchorage sizes, for a square anchorage device. It should be noted that this expression was developed for thin members, in which the ratios a/t and b/t were close to unity. Therefore, the values corresponding to very large concrete covers should be used with caution.
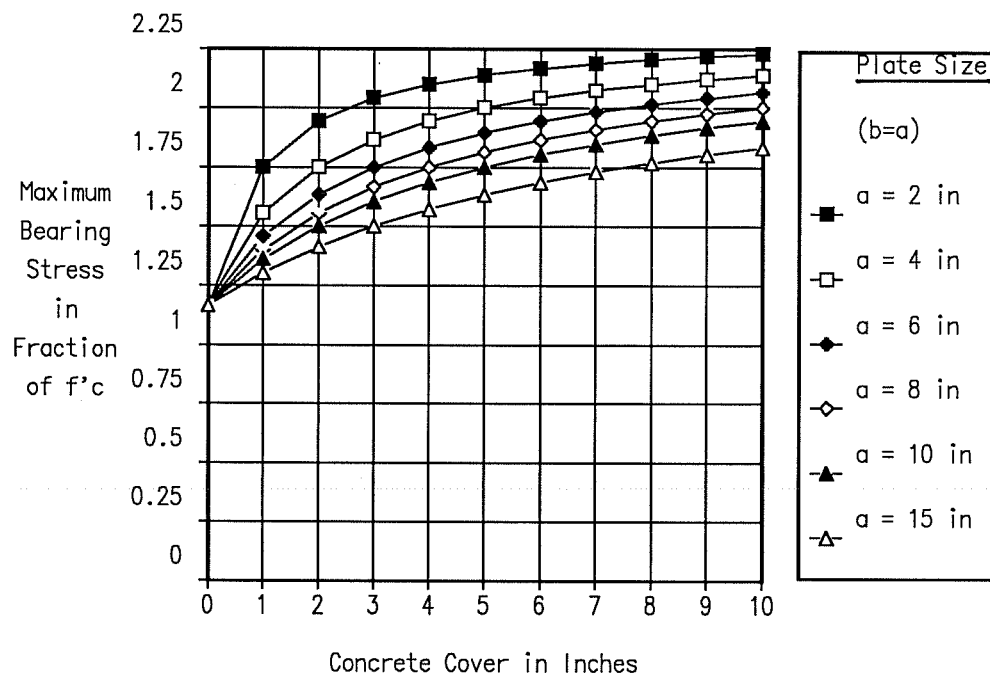
Figure 7.14   Maximum Bearing Stress Under the Anchorage Device as a Function of the Concrete Cover and the Dimension of the Anchorage Device, Based on the AASHTO Specification Proposal

The correction factor κ of Equation (9-33) was derived with the assumption that anchorage devices with a center to center spacing of more than two times the size of the anchorage device act independently from one another. Equation (9-33) is a linearization of the exact formula describing the increase in

stress caused by the reduction of the strut area in case of close spacing.

9.21.3.5 Bursting Force

9.21.3.5.1 The bursting force is the tensile force in the anchorage zone acting ahead of the anchorage device and transverse to the tendon axis. The magnitude of the bursting force, T_{burst}, and its distance from the loaded surface, d_{burst}, can be calculated using the Strut-and-Tie Model procedures of Section 9.21.4 or by integrating the tensile stresses determined from a Finite Element Analysis along the tendon path. Three-dimensional effects shall be considered for the determination of the bursting reinforcement requirements.

9.21.3.5.2 In the absence of a more accurate analysis, values for T_{burst} and d_{burst} can be estimated by Equations (9-34) and (9-35) respectively, provided that:

(1) The member has a rectangular cross section and its longitudinal extent is at least equal to the largest transverse dimension of the cross section.

(2) Only one anchorage device or one group of closely spaced anchorage devices is located in the anchorage zone considered. Anchorage devices can be considered as closely spaced if their center-to-center spacing does not exceed one and one half times the width of the anchorage device in the direction considered.

(3) The angle of inclination of the tendon as defined in Equations (9-34) and (9-35) is

between -5 degrees and +20 degrees.

In the application of Equations (9-34) and (9-35) the specified stressing sequence must be considered if more than one tendon is present.

$$T_{burst} = 0.25P_u \cdot (1-a/h) + 0.5P_u \cdot |\sin\alpha| \qquad (9\text{-}34)$$

$$d_{burst} = 0.5(h-2e) + 5e \cdot \sin\alpha \qquad (9\text{-}35)$$

where

P_u is the sum of the total factored tendon loads for the stressing arrangement considered;

a is the lateral dimension of the anchorage device or group of devices in the direction considered;

e is the eccentricity (always taken as positive) of the anchorage device or group of devices with respect to the centroid of the cross section;

h is the lateral dimension of the cross section in the direction considered;

α is the angle of inclination of the resultant of the tendon forces with respect to the centerline of the member, positive for concentric tendons or if the anchor force points toward the centroid of the section, negative if the anchor force points away from the centroid of the section.

9.21.3.5.3 Resistance to bursting forces shall be provided by non-prestressed or prestressed reinforcement, in the form of spirals, closed hoops, or well anchored transverse ties. This reinforcement is to be proportioned to resist the total factored bursting force. Arrangement and anchorage of bursting

reinforcement shall satisfy the following:
  (1) Bursting reinforcement shall extend over the full width of the member and must be anchored as close to the outer faces of the member as cover permits.
  (2) Bursting reinforcement shall be distributed ahead of the loaded surface along both sides of the tendon throughout a distance of 2.5 d_{burst} for the plane considered, but not to exceed 1.5 times the corresponding lateral dimension of the section. The centroid of the bursting reinforcement shall coincide with the distance d_{burst} used for the design.
  (3) Spacing of bursting reinforcement shall exceed neither 24 bar diameters nor 12 inches.

The guidelines for the determination of the bursting force and for the disposition of bursting reinforcement attempt to lead the designer toward reinforcement patterns which are relatively close to the elastic stress distribution. The experimental test results show that this leads to a satisfactory behavior under service loads, by limiting the extent and opening of cracks and at ultimate by limiting the required amount of redistribution of forces in the anchorage zone. The formulas to estimate the total bursting force and the location of the centroid of the tensile stresses were developed in Section 5.5.1. No investigations were made for the case of negative angles, but it is felt that a negative inclination of five degrees should not greatly modify the stress distribution and that the formula should also be adequate in this case.

9.21.3.6   Edge Tension Forces

9.21.3.6.1 Edge tension forces are tensile forces in the anchorage zone acting parallel and close to the transverse edge and longitudinal edges of the member. The transverse edge is the surface loaded by the anchors. The tensile force along the transverse edge is referred to as spalling force. The tensile force along the longitudinal edge is referred to as longitudinal edge tension force.

9.21.3.6.2 Spalling forces are induced in concentrically loaded anchorage zones, eccentrically loaded anchorage zones, and anchorage zones for multiple anchors. Longitudinal edge tension forces are induced in eccentrically loaded anchorage zones. The edge tension forces can be determined from a Finite Element Analysis, Strut-and-Tie Models, or in accordance with Section 9.21.3.6.4 and Section 9.21.3.6.5.

9.21.3.6.3 In no case shall the spalling force be taken as less than two percent of the total factored tendon force.

9.21.3.6.4 For multiple anchorages with a center-to-center spacing of less than 0.4 times the depth of the section, the spalling forces are adequately approximated by the requirement of Section 9.21.3.6.3. For larger spacings the spalling forces are similar to the tensile tie forces existing between footings in deep walls supported on individual footings and must be determined from a more accurate analysis, such as Strut-and-Tie Models or other analytical procedures.

9.21.3.6.5 If the centroid of all active tendons is located outside the kern of the section both spalling

forces and longitudinal edge tension forces are induced. The longitudinal edge tension force can be determined from an axial-flexural beam analysis at a section located at one half the depth of the section away from the loaded surface. The spalling force can be taken as equal to the longitudinal edge tension force but not less than specified in Section 9.21.3.6.3.

9.21.3.6.6 Resistance to edge tension forces shall be provided in the form of non-prestressed or prestressed reinforcement located close to the longitudinal and transverse edge of the concrete. Arrangement and anchorage of the edge tension reinforcement shall satisfy the following:

(1) Minimum spalling reinforcement satisfying Section 9.21.3.6.3 shall extend over the full width of the member.

(2) Spalling reinforcement between multiple anchorage devices shall effectively tie these anchorage devices together.

(3) Longitudinal edge tension reinforcement and spalling reinforcement for eccentric anchorage devices shall be continuous and shall extend over the full length of the anchorage zone and from the longitudinal edge to the other side of the eccentric anchorage device or group of anchorage devices.

The *Edge Tension Forces* is the name given in the proposed specification to the forces called *Spalling Forces* in this dissertation. They include spalling forces induced by the condition of compatibility and axial-flexural forces. The minimum

edge tension force for the design is two percent of the total post-tensioning force. This value is smaller than the four percent proposed by Guyon, and reflects both analytical and experimental findings which show that Guyon's values for spalling forces are high, that spalling cracks are very rarely observed in experimental tests, and that no direct evidence connects failures to spalling forces. In the case of eccentrically loaded anchorage zones, the edge tension force induced by the axial-flexural action can be simply computed by a combined axial load and flexure analysis. In the case of multiple anchorages, the tensile force between the anchors remains small as long as the distance between anchors is less than 0.4 times the lateral dimension of the member, as Fig. 6.12 shows. In cases where the tendons are located further apart, the deep wall analogy presented in Section 6.2.1 can be used to compute the multiple anchors tensile forces. It should be noted that these forces are likely to become large only in the case of two or three anchorages located as far apart from one another as possible. In all other cases, the minimum value will control.

7.3.7 Use of the Strut-and-Tie Model for the Design of Anchorage Zones

9.21.4   Application of the Strut-and-Tie Model to the Design of Anchorage Zones

9.21.4.1   General

9.21.4.1.1 The flow of forces in the anchorage zone may be approximated by a series of straight compression members (struts) and straight tension members (ties) which are connected at discrete points (nodes). Compression forces are carried by concrete compression struts, tension forces are carried by non-

prestressed or prestressed reinforcement.

9.21.4.1.2 The selected Strut-and-Tie Model shall follow a load path from the anchorages to the end of the anchorage zone. Other forces acting on the anchorage zone, such as reaction forces, tendon deviation forces, and applied loads, shall be considered in the selection of the Strut-and-Tie Model. The forces at the end of the anchorage zone can be obtained from an axial-flexural beam analysis.

9.21.4.2   Nodes

Local zone details in accordance with the provisions of Section 9.21.5 or Division II, Section 4.33.11 can be considered as properly detailed and are adequate nodes. The other nodes in the anchorage zone are adequate if the effective concrete stresses in the struts meet the requirements of Section 9.21.4.3 and the tension ties are properly detailed to fully develop the reinforcement yield strength.

9.21.4.3   Struts

9.21.4.3.1 The effective concrete compressive strength for the general zone shall usually be limited to $0.7\phi f'_{ci}$, where ϕ is 0.75, as specified in Section 9.14 and Section 9.21.3.2. In areas where the concrete may be extensively cracked at ultimate due to other load effects, or if large plastic rotations are required, the effective compressive strength shall be limited to $0.6\phi f'_{ci}$.

9.21.4.3.2 In anchorage zones the critical section for compression struts is ordinarily located at the interface with the local zone node. If special anchorage devices are used, the critical section of the strut can be taken as that section whose extension

intersects the axis of the tendon at a depth equal to the smaller of the depth of the local confinement reinforcement or the lateral dimension of the anchorage device.

9.21.4.3.3 For thin members the dimension of the strut in the direction of the thickness of the member can be approximated by assuming that the thickness of the compression strut varies linearly from the transverse lateral dimension of the anchor at the surface of the concrete to the total thickness of the section at a depth equal to the thickness of the section.

9.21.4.3.4 The compression stresses can be assumed as acting parallel to the axis of the strut and as uniformly distributed over its cross section.

9.21.4.4   Ties

9.21.4.4.1 Tension forces in the Strut-and-Tie Model are carried uniquely by non-prestressed or prestressed reinforcement. Tensile strength of the concrete shall be neglected.

9.21.4.4.2 Tension ties must be properly detailed and must extend beyond the nodes so that the full tension tie force is developed at the node. The reinforcement layout must follow closely the directions of the ties in the Strut-and-Tie Model.

The use of a Strut-and-Tie Model is permitted for the design of the anchorage zone. The stress limitations are the same as for the other analysis methods, except in cases where a large plastic redistribution of the internal forces is expected. This should be avoided in anchorage zones, because of their inherent lack of ductility. However, it is possible that, because of other load

effects, oblique cracks may be present in the anchorage zone. In this case, the use of a reduced compressive strength for the concrete in the struts is necessary. Because of the great freedom that is given to the designer in choosing the geometry of the Strut-and-Tie Model that will be used for design, it is very difficult to codify the application of the Strut-and-Tie Model to ensure that unsafe designs are impossible. Placing tight constraining limits on the use of the Strut-and-Tie Model would most likely make it useless for the many cases which cannot be anticipated by codes and regulations, but which can successfully be analyzed by the Strut-and-Tie Model. It is therefore recommended that only designers with a familiarity in the application of the Strut-and-Tie Model use it for the design of anchorage zones.

9.21.5   Design of the Local Zone

[not included]

7.3.8 Effect of the Tendon Curvature

9.29   Effects Of Tendon Curvature [new section]

9.29.1   General

Curved tendons induce deviation forces in the plane of tendon curvature. Curved post-tensioning tendons with multiple strands or wires also induce forces perpendicular to the plane of tendon curvature.

9.29.2   In-Plane Forces

9.29.2.1   In-plane forces are given by Equation (9-40).

$$F_r = P_u/R \quad (9-40)$$

where

F_r is the in-plane deviation force per length,

P_u is the total factored tendon force,

R   is the radius of curvature of the tendon at the considered location.

9.29.2.2   No reinforcement for in-plane forces is required if the radial tensile stresses induced by the in-plane forces are smaller than $2\phi f'_{ci}$ (Equation(9-41).

$$F_r \le 2\phi f'_{ci}(2 \cdot D) \quad (9\text{-}41)$$

where

F_r is the in-plane deviation force in pounds per inch;

f'_{ci} is the concrete compressive strength at the time of stressing in psi;

D   is the smaller of the tendon duct diameter or the concrete cover over the tendon duct in inches.

9.29.2.3   If the in-plane deviation forces are larger than specified in Section 9.29.2.2, fully anchored tie-back reinforcement to resist all of the in-plane deviation forces shall be provided in the form of prestressed or non-prestressed reinforcement.

9.29.3   Out-of-Plane Forces

9.29.3.1   Out-of-plane forces can be estimated using Equation (9-42):

$$F_{out} = F_r/\pi \quad (9\text{-}42)$$

9.29.3.2   No reinforcement for out-of-plane forces is required if the nominal shear stress induced across the concrete cover by these out-of-plane forces is smaller than $2\phi f'_{ci}$ (Equation (9-43)).

$$F_{out} \leq 2\phi f'_{ci}(2C) \qquad (9\text{-}43)$$

where

C is concrete cover over the tendon duct in inches;

f'_{ci} is the concrete compressive strength at the time of stressing in psi;

F_{out} is the out-of-plane force in kips.

9.29.3.3   If the nominal shear stress induced across the concrete cover is larger than $2\phi f'_{ci}$, local confining reinforcement shall be provided throughout the curved tendon segments to resist all of the out-of-plane forces, preferably in the form of spiral reinforcement.

4.33.17   Anchorage Zones [new section]

The constructor is responsible for the proper placement of all materials and correct performance of all stressing operations according to the design documents of the engineer of record and the requirements stipulated by the anchorage device supplier. Stressing operations may not be initiated before the minimum concrete strengths specified by the engineer of record and the anchorage device supplier are verified. Modifications to the local zone details verified under provisions of Section 9.21.5.3 in Division I and Section 4.33.11 in Division II shall be approved by the engineer of record.

Provisions covering transverse multi-strand effects are not a direct part of the present dissertation, but are part of the project statement of NCHRP. The formulas presented here are simplifications of the formulas originally proposed by Stone and

Breen [173] and implemented in the PTI Post-Tensioning Guide [140]. Equation (9-42) simply gives the deviation force caused by a circular cable of radius of curvature R. Assuming that the strands fill half of the tendon duct, Stone and Breen's formula can be rewritten as Equation (9-43) which gives the transverse force induced by the multi-strand effect. This force can be resisted by the concrete cover according to Equation (9-43), with a maximum shear stress of $2\sqrt{f'_{ci}}$. If the deviation force is larger than that value, confining reinforcement, preferably in the form of a spiral, shall be provided for the transverse deviation force F_{out}.

7.3.9 Example of Application of the Proposed Specification

The example chosen for this application of the approximate design method of the proposed specification is the sample problem which was submitted to the nations participating to the CEB survey [29] described in Chapter 1. Fig. 7.15 shows the geometry of the girder and the anchorage zone to be designed.

<u>Design Procedure</u>

- The individual tendon loads are 450 kN or 99 kips, for a total of 2,700 kN or 594 kips.
- The anchorage devices are assumed to be squares with a side dimension of 133 mm or 5.23 in instead of a circular plate with a diameter of 120 mm (4.7 in) as given in the CEB problem, so that the anchorage devices can be considered as closely spaced in both the main plane and across the thickness, according to Section 9.21.3.5.2, point (2). The size of the overall equivalent anchorage device is $300 + 133 = 433$ mm or 17.0 in, resulting in a ratio $a/h = 433/1,200 = 0.361$.
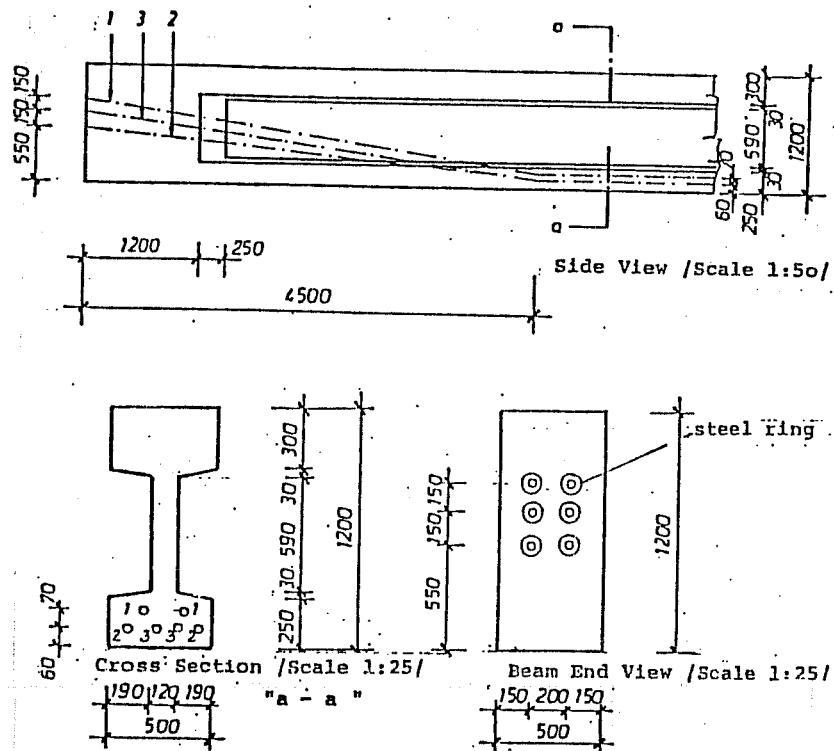
Figure 7.15   Geometry of the Sample Problem of the CEB Survey
(all dimensions in millimeters)

- The average eccentricity of the tendons is
  $700 - 1,200/2 = 100$ mm or 3.94 in, resulting in a ratio
  e/h of 0.083, well inside the kern of the rectangular
  section.

- The average angle of inclination of the tendons is
  7.7 degrees. The bursting force T_{burst} can be designed:

  $T_{burst} = 0.25 P_u \cdot (1-a/h) + 0.5 P_u \cdot |\sin\alpha|$ (9-34)

  $T_{burst} = 0.25 \cdot 2700 \cdot (1-0.361) + |0.5 \cdot 2700 \cdot \sin(7.7)| = 612$ kN
  or 134.6 kips

- The required area of reinforcement is:

  $1.3 \cdot 612/(0.75 \cdot 60/145) = 2,563$ mm^2 or 3.97 sq in

- The centroid of the reinforcement should be placed at the
  location d_{burst}:

$d_{burst} = 0.5(h-2e) + 5e \cdot \sin\alpha$ (9-35)

$d_{burst} = 0.5 \cdot (1,200-2\ 100) + 5 \cdot 100 \cdot \sin(7.7) = 567$ mm   or

22.3 in

- According to Section 9.21.3.5.3, point (2), the bursting reinforcement should be distributed over a distance of 1,420 mm or 55.9 in ahead of the anchorage device.

- Assuming that the anchorage devices are provided with a local zone confining reinforcement extending for 133 mm or 5.23 in, the increase in compressive stress caused by closely spaced anchorage devices in both directions is:

$\kappa = 1 + [2 - s/a] \cdot [0.3 + n/15] \leq 2.0$ (9-33)

$\kappa_{main\ plane} = 1 + [2 - (150/133))] \cdot [0.3 + (3/15)] = 1.44$

$\kappa_{transverse} = 1 + [2 - (200/133)] \cdot [0.3 + (2/15)] = 1.22$

$\kappa_{tot} = 1.44 \cdot 1.22 = 1.75$

- The compressive stress in the concrete at the interface between the local zone and the general zone is:

$f_{ca} = \kappa \cdot 0.6P/[a \cdot b(1 + a(1/b-1/t))]$ (9-32)

$f_{ca} = 1.75 \cdot 0.6 \cdot 1.3 \cdot 450,000/[133 \cdot 133 \cdot (1+133 \cdot (1/133-1/250))] = 23.7$ MPa or 3,355 psi.

- The concrete quality is C30, with a cube compressive strength of 30 MPa, or a cylinder compressive strength of 3,625 psi. In this case, the stresses in the concrete at the interface between the local zone and the general zone are 3,355 psi or $0.92f'_c$, which is more than the allowable value of $0.7 \cdot 0.75 \cdot 3,625 = 1,903$ psi or $0.52f'_c$. The minimum concrete strength for this application should be $0.92/0.52 \cdot 3625 = 6,500$ psi.

- Spalling reinforcement must be provided for the minimum value of 2% of the total force, of $0.02 \cdot 450 \cdot 6 = 54$ kN or 11.9 kips. The required cross sectional area is $54/(0.75 \cdot 60/145) = 174$ mm^2 or   0.20 sq in. Spalling reinforcement will be provided in both the main plane and

the transverse direction.

- The transverse bursting force is:

$T_{burst} = 0.25P_u \cdot (1-a/h) + 0.5P_u \cdot |\sin\alpha|$ (9-34)

$T_{burst, trans} = 0.25 \cdot 2700 \ (1-333/500) = 225$ kN or 49.5 kips

- The required area of reinforcement is:

$1.3 \ 225/(0.75 \cdot 60/145) = 942$ mm^2 or 1.43 sq in

- The location of the centroid for the transverse reinforcement is:

$d_{burst} = 0.5(h-2e) + 5e \cdot \sin\alpha$ (9-35)

$d_{burst, trans} = 0.5 \cdot (500) = 250$ mm or 10 in

- The length over which the transverse reinforcement needs to be distributed is 625 mm or 25 inches.
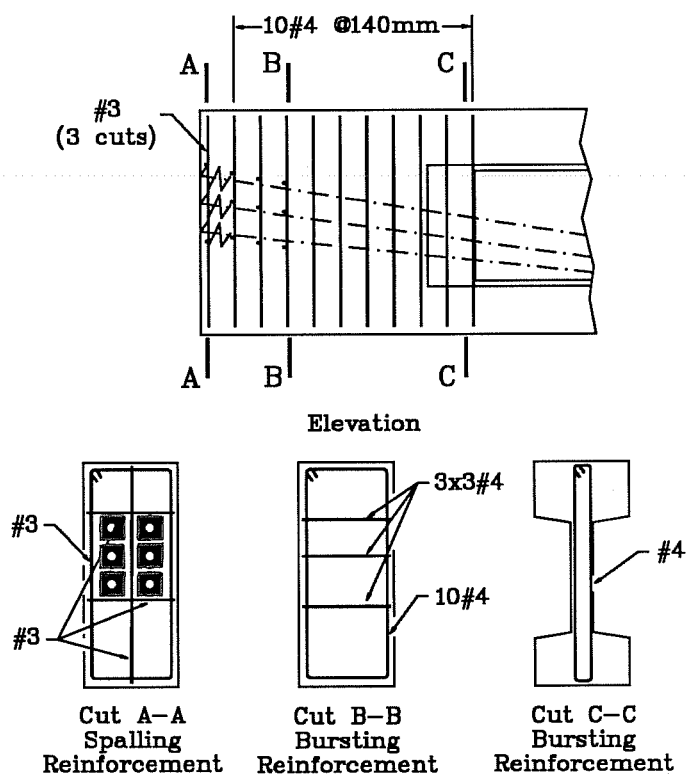
Figure 7.16   Final Reinforcement for the Example Problem of CEB
Survey According to Specification Proposal

Fig. 7.16 shows a possible reinforcement layout for the anchorage zone of the example problem. Fig. 7.17 shows the solution to the CEB problem using a Strut-and-Tie Model. The centroid of the reinforcement is slightly further from the anchorage device than given by the approximate formula, leading to a smaller amount of reinforcement (2220 mm^2). The compressive
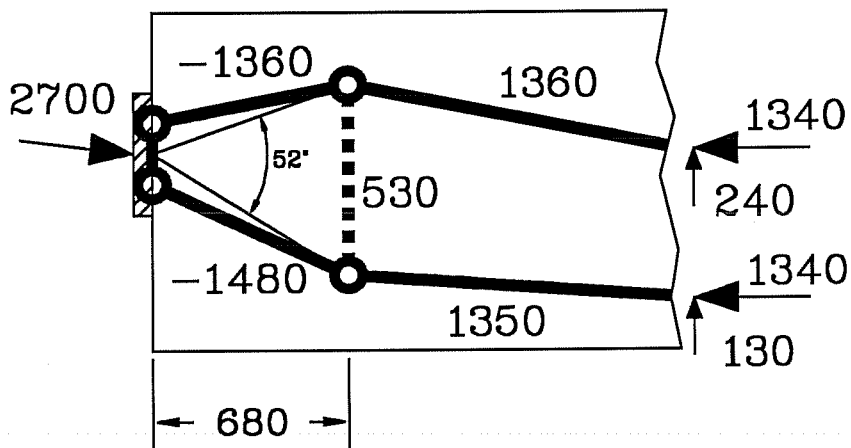
a) Strut−and−Tie Model
with Member Forces
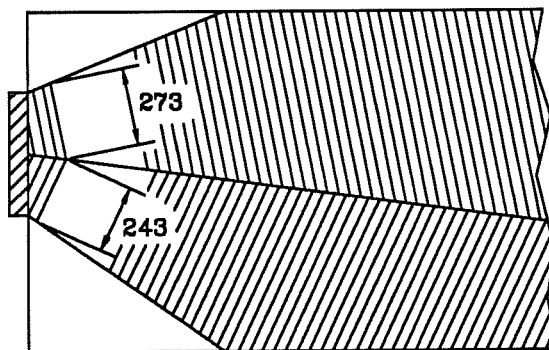
b) Check of the Critical Section
of the Compression Struts

Figure 7.17   Solution of the CEB Problem Using the Strut-and-Tie Model

stress at the interface between the local zone and the lower strut, which is the most critical, is

$$f_{ca} = 1.3 \cdot (1480 \cdot 220)/[(243/25.4) \cdot (328/25.4)] = 3,425 \text{ psi}$$
$$>1,903 \text{ psi}$$

As in the case of the approximate formula, the concrete strength given in the problem is not sufficient for the application of the post-tensioning load. The minimum concrete strength required for this application is $(3,425/1,903) \cdot 3,625 = 6,500$ psi.

The magnitude of the transverse force, the amount of reinforcement and the extent over which the reinforcement must be distributed are greater than the largest values obtained from the countries participating in the CEB survey on anchorage zones [29]. In the survey, the largest predicted tension force was 450 kN, with a corresponding reinforcement of 2000 mm^2. For more details on the CEB survey, see Section 2.8. Fig. 7.18 shows the transverse force obtained as answer to the CEB survey, compared with the proposed specification. The results are larger than any of the answers obtained by the CEB, but relatively close to the largest value, which probably did not consider the effect of the inclination of the tendons. It is significant that the concrete strength specified in the CEB example problem is clearly insufficient to prevent a failure in compression at the interface between the local zone and the general zone, which is predicted by both the Strut-and-Tie Model an the approximate code formula. This is caused by the very small center to center spacing of the anchorage devices in the main plane of the member. Manufacturer's specifications indicate that a center to center spacing of four third the plate size are generally recommanded in practice. If the center to center spacing is increased from 150 mm to 180 mm, the

compressive stress at the interface between the local zone and the general zone becomes 2,740 psi, or 0.76f'c. The minimum concrete stength for that layout of the anchorage devices is then 5,300 psi, which is a more reasonable value than the 6,500 psi obtained previously.
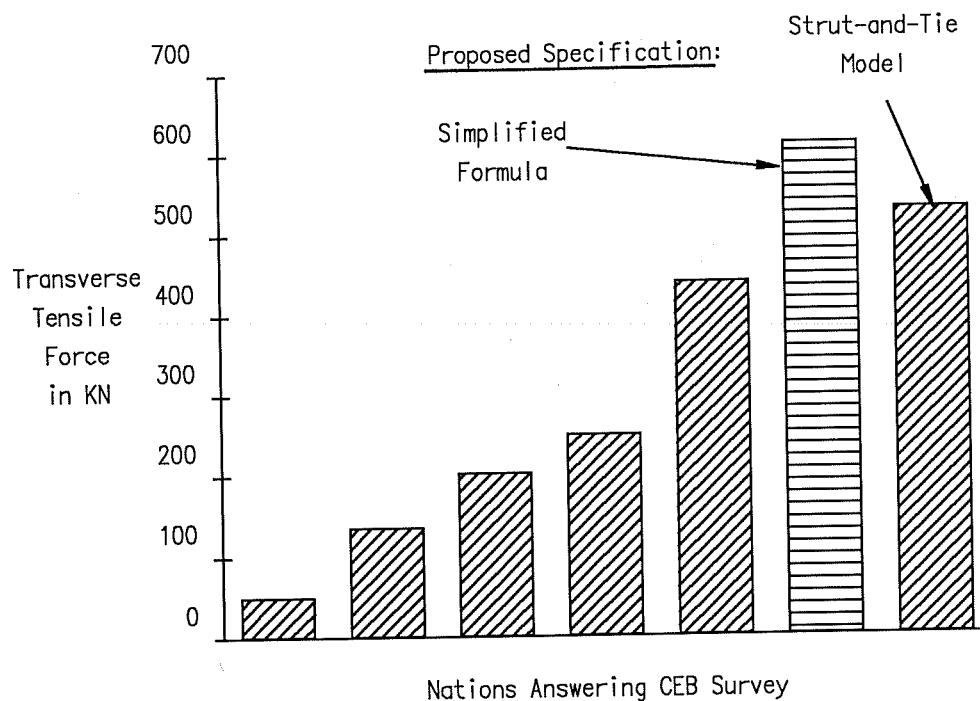
Figure 7.18 Results of the CEB Survey on Anchorage Zones Compared with the Results of the Proposed Specification

Chapter 8: Conclusions

8.1   Introduction

The original research statement by NCHRP which initiated the overall UT Austin research program on anchorage zones stated that:

> "*The AASHTO Standard Specification for Highway Bridges does not provide adequate guidance for designing reinforcement for tendon anchorage zones of post-tensioned concrete girders and slabs. Current designs can result in excessive cracking or congested reinforcing details. The wide variation of design practices currently suggests the need for research in this area. [...]*
>
> "*Design Criteria are needed for reinforcement details for inclined, sharply curved and highly eccentric tendons, and for intermediate anchorages.*"

At the conclusion of the first phase of the research project, and considering the concepts presented in the present dissertation, it is felt that decisive progress has been made toward ensuring more reliability, more consistency and more clarity in the design process of anchorage zones of post-tensioning tendons. The concept of the local zone and the general zone subdivision of the anchorage zone allows for more flexibility in the choice of the post-tensioning hardware, and at the same time ensures that the selection of a specific, satisfactory anchorage device does not have a major influence on the design of

405

the rest of the structure. The distinction between three possible modes of failure allows a better understanding of the behavior of the anchorage zone. It emphasizes the need to systematically combine adequate uniaxial compressive strength of the concrete, adequate confining reinforcement in the local zone and adequate reinforcement in the general zone in the design process. The elaboration by Roberts [144] of a testing procedure for local anchorage zones is an important step towards effective standardization of the performance of the anchorage devices. The present study, by focusing on failures occurring in the general zone, shows that the amount of reinforcement provided is not the only parameter to consider when computing the ultimate capacity of an anchorage zone. The hypotheses for the distinction between the various modes of failure were verified by comparing the theoretical predictions with the test results of Sanders [151] and Stone [167]. A good agreement was found between theoretical and experimental results. According to the model used in this dissertation, several of Stone's experimental test specimens failed in the local zone or at the interface between the local zone and the general zone, without mobilizing the bursting reinforcement provided in the general zone.

8.2 Analysis of Anchorage Zones Using the Finite Element Method

The results of linear Finite Element Analyses of anchorage zones can be used in various ways for the design of anchorage zones. Principal stress vector plots can used in constructing and evaluating the Strut-and-Tie Models discussed in the next section. The distribution of the elastic tensile stresses can be used to estimate the cracking load for the experimental specimens. The distribution of compressive stresses can be used to estimate the

maximum compressive strength of the anchorage zones. Because of the great flexibility of the Finite Element Method, a large number of parametric studies can be performed, exploring more general configurations which could not be experimentally tested within the limits of the current research project.

Estimations of the cracking load based on the maximum tensile stress in the bursting region, taking into account the presence of the tendon duct and using the tensile strength of the concrete as measured from split cylinder tests predict cracking loads slightly greater than the actual cracking load. In general, the results are within a reasonable range considering the uncertainties involved with concrete in tension. Some limited amount of cracking should be expected in most anchorage zones located in thin members. If the anchorage zone is otherwise properly designed, this cracking should not be a source of concern as far as the strength of the structure is concerned.

Using the results of the Finite Element Analyses, the maximum compressive force that can be applied on the anchorage zone can be estimated. Because of the presence of confining reinforcement in the local zone, the bearing stresses under the anchorage device can be in excess of the uniaxial compressive strength f'_c of the concrete. The concrete of the general zone, on the other hand, is unconfined and can resist only compressive stresses in the vicinity of $0.75f'_c$. The critical section for the compressive stresses is therefore generally located at the interface between confined and unconfined concrete. Because the length of the confining reinforcement is usually about equal to the lateral dimension of the anchorage device, it was found, that by allowing the compressive stress in the concrete at a distance equal to the lateral dimension of the anchorage device ahead of the anchorage to be $0.75f'_c$, a reasonable prediction of the ultimate compressive strength of the anchorage zones was obtained,

assuming that failure does not occur at a lower load for another reason such as local zone failure or tension tie failure.

An extensive series of parametric studies on the influence of the various geometric parameters of the anchorage zone confirmed the results of Guyon [74], and investigated the influence of additional parameters like the inclination and curvature of the tendon.

A practical design formula for the tensile bursting force T_{burst}, incorporating the influence of relative size of the anchorage device, the eccentricity of the tendon and the inclination of the tendon was developed, and is given in Equation 8.1.

$$T_{burst} = 0.25P(1-a/h) + 0.5 \cdot P \cdot \sin(\alpha) \quad \text{(Eq. 8.1)}$$

A corresponding equation giving the location of the centroid of the tensile stresses, d_{centr}, was also developed and is given in Equation 8.2. The quantities involved in the two equations are given after Eq. 8.2.

$$d_{centr} = 0.5 \cdot (1-2e/h) + 5 \cdot e \cdot \sin(\alpha) \quad \text{(Eq. 8.2)}$$

Where

P   is the total factored tendon load for the stressing arrangement considered,

a   is the lateral dimension of the anchorage device or group of devices in the direction considered,

e   is the eccentricity (always taken as positive) of the anchorage device or group of devices,

h   is the transverse dimension of the cross section in the direction considered,

α is the angle of inclination of the resultant of the tendon or tendons with respect to the centerline of the member,

positive for concentric tendons or if the anchor force points toward the centerline of the member, negative if the anchor force points away from the centroid of the section.

These two equations can be used for a very wide variety of applications, with angles of inclinations varying from -5 degrees (extrapolated) to 20 degrees. In the proposed specification for the AASHTO Bridge Design Specification, the use of this formula has also been proposed for closely spaced groups of tendons, making its range of applicability even wider.

Spalling stresses can be caused by compatibility in the case of concentric or slightly eccentric tendons or by flexural action in the case of eccentric tendons or between multiple anchorages. No anchorage zone failure was directly related to the spalling stresses or forces. In fact, spalling cracks were very rarely observed in concentric specimens and a tendency for redistribution of internal forces was observed in eccentric specimens.

8.3 Analysis of Anchorage Zones Using the Strut-and-Tie Model

One important concept at the beginning of the research project was the idea of trying to apply the Strut-and-Tie Model to the analysis and design of anchorage zones. In recent times, a large emphasis has been placed on the use of the Strut-and-Tie Models for the design of discontinuity regions in reinforced and prestressed concrete structures [20, 156]. However, little research had been done so far on the applicability of the Strut-and-Tie Model to regions like anchorage zones where, because of local confinement, the stresses in the concrete can exceed the uniaxial compressive strength and very strong gradients of stresses are present. The distinction made between failure of the

local zone and failure of the general zone made possible the application of normal Strut-and-Tie Model techniques to the general zone, excluding the local zone from the Strut-and-Tie Model and treating it as a separate problem.

While most applications of the Strut-and-Tie Model to design practice try to prevent a failure of the concrete in compression, this is not easily possible for anchorage zones, because the tensile strength of the concrete is much more significant than for cases involving bending or shear. In most cases, the ultimate load of the anchorage zone test specimens was less than two times the cracking load, which is a much smaller ratio than observed in bending for example. Only a few cracks typically develop before failure of the anchorage zone, leaving a large part of the concrete uncracked and able to resist substantial tensile forces. The presence of an important component of tensile stresses in the concrete makes the failure of an anchorage zone generally very brittle, and the ductility of an anchorage zone is relatively small. However, a series of tests showed that the distribution of the tensile bursting reinforcement in the bursting region can diverge from the elastic stress distribution without substantial deterioration of the performance. For design, it appears desirable that the Strut-and-Tie Models of anchorage zones be reasonably close to the elastic stress distribution. To that effect, the principal stress vectors and principal stress trajectories obtained from a linear elastic Finite Element Analysis are helpful.

Comparisons between the results of parametric studies using the Strut-and-Tie Model with parallel parametric studies using the Finite Element Method show that the results of both methods can give very close agreement. The main geometric parameter needed for the development of a Strut-and-Tie Model is the location of the centroid of the tensile bursting force. This location can be

determined by setting the diffusion angle of the compression forces to 26 degrees on either side of the tendon path, measured from the center of the anchorage device, or to a total of 52 degrees for cases with inclined or curved tendons. This is a very advantageous property, because, although Finite Element programs tend to be more and more available to the designer, it does not appear desirable nor likely that a Finite Element Analysis will be performed for each and every anchorage zone. The results of the Strut-and-Tie Model are sufficient to safely design the reinforcement. The stresses in the concrete struts at the interface between the local zone and the general zone must be considered and can often control the design. The accuracy of the prediction of the compressive strength based on the Strut-and-Tie Model decreases with increasing complexity of the specimens. For very complex configurations, it appears desirable to use the results of a numerical analysis.

8.3   Proposed Specification for AASHTO

Based on the results of the present analytical study and on the experimental results of Sanders [151] and Roberts [144], a proposal for an expanded section of the AASHTO Bridge Design Specification was made. The new sections clearly delineate the responsibilities of the parties involved in the analysis and design of anchorage zones, by attributing the responsibility for the performance of the local zone to the anchorage device supplier, the responsibility for the overall design and specifically the design of the general zone to the engineer of record, and the responsibility for the proper execution to the constructor. The forces that need to be considered for the design of anchorage zones are defined and the various possible modes of failure of the anchorage zone are described. Methods suitable for

the analysis and design of anchorage zones are presented, and approximate formulas are given for the design of anchorage zones located at the end of girders. A load factor of 1.3 on the maximum applied tendon force (generally $0.8F_{pu}$) is proposed, in conjunction with a ϕ-factor of 0.75. The maximum stress in the reinforcing steel can be assumed as the yield value for bonded reinforcement. The maximum compressive stress in the concrete can be assumed as $0.7f'_c$ for most cases. The tensile strength of the concrete is neglected. The use of Strut-and-Tie Models is allowed by the proposed code specifications, and guidelines are given for the design based on this analysis method.

8.4   Possible Areas of Future Research

The results of the present study constitute an important step in analytical and experimental investigations of anchorage zones of post-tensioning tendons. A rational model of the behavior of anchorage zones was proposed, and it can be expanded to configurations that are not included in the present study. Additional aspects are presently under investigation as part of the second phase of the overall UT Austin project on anchorage zones. These additional configurations include anchorage devices located in blisters, ribs and diaphragms, as well as slab anchors. The effect of a transverse reaction will also be investigated.

Further experimental research should include a more comprehensive treatment of the state of stresses at the interface between the local zone and the general zone, including the possible use of additional confining reinforcement in the general zone. Long term testing, as well as observation of actual structures should assess the dependability of concrete tensile stresses, possibly leading to the introduction of a contribution of concrete in tension in the design equation.

Additional analytical research should include the use of non-linear models for the behavior of the concrete. An analytical study of the influence of the tensile strength of the concrete on the behavior is highly desirable to allow comparison with experimental test results. Although it has mainly been used for stress fields with small gradients, the compression field theory of Collins et al. [36] offers promising possibilities for the modelling of concrete after cracking, including nonlinearities in tension as well as in compression.

The purpose of this dissertation was not to develop a perfect design equation that would fit every specific case, but rather to develop consistent and safe design methodologies that can be used in the absence of other information. The reader is reminded of the results of the CEB survey mentioned in Chapter 2, where the designs of anchorage zones according to the national codes of six developed countries exhibited a scatter of almost 1,000%. In this context, the economy of a given anchorage zone detail is secondary to its safety. The design procedures developed in the present dissertation should permit reduction of the scatter in the designs to maybe 10% when the simplified design formulas are applicable and maybe 20% when Strut-and-Tie Models need to be developed, which is a substantial improvement. If the proposed design guidelines were used to design experimental test specimens, it is expected that the scatter of the actual ultimate load of the specimen would be larger, maybe in excess of 25%. One specific area of research that will be generated by the implementation of the proposed design guidelines is the many questions that will unavoidably be raised by special details which are not covered in the present study. It is expected that Highway Departments or other organizations will desire that special anchorage detailing procedures be closely investigated in order to ensure consistent and economical designs.

Bibliography

[1]   Abeles, P.W., Bardan-Roy, B.K; "Prestressed Concrete Designer's Handbook, Chapter 10, End Blocks"; ViewPoint Publications, 3rd ed.; 1981; pp 253-279.

[2]   ACI 443 Comm; "Prestressed Concrete Bridge Design"; ACI Journal; Vol 73, No 11; November; 1976; pp 597-612.

[3]   ACI-American Society of Civil Engineers (ASCE) Comm. 423; "Recommendations for Concrete Members Prestressed with Unbonded Tendons"; Concrete International; Vol 5, No 7; July; 1983; pp 61-76.

[4]   Adeghe, L.N.; "A Finite Element Model for Studying Reinforced Concrete Detailing Problems"; Department of Civil Engineering, University of Toronto; Publ. No 86-12; October; 1986; pp 66-74.

[5]   Aldersebaes, J.K. and Wiedner, K.; "Containment Structure for Trojan Nuclear Plant"; ASCE Power Division Journal; Vol 97, No PO2 paper 7957; March; 1971; pp 351-366.

[6]   Almasi, J.; "Wieviel Spaltzugbewehrung ist nötig?"; (Publication Unknown).

[7]   American Association of State Highway Transportation Officials (AASHTO); "Standard Specification for Highway Bridges 13th edition"; 1983.

[8]   American Concrete Institute (ACI) 318-83; "Building Code Requirements for Reinforced Concrete"; American Concrete Institute; 1983.

[9]   Anderson, R.; "Behavior of CTT-Nodes in Reinforced Concrete Strut-and-Tie Models"; Master's Thesis, UT Austin; 1988.

[10] Ang, A.H.S, editor; "Structural Design, Analysis and Testing"; ASCE Proceedings of 1989 San Francisco Structures Congress; May; 1989.

[11] Arthur, P.D., Ganguli, S.; "Tests on End-Zone Stresses in Pretensioned Concrete 'I' Beams"; Magazine of Concrete Research; Vol 17, No 51; June; 1965; pp 85-100.

[12] ASCE; "Finite Element Analysis of Reinforced Concrete State of the Art Report"; 1982.

[13] ASCE-WRC; "Plastic Design in Steel"; ASCE Manuals and Reports on Engineering Practice; No. 41; 1971.

[14] Austrian Code for Prestressed Concrete, Post-Tensioning Systems; "ONORM B 4259"; December; 1979; German.

[15] Austrian Code for Prestressed Concrete-Road Bridges, Design and Construction; "ONORM B 4252"; December; 1975; German.

[16] Austrian Code for Reinforced Concrete Structures, Rules for Design and Construction I; "ONORM B 4200 Teil 8"; August; 1979; German.

[17] Bachmann, H.; "Stahlbeton II"; Institut für Baustatik und Konstruktion, Zürich; 1985; German.

[18] Ban, S., Mugurama, H., Ogaki, Z.; "Anchorage Zone Stress Distributions in Post-Tensioned Concrete Members"; Proceedings of World Conference on Prestressed Concrete California, San Francisco, CA; 1957; pp 16:1-14.

[19] Benabdallah, S., Ramirez, J.A., Lee, R.H.; "Computer Graphics in Truss-Model Design Approach"; ASCE Journal of Computing in Civil Engineering; Vol. 3, No. 3; July; 1989; pp 285-301.

[20] Bergmeister, K., Breen, J.E., Jirsa, J.O., Kreger, M.E.; "Detailing for Structural Concrete"; Center for Transportation Research, UT Austin; Report 1127-3F; November; 1989.

[21] Bleich, F.; "Der gerade Stab mit Rechteckquerschnitt als ebenes Problem"; Der Bauingenieur (Berlin); No 9 and 10; 1923; pp 225-259 and 304-307.

[22]   Boonman, C.L.F.; "Design of Intermediate Anchorages in Unbounded Tendons"; Magazine of Concrete Research; Vol 32, No 6; June; 1980; pp 344-351.

[23]   Bouadi, A.; "Behavior of CTT-Nodes in Structural Concrete for the Strut-and-Tie Model; Master's Thesis in Preparation, UT Austin; 1990.

[24]   Breen, J., Fenves, G., Sanders, D., Burdet, O.; "Anchorage Zone reinforcement for Post-Tensioned Concrete Girders"; University of Texas at Austin, Dept of Civil Engineering; August; 1987.

[25]   Breen, J.E., Cooper, R.L., Gallaway, T.M.; "Minimizing Construction Problems in Segmentally Precast Box Girder Bridges"; Research Report No. 121-6F Center for Highway Research, The University of Texas at Austin; August; 1975.

[26]   Burdet, O.L.; "Computation and Display of Principal Stresses Using PRIN6"; Unpublished User's Manual, UT Austin; 1990.

[27]   Burgess, J.A., Breen, J.E., Poston, R.W.; "Anchorage Zone Cracking of Post-Tensioned Bridge Decks with Closely-Spaced Anchors"; Masters Thesis, UT Austin.

[28]   Burns, N. and Hemakom, R.; "Test of Post-Tensioned Flat Plate with Banded Tendons"; ASCE Structural Division Journal; Vol 111, No 9; September; 1985; pp 1899-1915.

[29]   CEB; "Anchorage Zones of Prestressed Concrete Members"; No 181; April; 1987.

[30]   CEB-FIP (Comité Euro-International du Béton and Fédération Internationale de la Précontrainte); "Model Code for Concrete Structures"; 1990 (proposed); English Translation.

[31]   Cedolin, L., Dei Poli, S.; "Finite Element Nonlinear Plane Stress Analysis of Reinforced Concrete"; (Publication Unknown); pp 3-33.

[32] Chaikes, S.; "Calcul des abouts des poutres en béton précontraint"; Congrès International du Béton Précontraint à Gand; September; 1951; pp B41:1-27.

[33] Christodoulides, S.P; "The Distribution of Stresses Around the End Anchorages of Prestressed Concrete Beams. Comparison of Results Obtained Photoelastically with Strain Gauge Measurements and Theoretical Solutions"; IABSE Memoirs; Vol 16; 1956; pp 55-70.

[34] Christodoulides, S.P.; "A Photoelastic Investigation of Prestressed Concrete Anchorages"; Civil Engineering and Public Works Review; Vol 51, No 603; September; 1956; pp 994-997.

[35] Christodoulides, S.P.; "A Two-Dimensional Investigation of the End Anchorages of Post-Tensioned Concrete Beams"; The Structural Engineer; April; 1955; pp 120-133.

[36] Christodoulides, S.P.; "Three-Dimensional Investigation of the Stresses in the End Anchorage Blocks of a Prestress Concrete Gantry Beam"; The Structural Engineer; Vol 35, No 9; September; 1957; pp 349-356.

[37] Collins, M., Mitchell, D.; "Design of Disturbed Regions, Chapter 9"; Prestressed Concrete Basics, Canadian Prestressed Concrete Institute; 1987; pp 386-429.

[38] Construction Industry Research and Information Association; "A Guide to the Design of Anchor Blocks for Post-Tensioned Prestressed Concrete Members,"; CIRIA Guide 1, London; June; 1976.

[39] Cook, W.D., Mitchell, D.; "Studies of Disturbed Regions near Discontinuities in Reinforced Concrete Members"; ACI Structural Journal; March-April; 1988.

[40] CSA; "Design of Concrete Structures for Buildings"; Canadian Standards Associations, Rexdale; 1984.

[41] Csagoly, P., Holowka, M.; "Cracking of Voided Post-Tensioned Concrete Bridge Decks"; Ministry of Transportation and Communication; January; 1975.

[42] Csagoly, P., Holowka, M.; "The McCowon Bridge Test"; Ministry of Transportation and Communication; December; 1974.

[43] Csagoly, P., Holowka, M.; "Model Studies for Voided Post-Tensioned Concrete Slab Bridges"; Ministry of Transportation and Communication; August; 1974.

[44] Csagoly, P., Holowka, M.; "Finite Element Computer Program for Analysis of Plates with Bending and In-Plane Stresses"; Ministry of Transportation and Communication; November; 1974.

[45] De Borst, R.; "Computational Aspects of Smeared Crack Analysis"; Computational Modelling of Reinforced Concrete Structures; Pineridge Press, Swansea; 1986; pp 44-83.

[46] DeWolf, J.T.; "Axially Loaded Column Base Plates"; ASCE, Structural Division Journal; Vol 104, No ST5; May; 1978; pp 781-795.

[47] Dilger W.H., Ghali, A.; "Remedial Measures for Cracked Webs of Prestressed Concrete Bridges, Portland Cement Institute (PCI) Journal"; Vol 19, No 4; July-August; 1974; pp 76-85.

[48] Direction Générale des Transports Intérieurs, Paris; "Ponts en Encorbellement Contruits par Encorbellements Successifs"; Direction des Routes et de la Sécurité Routière; Complément au Bulletin technique No. 7; April; 1979; French.

[49] Douglas, D.J., Trahair, N.S.; "An Examination of the Stresses in the Anchorage Zone of a Post-Tensioned Prestressed Concrete Beam, Magazine of Concrete Research"; Vol 12, No 34; March; 1960; pp 9-18.

[50] Dowrick, D.J.; "Anchorage Zone Reinforcement for Post-Tensioned Concrete"; Civil Engineering and Public Works Review; September; 1964; pp 1101-1107.

[51] Drew, G.E.; "Post-Tensioning System Surveillance Program"; ASCE Structural Division Journal; Vol 105, No ST2; February; 1979; pp 347-357.

[52] Egeberg, J.L.; "A Finite Element Investigation of the Anchorage Zones of Prestressed Concrete Beams"; Department of Civil Engineering, University of California, Berkeley; No 363; August; 1968.

[53] Eibl, J.; "Innenverankerungen von Spanngliedern"; Beton- und Stahlbetonbau; No 2; 1973.

[54] Eibl, J., Ivanyi, G.; "Untersuchungen an Innenverankerungen im Spannbetonbau"; Schriftreihe des Deutschen Auschusses für Stahlbeton; 1966.

[55] El-Behairy S.; "Zugkräfte in der Nähe der Ankerplatten eines im inneren einer Rechteckscheibe verankerten Spanngliedes"; Beton- und Stahlbetonbau; 1968; p 135.

[56] Erickson, D.A.; "Problems Encountered with Post-Tensioned Unbonded Tendons"; Building Standards; Vol 54, No 5; September-October; 1985; pp 4-6.

[57] Evans, R.H., Marathe, M.S; "Micro-Cracking and Stress-Strain Curves for Concrete in Tension"; Matériaux et Constructions; Vol 1, No 1; January-February; 1968; pp 61-64.

[58] Falconer, B.A.; Post-Tensioning Anchorage Zones in Bridge Decks; Masters Thesis, UT Austin; May; 1990.

[59] Fenwick, R.C., Lee, S.C.; "Anchorage Zones in Prestressed Concrete Members"; Magazine of Concrete Research; Vol 38, No 135; June; 1986; pp 77-89.

[60] Figg, E.C.; "Segmental Bridge Design in the Florida Keys"; Concrete International; Vol 2, No 8; August; 1980; pp 17-22.

[61]   FIP Recommendations for Acceptance and Application of Post-Tensioning Systems; March; 1981.

[62]   Florida Department of Transportation Design Criteria..

[63]   Freyermuth, C.L.; "Post-Tensioning Details for Long Span Concrete Bridges"; PCI Journal; Vol 27, No 6; November-December; 1982; pp 48-65.

[64]   Fujii M., Kitamura, Y., Araki, T.; "Control of Horizontal Crack Width in Pretensioned Concrete Girders"; Journal of Japan Prestressed Concrete Association; Vol 16; May; 1971.

[65]   Fujii, M., Miyamoto, A., Kajimura, Y.; "Crack Control Design of Intermediate Anchorage Zone in Prestressed Concrete"; FIP Symposium on Partial Prestressing, Part; September; 1980; pp 44-51; Romanian.

[66]   Fujii, M., Miyamoto, A., Mizuno, H.; "Fundamental Study of Reinforcement of Rib-Anchorage Zone in Prestressed Concrete Member"; Journal of the Society of Materials Science,; Vol 29, No 318; March; 1980; pp 299-305; Japanese.

[67]   Gergely, P., Sozen, M.A.; "Design of Anchorage-Zone Reinforcement in Prestressed Concrete Beams"; PCI Journal; Vol 12, No 2; April; 1967; pp 63-75.

[68]   Gergely, P., Sozen, M.A., Siess,C.P.; "The Effect of Reinforcement on Anchorage Zone Cracks in Prestressed Concrete Members"; University of Illinois Civil Engineering Structural Research Series; No 271; July; 1963.

[69]   German Building Code; "DIN 1045"; Sec 17; German.

[70]   German Building Code Commentary; "Hilfsmittel zur Berechnung der Schnittgrossen und Formanderungen von Stahlbetontragwerken nach DIN 1045"; Heft 240; January; 1972; German.

[71]   Gerstner, R.W., Zienkiewicz, O.C.; "A Note on Anchorage Zone Stresses"; ACI Journal; July; 1962; pp 970-974.

[72] Greenberg, H.J, Prager, W.; "Limit Design of Beams and Frames"; ASCE Transactions; Separate No. 59; February; 1951; pp 447-484.

[73] Guyon, Y.; "Contraintes dans les pièces prismatiques soumises à des forces appliquées sur leurs bases, au voisinage de ces bases"; International Association for Bridge and Structural Engineering; Vol 11; 1961; pp 165-226.

[74] Guyon, Y.; "Limit-State Design of Prestressed Concrete, Vol 2, The Design of the Member"; John Wiley and Sons, New York; 1974.

[75] Guyon, Y.; "Prestressed Concrete"; John Wiley and Sons, New York; 1953.

[76] Hawkins, N.M.; "The Bearing Strength of Concrete Loaded through Rigid Plates"; Magazine of Concrete Research; Vol 20, No 62; March; 1968; pp 31-40.

[77] Hawkins, N.M.; "The Bearing Strength of Concrete Loaded Through Flexible Plates"; Magazine of Concrete Research; Vol 20, No 63; June; 1968; pp 95-102.

[78] Hawkins, N.M.; "The Bearing Strength of Concrete for Strip Loadings"; Magazine of Concrete Research; Vol 22, No 71; June; 1970.

[79] Hawkins, N.M.; "The Behavior and Design of End Blocks for Prestressed Concrete Beams"; Civil Engineering Transactions Institution of Engineers of Australia; October; 1966; pp 193-202.

[80] Hibbitt, Karlsson, and Sorenson Providence, RI.; "ABAQUS Users Guide".

[81] Higashida, K., Nakajima, H.; "Experimental Study on Reinforcement of Multiple Anchorages Zone in Post-Tensioned Concrete Member"; Journal of Japan Prestressed Concrete Engineering Association; Vol 16, extra number; 1974; pp 41-47.

[82] Hildebrand, J.F.; "Buttonheads for Tendon Wires of a Prestressed Concrete Reactor Vessel"; PCI Journal; Vol 16, No 5; September-October; 1971; pp 78-99.

[83] Hiltscher R., Florin, G.; "Die Spaltzugkraft in einseitig eingespannten am gegenüberliegenden Rande belasteten rechteckigen Scheiben"; Bautechnik; Vol 39, No 10; October; 1962; pp 325-328.

[84] Huang, T.; "Anchorage Take-Up Loss in Post-Tensioned Members"; PCI Journal; Vol 14, No 4; August; 1969; pp 30-35.

[85] Huang, T.; "Stresses in End Blocks of a Post-Tensioned Prestressed Beam"; ACI Journal; Vol 61, No 5; May; 1964; pp 589-601.

[86] Iyengar K.T.S.R.; "Ueber den Spannungszustand in einem elastischen Halbstreifen"; Oesterreichiche Ingenieur Archiv; Vol 16, No 3; 1962; pp 185-199.

[87] Iyengar, K.T.S.R.; "Two-Dimensional Theories of Anchorage Zone Post-Tensioned Prestressed Beams"; ACI Journal; Vol 59, No 10; October; 1962; pp 1443-1446.

[88] Iyengar, K.T.S.R., Prabhakara, M.K.; "Anchor Zone Stresses in Prestressed Concrete Beams"; ASCE Structural Division Journal; Vol 97, No ST3; March; 1971; pp 807-824.

[89] Iyengar, K.T.S.R., Yogananda, C.V.; "A Three-Dimensional Stress Distribution Problem in the Anchorage Zone of a Post-Tensioned Concrete Beam"; Magazine of Concrete Research; Vol 18, No 55; June; 1966; pp 75-84.

[90] Jofriet, J.C., McNeice. G.M., Csagoly, P.; "Finite Element Analysis of Prestressed Concrete Voided Bridge Decks"; PCI Journal; Vol 18, No 3; May-June; 1973; pp 51-66.

[91] Jones, T.R. Jr., Stephenson, H.K.; "Properties of Lightweight Concrete Related to Prestressing"; Proceedings of World Conference on Prestressed Concrete, Univ. of California, Berkeley, CA; 1957; pp A61-A612.

[92] Kammenhuber, J., Schneider, J.; "Arbeitsunterlagen für die Berechnung vorgespannter Konstruktionen"; Stahlton, Zürich; 1974.

[93] Komendant, A.E.; "Prestressed Concrete Structures"; McGraw-Hill; 1952; pp 172-173.

[94] Kruger, U.; "The Analysis of Patented Anchor Heads of Steel Wire Cable"; Der Bauingenieur; Vol 52, No 5; March; 1977; pp 105-11; German.

[95] Kupfer H.; "Bemessung von Spannbetonbauteilen"; Betonkalender; Part 1; 1981; p 1102.

[96] Lee, S.C.; "Bursting Stresses in the End Block of a Post-In Tensioned Prestressed Beam"; University of Auckland, Library School of Engineering; Report No 321; January; 1983.

[97] Lenschow, R., Sozen, M.A.; "Practical Analysis of the Anchorage Zone Problem in Prestressed Beams"; ACI Journal; November; 1965; pp 1421-1437.

[98] Leonhardt, F.; "Das Bewehren von Stahlbetontragwerken"; Beton Kalender von Wilhelm e. & Sohn; 1973.

[99] Leonhardt, F.; "Vorlesung über Massivbau, Teil 2"; Sonderfälle der Bemessung im Stahlbetonbau, Springer Verlag; 1986.

[100] Leonhardt, F.; "Vorlesung über Massivbau, Teil 5"; Spannbeton, Springer Verlag; 1980.

[101] Leonhardt, F.; "Prestressed Concrete--Design and Construction"; Wilhelm Ernest and Son, Berlin; 1964.

[102] Libby, J.R.; "Critique of a Post-Tensioned Roof Slab Failure"; Concrete International; Vol 7, No 10; October; 1985; pp 28-32.

[103] Libby, J.R.; "Segmental Box Girder Bridge Superstructure Design"; ACI Journal; Vol 73, No 5; May; 1976; pp 279-290.

[104] Lin, T.Y., Burns, N.H.; "Design of Prestressed Concrete Structures"; John Wiley & Sons, N.Y., 3rd ed.; 1981.

[105] Lin, T.Y., Redfield, C.; "Some Design Issues for American Constructors"; Proceedings of the Segmental Concrete Bridge Conference PC-7 Kansas City, MO; 1982.

[106] Littlejohn, G.S.; "Rock Anchor - State of the Art, Part 1:Design"; Ground Engineering; Vol 8, No 3; August; 1975.

[107] Losinger LTD, Bern; "Technical Documentation, Einleitung der Vorspannkräfte in den Beton"; Losinger, Bern; October; 1985.

[108] Losinger LTD, Bern; "VSL End Block Design in Post-Tensioned Concrete"; November; 1975.

[109] Ly K.T.; "Effet des forces de précontrainte concentrée dans les poutres caisson"; Rapport de recherche du Laboratoire des Ponts et Chaussées; No 68; September; 1977.

[110] MacGregor, J.; "Reinforced Concrete - Analysis and Design"; 1988.

[111] Magnel, G.; "Prestressed Concrete"; McGraw Hill, New York, 3rd Ed.; 1954.

[112] Marti, P.; "Basic Tools for Reinforced Concrete Beam Design"; ACI Journal; January-February; 1985; pp 46-56.

[113] Marti, P.; "Truss Models in Detailing"; Concrete International; December; 1985; pp 66-73.

[114] Marti, P.; "Zur plastischen Berechnung von Stahlbeton"; IBK ETH Zürich; Report No. 104; 1980.

[115] Meyer, C. , Okamura, H., editors; "Finite Element Analysis of Reinforced Concrete Structures"; ASCE; 1986.

[116] Meyerhof, G.G.; "The Bearing Capacity of Concrete and Rock"; Magazine of Concrete Research; Vol 4, No 12; April; 1953; pp 107-116.

[117] Middendorf, K.H.; "Anchorage Bearing Stresses in Post-Tensioned Concrete"; ACI Journal; November; 1960; pp 580-584.

[118] Middendorf, K.H.; "Practical Aspects of End Zone Bearing of Post-Tensioning Tendons"; PCI Journal; Vol 8, No 4; August; 1963; pp 57-62.

[119] Mitteilungen des Instituts für Bautechnik, Berlin; Heft 5; German.

[120] Mordecci, V.S.; "The Progress of Post-Tensioning Concrete"; Concrete, Journal of Concrete Society; Vol 18, No 10; October; 1984.

[121] Müller R.K., Schmidt, D.W.; "Zugkräfte in einer Scheibe, die durch eine zentrische Einzellast in einer rechteckigen Oeffnung belastet wird"; Die Bautechnik; Vol 11; 1964 S. 174 (IABSE); pp 165-226.

[122] Mörsch, E.; "Ueber die Berechnung der Gelenkquader"; Beton und Eisen; No 12; 1924; pp 156-161.

[123] Neal, B.G.; "The Plastic Methods of Structural Analysis"; John Wiley and Sons, N.Y.; 1963.

[124] Niyogi, S.K.; "Bearing Strength of Reinforced Concrete Blocks"; ASCE Structural Division Journal; Vol 101, No ST5; May; 1975.

[125] Niyogi, S.K.; "Bearing Strength of Concrete-Geometric Variations"; ASCE Structural Division Journal; Vol 99, No ST7; July; 1973; pp 1471-1490.

[126] North Carolina Department of Transportation Design Criteria..

[127] Ontario Highway Bridge Design Code; 1983.

[128] Ontario Highway Bridge Design Commentary; 1983.

[129] Ottosen, N.S.; "A Failure Criterion for Concrete"; ASCE Journal of Engineering Mechanics; Vol. 104, No. EM4; August; 1977; 527-535.

[130] Patran Users Guide; 1986.

[131] PCI Bridge Committee; "Tentative Design and Construction Specification for Precast Segmental Box Girder Bridges"; PCI Journal; Vol 20, No 4; July-August; 1975; pp 34-42.

[132] PCI Segmental Construction Committee; "Recommended Practice for Segmental Construction in Prestressed Concrete"; PCI Journal; Vol 20, No 2; March-April; 1975; pp 22-41.

[133] Picket, G., Iyengar, K.T.S.R; "Stress Concentration in Post-Tensioned Prestressed Concrete Beams"; Journal of Technology, Bengal Engineering College; Vol 1, No 2; December; 1956; pp 105-112.

[134] Podolny, W.; "The Cause of Cracking in Post-Tensioned Concrete Box Girder Bridges and Retrofit Procedures"; PCI Journal; Vol 30, No 2; March-April; 1985; pp 82-139.

[135] Podolny, W. and PCI-Post Tensioning Institute (PTI) Comm.; "Recommended Practice for Precast Post-Tensioned Segmental Construction"; PCI Journal; Vol 27, No 1; January-February; 1982; pp 15-61.

[136] Post-Tensioned Box Girder Bridge Manual; "PTI"; 1978.

[137] Post-Tensioned Box Girder Bridges, Design and Construction; "Western Concrete Reinforcing Steel Institute, PCI and Concrete Reinforcing Steel Institute"; 1969.

[138] Post-Tensioning Manual, 4th Ed.; "PTI"; 1986.

[139] Prestressing Part 2- Anchorages and End Blocks; " Concrete, Journal of the Concrete Society"; Vol 13, No 6; June; 1979; p 41.

[140] PTI; "Design and Construction Specifications for Segmental Concrete Bridges"; Post-Tensioning Institute; February; 1988.

[141] PTI Ad Hoc Committee for Unbounded Single Strand Tendons; PCI Journal; Vol 30, No 2; March-April; 1985; pp 22-39.

[142] Ramaswamy, G.S., Goel, H.; "Stresses in End Blocks of Prestressed Beams by Lattice Analogy"; Proceeding of World Conference on Prestressed Concrete, San Francisco; July; 1957; pp 231-234.

[143] Rasheeduzzafar, I.M.A., Al-Saadoum, S.S.; "A Photoelastic Investigation of Anchorage Bearing Stresses"; Magazine of Concrete Research; Vol 36, No 127; Jun-84; 1984; pp 81-91.

[144] Rejcha, C.; "Simplified Bearing Plate Computations for Post-Tensioning Anchorages"; PCI Journal; Vol 20, No 4; Jul-August; 1975; pp 102-111.

[145] Rhodes, B., Turner, F.H.; "Design of End-Blocks for Post-Tensioned Cables"; Concrete; Vol 1, No 12; December; 1967; pp 431-434.

[146] Roberts, C.; "Behavior and Design of the Local Anchorage Zone in Post-Tensioned Concrete"; Master's Thesis, UT Austin; May; 1990.

[147] Rogowsky, D.M., MacGregor, J.G.; "Design of Reinforced Concrete Deep Beams"; Concrete International; August; 1986; pp 49-58.

[148] Rowe, R.E.; "End Block Stresses in Post-Tensioned Concrete Beams"; The Structural Engineer; Vol 41, No 2; February; 1963; pp 55-67.

[149] Rowe, R.E., Zielinski, J.; "Distribution of Stress in Anchor Blocks"; Engineering; Vol 189, No 4899; Mar-11; 1960; pp 347-348.

[150] Rydezewski, J.R., Whitbread, F.J.; "Short End Blocks for Prestressed Beams"; The Structural Engineer; Vol 41, No 2; February; 1963; pp 41-53.

[151] Rüsch H.; "Spannbeton-Erlaüterungen zu DIN 4227: Richtlinien für Bemessung und Ausfürung."; Wilhelm Ernst und Sohn, Berlin; 1954.

[152] Rüsch H., Küpfer, G.; "Bemessung von Spannbetonbauteilen"; Beton Kalender von Wilhelm and Son; 1974.

[153] Sanders, D.H; "Design and Behavior of Post-Tensioned Concrete Anchorage Zones:; PhD Thesis, UT Austin; May; 1990.

[154] Sargious, M.; "Beitrag zur Ermittlung der Hauptzugspannungen am Endauflager vorgespannter Betonbalken"; Ph.D. dissertation Technische Hochschule Stuttgart; July; 1960.

[155] Schechter, E., Böcker, H.C.; "Wedge Anchorage System for Strand Post-Tensioning"; PCI Journal; Vol 16, No 4; July-August; 1971; pp 49-63.

[156] Schlaich, J., Scheef H.; "Concrete Box-Girder Bridges"; Structural Engineering Documents, 1e, IABSE; 1982.

[157] Schlaich, J., Schäfer, K.; "Konstruiren in Stahlbetonbau"; Beton Kalender; Part 2; 1989; pp 563-715; German.

[158] Schlaich, J., Schäfer, K., Jennewein, M.; "Toward a Consistent Design of Reinforced and Prestressed Concrete Structures"; PCI Journal; Vol 32, No 3; May-June; 1987; pp 74-151.

[159] Schlaich, M.; "Computerunteresützte Bemessung von Stahlbetonscheiben mit Fachwerkmodellen"; PhD Dissertation, ETH Zürich; 1989; German.

[160] Schleeh, L.K.; "Die Spannungszustände beim Auflager eines Spannbetonträgers"; Beton-und Stahlbetonbau, Berlin; Vol 58, No 7; July; 1963; pp 157-171; German.

[161] Schupack, M.; "Large Post-Tensioning Tendons"; PCI Journal; Vol 17, No 3; May-June; 1972; pp 14-28.

[162] Seible, F.; "Coupling Joints of Prestressing Tendons in Continuous Post-Tensioned Concrete Bridges.(Not Published Yet)".

[183] Vaughn, S.D.; "An Exploratory Photoelastic Investigation of Post-Tensioned Concrete Anchorage Zone Bursting Stresses"; unpublished M.S. thesis, The University of Texas at Austin; August; 1977.

[184] Vecchio, F.J., Collins, M.P.; "The Modified Compression-Field Theory for Reinforced Concrete Elements Subjected to Shear"; ACI Journal; March-April; 1986; pp 219-231.

[185] Virlogeux, M.; "Analyse de quelques problèmes spécifiques au calcul des ponts par encorbellements successifs"; Annales de l'Institut Technique du Bâtiment et des Travaux Publics; No. 391; February; 1981.

[186] Welsch, W.A. Jr, Sozen M.A.; "Investigation of Prestressed Reinforced Concrete Highway Bridges, Part 2, Analysis and Control of Anchorage Zone Cracking in Prestressed Concrete"; Engineering Experimental Station, Univ. of IL, Urbana; Bulletin No 497; 1968.

[187] Williams, A.; "The Bearing Capacity of Concrete Loaded Over a Limited Area"; Univ. of IL, Urbana; 1979.

[188] Wium, D., Buyukozturk, O.; "Problems in Designing Prestressed Segmental Bridges"; Massachussetts Institute of Technology; March; 1984.

[189] Wollmann, G.; Analysis and Design of Anchorage Zones; PhD Dissertation to be published, UT Austin.

[190] Woodward, R.J.; "Cracks in a Concrete Bridge"; Concrete; Vol 17, No 7; July; 1983; pp 49-45.

[191] Yankelvsky, D.Z., Reinhardt, H.W; "Uniaxial Behavior of Concrete in Cyclic Tension"; ASCE Journal of Structural Engineering; Vel 115, No. 1; January; 1989; pp 166-182.

[192] Yettram, A.L., Robbins, K.; "Anchorage Zone Stresses in Axially Post-Tensioned Members of Uniform Rectangular Section"; Magazine of Concrete Research; Vol 21, No 67; June; 1969; pp 103-112.

[193] Yettram, A.L., Robbins, K.; "Anchorage Zone Stresses in Axially Post-Tensioned I-Section Members with End-Blocks"; Magazine of Concrete Research; Vol 23, No 74; March; 1971; pp 37-42.

[194] Yettram, A.L., Robbins, K.; "Anchorage Zone Stresses in Post-Tensioned Uniform Members with Eccentric and Multiple Anchorages"; Magazine of Concrete Research; Vol 22, No 73; December; 1970; pp 209-218.

[195] Yong, Y.K., Gadugbeku, C., Nawy, E.; "Anchorage Zone Stresses of Post-Tensioned Prestressed Beams Subjected to Shear Forces"; ASCE Structural Division Journal; Vol 113, No 8; August; 1987; pp 1789-1805.

[196] Zielinski, J.L., Rowe, R.E; "The Stress Distribution Associated with Groups of Anchorages in Post-Tensioned Concrete Members"; Cement and Concrete Association, London; October; 1962.

[197] Zielinski, J.L., Rowe, R.E.; "An Investigation of the Stress Distribution in the Anchorage Zones of Post-Tensioned Concrete Members"; Cement and Concrete Association, London; Research Report No. 9; September; 1960.

[198] Zielinski, J.L., Scibak, W.; "Anchorage Zone of Post-Tensioned Concrete Members - Recent Tests and Design Provisions"; FIP - 10th International Congress, New Dehli; February; 1986; pp 281-288.

Olivier Laurent Burdet was born in Lausanne, Switzerland on March 9, 1960, the son of Jacques Edouard and Georgette Mai Burdet-Lugeon. He attended high school in Morges, Switzerland and Lausanne, Switzerland. He entered the Swiss Federal Institute of Technology in October 1978 and received the degree of Bachelor in Civil Engineering in January 1983. From April 1983 to August 1985, he was employed as a structural engineer by Glauser, Studer, Stüssi in Zürich, Switzerland. From September 1985 to July 1986 he attended the Geneva Bible Institute in Geneva, Switzerland. In August 1986, he entered the Graduate School of the University of Texas at Austin.

Permanent address: Les Sauges

                      CH-1136 Bussy-Chardonney (VD)

                      SWITZERLAND

This dissertation was typed by the author.